```
--    1   OF     2
-- 1 -  AD NUMBER: 719936
-- 6 -  UNCLASSIFIED TITLE:     NONLINEAR ACOUSTICS,
--11 -  REPORT DATE:       DEC    , 1970
--15 -  CONTRACT NUMBER:  N00014-70-A-0166-0001
```

```
-- END                Y  FOR NEXT ACCESSION                    END
P
--    2   OF     2
-- 1 -  AD NUMBER: 520010
-- 6 -  UNCLASSIFIED TITLE:     NONLINEAR ACOUSTICS.
--11 -  REPORT DATE:       MAR 16, 1972
--14 -  REPORT NUMBER:     ARL-TR-72-14
--15 -  CONTRACT NUMBER:  N00014-70-A-0166
```

(6)

Nonlinear Acoustics

(2)

(10)

Robert T. Beyer
Professor of Physics
Brown University
Providence, Rhode Island

Written for the Naval Ship Systems Command
Department of the Navy
1974

(12) 413

(15) N0002-72-C-1397

PREFACE

The idea of writing this book occurred to the author one night while he was in the hospital, between surgical operations. Whether he was under sedation at the time, or whether the idea was an hallucination, is best left to the judgment of the reader.

The opportunity to write the book was provided by a sabbatical leave from Brown University, spent in the Department of Electrical and Electronic Engineering at the University of Birmingham (U.K.) in 1971, and the writer extends his thanks to the Department Head, Professor David Tucker, Dr. O. H. Berktay, for their help in making the stay both possible and fruitful. Particular acknowledgment must be made to the University and Department librarians at Birmingham for their courtesy and helpful service.

The finishing of a book requires the assistance and cooperation of many. Thanks are of course due to Brown University on many points. The writer is also grateful to his colleagues in the Department of Physics at Brown, especially Professors A. O. Williams, Jr. and Peter J. Westervelt, for conversations on acoustical problems that have assisted in the preparation of this book. Special thanks are due Professor Mark B. Moffett of the University of Rhode Island who, in the spirit of "once a graduate student, always a graduate student," reviewed a good fraction of the book in some detail. The book was supported by the Naval Sea Systems Command under Contract N00024-72-C-1397 with Brown University.

The author acknowledges with thanks the cooperation of Academic Press for allowing him to use materials in this book from the author's previous publications with that company. Acknowledgment should also be made to various secretaries who worked on parts of the manuscript, with special thanks to Miss Maureen Byrne, who typed most of the text twice.

Finally, gratitude is due to my wife and family, for putting up once again with an author in the house.

Robert T. Beyer

February 14, 1974

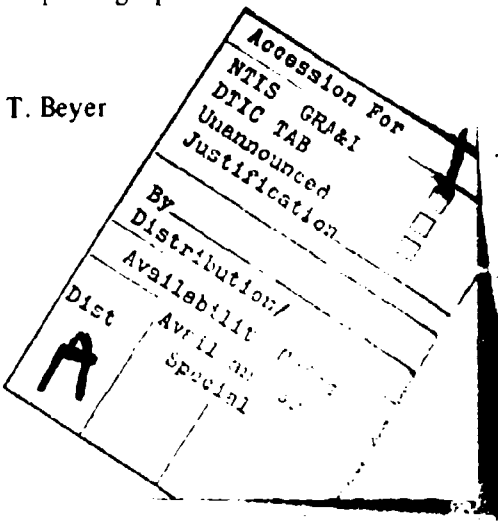

To my wife Ellen,

on our thirtieth anniversary

CONTENTS

INTRODUCTION

1. The Nature of Nonlinear Acoustics.

It is a commonplace remark to say that the theory of acoustics is an infinitesimal theory. The meaning here, of course, is that such quantities as the changes in pressure, density and temperature, produced by a sound wave are always small (i.e., infinitesimal) in comparison with the equilibrium values of the same quantities. However, one cannot make the same comparison for the displacement velocity of the hypothetical particle, since the theoretical treatment of sound propagation presupposes a continuous medium that is at rest in equilibrium. It is customary, and sensible, therefore, to require that the ratio of the particle velocity to the velocity of propagation of sound be sufficiently small. The question is, how small is small?

The answer to this question will be the burden of much of this book. To make a beginning, we first define the *acoustic Mach number M* as the ratio of the maximum particle velocity to the local sound velocity. We then require $M << 1$.

The significance of this definition, which parallels the more common Mach number of aerodynamics, can be gathered by considering the case of a plane harmonic wave in which the particle or displacement velocity u is expressed by

$$u = u_0 \sin \omega \left(t - \frac{x}{c_0} \right) \tag{1}$$

where u_0 is the amplitude of the displacement velocity and c_0 the sound velocity when the amplitude of the wave is infinitesimal.

The acoustic Mach number is then $M = u_0/c_0$. We now introduce the fact that the change in pressure δp associated with such a wave, is related to the particle velocity by the expression $\delta p = \rho_0 c_0 u$, where ρ_0 is the mean density of the medium. Then

$$M = \frac{u_0}{c_0} = \frac{\delta p_{\max}}{\rho_0 c_0^2} \quad . \tag{2}$$

For a gas under pressure p_0 and with an equilibrium density ρ_0, the sound propagation velocity is given by $c_0 = \sqrt{\gamma p_0/\rho_0}$, where γ is the ratio of specific heats.

The acoustic Mach number for a gas is therefore

$$M = \frac{\delta p_{\max}}{\gamma p_0}.$$

This ratio enters our problem in the following way. The usual one-dimensional wave equation for a particle displacement ξ

$$\frac{\partial^2 \xi}{\partial t^2} = c_0^2 \frac{\partial^2 \xi}{\partial x^2} \tag{3}$$

is in fact an approximation. The more accurate form (see Sec. 3.1) is

$$\left(1 + \frac{\partial \xi}{\partial x}\right)^{\gamma+1} \frac{\partial^2 \xi}{\partial t^2} = c_0^2 \frac{\partial^2 \xi}{\partial x^2}. \tag{4}$$

Equations (3) and (4) are compatible only if $\partial\xi/\partial x$ is entirely negligible, or if $\gamma = -1$. This latter is highly unlikely, although mathematical treatment of the case is not without significance. [1] We shall concentrate our attention on the first condition. In the case of the harmonic plane wave of Eq. (1), we can integrate over time to obtain

$$\xi = -\xi_0 \cos \omega\left(t - \frac{x}{c_0}\right)$$

so that

$$\left(\frac{\partial \xi}{\partial x}\right)_{\max} = \xi_0 \frac{\omega}{c_0} = \frac{u_0}{u} = M. \tag{5}$$

Thus the condition that $\partial\xi/\partial x$ be negligible compared with unity is equivalent to the previously stated condition $M \ll 1$.

It might appear that we have answered our question, but in fact we have not. For example, the sound of a jet engine at short range may be as intense as 140dB re 0.0002 dyne/cm^2, which corresponds to a value $M \simeq 1/1000$, a number that seems to be very small indeed. Nevertheless, the total effect of the factor $[1 + (\partial\xi/\partial x)]^{\gamma+1}$ will turn out to be quite considerable in this case.

The reason for this curious development is that the effect of the presence of a finite value is cumulative and while the influence of this term is only on the scale of 1 part in 1000 in a single wavelength, the wave will be seriously distorted by the term in $\partial\xi/\partial x$ after 1000 wavelengths.

The distinction between Eqs. (3) and (4) is, of course the difference between linear acoustics [Eq. (3)] and nonlinear acoustics [Eq. (4)].

It has been said that the mathematical analysis of physical problems is a series of rearguard actions. After we admit that a situation exists, we first suppose that it can be represented by a suitably chosen constant. When that fails, we switch to a linear dependence, and it is only as a last resort that we retreat to the use of nonlinear relations and nonlinear equations.

Only a few decades ago, nonlinear acoustics was little more than the analysis of shock waves and large amplitude mechanical vibrations. Gradually, however, more and more of acoustics has been examined for its nonlinear aspects until today one can write a nonlinear supplement to virtually every chapter of a text on acoustics and vibrations. This book might be regarded as a compendium of such supplements.

Because of the large attention that has already been given elsewhere to the topics of shock waves and nonlinear vibrations, these subjects will be treated rather sparingly here, and the reader is referred to well-known texts [2,3] for more detailed treatment.

2. Historical Aspects.

The reader who makes even a casual study of the earlier literature will be astonished, not at the lack of references to nonlinear phenomena at dates more than thirty years ago, but rather at the number of nonlinear processes that were observed and described in the distant past, studies that have frequently been neglected or forgotten until recently.

Aeroacoustics

Probably the oldest known nonlinear (acoustical) device is the Aeolian harp. In 1650, Athanasius Kircher [4] wrote a description of this instrument, but its existence goes back to early antiquity. In the Aeolian harp, a flow of wind (Aeolus, Roman god of the wind) past a string or wire can set that string in oscillation, and tradition has it that King David would set his harp so that the wind at night would strike it and produce sound. The wind whistling through tall grass or tree branches, the "singing" telephone wire and Lord Rayleigh's fingers in the baths at Bath* are all examples of the same phenomenon—the conversion of direct fluid flow to vibratory motion.

*"Bath, January, 1884:

I find in the baths here that if the spread fingers be drawn pretty quickly through the water (palm foremost is best) they are thrown into transverse vibration and strike one another. This seems like the aeolian string . . . ." Rayleigh's Notebook. [5]

An early analytic treatment (1878) of this phenomenon was that of Strouhal [6] who found experimentally that the frequency f is related to the airspeed v and diameter of wire d by

$$f \simeq 0.185\, v/d. \tag{6}$$

If f corresponds to the natural frequency of the wire, a substantial reinforcement of the vibration is obtained.

It was pointed out by Lord Rayleigh that the effect of the Aeolian harp must be due to the forces set in motion by the vortices that are created by the fluid flow past a solid cylinder. At very low speeds of flow the streamlines cling close to the cylinder on all sides, a behavior known as *potential* or *laminar flow* (Fig. 1a). However, even for rather modest speeds of flow, the stream lines break away from the cylinder in the rear (Fig. 1b). Helmholtz [7] attributed the drag resistance of a cylinder to the apparent "surface of discontinuity" AA'. Eddies or vortices are set up in this region (Fig. 1c). It was noted by Benard [8] and Mallock [9] that these eddies detach themselves from the region of the cylinder and move along the stream lines, very much as if they were small bits of matter caught up in the flow.

These vortices move off alternately from one side and the other. Their theoretical description was supplied by von Karman in a pair of classical papers [10] that resulted in the name *von Karman vortex trail* or *street* for the phenomenon. For a distance between the vortices at one side ℓ and spacing of the two lines of vortices h, von Karman found the relation

$$\frac{h}{\ell} \simeq 0.28\ . \tag{7}$$

The fact that the vortices drop off first from one side of the cylinder and then from the other results in a periodic force acting on the cylinder. The longitudinal component of this force opposing the flow direction always has the same sense, and contributes to the drag resistance, but the transverse component acts alternately in opposite directions, thus providing the stimulus for the Aeolian tones.

It is also of interest that Rayleigh noted in his famous book [11] that the Strouhal number, $= fd/v$ could depend on the shear viscosity η of the medium only through the combination $\eta/\rho vd$ (ρ = fluid density) a combination that was later exploited by Reynolds [12] in describing the transition from laminar to turbulent flow, and is hence known as the *Reynolds' number*.

A second sound source in fluid flow is that due to edge tones, first noted by Masson [13] and Sondhauss [14].

If air emerging from a narrow slit falls on a sharp wedge of wood or metal (Fig. 2), tones can be produced. Vortex trails pass out from the slit on either side, and a second street of vortices are produced at the wedge tip.

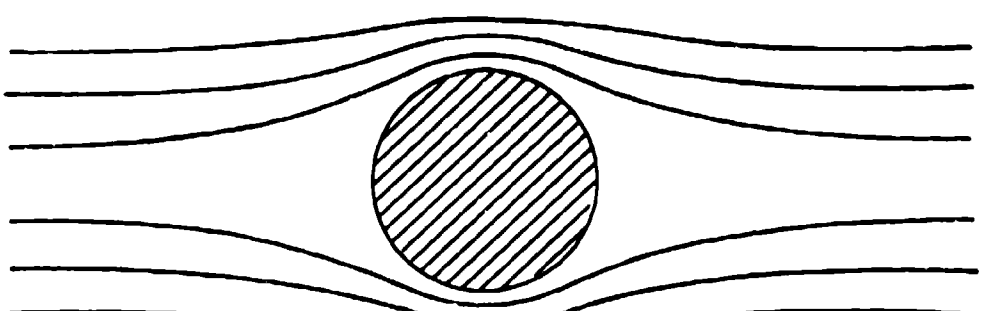

(a)

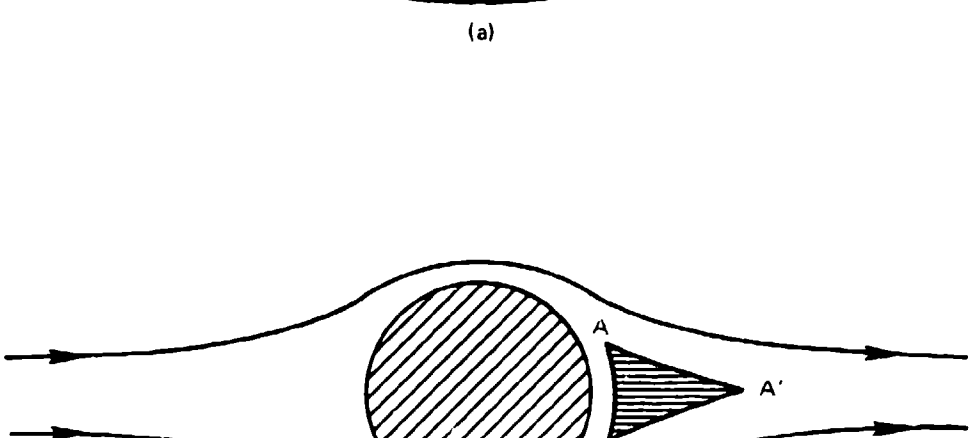

(b)

(c)

Figure 1.-Fluid flow around a rigid circular cylinder; (a) potential or laminar flow; (b) streamline breakaway with formation of surface of discontinuity AA'; (c) vortex formation behind cylinder.

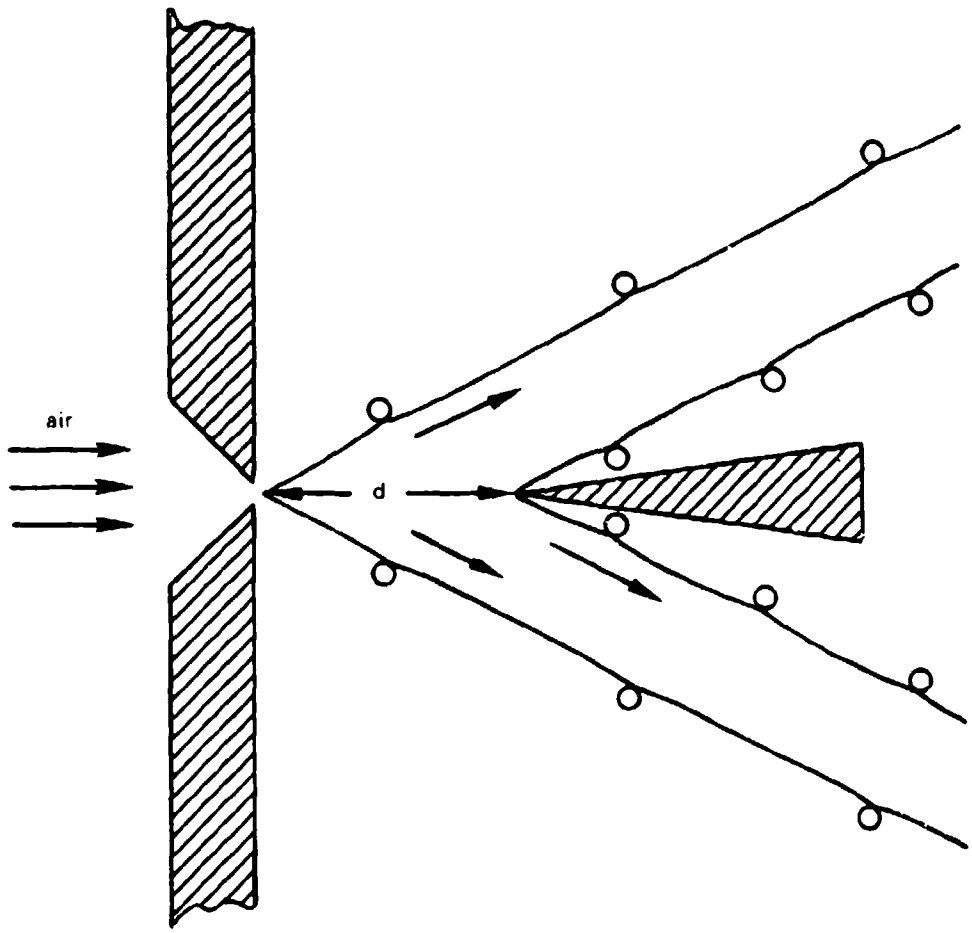

Figure 2.–Vortex formation and generation of edge tone in airflow through narrow slit onto facing wedge.

These vortices apparently must keep pace with the first set so that the distance *d* between slit and edge makes a kind of resonance distance.

Now the alternating nature of the detachment of vortices causes a vibration of the edge piece just as was the case for the wire. Here again the forces produced by the turbulent vortex street produce sound.

As early as 1877, Rayleigh had considered the effect of a rigid sphere undergoing periodic oscillations in a fluid, and showed that it would act in a fashion similar to that of an acoustic dipole, which was defined by him as "the limit of two equal opposite simple sources whose distance is diminished and intensity increased without limit in such a manner that the product of the intensity and distance is the same as for two unit sources placed a unit distance apart." [15]

Rayleigh also calculated the force exerted on the fluid by the oscillating sphere and observed that sound radiation occurred in the fluid flow past a wire when the wire was not permitted to vibrate. [16]

Thus the stage was set for the idea that sound generation from vortices might not require the presence of a solid surface, but more than half a century was to pass before it was stated directly by Yudin (1945) that he was "obliged to suppose that the origin of the vortex noise lies in the variable force acting on the medium." [17]

The next step was to regard turbulent motion of a fluid as a kind of inhomogeneity. Now the mathematical theory of the scattering of sound from small-scale inhomogeneities had been considered by Rayleigh. In this development, Rayleigh wrote down the expression for the D'Alembertian of the pressure,

$$\Box^2 p \equiv \nabla_p^2 - \frac{1}{c_0^2}\frac{\partial p}{\partial t^2} \quad . \tag{7}$$

He collected all other terms on the right side of the equation. These included terms dependent on the relative inhomogeneities in the sound velocity $\Delta c/c_0$ and the density $\Delta\rho/\rho_0$ of the medium, as well as other nonlinear terms in p and its derivatives. Since Rayleigh was interested in the effectiveness of these inhomogeneities in scattering an incident sound beam, he neglected the higher order terms not associated with the inhomogeneities. His equation then became

$$\Box^2 p = - \frac{2\Delta c}{c_0}\frac{\partial^2 p_s}{\partial t^2} - \frac{\partial}{\partial y}\left(\frac{\Delta\rho}{\rho_0}\right)\frac{\partial p_s}{\partial y} \tag{8}$$

where p_s is the pressure in the incident beam.

In 1952, Lighthill pointed out that, in the absence of inhomogeneities, the only terms remaining on the right side of Eq. (8) would be the higher order terms for a homogeneous medium, i.e., the terms discarded by Rayleigh. This led Lighthill to the equation

$$\Box^2 p = - \frac{\partial^2}{\partial y_i \partial y_j}(\rho u_i u_j + p_{ij} - c_0^2 \rho \delta_{ij}) \quad , \tag{9}$$

an equation that has become fundamental in subsequent studies of vortex-produced sound. (See Chapter 5 for identification of symbols and further development.)

Shock Waves

The history of the phenomenon of the shock wave begins with the observation in 1742 by a Belgian named Robens [18] that projectiles traveling faster than sound experienced surprisingly high resistance, but important progress waited upon improvement in experimental techniques.

In 1867 Poisson developed the *schlieren* method of sound visualization. Basically, this method involves the focussing of a light beam on the objective of a telescope or camera by means of a concave mirror. [19] If an opaque screen is drawn over half the objective lens, the mirror will appear to be quite dark. If the rays coming from the light source are disturbed by the presence of density changes in the medium (due, for example, to the passage of a shock wave), some additional light will bypass the screen and the mirror will appear illuminated. (Many variants of this technique have been developed. See A. B. Wood, [20] L. Bergmann [21] and Hargrove and Achyuthan. [22])

Töpler used this technique to show that an electrical spark discharge produced a compressed pulse in its neighborhood, while Mach and Gruess [23] used the same experiment to establish the fact that this pulse moved faster than sound and also that its speed increased with increase in the spark intensity.

The so-called shadow method, in which the shadow of the compressed regions of a spark induced pulse is photographed in the light produced by a second spark, made it possible to produce excellent photographs of the shock waves produced by a projectile in flight. [24]

At this stage, the experimental results were well ahead of theory, but Lord Rayleigh presented an analysis of shock waves in 1910 [25] and the fundamental equations governing shock wave propagation were derived by Rankine [26] and Hugoniot, [27] while the theory of shock thicknesses was treated by Becker. [28]

The problem of the "booms" resulting from the piling up of compressional waves in front of a supersonic source was treated by Prandtl [29] and later by Dumond et al. [30] while a definitive analysis of the patterns of such shocks at large distances waited until Whitham's work in 1952. [31]

Finite-amplitude Waves

Lying between linear acoustics and shock waves is the subject of small but finite amplitude waves. In 1808, Poisson [32] developed the form for the particle velocity

$$u = f[x - (c_0 + u)\, t] \tag{10}$$

that accurately describes the effect of a finite displacement u on the effective propagation speed of a given value of that velocity.

Poisson did not pursue the implications of this equation but Stokes [33] pointed out in 1848 that, since large values of u were propagated more rapidly than small values, the wave becomes progressively distorted as it travels through the medium, until ultimately a point is reached at which $\partial u/\partial x$ becomes negatively infinite, indicating a discontinuity. It remained for Earnshaw (1859) to produce an exact solution of Eq. (10), a solution that remained, however, in implicit form. [34] This relation of Earnshaw, which will be treated in detail in Chapter 3, remained in implicit form until 1935 when it was solved explicitly by Fubini. [35] The Fubini solution itself remained but little known for some years. The interesting history of this theory and its frequent rediscovery have been reviewed by Blackstock. [36]

A somewhat more limited but practical solution of the finite amplitude problem was developed by Riemann [37] in which the equation of motion (10) was linearized by using the first order expression for ξ to determine $\partial\xi/\partial x$ and by expanding

$$\left(1 + \frac{\partial \xi}{\partial x}\right)^{\gamma+1} \simeq 1 + (\gamma+1)\,\frac{\partial \xi}{\partial x} \quad .$$

This results in the production of a second harmonic component in the wave, the amplitude of which proportional to the distance from the source.

None of the foregoing analysis took sound absorption into account. In 1931, Fay developed his theory of the "almost stable wave." [38] The production of second and higher harmonics as a wave progresses, due to the nonlinear character of the acoustic wave equation, leading to the formation of a shock in the inviscid case, is counterbalanced at the higher frequencies (for most fluids, the absorption coefficient is proportional to the square of the frequency). In the almost stable wave, the two processes very nearly balance, so that the form of the distorted wave remains virtually constant.

Eckart [39] developed the perturbation analysis of the problem, and it was shown by Goldberg [40] and others [41] that the various harmonics rise to a maximum and then decay, a result confirmed experimentally by Krasilnikov et al. [42]

A somewhat different theoretical analysis was undertaken by Mendousse [43] who first noted the similarity between the acoustic equation and Burgers' equation, a general solution of which is known (Hopf, [44] Cole [45]). Khokhlov and coworkers [46] successfully carried out the analysis in 1962 and the work was continued by Blackstock, who also developed a model for the transition from the Fubini model to the Fay model of nonlinear propagation. [47]

Interaction of sound with sound.

One of the oldest observations in nonlinear acoustics was that made by Sorge in 1745 [48] and independently reported by Tartini in 1754 [49] (the latter claimed to have observed the effect as early as 1714). These two musi-

cians found that the sounding of two musical tones of high intensity results in the appearance of a lower tone, whose frequency is equal to the difference between the two original tones. The sounds have come to be known as "Tartini tones" or the Tartini pitch.

It was suggested by Lagrange [50] and later by Young [51] and Chladni [52] that the effect was the same as that of beats. The latter effect, which is the (low-frequency) modulation resulting from the sounding of two nearly similar tones, is a linear phenomenon. It was argued that, as the beat frequency increases, it goes over into a continuum tone, which is the difference frequency. These arguments found many supporters in the 19th century, even though it became known that the signals had to be quite intense before a difference tone could be observed, and that such a tone was a weak one, whereas beats are very evident even at relatively low intensities.

The problem therefore hung on for more than 100 years, until Helmholtz undertook his study of what he called *combination tones*, [53] and discovered the existence of a sum frequency as well as the difference frequency.

Even Helmholtz's discovery met with opposition, some observers completely denying its existence. An argument also developed as to whether these combination tones existed objectively, i.e., actual pressure waves propagating through the air, or "subjectively, being due to the nonlinear response of the ear." Helmholtz attributed the presence of the combination tones to nonlinearities within the ear, and modern research indicates the cochlea as the most probable source of such a nonlinear response.

Nevertheless, Rücker and Edser [54] were able to excite a tuning fork at the sum frequency, thus identifying the interaction as an objective one—i.e., actually occurring in the medium.*

In 1931, Lamb used a perturbation technique to consider the effect of two different primary frequencies propagating through a medium to show the existence of both sum and difference frequencies. His work was confirmed experimentally by Thuras, Jenkins and O'Neil. [56]

In 1950's, a controversy arose as to whether two sound beams intersecting at an arbitrary angle can produce sum and difference frequencies. The issue is a cloudy one and the author is an interested party. It is clear that two beams, traveling in the same direction, do produce sum and difference frequencies in the medium. The further development of this controversy will be treated in Chapter 9.

Radiation Pressure.

Three phenomena associated with the passage of intense sound beams are radiation pressure, streaming and cavitation, and some remarks on the history of each are in order.

*The issue is not a wholly settled one. See P. J. Westervelt, Proc. Symp. on Nonlinear Acoustics, Birmingham, U. K., 1971, p. 6.

When one attempts to determine the time average of the pressure at a fixed point in a medium traversed by a sound wave, one finds that an asymmetry has been produced by the fact that the hypothetical particle of the medium is itself displaced from its rest position. For equal displacements from the rest position, the first order density changes are the same, but the second order changes differ. The following quotation from Poynting (1905) gives an account of the situation:

"In sound waves there is at a reflecting surface a node—a point of no motion but of varying pressure. If the variations of pressure from the undisturbed value were exactly proportional to the displacements of a parallel layer near the surface, and if the displacements were exactly harmonic, then the average pressure would be equal to the normal undisturbed value. But consider a layer of air quite close to the surface. If it moves up a distance y towards the surface, the pressure is increased. If it moves an equal distance y away from the surface, the pressure is decreased, but by a slightly smaller quantity. To illustrate this, take an extreme case and, for simplicity, suppose that Boyle's law holds. If the layer advances half-way towards the reflecting surface the pressure is doubled. If it moves an equal distance outwards from its original position the pressure falls, but only by one-third of its original value; and if we could suppose the layer to be moving harmonically, it is obvious that the mean of the increased and diminished pressures would be largely in excess of the normal value. Though we are not entitled to assume the existence of the harmonic vibrations when we take into account the second order of small quantities, yet this illustration gives the right idea. The excess of pressure in the compressed half is greater than its defect in the extension half, and the net result is an average excess of pressure—a quantity itself of second order on the reflecting surface. This excess in the compression half of a wave train is connected with the extra speed which exists in that half, and makes the crests of intense sound waves gain on the troughs." [57]

It is not surprising to learn that Lord Rayleigh made substantial contributions to the theory of radiation pressure, defining a particular form that bears his name (Chapter 6). More recently, Brillouin [58] pointed out the tensor character of the pressure in the sound wave, and various aspects of the phenomenon have been studied in detail by Borgnis [59] and Westervelt. [60]

Streaming.

In 1831, Michael Faraday [61] noted that currents of air were set up in the neighborhood of vibrating plates—the first known observation of acoustic streaming. In 1876, Dvorak [62] reported that when Kundt's tube was excited to vigorous oscillation, currents of air were observed. Near the walls of the tube, this current flows from the loops to the nodes, with a return in the inner part of the tube from the nodes to the loops.

Once again, Lord Rayleigh put forth a fundamental theoretical explanation. In particular, he noted that, while the phenomenon depended on the viscosity of the fluid, it was one of second order, i.e., nonlinear. [63]

Rayleigh treated the problem of standing waves between parallel walls. The successive generalization of the problem to cylinders of various types is sketched in the review by Nyborg. [64]

In the 1920's, it was observed that a flow of fluid takes place in front of a quartz crystal used as a transducer, and the name "quartz wind" was attached to the phenomenon. The effect was observed by Meissner in liquids in 1926. [65] In 1948, Eckart [39] published a theoretical account of streaming in its relation with the so-called "bulk viscosity" of fluids, and for a time it was thought that an independent method of measuring this quantity had been determined. Subsequently, however, it was made clear that the streaming was in fact proportional to the total acoustic absorption coefficient in the fluid, so that what had been obtained was another method of measuring this quantity. [66]

Cavitation

The early history of cavitation research is marvelously summarized in the opening lines of Rayleigh's paper (1917) "On the Pressure Developed in a Liquid during the Collapse of a Spherical Cavity," lines that recall Poe's opening to "The Cask of Amontillado." [68] although with less ominous overtones:

"When reading O. Reynold's description of the sounds emitted by water in a kettle as it comes to the boil, and their explanation as due to the partial or complete collapse of bubbles as they rise through cooler water, I proposed to myself a further consideration of the problem thus presented; but I had not gone far when I learned from Sir C. Parsons that he also was interested in the same question in connexion with cavitation behind screw-propellers, and that at his instigation Mr. S. Cook, on the basis of an investigation by Besant, had calculated the pressure developed when the collapse is suddenly arrested by impact against a rigid concentric obstacle." [67]

We thus learn that research in cavitation had a wholly non-acoustic origin. Cavitation refers to the formation of holes in liquids, and it is a matter of indifference whether the holes are produced by local heating in a kettle of water, by the slashing of a propeller blade through the liquid, or by the oscillation of liquid particles under the action of a sound beam. Nevertheless, all three causes have strong interconnections and are of interest in acoustics.

Besant's calculation was made in 1859. [69] On the basis of it, it was concluded that enormous pressure could be generated in the collapse of a void existing inside an incompressible liquid. Thus, if bubbles are generated

near a propeller surface, their ensuing collapse generates large forces that can act on the blade and severely damage it. Hence cavitation is of great significance in engineering work.

Lord Rayleigh's reference to Reynolds suggests two other aspects of cavitation. Bubbles are developed in a heated liquid near its boiling point, apparently due to the local concentrations of heat, with impurities often playing the role of growth centers or nuclei. Cavitation therefore is of interest in the study of the phenomenon of boiling. Also, the collapse of such bubbles can be accompanied by noise.

For the acoustician, interest in cavitation divides between the origin of holes and the forces and sounds produced by bubble collapse.

A great amount of experimental research was carried on in the period 1930-1950, by which time it became clear that cavitation could involve bubbles filled with air that was previously dissolved in the liquid or filled with the vapor of the liquid itself. This second kind of cavitation was more difficult to achieve and apparently depended on a number of extraneous factors, including the purity of the liquid. In 1954, Galloway [70] estimated the threshold for this type of cavitation in water at overpressures of 200 atm.

The presence of bubbles in a liquid causes appreciable scattering and absorption, so that sound transmission through a bubbly medium will be greatly impeded. Studies of this phenomenon were pursued by E. Meyer and his associates. [71]

One of the most difficult problems with regard to cavitation is the determination of its onset. One technique is photographic, while another has been the recording of sound produced by the cavitating bubbles.

The fundamental problem of cavitation has remained the determination of the mechanism of bubble formation. Various theories of impurity seeds, entrapped air, thermal spikes, cosmic rays have all been advanced, but the picture remains unclear. As it says at the end of any research report, much more work remains to be done.

REFERENCES

(Throughout this text, JASA is used for "Journal of the Acoustical Society of America")

Introduction

1. In compressible flow problems, this is known as the von Karman-Tsien approximation. See A. H. Shapiro, *Dynamics and Thermodynamics Compressible Flow*, Ronald Press, N. Y., 1954, p. 344ff.
2. R. Courant and K. O. Friedrichs, *Supersonic Flow and Shock Waves*, Interscience, N. Y., 1948; J. N. Bradley, *Shock Waves in Chemistry and Physics*, J. Wiley, N. Y. (1962).
3. J. J. Stoker, *Nonlinear Vibrations*, Interscience, N. Y., 1950; A. A. Andronov, A. A. Vitt and S. E. Khaikin, *Theory of Oscillations* (translated from the second Russian edition), Addison Wesley, Reading, Mass., 1966.
4. A. Kircher, *Musurgia universalis*, Rome, 1650.
5. Cited in *The Life of the Third Baron Rayleigh*, by the Fourth Baron Rayleigh. E. Arnold, London, 1924, p. 136.
6. V. Strouhal, Wied, Ann. Phys. **5**, 216 (1878). For a more detailed historical treatment, see A. Powell, JASA **36**, 177 (1964).
7. H. L. Helmholtz, Berlin Akad. Wiss. Monatsber, 23 April, 1868, p. 215.
8. H. Bénard, Comp. rend. **147**, 970 (1908).
9. A. Mallock, Proc. Roy. Soc. (London) **A84**, 490 (1910).
10. T. von Karman, Nachr. Akad. Wiss Göttingen, Math.-Phys. Kl. **5**, 547 (1912); T. von Karman and H. Rubach, Phys. Z. **13**, 49 (1912).
11. Lord Rayleigh, *Theory of Sound* (reprint of the 2nd ed.), Dover, N. Y., 1945).
12. O. Reynolds, Phil. Trans. Roy. Soc. (London) **174**, 935 (1883).
13. A. Masson, Comp. rend. **36**, 257, 1004 (1855).
14. C. Sondhauss, Ann. d. Physik **91**, 214 (1854).
15. Ref. 11, vol. II, p. 147.
16. Lord Rayleigh, Phil. Mag. 7, 149 (1879); **29**, 433 (1915).
17. E. Y. Yudin, Z. Tekhn. Fiz. **14**, 501 (1945).
18. Cited in R.W.B. Stephens and A. E. Bate, *Acoustics and Vibrational Physics*, Edward Arnold Ltd., London, 1966, p. 486.
19. A. Töpler, Ann. d. Physik **131**, 33 (1867).
20. A. B. Wood, *Textbook of Sound* (2nd ed.), G. Bell, London, 1941.
21. L. Bergmann, Der Ultrascl all (6th ed.), S. Hirzel, Stuttgart, 1954.
22. C. E. Hargrove and K. Achyuthan, Use of Light Diffraction in Measuring the Parameter of Nonlinearity of Liquids and the Photoelastic Constants of Solids, *Physical Acoustics* (W. P. Mason, ed.), vol. IIB, Academic Press, N. Y., 1965.

23. E. Mach and G. Gruss, Wien. Ber. **78**, 2, 467 (1879).
24. C. V. Boys, Nature **47**, 415, 440 (1893).
25. Lord Rayleigh, Proc. Roy. Soc. (London) **84**, 247 (1910).
26. W. J. M. Rankine, Phil. Trans. Roy. Soc. (London) **160**, 277 (1870).
27. H. Hugoniot, J. de l'École Polytechnique **58**, 1 (1889).
28. R. Becker, Z. Physik **8**, 321 (1922).
29. L. Prandtl, Phys. Z. **5**, 599 (1904); **8**, 23 (1907).
30. J. W. M. Dumond, E. R. Cohen, W. K. H. Panofsky and E. Deeds, JASA **18**, 97 (1946).
31. G. B. Whitham, J. Fluid Mech. **1**, 290 (1956).
32. S. D. Poisson, J. de l'École Polytechnique **7**, 319 (1808).
33. G. G. Stokes, Phil. Mag. (ser. 3) **33**, 349 (1848).
34. S. Earnshaw, Phil. Trans. Roy. Soc. (London) **150**, 133 (1860).
35. E. Fubini, Alta Frequenza **4**, 539 (1935).
36. D. T. Blackstock, JASA **34**, 9 (1962).
37. B. Riemann, Gottingen Abhandlungen, 1860; reprinted in Collected Works, Dover Publications, N. Y., 1953, p. 156.
38. R. Fay, JASA **3**, 222 (1931).
39. C. Eckart, Phys. Rev. **73**, 68 (1948).
40. Z. A. Goldberg, Soviet Phys. Acoustics **3**, 157, 341 (1957).
41. G. D. Mikhailov, Soviet Phys. Doklady **1**, 409 (1957); see also N. N. Andreev, Soviet Phys. Acoustics **1**, 2 (1955).
42. V. A. Krasilnikov, V. V. Shklovskaya-Kordi and L. K. Zarembo, JASA **29**, 642 (1957).
43. J. S. Mendousse, JASA **25**, 51 (1953).
44. E. Hopf, Comm. Pure Appl. Math **3**, 201 (1950).
45. J. D. Cole, Quart. J. Appl. Math **9**, 225 (1951).
46. S. I. Soluyan, R. V. Khokhlov, Vestnik Fiz. Astron. Moscow Univ., No. 3, 52 (1961); Soviet Phys. Acoustics **8**, 170 (1962).
47. D. T. Blackstock, JASA **39**, 1019 (1966).
48. G. A. Sorge, *Anwesung zur Stimmung der Orgelwerke und des Claviers*; Hamburg, 1744, p. 40.
49. G. Tartini, *Trattato di Musica*, Padua, 1754.
50. J. Lagrange, Misc. Taurinens, vol. 1, Sec. 64, Ouevres de Lagrange Paris 1867, vol. 1, p. 142.
51. T. Young, Phil. Trans. Roy Soc. (London) 1800.
52. E. F. Chladni, Traité d'Acoustique, Paris, 1809, p. 251.
53. H. Helmholtz, *On the Sensations of Tone*, Reprinted by Dover, 1954, p. 155 and App. 12.
54. A. W. Rucker and E. Edser, Proc. Phys. Soc. (London) 13, 412 (1895).
55. H. Lamb, *Dynamical Theory of Sound*; 2nd ed. 1925, Reprint by Dover Publications, New York, 1960.
56. A. L. Thuras, R. T. Jenkins and H. T. O'Neil, JASA **6**, 173 (1935).
57. Poynting, Address on Radiation, Phys. Soc. (London) 1905; Phil. Mag. **14**, 749 (1907).

58. L. Brillouin, Ann. de Phys. (X) **4**, 528 (1925).
59. F. E. Borgnis, Rev. Mod. Phys. **25**, 653 (1953).
60. P. J. Westervelt, JASA **22**, 319 (1950).
61. M. Faraday, Phil. Trans. Roy. Soc (London) 121, 229 (1831).
62. V. Dvorak Pogg. Ann. Phys. **157**, 42 (1876).
63. Lord Rayleigh, Phil. Trans. Roy. Soc. (London) **175**, 1 (1884).
64. W. L. Nyborg, "Acoustic Streaming." *Physical Acoustics*, (W. P. Mason, ed.), Vol. IIB, Academic Press, New York, 1963.
65. A. Meissner, Z. Tech. Physik **7**, 585 (1926).
66. J. E. Piercy and J. Lamb, Proc. Roy. Soc. (London) **A 226**, 43 (1954).
67. Lord Rayleigh, Phil. Mag. 34, 94 (1917).
68. E. A. Poe, *The Cask of Amontillado*.
69. W. H. Besant, *Hydrostatics and Hydrodynamics* 1859, par. 158.
70. W. J. Galloway, JASA **26**, 849 (1954).
71. See for example, E. Meyer, 'High Intensity Sound in Liquids," *Underwater Acoustics*, Plenum Press, N. Y. 1962 pp. 139-157.

Chapter I

PRINCIPLES OF LINEAR ACOUSTICS

Since we have embarked on a text in which the world of vibrations and acoustics is divided into the part that is linear and the part that is not, it would be well to review first the part that is linear, which is supposed to be familiar to the reader. Actually, only the topics that bear on the nonlinear aspects of acoustics will be covered, and even here, the reader is encouraged if not urged to seek the fuller accounts in the references and bibliography given at the end of the chapter.

1.1 The Linear Oscillator.

The most familiar problem of vibratory motion is that of damped, linear oscillations. We consider a one-dimensional system in which a particle of mass m is attached to one end of a weightless spring of stiffness k.

If the particle undergoes a displacement ξ from its rest position, the restoring force is expressed by $-k\xi$. If the damping force is given by $-R\dot{\xi}$, where $\dot{\xi} = d\xi/dt$ and R is some constant of the system, we have the equation

$$m\ddot{\xi} = -k\xi - R\dot{\xi} \quad . \tag{1.1}$$

To solve (1.1), we set $\xi = Ae^{\lambda t}$. Then, substituting in (1.1), we obtain

$$\lambda^2 m + \lambda R + k = 0$$

or

$$\lambda = \frac{-R}{2m} \pm \frac{(R^2 - 4mk)^{1/2}}{2m} \quad . \tag{1.2}$$

Three cases can be distinguished here, depending on the relationship between R^2 and $4mk$:

Case 1: $R^2 > 4mk$ (overdamped motion)

$$\xi = A_1 \exp\left[\frac{-Rt}{2m} + \left(\frac{R^2}{4m^2} - \frac{k}{m}\right)^{1/2} t\right] + A_2 \exp\left[\frac{-Rt}{2m} - \left(\frac{R^2}{4m^2} - \frac{k}{m}\right)^{1/2} t\right] \tag{1.2a}$$

Case 2: $R^2 < 4mk$ (Underdamped motion)

$$\xi = A_1 \exp\left[\frac{-Rt}{2m} + i\omega_{nat}t\right] + A_2\left[\frac{-Rt}{2m} - i\omega_{nat}t\right] \tag{1.2b}$$

where $\omega_{nat} = (k/m - R^2/4m^2)^{1/2}$ is the *natural frequency* of the system.

Case 3: $R^2 = 4mk$ (critically damped motion)

A second solution is necessary here, in addition to $\exp(-Rt/2m)$. It can easily be established that $t \exp(-Rt/2m)$ is such a solution, so that the complete solution of (1.1) in this case is

$$\xi = (A_1 + A_2 t)\exp(-Rt/2m) \ . \tag{1.2c}$$

If our particle is now subjected to a harmonic force, such as $F_0 \cos \omega t$, the problem can be most easily solved by means of complex numbers. We therefore use the form $F_0 e^{j\omega t}$ for the force (F_0 real), so that Eq. (1.1) becomes

$$m\ddot{\xi} + R\dot{\xi} + k\xi = F_0 e^{j\omega t} \ . \tag{1.3}$$

If we use as our test solution $\xi = Ae^{j\omega t}$ (A complex), simple substitution yields

$$(-m\omega^2 + i\omega R + k)A = F_0$$

or (1.4a)

$$A = \frac{F_0}{i\omega R + k - m\omega^2} = \frac{F_0 e^{-i\phi}}{[\omega^2 R^2 + (k - m\omega^2)^2]^{1/2}}$$

where

$$\tan\phi = \frac{\omega R}{k - m\omega^2} \ . \tag{1.4b}$$

Our complex solution for ξ then becomes

$$\xi = \frac{F_0}{[\omega^2 R^2 + (k - m\omega^2)^2]^{1/2}} e^{j(\omega t - \phi)} \tag{1.4c}$$

for which it is understood that the real part is the solution for the real case.

Thus oscillations are forced at the frequency of the driving force. However, the amplitude of such oscillations will be small except in the neighborhood of the frequency for which

$$\frac{d}{d\omega}\left[\omega^2 R^2 + (k - m\omega^2)^2\right] = 0.$$

This *resonance* condition yields the frequency for maximum displacement, ω_d:

$$\omega_d = \left(\frac{k}{m} - \frac{R^2}{2m^2}\right)^{1/2} \tag{1.5}$$

It is worth noting here that the use of the complex variable technique relies on the principle of superposition–i.e., that if $f_1(t)$ is a solution of a given equation and $f_2(t)$ is a second solution, then $f \equiv af_1 + bf_2$ is also a solution. In particular, if $a = 1, b = i$, (f_1 f_2 real) Then the fact that f is a solution guarantees that the real (f_1) and imaginary (if_2) parts are also solutions. The principle of superposition in turn requires that the governing equation be linear, so that this technique cannot be used for nonlinear problems without special consideration.

In most of the problems with which we shall deal, it is of greater interest to consider the displacement velocity $\dot{\xi}$ rather than the displacement itself. If we form the time derivative of (1.3) and set $\dot{\xi} \equiv u$, we have

$$m\ddot{u} + R\dot{u} + ku = i\omega F_0 e^{i\omega t} . \tag{1.6}$$

Proceeding as above, we try $u = Ae^{i\omega t}$. Substitution in (1.6) then yields

$$[-\omega^2 m + i\omega R + k]A = i\omega F_0$$

or

$$A = \frac{F_0}{R + i\left(m\omega - \frac{k}{\omega}\right)} \equiv \frac{F_0 e^{-i\phi}}{\left[R^2 + \left(m\omega - \frac{k}{\omega}\right)^2\right]^{1/2}} \tag{1.7a}$$

with

$$\tan\phi = \frac{m\omega - \frac{k}{\omega}}{R}. \tag{1.7b}$$

The maximum particle velocity is therefore obtained when the imaginary part of the denominator of Eq. (1.7a) vanishes, i.e.,

$$\omega_r^2 = \frac{k}{m} . \tag{1.8}$$

This frequency is known as the *resonance frequency*, since it is the one for which the displacement velocity is exactly in phase with the forcing term. It should be noted that this was not the case when we considered displacement. The maximum displacement [Eq. (1.4a)] occurs when $\omega = \omega_d$ [Eq. (1.5)] which is a lower frequency than ω_r.

1.2 The Vibrating String.

A second important problem of linear theory is that of the vibrating string. If a string is attached to rigid supports and given a small displacement, (Fig. 1-1a), the resultant restoring force will cause the string to vibrate.

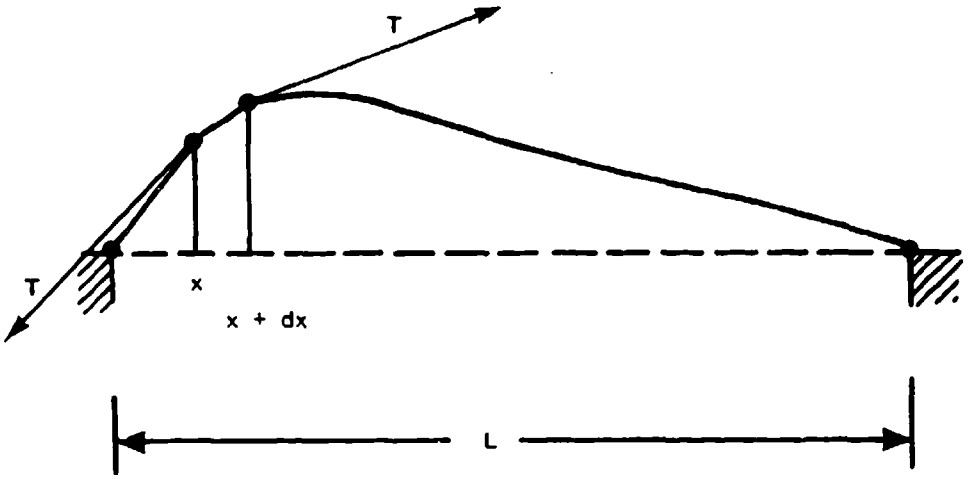

Figure 1-1a.–Displacement of a vibrating string under uniform tension *T*.

The details of the situation are indicated in the enlarged Fig. 1-1b. The string is assumed to be uniform, with a mass per unit length equal to σ, the magnitude of the tension in the string, T, is assumed to be constant, and all displacements are small ($\xi/L << 1$, where L is the length of the string).

The force in the y direction at the left end of our string segment (at x) is given by

$$T_y = -T\frac{\partial \xi}{\partial x} .$$

while that at the right end (at $x + dx$) is

$$T_y' = T\left(\frac{\partial \xi}{\partial x} + \frac{\partial^2 \xi}{\partial x^2}dx\right)$$

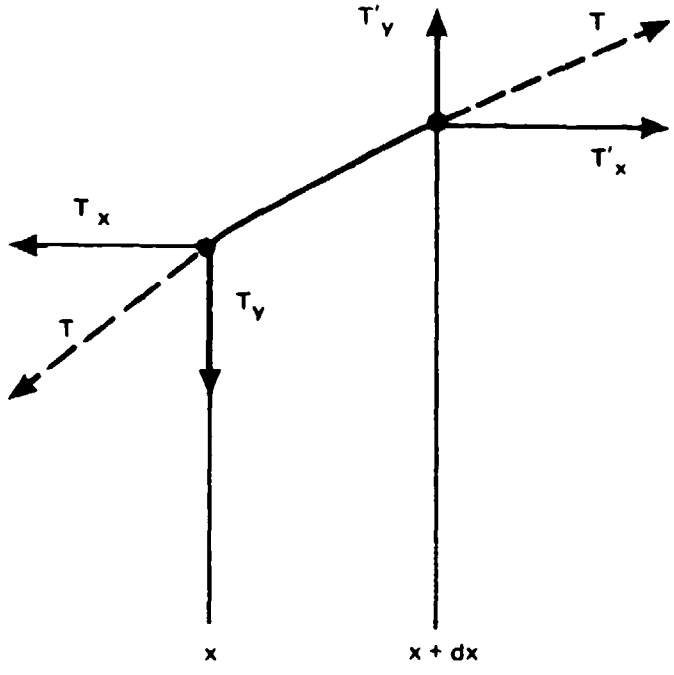

Figure 1-1b.–Enlarged view of segment of string from Fig. 1b. Motion is restricted to xy plane.

so that the net restoring force on the element is

$$T_y - T'_y = -T\frac{\partial^2 \xi}{\partial x^2}\,dx. \tag{1.9}$$

The mass of the length of string dx is σdx, where σ is the mass per unit length of the string. Then the equation of motion becomes

$$-T\frac{\partial^2 \xi}{\partial x^2}\,dx = -\sigma dx\ddot{\xi}$$

or

$$T\frac{\partial^2 \xi}{\partial x^2} = \sigma\frac{\partial^2 \xi}{\partial t^2}\,. \tag{1.10}$$

This is the same equation as Eq. (3) of the INTRODUCTION if $c_0^2 = T/\sigma$. Hence waves can propagate along the string with velocity $c_0 = \sqrt{T/\sigma}$.

The general solution of Eq. (1.10) can be easily demonstrated to be

$$\xi = Af(x - c_0 t) + Bg(x + c_0 t) \tag{1.11}$$

since

$$\dot{\xi} = Af'(x - c_0t)(-c_0) + Bg'(x + c_0t)c_0$$

$$\ddot{\xi} = c_0^2 Af''(x - c_0t) + c_0^2 Bg''(x + c_0t);$$

and

$$\frac{\partial \xi}{\partial x} = Af' + Bg' ,$$

$$\frac{\partial^2 \xi}{\partial x^2} = Af'' + Bg'' ,$$

so that

$$c_0^2 \frac{\partial^2 \xi}{\partial x^2} = c_0^2 Af'' + c_0^2 Bg''$$

which is exactly equal to $\ddot{\xi}$..

Equation (1.11) represents two transverse waves traveling in opposite directions. It is an entirely general solution. The particular form that the displacement of the string takes depends on the way the string is initially plucked.

This initial plucking could lead to a complicated form for the solution, and be a very difficult problem but for the principle of superposition, to which we have already referred, and for the procedures of Fourier analysis. So long as we are dealing with a linear equation, any linear combinations of solutions will also be a solution. But virtually any physically realizable displacement of the string can be decomposed by Fourier analysis into sinusoidal components, each one of which can be studied separately, with the final answer represented by the sum of the Fourier components.

In the problem at hand, only the sine series will be needed, since the end points of the string are fixed. Let us therefore look at the simplest possible case, in which the initial displacement is given by a sinusoidal curve:

$$\xi(x, 0) = \xi_0 \sin kx \quad . \tag{1.12}$$

If the length of the string is L, the condition that the ends of the string are fixed yields

$$\xi(L, 0) = \xi_0 \sin kL = 0, \quad \text{or} \quad kL = n\pi, n = 1,2,3, \ldots . \tag{1.13}$$

The solution of (1.10) for this case is given by (1.11):

$$\xi = A \sin k(x - c_0 t) + B \sin k(x + c_0 t) \tag{1.14}$$

or

$$\xi = (A + B) \sin kx \cos \omega t - (A - B) \cos kx \sin \omega t$$

with $\omega = kc_0$. Since $\xi(0,t) = 0$ for all t, it follows that $A = B$. Then, recalling (1.13) we obtain

$$\xi_0 = A + B = 2A$$

or

$$A = \xi_0/2 \ .$$

Hence Eq. (1.14) becomes

$$\xi = \xi_0 \sin kx \cos \omega t \tag{1.15}$$

which corresponds to a standing wave. Finally, substitution of the boundary condition (1.13) leads to the result for the nth harmonic:

$$\xi = \xi_0 \sin \frac{n\pi x}{L} \cos n\omega t . \tag{1.16}$$

1.3 Beats.

The "beating" of two oscillations of different frequencies is a linear phenomenon. The two oscillations might be sound waves traveling in the same direction, two oscillations superposed on a string or two separate vibrators forcing a mechanical system. For simplicity, we assume the two oscillations to have the same initial phase. Then

$$\begin{aligned} \xi_1 &= A \sin \omega_1 t \\ \xi_2 &= mA \sin \omega_2 t \end{aligned} \tag{1.17}$$

where $\omega_2 > \omega_1$, and m lies between 0 and 1, we shall further assume that the

difference between ω_1 and ω_2 is small, and introduce the notation for the difference (Ω) and mean (ω_0) frequencies

$$\Omega = \omega_2 - \omega_1$$

$$\omega_0 = (1/2)(\omega_2 + \omega_1) .$$

Then, by simple trigonometry, the sum of the two displacements $\xi_1 + \xi_2$ becomes

$$\begin{aligned} \xi = \xi_1 + \xi_2 &= A \sin \omega_1 t + mA \sin \omega_2 t \\ &= A(1+m) \sin \omega_0 t \cos \frac{\Omega t}{2} - A(1-m) \cos \omega_0 t \sin \frac{\Omega t}{2}. \end{aligned} \tag{1.18}$$

We restrict ourselves to two signals of equal amplitude, so that m (the modulation index) = 1. A plot of Eq. (1.18) in this case for $\omega_1 = 10\pi$, $\omega_2 = 12\pi$ is shown in Fig. 1-2.

The human ear hears the pulsations of sound in the vicinity of the extremal values (± 1) of $\cos \Omega t/2$ and therefore perceives a beat frequency Ω, which is also the difference frequency.

1.4 Plane Waves, Nondissipative Case.

A number of features of linear acoustic waves will be used throughout the book and will be summarized here.

In many problems, one uses the simplification of *plane waves*, in which the wave fronts are plane surfaces traveling perpendicular to their surface. For a harmonic wave traveling in the $+x$ direction, the displacement velocity $u = \partial\xi/\partial t$ of the plane wave was given by Eq. (1) of the INTRODUCTION:

$$\begin{aligned} u &= u_0 \sin \omega \left(t - \frac{x}{c} \right) \\ &= u_0 \sin (\omega t - kx) \end{aligned} \tag{1.19}$$

with $k = \omega/c$, $u_0 = \dot{\xi}_0 = \omega \xi_0$.

A common way of describing wave motion in the linear case is that of the velocity potential. For irrotational motion (curl $\mathbf{u} = 0$), there exists a function $\phi(\mathbf{r}, t)$ for which the velocity displacement vector can be written

$$\mathbf{u} = \Delta\phi \tag{1.20}$$

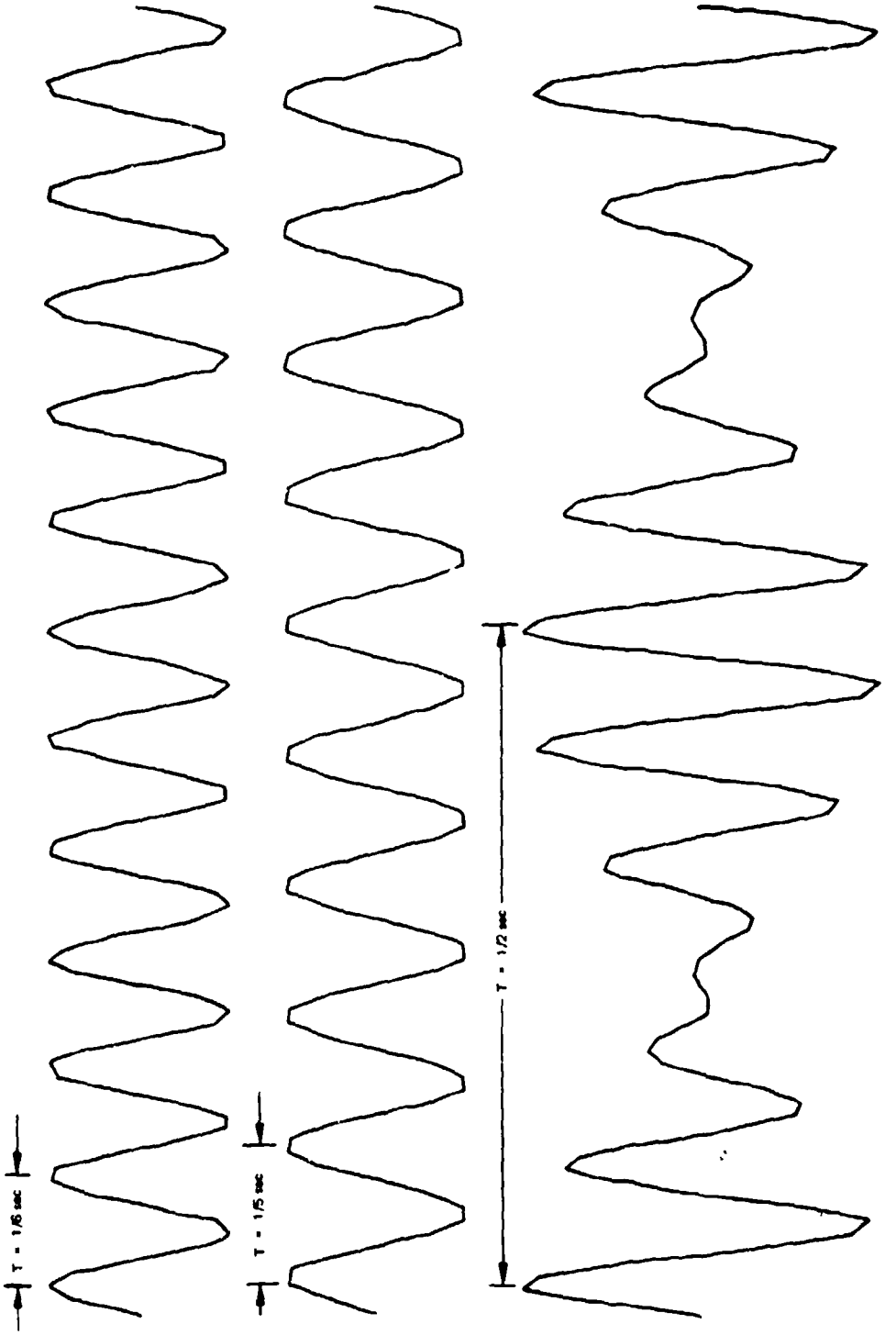

Figure 1-2. – A computer trace of beats. The first trace is that of $\omega_1 = 10\pi$ra/sec ($T = 1/5$ sec), the second that of $\omega_2 = 12\pi$ra/sec ($T = 1/2$ sec). Beat frequency $\Omega = 2\pi$ra/sec.

(Courtesy of Prof. A. M. Shapiro, Brown University.)

or, for plane waves, $u = \partial\phi/\partial x$. This quantity ϕ is known as the *velocity potential*.

The pressure due to the presence of an acoustic wave can be introduced by considering a small volume element (Fig. 1-3*a*). At rest, the volume dV_0 is given by $dV_0 = dxdydz$.

If a disturbance now passes in the $+x$ direction, the force exerted on this element from the left will be pdA, where p is the total pressure at the plane x.

In the plane $x + dx$, the corresponding pressure will be

$$p + \frac{\partial p}{\partial x}\,dx$$

and the force exerted by this pressure on the material that was in the original element will be

$$-\left(p + \frac{\partial p}{\partial x}dx\right)dA \ .$$

The net force on dV_0 is then

$$pdA - pdA - \frac{\partial p}{\partial x}\,dxdA = -\frac{\partial p}{\partial x}dV_0 \ .$$

By Newton's equation of motion, we obtain

$$-\frac{\partial p}{\partial x}dV_0 = (\rho_0 dV_0)\ddot{\xi}$$

or

$$\rho_0\ddot{\xi} = \frac{\partial p}{\partial x} \ . \tag{1.21}$$

From Eq. (1.20), this can be written in terms of the velocity potential:

$$-\frac{\partial p}{\partial x} = \rho_0\frac{\partial\dot{\xi}}{\partial t} = \rho_0\frac{\partial^2\xi}{\partial x\partial t} \ . \tag{1.22}$$

Integrating (1.22) with respect to x, we obtain

$$-p = \rho_0\frac{\partial\xi}{\partial t} + f(t) + \text{const} \ .$$

Since this relation must also hold in the absence of sound (when $\partial\phi/\partial t = 0$), it is clear that the function $f(t)$ must vanish and that the constant must equal $-\rho_0$, the negative of the equilibrium pressure. Hence

$$p \quad p_0 = -\rho_0 \frac{\partial \phi}{\partial t} = p_e = \text{excess pressure due to sound wave.} \quad (1.23)$$

The density changes can also be introduced by defining the *condensation* as the fractional increase in the density:

$$s = \frac{\rho - \rho_0}{\rho_0} . \quad (1.24)$$

If we refer to Fig. 1-3*b*, and observe that the particle displacement at x is ξ, while that at $x + dx$ is $\xi + (\partial\xi/\partial x)\, dx$, we can see that the original volume element dV_0 is now distorted into the new volume

$$dV = dydz \left[x + dx + \xi + \frac{\partial \xi}{\partial x} - (x + \xi) \right]$$

$$= dxdydz \left(1 + \frac{\partial \xi}{\partial x} \right) .$$

Since the mass of the element remains constant, we have

$$\rho_0 dV_0 = \rho dV$$

or

$$\rho_0 dV_0 = \rho dV_0 \left(1 + \frac{\partial \xi}{\partial x} \right) .$$

Finally,

$$\rho = \frac{\rho_0}{1 + \dfrac{\partial \xi}{\partial x}} . \quad (1.25)$$

The condensation s can then be written

$$s = \frac{1}{1 + \dfrac{\partial \xi}{\partial x}} - 1 \simeq - \frac{\partial \xi}{\partial x} . \quad (1.26)$$

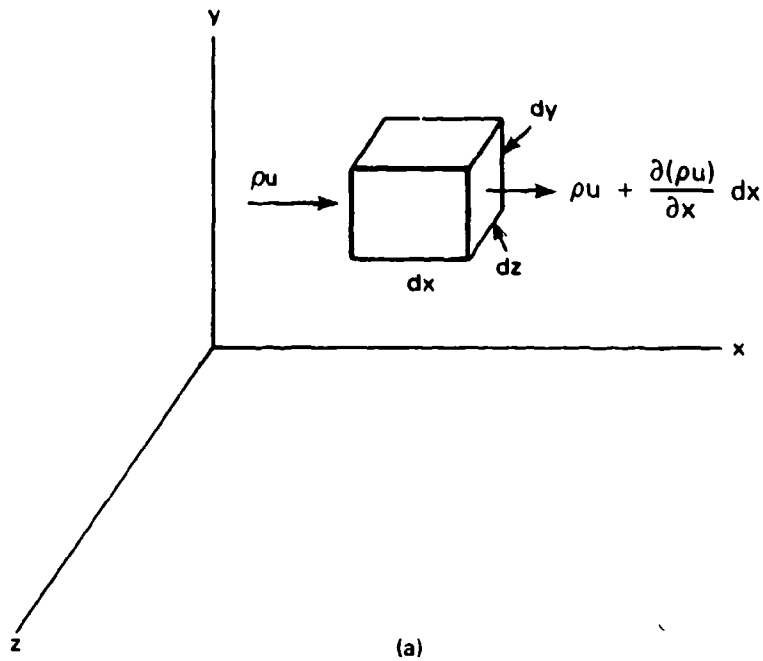

(a)

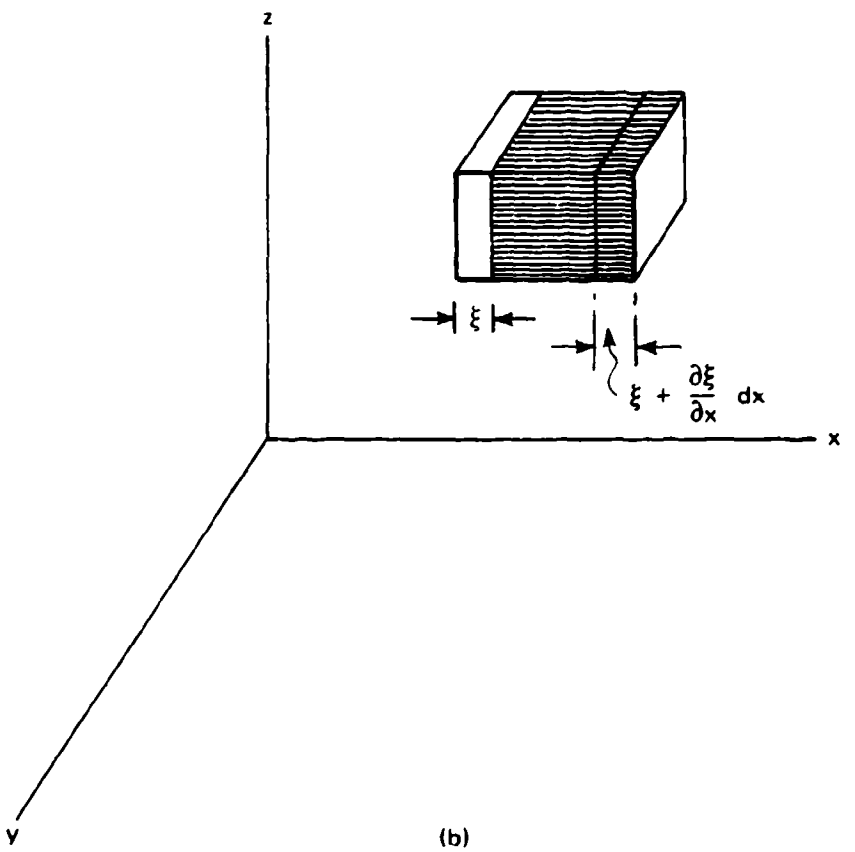

(b)

Figure 1-3.–(a) Element of volume; (b) linear displacements in volume element.

We also need the expression for the energy in the wave. Let us consider a volume element ΔV. In the presence of the sound wave, the element will have a displacement velocity $\dot{\xi}$ and condensation s.*

The energy of the volume element will be $E\Delta V$, where E is the energy per unit volume at time and position x (the energy density). This in turn can be broken up into kinetic (E_{kin}) and potential (E_{pot}) energy terms:

$$E\Delta V = E_{\text{kin}}\,\Delta V + E_{\text{pot}}\,\Delta V = \frac{1}{2}\rho\dot{\xi}^2\,\Delta V - \int_{\Delta V} p_e dV. \qquad (1.27)$$

The sound velocity is related to the pressure through the isentropic equation

$$c^2 = \left(\frac{\partial p}{\partial \rho}\right)_s. \qquad (1.28)$$

For small changes in density, $\delta p = c^2\delta\rho$, so that $p_e = \rho_0 c^2 s$. Making use also of the fact that $dV/\Delta V = -\,d\rho/\rho_0$ or $dV = -\,\Delta V ds$, we can convert the potential energy term as follows

$$-\int_{\Delta V} p_e dV = \rho_0{}^2\Delta V \int_0^s s ds = \frac{1}{2}\rho_0 c^2 s^2 \Delta V$$

and Eq. (1.22) becomes

$$E = \frac{1}{2}\rho_0\dot{\xi}^2 + \frac{1}{2}\rho_0 c^2 s^2 \ . \qquad (1.29)$$

We now define the intensity of a sound beam as the average rate of energy flux across a unit area perpendicular to the direction of propagation of the wave. If we write $\bar{E}$ as the mean energy density, then

$$I = c\bar{E} \ . \qquad (1.30)$$

If we are dealing with a plane harmonic wave, such as is described by Eq. (1) of the INTRODUCTION, then

$$\dot{\xi} = \dot{\xi}_0 \sin(\omega t - kx)$$

*These are the mean quantities for the element ΔV. As $\Delta V \to 0$ these become identical with the $\dot{\xi}$ and s introduced previously, as can be demonstrated by application of the theorem of the mean.

$$\xi = -\left(\frac{\dot{\xi}_0}{\omega}\right)\cos(\omega t - kx) = -\xi_0 \cos(\omega t - kx)$$

$$\phi = \frac{\dot{\xi}}{k}\cos(\omega t - kx) = \xi_0 c \cos(\omega t - kx) \tag{1.31}$$

$$p = \rho_0 \xi_0 c\omega \sin(\omega t - kx) = \rho_0 c u_0 \sin(\omega t - kx)$$

$$s = \xi_0 \frac{\omega}{c}\sin(\omega t - kx) = k\xi_0 \sin(\omega t - kx) .$$

The energy density is given by

$$E = \frac{1}{2}\rho_0 \dot{\xi}_0^2 \sin^2(\omega t - kx) + \frac{1}{2}\rho_0 c_0^2 \frac{\dot{\xi}_0}{c_0^2}\sin^2(\omega t + kx)$$

$$= \rho_0 \dot{\xi}_0^2 \sin^2(\omega t - kx) \tag{1.32}$$

so that its mean value $\bar{E}$ is

$$\bar{E} = \rho_0 \dot{\xi}_0^2 \frac{1}{T}\int_0^T \sin^2(\omega t - kx)\, dt = \frac{1}{2}\rho_0 \dot{\xi}_0^2 \tag{1.33}$$

and

$$I = \frac{1}{2}\rho_0 c_0 \dot{\xi}_0^2 = \frac{p_{e0}^2}{2\rho_0 c_0} \tag{1.34}$$

where p_{e0} is the pressure amplitude in the wave, equal to $\rho_0 c_0 u_0$.

The set of Eqs. (1.31) can be repeated for the complex notation:

$$\dot{\xi} = -i\dot{\xi}_0 e^{i(\omega t - kx)}$$

$$\xi = -\xi_0 e^{i(\omega t - kx)}$$

$$s = -ik\xi_0 e^{i(\omega t - kx)} \tag{1.35}$$

$$\phi = \frac{\dot{\xi}_0}{k} e^{i(\omega t - kx)}$$

$$p_e = -i\rho_0 c_0 \dot{\xi}_0 e^{i(\omega t - kx)}$$

where we are interested in the real portions only. Since E and I depend on the squares of ξ and $\dot{\xi}$, the complex form cannot be used in the simple product form. However, a check with Eqs. (1.35) will show that the intensity is given by the form

$$I = \frac{1}{2} p\dot{\xi}^* \tag{1.36}$$

where the asterisk denotes the complex conjugate.

1.5 Spherical and Cylindrical Waves.

The one-dimensional wave equation

$$\frac{\partial^2 \xi}{\partial t^2} = c_0^2 \frac{\partial^2 \xi}{\partial x^2}$$

cited in the INTRODUCTION [Eq. (3)] is a special case of the more general relation

$$\frac{\partial^2 \xi}{\partial t^2} = c_0^2 \nabla^2 \boldsymbol{\xi} \tag{1.37a}$$

or, in terms of velocity potential,

$$\frac{\partial^2 \phi}{\partial t^2} = c_0^2 \nabla^2 \phi \ . \tag{1.37.b}$$

Here $\boldsymbol{\xi}$ is the vector displacement at the point $\mathbf{r}$ and ∇^2 is the differential operator div grad. Equation (1.37b) can easily be converted to Eq. (1.37a) by taking its gradient

$$\frac{\partial^2 \nabla \phi}{\partial t^2} = c_0^2 \nabla^2 (\nabla \phi)$$

which becomes

$$\frac{\partial^2 \dot{\xi}}{\partial t^2} = c_0^2 \nabla^2 \dot{\xi}$$

or

$$\frac{\partial}{\partial t}\left[\frac{\partial^2 \xi}{\partial t} = c_0^2 \nabla^2 \xi\right]$$

whereupon simple integration produces Eq. (1.37a).

In the case of a spherical wave, the equivalent to Eq. (1.37b) can be written as

$$\frac{1}{r}\frac{\partial^2 (r\phi)}{\partial r^2} = \frac{1}{c^2}\frac{\partial^2 \phi}{\partial t^2} \tag{1.38}$$

which has the solution

$$\phi = \frac{1}{r} f\left[t \pm \frac{r}{c}\right] . \tag{1.39}$$

Similarly, for cylindrical waves, Eq. (1.37b) is replaced by

$$\frac{1}{\rho}\frac{\partial}{\partial \rho}\left[\rho \frac{\partial \varphi}{\partial \rho}\right] = \frac{1}{c^2}\frac{\partial^2 \phi}{\partial t^2} \tag{1.40}$$

where ρ is the radial coordinate. For large values of ρ, this equation possesses solutions of the form

$$\phi = \frac{f\left[t \pm \frac{r}{c}\right]}{\rho^{1/2}} \tag{1.41}$$

This solution is valid whenever ρ is large compared with the acoustic wavelength ($k\rho >> 1$).

1.6 Sound Absorption.

A great deal of attention has been devoted to the theory of sound absorption in various media, and the reader is referred to the extensive treatment given in Beyer and Letcher (1969), Chapters 4 and 5. Here we shall be mainly interested in the simplest case, that of absorption due to viscosity. The original theory was developed by Stokes more than 100 years ago.[1]

In the derivation here, we shall consider waves of infinitesimal amplitude, so that products of first order quantities can be neglected.

We begin with the equation of continuity (or conservation of mass). If we again consider a fixed volume element $dxdydz$ (Fig. 1-3a), the influx of mass per second from the left will be $\rho u dydz$ while the outflow will be

$$\left[\rho u + \frac{\partial}{\partial x}(\rho u)\, dx\right] dydz$$

so that the net mass increase in the volume will be

$$\rho u dydz - \left[\rho u + \frac{\partial}{\partial x}(\rho u)\, dx\right] dydz = -\frac{\partial}{\partial x}(\rho u)\, dV$$

which is also equal to the rate of mass increase

$$\frac{\partial \rho}{\partial t} dV .$$

[The density ρ in the last equation is a mean value, just as the s in Eq. (1.29), a value which the ρ of the previous equation approaches in the limit as $dV \to 0$.]

Hence

$$-\frac{\partial}{\partial x}(\rho u) = \frac{\partial \rho}{\partial t} . \tag{1.42}$$

The second equation is the equation of motion (conservation of momentum), Eq. (1.21)

$$\rho_0 \ddot{\xi} = -\frac{\partial p}{\partial x} . \tag{1.21}$$

The third equation will be the first law of thermodynamics, or the conservation of energy. The first law can be written

$$\Delta Q = dU - \Delta W \tag{1.43}$$

where ΔQ is the heat added (per mole) to the system of an infinitesimal process, dU the corresponding increase in the internal energy of the system, and ΔW the work done on the system during the process. In particular, we use the equation under the adiabatic condition; that is, we assume that no

heat enters or leaves the system during the process. In such a case, $\Delta Q = 0$. Furthermore, ΔW can be replaced by

$$\Delta W = -pdV = M(p/\rho^2)\,d\rho \tag{1.44}$$

where M is the gram molecular weight of the gas, while $dU = C_V dT$, where C_V is the heat capacity per mole at constant volume.

In the general case, the fourth equation (the equation of state) is an expression of the form

$$p = p(\rho, T)\,. \tag{1.45}$$

In the case of an ideal gas, $p = \rho RT/M$, where R is the gas constant (per mole). In many cases, however, the more general form of Eq. (1.45) is satisfactory.

Now let us suppose that a plane harmonic wave travels through the medium in the $+x$ direction. We shall write the expressions for the change in the pressure (p_e), the condensation [$s = (\rho - \rho_0)/\rho_0$], the change in temperature ($\theta = T - T_0$) and the velocity ($u = \dot{\xi}$) associated with this wave, all in complex form

$$\begin{aligned} p_e &= p_{0e}e^{j(\omega t - kx)} & \theta &= \theta_0 e^{j(\omega t - kx)} \\ s &= s_0 e^{j(\omega t - kx)} & u &= u_0 e^{j(\omega t - kx)} \end{aligned} \tag{1.46}$$

We now substitute these values in (1.42), (1.21), (1.44), (1.46), neglecting all products of small quantities. This results in the four equations

$$\begin{aligned} &\text{(a)} \quad -\frac{\partial u}{\partial x} = \frac{\partial s}{\partial t} & &\text{(c)} \quad C_V\theta = \frac{Mp_0}{\rho_0}s \\ &\text{(b)} \quad -\frac{\partial u}{\partial t} = \frac{1}{\rho_0}\frac{\partial p_e}{\partial x} & &\text{(d)} \quad p_e = \left(\frac{\partial p}{\partial \rho}\right)_T \rho_0 s + \left(\frac{\partial p}{\partial T}\right)_\rho \theta \end{aligned} \tag{1.47}$$

or, for the plane harmonic wave of Eq. (1.46),

$$\begin{aligned} iku - i\omega s + 0 + 0 &= 0 \\ i\omega u + 0 - \left(\frac{ik}{\rho_0}\right) p_e + 0 &= 0 \end{aligned} \tag{1.48}$$

$$0 \quad - M\left(\frac{p_0}{\rho_0}\right) s \quad + 0 \qquad + C_V\theta \quad = 0$$

$$0 \quad - \left(\frac{\partial p}{\partial \rho}\right)_T \rho_0 s + p_e \qquad - \left(\frac{\partial p}{\partial T}\right)_\rho \theta = 0 \ .$$

In order that (1.48) have a non-trivial solution, it is necessary that the determinant of the coefficients of (1.48) vanish. This yields the following expression for the sound velocity $c_0 = \omega/k$

$$c_0^2 = \left(\frac{\partial p}{\partial \rho}\right)_T + \left(\frac{Mp_0}{\rho_0^2} C_V\right)\left(\frac{\partial p}{\partial T}\right)_\rho \ . \tag{1.49}$$

For an ideal gas,

$$\left(\frac{\partial p}{\partial \rho}\right)_T = \frac{p_0}{\rho_0}$$

$$\left(\frac{\partial p}{\partial T}\right)_\rho = \frac{p_0}{T} = \frac{\rho_0 R}{M} \tag{1.50}$$

so that

$$c_0^2 = \frac{p_0}{\rho_0}\left(1 + \frac{R}{C_V}\right) = \partial \frac{p_0}{\rho_0} \ .$$

All of the treatment thus far has assumed the absence of dissipation in the medium. The presence of viscosity adds new force terms to the righthand side of the equation of motion. In its most general form, the resultant equation of motion is known as the Stokes-Navier equation.[2] For the one-dimensional case, this equation can be written

$$\frac{\partial(\rho\dot{\xi})}{dt} = -\frac{\partial p}{\partial x} + \left(\frac{4}{3}\eta + \eta'\right)\frac{\partial^2 \xi}{\partial x^2} \tag{1.51}$$

where η is the shear viscosity coefficient. The quantity η' is known as the second or bulk viscosity coefficient, and corresponds to the viscous drag that would be experienced in a pure volume dilatation, in which no shearing motions can occur.

The nature and value of η' forms one of the most interesting problems in the historical development of ultrasonic wave propagation.[3] Stokes assumed that η' was identically zero, and to a large extent, this assumption marks the difference between classical and modern theories of ultrasonic absorption and dispersion. We shall leave η' in Eq. (1.51) so that it can be used to cover both classical and modern theories.

If we now make the linear approximation in Eq. (1.51), we obtain

$$\frac{\partial u}{\partial t} = -\frac{1}{\rho_0}\frac{\partial p_e}{\partial x} + \frac{\left(\frac{4}{3}\eta + \eta'\right)}{\rho_0}\frac{\partial^2 u}{\partial x^2} \tag{1.51a}$$

or, for harmonic waves of frequency ω,

$$i\omega u = + i\left(\frac{k}{\rho_0}\right) p_e - \left(\frac{4}{3}\eta + \eta'\right)\left(\frac{k^2}{\rho_0}\right)u$$

which now replaces Eqs. (1.21), (1.47b), and the second line of Eq. (1.48) becomes

$$\left[i\omega + \left(\frac{4}{3}\eta + \eta'\right)\left(\frac{k^2}{\rho_0}\right)\right]u - \left(\frac{ik}{\rho_0}\right)p_e = 0 \ .$$

This leads to the result

$$\frac{k^2}{\omega^2} = \left[c_0^2 + i\left(\frac{4}{3}\eta + \eta'\right)\frac{\omega}{\rho_0}\right]^{-1} . \tag{1.52}$$

The presence of the imaginary term on the right side of (1.52) makes k complex. We therefore set $k = k_r - i\alpha$, so that all the Eqs. (1.46) can be written in the form

$$u = u_0 \exp(-\alpha x) \exp i(\omega t - k_r x) \ , \tag{1.53}$$

in which α is the amplitude absorption coefficient, while k_r is the real wave number, equal to ω divided by the phase velocity c.

The substitution $k_r - i\alpha$ in Eq. (1.53) leads to the two equations

$$k_r^2 - \alpha^2 = \frac{\omega^2 c_0^2}{c_0^4 + \left(\frac{4}{3}\eta + \eta'\right)^2 \frac{\omega^2}{\rho_0^2}} \tag{1.54}$$

$$2k_r\alpha = \frac{\left(\frac{4}{3}\eta + \eta'\right)\frac{\omega^3}{\rho_0}}{c_0^4 + \left(\frac{4}{3}\eta + \eta'\right)^2 \frac{\omega^2}{\rho_0^2}} .$$

In virtually all cases, $k_0^2 >> \alpha^2$ [and hence $(4\eta/3 + \eta')^2\, \omega^2/\rho_0^2 << c_0^4$] so that, to an excellent approximation, we have

$$k_r = \frac{\omega}{c_0}$$

$$k_r\alpha = \frac{1}{2}\left(\frac{4}{3}\eta + \eta'\right)\frac{\omega^3}{\rho_0 c_0^4} . \tag{1.55}$$

$$\alpha = \frac{1}{2}\left(\frac{4}{3}\eta + \eta'\right)\frac{\omega^2}{\rho_0 c_0^3} .$$

Thus the ordinary propagation of a plane harmonic wave of infinitesimal amplitude is non-dispersive. Experiment has shown that most fluids obey the quadratic dependence of α on ω, but the value of α is much larger than is predicted under the Stokes assumption that $\eta' = 0$. The keeping of η', therefore, provides a mechanism for describing this additional absorption.

1.7 Relaxation Phenomena.

In the decisive equations of the previous section [(1.54), (1.55)], the sound absorption coefficient is proportional to ω^2. In many gases and liquids, however α is not proportional to ω^2 over a significant range of frequencies. The reason for this behavior lies in the lag of the internal processes in the medium behind the externally applied changes in pressure that derive from the sound wave.

If we look back at Eq. (1.47), we can see that (*c*) and (*d*) (the equation of energy conservation and the equation of state) could have been combined into a single relation involving only the pressure and the condensation:

$$p_e = \left[\left(\frac{\partial p}{\partial \rho}\right)_T \rho_0 + \left(\frac{\partial p}{\partial T}\right)_\rho \frac{Mp_0}{C_V \rho_0}\right] s . \tag{1.56}$$

The determinant of Eq. (1.48) could then have been written in 3 X 3 form. For an ideal gas, (1.56) reduces to

$$p_e = \gamma p_0 s = \rho_0 c_0^2 s \ . \tag{1.57}$$

Any process that removes energy from the sound beam and returns it at an appreciably later time in the wave cycle causes a dissipation of the acoustic energy, i.e., attenuation of the beam. This destroys the isentropic character of the sound propagation (even though it may still be adiabatic) and properly requires the use of irreversible thermodynamics for a rigorous description. We shall not make such an exposition here, but only make a few explanatory remarks and write down the resultant equations, the derivation of which can be found in the literature.[4]

The analysis of these processes, which transfer energy from the translational mode of motion (the sound wave) to other modes such as vibration or rotation of atoms or groups of atoms within the molecule, or to the potential energy of some structural rearrangement (including chemical reactions and electrolytic processes) is aimed at obtaining a time-dependent equation connecting the instantaneous values of the pressure and density that is often called the "acoustic equation of state." This type of equation is known as a relaxation equation and the process is usually referred to as a relaxation process. The rate of this relaxation is defined in terms of quantity known as the relaxation time. This is a measure of the time required to complete some specified reaction, subject to the condition that an appropriate set of thermodynamic variables is held constant. It should be noted that there exists no unique relaxation time for a given process, although the differences among those defined for liquids are usually negligibly small.

In the simplest case, that of an ideal gas, in which one can still neglect the changes in entropy that do occur, the acoustic equation of state takes the form

$$\rho_0 \tau_{ps} \dot{s} + \rho_0 s = \frac{\tau_{ps}}{c_0^2} \dot{p}_e + \frac{1}{c_0^2} p_e \tag{1.58}$$

where c_∞, c_0 are the values of the sound speed measured at very high and very low frequencies, respectively, and τ_{ps} is the relaxation time measured under conditions of constant pressure and entropy. If we again introduce a harmonic time dependence, Eq. (1.58) takes the form

$$(1 + i\omega\tau_{ps})\, \rho_0 s = \left(\frac{1}{c_0^2} + \frac{i\omega\tau_{ps}}{c_\infty^2} \right) p_e \ . \tag{1.59}$$

The quantity τ_{ps} is the relaxation time measured under conditions of constant pressure and entropy. If we consider Eq. (1.59) at very low frequency, it can be seen to reduce to Eq. (1.57), with the previously calculated expression for the absorption coefficient. A similar equation is also obtained at very high frequency, except that the sound speed to be used in that case is c_∞.

For the general case, however, the expression for c will be quite different. If we write our three equations

$$\begin{aligned} iku - i\omega s &= 0 \\ i\omega u - \left(-\frac{ik}{\rho_0}\right) p_e &= 0 \\ (1 + i\omega\tau_{ps})\rho_0 s - \left(\frac{1}{c_0^2} + \frac{i\omega\tau_{ps}}{c_\infty^2}\right) p_e &= 0 \end{aligned} \tag{1.60}$$

and set the determinant of the coefficients equal to zero, we ultimately obtain the expressions for the sound velocity c and the absorption coefficient per unit wavelength $\mu \equiv \alpha\lambda$:

$$\frac{c^2}{c_0^2} = \frac{1 + \omega^2\tau_{ps}^2}{1 + \left(\frac{c_0}{c_\infty^2}\right)\omega^2\tau_{ps}^2}$$

$$\mu = \alpha\lambda = \frac{c}{c_0^2}\,\frac{\epsilon\pi\omega\tau_{ps}}{1 + \omega^2\tau_{ps}^2}, \tag{1.61}$$

where the quantity $\epsilon = (c_\infty^2 - c_0^2)/c_0^2$ is known as the relaxation strength.

While more complicated expressions can be obtained for other specific relaxation processes, the general structure of the final result remains the same as Eqs. (1.61), and we shall content ourselves with making use of these equations.

1.8 Radiation Field of a Piston Source. Diffraction.

In Section 1.5 we discussed the case of plane waves at some length, while Section 1.6 gave a brief account of spherical and cylindrical waves. Actual sound sources usually differ considerably from these idealized cases,

the commonest being a flat plate of finite dimensions that vibrates perpendicular to its plane (the plane piston). The next step in the case of linear acoustics is the analysis of the radiation field from such a sound source, whose dimensions are many times the wavelength of the radiation.

Such an analysis usually begins with the statement of Green's theorem. Given two continuous functions with continuous first derivatives, in a region bounded by the closed surfaces, we have

$$\int_V (\phi \nabla^2 \psi - \psi \nabla^2 \phi)\, dV = \int_S \left(\psi \frac{\partial \phi}{\partial n} - \phi \frac{\partial \psi}{\partial n}\right) dS \tag{1.62}$$

where n is the inward drawn normal to the surface (Fig. 1-4).

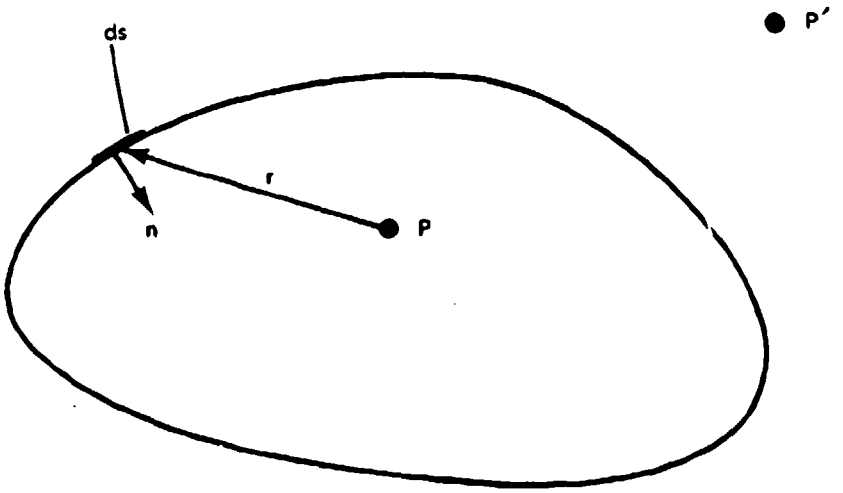

Fig. 1-4.–Surface for Green's theorem. P, P' are inside and outside the closed surface, respectively.

Now suppose that both ϕ and ψ are solutions of the wave equation (1.37a), where the time dependence is assumed to be given by $e^{j\omega t}$. Then the left-hand side of (1.62) vanishes, leaving

$$\int_S \left(\phi \frac{\partial \psi}{\partial n} - \psi \frac{\partial \phi}{\partial n}\right) dS = 0 \,. \tag{1.63}$$

Since ψ is an arbitrary solution of the wave equation, it can be chosen so as to provide a relatively simple solution of the boundary value problem at hand. Such a function is known as the Green's function of the problem. Here we shall use for ψ the spherical wave solution of the wave equation: ψ =

$e^{-i\mathbf{k}\cdot\mathbf{r}}/r$. We must of course surround the point P by a small sphere so as to avoid the singularity at $r = 0$. Then Eq. (1.63) becomes

$$\int \phi \frac{\partial}{\partial n}\left(\frac{e^{i\mathbf{k}\cdot\mathbf{r}}}{r}\right) ds - \int \frac{e^{i\mathbf{k}\cdot\mathbf{r}}}{r} \frac{\partial \phi}{\partial n} dS \tag{1.64}$$

$$+ \phi_P \frac{\partial}{\partial n}\left(\frac{e^{-ik\rho}}{\rho}\right) 4\pi\rho^2 - \frac{e^{-ik\rho}}{\rho} \frac{\partial \phi}{\partial n}\bigg|_P 4\pi\rho^2 = 0$$

where ρ is the radius of the small sphere centered at P. Now $\partial\rho/\partial n = 1$, so that the last two terms in Eq. (1.64) become

$$\phi_P 4\pi\rho^2 e^{-ik\rho}\left(-\frac{ik}{\rho} - \frac{1}{\rho^2}\right) - 4\pi\rho e^{-ik\rho} \frac{\partial \phi}{\partial n}\bigg|_P$$

and in the limit as $\rho \to 0$, Eq. (1.58) becomes

$$\phi_P = -\frac{1}{4\pi}\int \frac{e^{-i\mathbf{k}\cdot\mathbf{r}}}{r} \frac{\partial \phi}{\partial n} dS + \frac{1}{4\pi}\int \phi \frac{\partial}{\partial n}\left(\frac{e^{-i\mathbf{k}\cdot\mathbf{r}}}{r}\right) dS \,. \tag{1.65}$$

Note that r is the distance from a surface point to the point P. If the point P were outside the surface (e.g., p' in Fig. 1-4), the right-hand side of Eq. (1.65) would be equal to zero, since the last two terms in Eq. (1.64) would not have appeared.

Equation (1.65) can be further simplified by imposing on the function ϕ an additional requirement such that one or the other of the integrals vanishes. This can be done, for example, by repeating the above derivation for a point P' external to the surface S. Under such circumstances we get

$$0 = -\frac{1}{4\pi}\int \frac{e^{-i\mathbf{k}\cdot\mathbf{r}}}{r} \frac{\partial \phi'}{\partial n'} dS + \frac{1}{4\pi}\int \phi' \frac{\partial}{\partial n'}\left(\frac{e^{-i\mathbf{k}\cdot\mathbf{r}}}{r}\right) dS \,. \tag{1.66}$$

It is, of course assumed that ϕ' vanishes sufficiently rapidly over the remaining portions of the surface at $r = \infty$ so that the integral over this surface also vanishes. If we add Eqs. (1.65) and (1.66) and make use of the fact that $\partial/\partial n' = -\partial/\partial n$, we get

$$\phi_P = -\frac{1}{4\pi}\int_S \frac{e^{-i\mathbf{k}\cdot\mathbf{r}}}{r}\left(\frac{\partial \phi}{\partial n} - \frac{\partial \phi'}{\partial n}\right) dS + \frac{1}{4\pi}\int_S (\phi - \phi')\frac{\partial}{\partial n}\left(\frac{e^{-i\mathbf{k}\cdot\mathbf{r}}}{r}\right) dS \,. \tag{1.67}$$

[Since the integration in (1.67) is carried out only over the surface S, we can still measure r from the point P without encountering a singularity, so that r is the same for both ϕ and ϕ'.] We shall now take S to be a plane perpendicular to the x axis. We can then take either $\varphi = \phi'$ or $\partial\phi/\partial n' = \partial\phi/\partial n$ on the surface.

(a) $\phi(-x,y,z) = \phi(x,y,z)$. Then $\partial\phi/\partial n = -\partial\phi/\partial n$ and we get

$$\phi_P = -\frac{1}{2\pi}\int\int \frac{e^{-i\mathbf{k}\cdot\mathbf{r}}}{r}\frac{\partial\phi}{\partial n}\,dS \tag{1.68}$$

(b) $\partial\phi(-x,y,z)/\partial n = +\partial\phi'(x,y,z)/\partial n$. Then $\phi \equiv \phi'$ on the surface and we have

$$\phi_P = \frac{1}{2\pi}\int\int \phi\frac{\partial}{\partial n}\left(\frac{e^{-i\mathbf{k}\cdot\mathbf{r}}}{r}\right)dS\ . \tag{1.69}$$

Case (a) [Eq. (1.68)] is the diffraction integral used by Rayleigh. It can be thought of as representing the radiation field due to a distribution of simple spherical wave sources over the plane surface S. The density of source distribution is then 2ϕ. In the same way, case (b) represents the radiation field due to a distribution of acoustic dipoles of density 2 ($\partial\phi/\partial n$. Either equation can be used for the determination of the radiation field in the positive half space, provided that $\partial\phi/\partial n$ or ϕ is known on the bounding plane. While the form of the integral is simple, the detailed computation of the field remains a complicated one. In addition, the requirement that $\partial\phi/\partial n$ or ϕ be known over the boundary makes it necessary to introduce certain rather arbitrary simplifications in the boundary conditions in order to make solutions practical.

As an example of solutions of this type, we consider the problem of a vibrating circular piston. To take care of the boundary condition, we further assume that the plate is mounted in an infinite rigid wall or baffle. (In practice, of course, the term "infinite" here usually means distances of a few centimeters.) We therefore require the boundary conditions (Fig. 1-5):

$$\dot{\xi} = \frac{\partial\phi}{\partial n} = \dot{\xi}_0 e^{j\omega t} \qquad \rho \leqslant a$$

$$= 0 \qquad \rho > a\ .$$

This is the condition for the ideal plane piston of circular cross section. It is obvious that such conditions are not fully obtained in practice. In the use of an ordinary crystal or ceramic plate, for example, the edges are more or less clamped, so that we may expect $\dot{\xi}_0$ to be smaller in these regions. The crystal itself may vibrate more strongly on certain portions of its surface. Finally, no

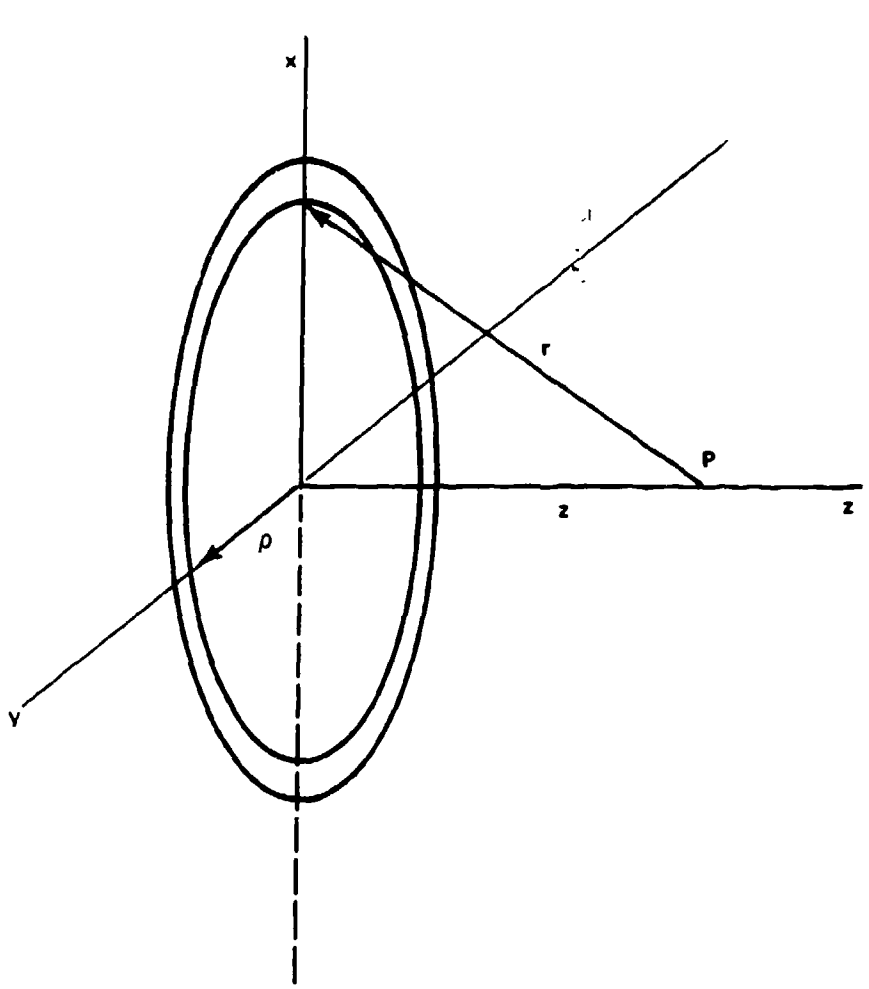

Figure 1-5.–Circular ring on the surface of plane piston in the xy plane.

baffle is either infinite or completely rigid. It is therefore a stroke of good fortune that the results of the analysis that follows below have been quite accurately confirmed.

As a first step in our analysis, we shall determine the value of the intensity I along the axis of the piston.

Since $\partial\phi/\partial n = \dot{\xi}_0 e^{j\omega t}$ for $r \leqslant a$, $dS = 2\pi\rho d\rho$, $r^2 = \rho^2 + z^2$, Eq. (1.68) becomes

$$\phi_P = -\dot{\xi}_0 e^{j\omega t} \int_0^a \frac{e^{-ikr}}{r} \rho d\rho \ . \tag{1.70}$$

By simple integration, this results in the expression

$$\phi_p = - i \frac{\xi_0 e^{j\omega t}}{k} \left(e^{-ik\sqrt{z^2 + a^2}} - e^{-ikz} \right) \tag{1.70}$$

By Eq. (1.23), the acoustic pressure p_e is then

$$p_e = - \rho_0 \phi = - \dot{\xi}_0 \rho_0 c e^{j\omega t} \left(e^{-ik\sqrt{z^2 + a^2}} - e^{-ikz} \right) \quad . \tag{1.71}$$

To find the intensity, we need the real part of Eq. (1.71)

$$\mathrm{Re}\, p_e = -\rho_0 c \dot{\xi}_0 \left[\cos\left(\omega t - k\sqrt{z^2 + a^2} \right) - \cos(\omega t - kz) \right]$$

which can be transformed to

$$\mathrm{Re}\, p_e = -2\rho_0 c \dot{\xi}_0 \sin\left(\frac{k}{2} \left\{ \sqrt{z^2 + a^2} - z \right\} \right) \sin\left[\omega t - \frac{k}{2} \left(\sqrt{z^2 + a^2} + z \right) \right] \tag{1.72}$$

so that

$$I = \frac{\langle (\mathrm{Re}\, p_e)^2 \rangle}{\rho_0 c} = 2\rho_0 c \dot{\xi}_0^2 \sin^2 \frac{k}{2} \left(\sqrt{z^2 + a^2} - z \right) . \tag{1.73}$$

where $\langle \cdot \cdot \cdot \rangle$ denotes the time average.

At large distances from the source, $a^2/z^2 \ll 1$ and $\sqrt{z^2 + a^2} - z \simeq a^2/2z$ so that

$$I \simeq 2\rho_0 c \dot{\xi}_0^2 \sin^2 \frac{ka^2}{4z} = 2\rho_0 c \dot{\xi}^2 \sin^2 \frac{\pi a^2}{2z\lambda} \quad . \tag{1.74}$$

A graph of this function is given in Fig. 1-6, where z is plotted in units of a^2/λ.

The location of the last maximum of this curve, at $z = a^2/\lambda$, is usually taken as the dividing line between the *near field* (Fresnel diffraction) and the *far field* (Fraunhofer diffraction).

For the determination of the radiation field at points off the axis, other analyses have been developed which yield approximate solutions in certain specific cases. A particularly useful approximation (in audio acoustics) has

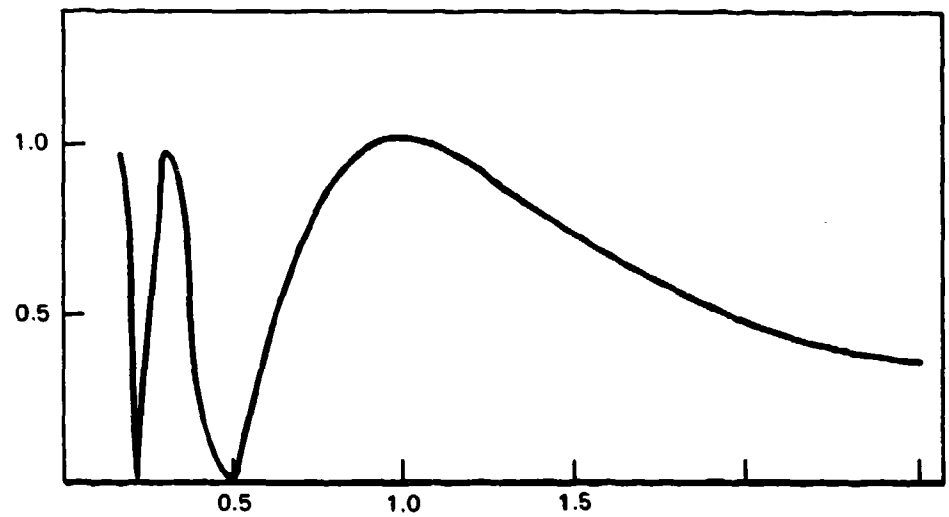

Figure 1-6.–Axial intensity of harmonic plane piston.

been that of the far field ($\rho \ll r$) and low frequencies ($k\rho \ll 1$) (see Fig. 1-7). The variable r' in the figure is given by the relation

$$r'^2 = r^2 \cos^2\theta + q^2 = r^2 + \rho^2 - 2r\rho \sin\theta \cos\psi \ .$$

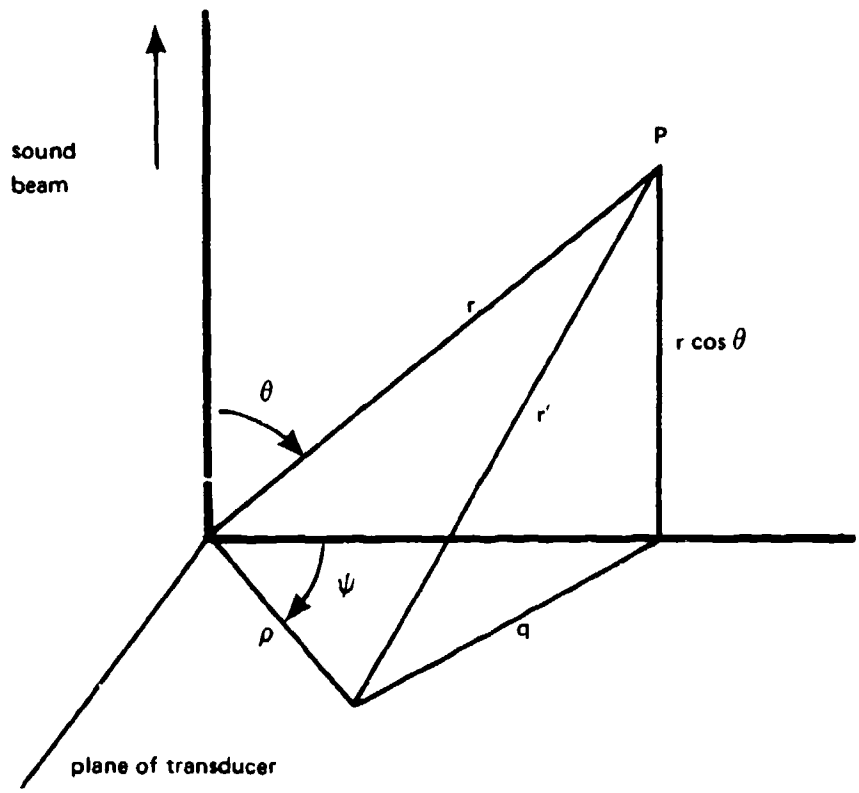

Figure 1-7.–Geometry for plane piston calculation.

Under the approximations $\rho << r$ and $k\rho << 1$, we expand the expression for r':

$$r' = [r^2 + \rho^2 - 2r\rho \sin\theta \cos\psi]^{1/2} \simeq r - \rho \sin\theta \cos\psi \ .$$

Then (1.69) becomes

$$\phi = - \frac{\dot{\xi}_0 e^{i\omega t}}{2\pi} \int\int \frac{e^{-ikr}}{r} \exp(ik\rho \sin\theta \cos\psi)\, \rho d\rho d\psi$$

or

$$\phi = - \frac{\dot{\xi}_0 e^{i\omega t}}{2\pi} \cdot \frac{e^{-ikr}}{r} \int_0^a \rho d\rho \int_0^{2\pi} \exp(ik\rho \sin\theta \cos\psi)\, d\psi \ .$$

The integral over ψ is the integral representation of the Bessel function of order zero and is equal to $2\pi J_0(k\rho \sin\theta)$. Then

$$\phi = \frac{- \xi_0 e^{j(\omega t - kr)}}{rk^2 \sin^2\theta} \int_0^a J_0(k\rho \sin\theta)\ \rho k \sin\theta\ \rho k \sin\theta\, d(\rho k \sin\theta) ;$$

but $\int xJ_0(dx) = xJ_1(x)$, so that

$$\phi = - \dot{\xi}_0 \frac{a^2 e^{j(\omega t - \mathbf{k}\cdot\mathbf{r})}}{2r} \frac{2J_1(ka \sin\theta)}{ka \sin\theta} \ . \tag{1.75}$$

or

$$p_c = i\omega\rho_0 a^2 \dot{\xi}_0^2 \frac{e^{j(\omega t - \mathbf{k}\cdot\mathbf{r})}}{2r} \frac{2J_1(ka \sin\theta)}{ka \sin\theta} \ . \tag{1.76}$$

A polar plot of $2J_1(ka \sin\theta)/ka \sin\theta \equiv f(\theta)$ is shown in Fig. 1-8 for $\lambda \simeq a$ and for $\lambda = 2a$.

Of particular interest are the side lobes. As the ratio λ/a is decreased, more and more of these lobes will appear. Thus, if an acoustic detector is moved across the radiation field at some distance from the source, maxima and minima of the intensity will be noted—the characteristic of a diffraction pattern.

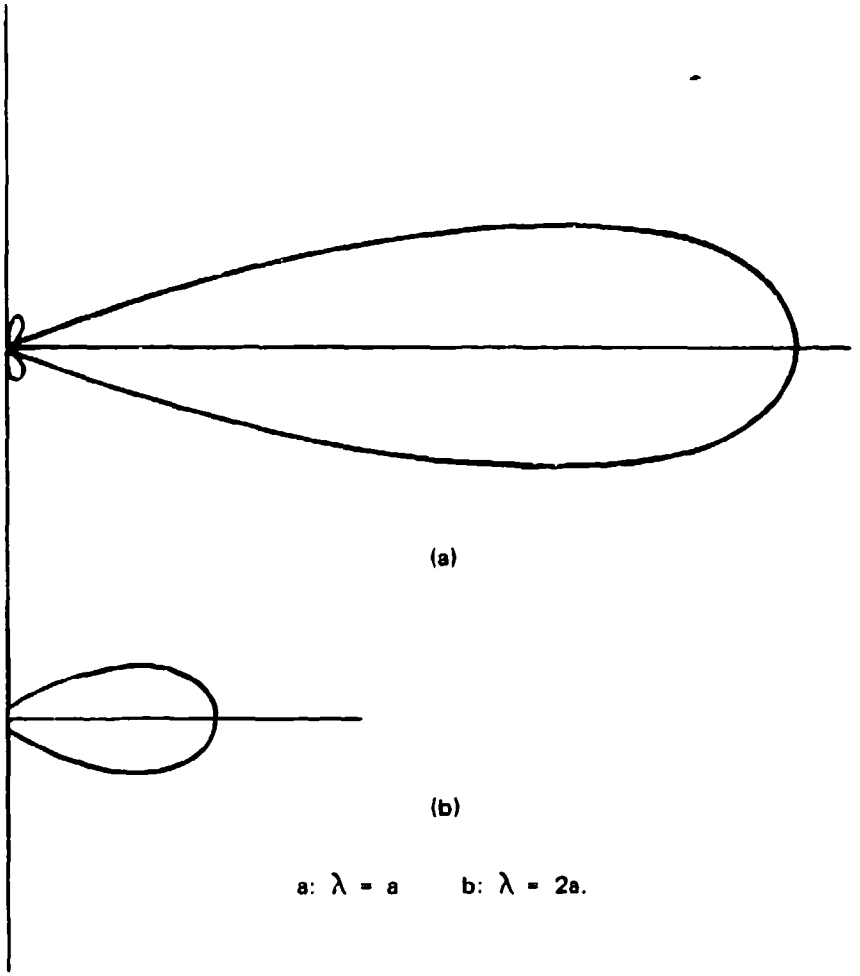

Figure 1-8.–Directivity of harmonic plane piston of radius a: (a) wavelength $\lambda = a$; (b) $\lambda = 2a$.

1.9 Refraction, Reflection and Scattering of Acoustic Waves.

As a sound beam passes from one medium to another, the beam will be both reflected and refracted. For oblique incidence, the law of reflection is the same as in optics, namely, the angle of incidence is equal to the angle of reflection.*

The law of refraction is also the same. For transmission as shown in Fig. 1-9, $\cos\theta_1/\cos\theta_2 = c_1/c_2$ where c_1, c_2 are the velocities of sound in the two media.

*Provided that we are dealing only with the case of longitudinal waves. When one deals with a solid medium, where transverse waves may exist, mode conversion is possible and the problem becomes complicated. See Beyer & Letcher, op. cit., pp. 30ff.

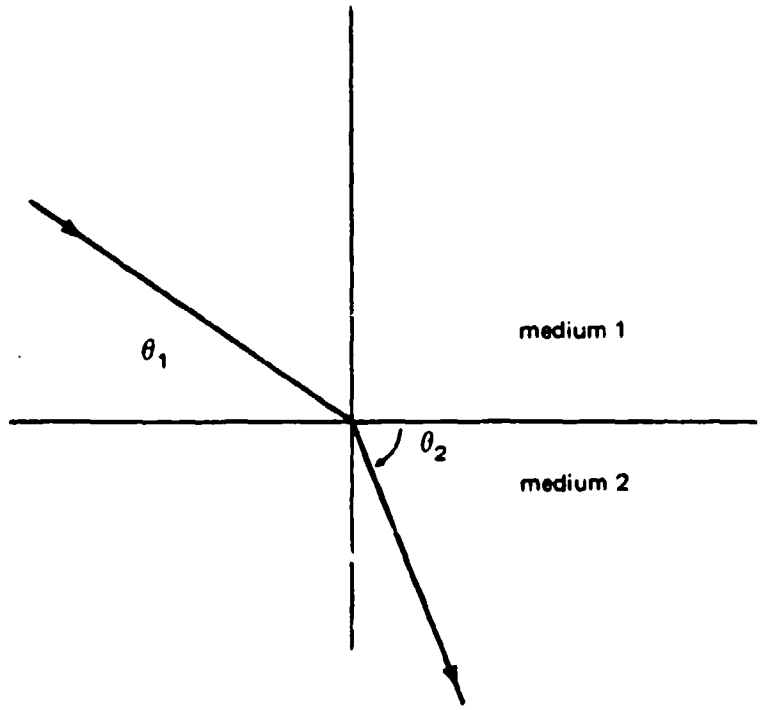

Figure 1-9.–Transmission of sound beam through interface.

The calculation of the amount of energy transmitted and reflected can be performed simply for the case of normal incidence. We shall consider two non-dissipative media (Fig. 1-10). The incident, reflected and transmitted displacements are indicated.

As we pass from one medium to another, there are two continuity conditions. First, the particle displacement must be the same in the two media at the boundary. Otherwise there would either be holes or the occupation of the same point by two different bits of matter. The pressure must also be continuous across the boundary; otherwise accelerations of the interface would occur.

The first of these conditions yields the equation.

$$A_1 + A_2 = B \ . \tag{1.77}$$

We now recall that the pressure in a plane wave is given by

$$p_e = \rho c \dot{\xi} = i\omega\rho c\xi$$

Hence the second condition will be

$$i\omega\rho_1 c_1 (A_1 - A_2) = i\omega\rho_2 c_2 B$$

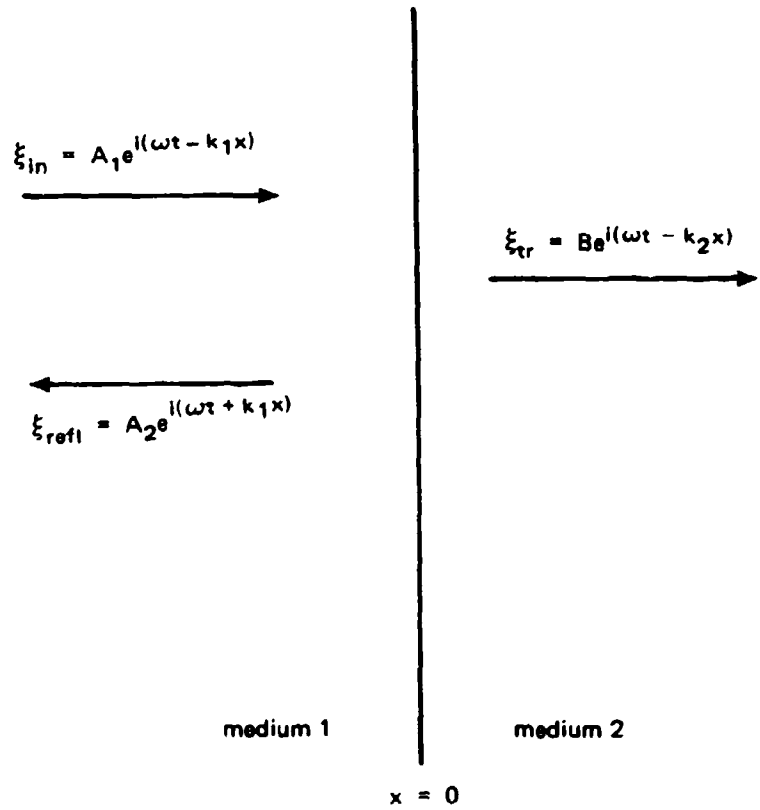

Figure 1-10.–Transmission and reflection of a plane wave.

or

$$A_1 - A_2 = \frac{\rho_2 c_2}{\rho_1 c_1} B \quad . \tag{1.78}$$

Solving for B and A_2 in terms of A_1, we get

$$A_2 = \frac{\rho_1 c_1 - \rho_2 c_2}{\rho_1 c_1 + \rho_2 c_2} A_1$$

$$B = \frac{2\rho_1 c_1}{\rho_1 c_1 + \rho_2 c_2} A_1 \tag{1.79}$$

The power transmitted and reflected can also be determined. The initial intensity I_1 is given by

$$I_1 = \frac{1}{2} \rho_1 c_1 \omega^2 A_1^2$$

so that the power transmission ratio T, defined as

$$T = \frac{I_{\text{trans}}}{I_1}$$

will be

$$T = \left(\frac{2r}{1+r}\right)^2 \qquad r = \frac{\rho_2 c_2}{\rho_1 c_1} \tag{1.80}$$

while the power reflection ratio R will be

$$R = 1 - T = \frac{I_{\text{refl}}}{I_1} = \left(\frac{1-r}{1+r}\right)^2 . \tag{1.81}$$

These have been calculated without account of losses in the media. (For an account of the more involved dissipation, see Lindsay, *Mechanical Radiation*, McGraw-Hill, N. Y. 1960, pp. 77ff.)

We have already seen how a sound source, such as a plane piston, can give rise to a diffractive radiation pattern. Similar results can be expected when a sound wave encounters an obstacle. Obviously there are many possible combinations (plane wave–rigid sphere, plane wave–soft cylinder, spherical wave–soft cylinder, and so on). We shall consider only the first case of scattering of plane waves by a rigid cylinder, following the presentation given by Lindsay and referring the reader to his work for a more detailed discussion of the problem.

We therefore consider a plane wave in a fluid incident on a rigid right circular cylinder of radius a where axis is normal to the direction of propagation (Fig. 1-11).

When a plane wave encounters such an obstacle, we expect that some signal will be deflected in all directions, and that the resultant pattern will have cylindrical symmetry. The full wave equation (neglecting absorption and adhering to the assumption of linearity) in the cylindrical coordinates r, θ, z will be

$$\frac{\partial^2\phi}{\partial r^2} + \frac{1}{r}\frac{\partial\phi}{\partial r} + \frac{1}{r^2}\frac{\partial^2\phi}{\partial\theta^2} + \frac{\partial^2\phi}{\partial z^2} = \frac{1}{c_0^2}\frac{\partial^2\phi}{\partial t^2}. \tag{1.82}$$

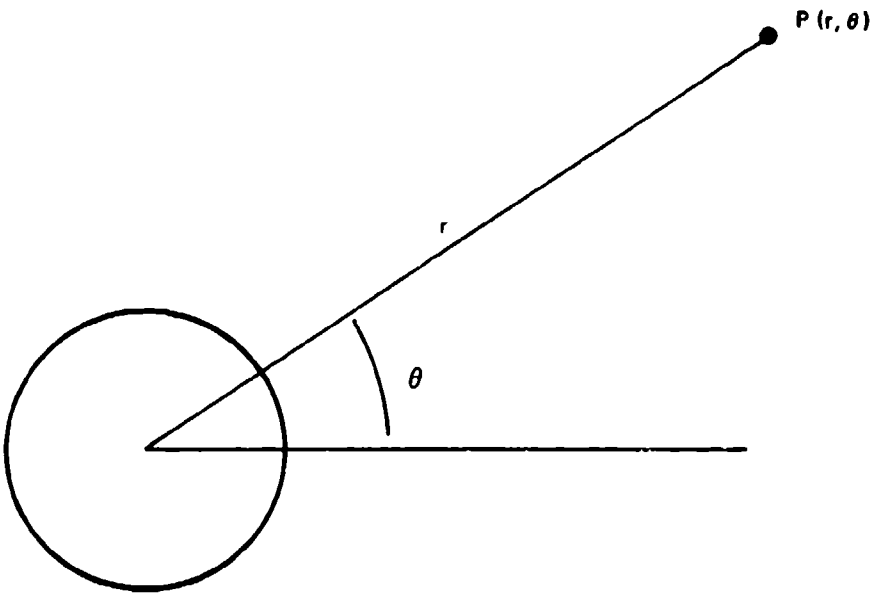

Figure 1-11.–Geometry for scattering from a circular cylinder.

In the usual way of solving this equation[5] we represent the solution in the form of a product

$$\phi(r, \theta, z) = R(r)\Theta(\theta)Z(z) \quad . \tag{1.83}$$

By the introduction of suitable integers m', ℓ, and use of the harmonic wave dependence

$$\phi \propto e^{j\omega t}, \ddot{\phi} = - \omega^2 \phi ,$$

Eq. (1.83) can be broken up into the three ordinary differential equations

$$\frac{d^2\Theta}{d\phi^2} + m^2\Theta = 0$$

$$\frac{d^2Z}{dz^2} + \ell^2 Z = 0 \tag{1.84}$$

$$\frac{d^2R}{dr^2} + \frac{1}{r}\frac{dR}{dr} + \left(k^2 - \ell^2 - \frac{m^2}{r^2}\right) R = 0$$

we shall also introduce $q^2 = k^2 - \ell^2$.

The the first two equations have solutions of well known harmonic form, while the third is Bessel's equation, the general solution of which is of the form

$$R = AJ_n(qr) + BN_n(qr) \quad . \tag{1.85}$$

Here J_n is the nth order Bessel function of the first kind:

$$J_n(x) = \left(\frac{x}{2}\right)^n \sum_{j=0}^{\infty} \frac{(-1)^j}{j!(m+j)!} \left(\frac{x}{2}\right)^{2j} \tag{1.86}$$

and N_n is the nth order Bessel function of the second kind (also called the *Neumann function).*

This latter has a rather involved series form and has the disadvantage that it becomes infinite at $x = 0$. It can be avoided by defining Bessel functions of a third kind, usually known as *Hankel functions*:

$$\begin{aligned} H_n^{(1)} &= J_n(x) + iN_n(x) \\ H_n^{(2)} &= J_n(x) - iN_n(x) . \end{aligned} \tag{1.87}$$

The basic procedure to be followed in solving the scattering problem is to expand the plane wave in a series of Bessel functions of the first kind and to express the scattered wave in terms of Hankel functions. Application of boundary conditions then will serve to produce the desired solution.

(i) **Expansion of the plane wave.**

We first represent the plane wave spatial dependence in the form (see Fig. 1·11)

$$e^{-ikx} = e^{-ikr\cos\theta} = \sum_{n=0}^{\infty} C_n(r) \cos n\theta \quad .$$

Here the coefficients $C_n(r)$ will be given by the integral

$$C_n(r) = \frac{1}{\pi}\int_0^{\pi} e^{-ikr\cos\theta} \cos n\theta d\phi$$

$$= 2(-1)^n J_n(kr) \qquad n \geqslant 1$$

$$= J_0(kr) \qquad n = 0 \ .$$

Hence the velocity potential for the plane wave will be

$$\phi_p = A_p e^{j(\omega t - kx)} = A_p \left[J_0(kr) + 2 \sum_{n=1}^{\infty} (-1)^n J_n(kr) \cos n\theta \right] \tag{1.88}$$

(ii) **Scattered wave.**

To treat the scattered wave, we first note that the form of the scattered wave should be proportional to e^{-ikr} at large distances from the cylinder. Now the asymptotic form of the Hankel functions for large argument x will be given by

$$H_n^{(1)}(x) \simeq \sqrt{\frac{2}{\pi x}}\, e^{i\left[x - \frac{2n+1}{4}\pi\right]}$$

$$H_n^{(2)}(x) \simeq \sqrt{\frac{2}{\pi x}}\, e^{-i\left[x - \frac{2n+1}{4}\pi\right]} \tag{1.89}$$

from which we can see that the function of the second kind, $H_n^{(2)}(x)$, is the one to be used. (If we had used the time dependence $e^{-i\omega t}$, then $H_n^{(1)}(x)$ would have been the appropriate form.) We therefore try the scattering form

$$\phi_s = e^{j\omega t} \sum_{n=0}^{\infty} B_n H_n^{(2)} \cos n\theta \ . \tag{1.90}$$

We must now apply the boundary condition that the particular velocity normal to the cylinder be zero at the surface of the cylinder, since the cylinder is assumed to be rigid. That is,

$$u_r\Big|_{r=a} = \frac{\partial}{\partial r}(\phi_p + \phi_s)\Big|_{r=a} = 0 \ . \tag{1.91}$$

If Eqs. (1.88), (1.90) are substituted in Eq. (1.19) and the lengthy mathematical manipulations are carried out, the following is obtained for the pressure in the scattered wave:

$$p_s = -\rho_0 \dot{\phi}_s = -\rho_0 A_p e^{i\omega t} \left[-i \sin \gamma_0 e^{-i\gamma_0} H_0^{(2)}(kr) + 2 \sum_{n=1}^{\infty} (-1)^{n+1} \sin \gamma_n e^{-\gamma_n} H_n^{(2)}(kr) \cos n\theta \right] \tag{1.92}$$

or if $kr >> 1$

$$p_s = -\rho_0 A_p \sqrt{\frac{2}{\pi kr}}\, e^{i(\omega t - kr)} \left[-i \sin \gamma_0 e^{-i \frac{(\gamma_0 - \pi)}{4}} + 2 \sum_{n=1}^{\infty} (-1)^{n+1} \sin \gamma_n e^{-i \left(\gamma_n - \frac{2n+1}{4} \right) \pi} \cos n\theta \right]$$

$$\equiv -\rho_0 A_p \sqrt{\frac{2}{\pi kr}}\, e^{i(\omega t - kr)} \psi_s(\theta) \, . \tag{1.93}$$

Hence the scattered intensity will be

$$I = \frac{\rho_0 A_p^2}{\pi r \omega} [\psi_s(\theta)]^2 \, . \tag{1.94}$$

The scattered intensity function $|\psi_p(\theta)|^2$ for two different cylinders is given in Fig. 1-12.

From these relations it is clear that there is no shadow zone but that in fact, the forward scattering reaches a maximum at $\theta = 0$. Also, as the frequency increases, the number of maxima and minima also increases.

1.10 Surface Waves.

In addition to waves passing through the volume of a medium, there are waves that are constrained to move mainly on the surface. We shall discuss the most important of these briefly.

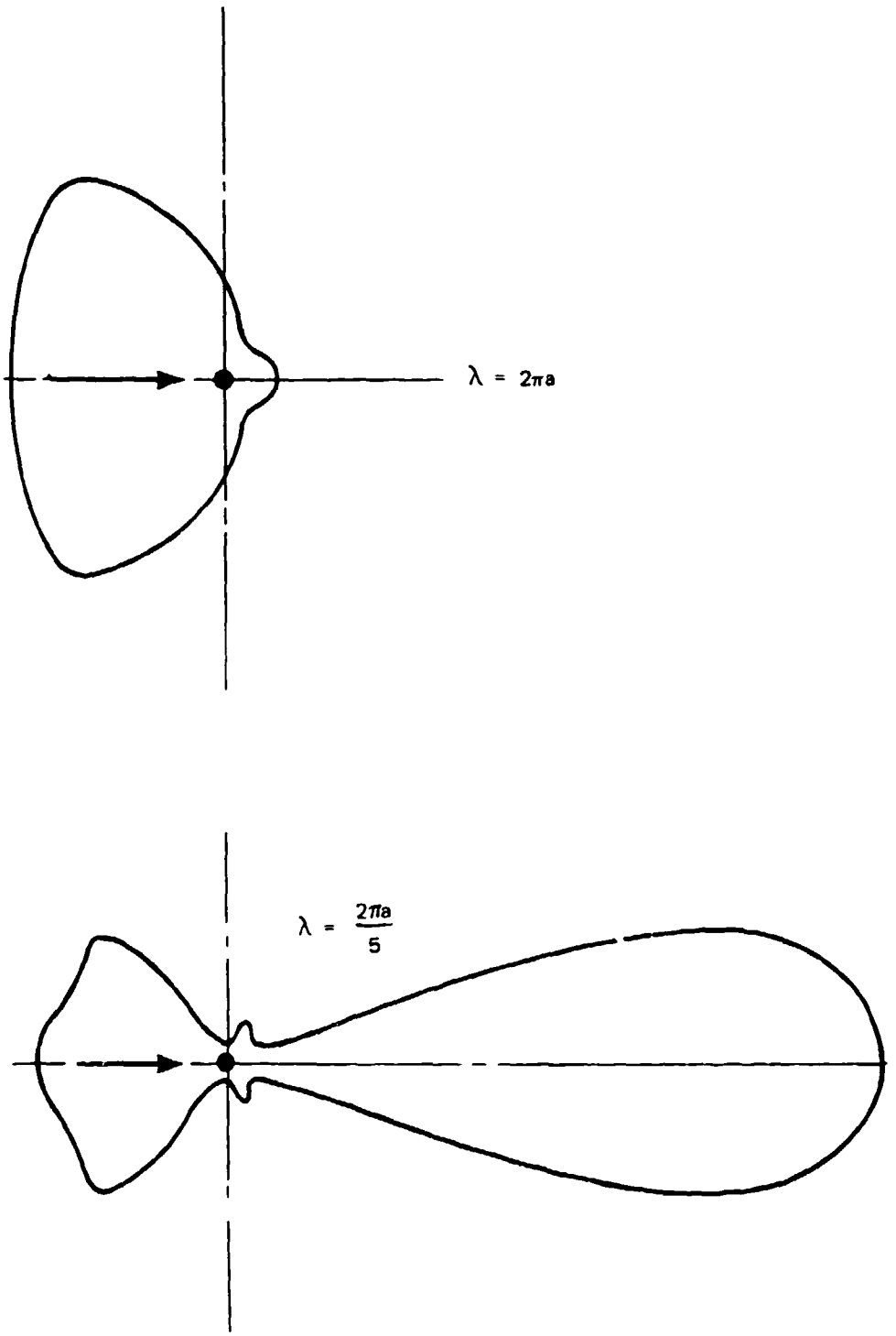

Figure 1-12.–Scattering of sound from solid cylinder of radius a for the wavelength $\lambda = 2\pi a, 2\pi a/5$. Direction of incident beam is indicated by arrows.

Waves on a liquid surface.

From classical hydrodynamics, the equation for the velocity potential of a disturbance on the surface of liquid subject to gravity is

$$\rho g \frac{\partial \phi}{\partial z} + \rho \frac{\partial^2 \phi}{\partial t^2} - \sigma \frac{\partial}{\partial z}\left(\frac{\partial^2 \phi}{\partial x^2} + \frac{\partial^2 \phi}{\partial y^2}\right) = 0 \tag{1.95}$$

where the z direction is perpendicular to the free surface of the liquid. Here g is the acceleration due to gravity and σ is the surface tension of the liquid.

We consider a plane wave traveling along the surface in the x direction, exponentially damped in the z direction

$$\phi = Ae^{+kz} \cos(kx - \omega t) \qquad (z < 0) \ . \tag{1.96}$$

If the medium is of some finite depth h, there will be a second solution

$$\phi = Be^{-kz} \cos(kx - \omega t) \tag{1.97}$$

and, by application of the boundary condition that the pressure be continuous, we obtain the following expression for the relation for the velocity of the surface wave

$$c^2 = \left[\frac{g}{k} + \frac{k\sigma}{\rho}\right] \tanh kh \ . \tag{1.98}$$

The resultant expression for ϕ becomes

$$\phi = A \cos(kx - \omega t) \cosh k(z + h) \ . \tag{1.99}$$

Two special cases are included here. If the wavelength is long (or the surface tension low) the first term predominates and we have *gravity waves*. On the other hand, at high frequency (or high surface tension) the second term is dominant, and we have *capillary waves*.

One can also distinguish the results for shallow water, where $\tanh kh = kh$, and deep water, where $\tanh kh \simeq 1$

shallow water

$$c^2 = gh + \frac{\sigma}{\rho} k^2 \tag{1.100}$$

deep water

$$c^2 = \frac{g}{k} + \frac{k\sigma}{\rho} . \tag{1.101}$$

In the case of deep water, where we need consider only Eq. (1.96), it can be seen that the displacement from equilibrium in the x and z direction $\delta x, \delta z$ are both sinusoidal in time:

$$\delta x = - \frac{Ak}{\omega} e^{kz} \cos (kx - \omega t)$$

$$\delta z = - \frac{Ak}{\omega} e^{kz} \sin (kx - \omega t) \tag{1.102}$$

so that individual fluid particle undergoes a circular motion. On the other hand, the crests of the waves described by Eq. (1.102) will be narrow and the troughs wide, so that the wave is spatially nonlinear.

If we consider the shallow water case (Eq. 1.99) the pressure of the cosh $k(h + z)$ term makes the displacements of different size in the x and z directions, so that the particle motion becomes elliptical.

Waves on a solid surface.

In the case of surface waves on a solid surface, one also distinguishes two types. In the *Rayleigh waves*, the motion of the particle in the solid is similar to that of gravity waves, i.e., the particle undergoes displacements in directions perpendicular and horizontal to the surface, but is damped exponentially as one penetrates the medium. A visualization of a Rayleigh wave is shown in Fig. 1-13.

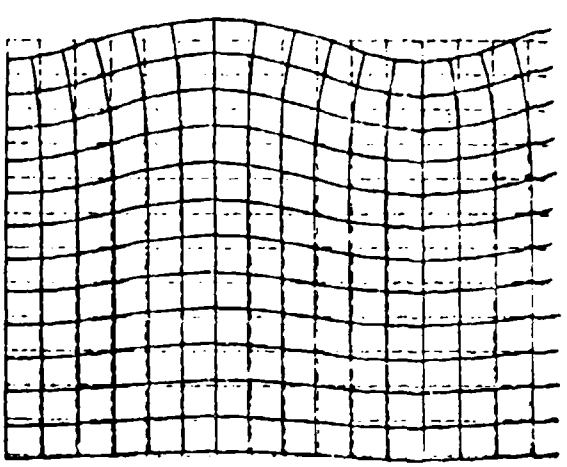

Figure 1-13.–Deformation of surface layers by a Rayleigh wave (after L. Kremer and M. Heckl, Körperschall, Springer Verlag, Berlin/Heidelberg, 1967, p. 150).

The velocity of propagation of a Rayleigh wave is an involved function of the elastic properties of the medium, but is usually slightly smaller than the propagation velocity of a shear wave in the unbounded medium. Figure 1-14 gives a plot of the ratio c_R/c_t as a function of Poisson's ratio.

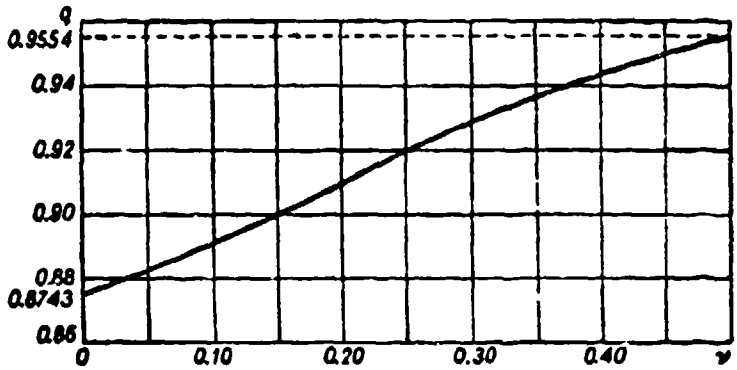

Figure 1-14.–Ratio q of the Rayleigh wave velocity c_R to the shear wave velocity c_t as a function of the Poisson ratio ν [after I. Malecki, Physical Foundations of Technical Acoustics (English translation, Pergamon Press, N.Y., 1969, p. 88)].

If a transverse surface wave is propagated in layered material, so that all the displacements are parallel to the surface, the wave is known as a *Love wave.*

BIBLIOGRAPHY

Chapter 1

R. B. Lindsay, *Mechanical Radiation*, McGraw-Hill N. Y., 1960.

P. M. Morse and K. U. Ingard, *Theoretical Acoustics*, Academic Press, N. Y., 1969.

R. T. Beyer and S. V. Letcher, *Physical Ultrasonics*, Academic Press, N. Y., 1969.

R. W. B. Stephens and A. E. Bate, *Acoustics and Vibrational Physics*, E. Arnold, London, (2nd ed.) 1966.

E. Skudrzyk, *The Foundations of Acoustics*, Springer, N. Y., 1971.

L. E. Kinsler and A. K. Frey, *Fundamentals of Acoustics*, Wiley, N. Y., (2nd ed.) 1962.

REFERENCES

Chapter 1

1. G. C. Stokes, Trans. Camb. Phil. Soc. 8, 287 (1845).
2 See the article by F. V. Hunt on "Propagation of Sound in Fluids," AIP Handbook (3rd ed.), McGraw-Hill, N. Y., 1972, esp. p. 3-41.
3. See "A Discussion of the First and Second Viscosities of Fluids," under the leadership of L. Rosenhead, Proc. Roy. Soc. London **226A**, 1, (1954).
4. R. T. Beyer and S. V. Letcher, *Physical Ultrasonics*, Academic Press, N. Y., 1969, Chapters 4 and 5.
5. See, e.g., J. Mathews and R. L. Walker, *Mathematical Methods of Physics* (2nd ed.), W. A. Benjamin, N. Y., 1970, pp. 226ff. P. M. Morse and K. U. Ingard, *Theoretical Acoustics*, McGraw-Hill, N. Y., 1968, pp. 332ff.

Chapter 2

SOME SOURCES OF NONLINEAR OSCILLATIONS

In undertaking a study of nonlinear systems, one is confronted with the wide variety and diverse character of the phenomena. To paraphrase Tolstoy,* the vibrations of linear systems are all alike, but each nonlinear system is nonlinear in its own way. That is, the form of the partial differential equation governing the process, or the mutual variation of the parameters involved may be quite different from one another.

The nonlinearity may occur in the source, in the medium, or even in the detection system. In this chapter, we shall discuss relatively simple nonline oscillations and several examples of nonlinear sources.

2.1 The Simple Pendulum.

The simple pendulum is a typical example of a nonlinear system which generally receives an approximate linear treatment. The arrangement is shown in Fig. 2-1. If a bob of mass m, suspended from the point P, is displaced through the angle θ and released, a restoring force $-mg \sin \theta$ is set up. This force exerts a torque $-mg\ell \sin \theta$ about the axis through the support point, so that the equation of motion will be, in the absence of dissipation,

$$I\ddot{\theta} = -mg\ell \sin \theta .$$

For a massless rod and a bob of concentrated mass, the moment of inertia I about the point of suspension can be set equal to $m\ell^2$. Then our equation becomes

$$\ddot{\theta} = \frac{-g}{\ell} \sin \theta \quad . \tag{2.1}$$

The usual approximation is that of small angular displacements so that we can set $\sin \theta \simeq \theta$. Then Eq. (2.1) becomes identical with Eq. (1.1), and simple

*Leo Tolstoy, *Anna Karenina*, p. 1. A somewhat similar note has been sounded by Werner Heisenberg: "It has been argued that every nonlinear problem is really individual, that it requires individual methods, usually very complicated and difficult methods." (Physics Today, Vol. 20, p. 27, May, 1967.)

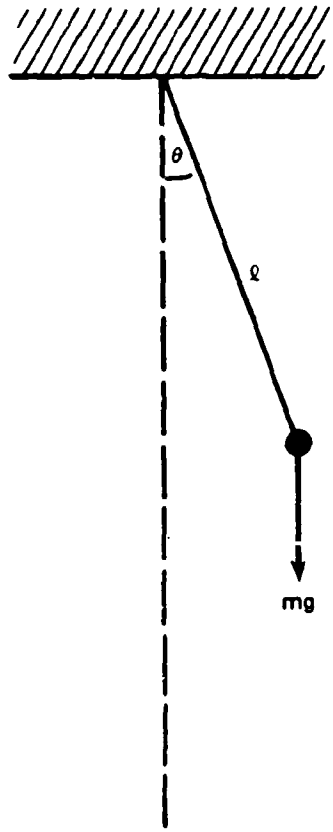

Figure 2-1.–Simple pendulum.

harmonic motion results, with the circular frequency ω given by $\omega = \sqrt{g/\ell}$. If the pendulum is released from rest at an angular displacement θ_0, then

$$\theta = \theta_0 \cos \omega t \ . \tag{2.2}$$

If the angle θ exceeds 10° however, the approximation is no longer satisfactory. While an effective solution can be obtained in terms of elliptic integrals, [1] it is instructive for our purposes to include the next approximation in the series expansion of $\sin \theta = \theta - \theta^3/3! + \ldots$, and consider the equation

$$\theta = \frac{-g}{\ell}\theta + \frac{g}{6\ell}\theta^3 \tag{2.3}$$

which we shall write

$$\theta = -a\theta - b\theta^3 \ . \tag{2.3'}$$

To solve this equation, we employ an iteration technique. We first substitute Eq. (2.2) in the second (hopefully small) term on the right side of Eq. (2.3′). That is, we write

$$\theta = -a\theta - b\theta_0^3 \cos^3 \omega t$$

or since $\cos^3 \omega t = (3/4) \cos \omega t + (1/4) \cos 3\omega t$,

$$\theta = -a\theta - \frac{3b\theta_0^3}{4} \cos \omega t - \frac{b}{4} \theta_0^3 \cos 3\omega t \ . \tag{2.4}$$

Thus our procedure has led to the linearization of the original equation. We now attempt a new approximate solution

$$\theta = A_1 \cos \omega t + A_3 \cos 3\omega t \ . \tag{2.5}$$

Substitution of (2.5) in (2.4) yields

$$\left(-\omega^2 A_1 + aA_1 + \frac{3b\theta_0^3}{4}\right) \cos \omega t +$$

$$\left(-9\omega^2 A_3 + aA_3 + \frac{b}{4} \theta_0^3\right) \cos 3\omega t = 0 \ .$$

Since $\cos \omega t$ and $\cos 3\omega t$ are linearly independent, we can equate the separate coefficients to zero. Then

$$\omega^2 = a + \frac{3b\theta_0^3}{4A_1} \cong a + \frac{3}{4} b\theta_0^2$$

$$A_3 = \frac{b\theta_0^3}{4} \frac{1}{9\omega^2 - a} = \frac{b\theta_0^3}{32a + 27b\theta_0^2} \tag{2.6}$$

Replacing the substitutions of (2.3′), namely, $a = g/\ell \equiv \omega_0^2$, $b = -g/6\ell = -\omega_0^2/6$, we see that

$$\omega^2 = \omega_0^2 \left(1 - \frac{\theta_0^2}{8}\right) . \tag{2.7}$$

This result was obtained by Daniel Bernoulli in 1747.

Of course, our method is still highly approximate. For example, Eq. (2.5) will now be written

$$\theta = \theta_0 \cos \omega t + \frac{b\theta_0^3}{32a + 27b\theta_0^2} \cos 3\omega t \tag{2.8}$$

which would give an incorrect value of the displacement at $t = 0$ unless the quantity θ were redefined. One can, of course, make such a redefinition and continue the iteration process.

2.2 Nonlinear Springs.

In Section 1.1, we discussed the free and forced oscillations of a linear spring. We shall now treat the corresponding nonlinear cases.

Let us rewrite Eq. (1.1) in a more general form

$$\ddot{\xi} + R(\dot{\xi}) + f(\xi) = F(t) \ . \tag{2.9}$$

Here $f(\xi)$ is the internal restoring force per unit mass, $F(t)$ the corresponding external forcing term and $R(\dot{\xi})$ the dissipation term.

Some possible forms of $f(\xi)$ are sketched in Fig. 2-2. If $f(\xi) = k\xi$, we have the simple linear case. If $f(\xi) = k\xi + b\xi^3$, $b > 0$ the restoring force will always be greater in magnitude than in the linear case that corresponds to the pendulum case just considered. Hence for free oscillations $[F(t) = 0]$, the frequency of vibration will be increased above the value in the linear case. This situation is somewhat equivalent to a stiffer or "harder" spring. On the other hand, if $b < 0$, as in the case of the simple pendulum, the frequency of oscillation decreases and we have a spring with a lower effective stiffness, i.e., a "softer" spring.

Equation (2.9) covers a great number of different nonlinear cases, depending on the form of terms $R(\dot{\xi})$ and $f(\xi)$. Since this subject has been treated very extensively in the literature (e.g., Stoker, 1950 [2]) we shall only review those cases here that are of particular interest to us in nonlinear acoustics.

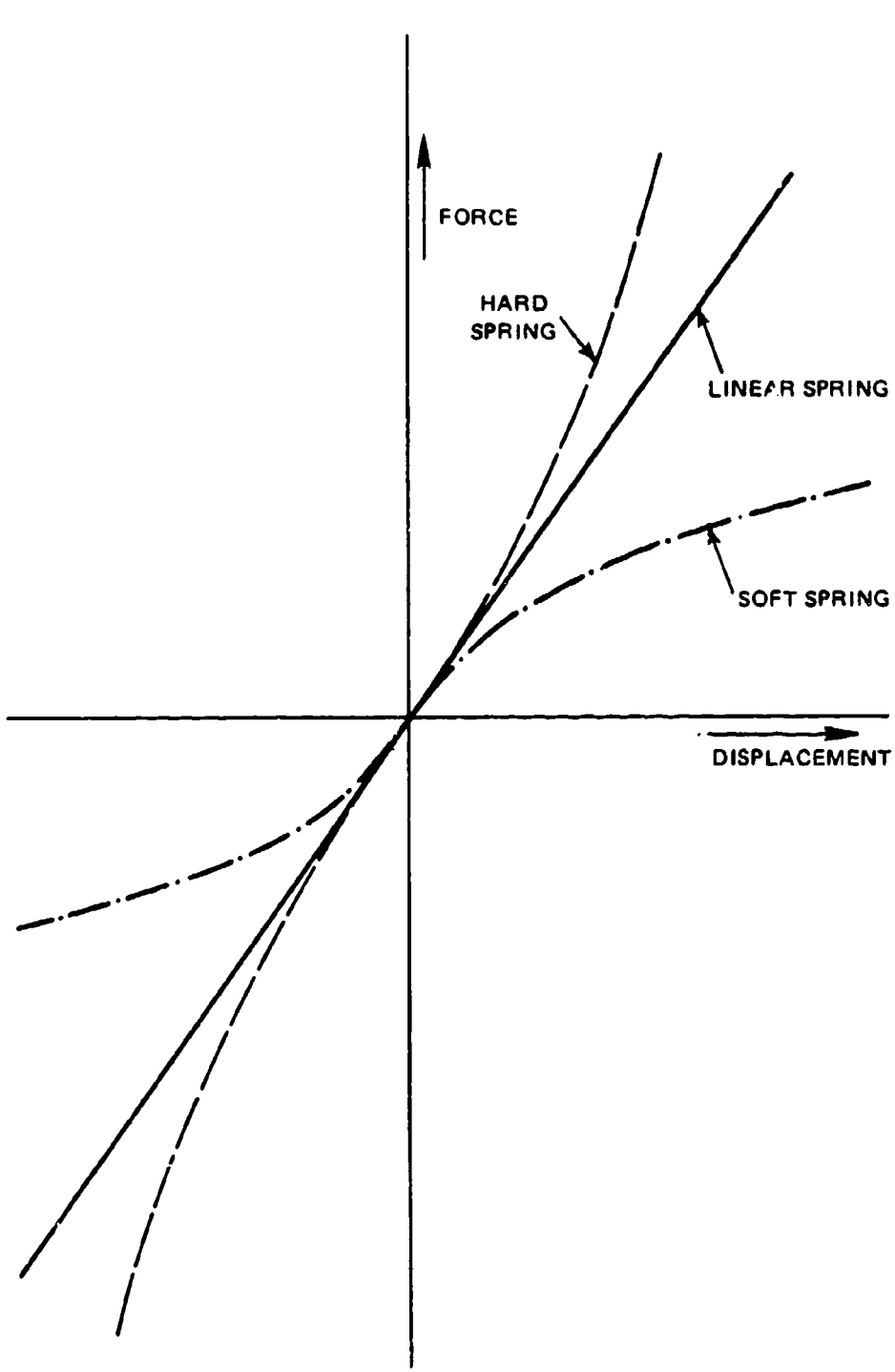

Figure 2-1.–Force-displacement curves for various springs.

2.3 Undamped Forced Oscillations with Nonlinear Restoring Force.

In this case $R(\dot{\xi}) = 0$. We shall first consider $F(t) = F_0 \cos \omega t$, $f(\xi) = k\xi + \epsilon\xi^3$. Then

$$m\ddot{\xi} = -k\xi - \epsilon\xi^3 - F_0 \cos \omega t \quad . \tag{2.10}$$

When $F_0 = 0$, this corresponds to a simple pendulum with small-amplitude frequency $\omega_0^2 = k/m$. Our first order solution will be

$$\xi_1 = A \cos \omega t \quad . \tag{2.11}$$

If this value of ξ_1 is substituted on the right side of (2.10), we next obtain

$$m\ddot{\xi}_2 = -kA \cos \omega t + F_0 \cos \omega t - \epsilon A^3 \cos^3 \omega t$$

or, using the trigonometric identity for $\cos^3 \omega t$, we have for the second approximation

$$\ddot{\xi}_2 = \left(-\frac{3}{4}\frac{\epsilon}{m} A^3 - \frac{k}{m} A + \frac{F_0}{m} \right) \cos \omega t - \frac{\epsilon A^3}{4m} \cos 3\omega t \quad . \tag{2.12}$$

Integration of (2.12) yields

$$\xi_2 = \frac{1}{\omega^2} \left(\frac{k}{m} A + \frac{3}{4}\frac{\epsilon}{m} A^3 - \frac{F_0}{m} \right) \cos \omega t + \frac{\epsilon A^3}{36m\omega^2} \cos 3\omega t \, . \tag{2.13}$$

Equation (2.13) is subject to a number of limitations: ϵ/m must be small if we are to have a converging process; for other reasons, k/m, A, and F_0/m also need to be small.

It would seem at this point that all we need do is proceed with further iterations. However, there are difficulties lurking, as has been pointed out by Duffing. [4] We can regard Eq. (2.13) as giving us the value of A for a fixed value of ω, or, of giving us ω for prescribed values of A. Thus, let us suppose that our solution for ξ_2 must remain close to the original solution $\xi_1 = A \cos \omega t$. We therefore require

$$\xi_2 = A_1 \cos \omega t + \frac{\epsilon A^3}{36m} \cos 3\omega t$$

to be the same as

$$\xi_1 = A \cos \omega t$$

so far as the term in the frequency ω is concerned. Then

$$A\omega^2 = \frac{kA}{m} + \frac{3}{4}\frac{\epsilon}{m} A^3 - \frac{F_0}{m} \tag{2.14}$$

or

$$\omega^2 = \frac{k}{m} + \frac{3}{4}\frac{\epsilon}{m} A^2 - \frac{F_0}{mA} \; . \tag{2.14'}$$

Let us pause a moment and consider the meaning of this relation by rewriting Eq. (2.14) in parametric form:

$$y_1 = \frac{3}{4}\frac{\epsilon}{m} A^3$$

$$y_2 = (\omega_0^2 - \omega^2) A - \frac{F_0}{m} \; ; \quad \omega_0^2 = \frac{k}{m} \; .$$

Figure 2-3 gives the curve for y_1 in the case $\epsilon > 0$. If ω is very large, y_2 will have a negative slope. The solution is then given by the point P_1.

We now consider decreasing values of ω. The line for y_2 swings around and ultimately takes a positive slope, the y intercept point being fixed at $-F_0/m$. The magnitude of A increases as the solution point moves down the curve y_1 to P_2. But now consider the points P_3, P_3'. Here the solution has two values. A plot of the possible values of A^2 as a function of ω is shown in Fig. 2-4. It is evident from the figure that A^2 will pass through a maximum and then decrease as ω is reduced. When the frequency goes beyond ω_{c1}, however, the amplitude falls suddenly, by a jump, to a much lower value. The amplitude then continues to decrease with decreasing ω.

If we now reverse the situation and increase ω, A^2 will increase gradually until $\omega = \omega_{c2}$, at which point the amplitude jumps to a much larger value.

Before continuing with our study, let us take a step back and redo the above problem in a slightly different form. Following Stoker, we rewrite Eq. (2.10) as

$$\ddot{\xi} + \omega^2 \xi = (\omega^2 - \omega_0^2)\, \xi - \beta \xi^3 + F \cos \omega t \tag{2.15}$$

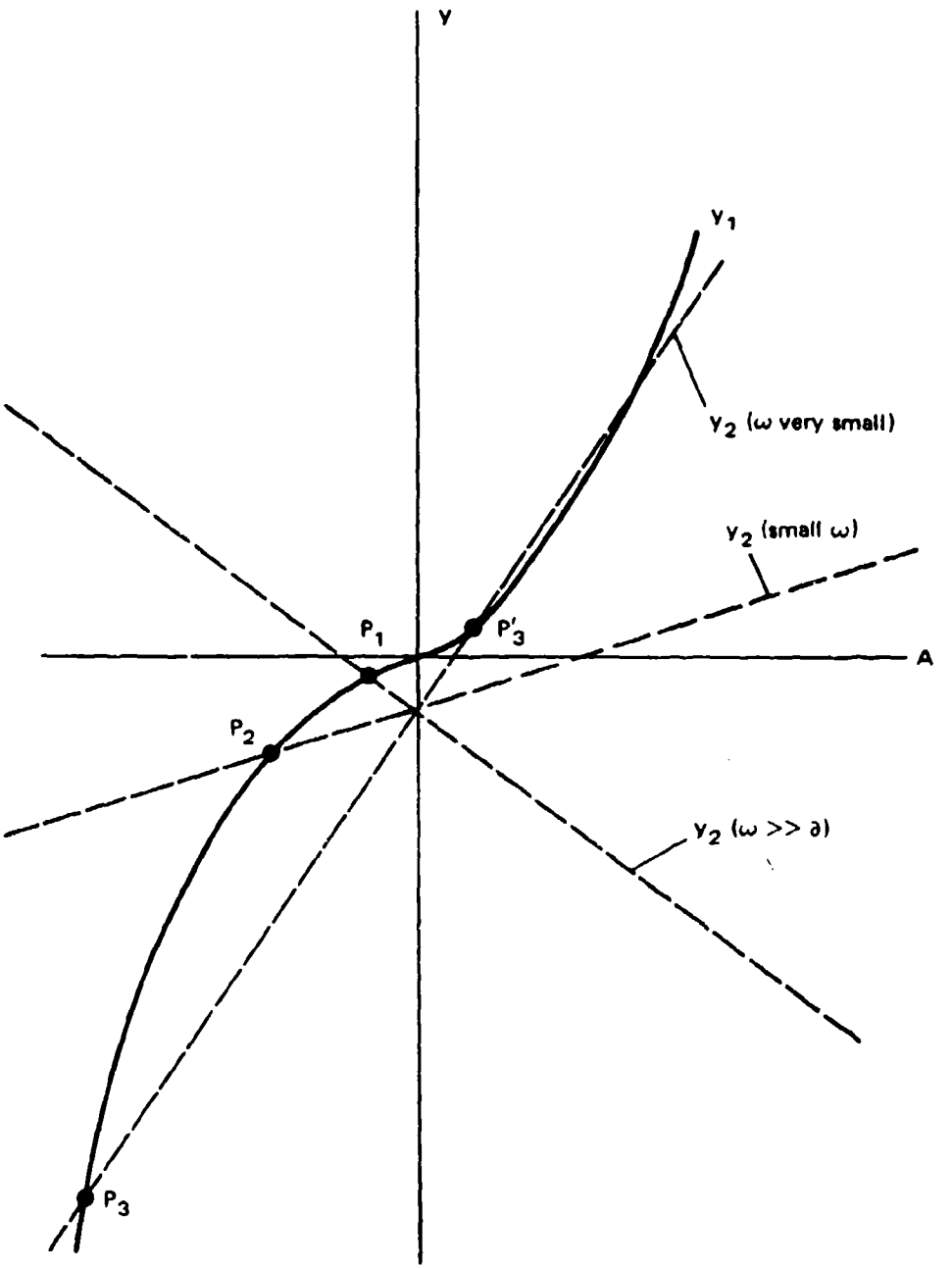

Figure 2-3.–Parametric form of Eq. (2.14): solid curve–y_1; broken curves–y_2 for various ω.

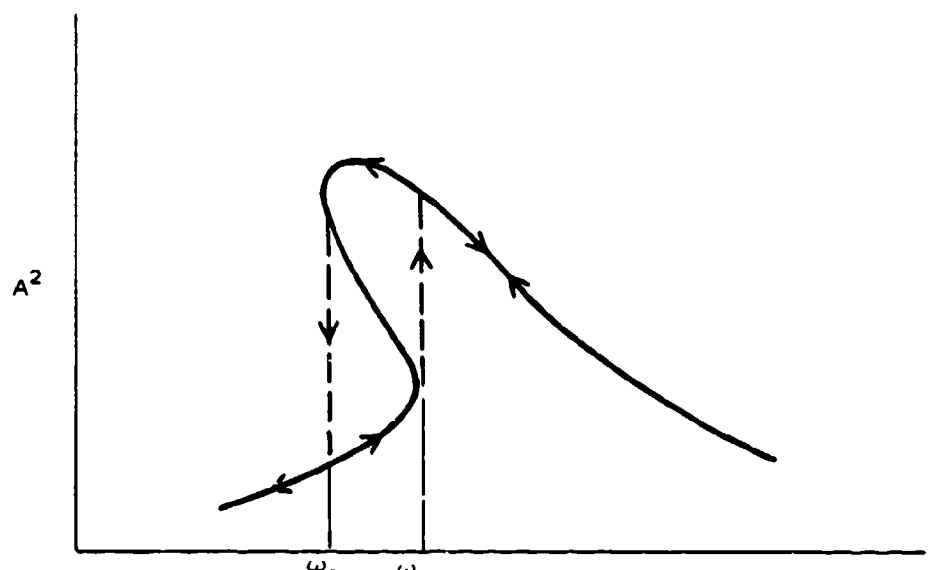

Figure 2-4.–Behavior of nonlinear spring.

where $\beta = \epsilon/m$ and $F_0 = F/m$.

We again make the first approximation

$$\xi = A \cos \omega t$$

and substitute on the right in Eq. (2.10)

$$\ddot{\xi}_2 + \omega^2 \xi_2 = \left[(\omega - \omega_0^2) A - \frac{3}{4} \beta A^3 + F \right] \cos \omega t - \frac{1}{4} \beta A^3 \cos 3\omega t \,. \tag{2.16}$$

It should be clear here that the coefficient of cos ωt on the right side of (2.16) must vanish, since cos ωt is a solution of the homogeneous equation $\ddot{\xi}_2 + \omega^2 \xi_2 = 0$. We therefore obtain

$$\omega^2 = \omega_0^2 + \frac{3}{4} \beta A^2 - \frac{F}{A} \,, \tag{2.17}$$

which is identical with Eq. (2.14′). Hence

$$\ddot{\xi}_2 + \omega^2 \xi_2 = - \frac{1}{4} \beta A^3 \cos 3\omega t \,.$$

It is evident that

$$\xi_2 = A_1 \cos \omega t + C \cos 3\omega t$$

must be a solution of (2.16); for, adding the expressions for ξ_2 and $\omega^2 \xi_2$, we obtain

$$\ddot{\xi}_2 = -\omega^2 A_1 \cos \omega t - 9\omega^2 C \cos \omega t$$

$$\omega^2 \xi_2 = \omega^2 A_1 \cos \omega t + \omega^2 C \cos \omega t$$

$$-\frac{1}{4} \beta A^3 \cos \omega = -8\omega^2 C \cos \omega t$$

or

$$C = \frac{1}{32} \beta A^3 = \frac{\epsilon A^3}{32m}$$

and

$$\xi_2 = A_1 \cos \omega t + \frac{\epsilon A^3}{32m\omega^2} \cos 3\omega t \ . \tag{2.18}$$

Equations (2.17) and (2.18) constitute the second approximation. It should be noted that the second term on the right in (2.18) differs slightly from that in the first attempt (2.13), because of the different levels of approximations involved.

The reason for introducing the second mode of solution above is that it affords a consistent method for obtaining higher order approximations. If (2.18) is substituted on the right side of Eq. (2.15), the new alignment on the right leads to terms in ω, 3ω, 5ω and higher orders. If we write these as

$$\ddot{\xi}_3 + \omega^2 \xi_3 = P \cos \omega t + Q \cos 3\omega t + R \cos 5\omega t \tag{2.19}$$

$$P = P(A, \omega), \text{ etc.}$$

Here $P = 0$, for the same argument given after (2.16), which would improve the approximations in ω and A, etc.

2.4 Effect of Damping. Duffing's Equation.

Thus far, we have neglected the effect of damping, so that it is unrealistic to close off the top of our curve in Fig. 2-4. If we have damping we must also expect a phase difference between the impressed force and the displacement. To take this into account, it is convenient to write the force in the form $F_1 \cos \omega t + F_2 \sin \omega t$, so that $|F| = \sqrt{F_1^2 + F_2^2}$ and our differential equation becomes

$$\ddot{\xi} + r\dot{\xi} + \omega_0^2 \xi + \beta \xi^3 = F_1 \cos \omega t + F_2 \sin \omega t \ , \tag{2.20}$$

which is the complete form of *Duffing's equation*. As before, we assume such quantities as r, F_1, F_2 to be small. We begin with the linear approximation

$$\xi_1 = A \cos \omega t$$

and substitute throughout (2.20), expand $\cos^3 \omega t$ and then neglect the terms in $3\omega t$ for the time being, we obtain

$$\begin{aligned} (\omega_0^2 - \omega^2) A + \frac{3}{\delta} \beta A^3 &= F_1 \\ - A\omega r &= F_2 \ . \end{aligned} \tag{2.21}$$

By squaring and adding together the two equations in (2.21), we get

$$\left((\omega_0^2 - \omega^2) A + \frac{3}{4} \beta A^3 \right)^2 + A^2 \omega^2 r^2 = F^2 \ . \tag{2.22}$$

If we introduce the response function

$$S(\omega, A) = (\omega_0^2 - \omega^2) A + \frac{3}{4} \beta A^3 \ .$$

Then Eq. (2.22) becomes

$$S^2(\omega, A) + A^2 \omega^2 r^2 = F^2 \ . \tag{2.23}$$

This is the more general form of the frequency relation (2.17), since setting $r = 0$ in (2.23) will recover that equation. We shall not continue the further anlaysis of this situation, but instead reproduce the curves for damped and undamped harmonic responses as given by Stoker [2] and reproduced in Figs. 2-5 a,b,c,d.

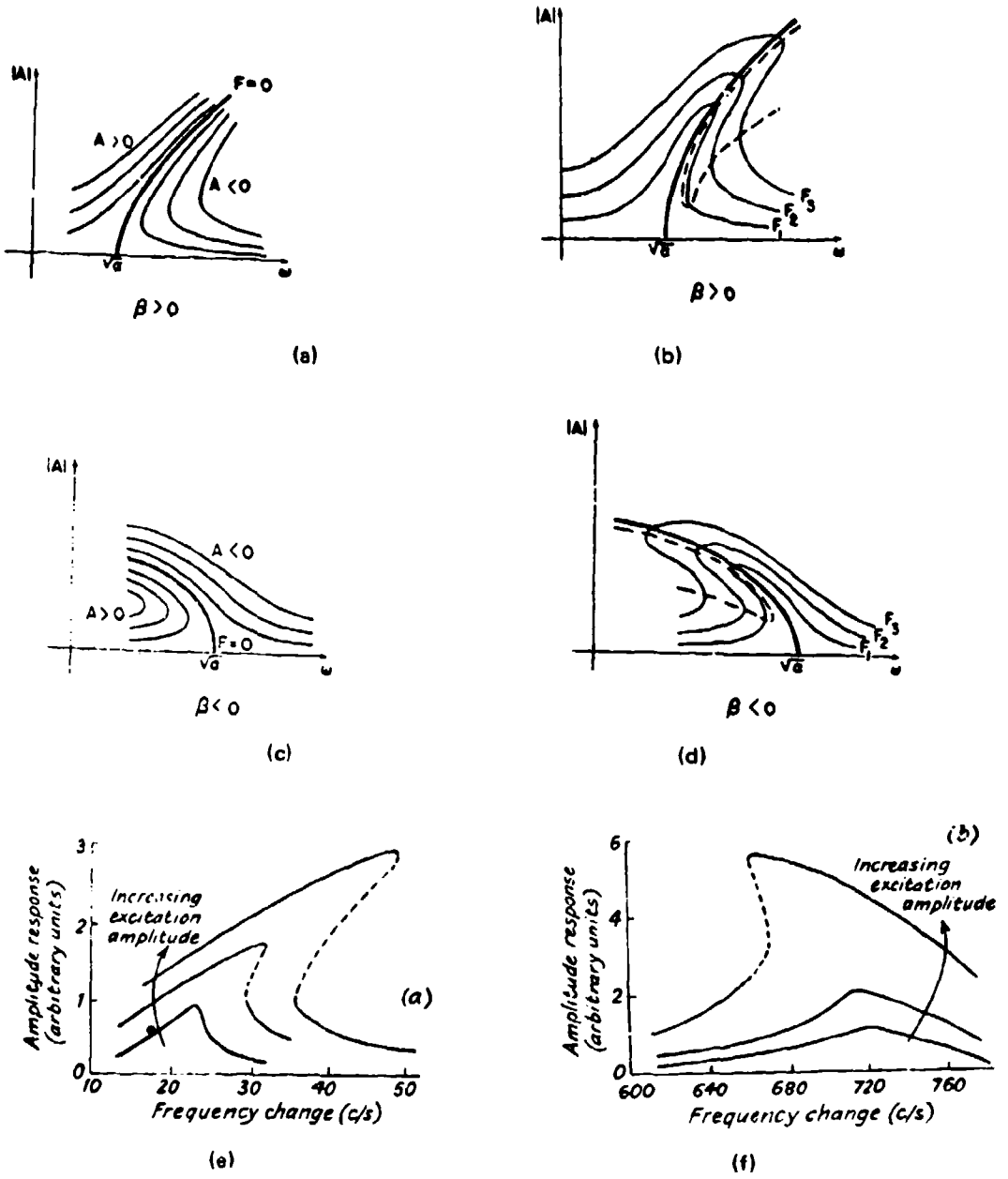

Figure 2-5.–Nonlinear spring response

a) hard spring, no damping

b) hard spring, with damping

c) soft spring, no damping

d) soft spring, with damping.

In the case of a linear spring, the bold-face curve would be a vertical line in each case (after Stoker, [2] pages 88, 92).

e) AT-cut quartz crystal with resonance frequency 4.895 MHz at large excitation amplitudes.

f) BT-cut quartz crystal with resonance frequency 4.990 MHz at large excitation amplitudes (e, f from Stephens and Bate [3]).

Another manifestation of this nonlinear behavior is that reported by Seed [3] for resonating quartz crystals. Seed obtained amplitude-frequency response curves for AT and BT cut quartz crystals. These are shown in Figs. 2-5 e,f. The resemblance of these to Figs. 2-5 c,d can easily be seen.

2.5 Subharmonics.

Before completing our discussion of Duffing's equation, some comment should be made about subharmonic responses. Again we shall follow Stoker, treating only the case of the subharmonic $\omega/3$.

In the undamped linear system

$$\ddot{\xi} + \omega_0^2 \xi = F \cos \omega t \ ,$$

where $\omega_0 = \omega/n$, we can get the solution

$$\xi = A \cos \frac{\omega}{n} t \ \ (n \text{ an integer}),$$

in addition to the solution at the frequency ω. However, the presence of damping will remove this essentially transient solution. Let us now look once again at Eq. (2.20). As a special case, we shall look for oscillations of the frequency $\omega/3$. We therefore form the Fourier series of the displacement. (It can be shown that the term in $\sin(\omega t/3)$ vanishes and will be omitted.) Then

$$\xi = C_1 \cos \frac{\omega t}{3} + A_1 \cos \omega t + B_1 \sin \omega t \ . \tag{2.24}$$

Substitution of (2.24) in (2.20) with use of various trigonometric identities leads to the results

$$\begin{aligned}
&\left(\omega_0^2 - \frac{\omega^2}{9}\right) C + \frac{3}{4}\beta(C^3 + C^2 A + 2AC^2 + 2CB^2) = 0 \\
&\frac{-\omega r}{3} + \frac{3}{4} BC = 0 \\
&(\omega_0^2 - \omega^2) A + \frac{1}{4}\beta(C^3 + 6C^2 AB + 3A^3 + 3AB^2) + r\omega B = F_1 \\
&(\omega_0^2 - \omega^2) B - \frac{3}{4}\beta(2C^2 + B^2 + A^2) - r\omega A = F_2 \ .
\end{aligned} \tag{2.25}$$

These rather messy algebraic relations can be rearranged to yield

$$\omega^2 = 9\omega_0^2 + \frac{27}{4}\beta\left(C^2 - \frac{FC}{8\omega_0^2} + \frac{F_1^2}{32\omega_0^4}\right) \tag{2.26}$$

where $F^2 = F_1^2 + F_2^2$ as before. This relation, which determines the value of the subharmonic amplitude $|C|$, is valid only if

$$r < \frac{3}{32}\frac{|\beta CF|}{\omega_0^3} \tag{2.27}$$

i.e., the damping must be small if the subharmonics are to exist.

Figure 2-6, which is also from Stoker (p. 107), shows a plot of the relation between the amplitude C of the subharmonic and the driving frequency ω for the case of a hard nonlinear spring, without damping. [The curve in the figure is for the case $F = F_1$ in Eq. (2.26).]

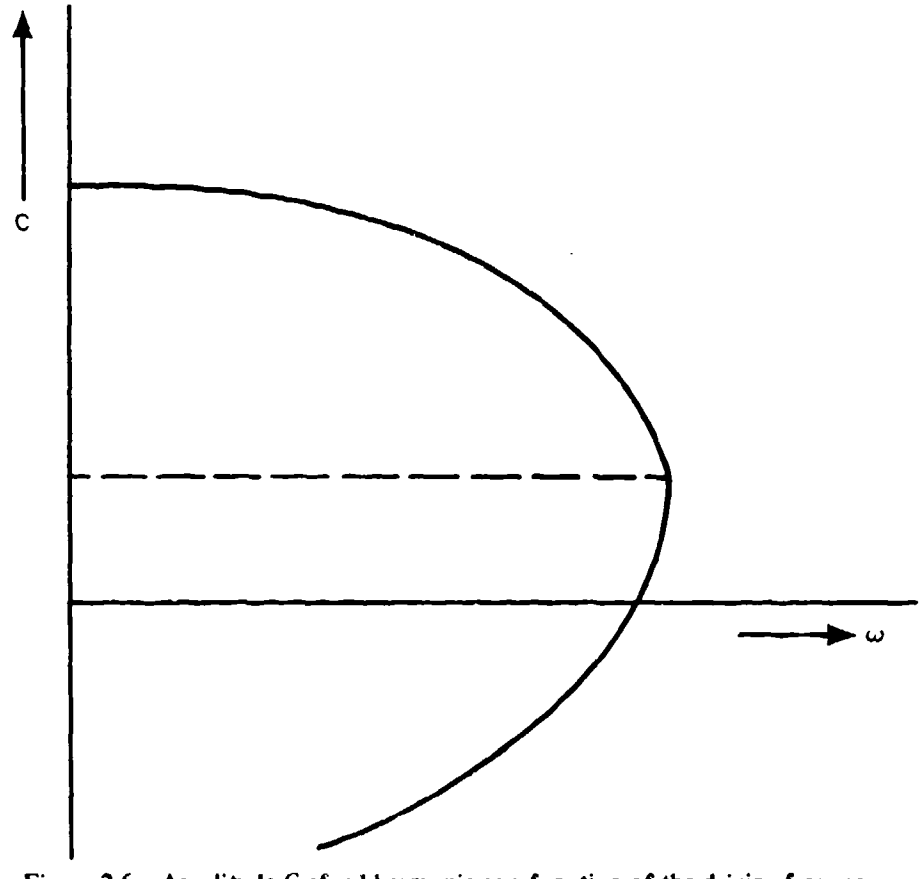

Figure 2-6.–Amplitude C of subharmonic as a function of the driving frequency ω for the case of a hard, nonlinear spring with damping (after Stoker, [2], p. 107).

Since this is the case for which $\beta < 0$, the relation between the driving frequency ω and the natural frequency of the system must always be such that $\omega < 3\omega_0$ for the subharmonic vibration $\omega/3$ to occur.

2.6 Nonlinear Strings.

Our linear treatment of the vibrating string of Section 1.2 involved many simplifying assumptions, including uniform tension and small amplitudes of oscillation. Let us now consider the case in which these limitations are removed. We shall also allow for the possibility of motion in three dimensions, and indicate how damping can be introduced in the motion.

A string at rest has a length ℓ measured along the x axis. If the displacements from the rest position at x are given by ξ, η, ζ, then the segment x will have in general the length ds:

$$ds = \left[\left(1 + \frac{\partial \xi}{\partial x}\right)^2 + \left(\frac{\partial \eta}{\partial x}\right)^2 + \left(\frac{\partial \zeta}{\partial x}\right)^2\right]^{1/2} dx$$

or, in reduced notation,

$$ds^2 = \left[(1 + \xi_x)^2 + \eta_x^2 + \xi_x^2\right] dx^2 . \tag{2.28}$$

The tension in the string at rest is T_0. To find the tension at any time for the point that was at x when at rest, we use Hooke's law, writing

$$T - T_0 + YA\left(\frac{ds - dx}{dx}\right) \tag{2.29}$$

where Y = Young's modulus and A is the cross sectional area of the string. From (2.28), (2.29) we then have

$$T = T_0 + YA\left\{\left[(1 + \xi_x)^2 + \eta_x^2 + \xi_x^2\right]^{1/2} - 1\right\} . \tag{2.30}$$

We can now write down the formal expression for the equation of motion. The x component of the tension will be

$$(x,t)(1 + \xi_x) \frac{d}{dx} \tag{2.31}$$

so that the net force on the element shown in Fig. 2-7 in the x direction will be

$$A \frac{\partial}{\partial x}\left[T(1 + \xi_x) \frac{dx}{ds}\right]$$

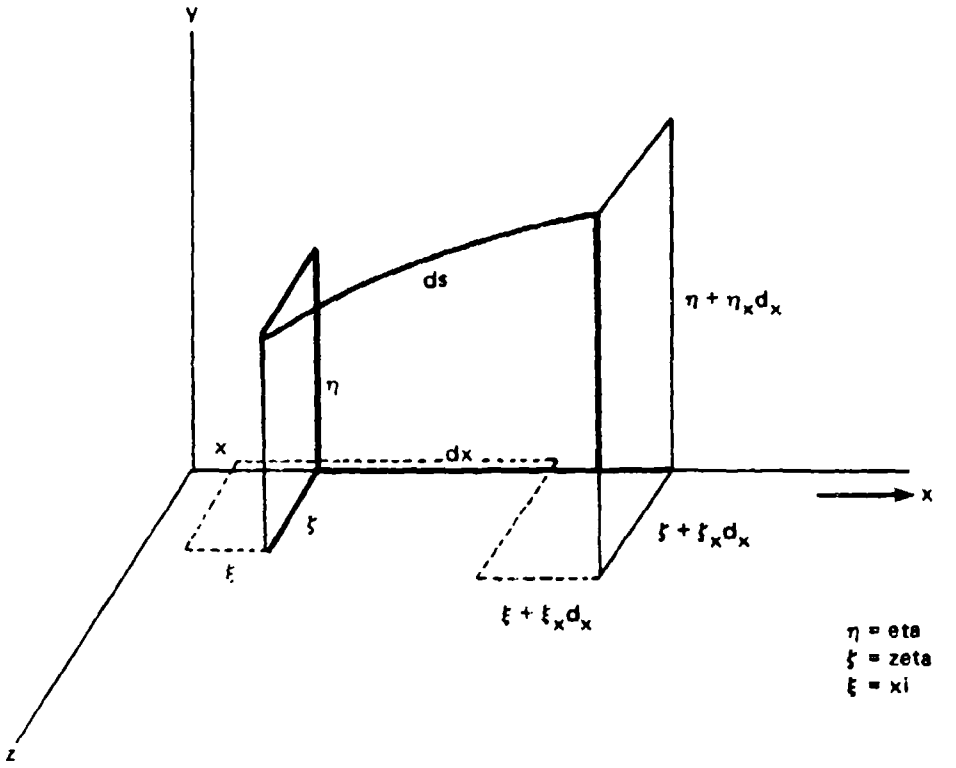

Figure 2-7.–Displacement of a string segment in three dimensions.

so that

$$\frac{\partial}{\partial x}\left[T(1 + \xi_x) \frac{dx}{ds}\right] = \sigma \xi_{tt} \tag{2.32}$$

where σ is the mass of the string per unit length.

Since we are interested here in improving on the linear treatment, it is appropriate to use approximate forms of Eq. (2.28) and (2.30):

$$\begin{aligned} ds &\simeq \left(1 + \xi_x + \frac{1}{2}\eta_x + \frac{1}{2}\zeta_x^2\right) dx \\ T &\simeq T_0 + YA\left(\xi_x + \frac{1}{2}\eta_x^2 + \frac{1}{2}\zeta_x^2\right) \end{aligned} \tag{2.33}$$

and Eq. (2.32) becomes

$$\frac{\partial}{\partial x}\left\{\left[T_0 + YA\left(\xi_x + \frac{1}{2}\,\eta_x^2 + \frac{1}{2}\,\zeta_x^2\right)\right](1+\xi_x) \times\left(1 - \xi_x - \frac{1}{2}\,\eta^2 - \frac{1}{2}\,\zeta^2\right)\right\} = \sigma\xi_{tt} \quad .$$

Carrying out the indicated operations, but keeping only the lowest combination for each of the displacements, we get the result

$$\sigma\xi_{tt} - YA\xi_{xx} = \frac{1}{2}\,(T_0 - YA)\,\frac{\partial}{\partial x}\left(\eta_x^2 + \zeta_x^2\right) \quad . \tag{2.34}$$

If we introduce the notation

$$c_0^2 = \frac{T_0}{\sigma} \qquad c_1^2 = \frac{YA}{\sigma} \quad ,$$

Eq. (2.34) takes the compact form

$$\xi_{tt} - c_1^2\xi_{xx} = \frac{1}{2}\left(c_0^2 - c_1^2\right)\frac{\partial}{\partial x}\left(\eta_x^2 + \zeta_x^2\right) \quad . \tag{2.35}$$

The corresponding equations for the y and z directions, which are identical in form with one another, can be obtained in this same manner, with only the replacement of Eq. (2.31) by the form for the y component of T:

$$T\,\frac{dy}{ds} = T\eta_x\,\frac{dx}{ds} \text{ , etc.}$$

After simple transformations, one gets

$$\begin{aligned} \eta_{tt} - c_0^2\eta_{xx} &= (c_1^2 - c_0^2)\,\frac{\partial}{\partial x}\left[\eta_x\left(\xi_x + \frac{1}{2}\,\eta_x^2 + \frac{1}{2}\,\zeta_x^2\right)\right] \\ \zeta_{tt} - c_0^2\zeta_{xx} &= (c_1^2 - c_0^2)\,\frac{\partial}{\partial x}\left[\zeta_x\left(\xi_x + \frac{1}{2}\,\eta_x^2 + \frac{1}{2}\,\xi_x^2\right)\right] . \end{aligned} \tag{2.36}$$

All of these relations have neglected the damping. Since we are mainly interested in the transverse vibration, we shall enter this in Eq. (2.36) by the addition of a damping term $R\eta_t$ on the left hand side.

In order to solve the set (2.35), (2.36) it is convenient to make further approximations. For wires, $c_1^2 >> c_0^2$, and the longitudinal vibrations are well below the resonance frequency for such vibrations. We can therefore neglect ξ_{tt} in (2.35) and rewrite the equation as

$$\xi_{xx} = -\frac{1}{2}\frac{\partial}{\partial x}(\eta_x^2 + \zeta_x^2)$$

which can be solved in the form

$$\xi_x = -\frac{1}{2}(\eta_x^2 + \xi_x^2) + f(y,z)$$

$$\xi = -\frac{1}{2}\int_0^x (\eta_x^2 + \zeta_x^2)\,dx + xf(y,z) + \text{const.}$$

By using the boundary conditions $\xi(0,t) = \xi(\ell,t) = 0$, we can establish the constant and $f(y,z)$, so that finally,

$$\xi = -\frac{1}{2}\int_0^x (\eta_x^2 + \zeta_x^2)\,dx + \frac{x}{2\ell}\int_0^\ell (\eta_x^2 + \xi_x^2)\,dx$$

$$\xi_x = -\frac{1}{2}(\eta_x^2 + \zeta_x^2) + \frac{1}{2\ell}\int_0^\ell (\eta_x^2 + \zeta_x^2)\,dx \quad . \tag{2.37}$$

We can therefore write Eqs. (2.36) (with account of damping) as

$$\eta_{tt} + R\eta_t - c_0^2\eta_{xx} = \frac{c_1^2\eta_{xx}}{2\ell}\int_0^\ell (\eta_x^2 + \zeta_x^2)\,dx$$

$$\zeta_{tt} + R\zeta_t - c_0^2\zeta_{xx} = \frac{c_1^2}{2\ell}\zeta_{xx}\int_0^\ell (\eta^2 + \zeta^2)\,dx \quad . \tag{2.38}$$

The solution of Eq. (2.38) is still a very complicated problem. Partial solutions can be found in the literature. [5,6]

We shall limit ourselves to the simplest example. Neglecting damping, we assume a first order solution of the vibrating string as

$$\eta = \eta_0 \sin \omega t \sin \frac{\pi x}{\ell}\,; \quad \xi = 0, \zeta = 0 \quad .$$

Equation (2.37) can then be solved for ξ:

$$\xi = - \frac{\eta_0^2 \pi}{8\ell} \sin^2 \omega t \sin \frac{2\pi x}{\ell} \tag{2.39}$$

The first of Eqs. (2.38) in this case can now be written as

$$\eta_{tt} - c_0^2 \eta_{xx} = - \frac{c_1^2}{4} \eta_0^3 \left(\frac{\pi}{\ell}\right)^4 \sin^3 \omega t \sin \frac{\pi x}{\ell} \tag{2.40}$$

and will yield a second order particular solution involving the third harmonic in time.

Finally, the second equation of (2.38) remains $\zeta = 0$ as before. To this level of approximation then, coupling exists between the longitudinal mode and the already excited transverse mode, and the transverse mode develops higher harmonics in its temporal variable.

As we have already emphasized, it is not the purpose of this book to explore the entire field of vibrating systems, but only those which touch upon the area of acoustics. It suffices to remark, therefore, that one of the simplest of vibrating systems–the string–can easily become nonlinear in its motions and thus produce harmonics of the original signal.

2.7 Nonlinearity in Membranes.

The nonlinear string is complex enough; the move to the two-dimensional problem of the nonlinear membrane is that much worse. We shall give only a very brief description, following the analysis of Chobotov and Binder. [7] The forces on a segment of an undamped circular membrane are depicted in Fig. 2-8. The quantities N_r and N_θ refer to the radial and tangential stresses. The rest of the notation is self-explanatory.

The equations of motion that result from these forces are given by

$$\frac{\partial}{\partial r}[(r+u) N_r \cos\phi] - \frac{\left(1 + \frac{\partial u}{\partial r}\right) N_\theta}{\cos\phi} = \frac{\rho h (r+u)}{\cos\phi}\left(1 + \frac{\partial u}{\partial r}\right)\frac{\partial^2 u}{\partial t^2} \; ;$$

$$\frac{\partial}{\partial r}[(r+u) N_r \sin\phi] = \frac{\rho h (r+u)}{\cos\phi}\left(1 + \frac{\partial u}{\partial r}\right)\frac{\partial^2 w}{\partial t^2} \; . \tag{2.41}$$

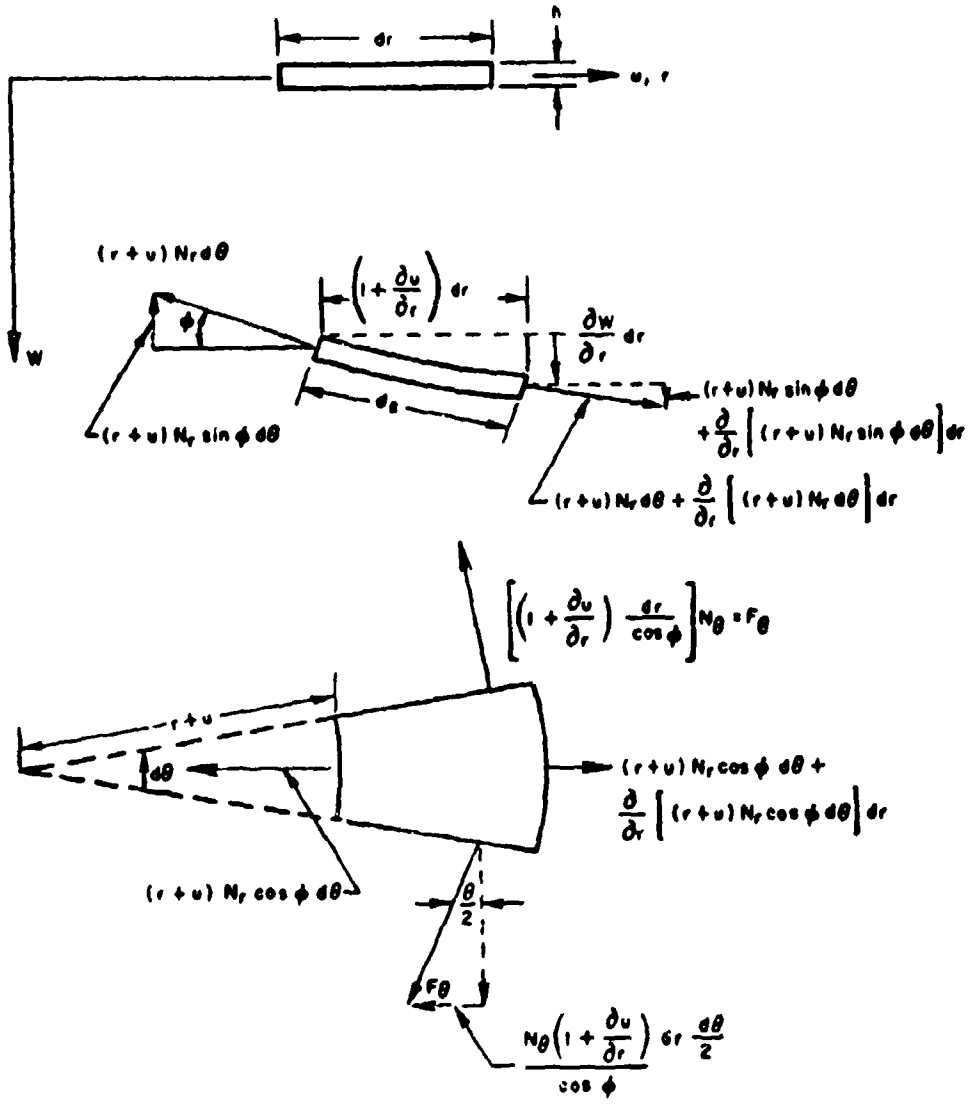

Figure 2-8.–Forces on an element of a circular membrane (after Chobotov and Bender, [7] p. 60).

In the case of a linear membrane, $u = 0$, $N_r = \text{const}$, $\sin \phi \cong \phi \simeq \partial w/\partial r$ and $\cos \phi \simeq 1$. The second equation above becomes the linear form

$$\frac{1}{r} \frac{\partial}{\partial r}\left(r \frac{\partial u}{\partial r}\right) = \frac{\rho h}{N_r} \frac{\partial^2 w}{\partial t^2} \quad . \tag{2.42}$$

Even to begin the solution of Eq. (2.41) requires a number of approximations. If we consider the deformed length ds, it has the approximate form (see Fig. 2-8)

$$ds = \left[\left(1 + \frac{\partial u}{\partial r}\right)^2 + \left(\frac{\partial w}{\partial r}\right)^2\right]^{1/2} dr \simeq \left[1 + \frac{\partial u}{\partial r} + \frac{1}{2}\left(\frac{\partial w}{\partial r}\right)^2 + \cdots\right] dr$$

so that the radial strain ϵ_r is given approximately by

$$\epsilon_r = \frac{ds - dr}{dr} \simeq \frac{\partial u}{\partial r} + \frac{1}{2}\left(\frac{\partial w}{\partial r}\right)^2 . \tag{2.43}$$

This is a form that also is valid in the case of plates (see below).

By expressing N_r and N_θ in terms of the radial strain ϵ_r and the tangential strain $\epsilon_\theta = u/r$ through Hooke's law, and making the approximation of small angle ϕ, approximate differential equation can be deduced. It is convenient to write these in non-dimensional form, measuring lengths in terms of the fraction of the membrane radius a:

$$\bar{\eta} = r/a$$

$$\bar{u} = u/a \qquad \tau = \left(\frac{N_0}{\rho h}\right)^{1/2} \frac{t}{a} \tag{2.44}$$

$$\bar{w} = w/a$$

and writing the initial strain e_0 in the membrane in terms of the initial stress N_0:

$$e_0 = (1 - \mu) N_0 \frac{E}{h} . \tag{2.45}$$

We than have the equations

$$(1 - \mu)\left(1 + \frac{\partial \bar{u}}{\partial \eta}\right)\left[\frac{\partial \bar{u}}{\partial \eta} - \frac{\bar{u}}{\eta} + \frac{1}{2}\left(\frac{\partial \bar{w}}{\partial \eta}\right)^2\right]$$

$$+ (\eta + \bar{u})\left[\frac{\partial^2 \bar{u}}{\partial \eta^2} + \frac{\partial w}{\partial \eta} \cdot \frac{\partial^2 w}{\partial \eta^2} + \mu\left(\frac{\partial u}{\eta \partial \eta} - \frac{\bar{u}}{\eta^2}\right)\right]$$

$$= e_0 (1 + \mu)(\eta + \bar{u})\left(1 + \frac{\partial \bar{u}}{\partial \eta}\right) \frac{\partial^2 \bar{u}}{\partial \tau^2}$$

and

$$\frac{\partial \bar{w}}{\partial \eta}\left\{\left(1+\frac{\partial \bar{u}}{\partial \eta}\right)\left[\frac{\partial \bar{u}}{\partial \eta}+\frac{1}{2}\left(\frac{\partial w}{\partial \eta}\right)^2+\mu\frac{\bar{u}}{\eta}+(1+\mu)e_0\right]\right.$$

$$\left.+(\eta+\bar{u})\left[\frac{\partial^2 \bar{u}}{\partial \eta^2}+\frac{\partial w}{\partial \eta}\cdot\frac{\partial^2 \bar{w}}{\partial \eta^2}+\mu\left(\frac{\partial u}{\eta\partial \eta}-\frac{\bar{u}}{\eta^2}\right)\right]\right\}$$

$$+\frac{\partial^2 \bar{w}}{\partial \eta^2}\left\{(\eta-\bar{u})\left[\frac{\partial \bar{u}}{\partial \eta}+\frac{1}{2}\left(\frac{\partial \bar{w}}{\partial \eta}\right)^2+\frac{\mu\bar{u}}{\eta}+(1+\mu)e_0\right]\right\}$$

$$=e_0(1+\mu)(\eta+\bar{u})\left(1+\frac{\partial \bar{u}}{\partial \eta}\right)\frac{\partial^2 \bar{w}}{\partial r^2}\quad . \tag{2.46}$$

These equations can be solved approximately by a perturbation technique, done in [7], in powers of the square root of the initial strain e_0:

$$\bar{u}=e_0{}^{1/2}u_1+e_0u_2+e_0{}^{3/2}u_3+\ldots$$

$$\bar{w}=e_0{}^{1/2}w_1+e_0w_2+e_0{}^{3/2}w_3+\ldots\quad . \tag{2.47}$$

These quantities are now substituted in Eq. (2.45) and the coefficients of corresponding powers of $e_0{}^{1/2}$ equation. It follows from this step that $u_1\equiv 0$ from the first of these coefficients. The other equations are then

$$(e_0):\quad \frac{\partial u_2}{\partial \eta}-\frac{u_2}{\eta}+\frac{1}{2}\left(\frac{\partial w_1}{\partial \eta}\right)^2(1-\mu)$$

$$+\eta\left(\frac{\partial^2 u_2}{\partial \eta^2}+\frac{\partial w_1}{\partial \eta}\cdot\frac{\partial^2 w_1}{\partial \eta^2}\right)=0\quad , \tag{2.48}$$

$$(e_0{}^{3/2}):\quad \frac{\partial w_1}{\partial \eta}\left[\frac{\partial u_2}{\partial \eta}+\frac{1}{2}\left(\frac{\partial w_1}{\partial \eta}\right)^2(1+\eta)\right.$$

$$\left.+\eta\left(\frac{\partial^2 u_2}{\partial \eta^2}+\frac{\partial w_1}{\partial \eta}\cdot\frac{\partial^2 w_1}{\partial \eta^2}\right)+\mu\frac{\partial u_2}{\partial \eta}\right]$$

$$+ \eta \frac{\partial^2 w_1}{\partial \eta^2}\left[\frac{\partial u_2}{\partial \eta} + \frac{1}{2}\left(\frac{\partial w_1}{\partial \eta}\right)^2 + \frac{\mu u_2}{\eta} + (1+\mu)\right]$$

$$= (1+\mu)\eta \frac{\partial^2 w_1}{\partial r^2} \quad . \tag{2.49}$$

If it is assumed that

$$u_1 = \alpha q(\tau)(1-\eta^2) \tag{2.50}$$

where $\alpha = w_0/ae_0^{1/2}$ and $q(\tau)$ is a function of dimensionless time that is no greater than unity, the equation for q becomes

$$\frac{d^2q}{d\tau^2} + 6q + \alpha^3 \frac{(13+21\mu-4\mu^2)}{5(1+\mu)} q^3 = 0 \tag{2.51}$$

which is a Duffing equation for the fundamental mode of a circular membrane [cf. Eq. (2.20)].

It can be shown from the solution of Eq. (2.51) that the ratio of the nonlinear period T^* to the linear period T is given by the form

$$\frac{T^*}{T} = \frac{2K(k)}{\pi\left(1 + \dfrac{\alpha^2(13+21\mu-4\mu^2)}{30(1+\mu)}\right)^{1/2}} \tag{2.52}$$

which is plotted vs. $\alpha = 0.3$ in Fig. 2-9. Here $K(k)$ is the complete elliptic integral and

$$k^2 = \left[2\left(1 + \frac{30(1+\mu)}{\alpha^2(13+21\mu-4\mu^2)}\right)\right]^{-1} .$$

A corresponding analysis can be carried out for forced oscillations. An example taken from [7] is shown in Fig. 2-10, when the resonance response of a test membrane is plotted as a function of the sound pressure level in front of the membrane. The solid curve is the expression obtained theoretically.

2.8 Nonlinearity of Plates.

The vibration of plates brings into play one or more complicating factors in the thickness dimension of the vibration. The starting point for such

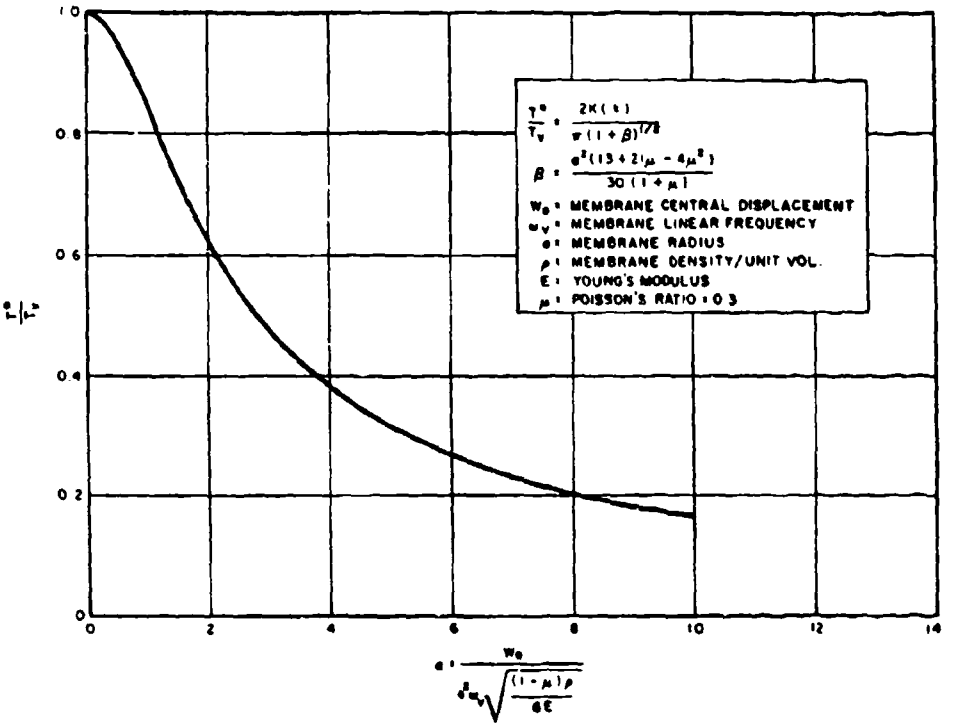

Figure 2-9.–Ratio of nonlinear period to linear period as a function of the nondimensional displacement for vibration of a circular membrane in vacuum (fundamental mode) (after Chobotov and Bender, [7] p. 64).

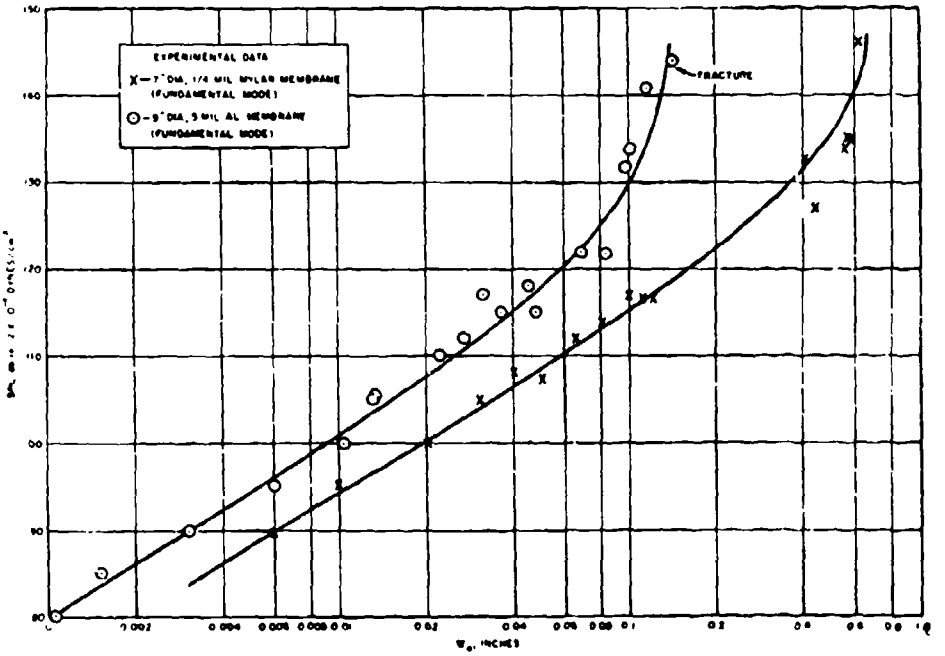

Figure 2-10.–Relation between resonant amplitude response and incident (blocked membrane) sound-pressure level (after Chobotov and Bender, [7] p. 68).

analysis is the expression for the total energy U of a plate under deformation. [8]

$$U = \frac{D}{2}\int\int\left[(\nabla^2 w)^2 + \frac{12}{h^2}\ e^2\right] - 2(1-\nu)$$

$$\times\left[\frac{12}{h^2}\ e_2 + \frac{\partial^2 w}{\partial x^2}\ \frac{\partial^2 w}{\partial y^2} - \left(\frac{\partial^2 w}{\partial x \partial y}\right)^2\right] dxdy \qquad (2.53)$$

where D is the bending rigidity $= \dfrac{Eh^2}{12(1-\nu^2)}$,

E the modulus of elasticity,

ν Poisson's ratio,

w deflection of plate in the Z direction,

e the first invariant of middle surface strains, $= \epsilon_x + \epsilon_y$,

e_2 the second invariant of middle surface strains, $= \epsilon_x\ \epsilon_y - \dfrac{1}{4}\ \gamma_{xy}$,

γ_{xy} = shearing strains of middle surface $= \dfrac{\partial u}{\partial y} + \dfrac{\partial v}{\partial x} + \dfrac{\partial w}{\partial x}\ \dfrac{\partial w}{\partial y}$,

$$\epsilon_x = \frac{\partial u}{\partial x} + \frac{1}{2}\left(\frac{\partial w}{\partial x}\right)^2 \qquad \epsilon_y = \frac{\partial v}{\partial y} + \frac{1}{2}\left(\frac{\partial w}{\partial y}\right)^2 \qquad (2.54)$$

h = thickness of plate. Note the correspondence of the expressions for ϵ_x, ϵ_y with Eq. (2.43).

Arguing from the exact solutions for uniformly loaded plates [9] Berger neglected terms in Eq. (2.53) arising from the second strain in variant e_2 [10]. From this assumption Berger immediately obtained the equations

$$e = \frac{\alpha^2 h^2}{12}$$

$$\nabla^4 w - \alpha^2 \nabla^2 w = \frac{8}{D} \qquad (2.55)$$

where α is a normalized constant of integration and q is the intensity of the uniform load.

The second of Eqs. (2.53) is a linear form for fixed α and can be solved for w. Then substitution of w in the expression for e [Eq. (2.54)] gives a second linear form for u, v.

In addition to this *Berger approximation*, a perturbation procedure, similar to that used for membranes, has been developed by Chu and Hermann, [11] and applied to a variety of problems by Wu and Vinson. [12]

The nonlinearity of both plates and membranes is reflected in acoustics by distortions produced in the transduction of sound waves by loudspeakers and microphones. It is a matter of higtorical interest that the problems of loudspeaker distortion led to a detailed mathematical study of finite amplitude wave propagation in horns by McLachlan in 1934, [13] and to some of the earliest experimental work on such propagation in air by Thuras, Jenkins and O'Neill in 1935. [14]

2.9 Tartini Tones.

That the ear, like the mechanical systems discussed earlier in this chapter, could exhibit nonlinear characteristics has long been known, although the associated phenomena were long misunderstood. While these physiological phenomena have had little interconnection with the types of nonlinearity that form the bulk of this book, reasonable completeness demands a brief review of the subject. More detail can be found in the references, especially in the historical note of Jones, [15] and in the reviews by Wever and Lawrence [16] and by Tonndorf. [17]

At about the middle of the 18th century, a number of musicians observed that when two musical tones of high intensity are sounded, one can hear a lower tone whose frequency is equal to the difference of the two original tones. Subsequently, other difference tones were discovered between higher harmonics of the fundamentals present in each of the original notes. All such difference tones are called *Tartini tones* or *Tartini pitch* after their first discoverer.*

For the first 100 years after their discovery, these tones were thought to be a high frequency beat phenomenon (recall Section 1.3). This would have made the phenomenon a linear one. Helmholtz disposed of this idea by reporting the existence of sum tones, whose frequencies were the sum of the two original tones. Today, all such sum and difference tones are called *combination* tones. If h and ℓ are the fundamental frequencies of the original tones, then the frequencies are given by

$$f_{mn} = mh \pm \ell n \tag{2.56}$$

where m,n are positive integers or zero. Thus if $n = 0$, we have the possibility of existence of all harmonics from an intense, single-frequency source.

*There is some uncertainty as to which of several individuals first observed the phenomenon. A. T. Jones has assigned the honor to Tartini after a detailed study. [15]

Experimental verification of the existence of these harmonics of an originally pure tone is shown in Fig. 2-11 which is the electrical response, in microvolts, of a cat's ear, resulting from a stimulation of the outer ear by a pure 1000-Hz tone of varying intensity. [16,18] Curve 1 is the response at the fundamental frequency, which is linear to above incident intensities of 0.1 dyn/cm^2, but becomes nonlinear in that region. The curve labeled 2 is the response at the second harmonic, and first becomes appreciable in the region where the fundamental response is no longer linear. The other curves indicate the response at selected higher harmonics. The reality of combination tones in the middle ear is confirmed by the results of Fig. 2-12, which gives the electrical responses of a guinea pig's ear to tones of 1000 and 2800 Hz. The various difference tones are shown in (a) and the summation tones in (b).

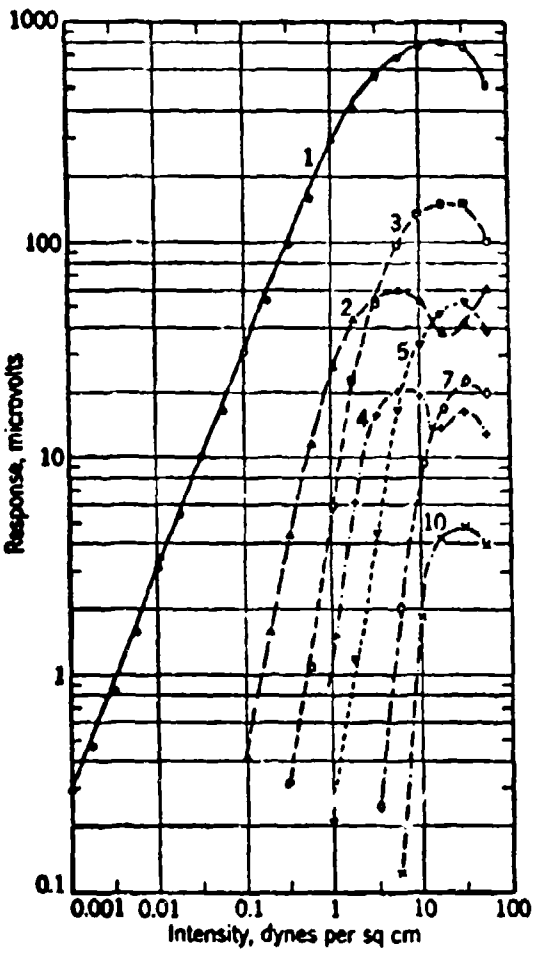

Figure 2-11.–Response of a cat's ear with a pure tone of 1000 Hz. The numbers on each curve indicate the harmonic (after Wever and Bray [18]).

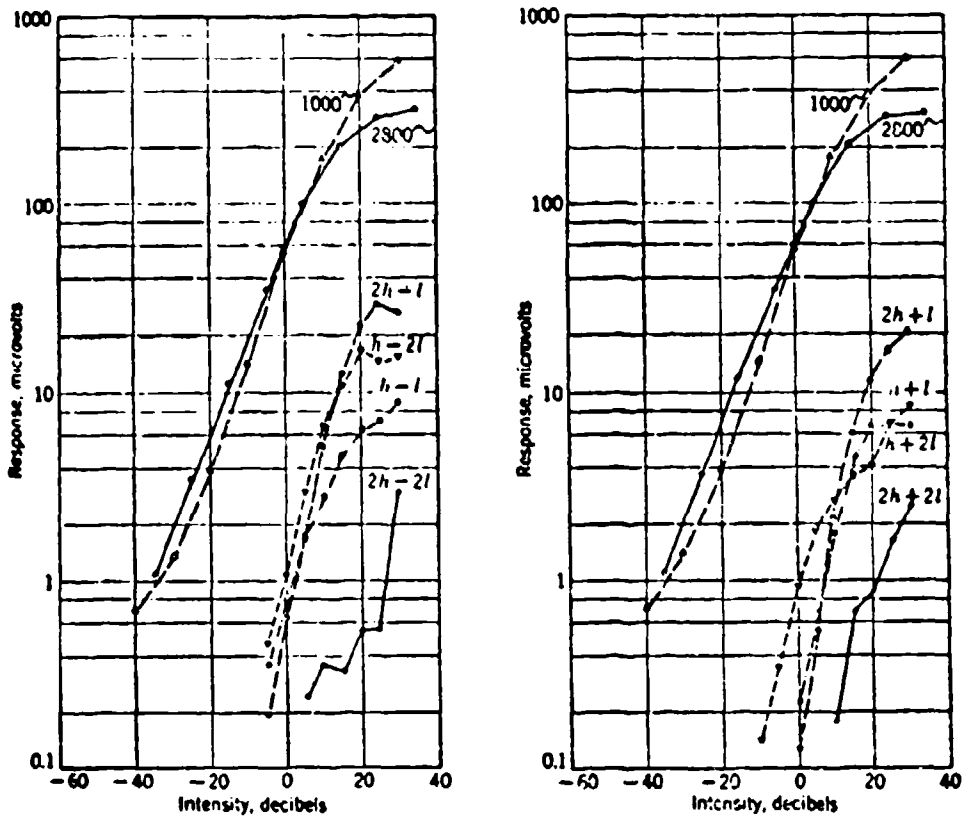

Figure 2-12.--Difference and summation tone responses of an intact guinea pig ear produced by aerial stimulation at 1000 Hz and 2800 Hz. Functions are shown for primaries (h,f) and various combinations (after Wever and Lawrence, [16] p. 161).

Helmholtz recognized the fundamental nonlinearity of the problem, and suggested that the source of the nonlinearity was the middle ear, in particular, the eardrum mechanism and the joint between the malleus and incus (hammer and anvil) bones (see Fig. 2-13). It is of interest that an opposite viewpoint was taken by Riemann who maintained the essential linearity of the middle ear.

The position of Helmholtz was a consequence of his theory of hearing. Helmholtz argued that every individual frequency had a specific location of action of the basilar membrane (which is part of the material dividing the two fluid-filled portions of the cochlea). Thus there would be a resonance action in the cochlea that leaves no room for the creation of combination frequencies.

A great deal of research has been done on the response of separate portions of the middle ear, as well as on the effect of actual removal of the middle ear all the way to the stapes (anvil) (see Wever and Lawrence). The

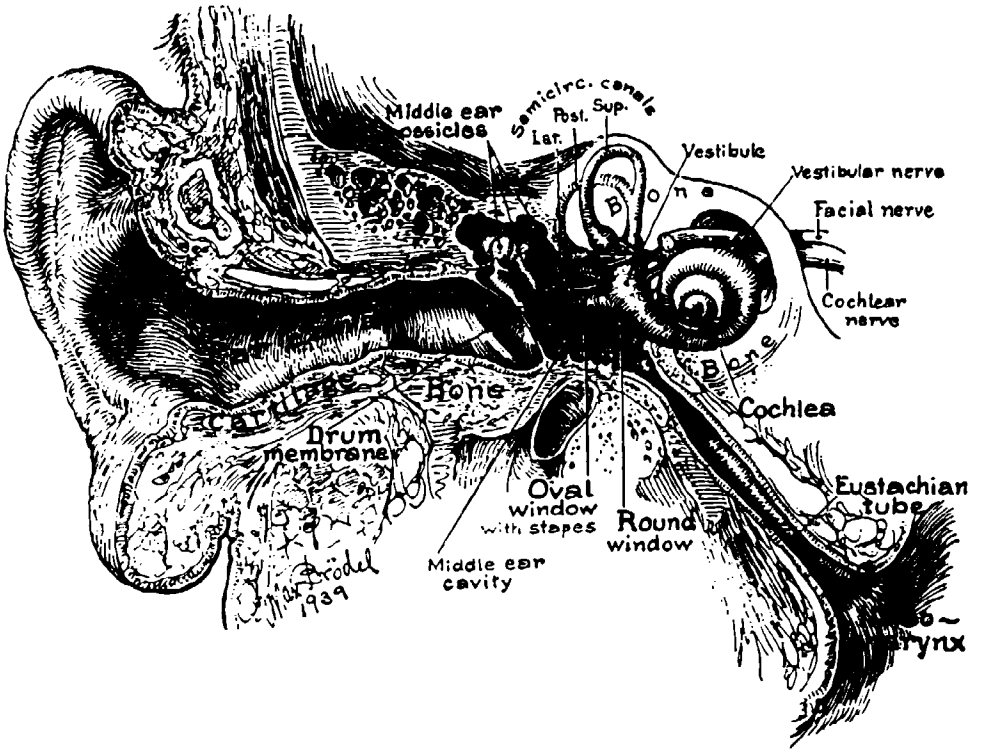

Figure 2-13.–Details of the human ear (Max Brödel, "Three Unpublished Drawings of the Anatomy of the Human Ear," W. B. Saunders Co., Philadelphia, Penna.)

conclusion is that the middle ear is a linear mechanism for the range of pressures represented by sound waves.

It was therefore necessary to develop a nonlinear theory of the cochlea. This work was pioneered by von Bekesy [see the review by Tonndorf [17] (1970)], and the concepts of nonlinear hydrodynamics have provided considerable insight into the action of the cochlea. According to these theories, the fluid in the cochlea is stimulated into surface waves which are strongest (naturally) near the surface that is formed by the basilar membrane.

The analogy to surface waves is indicated in Fig. 2-14.

As pointed out by Tonndorf, surface waves are inherently nonlinear. We forego a mathematical discussion at this point (see Chapter 11) but point out that gravitational surface waves have narrow crests and broad troughs.

Down the middle of the cochlea is the membrane known as the helicotrema. von Bekesy noted that the effects of stimulation of this membrane by the sound pulse produces eddies in the cochlear fluid (Fig. 2-15). The combined effect of all of these complications is therefore sufficient to account for the existence of sum-and-difference frequency stimulations of the brain when two intensive sounds of different frequency impinge upon the inner ear.

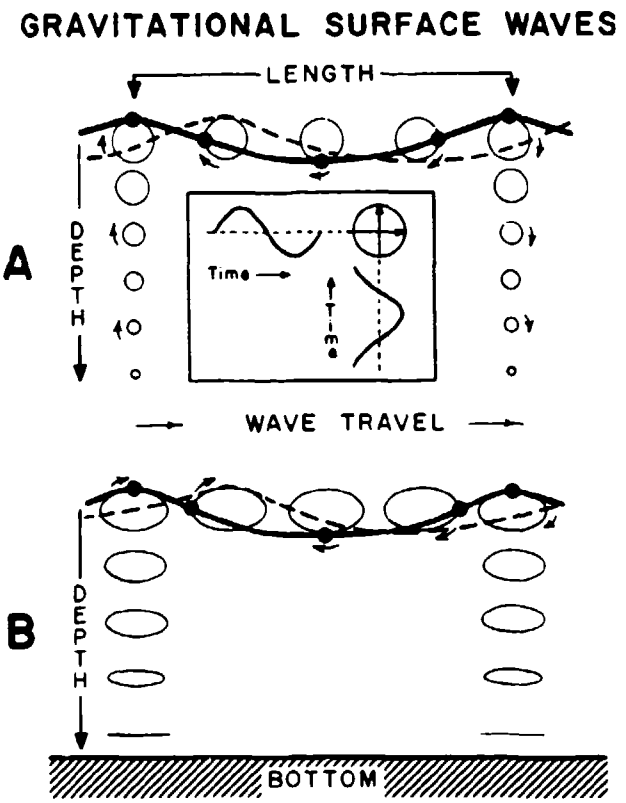

Figure 2-14.–Gravitational surface waves (schematic): (a) in deep water; (b) in shallow water of constant depth. Wave progression is from left to right, the dashed outline occurring $\pi/2$ later than the solid one. Note the asymmetry of the waveform in both cases. Individual fluid particles roll along their trochoidal closed orbits, clockwise in the present graph (see arrows). Each orbit (see insert) is the vectorial resultant of two force vectors acting at right angles to each other and being 90° apart in phase, with the vertical vector leading the horizontal one. Note the exponential decline of orbital diameter with depth in deep water (top); in shallow water (bottom) the decline is limited to the vertical vectors giving the orbits an elliptical shape, even along the surface (from J. Tonndorf, [17] p. 581).

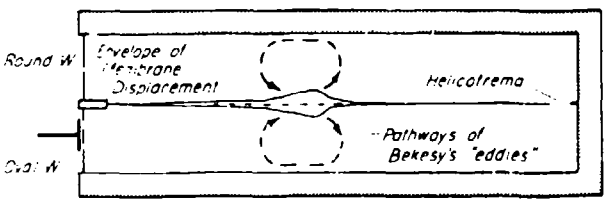

Figure 2-15.–Schematic of von Bekesy's eddies. These eddies fill the space fully at low frequencies, but shrink at high frequency. The particle velocity in the eddy is at first proportional to the square of the amplitude but the dependence flattens at high intensities (from J. Tonndorf, [17] p. 586).

REFERENCES

Chapter 2

1. See, e.g., P. M. Morse and K. U. Ingard, *Theoretical Acoustics*, McGraw-Hill, New York, 1968.
2. J. J. Stoker, *Nonlinear Vibrations*, Interscience, New York, 1950.
3. R. W. B. Stephens and A. E. Bate, *Acoustics and Vibrational Physics*, 2nd ed., Edward Arnold, London, 1966, p. 587; see also A. Seed, J. Sci. Instr. **41**, 242 (1964); Brit. J. Appl. Phys. **16**, 87, 1341 (1965).
4. G. Duffing, Erzwungene Schwingungen bei veränderlicher Eigenfrequenz, Braunschweig, 1918.
5. G. Carrier, Quart. Appl. Math. **3**, 157 (1945).
6. G. V. Anand, JASA **45**, 1089 (1969).
7. V. A. Chobotov and R. C. Binder, JASA **36**, 59 (1964).
8. S. Timoshenko, *Theory of Plates and Shells*, McGraw-Hill, New York, 1940, pp. 95, 315.
9. S. Way, Trans. ASME **56**, 627 (1934).
10. H. M. Berger, J. Appl. Mech. **22**, 465 (1968).
11. H. N. Chu and G. Hermann, J. Appl. Mech. **23**, 532 (1967)
12. C. I. Wu and J. R. Vinson, JASA **49**, 1561 (1971).
13. N. McLachlan, *Loudspeakers*, 1934 (Dover reprint, 1960).
14. A. L. Thuras, R. T. Jenkins and H. T. O'Neill, JASA **6**, 173 (1935).
15. A. T. Jones, Am. J. Phys. **3**, 49 (1935).
16. E. G. Wever and M. Lawrence, *Physiological Acoustics*, Princeton, 1954.
17. J. Tonndorf, JASA **47**, 579 (1970).
18. E. G. Wever and C. W. Bray, JASA **9**. 227-233 (1938).

CHAPTER 3

NONLINEAR PROPAGATION IN FLUIDS

3.1 Formulation of the Wave Equation, Lagrangian and Eulerian Coordinates.

In Chapter 1, we deliberately avoided the fact that an ambiguity can be introduced in our elementary derivation of the wave equation. That is, we have a choice, in describing the vibrations of a "particle," to refer to the displacement of a single particle, which at rest lies at the point $x = a$, or to the displacement of the particle which at any instant of time happens to be at the point x. The first of these descriptions then describes the motion of a single particle, while the second involves a succession of particles at a particular point.

If we follow the specific particle, we are said to be operating in Lagrangian, or material, coordinates. We consider a fluid particle (Fig. 3-1) at rest at the point a. Under the action of a harmonic wave, the particle will undergo oscillations about this point. The instantaneous position of this particle will be labeled x:

$$x = a + \xi \ . \tag{3.1}$$

We therefore say that the displacement of the particle originally at a is ξ. The quantity a defines the points along the "x" axis of our coordinate system, and is a variable. The coordinates a,t are known as the *Lagrangian coordinates.*

We can then describe the particle velocity in these coordinates, $u^L(a,t)$, as

$$u^L(a,t) = \frac{\partial x}{\partial t} = \frac{\partial \xi}{\partial t} \tag{3.2}$$

and the Lagrangian acceleration as

$$\frac{\partial u^L}{\partial t} = \frac{\partial^2 \xi}{\partial t^2} \ . \tag{3.3}$$

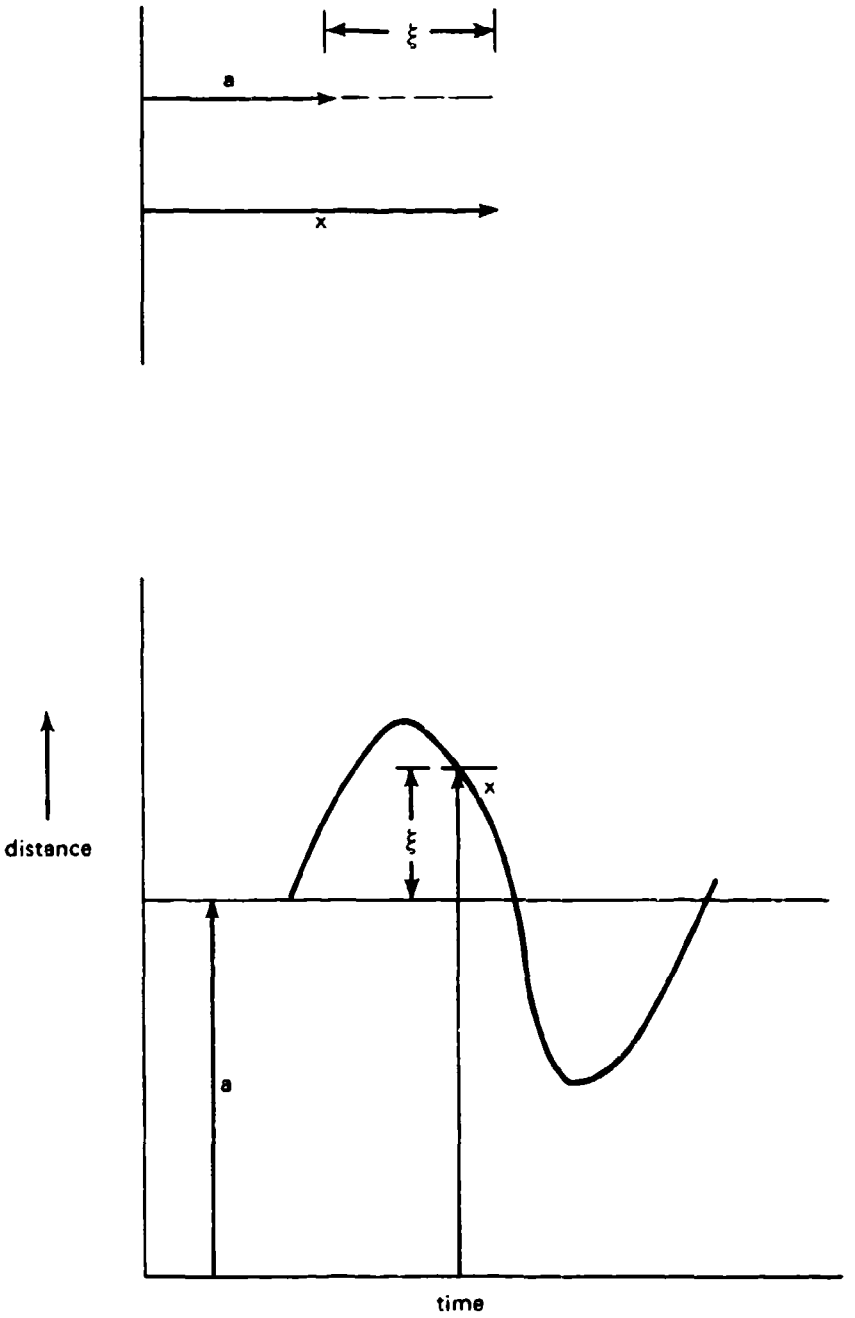

Figure 3-1.–Displacements in Lagrangian and Eulerian coordinates.

On the other hand, if we concentrate on a particular point in the laboratory system of coordinates, and specify the displacements at that point, we are said to be using the *Eulerian*, or *spatial*, coordinates.

Any Lagrangian coordinate q^L can easily be related to the Eulerian coordinates by employing a series expansion [1]

$$q^L(a,t) = q^E(x,t)\Big|_{x=a+\xi(a,t)} = q^E(x,t)\Big|_{x=a} + \frac{\partial q^E}{\partial x}(x,t)\Big|_{x=a}\xi(x,t) + \ldots . \tag{3.4}$$

where we have written out only the first two terms, which is usually sufficient. Similarly, we could express the Eulerian coordinate q^E in terms of the Lagrangian

$$q^E(x,t) = q^L(a,t)\Big|_{a=x-\xi(a,t)} = q^L(x,t)\Big|_{a=x} - \frac{\partial q^L}{\partial a}(a,t)\Big|_{a=x}\xi(a,t) + \ldots . \tag{3.5}$$

It should be noted that the displacement ξ is common to both systems. In the Lagrangian, it is to be understood as the displacement of the particle originally located at a, and is therefore a function of a and t. In Eulerian coordinates, ξ is the instantaneous displacement of whatever particle is at the coordinate x; ξ here is then a function of x and t.

As an example, we can write the Eulerian particle velocity u^E as

$$u^E = u^L - \left(\frac{\partial u^L}{\partial a}\right)\xi + \ldots = \frac{\partial \xi}{\partial t} - \left(\frac{\partial^2 \xi}{\partial t \partial a}\right)\xi + \ldots . \tag{3.6}$$

Now let us look at the dynamic situation. Figure 3-2 shows a small element of fluid *dadydz* at rest. Let us suppose that a plane wave is traveling to the right through the fluid, so that, at a given instant, the particles originally at rest at a will be displaced a distance ξ, while those ordinarily at rest at $a + da$ will be displaced a distance $\xi + d\xi$. Since these new boundaries of our fluid element could also have been written as x^L and $x^L + dx^L$, the displaced

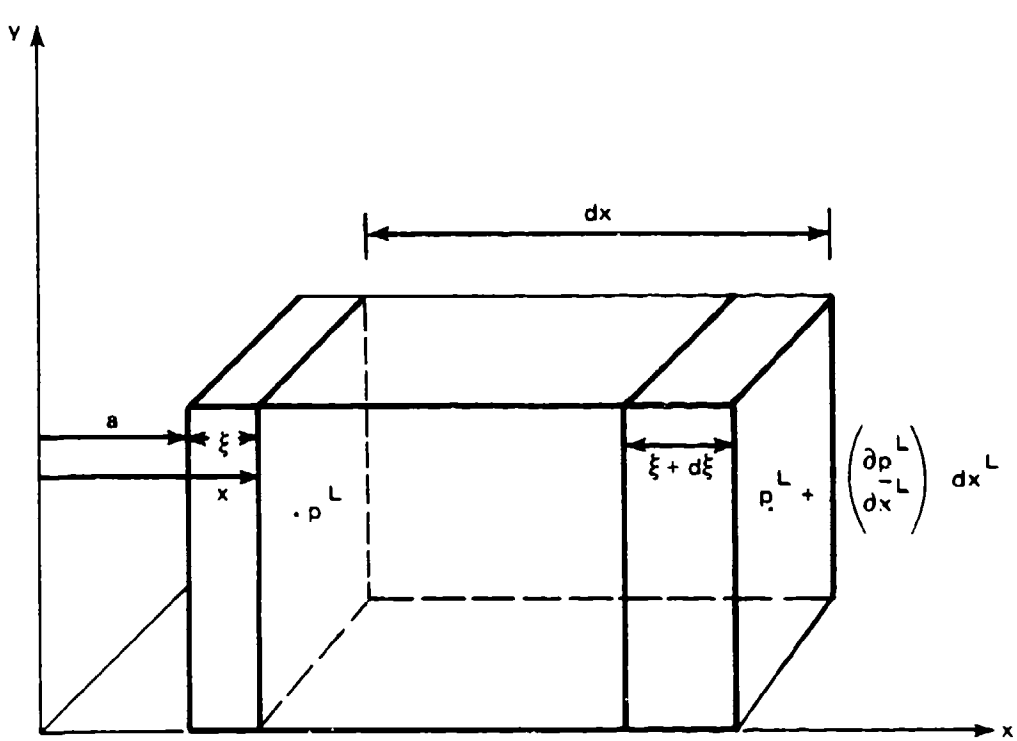

Figure 3-2a.–Pressure gradients in Lagrangian coordinates.

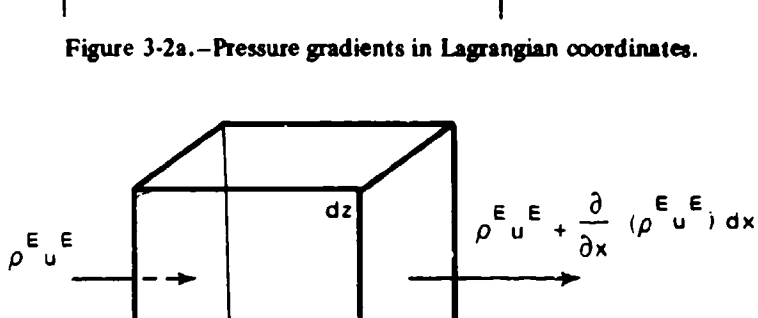

Figure 3-2b.–Rate of mass flow in Eulerian coordinates.

and distorted volume dV could also have been written $dxdydz$. (Since we have supposed no fluid motion in the y and z directions, there is no need of distinguishing between Lagrangian and Eulerian coordinates for them.) If we now represent the density of the fluid at rest by ρ_0 and that of the displaced fluid (in the Lagrangian system) by ρ^L, we must have

$$\rho^L dx^L dydz = \rho_0 dadydz$$

since the total mass in the box must be the same in the two cases. We therefore have

$$\rho^L = \rho_0 \frac{da}{dx^L}$$

or, since $x^L = a + \xi$, we have

$$\rho^L = \rho_0 \left(1 + \frac{\partial \xi}{\partial a}\right)^{-1}. \tag{3.7}$$

The Langrangian formulation makes it particularly easy to write down the equation of motion. If the pressure at any instant at the left side of the volume element (Fig. 3.2a) is p^L, while that on the right is $p^L + (\partial p^L / \partial x^L)\, dx^L$ then the net force (to the right on the fluid in the volume element dV) is $-(\partial p^L / \partial x^L) dx^L dydz$ and the equation of motion becomes

$$-\frac{\partial p^L}{\partial x^L} dx^L dydz = (\rho_0 dadydz)\, \ddot{\xi}$$

or

$$-\frac{\partial p^L}{\partial x^L}\frac{\partial x^L}{\partial a} = -\frac{\partial p^L}{\partial a} = \rho_0 \ddot{\xi}.$$

It is instructive to develop the equation of continuity in Eulerian coordinates also. We consider a volume element $dxdydz$ in Eulerian coordinates (see Fig. 3.2b). The rate of mass influx at the left will be $\rho^E u^E\, dydz$, while the outflow at the right will be

$$\left[\rho^E u^E + \frac{\partial(\rho^E u^E)}{\partial x}\right] dydz,$$

so that the net influx will be

$$\rho^E u^E dydz - \left[\rho^E u^E + \frac{\partial(\rho^E u^E)}{\partial x}\, dx\right] dydz = -\frac{\partial(\rho^E u^E)}{\partial x}\, dV.$$

(3.9)

This must in turn be equal to the rate of mass increase in the element, $(\partial \bar{\rho}^E/\partial t)(dxdydz)$, where $\bar{\rho}^E$ is the mean (Eulerian) density over the distance interval dx. Hence

$$\left(\frac{\partial \bar{\rho}^E}{\partial t}\right) dV = - \left(\frac{\partial(\rho^E u^E)}{\partial x}\right) dV$$

or, in the limit as $dx \to 0$,

$$- \frac{\partial \rho^E}{\partial t} = \frac{\partial(\rho^E u^E)}{\partial x} \tag{3.10}$$

which is the equation of continuity for one dimensional motion. In three dimensions, this equation can be rewritten as

$$- \frac{\partial \rho^E}{\partial t} = \frac{\partial \left(\rho^E u^E{}_x\right)}{\partial x} + \frac{\partial \left(\rho^E u^E{}_y\right)}{\partial y} + \frac{\partial \left(\rho^E u^E{}_z\right)}{\partial z} \equiv \nabla(\rho^E \underset{\sim}{u}^E) \, . \tag{3.11}$$

We now define the speed of sound c by the relation

$$c^2 = \frac{\partial p^L}{\partial \rho^L} = \frac{\partial p^E}{\partial \rho^E} \tag{3.12}$$

where the derivative is taken under adiabatic conditions. Then, by use of Eq. (3.7), we get

$$- \frac{\partial p^L}{\partial a} = - \frac{\partial p^L}{\partial \rho^L} \frac{\partial \rho^L}{\partial a} = \frac{c^2 \rho_0}{\left(1 + \frac{\partial \xi}{\partial a}\right)^2} \frac{\partial^2 \xi}{\partial a^2}$$

and Eq. (3.8) becomes

$$\frac{\partial^2 \xi}{\partial t^2} = \frac{c^2}{\left(1 + \frac{\partial \xi}{\partial a}\right)^2} \frac{\partial^2 \xi}{\partial a^2} \tag{3.13}$$

which is the equation of motion for an acoustic wave in one dimension. For the special case of an ideal gas, the adiabatic relation can be written

$$p = p_0 \left(\frac{\rho}{\rho_0}\right)^{\gamma} \tag{3.14}$$

where γ is the ratio of specific heats. Then

$$c^2 = \frac{\partial p^L}{\partial \rho^L} = \frac{\gamma \rho_0}{\rho_0}\left(\frac{\rho}{\rho_0}\right)^{\gamma-1} = \frac{\gamma p_0}{\rho_0} \frac{1}{\left(1 + \frac{\partial \xi}{\partial a}\right)^{\gamma-1}}$$

whence (3.12) becomes

$$\frac{\partial^2 \xi}{\partial t^2} = \frac{c_0^2}{\left(1 + \frac{\partial \xi}{\partial a}\right)^{\gamma+1}} \frac{\partial^2 \xi}{\partial a^2} . \tag{3.15}$$

This is the form of the nondissipative wave equation in one dimension in Lagrangian coordinates.

We have already obtained the equation of continuity in Eulerian coordinates [Eq. (3.10)]. To find the equation of motion in these coordinates of motion, we need only recall that we can follow the velocity changes of an element of the fluid by using the total derivative, so that the equation of motion is given by

$$\frac{d\mathbf{u}}{dt} = -\frac{\nabla p}{\rho} \text{ (Eulerian coordinates)}$$

or

$$\dot{\mathbf{u}} + (\mathbf{u} \cdot \nabla)\mathbf{u} = -\frac{\nabla p}{\rho} ,$$

which, in one dimension, is

$$\ddot{\xi} + \dot{\xi} \frac{\partial \dot{\xi}}{\partial x} = -\frac{1}{\rho} \frac{\partial p}{\partial x} . \tag{3.16}$$

This equation, together with (3.10), gives us the wave equation in parametric form.

If one is dealing with a liquid, some other relation must be found between p and ρ than that given in Eq. (3.14). The form

$$p = P\left(\frac{\rho}{\rho_0}\right)^{\gamma} - Q \tag{3.17}$$

is sometimes used, where P, Q, and γ are three constants to be determined from the experimental data. Such a form is commonly used in hydrodynamics for water, with the values $\gamma = 7$, $P = 3001$ atm, $Q = 3000$ atm, and is known as the Tait equation. Note that in this case γ is no longer the ratio of specific heats, but is a parameter chosen to fit the experimental form of the $p - \rho$ curve.

An alternative representation is obtained by the use of the Taylor expansion of the pressure in terms of the density for the isentropic case:

$$p = p_0 + \left(\frac{\partial p}{\partial \rho}\right)_{S,\rho=\rho_0} (\rho - \rho_0) + \frac{1}{2}\left(\frac{\partial^2 p}{\partial \rho^2}\right)_{S,\rho=\rho_0} (\rho - \rho_0)^2 + \cdots \tag{3.18}$$

or

$$p = p_0 + As + \frac{B}{2!}s^2 + \frac{C}{3!}s^3 + \cdots \tag{3.19}$$

where

$$A = \rho_0\left(\frac{\partial p}{\partial \rho}\right)_{S,\rho=\rho_0} = \rho_0 c_0^2$$

$$B = \rho_0^2\left(\frac{\partial^2 p}{\partial \rho^2}\right)_{S,\rho=\rho_0} \qquad s = \frac{\rho - \rho_0}{\rho_0} \tag{3.20}$$

$$C = \rho_0^3\left(\frac{\partial^3 p}{\partial \rho^3}\right)_{S,\rho=\rho_0}$$

The parameters A, B, C... are temperature-dependent quantities. In most situations, only the terms involving A and B are necessary.

We could use Eq. (3.19) in conjunction with Eq. (3.20) to obtain an expression for c^2 to be substituted in Eq. (3.13). This expression is

$$c^2 = c_0^2 \left[1 + \left(\frac{B}{A}\right) s + \left(\frac{C}{2A}\right) s^2 + \ldots\right]. \tag{3.21}$$

This would give a rather cumbersome form to Eq. (3.13) and it has proved to be more convenient (and equally accurate, to terms of second order) to establish the relation between the parameter γ in Eqs. (3.14) and (3.17) with the ratio B/A.

If we expand Eq. (3.14) in powers of the condensation s,

$$p = p_0(1+s)^\gamma = p_0 \left[1 + s + \frac{\gamma(\gamma-1)}{2} s^2 + \ldots\right]$$

and comparing the result, term by term, with Eq. (3.19), it can be established that $B/A = \gamma - 1$ for the ideal gas. If therefore we use the form of Eq. (3.14), but replace γ by $B/A + 1$, we can rewrite Eq. (3.15) in the form

$$\frac{\partial^2 \xi}{\partial t^2} = \frac{c_0^2}{\left(1 + \frac{\partial \xi}{\partial a}\right)^{2 + \frac{B}{A}}} \frac{\partial^2 \xi}{\partial a^2} \tag{3.15}$$

that will be good for all fluids for which C/A can be neglected.*

The ratio B/A plays a significant role in nonlinear acoustics, so that its experimental determination is of some importance. To make this determination, we first observe that, from Eq. (3.20),

$$\frac{B}{A} = \frac{\rho_0}{c_0^2} \left(\frac{\partial^2 p}{\partial \rho^2}\right)_{S,\rho=\rho_0} = \frac{\rho_0}{c_0^2} \left(\frac{\partial c^2}{\partial \rho}\right)_{S,\rho=\rho_0}$$

$$= 2 \frac{\rho_0}{c_0} \left(\frac{\partial c}{\partial p}\right)_{S,\rho=\rho_0} \cdot \left(\frac{\partial p}{\partial \rho}\right)_{S,\rho=\rho_0}$$

$$= 2\rho_0 c_0 \left(\frac{\partial c}{\partial p}\right)_{S,\rho=\rho_0}.$$

*Had we expanded Eq. (3.17) instead of (3.14), we would have obtained the same relation between γ and B/A. In such a case, $P - Q = p_0$ and $P = \rho_0 c_0^2/\gamma$, where $\gamma = B/A + 1$.

By means of simple thermodynamic transformations, this expression can be converted to the form

$$\frac{B}{A} = 2\rho_0 c_0 \left(\frac{\partial c}{\partial p}\right)_{T,\rho_0} + \frac{2\beta T c_0}{c_p} \left(\frac{\partial c}{\partial T}\right)_{p,\rho_0}$$

where $\beta = (1/V)(\partial V/\partial T)_p$ = volume coefficient of thermal expansion, and c_p is the specific heat at constant pressure.

A similar analysis for C/A leads to the relation

$$\frac{C}{A} = \frac{3}{2}\left(\frac{B}{A}\right)^2 + 2\rho_0^2 c_0^3 \left(\frac{\partial^2 c}{\partial p^2}\right)_S . \tag{3.22}$$

Analysis of the case of water at 20° for an excess pressure of 6 atmospheres has indicated that the relative size of the A, B and C terms of Eq. (3.20) is

$$1. \quad 6.75 \times 10^{-4}, \quad 4.56 \times 10^{-7} .$$

Except at very high pressures then, it is safe to neglect the cubic and higher order terms in (3.20), at least in water. [2]

Some typical values of the ratio B/A are given in Table 3-1. The range of variation is very slight, as is the variation with temperature and pressure.

A plot of B/A vs $1/c$ (Fig. 3.3) is a useful way of presenting these data. Points corresponding to liquid metals are indicated by the black circles. The line drawn on the graph is one suggested by J. F. Ballou, and known in the author's research group as Ballou's rule: [2a]

$$\frac{B}{A} = \frac{1.2 \times 10^6}{c} - 0.5$$

where c is the speed of sound in the medium in cm/sec. While the data are scattered it is clear that B/A in general increases as c decreases.

In the rest of the chapter, we shall replace $\gamma + 1$ in (3.16) by $B/A + 2$ whenever we are dealing with liquids.

Table 3-1. Values of B/A. Except where indicated, all values are at atmospheric pressure.

Substance	T, °C	B/A	Substance	T, °C	B/A
distilled water	0	4.2	methyl acetate	30	9.7
	20	5.0	cyclohexane	30	10.1
	40	5.4	nitrobenzene	30	9.9
	60	5.7	mercury	30	7.8
	80	6.1	sodium	110	2.7
	100	6.1	potassium	100	2.9
Pressure			tin	240	4.4
1 atm	30	5.2	indium	160	4.6
200 kg/cm^2	30	6.2	bismuth	318	7.1
4000	30	6.2			
8000	30	5.9	monatomic gas	20	0.67
			diatomic gas	20	0.40
sea water (3.5%)	20	5.25	methyl iodide	30	8.2
methanol	20	9.6	sulfur	121	9.5
ethanol	0	10.4	glycerol (4% H_2O)	30	9.0
	20	10.5	1,2 – dichloro-hexafluoro-cyclopentene (DHCP)	30	11.8
	40	10.6			
n-propanol	20	10.7			
N-butanol	20	10.7			
acetone	20	9.2			
beneze	20	9.0			
chlorobenzene	30	9.3			
liquid nitrogen	b.p.	6.6			
benzyl alcohol	30	10.2			
diethylamine	30	10.3			
ethylene glycol	30	9.7			
ethyl formate	30	9.8			
heptane	30	10.0			
hexane	30	9.9			

3.2 Earnshaw Solution of the Wave Equation. The Discontinuity Solution.*

Equation (3.16) was solved in implicit fashion by Earnshaw in 1860. [3] His analysis began with the fact that the Lagrangian particle velocity $u = \dot{\xi}$ must be some function of the local density, which is in turn a function of $\partial\xi/\partial x$ through (3.7). We therefore write $u = f(\partial\xi/\partial x)$. Then

$$\ddot{\xi} = f' \cdot \frac{\partial^2 \xi}{\partial x \partial t} , \frac{\partial^2 \xi}{\partial x \partial t} = f' \cdot \frac{\partial^2 \xi}{\partial x^2} \tag{3.23}$$

*Beginning with this section, we shall cease using a to denote Lagrangian coordinates, replacing it with the more conventional x.

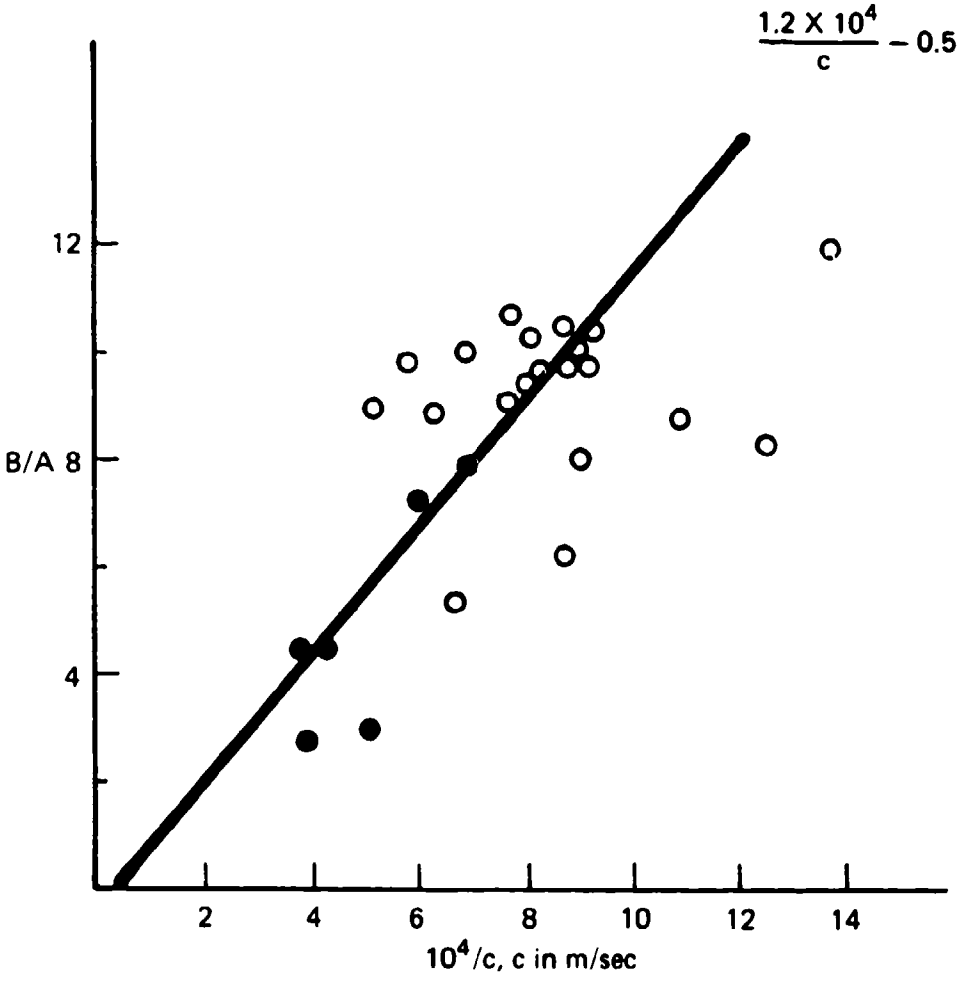

Figure 3-3.–Ratio of B/A for liquids as a function of inverse sound velocity: Solid curve indicates Ballou's rule
• liquid metals
○ other liquids.

where f' denotes the derivative of f with respect to its argument, so that

$$\ddot{\xi} = (f')^2 \frac{\partial^2 \xi}{\partial x^2} . \tag{3.24}$$

By comparison of Eq. (3.24) with (3.16) we obtain

$$f'\left(\frac{\partial \xi}{\partial x}\right) = \frac{\pm c_0}{\left(1 + \frac{\partial \xi}{\partial x}\right)^{1 + \frac{B}{2A}}} . \tag{3.25}$$

Integrating (3.25), we get

$$f\left(\frac{\partial \xi}{\partial x}\right) = u = \frac{\pm c_0}{\left(1 + \frac{\partial \xi}{\partial x}\right)^{\frac{B}{2A}}} \left(-\frac{2A}{B}\right) + \text{const.} \tag{3.25a}$$

When there is no sound, $\partial \xi / \partial x = 0$ and $u = 0$, so that

$$\pm \left(\frac{2A}{B}\right) c_0 + \text{const} = 0$$

or

$$u = \pm \frac{2A}{B} c_0 \left[1 - \frac{1}{1 + \left(\frac{\partial \xi}{\partial x}\right)^{\frac{B}{2A}}}\right] \tag{3.26}$$

$$= \frac{2A}{B} c_0 \left[1 - (1+s)^{\frac{B}{2A}}\right] .$$

The rate at which a particular value of s, u or $\partial \xi / \partial x$ is propagated is given by the square root of the coefficient of $\partial^2 \xi / \partial x^2$ in (3.24), i.e., f', to which we attach the symbol v. From (3.25),

$$v = \pm c_0 (1+s)^{1 + \frac{B}{2A}} .$$

We confine our attention to waves traveling in the positive x direction and eliminate s from Eqs. (3.26) and (3.27), thus obtaining the rate of propagation of the wave as a function of the particle velocity:

$$v = c_0 \left(1 + \frac{B}{2A} \frac{u}{c_0}\right)^{\frac{2A}{B} + 1} . \tag{3.28}$$

Since the general form of the solution of (3.16) is

$$u = F\left[\omega\left(t \pm \frac{x}{v}\right)\right], \tag{3.29}$$

a wave with the boundary condition

$$u(0, t) = u_0 \sin \omega t \tag{3.30}$$

will have the solution

$$u(x,t) = u_0 \sin \left[\omega t - \frac{\omega x}{c_0}\left(1 + \frac{B}{2A}\frac{u}{c_0}\right)^{-\frac{2A}{B} - 1}\right] \tag{3.31}$$

which is the implicit solution of Eq. (3.16).

A simple plotting of Eq. (3.31) as a function of x for specific values of u will demonstrate that the points of high particle velocity will move more rapidly than those of low velocity, so that the waveform becomes progressively steeper (in the neighborhood of $u = 0$) as x increases (see Fox and Wallace [4]). If we therefore take the derivative with respect to x in (3.31) and evaluate $\partial u/\partial x$ at $u = 0$, we obtain the result

$$\frac{\partial u}{\partial x} = \frac{\frac{-\omega}{c_0}}{\frac{1}{u_0} - \frac{\omega x}{c_0^2}\left(1 + \frac{B}{2A}\right)} . \tag{3.32}$$

Thus, $\partial u/\partial x$ becomes more negative with increasing x, becoming negatively infinite at a distance ℓ from the origin, where

$$\frac{1}{\ell} = \left(1 + \frac{B}{2A}\right) \frac{\omega u_0}{c_0^2} = \beta M k; \quad \beta = 1 + \frac{B}{2A}. \tag{3.33}$$

Here M is the acoustic Mach number, and the symbol $\beta=(1+B/2A)[=(\gamma+1)/2$ for gases] measures the nonlinearity; ℓ is called the *discontinuity distance*. It is, of course, defined for the idealized case of zero viscosity, but it gives a measure of how rapidly distortions appear even in a wave of very modest amplitude. Some values of ℓ are shown in Table 3-2.

Table 3.2 Values of the discontinuity distance ℓ for various sound levels and frequencies ($T = 20°$, $p_0 = 1$ atm).

Water

P_{ac} in atm	M	ℓ, in cm (at 100 kHz)	ℓ, in cm (at 1.0 MHz)
0.1	0.0046×10^{-3}	14,800	1480
1	0.046×10^{-3}	1,480	148
10	0.46×10^{-3}	148	15

Air

P_{ac} in atm dyne/cm^2	dB re 0.0002	M	ℓ, in cm (10 kHz)	ℓ, in cm (100 kHz)
20	100	0.014×10^{-3}	32,000	3200
200	120	0.14×10^{-3}	3,200	320
2000	140	1.4×10^{-3}	320	32

3.3 Riemann's Solution.

At about the same time as Earnshaw, Riemann attacked the finite amplitude problem in quite a different way.[5] He began with the equations of mass and momentum conservation, which we write in Eulerian form [see Eqs. (3.10), (3.16)]

$$\frac{\partial u}{\partial t} + u\frac{\partial u}{\partial x} = -\frac{c^2}{\rho}\frac{\partial \rho}{\partial x} \tag{3.34}$$

$$\frac{1}{\rho}\frac{\partial \rho}{\partial t} + \frac{u}{\rho}\frac{\partial \rho}{\partial x} = -\frac{\partial u}{\partial x}. \tag{3.35}$$

We then multiply (3.35) by $\pm c$ and add the result to (3.34). This gives us two equations, which we write as

$$\frac{\partial P}{\partial t} = - (u + c) \frac{\partial P}{\partial x}$$
$$\frac{\partial Q}{\partial t} = - (u - c) \frac{\partial Q}{\partial x} \tag{3.36}$$

where

$$P = u + \int_{\rho_0}^{\rho} \frac{c}{\rho} d\rho \equiv u + w(\rho)$$
$$Q = u - w(\rho). \tag{3.36a}$$

We now consider P as a function of x and t, and form its differential

$$dP = \frac{\partial P}{\partial x} dx + \frac{\partial P}{\partial t} dt .$$

Then, using (3.36), we get

$$dP = \frac{\partial P}{\partial x} [dx - (u + c) dt] .$$

Hence P will be invariant along the curve defined by $dx/dt = u + c$. Similarly, Q will be invariant along the curve $dx/dt = u - c$. The quantities P and Q are known as the *Riemann invariants*.

The behavior of the fluid is completely determined by a knowledge of P,Q everywhere in the x,t plane. The significance of the Riemann invariants is that, if P is originally known as a function of x at some time t_0, then the particular values of P will remain the same as the initial values along the curve defined by $dx/dt = u + c$.

Let us look at this in terms of a wave that was initially sinusoidal. At $t = 0$, $u_0 \sin kx$. This is indicated in Fig. 3-4 by the heavy sinusoidal curve. (One should think of this curve as plotted in a plane perpendicular to the paper. Only the first half cycle will be studied.)

As time passes a particular value of the particle velocity, u_1, will be propagated along the straight line $dx/dt = u_1 + c$. A number of such lines are also plotted for various points in the wave, the slope dt/dx becoming smaller

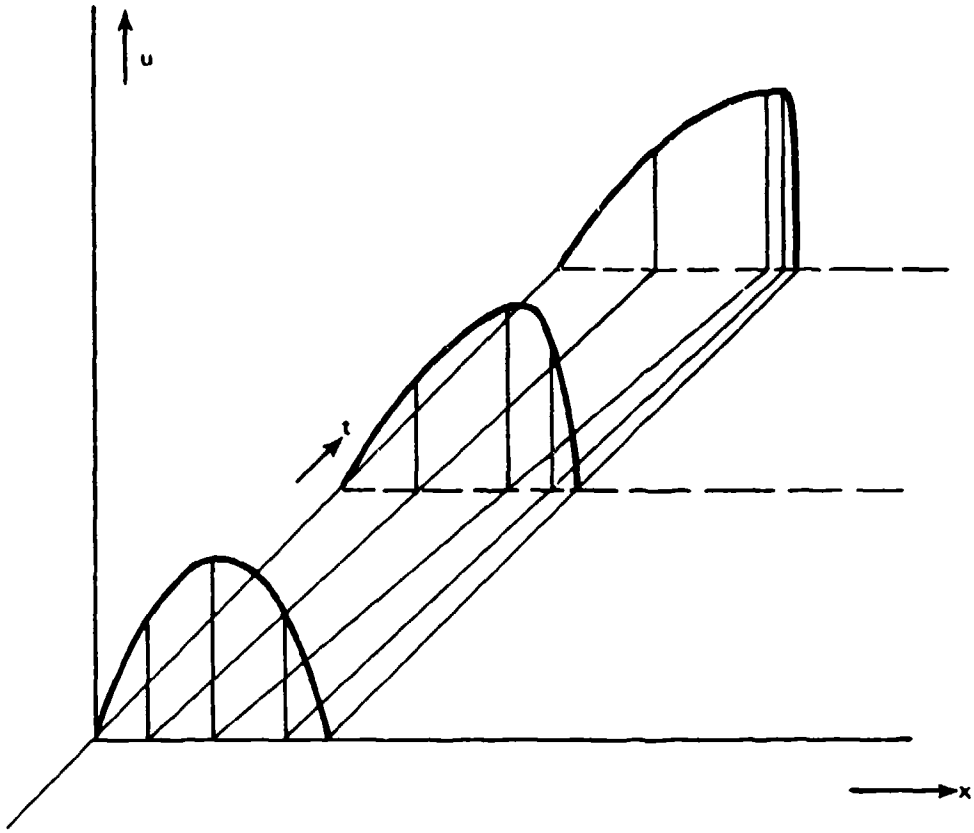

Figure 3-4.–Wave distortion as described by method of characteristics.

as u becomes larger. We can therefore reconstruct the curve at later position in time and space, as is shown in the figure. The steepening of the wave profile as it progresses is plainly indicated by this method.

Such curves as the straight lines in Fig. 3-4, along which P,Q remain invariant are known as the characteristics of the flow, and the technique used for their solution is known as the *method of characteristics.* It is widely used in fluid dynamics and shock wave theory (see Chapter 4).

3.4 The Fubini Solution.

The explicit solution of Eq. (3.31) was obtained by Fubini in 1935 for low Mach numbers. [6] The parenthetical expression in (3.31) is expanded in a bionomial series and only the first two terms are kept. This results in the equation

$$u(x, t) = u_0 \sin \left[\omega t - \frac{\omega x}{c_0}\left(1 - \beta \frac{u}{c_0}\right)\right]$$

so that [recall Eq. (3.33)]

$$\frac{u}{u_0} = \sin\left(\omega t - kx + \frac{x}{\ell}\frac{u}{u_0}\right) \tag{3.37}$$

where $k = \omega/c$. We now expand u/u_0 in a Fourier series

$$\frac{u}{u_0} = \sum_{n=1}^{\infty} B_n \sin n(\omega t - kx) \tag{3.38}$$

where

$$B_n = \frac{1}{n}\int_0^{2\pi} \frac{u}{u_0} \sin n(\omega t - kx)\, d(\omega t - kx) \; . \tag{3.39}$$

Substitution of Eq. (3.34) in (3.36) and manipulation of the result ultimately leads to the values of B_n:

$$B_n = \left(\frac{2\ell}{nx}\right) J_n\left(\frac{nx}{\ell}\right) \tag{3.40}$$

where J_n is the Bessel function of the first kind of order n. The explicit solution is then

$$\frac{u}{u_0} = 2 \sum_{n=1}^{\infty} \frac{J_n\left(\frac{nx}{\ell}\right)}{\frac{nx}{\ell}} \sin n(\omega t - kx) \; . \tag{3.41}$$

It should be noted that when $x > \ell$, Eq. (3.37) becomes multivalued in u, and cannot be used without modification (see Section 3.8). In the actual physical case, such an infinite steepness will occur first at the point $u = 0$ and then in its neighborhood, so that a shock front is formed with a very small discontinuity in pressure. Such a discontinuity increases in strength with the propagation distance and the wave becomes more and more nearly sawtooth in shape.

It is of some interest to note that in the corresponding case of transverse waves in water, multivaluedness is possible, as anyone who has had a surf wave break over his head can testify.

Before leaving the nondissipative case, it is worth introducing a graphical representation made popular by Soluyan and Khokhlov [6a]. If we return to Eq. (3.37) and let $W = u/u_0$, $Z = \omega t - kx$, $\sigma = x/\ell$, we have

$$W = \sin\ (Z + \sigma W)$$

or

$$Z = \sin^{-1}\ W - \sigma W\ . \tag{3.42}$$

We now plot a graph of Z vs. W (Fig. 3-5). If we indicate the two terms separately, the distortion of the wave form can easily be seen. Forward progress of the wave corresponds to clockwise rotation of the curve II. When $\sigma = 1$, the negative slope of curve II is the same magnitude of the positive slope of $\sin^{-1} W$ at the origin so that infinite steepness (shock) of W as a function of Z is achieved at that point.

3.5 The Viscous Case. Perturbation Analysis.

We shall now take dissipation into account. The distortions of the wave form brought about by nonlinearity are equivalent to the production of higher harmonics of the original wave, as is explicitly indicated in Eq. (3.38). Since $\alpha \propto \omega^2$ for fluids at frequencies far removed from a relaxation frequency, this means that the higher harmonics will be attenuated more rapidly. Hence the net growth of these harmonics will be smaller than that predicted by Eq. (3.38) so that the presence of viscosity should delay or even prevent the appearance of a shock front. There is then a region along the path of propagation in which the rate of energy conversion from the lower to the higher harmonics is roughly counterbalanced by the increase dissipation of these higher frequency components, so that the wave form remains very nearly constant. This is sometimes called the region of the *comparatively stable wave.* Experimentally, its presence has been clearly demonstrated by Krasilnikov and coworkers. [7]

The theoretical analysis of the wave propagation for the case of finite but moderate amplitude by means of a perturbation analysis was first carried out over one hundred years ago by Airy in studying tidal motion.[8] The perturbation is performed in the acoustic case in terms of the initial Mach number $M_0 = u_0/c_0$. It is assumed that the hydrodynamic variables, such as the displacement ξ, can be written in series of the form

$$\xi = \xi_1 + \xi_2 + \cdots$$

in which each term is smaller than its predecessor by the factor M_0.

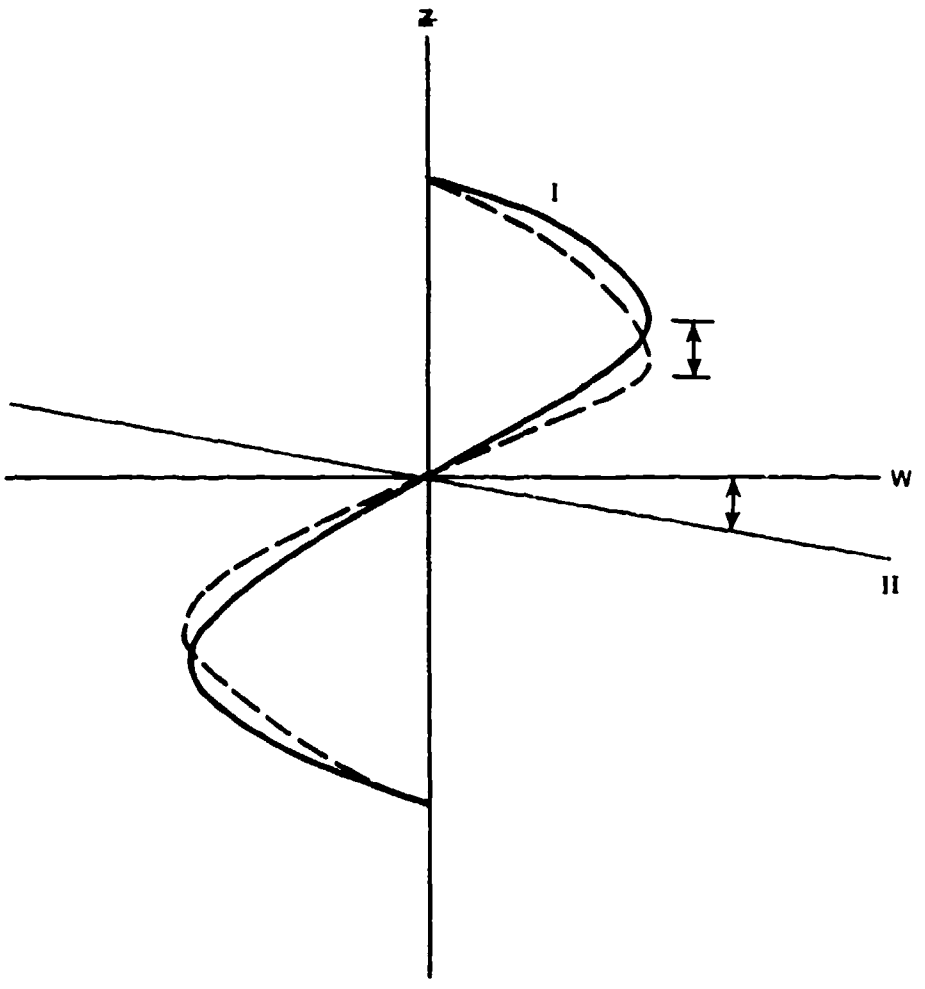

Figure 3·5.–Plot of terms in Eq. (3.42). *I*– $\sin^{-1} W$; *II*– $-\sigma W$; broken line– Z.

In the case of viscous medium, Eq. (3.38) can be replaced by the Stokes-Navier equation (1.51)

$$\rho_0 \ddot{\xi} = - \frac{\partial p^L}{\partial x} + \left(\frac{4}{3}\eta + \eta'\right) \frac{\partial^2 \dot{\xi}^L}{\partial x^2} \tag{3.43}$$

(Where we have continued the notational change $a \rightarrow x$ mentioned on p. 3-11) so that the nonlinear Eq. (3.16) is replaced by

$$\left(1 + \frac{\partial \xi}{\partial x}\right)^{\frac{B}{A}+2} \left(\ddot{\xi} - \nu b \frac{\partial^3 \xi}{\partial x^2 \partial t}\right) = c_0^2 \frac{\partial^2 \xi}{\partial x^2}, \tag{3.44}$$

where ν is the *kinematic shear viscosity*, equal to η/ρ_0 and $b = 4/3 + \eta'/\eta$ is the *viscosity number*. (This analysis is not valid in the neighborhood of a relaxation frequency, where b would have to be a function of frequency) (see Section 3.10).

We now substitute our expansion of ξ in (3.44) and equate terms of corresponding order in ξ. The resulting equation can be written in compact form by defining the differential operator Ω:

$$\Omega \equiv \frac{1}{c_0^2}\frac{\partial^2}{\partial t^2} - \frac{\nu b}{c_0^2}\frac{\partial^3}{\partial x^2 \partial t} - \frac{\partial^2}{\partial x^2} . \tag{3.45}$$

Then $\Omega\xi_1 = 0$,

$$\Omega\xi_n = \beta\frac{\partial}{\partial x}\sum_{i=1}^{n-1}\frac{\partial \xi_i}{\partial x}\frac{\partial \xi_{n-1}}{\partial x} , \quad n > 1 . \tag{3.46}$$

In deriving these equations, the further approximation that $\alpha/k << 1$ has been made; this is virtually always a safe assumption. In this approximation, terms that are smaller by the factor α/k than otherwise similar terms have been neglected.

Equations (3.45) and (3.46) can now be solved in their homogeneous and inhomogeneous parts, subject to the boundary condition

$$\xi(0,t) = -\xi_0 \cos \omega t ,$$

corresponding to $\dot{\xi}(0,t) = u_0 \sin \omega t$ as used in the nondissipative case.

The solutions of (3.46) have been carried out up to $n = 6$.[9] The most interest attaches to the series representations of the fundamental and second harmonics, the early terms in which have the form

$$u_1 = u_0 R^{1/2} \sin(\omega t - kx)\left[1 - \frac{1}{1!2!}\left(\frac{1-R}{4\alpha\ell}\right)^2 + \frac{1}{2!3!}\left(\frac{1-R}{4\alpha\ell}\right)^4 (4 - 2R - R^2) + \cdots\right]$$

$$u_2 = u_0 R \sin 2(\omega t - kx)\left[\left(\frac{1-R}{4\alpha\ell}\right) - \frac{4}{3}\left(\frac{1-R}{4\alpha\ell}\right)^3\left(\frac{3+R}{4}\right) + \ldots\right] \tag{3.47}$$

where $R = e^{-2\alpha x}$.

Graphs of u_1, u_2, u_3, u_4 are shown in Fig. 3-6 which corresponds to the case $\omega/2\pi = 2.5$ MHz in water, initial pressure amplitude 3.0 atm. Here $\alpha = 0.0016$ cm^{-1}, $\ell = 21$ cm. As the graph indicates, the calculations can be carried beyond the point $x = \ell$, but to a lesser extent for each succeeding harmonic.

It has been proved by Blackstock[10] that the series represented by solutions such as Eq. (3.43) converge everywhere. However, the complete form of the series has never been obtained, so that the partial solutions represented by the first few terms may or may not be an entirely valid solution of the problem. It should also be noted that when $4\alpha\ell$ is large, the Keck-Beyer solutions (Eq. 3.47) are always a good approximation.

We can also compute the total absorption coefficient by forming the expression for the energy density in each harmonic and using the relation

$$\alpha_{\text{fin}} = -\frac{1}{2I}\frac{dI}{dx} .$$

As a result, we obtain

$$\frac{\alpha_{\text{fin}}}{\alpha} = 1 + 3e^{-2\alpha x}\left(\frac{1 - e^{-2\alpha x}}{4\alpha\ell}\right)^2 + O\left(\frac{1}{4\alpha\ell}\right)^2 . \tag{3.48}$$

Here $O(\ldots)$ denotes "order of".

3.6 Other Methods of Solution.

Before taking up the analysis of finite-amplitude wave propagation by means of Burgers' equation, it is appropriate to discuss several other approaches that have shed light on the problem.

A. Fay's solution. The most important of the other methods, particularly from the historical viewpoint, has been that given by Fay in 1931.[11] He made use of an equation of the form of (3.40) and expanded the excess pressure in a power series in $\partial\xi/\partial x$. At the same time, he expressed $\partial\xi/\partial x$ as a Fourier series whose coefficients depend on x and include exponential decay factors. The details of the derivation are quite involved. Among other assumptions, Fay limited his region of application to that of the comparatively stable waveform. From Fay's analysis one ultimately obtains the following expression for the acoustic pressure $p_{\text{ac}} = p - p_0$:

$$p_{\text{ac}} = \frac{b\eta\omega}{\beta}\sum \frac{\sin n(\omega t - kx)}{\sinh n\alpha(x + x_0)} . \tag{3.49}$$

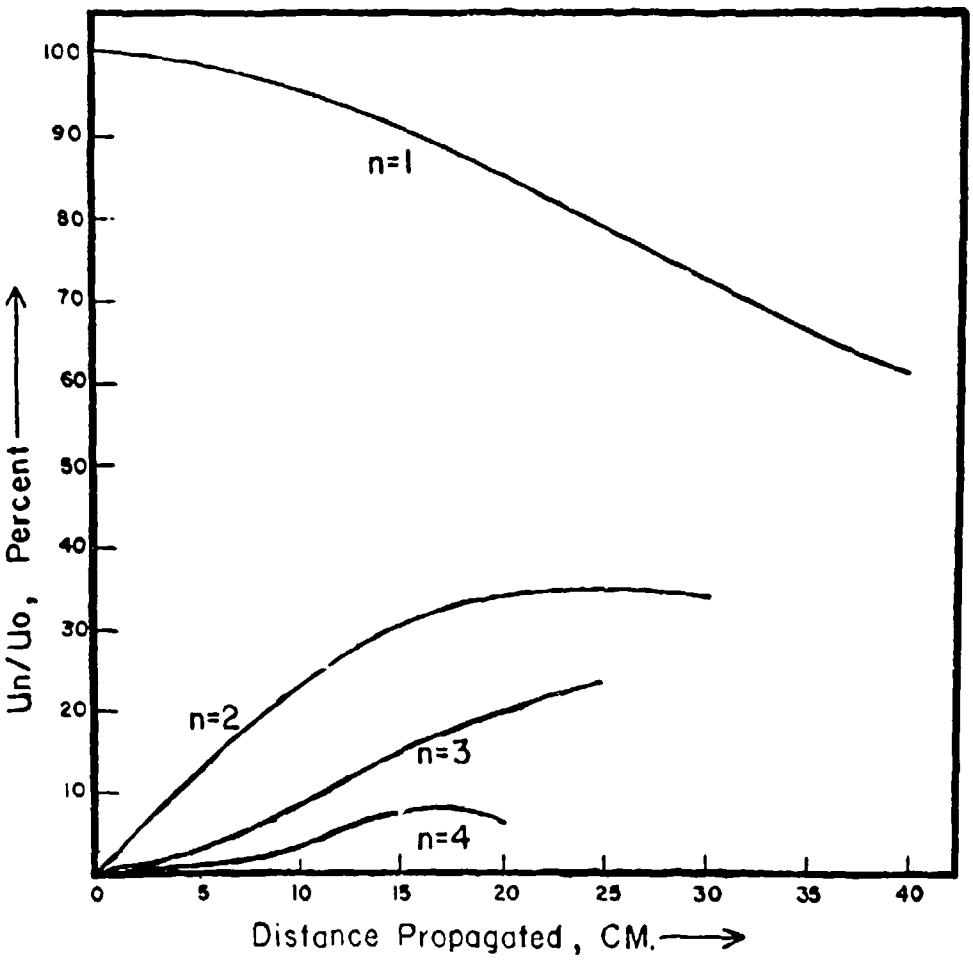

Figure 3-6.–Fundamental and several harmonics as a function of distance traveled in water. Frequency = 2.5 MHz, pressure amplitude 3.0 atm (from R. P. Ryan [9a]).

To evaluate x_0, we consider the asymptotic form of the sawtooth part of the solution in the analysis of Blackstock's bridging function [see discussion after Eq. (3.79) below]. This gives the amplitude of the fundamental component in a decaying sawtooth as

$$\frac{2p_{10}}{1+\sigma} \tag{3.49a}$$

where p_{10} is the amplitude of the original sinusoidal signal at $x = 0$ and $\sigma = x/\ell$. This is to be compared with the first term on the right side of Eq. (3.49)

$$\frac{b\eta\omega}{\beta \sinh \alpha(x+x_0)} \simeq \frac{b\eta\omega}{\beta\alpha(x+x_0)} = \frac{2p_{10}\ell}{x+x_0}. \tag{3.49b}$$

By comparing the second and third terms in Eq. (3.49b), we see that x_0 should be identified with the discontinuity distance ℓ.

An approximate evaluation of (3.49) can be carried out by noting that $\sinh n\alpha(x + x_0)$ can be approximated by $n\alpha(x + x_0)$ for the first few terms of the series (which are the most significant ones). No major error is then introduced by replacing the hyperbolic sine function by its argument for all n and writing

$$p_{ac} = \frac{2p_{10}\ell}{\omega(x+x_0)} \sum_{n=1}^{\infty} \frac{\sin n(\omega t - kx)}{n} \tag{3.50}$$

where the summation is the expression for the Fourier series of the sawtooth. This can be rewritten as

$$p_{ac} = \frac{2p_{10}\ell}{x+x_0}\left[-\frac{\omega t + kx + \pi}{2}\right] \tag{3.51}$$

with the bracketed term running from $-\pi/2$ to $+\pi/2$. Hence the step in the pressure will be

$$p_{10}\frac{2\ell}{x_0+x}\pi \tag{3.52}$$

with the maximum departure of the pressure from equilibrium being half this amount. It is evident that the peak pressure does not decay exponentially. If we try to fit an effective absorption coefficient to this case, then

$$\alpha_{\text{eff}} = -\frac{1}{p_{\max}}\frac{dp_{\max}}{dx} = \frac{1}{x_0 + x}. \tag{3.53}$$

Another way of expressing this result is to consider the ratio $\alpha_{\text{eff}}/\nu^2$ to $p_{\max}/\nu$:

$$\frac{\alpha_{\text{eff}}/\nu^2}{p_{\max}/\nu} = \frac{2}{p_{10}\ell\omega} = \frac{2\beta}{\rho_0 c_0^3} \tag{3.54}$$

so that $\alpha_{\text{eff}}/\nu^2$ is directly proportional to $p_{\max}/\nu$, provided that $p_{\max}$ is evaluated at the same point as α_{eff}.

A number of other approximate treatments have been developed. Mendousse[12] suggested that the approximate stable waveform can be split into two parts (Fig. 3-7). Over most of the wave, the particle velocity will be proportional to x so that the value of $-(\partial u/\partial x)$ is as shown in the second part of the figure. The viscous force, $-(\partial^2 u/\partial x^2)$, is then equal to zero except in

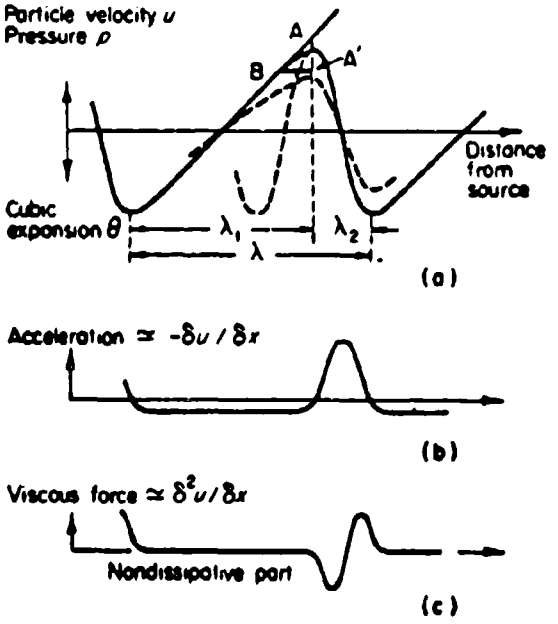

Figure 3-7.–Treatment of nearly sawtooth wave by Mendousse [12]. (a) particle displacement velocity; (b) particle acceleration; (c) viscous force.

the immediate neighborhood of the crest, in which region its fluctuations can be approximated by a sine wave of much higher frequency. Mendousse was able to show that the attenuation predicted by this analysis was consistent with the decrease in the height of the near sawtooth wave as propagated in gases.

By a somewhat similar analysis, Rudnick[13] derived an expression for the attenuation coefficient for the fundamental component of the wave, arriving at the result

$$\frac{\alpha_{\text{fund}}}{\alpha} = \left[1 + \left(\frac{\pi\beta p_{10}\nu}{\alpha\rho_0 c_0^3}\right)^2\right]^{1/2} = \left[1 + \frac{1}{(2\alpha\ell)^2}\right]^{1/2} . \tag{3.55}$$

B. Numerical Analysis. In 1954, Fox and Wallace[4] attempted a graphical analysis of the distortion of the wave. Taking the implicit solution of one-dimensional propagation in a nondissipative medium, they divided the discontinuity distance into ten equal parts and determined the harmonic content of the wave at the end of each such interval. From this they derived a numerical growth factor $\delta_k^{(n)}$ such that the content of the nth harmonic at the end of the $(k + 1)$th interval was given by

$$(u_n)_{k+1} = (u_n)_k \exp \delta_k^{(n)} . \tag{3.56}$$

They then inserted an attenuation factor appropriate to the given harmonic. For a nonrelaxing medium with infinitesimal absorption coefficient at the original frequency given by α, the modified form for harmonic growth was

$$(u_n)_{k+1} = (u_n)_k \exp\left[a_k^{(n)} - n^2\alpha\Delta x\right] \tag{3.57}$$

where Δx was the propagation interval.

Essentially the same procedure has been adapted by Cook[14] for analysis by a high-speed computer. In addition, he made use of the Bessel-Fubini explicit solution, Eq. (3.41) as a starting point, instead of the graphical method used by Fox and Wallace. Cook has presented his results for both harmonic content and effective absorption coefficient in terms of the reduced distance $\sigma = x/\ell$ (ℓ is the discontinuity distance) and for various values of α. The shape of such curves is indicated in Fig. 3-8.

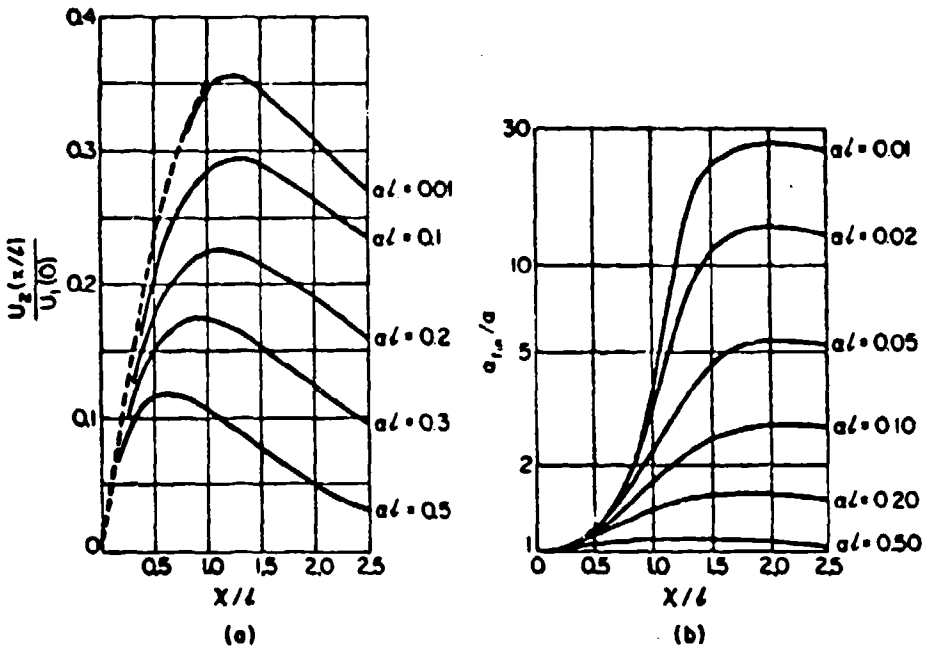

Figure 3-8a.–Calculated values of second harmonic particle velocity as a function of the reduced distance x/ℓ for different values of $\alpha\lambda$. Figure 3-8b.–Total absorption coefficient α_{fin} as a function of the reduced distance x/ℓ for various values of $\alpha\ell$. ℓ is the discontinuity length, α the infinitesimal-amplitude absorption coefficient (from Cook [14]).

3.7 Burgers' Equation.

The analysis of finite amplitude waves in fluids has recently been stimulated by a fresh approach. Consider an equation of the form

$$v_t + vv_x = \delta v_{xx} \tag{3.58}$$

where δ is a constant, and where we have introduced the reduced notation v_x, $\equiv \partial v/\partial x$, v_{xx}, $= \partial^2 v/\partial x^2$, etc. This equation, which is known as Burgers' equation, has two interesting properties. If $\delta = 0$, Eq. (3.58) has the general solution $v = f(x - vt)$, which resembles wave propagation in a nondissipative medium [cf. Eq. (3.29)]. On the other hand, if one assumes the linear approximation of Eq. (3.58) with $\delta \neq 0$, then the solution is in the form of damped waves. Thus, Burgers' equation resembles both extreme cases of the finite amplitude propagation under study. However, unlike the case of Eq. (3.44), Burgers' equation has a known exact solution.

A large number of authors have, with increasing success, attempted to modify the writing of the equations of finite amplitude sound propagation so

as to fit an equation of the Burgers type. In the early (non-acoustic) analyses, the use of the equation was limited to initial value problems. The work of Mendousse (1953) broke new ground,[12] although its meaning for acoustics was not fully appreciated until nearly a decade later.

Let us begin with the Lagrangian formulation of the wave equation for a dissipative medium (in reduced notation)

$$\rho_0 \xi_{tt} = - p_x + \left(\frac{4}{3}\eta + \eta'\right) \xi_{xxt} . \qquad (3.43)$$

To quote from Mendousse's paper:

"In the approximation that will now be described, the only physical feature that needs to be used is the relative stability of the wave, regardless of any assumption of a particular shape. That is, one imagines an observer moving with the wave velocity c, riding the wave, so to speak; and one assumes that only slow changes occur in the state of the medium near this observer (there would be no change at all for a nondissipated, nondistorted wave). In a suitable system of coordinates some of the partial derivatives are then very small and can be neglected in many places where they occur."

As a first step, we use the pressure-density relation (3.19), stopping with the quadratic term, and recall that $s = 1/(1 + \xi_x) - 1$ [Eq. (1.26)], so that approximately

$$p_x = - A\xi_{xx} + 2A\beta\xi_x\xi_{xx} . \qquad (3.59)$$

Equation (3.43) now can be rewritten as

$$\rho_0 \xi_{tt} - b\eta\xi_{xxt} = A\xi_{xx} - 2A\beta\xi_x\xi_{xx} . \qquad (3.60)$$

Since our observer is going to move with the speed c_0, we are in effect making the coordinate transformation $z = x - c_0 t$, $\tau = t$. The various derivatives then transform as follows:

$$\xi_t(z,\tau) = \xi_x z_t + \xi_\tau \tau_t$$

Which, from the definition of z,τ becomes

$$\xi_t(z,\tau) = - c_0\xi_z + \xi_\tau .$$

Similarly,

$$\xi_{tt} = c_0^2 \xi_{zz} - 2c_0 \xi_{x\tau} + \xi_{\tau\tau}$$
$$\xi_x = \xi_z$$
$$\xi_{xx} = \xi_{zz} \tag{3.61}$$

so that Eq. (3.60) becomes

$$\rho_0 \xi_{\tau\tau} - 2\rho_0 c_0 \xi_{z\tau} + 2\rho_0 c_0^2 \beta \xi_z \xi_{zz} - \left(\frac{4}{3}\eta + \eta'\right) \xi_{zz\tau} + \left(\frac{4}{3}\eta + \eta'\right) c_0 \xi_{zzz} = 0 \tag{3.62}$$

with $\beta \equiv 1 + B/2A$, $A = \rho_0 c_0^2$.

Thus far, we would have appeared to make things worse, but there is hope. We recall from our previous analysis that the linear approximation for the particle displacement ξ is

$$\xi = \xi_0 e^{-\alpha x} \cos(\omega t - kx) ,$$

or, in the transformed variables,

$$\xi(z,\tau) = - \xi_0 e^{-\alpha(z + c_0\tau)} \cos kz . \tag{3.63}$$

We now attempt to estimate the relative size of the terms in (3.62). We recall that $\alpha^2 << k^2$, so that $\alpha = (1/2)(b\omega^2 n/\rho_0 c_0^3)$.

In magnitude, differentiation with respect to τ multiplies the function ξ by αc_0 while differentiation with respect to z multiplies it by k. Using the definitions of α, b, we can write the orders of the terms in (3.62) as

Term	Order of Magnitude
$\rho_0 \xi_{\tau\tau}$	$\xi_0 \rho_0 c_0^2 \alpha^2$
$- 2\rho_0 c_0 \xi_{z\tau}$	$\xi_0 \rho_0 c_0^2 \alpha k$
$2\rho_0 c_0^2 \beta \xi_z \xi_{zz}$	$\xi_0 \rho_0 c_0^2 k^3 \beta \xi_0$
$-\left(\frac{4}{3}\eta + \eta'\right) \xi_{zz\tau}$	$\xi_0 \rho_0 c_0^2 \alpha^2$
$\left(\frac{4}{3}\eta + \eta'\right) c_0 \xi_{zzz}$	$\xi_0 \rho_0 c_0^2 \alpha k$.

(3.64)

It is evident that the first and fourth terms are of higher order. We therefore neglect them and rewrite our equation as

$$-2\rho_0 c_0 \xi_{z\tau} + 2\rho_0 c_0^2 \beta \xi_z \xi_{zz} + b\eta c_0 \xi_{zzz} = 0 \tag{3.65}$$

which is of the form of Burgers' equation if we set $v = \partial\xi/\partial z = \xi_z$.

One could just as well have employed a retarded time $\tau = t - x/c_0$, $z = x$ (so that $\xi = \xi_0 e^{-\alpha z} \cos \omega\tau$), and make similar approximations. The derivation is somewhat lengthier, but eventually one emerges with the result

$$c_0^3 u_z - \beta c_0 u u_\tau = \frac{1}{2}\frac{b\eta}{\rho_0} u_{\tau\tau} = \frac{c_0^3 \alpha}{\omega^2} u_{\tau\tau} \tag{3.66}$$

which is the form of Burgers' equation used by Blackstock. [15]*

Equation (3.66) can be further reduced, to nondimensional form, by dividing by $\beta u_0^2 c_0 (2\pi/x)$ and introducing the notation $W = u/u_0$, $\sigma = z/\ell$, $y = \omega\tau$ and $\Gamma = \beta (u_0/c_0\alpha)(2\pi/\lambda) = 1/\alpha\ell$.** The result is

$$W_\sigma - WW_y = \frac{1}{\Gamma} W_{yy} \tag{3.67}$$

---

*Blackstock also includes the heat conduction losses, which have the effect of adding the quantity $(\gamma - 1)/Pr$ to the viscosity number b in the term on the right in Eq. (3.66). Here γ is the ratio of specific heats and Pr is the Prandtl number $= \eta c_p/\kappa$, where κ is the thermal conductivity. The relation $(1/2)(\eta/\rho)[b + (\gamma - 1)/Pr]$ is equal to $\alpha c_0(\lambda/2\pi)^2$ for a sound wave of length λ and absorption coefficient α.

**Soviet writers often speak of the Reynolds number (Re) in this connection, but the definition varies. Thus Khokhlov and Soluyan [16] use

$$\mathrm{Re} = \frac{\beta}{2\alpha}\frac{u_0}{c_0^2}\omega = \frac{\Gamma}{2}$$

while Naugolnykh [17] and Goldberg [18] use

$$\mathrm{Re} = \frac{\rho_0 v_0 \lambda}{2\pi b} = \frac{1}{2\alpha}\frac{u_0}{c_0^2}\omega = \frac{\Gamma}{2\beta}.$$

We have avoided its use, because of the ambiguity, and retain Γ to which the name *Goldberg number* is sometimes given.

which is of the same form as Eq. (3.58). If we make the change of variable

$$W = \frac{2}{\Gamma\zeta}\,\zeta_y = \frac{2}{\Gamma}\,\frac{\partial \ln \zeta}{\partial y} \tag{3.68}$$

Eq. (3.67) reduces to the diffusion equation

$$\zeta_\sigma = \frac{1}{\Gamma}\,\zeta_{yy} \,. \tag{3.69}$$

The solution satisfying the usual boundary conditions has been developed in detail by Blackstock. The final form for ζ is

$$\zeta = I_0\left(\frac{\Gamma}{2}\right) + 2\sum_{n=1}^{\infty}(-1)^n\, I_n\left(\frac{\Gamma}{2}\right) e^{-n^2\alpha x}\,\cos ny$$

We can then recover $u = u_0 W$ from (3.68):

$$\frac{u}{u_0} = \frac{\displaystyle\sum_{n=1}^{\infty}(-1)^{n+1}\, nI_n\left(\frac{\Gamma}{2}\right) e^{-n^2\alpha x}\,\sin\, n(\omega t - kx)}{I_0\left(\frac{\Gamma}{2}\right) + 2\displaystyle\sum_{n=1}^{\infty}(-1)^n\, I_n\left(\frac{\Gamma}{2}\right) e^{-n^2\alpha x}\,\cos\, n\,(\omega t - kx)} \tag{3.70}$$

where I_n is the Bessel function of order n of imaginary argument:

$$I_n(z) = i^{-n} J_n(iz) \,.$$

The solution (3.70) is quite a complete one, but its form has thus far prevented any simple expression of it. As Blackstock has pointed out, what we desire is the Fourier series

$$\frac{u}{u_0} = \sum_{n=1}^{\infty} B_n\,\sin\, n\,(\omega t - kx) \tag{3.71}$$

but what we have is its logarithmic derivative. Various computer methods exist to evaluate (3.70), the results of which are very similar to those obtained by Cook (see Fig. 3-8). The extra attenuation of the fundamental, due to finite amplitude effects

$$EXDB = - 20 \log_{10} \frac{B_1}{e^{-\alpha x}} \tag{3.72}$$

has been computed by Blackstock for various values of Γ (Fig. 3-9).

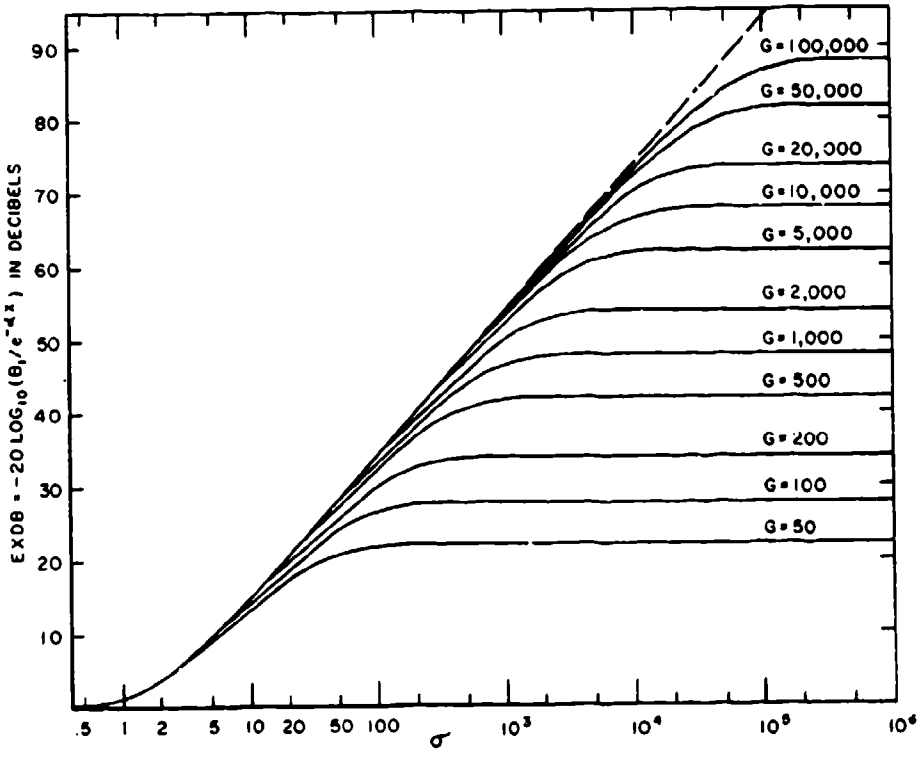

Figure 3-9.–Curves of *EXDB* for values of Γ (written *G* in figure) computed for Eq. (3.73) and similar approximation. The dashed curve is the asymptote *EXDB* = 20 log [(σ + 1)/2] (from Blackstock [15]).

The asymptotic form of (3.63) for large Γ has also been studied by Blackstock, following the original treatment of Cole.[19] Several orders of approximation are given, the highest being

$$\frac{u}{u_0} = \frac{2}{\Gamma} \sum \frac{\left[1 - \frac{n}{\Gamma^2} \coth \frac{n}{\Gamma}(1+\sigma)\right]}{\sinh \frac{n}{\Gamma}(1+\sigma)} \sin n\,(\omega t - kx) \,. \tag{3.73}$$

If the coth term is neglected, Eq. (3.73) reduces to the Fay solution (3.49), provided that $x_0 = \ell$ in that equation.

Equation (3.73)—the "improved" Fay solution—is highly reliable for $\sigma > 3$, $\Gamma \geq 50$.

3.8 Blackstock's Bridging Function.

In 1966, Blackstock[20] proposed a method for connecting the Fubini solution at short distances from the source with the approximate sawtooth solution of Fay that is valid at larger distances.* To establish this connection, we assume that the particle velocity at $x = 0$ is given by $u = u_0 \sin \omega t$ or

$$W = \sin \Phi \tag{3.74}$$

where $W = u/u_0$ and $\Phi = \omega t$, t being the time.

A particular value of the particle velocity u (or W) travels at the constant speed v in a nondissipative medium, where v is given by Eq. (3.28)

$$v = c_0 \left(1 + \frac{B}{2A} \cdot \frac{u}{c_0}\right)^{\frac{2A}{B} + 1} . \tag{3.28}$$

This displacement velocity at the space point x and time t would have originated from the point $x = 0$ at an earlier time t' given by

$$t - t' = \frac{x}{v} \simeq \frac{x}{c_0} \left(1 - \beta \frac{u}{c_0}\right) \tag{3.75}$$

where the binomial expansion has been used for the expression in parentheses in Eq. (3.28) under the assumption that $Bu/2Ac_0 \ll 1$ (small Mach number).

The amplitudes B_n of the various harmonics of the distorted wave [Fubini solution, Eq. (3.38)] are given by Eq. (3.39), which we now write in the notation

$$B_n = \frac{2}{\pi} \int_0^{\pi} W \sin ny \, dy \tag{3.76}$$

where $y = \omega t - kx$.

*It has been noted by at least one observer that this actually is a separate approximate solution, valid for intermediate ranges.

As the wave travels out from the source, it undergoes progressive distortion until the point $x = \ell$ is reached at which the shock front first appears, with the slope dW/dy becoming negatively infinite at that point. As the wave progresses further, the interval of infinite negative slope becomes steadily greater, i.e., the step in the velocity profile (the shock front) increases in strength. All that we are saying is that, since the quantity W cannot become multivalued, more and more of the wave "piles up" at the front marked by $u = 0$. This process is illustrated in Fig. 3-10.

The initially sinusoidal wave at $x = 0$ (Fig. 3-10a) has just reached the condition where $\partial W/\partial y \to \infty$ at just the point $u = 0$ in (b). In (c), a considerable part of the wave has reached the shock front, so that a large velocity jump appears at $u = 0$. Fig. 3-10*d* shows the virtually completed sawtooth formation.

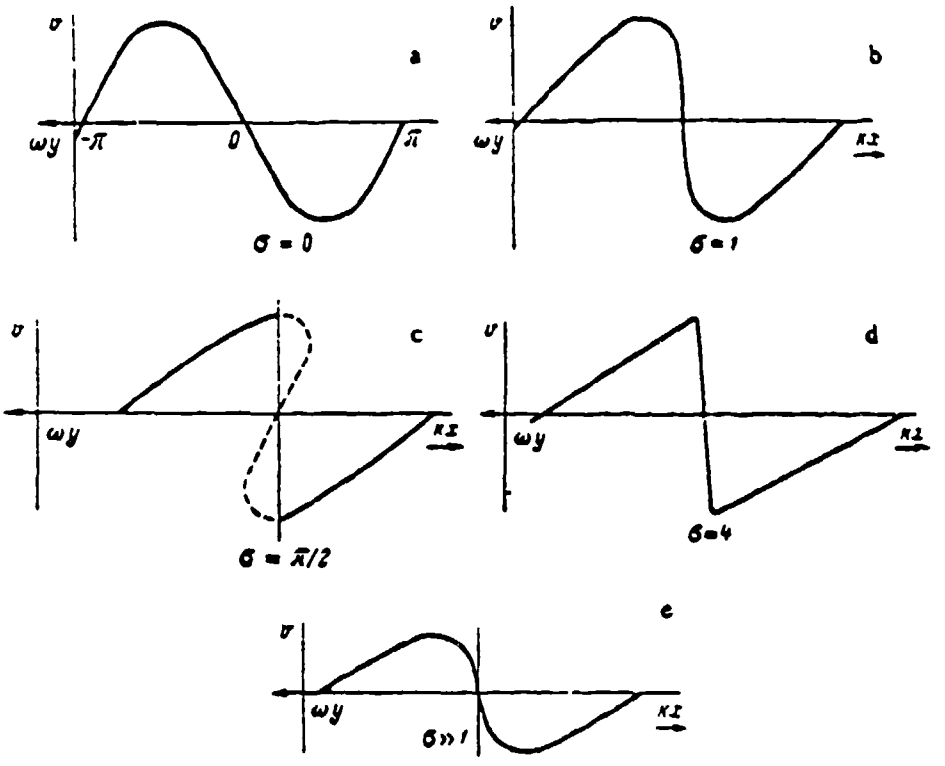

Figure 3-10.–Distortion of waveform during propagation (after Naugol'nykh [17], p. 16).

In order to treat the altered conditions for $x > \ell$, we rewrite Eq. (3.75) in the form

$$t' = t - \frac{x}{c_0} + \beta \frac{ux}{c_0^2}$$

or, using the definition of Eq. (3.33)

$$t' = t - \frac{x}{c_0} + \frac{x}{\omega \ell} \frac{\mu}{u_0}$$

so that

$$\Phi = \omega t' = \omega t - kx + \frac{x}{\ell} W$$

or

$$\Phi = y + \sigma \sin \Phi \ . \tag{3.77}$$

if we now return to Eq. (3.76), we have

$$B_n = \frac{2}{\pi} \int_{y=0}^{y=\pi} \sin \Phi \sin ny \, dy$$

$$= \frac{2}{n\pi} \left[- \sin \Phi \cos ny \Big|_{y=0}^{y=\pi} + \int_{y=0}^{y=\pi} \cos ny \cos \Phi \, d\Phi \right]. \tag{3.78}$$

When $\Phi = \pi$, $y = \pi$ [from Eq. (3.77)]. As y decreases, Φ falls, not necessarily to zero, but to Φ_{min}, where

$$\Phi_{\min} = \sigma \sin \Phi_{\min} \ .$$

We can then rewrite Eq. (3.78)

$$B_n = \frac{2}{n\pi} \sin \Phi_{\min} + \frac{2}{n\pi\sigma} \int_{y=0}^{y=\pi} \cos ny \, d(\Phi - y) \ ,$$

since $d(\Phi - y) = \sigma \cos \Phi \, d\Phi$ from (3.77). But

$$\int_0^{\pi} \cos ny \, dy = 0$$

so that B_n finally becomes

$$B_n = \frac{2}{n\pi} \sin \Phi_{\min} + \frac{2}{n\pi\sigma} \int_{\Phi_{\min}}^{\pi} \cos n(\Phi - \sigma \sin \Phi)\, d\Phi \ . \quad (3.79)$$

If $\sigma \leqslant 1$, $\Phi_{\min} = 0$, the first term on the right-hand side of (3.79) vanishes, while the second becomes the Fubini amplitudes of (3.39). For $\sigma > 1$, i.e., in the shock region, the first term begins to increase. It can be shown that for very large values of σ, this term has the asymptotic value of $2/n\ (1 + \sigma)$, which defines the relative amplitudes of the components of a sawtooth. At the same time, $\Phi_{\min} \to \pi$, so that the second term on the right vanishes. Thus a smooth transition is made from one solution to the other. A sample of this transition is shown in Fig. 3-11.

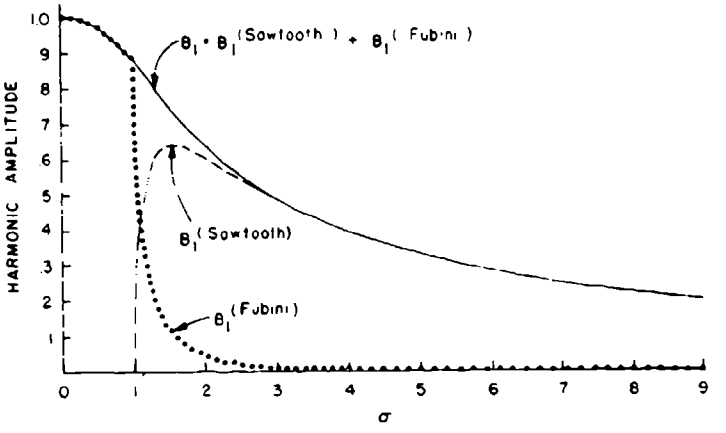

Figure 3-11.–Amplitude of first harmonic vs. distance. 1–first term on right side of eq. (3.79) (n = 1); 2–second term; 3–total B_1 (after Blackstock [20]).

3.9 Work of Soluyan and Khokhlov.

An excellent summation of our understanding of the distortion problem has been made by Khokhlov and Soluyan. [16] They examined in detail the representation for ζ in Eq. (3.68). This solution can be written as the summation

$$\zeta = 2 \sum_{n=0}^{\infty} (-1)^n J_n \left(\frac{\Gamma}{2}\right) e^{-n^2 \alpha x} \sin nZ \quad (3.80)$$

where $Z = \omega t - kx$, or as an integral,

$$\zeta = \frac{1}{\sqrt{4\pi\alpha x}} \int_{-\infty}^{\infty} \exp\left[-\frac{\Gamma \cos Z}{2} - \frac{\Gamma (Z - Z_0)^2}{2}\right] dZ . \qquad (3.81)$$

If one considers the integrand of Eq. (3.81)

$$Y = \exp\left[-\frac{\Gamma \cos Z}{4\ell} - \frac{\Gamma (Z - Z_0)^2}{2\ell}\right] \qquad (3.82)$$

one can see that for Γ ($= 1/\alpha\ell$) small, the first term is small and the principal contribution to the integral comes from the second term in the neighborhood of $Z = Z_0$. If Γ becomes large, however, the function will have peaks in the neighborhood of $Z = \pm \pi$. This latter condition leads to the result

$$W = \frac{u}{u_0} = \frac{1}{1 + \sigma}\left[-Z + \pi \tanh \frac{\pi\Gamma Z}{2(1 + \sigma)}\right]. \qquad (3.83)$$

Here it is required that $\sigma > 1 + 2/\Gamma$.

Soluyan and Khokhlov therefore break up the solution of Burgers' equation into three zones.

(1) From the source to a point x such that $\sigma_1 = x_1/\ell < 1$. Here the dissipative effects can largely be ignored and the Fubini solution applies.

(2) From the neighborhood of x_1 to some point x_2; here, both dissipative and nonlinear effects must be considered simultaneously. The point x_2 is defined as

$$x = \frac{2\Gamma}{Mk} = \frac{2\beta}{\alpha} .$$

(3) From x_2 on. Here the sawtooth has decayed into what is predominantly a damped harmonic. In fact the first two terms are

$$\frac{u}{u_0} = \frac{4}{\Gamma}\left[e^{-\alpha x} \sin Z + e^{-2\alpha x} \sin Z\right]. \qquad (3.84)$$

The wave shape in the second region can easily be calculated from Eq. (3.83). Figure 3-12 shows u/u_0 for the case $\Gamma = 10$, which corresponds to a peak initial p/f of 1.5 atm/MHz. The plot is shown for the values of $\sigma = 1, 5, 29$—the vertical scale in the last case being multiplied by 50. This relation

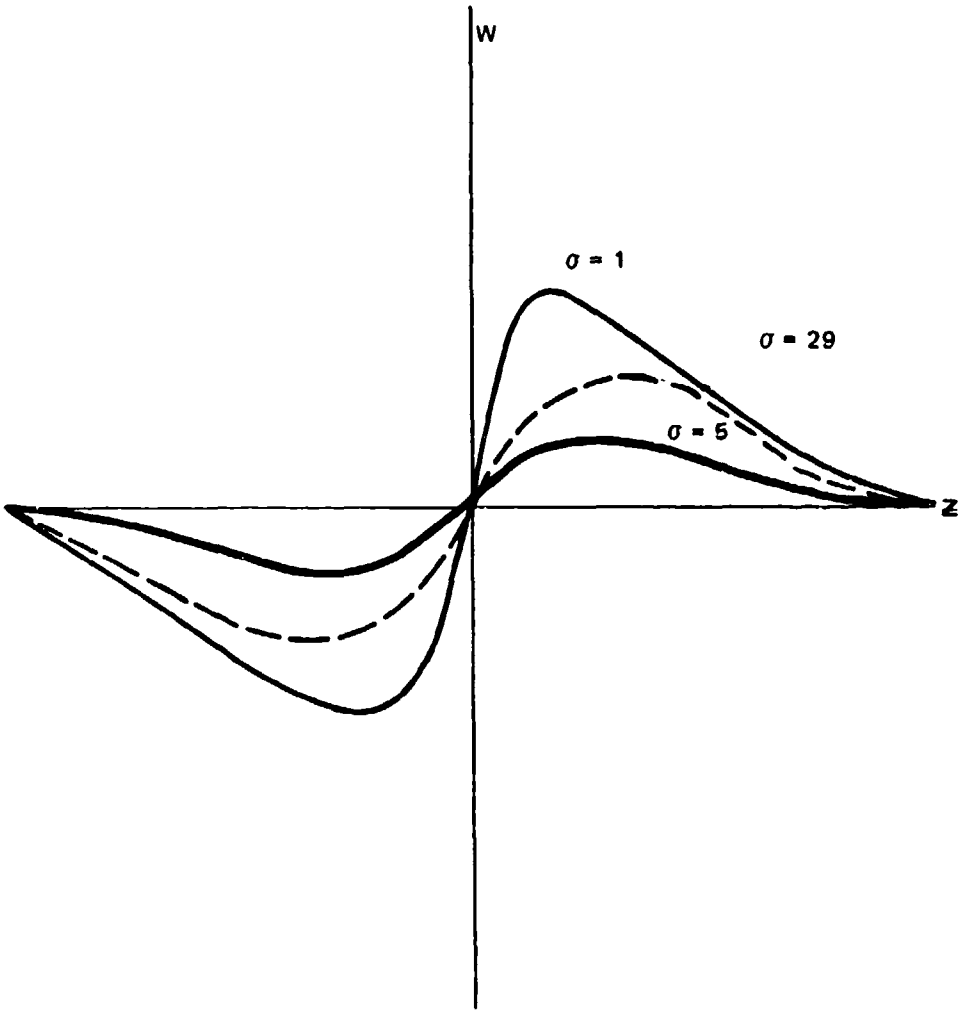

Figure 3-12.–Wave form from Eq. (3.83) for various σ.

(3.83) has suffered surprising neglect in the study of nonlinear propagation although, as Blackstock has pointed out, Eq. (3.83) is an exact solution of the Burgers' Eq. (3.67).

From Eq. (3.83) we can also deduce an expression for the effective thickness of the wave front–the distance between the crest and trough of the wave. Neglecting the slight variation of σ over a distance of a single wavelength, we have

$$\frac{dW}{dZ} = \frac{1}{1 + \sigma}\left[1 + \frac{\pi}{\Delta}\operatorname{sech}^2\frac{Z}{\Delta}\right] \tag{3.85}$$

where $\Delta = 2(1 + \sigma)/\pi\Gamma$. The extrema therefore occur at Z_m such that

$$Z_m = \pm \Delta \cosh^{-1} \sqrt{\pi/\Delta} \tag{3.86}$$

so that the thickness T will be

$$T = 2Z_m = 2\Delta \cosh^{-1} \sqrt{\pi/\Delta} \, . \tag{3.87}$$

Since $Z = \omega t - kx$, T is measured in radians. The physical distance corresponding to T will be

$$\frac{T}{2\pi} \lambda = \frac{\omega' \Gamma}{c} .$$

Table 3.3 shows the thickness of the front for the cases examined in Fig. 3-12.

Table 3.3

Γ = 10

σ	Δ, ra	T	$T/2\pi$ (fraction of a period)
1	0.127	0.58	0.092
5	0.382	1.30	0.207
29	1.91	2.87	0.465
sine wave			0.5

3.10 Spherical and Cylindrical Waves of Finite Amplitude.

Thus far, our analysis of finite amplitude wave in this chapter has been limited to plane waves. We must now consider spherical and cylindrical waves. We shall not repeat the complexities of Section 3.5 in the adaptation of the

acoustic equation to fit Burgers' equation, but point out that a general form corresponding to Eq. (3.66) can be obtained. [10] It is

$$u_r + n\frac{u}{r} - \frac{\beta}{c_0} uu_\tau = \frac{b\eta}{2\rho_0 c_0^3} u_{\tau\tau} . \tag{3.88}$$

Here $n = 1, 1/2$ and 0 for spherical, cylindrical and plane waves.

A number of attempts have been made to generalize Burgers' equation to include the cylindrical and spherical cases. The most significant of these are those of Naugolnykh and coworkers [21] and the stretched coordinate concept of Blackstock. [22] A summary of work in this area has been given by Cary. [24]

In the stretched coordinate representation, Burgers' equation can be written as

$$W_f - WW_Z = EW_Z \tag{3.89}$$

where

$$W = \left(\frac{\sigma}{\sigma_0}\right)^a \frac{u}{u_0}$$

$$Z = \omega\left(t - \frac{x}{c_0}\right)$$

$$\sigma = \frac{x}{\ell}$$

$$\sigma_0 = \frac{x_0}{\ell}$$

x_0 = source radius (for spheres and cylinders)

x = field position in all three cases

(3.89a)

The definitions a, f and E are given in Table 3.4.

While this representation appears to make the spherical and cylindrical cases solvable by analogy with the plane wave case, that is not so. This is due especially to the variable behavior of the coefficient E.

Table 3.4

Notation in Generalized Burgers' Equation

Type of wave	a	W	f	E
Plane	0	u/u_0	σ	Γ^{-1}
Cylindrical	1/2	$\left(\frac{\sigma}{\sigma_0}\right)^{1/2}\frac{u}{u_0}$	$2[(\sigma\sigma_0)^{1/2}-\sigma_0]$	$\left(1+\frac{f}{2\sigma_0}\right)^{\Gamma-1}$
Spherical	1	$\left(\frac{\sigma}{\sigma_0}\right)\frac{u}{u_0}$	$\sigma_0 \ln\frac{\sigma}{\sigma_0}$	$\exp\left(\frac{f}{\sigma_0}\right)^{\Gamma-1}$

An interesting technique has been developed by Banta [23] and Cary [24] for the problem at hand. In this method, the function $W(f,Z)$ is expanded in a Taylor's series about the point $f=0$:

$$W(f,Z) = \sum_{n=0}^{\infty} \frac{f^n}{n!} \frac{\partial^n}{\partial f^n} W(0,Z) \equiv \sum_{n=0}^{\infty} \frac{f^n}{n!} D_f^n W(0,Z) \ . \qquad (3.90)$$

Further use of Eqs. (3.89), (3.90) involve approximations. A few special examples will be considered here. If we limit ourselves to zone 1 of Sec. 3.9 and large values of the Goldberg number Γ, ($\Gamma > 5$) we can assume that the terms containing Γ^{-1} in Eq. (3.89) (EW_{ZZ}) are small in comparison with WW_Z.

We therefore expand the various derivatives D_f^n. By repeated use of the approximations just stated, one can obtain a simplified expression for the derivatives. The final solution for plane wave is then

$$W(f,Z) = \sum_{n=0}^{\infty} \frac{f^n}{(n+1)!} \left[D_Z^n W^{n+1}(0,Z)\right] + ED_Z \sum_{n=1}^{\infty} \frac{f^n}{n!} D_Z^n \left[\frac{W^n(0,Z)}{n}\right] . \qquad (3.91)$$

A similar expression can be obtained for spherical waves. Since it is quite cumbersome, it will not be written out here (see ref. 24, p. 1371).

These expressions can be used with the computer to give detailed information about the initial stages of the finite amplitude beam and are especially useful in treating parametric arrays (see Chapters 9, 10).

3.11 Case of a Relaxing Medium.

Thus far, we have considered the propagation of a finite-amplitude wave only in a nonrelaxing medium, in which α is proportional to ω^2. We shall now consider the relaxing case, under the limitation that the velocity dispersion is small, i.e., that the relaxation strength $\epsilon = (c_\infty^2 - c_0^2)/c_0^2 \ll 1$.

The derivation involves the addition of a quadratic term in ρ to the relationship between p and ρ and the introduction of the quantity ζ,* known as the degree of reaction in the equation for the Helmholtz free energy F:

$$dF = -SdT - pdV - Ad\zeta \tag{3.92}$$

where A is known as the chemical affinity. As ζ goes from 0 to 1, the reaction (which here would be the internal state of the system) proceeds from a state where there are only reactants to a state where there are only products. An equation such as (3.92) was used in the derivation of (1.58).

We now form the expression for the sound velocity. Since $c^2 = (\partial p/\partial \rho)_s$, we need to evaluate $\partial p/\partial \rho$ in terms of the new variable ζ:

$$dP = \left(\frac{\partial p}{\partial \rho}\right)_\zeta d\rho + \left(\frac{\partial p}{\partial \zeta}\right)_\rho d\zeta$$

or

$$\left(\frac{dP}{d\rho}\right)_s = \left(\frac{\partial p}{\partial \rho}\right)_\zeta + \left(\frac{\partial p}{\partial \zeta}\right)\left(\frac{\partial \xi}{\partial \rho}\right)_s . \tag{3.93}$$

If we now introduce the rate equation

$$\tau_r \frac{\partial \zeta}{\partial t} = -(\zeta - \zeta_0) , \tag{3.94}$$

where the subscript r has been added to the symbol for the relaxation time to distinguish it from the τ used for the retarded time in the Burgers analysis, we

*For a more complete discussion of the degree of reaction, see Beyer and Letcher, Chapter 4.

can parallel the development given by Beyer and Letcher* to obtain the relaxational equation

$$\dot{p}_e - \left(c_\infty^2 + \frac{B}{A} c_0^2 s\right) \rho_0 \dot{s} + \frac{1}{\tau_r}\left(p_e - \rho_0 c_0^2 s - \rho_0 c_0^2 \frac{B}{A} s^2\right) = 0 . \tag{3.95}$$

Then making the transition to the retarded time representation, we have approximately

$$\frac{\partial u}{\partial z} - \frac{\beta}{c_0^2} u \frac{\partial u}{\partial \tau} = -\frac{P\tau_r}{2\rho_0 c_0^2} \frac{\partial^2 \zeta}{\partial \tau^2}$$
$$\tau_r \frac{\partial \zeta}{\partial \tau} + \zeta = -\frac{\epsilon \rho_0 c_0 u}{P} . \tag{3.96}$$

Here $P = (\partial p/\partial \zeta)\rho_0$ and ϵ are both small quantities.

In an effort to provide at least a partial solution of Eqs. (3.96), Soluyan and Khokhlov [25] examined possible solutions in the limiting cases $\omega\tau \ll 1$ and $\omega\tau \gg 1$.

(1) $\omega\tau \ll 1$.

As before, we divide the path of propagation into three parts:

(a) In the first region, the dissipative effects are negligible. This is equivalent to setting the right side of the first of Eqs. (3.96) equal to zero; i.e.,

$$\frac{\partial u}{\partial z} - \frac{\beta}{c_0^2} u \frac{\partial u}{\partial \tau} = 0 \tag{3.97}$$

subject to the boundary condition $u = u_0 \sin \omega t$ for $x = 0$. This equation has the solution given by Eq. (3.42),

$$Z = \sin^{-1} \frac{u}{u_0} - \sigma \frac{u}{u_0} \tag{3.98}$$

($Z = \omega t - kx$), i.e., the same result that was obtained in the nonrelaxing case.

Op. cit., pp. 99-102.

(b) Beginning at $\sigma = 1$, the second region is that for which the approximate sawtooth is undergoing slow decay. To solve Eqs. (3.96) in this case, we write

$$\frac{\partial u}{\partial z} + \frac{\partial G}{\partial \tau} = 0$$
$$\tau_r = \frac{\partial \zeta}{\partial \tau} + \zeta = - \frac{\epsilon \rho_0 c_0}{P} u \tag{3.99}$$

where

$$G = - \frac{\beta}{2c_0^2} u^2 + \frac{P \tau_r}{2\rho c_0^2} \frac{\partial \zeta}{\partial \tau} . \tag{3.100}$$

If dissipation is neglected, $P = 0$ and a plot of $-G$ vs. τ would be the solid curve in Fig. 3-13. This curve is equivalent to a perfect sawtooth at $\tau = 0$.

When the relaxation loss is taken into account, the wave front takes on a finite steepness, as in the case of Fig. 3-12. In such a case, u is a rapidly decreasing function of τ near $\tau = 0$, so that the second term on the right in Eq. (3.100) is virtually a constant near $\tau = 0$, giving (3.100) the dashed form in Figure 3-13. Hence G is constant over most of the wave front. This is equivalent to the condition $\partial u/\partial z = 0$ and yields the solution

$$\frac{\partial u}{\partial \tau} = \frac{1}{2\tau_r} \frac{u_1^2 - u^2}{\frac{\epsilon c_0}{2\beta} + u} \tag{3.101}$$

where

$$u_1 = \frac{u_0}{1 + \beta\omega \frac{u_0^2}{c_0^2}} \tag{3.102}$$

is the limiting jump in the amplitude of the (velocity) sawtooth.

If Eq. (3.101) is integrated, one gets

$$\frac{Z + Z_0}{\tau} = \ln \frac{(u_1 + u)^{\kappa - 1} u_1^2}{(u_1 - u)^{\kappa + 1}} \tag{3.103}$$

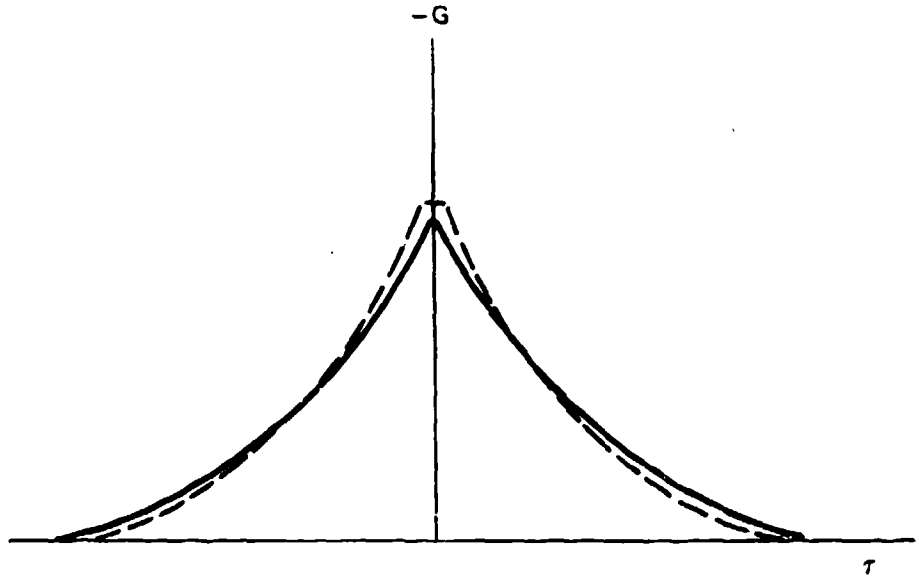

Figure 3-13.–Plot of Eq. (3.100) (after Soluyan and Khokhlov [25]).

where

$$\kappa = \frac{c_\infty^2 - c_0^2}{2\beta c_0 u_2} \tag{3.104}$$

For large κ, this combination yields the result

$$u - u_1 \tanh\left(\frac{Z}{2\kappa\tau_r}\right) \tag{3.105}$$

which, when matched with the sawtooth, gives

$$u = \frac{u_0}{1+\sigma}\left[-Z + \pi \tanh\left(\frac{Z}{\Delta}\right)\right] \tag{3.106}$$

which is similar to (3.83), except that Δ here has the form

$$\Delta = \frac{1+\sigma}{\pi}\,\frac{2}{\Gamma'} \tag{3.107}$$

where $\Gamma' = u_0/c_0\epsilon\omega\tau_r$.

Actually, this presents nothing basically new. As long as $\omega\tau_r \ll 1$, the absorption coefficient is proportional to ω^2 and could have been introduced

through a bulk viscosity added to $(4/3)\eta$ (η is the shear viscosity). Thus, if we express the shear viscosity in terms of a relaxation time τ_{sh}, then

$$\frac{4\eta}{3} = \tau_{sh}\rho_0\epsilon c_0^2 \ , \ \Gamma' \to \Gamma$$

and Eq. (3.106) reduces to the precise form of (3.83).

(2) $\omega\tau >> 1$

We first write the integral solution of the second of Eqs. (3.96):*

$$\zeta = -\frac{\epsilon\rho_0 c_0}{P\tau_r}\int_{\tau-\frac{2\pi}{\omega}}^{\tau} u(\tau')\exp\left(\frac{\tau'-\tau_r}{\tau_r}\right)d\tau' \cdot \left[1-\exp\left(\frac{-2\pi}{\omega\tau_r}\right)\right]^{-1} . \tag{3.108}$$

An approximate expression for $\partial^2\zeta/\partial\tau^2$ can be found by expanding the exponential in the integrand of Eq. (3.108) in a power series and differentiating the resultant expression for ζ twice with respect to τ:

$$\frac{\partial^2\zeta}{\partial\tau^2} = -\frac{\epsilon\rho_0 c_0}{P\tau_r}\left[\frac{\partial u}{\partial\tau} - \frac{1}{\tau_r}(u-u_{av})\right] \tag{3.109}$$

where u_{av}, the constant part of the velocity, is given by

$$u_{av} = \frac{\omega}{2\pi}\int_{\tau-\frac{2\pi}{\omega}}^{\tau} u(\tau')\,d\tau' = 0$$

for our original boundary conditions.

Equation (3.109) can then be substituted in Eqs. (3.97), (3.100) to yield

$$\frac{\partial u}{\partial z} - \frac{\beta}{c_0^2}\left(u+\frac{\epsilon c_0}{2\beta}\right)\frac{\partial u}{\partial\tau} + \frac{\epsilon}{2c_0\tau_r}u = 0 \tag{3.110}$$

*Sotuyan and Khokhlov, ref. 25, p. 172.

which has the solution

$$\omega\tau = \sin^{-1}\left(\frac{ue^{\lambda x}}{u_0}\right) = \frac{\beta\omega u_0}{\lambda c_0^2}\left(1 - e^{-\lambda x}\right)\frac{u}{u_0}e^{\lambda x} \tag{3.111}$$

$$- \omega\tau_r\lambda x$$

where

$$\lambda = \frac{\epsilon}{2c_o\tau_r} . \tag{3.112}$$

The third term in (3.103) is the modification of the equation due to the velocity change from c_0 to c_∞. The rest of the equation can be seen to be of the same form as Eq. (3.42) and can therefore be analyzed graphically in the same way. That is, we plot $\omega\tau$ vs. $ue^{\lambda x}/u_0$ which is then the sum of the inverse sine function and a straight line with slope $-Z$, where

$$Z = \frac{\beta\omega u_0}{c_0^2\lambda}\left(1 - e^{-\lambda x}\right) \equiv \frac{1}{\ell\lambda}\left(1 - e^{-\lambda x}\right) .$$

Soluyan and Khokhlov refer to Z, which has the dimension of a length in angular units, as the reduced distance. It rises from zero at $x = 0$ to the limiting value $Z_\infty = 2c_0\tau/\epsilon\ell$ as $x \to \infty$.

Now Eq. (3.42) indicates the formation of a shock discontinuity at $\sigma = 1$ (or $x = \ell$). Since Z is the generalization of σ, it follows that no shock front can form if $Z < 1$, and the distortions will be given by Eq. (3.111), which can now be written in the form

$$\omega\tau' = \sin^{-1} We^{\lambda x} - \frac{i}{\lambda\ell}\left(1 - e^{\lambda x}\right)e^{\lambda x} \tag{3.113}$$

where $\tau' = \tau + \epsilon\omega x/2c_0$.

If the initial u_0 is large enough that $Z_\infty >> 1$, the nonlinear effects dominate virtually from the beginning, and one is dealing with a decaying shock wave from $x = \ell$ onwards.

The nonlinear effects in a relaxing medium are summed up by Soluyan and Khokhlov in a graph of the waveform for relatively large distances from the source, but all for the case $\sigma < 1$ (Fig. 3-14).

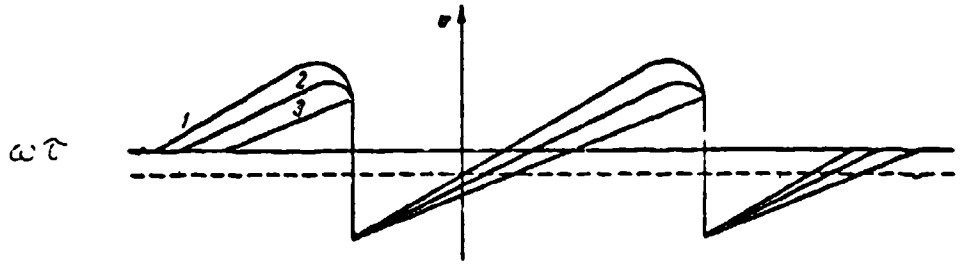

Figure 3-14.–Profile of a finite-amplitude wave in a relaxing medium (after Khokhlov and Soluyan [16]).

Curve 1 corresponds to the case $\omega\tau << 1$, curve 3 to $\omega\tau >> 1$. Since $\omega\tau \simeq 1$ is an intermediate case, involving no special effects, it should be contained between the two curves and is suggested by the dashed curve (z).

The problem of the intermediate case has also been treated approximately in a perturbation analysis. [26] In Eq. (3.45) the term νb refers to the effects of shear and bulk viscosity (we neglect thermal conductivity so that $\nu b = (4\eta/3 + \eta')/\rho_0$. When we operate at a frequency well below the relaxation frequency, α is related to νb by the expression

$$\alpha = \frac{1}{2}\,\frac{\eta b \omega^2}{\rho_0 c_0^3}\,. \tag{3.114}$$

Ryan, Attanasio and Beyer [26] used Eq. (3.114) to replace νb in Eqs. (3.44) ff., employing the value of α corresponding to the frequency involved in each individual term of the inhomogeneous and homogeneous equations. Expressions were found by them for the first few harmonics as a function of distance. In this analysis, all effects of dispersion have been neglected. The terms corresponding to Eqs. (3.47) are

$$u_1 = u_0 e^{-\alpha_1 x} \sin(\omega t - kx) \times$$

$$\left\{1 - \frac{1}{(2\ell)^2(\alpha_2 - 2\alpha_1)}\left[\frac{1}{2\alpha_1} - \frac{1}{\alpha_2} - \frac{1}{2\alpha_1}\,e^{-2\alpha_1 x} + \frac{1}{\alpha_2}\,e^{-\alpha_2 x}\right]\right\} + \cdots$$

$$u_2 = u_0 e^{-2\alpha_1 x} \sin 2(\omega t - kx) \left[1 - e^{-(\alpha_2 - 2\alpha_1)x}\right] \frac{2}{(\alpha_2 - 2\alpha_1)} + \cdots \tag{3.115}$$

3.12 Experimental Verification.

A. Electrical Method. The relations derived in the previous sections have been subjected to a number of experimental tests. It has long been known that the use of too high an intensity in ultrasonic absorption measurements would lead to a higher measured value of α than that obtained at very low intensities. Eventually, a number of observers attempted to measure the absorption coefficient as a function of the initial intensity. Unfortunately, it was not realized in a number of these researches that the value of the effective absorption coefficient would vary with distance from the source, so that this valuable parameter--the range over which the measurement occurred--was not always recorded. Such measurements gave an average effective absorption coefficient over some range, usually 10-40 cm.

Another problem was raised by the fact that the usual detecting instrument was a quartz or ceramic transducer that was sensitive only to odd harmonics of the distorted wave. Nevertheless, surprisingly consistent results were obtained.

In 1935, Thuras, Jenkins and O'Neil [27] made absorption measurements in air. Sound in the frequency range 300-2000 Hz was generated in an air-filled tube 3.8 cm in diameter and 15 m long. The second harmonic signal developed in the tube was measured. While exact quantitative agreement was not to be expected, because of the many approximations involved in this early work, the qualitative aspects of the nondissipative theory were confirmed; namely, that the acoustic pressure of the second harmonic generated was approximately proportional to the distance traveled by the sound, to the frequency used, and to the pressure of the original signal.

In 1954, Fox and Wallace [28] reported measurements on a 5 MHz sound beam with initial intensities up to 4.00 watts/cm^2. Measurements were reported in water and in carbon tetrachloride. In the case of water, at points several centimeters from the source, the rate at which the intensity fell off was equivalent to an absorption coefficient about five times that due to an infinitesimal wave. While they were not able to observe the initial rise in the total absorption coefficient predicted by Eq. (3.48), their results were consistent with a numerical and graphical analysis which they presented.

In 1957, Krasilnikov et al. [29] made a striking improvement in technique by measuring the harmonic content of a beam from a 1.5 MHz source in water. To filter out unwanted harmonics, they used glass or metal plates set at some appropriate angle with respect to the direction of the beam. By suitable choice of plate composition and thickness, as well as the setting angle, they were able to reduce undesired harmonics to a very small amount and thus achieve a harmonic analysis.

A reason for this success can be found in the following way, when one is dealing with the case in which $x > \ell$. In Eq. (3.48) the absorption coefficient

remains fairly constant over the measured region, so that the first objection becomes less significant. In the second place, since the piezoelectric receiver is nearly equally sensitive to all the odd harmonics, we can replace Eq. (3.50) by

$$(p_{ac})_{odd} = \frac{b\eta\omega}{\beta\alpha(x + x_0)} \sum_{1,3,5\ldots} \frac{\sin n(\omega t - kx)}{n}$$

The acoustic intensity will then be

$$I \propto (p_{ac})^2 \text{ odd} = \left[\frac{\eta\omega}{\beta\alpha(x + x_0)}\right]^2 \sum \frac{1}{n^2}$$

and the effective absorption coefficient α_{eff} will be

$$\alpha_{eff} = -\frac{1}{2I}\frac{dI}{dx} = -\frac{d \ln I}{dx} = -\frac{\phi \ln(x + x_0)^{-2}}{dx} = \frac{1}{x + x_0}$$

exactly as before.

Figure 3-15 shows the measured values of the absorption coefficient α_{eff} in water. Here α_{eff}/ν^2 is plotted against $(p_{ac})/\nu$. The slope of the straight portion of this curve is 2×10^{15} cgs units, while the computed slope from Eq. (3.54) is 2.1×10^{15} cgs units, which is far better agreement than the approximate analysis warrants.

Krasilnikov and his coworkers also used a thermal detector to measure the total incident acoustic radiation and recorded effective absorption coefficients up to 30 times the infinitesimal amplitude value.

A modification of the radiation pressure microphone was used by Barnes and Beyer [30] to determine the effective absorption coefficient. In this experiment, the rf carrier wave applied to the transducer is 100% modulated by an audio frequency square wave. As a result, the radiation pressure oscillates at the audio frequency. This signal, whose amplitude is proportional to the ultrasonic intensity, is detected by means of a condenser microphone. In this way, the ultrasonic intensity can be measured at a variety of distances from the source.

The ultrasonic intensity for a specific case is shown in Fig. 3-16, together with the relative intensity obtained from the perturbation analysis. The slope of the continuous curves, which is in each case proportional to the effective absorption coefficient, is seen to begin at the infinitesimal rate (the dashed lines) close to the source, increase to a maximum, and then fall off gradually, once again approaching the infinitesimal amplitude value at the largest distances measured.

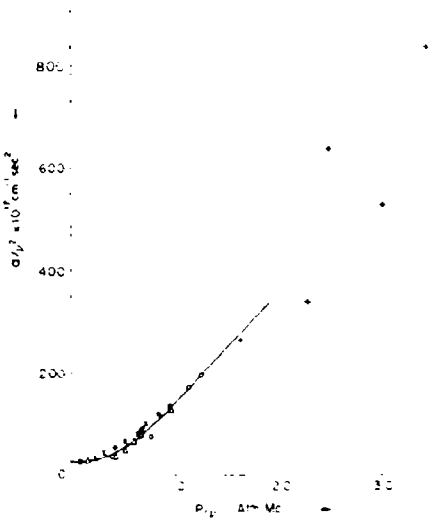

Figure 3-15.–Values of the measured absorption coefficient α in water as a function of the initial pressure p and frequency ν. (+) 1.5 MHz [29]; (○) 3.85 MHz; (○) 5.85 MHz; (×) 6.80 MHz; (△) 8.74 MHz; (○,●,×,△) [29a].

A comparison can also be made here with the Fay theory. From (3.48), the ultrasonic intensity in the sawtooth region is proportional to $1/(x + x_0)^2$, so that

$$\log I = \text{const} - 2 \log (x + x_0) .$$

If $\log I$ is plotted against x, the result will be a curve of fixed shape, which has the limiting value shown in the figure for the case $x_0 = 0$, which corresponds to an infinite source intensity. As x_0 increases, the curve shifts to the left in the diagram. The Fay region for each of the experimental curves can thus be established.

The distorted wave form has also been studied in detail. Progressive distortion of a finite-amplitude wave is shown in Fig. 3-17, while Figs. 3-18, 3-19 show experimental values of the components of initially sinusoidal waves, compared with the theoretical values obtained by perturbation analysis.

B. Optical Methods. Many optical methods have been developed for the study of ultrasonic waves, but the method of optical diffraction has been especially useful in the study of finite-amplitude waves. A schematic diagram of the method is shown in Fig. 3-20. A collimated monochromatic light beam is passed through a tank containing the liquid and the ultrasonic beam. The light is then focused on a screen. Since the sound beam represents a variation in the local index of refraction that is equal to the wavelength of the sound λ,

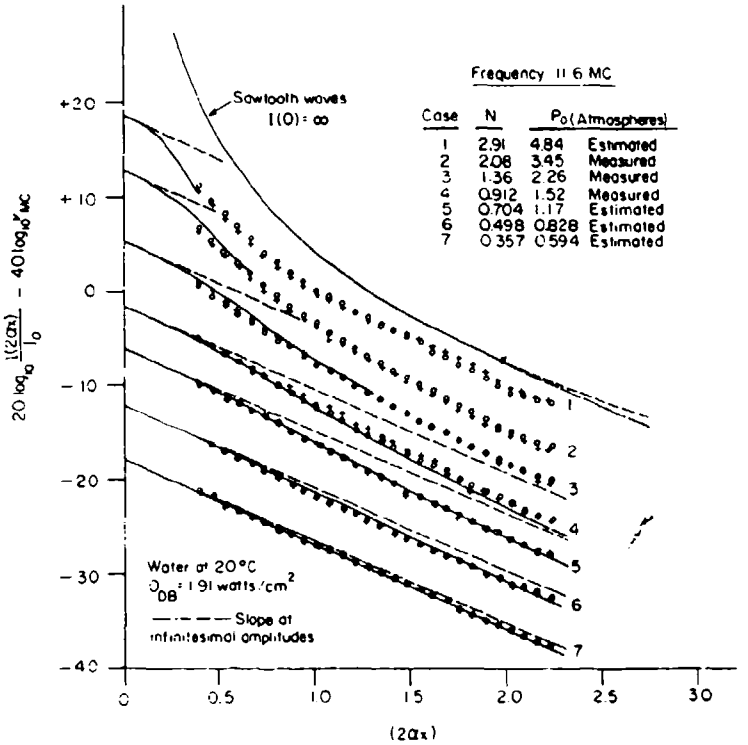

Figure 3-16–Comparison of theoretical and experimental values of the intensity of an 11.6 MHz sound beam in water. The solid line represents values computed from formulas of Keck and Beyer [9], except that the uppermost curve is computed from the Fay [11] theory with $x_0 = 0$. Broken curves indicate intensity computed with the use of infinitesimal amplitude absorption α. $N = 1/4\alpha\ell$ (from Barnes and Beyer [30]).

the system is akin to a diffraction grating. The focusing lens merely assures that the resultant Fraunhofer diffraction pattern will be registered on the screen. Under these circumstances, λ is the grating spacing, and the diffraction formula for the maxima in the diffraction pattern becomes

$$\sin \theta = \frac{n\lambda_\ell}{x}$$

where λ_ℓ is the optical wavelength, θ the angle made by the diffracted way with the horizontal and n is the order of the diffraction image.

The theoretical analysis of this problem for an infinitesimal-amplitude wave was first performed by Raman and Nath, [31] who showed that the intensity of the light in the nth order diffraction image was related to the peak change in the index of refraction $\delta\mu$ in the following way

$$I \propto J_n \left(\frac{2\pi\delta\mu L}{\lambda_\ell}\right)$$

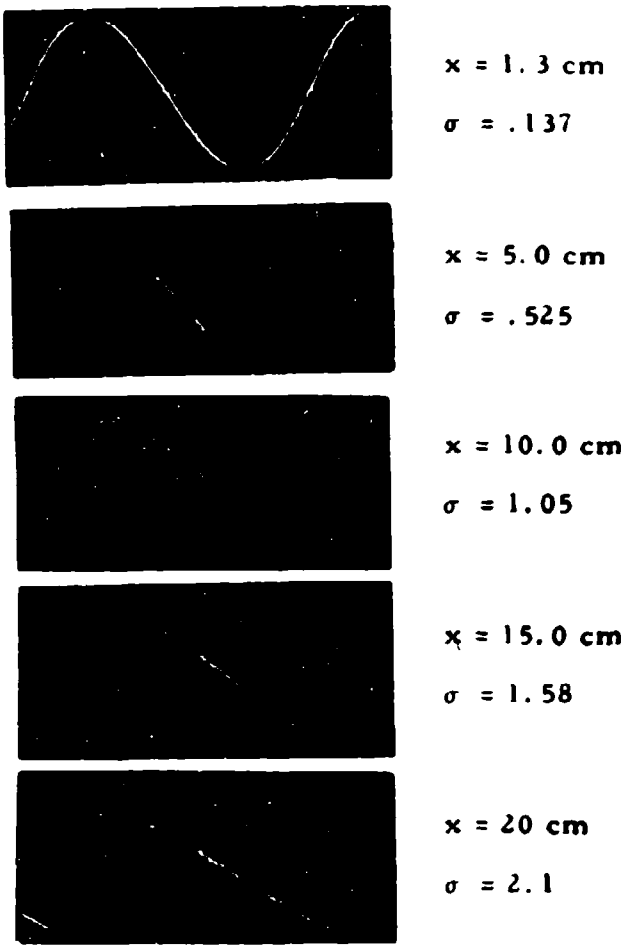

Figure 3-17.–Progressive distortion of waveform in an originally sinusoidal signal. ν = 2.58 MHz, initial acoustic pressure 6.0 atm. The medium was water at 22°C; x is the distance from the source, σ = reduced length = x/ℓ. (a) x = 1.3 cm, σ = 0.137; (b) x = 5.0 cm, σ = 0.525; (c) x = 10.0 cm, σ = 1.05; (d) x = 15.0 cm, σ = 1.58; (e) x = 20 cm, σ = 2.1 (from R. P. Ryan, Ph.D. thesis, Brown University, 1963).

where L is the width of the ultrasonic beam traversed by the light and J_n is the Bessel function of order n. Since $\delta\mu$ is related to the density change $\delta\rho$ by the expression of Lorenz-Lorentz

$$\frac{\delta\mu}{\mu} = \frac{\delta\rho}{\rho_0}\left[\frac{(\mu^2+2)(\mu^2-1)}{6\mu^2}\right] \tag{3.116}$$

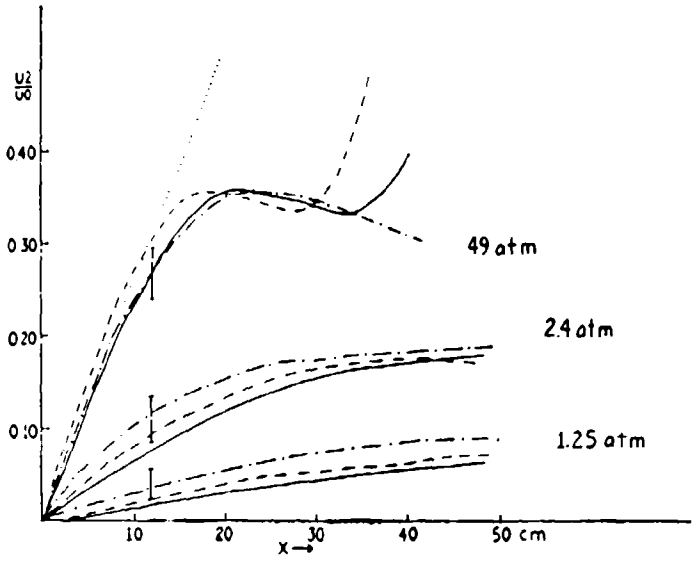

Figure 3-18.–Comparison of theoretical and experimental values of the relative second harmonic content of 1.5 MHz waves in water:. . . . . theoretical [18]; .__.__. experimental [29]; _____ B/A = 5.5 and _ _ _ _ _ B/A = 7.0, theoretical [9]. The symbol (I) indicates the spread of experimental data.

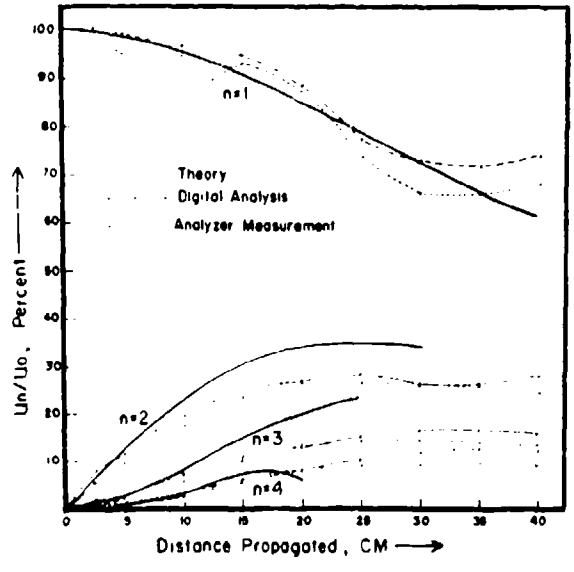

Figure 3-19.–Comparison of theoretical and experimental values of harmonic growth and decay for 2.5 MHz sound waves in water, compared with theoretical predictions: (–) theory; (×) digital analysis; (•) analyzer measurement. Initial pressure amplitude 3.0 atm. The curves marked "digital analysis" were obtained by a computer analysis of waveforms photographed on an oscilloscope screen. Those marked "analyzer measurement" represent data obtained by passing detected signal through an electric filter tuned to the appropriate harmonic (from Ryan, Lutsch and Beyer [39]).

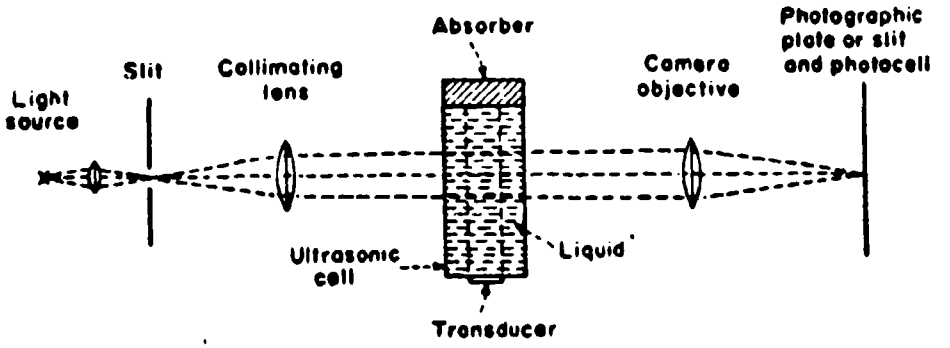

Figure 3-20.–Schematic diagram of the Debye-Sears method [from H. J. McSkimin, "Physical Acoustics" (W. P. Mason, ed.), Vol. 1A, P. 280, Academic Press, N. Y., 1964].

the light intensity is an excellent measure of the intensity of the sound wave. An example of these diffraction results is shown in Fig. 3-21.

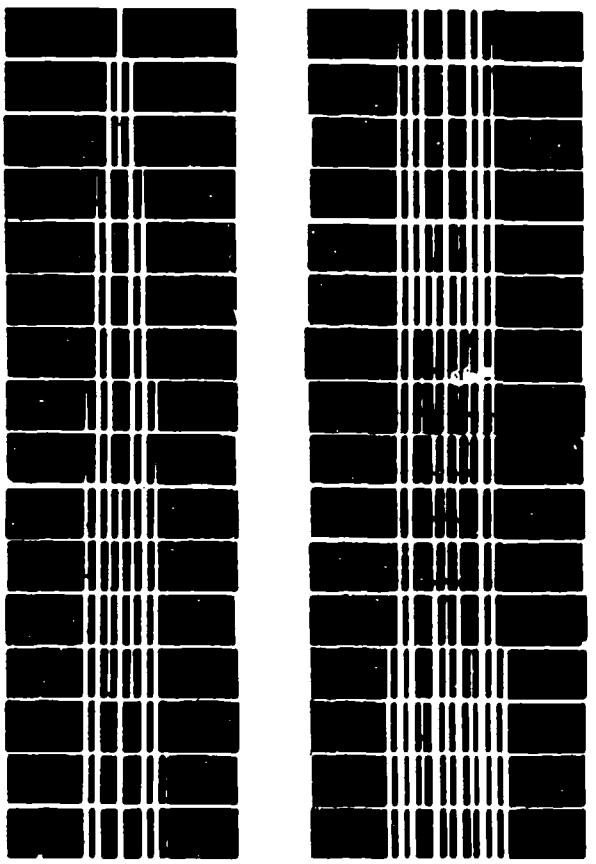

Figure 3-21.–Optical diffraction in a traveling sound wave at various relative intensities [from O. Nomoto, Proc. Phys. Math. Soc. Japan *22*, 314 (1940)].

Shortly after the initial work on the optical diffraction by sound, Sanders [32] noted a slight asymmetry between the intensities of the positive and negative diffraction orders. At the time, it was suggested that a second harmonic signal was present in the source. Some twenty years passed, however, before it was realized that the true explanation of the asymmetry lay in the presence of distortion in the medium rather than in the inadequacies of the generator. Almost simultaneously, Mikhailov and Shutilov [33] in the USSR and Hiedemann and coworkers in the USA [34] demonstrated this finite-amplitude asymmetry in optical diffraction. We shall give a brief discussion of both methods, beginning first with that of Mikhailov and Shutilov, since it is much simpler mathematically.

If the optical diffraction experiment is carried out at very high intensities, many diffraction orders are excited (Fig. 3-22). A diffraction order of maximum intensity can be seen on each side of the central line. As long as the sound intensity is very weak, the location of these maxima is symmetric (see Fig. 3-21), but as the sound intensity is increased, the negative-order maximum becomes the brighter one; in addition, it occurs at a lower order number than the maximum among the positive order lines.

The net effect of the ultrasonic beam at low sound intensities is to modulate the phase but not the amplitude of the light passing through the cell. As a result, the wavefront of the light emerging from the cell has the

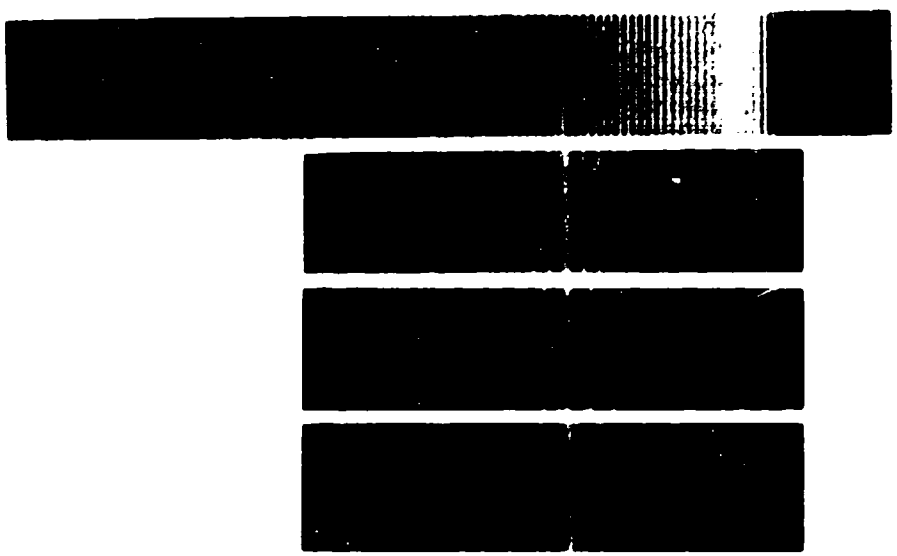

Figure 3-22.–Optical diffraction at high acoustic intensity. (a) Pattern with direct ultrasonic beam of 15.1 W/cm^2, ν = 583 kHz. The remaining photographs correspond to the same experimental arrangements but with the acoustic filter passing only the second harmonic (b), third (c), and fourth (d) (from Mikhailov and Shutilov [33].)

form pictured in Fig. 3-23a. The resultant "corrugation" of the wavefront of the diffracted light beam would then have the same shape. Since the slope of each side of the sawtooth wave is proportional to the value of the pressure gradient in that portion of the cycle (recall Fig. 3-7), and since the portion of the wave cycle during which the gradient of the condensation is positive is now smaller than that during which it is negative, the light intensity of the maximum in the forward direction is less than in the back direction. Furthermore, the order of the diffraction image for which refraction occurs must be greater in the forward direction. Shutilov was able to show that $\phi_1 = \lambda_\varrho m_1/\lambda$, $\phi_2 = -\lambda_\varrho m_2/\lambda$, where λ is the acoustic and λ_ϱ the optical wavelength and m_1, m_2 are the orders of the positive and negative intensity maxima.

Mikhailov and Shutilov worked at a frequency of 583 KHz and with sound intensities up to 20 W/cm^2, corresponding to an excess pressure of nearly 8 atm, a much higher value, especially for such a low frequency, than any at which Hiedemann et al. operated. Therefore, the approximation of a nearly sawtooth waveform was reasonable in their case.

In the measurements of Hiedemann and his students, the intensity of the sound was sufficiently low that only a small number of harmonics had to be considered. In their analysis, which we shall now summarize, it is further assumed that the odd harmonics are in phase with the fundamental and that the even harmonics are 180° out of phase.

The Hiedemann analysis is an enlargement of the infinitesimal-amplitude diffraction theory of Raman and Nath. In essence, the distorted wave is analyzed into its Fourier components. The diffraction effect of each of these components is then combined to obtain the total result for the case of a light beam whose width is very large compared with the ultrasonic wavelength. The light intensity of the nth order image is

$$I_n \propto \Phi_n^2$$

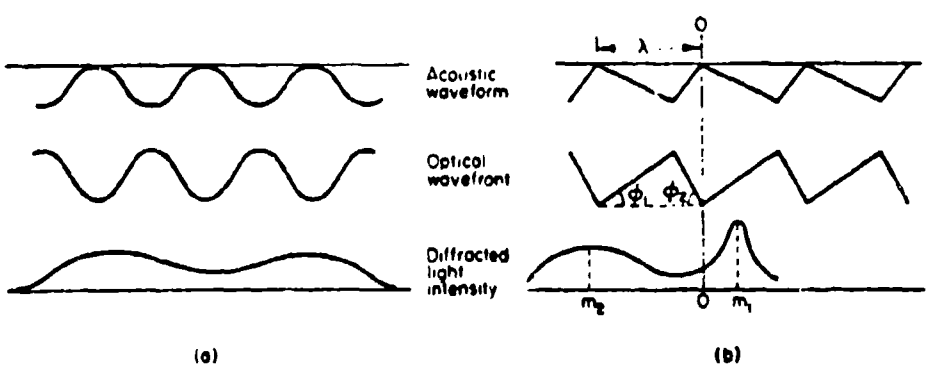

Figure 3-23.–Wave shapes in optical diffraction: (a) low acoustic intensity; (b) high acoustic intensity (after Mikhailov and Shutilov [33]).

where Φ_n is the amplitude:

$$\Phi_n = \sum_{\substack{k_2,k_3,k_4,\ldots \\ =-\infty}}^{\infty} J_{n-2k_2-3k_3} \cdots (w) J_{k_2}(a_2 w) J_{k_3}(a_3 w) + \cdots . \tag{3.117}$$

Here $w = 2\pi\mu L/\lambda$. The term a_j is the amplitude of the jth harmonic in the distorted waveform, relative to the fundamental. The operation of Eq. (3.117) is best understood by an example. If one is looking at the third-order diffraction image ($n = 3$), and if the sound intensity is so small that only a_2 among the harmonic amplitudes is appreciable, then

$$\Phi_3 = \sum_{k_2=-\infty}^{\infty} J_{3-k_2}(w) \; J_{k_2}(w) \; . \tag{3.118}$$

If, further, the only J_p of importance are those for $p = 0, \pm 1, \pm 2, \pm 3$, we have

$$\begin{aligned} \Phi_3 &= J_3(w)\, J_0(a_2 w) + J_1(w)\, J_1(a_2 w) \\ &\quad + J_{-1}(w)\, J_2(w) + J_{-3}(w)\, J_3(a_2 w) \; . \end{aligned} \tag{3.119}$$

In the undistorted case, of course, $\Phi_n = J_n(w)$ and the solution reduces to that of Raman and Nath. By making use of the theoretical values for a_2 from the perturbation analysis, one can compute the relative intensity of the diffraction order under study. Some typical examples are shown in Fig. 3-24. These experimental and theoretical results are seen to be in excellent agreement with each other.

3.13 Practical Sources of Finite Amplitude Sound.

The numerous studies described in this chapter have concentrated on two simple cases–the plane wave and the spherical wave. In practice, however, we deal with sources of limited extent–usually a rectangular or circular

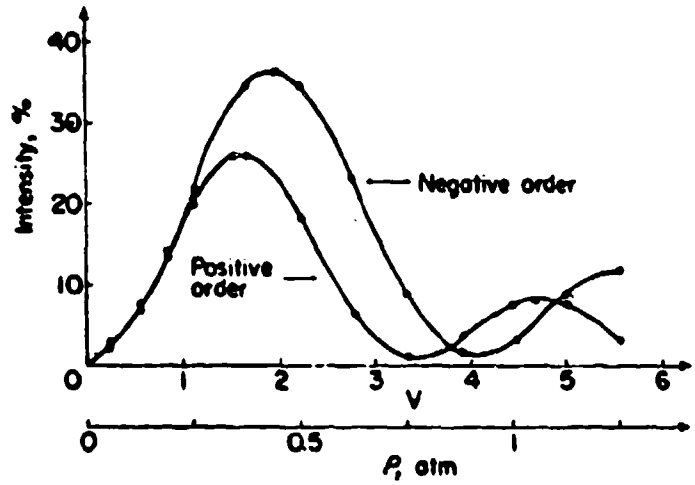

Figure 3-24.–Experimental values of the intensity of the first diffraction order as a function of the original pressure p for water at 2 MHz (from Hiedemann and Zankel [34]).

vibrating disk on the one hand, or a portion of a spherical surface on the other. In each case, the distortion of an originally sinusoidal wave form is complicated by the diffraction of the infinitesimal beam. The theoretical and experimental studies of this problem have thus far been quite limited.

The Plane Piston. A. The Near Field. Ingenito and Williams [32] have produced a partial solution for the near field of the finite amplitude plant piston. They began with the presumed existence of a velocity potential

$$\Phi = \sum_i \Phi_i$$

where the Φ_i are the potentials applicable to each harmonic. Then, following Heaps, [33] they deduced the equation for the second harmonic Φ_2:

$$\Box^2 \Phi_2 = \frac{-1}{2c^2} \frac{\partial}{\partial t} \left[\Box^2 \left(\Phi_1^2 \right) + \frac{2\beta}{c^2} \left(\frac{\partial \Phi_1}{\partial t} \right)^2 \right] \tag{3.120}$$

where $\Box^2$ is the d'Alembertain operator $\nabla^2 - (1/c^2)(\partial^2/\partial t^2)$ and β is the parameter of nonlinearity. The authors further assumed that all harmonics higher than the second can be neglected and that the function Φ_1 is unaffected by the growth of Φ_2. These are the usual assumptions of a perturbation theory and parallel in spirit the early treatment of the plane wave problem.

By assuming the fumdamental velocity potential Φ_1 to have the form

$$\Phi_1 = \text{Re}\left[\phi_1(x,y,z)\, e^{-i\omega t}\right].$$

Ingenito and Williams transformed Eq. (3.120) to the form

$$[\nabla^2 + (2k)^2]\ \phi_2(x,y,z) = \left(\frac{ik}{2c}\right)\left\{[\nabla^2 + (2k^2)]\ \phi_1{}^2 - 2\beta k^2 \phi_1{}^2\right\}. \tag{3.121}$$

The authors were then able to show that the most significant effects were produced by the last term in the curly brackets on the right.

By the use of a Green's function technique, plus an expansion of an exponential factor in terms of Bessel function, Ingenito and Williams arrived at an approximate expression for ϕ_2 in cylindrical coordinates

$$\phi_2(r,z) \simeq -\frac{\beta k^2}{4c}\int_{\sigma=0}^{z} e^{ik\sigma}\ \phi_1{}^2\left(r, z-\frac{\sigma}{2}\right)\, d\sigma\ . \tag{3.122}$$

The authors carried out explicit solutions of Eq. (3.122) in three cases.

(1) A collimated beam

$$\begin{aligned}\phi_1(r,z) &= \frac{iv}{r}\ e^{ikz} \quad r < a \\ &= 0 \qquad\quad r > a\ .\end{aligned} \tag{3.123}$$

Application of Eq. (3.123) to Eq. (3.122) yields

$$\begin{aligned}\phi_2(r,z) &= \frac{\beta}{4c}\ v^2 z e^{ikz} \quad r < a \\ &= \qquad\qquad r > a\ .\end{aligned} \tag{3.124}$$

This yields a second harmonic that increases in amplitude with z, thus resembling the first correction to the plane wave case [Eq. (3.41)].

(2) Average value

$$\phi_2\ (r,z) = \frac{\beta}{4c}\ v^2\ \exp\left[2(ik-\alpha)z\right]\ (z + \ell \sin z/\ell) \tag{3.125}$$

It is common practice to use a receiving transducer of the same radius as the source, so that the average value of ϕ_2 over a plane area of the same size as that of the source, centered perpendicularly on the axis is of interest. Their final expression is of the form

$$\langle \phi_2 (r,z) \rangle = - \frac{k}{4c} \int_{\sigma=0}^{z} e^{jk\sigma} \left[\left\langle \phi_1 \left(r, z - \frac{\sigma}{2} \right) \right\rangle \right]^2 d\sigma \, . \quad (3.126)$$

When a specific expression used for ϕ_1 [such as that obtained by Bass (34)], Eq. (3.126) can be evaluated numerically. A plot of the results [essentially, of the integral in Eq. (3.126)] is shown in Fig. 3-25, along with the linear relation of Eq. (3.124).

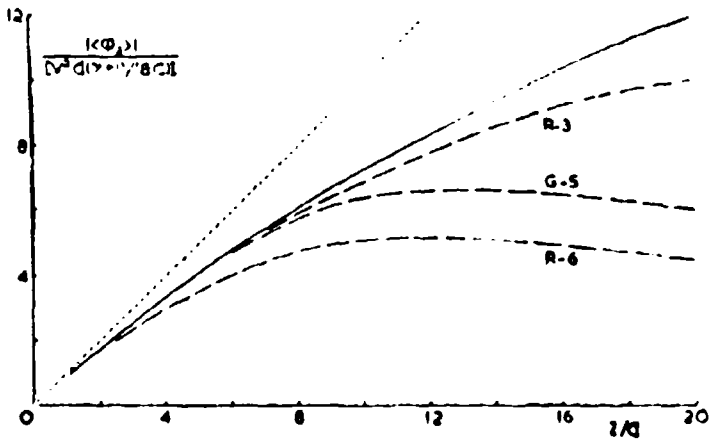

Figure 3-25.–Magnitude $|\langle \phi_2 \rangle|$ of averaged second harmonic velocity potential in dimensionless form versus axial distance z/a. k = 109.9 cm^{-1}, a = 1.042 cm, B/A = 5. – – –: Eq. (3.124). ——— (3.125). (R – 3): Figure 7 of Ref. 39. (R – 6): Figure 8 of Ref. 39. (G – 5): Figure 3 of Ref. 38. Numbers 3, 6 and 5 and source pressures in atmospheres (from Ingenito and Williams [35]).

Since this is a nondissipative theory, it is difficult to make a realistic experimental comparison. However, Ingenito and Williams have plotted three experimental cases of signals of initial pressure of 5 atm [38] and 3, 6 atm [39] obtained with a receiver 2.5 times the radius of the source. Good agreement is evident between the theory and the 3-atm curve. The curves for the higher pressures deviate considerably from the theory. As can be seen from Fig. 3-19 (from which the curve R – 3 is taken) at a point corresponding to z/a = 15 (a = 1 cm) the amplitude of third harmonics is a considerable fraction of the second while the fundamental amplitude has decreased slightly. For 6 MHz however the data from the same paper show a 25% drop

in the fundamental amplitude at $z/a = 15$ cm while the amplitude of the third harmonic is more than that of the second, so that two of the approximations of the Ingenito-Williams theory have lost their validity.

(3) Axial value

In the case of waves of infinitesimal amplitude, the axial value of the velocity potential has long been known [Eq. (1.64)]. Ingenito and Williams have found an expression for the finite amplitude case that appears to be the most accurate of their formulas:

$$\phi_2(0,z) = \frac{\beta v^2 k a^2}{4c}\, e^{2ikz}\left[\int_{t_0}^{t_1} t^{-2}e^{2it}\, J_0\left(\frac{2t}{t_0}\right)(t - t_0)\, dt - 2\int_{t_0}^{t_1} t^{-2}e^{jt}dt + \left(\frac{z}{ka^2}\right)\right] . \tag{3.127}$$

An evaluation has been carried out of the second harmonic pressure amplitude based on this equation (Fig. 3.26) and compared with experiment. The agreement is astonishingly good.

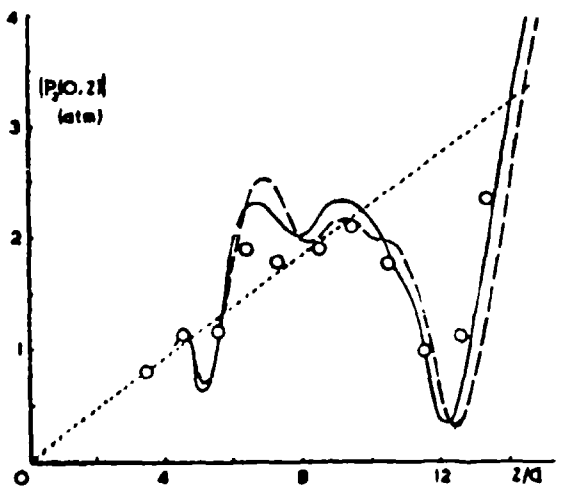

Figure 3-26.—Magnitude $|p_e|$ of axial second harmonic pressure in atmospheres versus axial distance z/a. Source pressure 5.0 atm, $k = 109.9$ cm^{-1}, $a = 1.042$ cm, $B/A = 5$. ——— Eq. (3.127) including coupling function. — — Eq. (3.127) with coupling function unity. — — — Perfectly collimated plane waves (from Eq. (3.124)2. ○: measured values of Ref. 38 (from Ingenito and Williams [35]).

The Plane Piston. B. The Farfield. The problem of the nonlinearities of the farfield of the plane piston can be shown to be essentially that of a spherical source with boundary conditions at the effective starting point of spherical spreading superposed. We shall therefore follow this treatment of Lockwood, Muir and Blackstock [40] and assume that the particle velocity amplitude u_0 at this point r_0 is given by $(u_0/c_0)D(\theta)$, where $D(\theta)$ is the infinitesimal amplitude directivity function in the farfield of a circular, baffled, plane piston:

$$D(\theta) = \frac{2J_1(ka \sin \theta)}{ka \sin \theta} \quad . \tag{3.128}$$

An additional assumption is that the farfield distortion of the wave form derives almost wholly from disturbances that were purely sinusoidal at the point r_0, i.e., that the nearfield distortions do not play a significant role in the farfield. [41]

The analysis of Lockwood et al. is based on the weak shock theory of Blackstock. [20] The acoustic pressure for the spherical wave is given by Blackstock as

$$p = \rho_0 c_0 u_0 D(\theta) \frac{r_0}{r} \sin \Phi \tag{3.129}$$

where Φ is the function defined by Eq. (3.77)

$$\Phi = y + \sigma \sin \Phi \tag{3.77}$$

where y is given by

$$y = \omega t - \frac{(r - r_0)}{c_0} \tag{3.130}$$

in the spherical case and σ is given by

$$\sigma = \frac{\beta u_0}{c_0} D(\theta) \, kr \, ln \left(\frac{r}{r_0}\right) \quad . \tag{3.131}$$

If the Blackstock bridging technique (Section 3.8) is used, the Fourier coefficient B_n can be written as

$$B_n = \frac{2}{n\pi} \sin \Phi_{min} + \frac{2}{n\pi\sigma} \int_{\Phi_{min}}^{\pi} \cos n(\Phi - \sigma \sin \Phi) \, \theta\Phi \tag{3.79}$$

= Fay contribution + Fubini contribution .

At large $\sigma(\sigma > 3)$ the Fubini contribution becomes negligible and $B_n \to 2/n(1 + \sigma)$.

The pressure at the point r can now be written as

$$P = \rho_0 c_0 u_0 D(\theta) \frac{r_0}{r} \sum_{n=1}^{\infty} B_n \sin ny . \tag{3.132}$$

Since B_n is a function of σ, it also depends on $D(\theta)$ through Eq. (3.131). The directivity of the nth harmonic in (3.132) $[D_n(\theta)]$ is therefore proportional to $D(\theta)\, B_n(\sigma)$. If we define σ_1 as the value of σ at which $D(\theta) = 1$, then $D_n(\theta)$ can be written as

$$D_n(\theta) = \frac{D(\theta)\, B_n(\sigma)}{[D(\theta)\, B_n(\theta)]_{\theta=0}} = D(\theta) \frac{B_n(\sigma)}{B_n(\sigma_1)} . \tag{3.133}$$

We distinguish two cases:

$\sigma < 1$.

Here the Fubini solution $B_n(\sigma) = (2/n_\sigma) J_n(n\sigma)$ prevails, so that

$$D_n(\theta) = \frac{J_n[nD(\theta)\ \sigma_1]}{J_n(n\sigma_1)} . \tag{3.134}$$

For small values of σ_1, $D_n(\theta) \simeq [D(\theta)]^n$ so that the higher frequency components of the beam become progressively narrower.

$\sigma >> 1$.

Here

$$D_n(\theta) = D(\theta) \frac{1 + \sigma_1}{1 + \sigma} = \frac{D(\theta)(1 + \sigma_1)}{1 + D(\theta)\sigma_1} \tag{3.135}$$

i.e., the directivity is independent of the order of the harmonic and is somewhat broader.

Experimental measurements have been also carried out by Lockwood et al. with a 3-in.-diameter piston source operating at a fundamental frequency of 454 kHz. The measurements were made distances of 41 and 117 yd, both

of which are well into the farfield ($a^2/\lambda \simeq 2$ yd). The results are shown in Fig. 3-27.

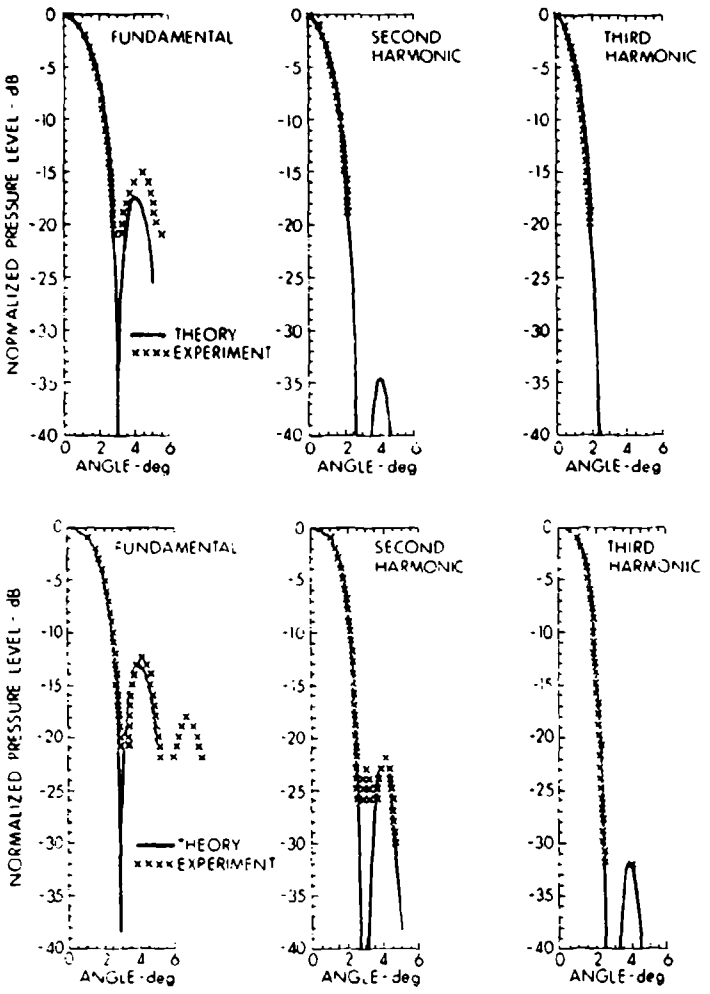

Figure 3-27.–Finite amplitude effects of circular piston: (a) harmonic beam patterns at a range of 117 yd. Source level 109 dB, frequency 454 kHz; (b) range 41 yd, source level 127 dB, frequency 450 kHz (from Lockwood, Muir and Blackstock [40]).

In the case of the theoretical curves, a value of $r_0 = 1$ yd was chosen.

The Spherical Cap. In 1969, Smith and Beyer carried out an experimental study of the radiation from a focusing spherical cap at finite amplitudes. [42] To date, there exists no theory for this case. There is a theory for the finite amplitude spherical wave [21] and another for a spherical cap under infinitesimal amplitude conditions. [43] A comparison of experimental data

with the two theories is shown in Fig. 3-28. It can be seen from the figure that there is fair qualitative agreement among the three curves for the fundamental, but not much agreement between experiment and theory for the second harmonic.

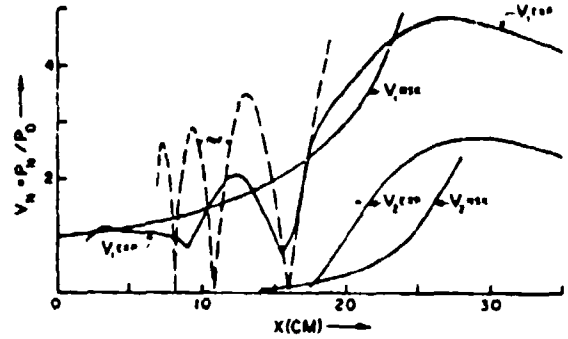

Figure 3-28.–Theoretical and experimental values of axial acoustic pressure amplitude for initial pressure of 0.5 atm. – – – –Values computed from infinitesimal amplitude theory. Subscripts 1, 2 refer to fundamental and second-harmonic components (from Smith and Beyer [42]).

A second comparison with the finite amplitude theory is shown in Fig. 3-29 for a source pressure of 1 atm. Here the averaged value of the experimental curve is reasonably close for both the fundamental and second harmonic.

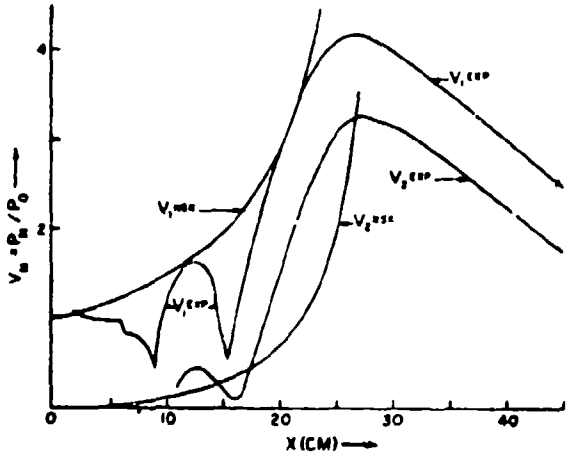

Figure 3-29–Theoretical and experimental values of the axial acoustic pressure amplitude for initial pressure of 1.0 atm. Subscripts 1, 2 refer to fundamental and second harmonic components (from Smith and Beyer [42]).

3.14 Finite-Amplitude Propagation in Tubes.

All of the previous analysis has been concerned with unbounded waves. A body of literature has also accumulated on the propagation of finite-amplitude sound waves in fluid-filled tubes. This section contains a brief review of such propagation.

Earlier theoretical and experimental work on the propagation of finite-amplitude waves in air-filled ducts was carried out by Thuras, Jenkins and O'Neil in 1935 in the work cited previously. [27] A more modern repetition of these measurements was made by Cruikshank [44] in 1966. A 24-ft pipe of 2-in diameter was used with an absorbing termination. The results shown in Fig. 3-30 give the magnitude of the second harmonic in the case of a 1000-Hz

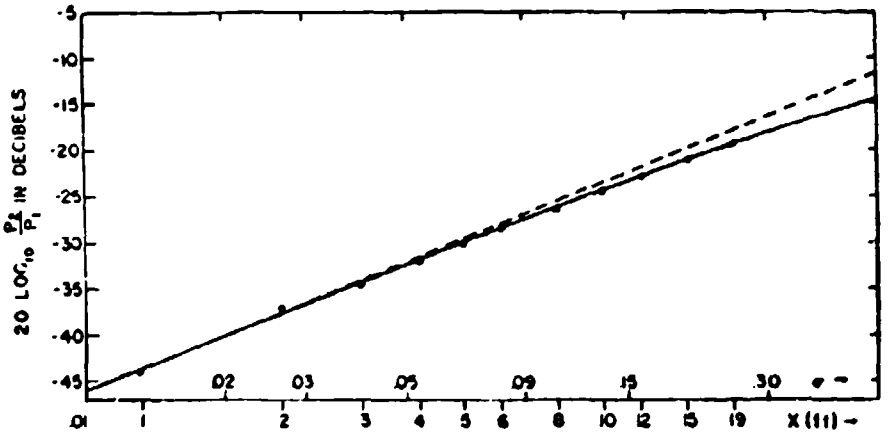

Figure 3-30.–Second harmonic generation in a tube as a function of distance from the source. Fundamental: 1 kHz at SPL of 140 dV. _ _ _ _ lossless theory, $P_2/P_1 = \sigma/2$. ——— : Theory corrected for viscous and thermal wall effects. . . . . : Experimental data (from D. B. Cruikshank, Jr. [44]).

source. The measurements are clearly in the near field. The theoretical curve, which takes viscosity and heat conduction at the walls into account, is a refinement of the work of Thuras et al., carried out by Blackstock. [45]

$$\frac{p_2}{p_1} = \frac{\sigma}{2} \frac{e^{-\alpha_1 x/\sqrt{2}}}{(2-\sqrt{2})\alpha_1 x} \left\{ [\cosh [(2-\sqrt{2})\ \alpha_1 x] \right. \tag{3.136}$$

$$\left. - \cos\ [2-\sqrt{2})\ \alpha_1 x] \right\}^{1/2}$$

where α_1 is the infinitesimal-amplitude sound absorption at the fundamental frequency and p_1, p_2 are the pressure amplitudes of the fundamental and second harmonic.

A much more exhaustive treatment of this problem has been presented by Burns. [46] An initially sinusoidal wave was studied for propagation in a fluid filled tube. Equations for the scalar and vector potentials were set up and solved by fourth order perturbation theory. The theoretical results are too cumbersome to be repeated here, but it should be noted that reasonably good experimental confirmation was obtained for 445 Hz waves in air. These measurements were also nearfield in character. A sample of the results are shown in Fig. 3-31 for Mach number $M = 0.0316$ in air. Here the fundamental and second harmonic are plotted for three different tube diameters.

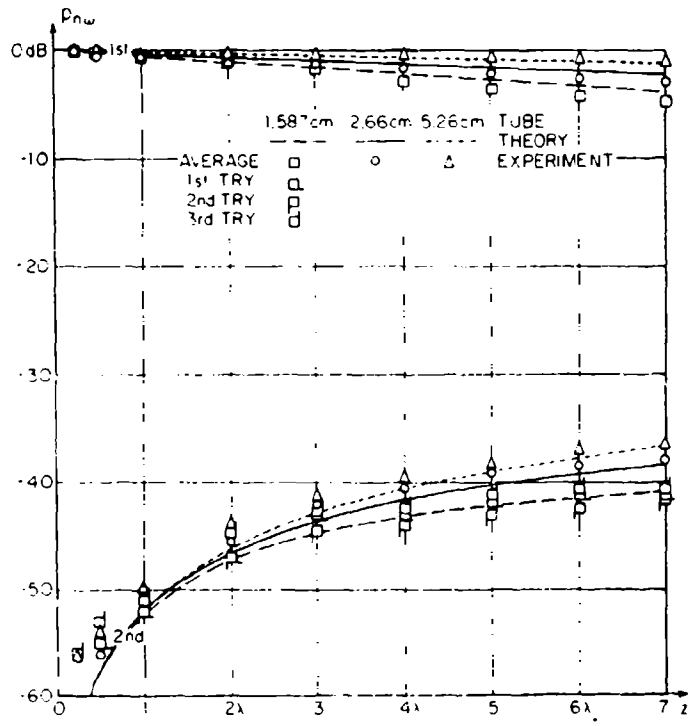

Figure 3-31.—Fundamental and second harmonic for air-filled tubes. Frequency = 445 Hz, initial Mach number 0.0316 (from S. H. Burns [46]).

Another analysis of the problem has been given by Coppens. For a duct with rigid walls, the one-dimensional wave equation for a dissipative fluid can be written as

$$\sum \left(\frac{\partial^2}{\partial x^2} - \frac{1}{c_0^2} \frac{\partial^2}{\partial t^2} + D_n \right) u_n = \beta \frac{\partial^2}{\partial x \partial t} \left(\frac{\partial \xi}{\partial x} \right)^2 \tag{3.137}$$

where

$$D \simeq -\delta n \left(\frac{\partial^2}{\partial x^2} + \frac{1}{n\omega} \frac{\partial^3}{\partial x^2 \partial t} \right)$$

$$\delta_n \simeq \left(\frac{G}{S} \right) \frac{1}{(2n\omega)^{1/2}} \left[\nu^{1/2} + (\gamma - 1) \left(\frac{\nu'}{\gamma} \right)^{1/2} \right].$$

Here the particle velocity $u = \partial \xi / \partial t$ is formed from the sum Σu_n of the harmonic components, c_0 is the phase velocity when $\beta = 0$, $\delta_n = 0$, γ is the ratio of specific heats, ν the kinematic viscosity and ν' the thermometric conductivity. S is the cross sectional area of the duct and G its perimeter. Equation (3.137) is the dissipation generalization of Eq. (3.46) and holds, subject to the conditions that the boundary layer separating the main stream of the fluid from the walls be small compared with the wave-length or physical dimensions of the duct, and that the wave fronts be essentially planar across it.

If we take the limiting case of a linear process ($\beta = 0$) and use the boundary conditions

$$u(0,t) = u_0 \sin \omega t \tag{3.138}$$

the solution reduces to that of Kirchhoff for sound propagation in a tube

$$\frac{u}{u_0} = e^{-\alpha_1 x} \sin \left[\omega t - (k_0 + \alpha_1) x \right] \tag{3.139}$$

where the absorption coefficient is given by

$$\alpha_1 \simeq \frac{1}{2} \frac{\omega}{c_0} \delta_1 \tag{3.140}$$

and the dispersion of the primary frequency is given by

$$\left(\frac{c_1}{c_0} \right)^2 = 1 - \delta_1 . \tag{3.141}$$

For the nonlinear case, Coppens has carried out both perturbation analysis and computer solutions by Fourier expansion. He has expressed his results in the form of the following parameters:

$$\frac{M\beta}{\delta_1} = \frac{\frac{1}{2} M\beta}{\alpha_1 k_0}, \tag{3.142}$$

where M is the acoustic Mach number, $M\beta/\delta_1$, which is the ratio of the "waveform strength" $M\beta$ to the fractional loss per wavelength $2\alpha_1 k_0$, is called by him the strength parameter. A second parameter is modeled on the discontinuity length ℓ for a plane wave [Eq. (3.33)]. If we define a dimensionless distance d,

$$d = \alpha_1 x \tag{3.143}$$

then the dimensionless discontinuity length could be represented as

$$\ell_s = \alpha_1 \ell. \tag{3.144}$$

A few samples of Coppens calculation follows. Figure 3-32 shows the relative harmonic distortions for values of the parameters just mentioned, while Fig. 3-33 shows the profile of the waveform. The asymmetry of the positive and negative portions of the curve should be noted.

Two other recent studies deserve mention. Keller and Millmann have carried out a perturbation analysis of a finite amplitude wave propagating in a wave guide of nonrectangular cross section in the absence of dissipation. [48] The propagation wave numbers k_n of the waves corresponding to the modes of linear theory are found to be functions of the amplitude ξ_0.

Finally, Cruikshank [49] has carried out an experimental study of the pressure waveforms of a piston vibrating in a closed resonance tube. The results are in good agreement with the basic theory of Chester. [50] Cruikshank also gives an excellent historical review of work in this field.

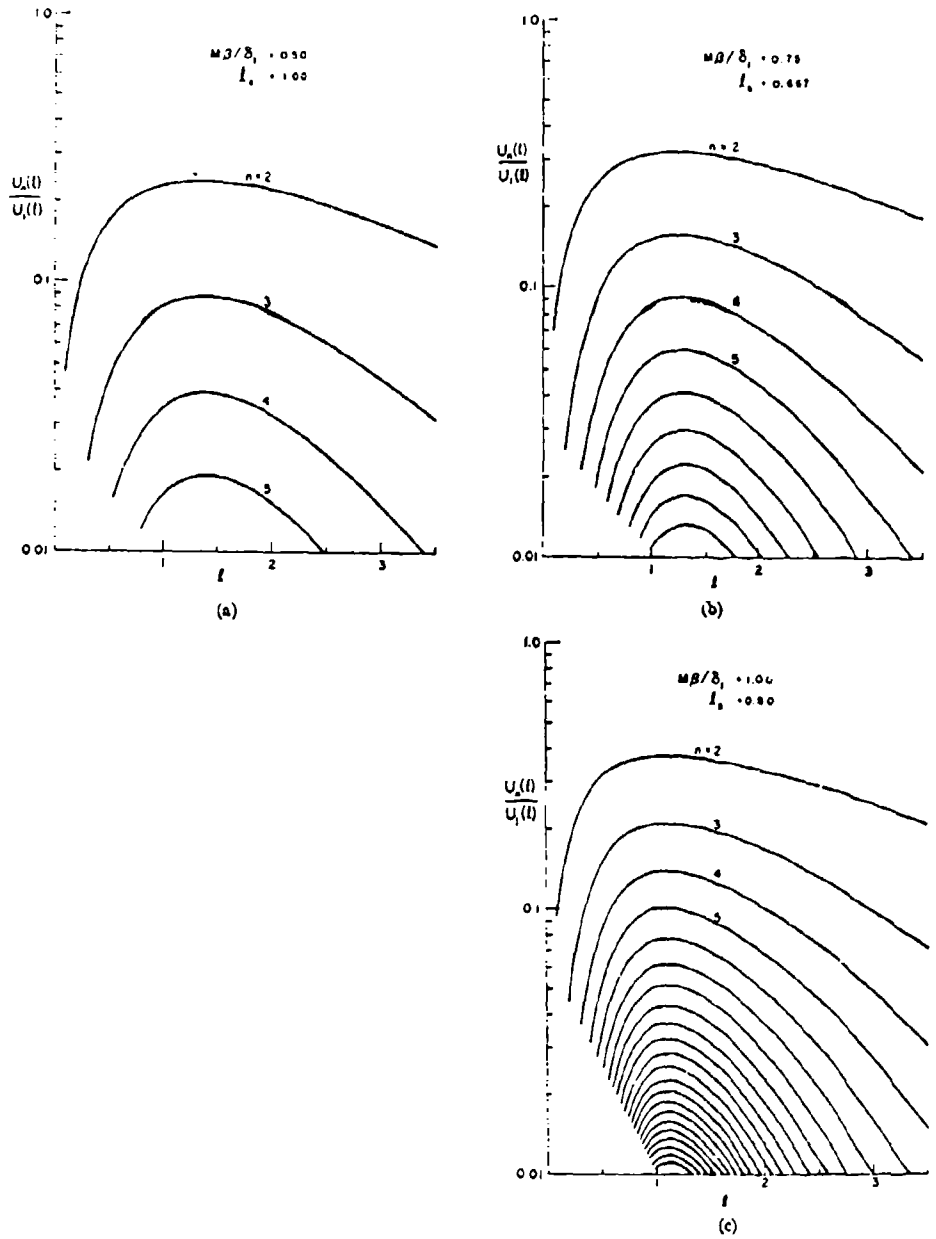

Figure 3-32.–Relative harmonic distortions in wave form as a function of the dimensionless distance for various values of the strength parameter. n = number of harmonic (from Coppens [47]).

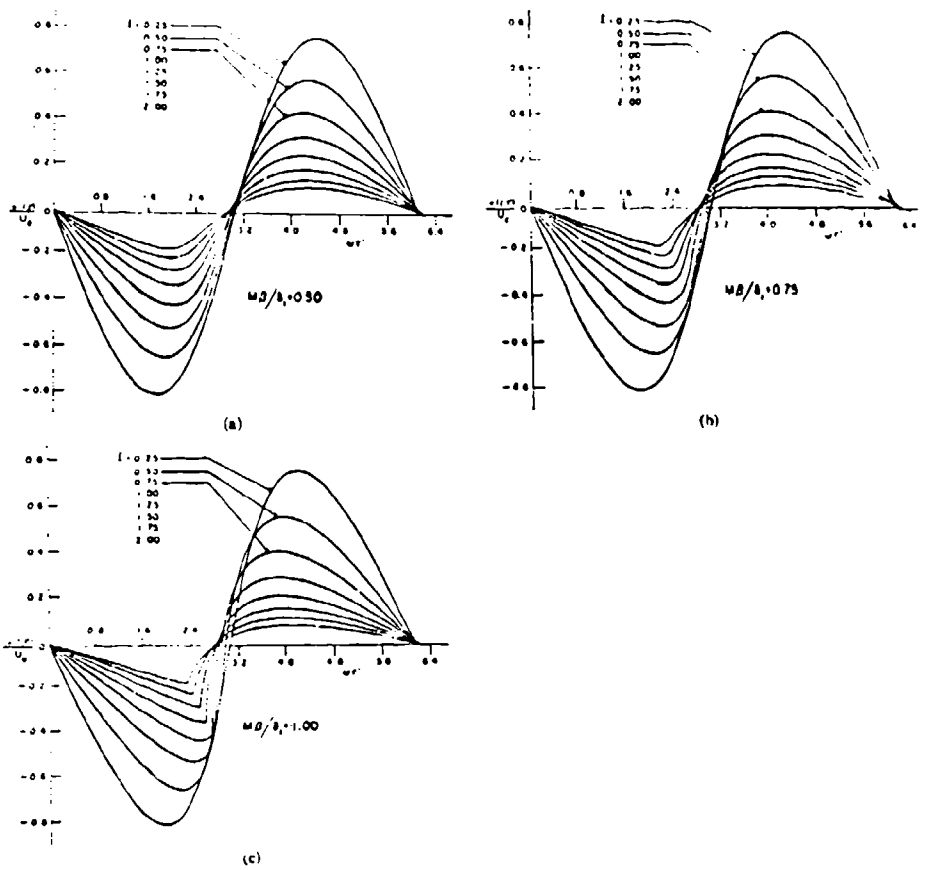

Figure 3-33.–Profiles (in time) of the wave form at various values of ℓ for different values of the strength parameter (from Coppens [47]).

REFERENCES

Chapter 3

1. F. V. Hunt, JASA **27**, 1019 (1955).
2. For a more detailed consideration, see M. P. Hagelberg, G. Holton and S. Kao, JASA **41**, 564 (1967).
3. S. Earnshaw, Phil. Trans. Roy. Soc. (London) **150**, 133 (1860).
4. F. E. Fox and W. A. Wallace, JASA **26**, 994 (1954).
5. B. Riemann, Göttingen Abhandlungen, 1860; reprinted in Collected Works, Dover Publications, N. Y., 1953, p. 156.
6. E. Fubini, Alta Frequenza, **4**, 539 (1935).

6a. S. I. Soluyan and R. V Khokhlov, Vestnik, Moscow State University **3**, 52 (1961).

7. V. A. Krasilnikov, V. V. Shklovskaya-Kordy and L. K. Zarembo, JASA **29**, 642 (1957).
8. G. B. Airy, Encyclopedia Metropolitana, London, 1845, Vol. 5, p. 241.
9. W. Keck and R. T. Beyer, Phys. Fluids **3**, 346 (1960).
9a. R. P. Ryan, Ph.D. thesis, Brown University, 1963.
10. D. T. Blackstock, JASA **39**, 411 (1966).
11. R. Fay, JASA **3**, 222 (1931).
12. J.S. Mendousse, JASA **25**, 51 (1953).
13. I. Rudnick, JASA **30**, 565 (1958).
14. B. D. Cook, JASA **34**, 941 (1962).
15. D. T. Blackstock, JASA **36**, 534 (1964).
16. R. V. Khokhlov and S. I. Soluyan, Acustica **14**, 241 (1964).
17. K. A. Naugol'nykh, "Absorption of Finite Amplitude Waves," in *High Intensity Ultrasonic Fields*, L. D. Rozenberg, ed. (English translation, Plenum Press, N. Y. 1971) p. 14.
18. Z. A. Goldberg, Sov. Phys. Akust. **3**, 346 (1956); 340 (1957).
19. J. D. Cole, Quart. Appl. Math. **9**, 225 (1951).
20. D. T. Blackstock, JASA **39**, 1019 (1966).
21. K. Naugol'nykh, Soviet Phys.-Acoustics **5**, 79 (1959); K. Naugol'nykh, S. I. Soluyan and R. V. Khokhlov, Soviet Phys.–Acoustics **9**, 42 (1963).
22. D. T. Blackstock, JASA **36**, 217 (1964).
23. E. Banta, J. Math. Anal. Applications **10**, 166 (1965).
24. B. B. Cary, JASA **43**, 1364 (1968).
25. S. I. Soluyan and R. V. Khokhlov, Soviet Phys.-Acoustics **8**, 170 (1962); see also A. L. Polyakova, S. I. Soluyan and R. V. Khokhlov, Soviet Phys.-Acoustics **8**, 78 (1962).
26. R. P. Ryan, C. R. Attanasio and R. T. Beyer, JASA **37**, 602 (1965).
27. A. L. Thuras, R. T. Jenkins and H. T. O'Neil, JASA **6**, 173 (1935).
28. F.E. Fox and W. A. Wallace, JASA **26**, 994 (1954).
29. V. A. Krasilnikov, V. V. Shklovskaya-Kordi and L. K. Zarembo, JASA **29**, 642 (1957).
29a. V. Narasimhan and R. T. Beyer, JASA **28**, 1233 (1956); **29**, 532 (1957).
30. R. P. Barnes, Jr. and R. T. Beyer, JASA **36**, 1371 (1964).
31. C. V. Raman and N.S.N. Nath, Proc. Ind. Acad. Sci. Sect. **A2**, 406, 413 (1935); 3, 75 (1936).
32. F. H. Sanders, Nature **138**, 285 (1936); Canad. J. Res. **A14**, 158 (1936).
33. I. G. Mikhailov and V. A. Shutilov, Soviet Phys.-Acoustics **4**, 174 (1958); **5**, 75, 230 (1959).
34. E. Hiedemann and K. L. Zankel, Acustica **11**, 213 (1961); L. E. Hargrove and K. Achyuthan, *Physical Acoustics* (W. P. Mason, ed.), Vol. 2B, Academic Press, N. Y., 1965.
35. F. Ingenito and A. O. Williams, Jr., JASA **49**, 319 (1971).

36. H. S. Heaps, JASA **34**, 355 (1962).
37. R. Bass, JASA **30**, 602 (1958). [Note that the i before $J_1(\xi)/\xi$ of Eq. (14) of this paper should be replaced by unity.]
38. R. K. Gould, C. W. Smith, A. O. Williams, Jr. and R. P. Ryan, JASA 40, 421 (1966).
39. R. P. Ryan, A. G. Lutsch and R. T. Beyer, JASA **34**, 31 (1962).
40. J. C. Lockwood, T. G. Muir and D. T. Blackstock, JASA **53**, 1148 (1973).
41. J. C. Lockwood, JASA **52**, 115 (A) (1972).
42. C. W. Smith and R. T. Beyer, JASA **46**, 806 (1969).
43. H. T. O'Neil, JASA **21**, 516 (1949).
44. D. B. Cruikshank, Jr., JASA **40**, 731 (1966).
45. D. T. Blackstock, Paper 0-15 Fourth ICA on Acoustics, Copenhagen, 1962.
46. S. H. Burns, JASA **41**, 1157 (1967).
47. A. B. Coppens, JASA **49**, 306 (1971).
48. J. B. Keller and M. H. Millmann, JASA **49**, 329 (1971).
49. D. B. Cruikshank, Jr., JASA **52**, 1034 (1972).
50. W. Chester, J. Fluid Mech. **18**, 44 (1964).

Chapter 4

SHOCK WAVES

The literature on shock waves is probably larger than that of all other fields of nonlinear acoustics combined. Large numbers of books have also been devoted to the problem. [1] Here, therefore, we shall give it only the briefest of treatments, emphasizing fundamentals and those aspects of the subject that have a bearing on other topics covered in this text.

4.1 The Rankine-Hugoniot Equation.

The concept of the shock wave is familiar to nearly everyone today through the phenomenon of the sonic boom. It also, however, appears as the result of explosions or in the flight of a high speed projectile. The passage of a body through the air at supersonic speeds (bullet, sonic boom), or the sudden release of a high pressure (air blast, shock tube), results in a rapid rise in pressure that is propagated through the medium. Because this jump in pressure takes place over a very short distance along the direction of propagation, it is a useful and convenient approximation to assume that the rise is instantaneous, i.e., that there is a discontinuity in the pressure. The actual "thickness" of the jump region is only of the order of a few free path lengths and will be discussed in Section 4.

We shall also assume the gas to be ideal, so that $p = n\rho RT$, and that such properties of the gas as the specific heats remain constant over the pressures and temperatures of interest.

Let us now consider flow taking place along a straight line in a tube, or along a stream tube, of constant cross section area S. In Fig. 4-1 AA' represents the shock front, which moves to the right at velocity V. The lines OO' and PP' represent plane surfaces behind and in front of the shock respectively, that are also moving to the right with velocity V. In the undisturbed gas in front of the shock, the pressure p_0, density ρ_0 and velocity of flow v_0 represent equilibrium values. Behind the front (to the left of the line AA'), these same quantities have the constant values p_1, ρ_1, v_1.

Conservation of mass (equation of continuity) requires that the mass flow across any plane surface OO' behind the shock must be equal to that across any similar plane surface PP' in front of the shock. In this notation the surface PP' moves with a speed $V - v_0$ relative to the local fluid, so that a

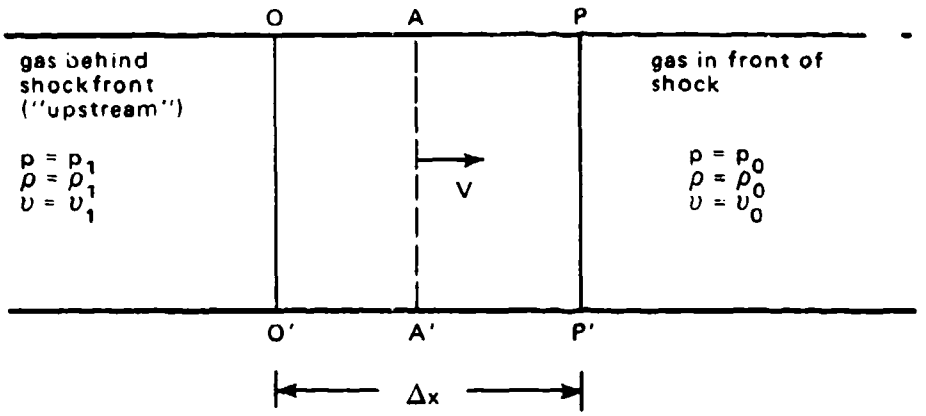

Figure 4-1.–Passage of idealized shock wave in a tube.

mass $(V - v_0)\rho_0$ passes through PP' (from right to left) per second. Similarly, the mass $(V - v_1)\rho_1$ passes through OO', so that

$$(V - v_1)\rho_1 = (V - v_0)\rho_0 \equiv m_t. \tag{4.1}$$

We call this mass flow per unit time the *mass velocity* m_t (after Rankine).*

For the *conservation of momentum*, the net force acting on the volume of gas between OO' and PP' will be $(p_1 - p_0)S$. This must be equal to the increase in momentum of the gas. Now the mass entering the volume element per unit time is m_t, so that the momentum added per second at the left is $m_t v_1$, while that removed at the right will be $m_t v_0$, we have

$$(p_1 - p_0) = m_t(v_1 - v_0). \tag{4.2}$$

We now consider the *conservation of energy*. If E is the internal energy per unit mass of gas, the increase of energy per second in our volume element (between OO' and PP') will be

$$m_t\left[\frac{1}{2}v_1^2 + E_1\right] - m_t\left[\frac{1}{2}v_0^2 + E_0\right],$$

which must equal the work done in increasing the velocity from v_0 to v_1, $p_1v_1 - p_0v_0$:

$$m_t\left[\frac{1}{2}v_1^2 + E_1\right] - m_t\left[\frac{1}{2}v_0^2 + E_0\right] = p_1v_1 - p_0v_0. \tag{4.3}$$

*it is customary to use m for this mass flow rate, but the author finds it dimensionally confusing and has added the subscript t.

Equations (4.1), (4.2), (4.3) are known as the ***Rankine-Hugoniot relations***, and form the basis of virtually all shock theory.

We can eliminate v_0, v_1 from the first two equations, obtaining

$$p_1 + \frac{m_t^2}{\rho_1} = p_0 + \frac{m_t^2}{\rho_0} = \text{constant}. \tag{4.4}$$

We can also calculate the change in the entropy across the shock front. If S_0 and S_1 are the entropies per unit mass on the two sides of the front

$$\rho_0 S_0 (V - v_0) \lesseqgtr \rho_1 S_1 (V - v_1)$$

or,

$$m_t S_0 \lesseqgtr m_t S_1 , \tag{4.5}$$

i.e., since we are dealing with an irreversible process, the entropy cannot decrease.

For an ideal gas, $P = \rho R' T$, where $R' = R/M$ = gas constant per unit mass, so that we can write for E

$$E = c_V T = \frac{c_V P}{\rho R' T}$$

where c_V = specific heat per unit mass (at constant volume). Then, since

$$\gamma = \frac{c_p}{c_V} = 1 + \frac{R}{c_V} = 1 + \frac{R'}{c_V},$$

$$E = \frac{1}{\gamma - 1} \frac{p}{\rho}. \tag{4.6}$$

That is, the energy density increase across the shock is

$$\Delta E = E_1 - E_0 = \frac{1}{\gamma - 1}\left[\frac{p_1}{\rho_1} - \frac{p_0}{\rho_0}\right]. \tag{4.7}$$

We can rewrite Eq. (4.3) in a more convenient form:

$$p_1 v_1 - p_0 v_0 = \frac{m_t}{2} (v_1^2 - v_0^2) + m_t \Delta E \tag{4.3'}$$

which, by application of (4.2), becomes

$$\frac{1}{2}(p_1 + p_0)(v_1 - v_0) = m_t \Delta E.$$

A second application of (4.2) gives

$$\frac{1}{2m_t}(p_1 + p_0)(p_1 - p_0) = m_t \Delta E = \frac{m_t}{\gamma - 1}\left[\frac{p_1}{\rho_1} - \frac{p_0}{\rho_0}\right]. \tag{4.8}$$

Since (from 4.4)

$$p_1 - p_0 = -m_t^2\left[\frac{1}{\rho_1} - \frac{1}{\rho_0}\right] \tag{4.4'}$$

Eq. (4.5) becomes

$$-\frac{1}{2}(p_1 + p_0)\left[\frac{1}{\rho_1} - \frac{1}{\rho_0}\right] = \left[\frac{1}{\gamma - 1}\right]\left[\frac{p_1}{\rho_1} - \frac{p_0}{\rho_0}\right].$$

Simple algebraic transformations then lead to the final result:

$$\frac{\rho_1}{\rho_0} = \frac{p_1(\gamma + 1) + p_0(\gamma - 1)}{p_0(\gamma + 1) + p_1(\gamma - 1)}. \tag{4.9}$$

Equation (4.9) is known as the *Rankine-Hugoniot equation.*

Let us now obtain an expression for the velocity V with which the shock moves forward. If we solve Eq. (4.4') for m_t and use Eq. (4.1), we find

$$V - v_0 = \frac{1}{\rho_0}\sqrt{\frac{p_1 - p_0}{\rho_0^{-1} - \rho_1^{-1}}}. \tag{4.10}$$

If we now consider a shock of very small amplitude, such that $p_1 = p_0 + \delta p$, $\rho_1 = \rho_0 + \delta\rho$, $\delta p/p_0$, $\delta\rho/\rho_0 \ll 1$, Eq. (4.10) reduces to

$$V - v_0 = \sqrt{\frac{\delta p}{\delta \rho}}. \tag{4.11}$$

If the fluid in front of our weak shock is at rest, $v_0 = 0$. In any event, the quantity $V - v_0$ is the speed of the shock relative to the fluid in front of it, and its value is correctly given by Eq. (4.10). Appropriate substitution for p_1, ρ_1 in Eq. (4.9) will also lead to the result $\lim_{\delta\rho\to 0} \frac{\delta p}{\delta \rho} = \frac{\gamma p_0}{\rho_0}$, i.e., the shock speed becomes equal to the small amplitude value of the sound propagation speed.

Equation (4.9) can also be solved for the ratio p_1/p_0:

$$\frac{p_1}{p_0} = \frac{\rho_1(\gamma + 1) - \rho_0(\gamma - 1)}{\rho_0(\gamma + 1) - \rho_1(\gamma - 1)}. \tag{4.12}$$

It is useful to express the values of the various parameters before and after the shock in terms of the shock strength η, defined as the ratio of the pressure jump to the quiescent pressure in front of the shock:

$$\eta = \frac{p_1 - p_0}{p_0} \quad \text{or} \quad \frac{p_1}{p_0} = 1 + \eta. \tag{4.13}$$

The speed of the shock front $u(= V - v_0)$ relative to the fluid ahead of it is then given [Eq. (4.12)] by

$$u \equiv V - v_0 = \left[\frac{p_0\eta}{\rho\left[1 - \frac{\rho_0}{\rho_1}\right]}\right]^{1/2} \tag{4.14}$$

where use has also been made of Eqs. (4.9) and (4.13). A further application of Eq. (4.9) and collection of terms yields

$$u = \sqrt{\frac{\gamma p_0}{\rho_0}}\sqrt{1 + \frac{\gamma + 1}{2\gamma}\eta}$$

$$= c_0\sqrt{1 + \frac{\gamma + 1}{2\gamma}\eta} \simeq c_0\left[1 + \frac{\gamma + 1}{4\gamma}\eta\right]. \tag{4.15}$$

The similarity of this equation to the propagation velocity of a finite amplitude harmonic wave [Eq. (3.28)] should be noted. For an ideal gas, Eq. (3.28) becomes

$$v = c_0\left[1 + \frac{\gamma - 1}{2}\frac{u}{c_0}\right]^{\frac{\gamma+1}{\gamma-1}}. \tag{3.28'}$$

For waves of modest amplitude, we expand the bracketed expression in (3.28'), keeping only the first two terms. Then

$$v \simeq c_0\left[1 + \frac{\gamma + 1}{2}\frac{u}{c_0}\right] \tag{4.16}$$

which is the same as the corresponding expansion of Eq. (4.15) if we identify $2\gamma u_0/c_0$ as the equivalent of the shock strength.

The temperature ratio T_1/T_0 across the shock front can also be found. From the general gas law,

$$\frac{T_1}{T_0} = \frac{p_1}{p_0}\frac{\rho_0}{\rho_1} = (1 + \eta)\frac{\rho_0}{\rho_1} \tag{4.17}$$

while Eq. (4.9) can be put in the form

$$\frac{\rho_1}{\rho_0} = \frac{2\gamma + \eta(\gamma + 1)}{2\gamma + \eta(\gamma - 1)}. \tag{4.18}$$

Combining Eqs. (4.17), (4.18) we get

$$\frac{T_1}{T_0} = (1 + \eta)\frac{2\gamma + \eta(\gamma - 1)}{2\gamma + \eta(\gamma + 1)}. \tag{4.19}$$

Some interesting consequences follow from these equations. Suppose, for example, that p_0 is equal to atmospheric pressure, while p_1 is 101 atm. Then the shock strength $\eta = 100$. For air, $\gamma = 1.4$, and we have

$$\frac{\rho_1}{\rho_0} = 5.7, \quad \frac{T_1}{T_0} = 17.7.$$

Actually, in the limit of large η (strong shocks),

$$\frac{\rho_1}{\rho_0} \to \frac{\gamma + 1}{\gamma - 1} = 6 \text{ (air)}$$

and

$$\frac{T_1}{T_0} \to (1 + \eta)\left[\frac{\gamma - 1}{\gamma + 1}\right] = \frac{1 + \eta}{6} \text{ (air)}.$$

That is, the density cannot become greater than 6 times the density of the gas ahead of the shock front, but the temperature can increase linearly with the shock strength. We therefore have a mechanism of achieving very high gas temperatures with only relatively modest density changes, that has been used in investigation of gas reactions under such conditions. [2]

4.2 The Shock Tube.

While much experimental information can be gathered from a study of blast waves, sonic booms, etc. in the open atmosphere, the most detailed comparison of theory and experiment has been provided with the use of the shock tube. Such a tube is pictured in Fig. 4-2.

Such tubes are usually constructed of glass or metal with diameters of a few inches and lengths of about one hundred diameters. The tube is made in two sections, separated by a thin, expendable diaphragm. Each section has separate pumping facilities. The high pressure end is usually about 1/6 the entire length of the tube. A window is placed in the side of the tube for photographic purposes.

In operation, the high pressure end is raised to a level ranging from a few to several thousand atmospheres. The diaphragm is then ruptured and the gas rushes down the tube. A shock front will be formed in a distance equal to about 10 diameters. The structure of the wave as it passes down the tube is indicated in Fig. 4-3. When the diaphragm is ruptured, high pressure gas moves forward. The most advanced front of this moving gas is known as the *contact surface C*. It begins at the diaphragm position and moves forward with the flow velocity v. This plane corresponds to the position defined by $m_t = 0$ in the Rankine-Hugoniot relation. We can see immediately from Eq. (4.4) that the pressure will have the same value in either side of this surface, while Eq. (4.3′) indicates that the velocity will also be continuous.

The shock front S travels with supersonic velocity and pulls away from the contact plane. At the same time, the expansion of the gas, initially to the

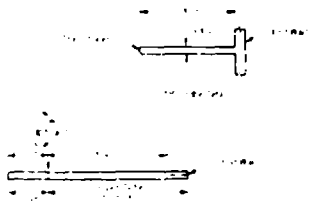

(a)

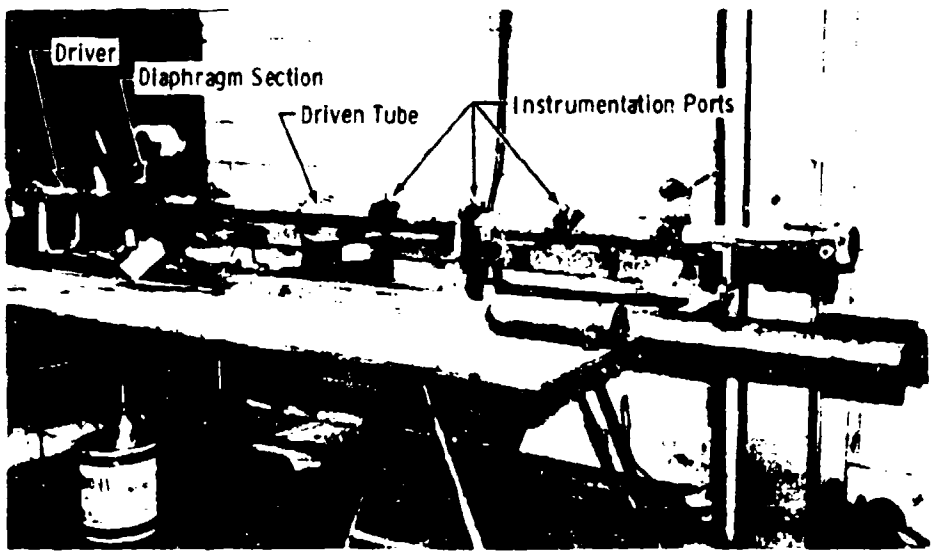

(b)

Figure 4-2.–Form of shock tube: (a) sketch of longitudinal cross section; (b) photograph of actual installation (from J.J. Lacey, Jr. [3] p. 135).

left of the diaphragm, results in a region of reduced pressure or rarefaction that moves to the left from the diaphragm. The foremost part of this wave is known as the "head" H, while the trailing part is called the "tail", T.

Another way of expressing these curves is by a plot in the t,x plane (the so-called x/t diagram). Here t measures the time elapsed after rupture of the diaphragm and x is measured from the diaphragm, positive in the direction of propagation of the shock.

The four dividing plane surfaces in Fig. 4-3 correspond to the four lines in Fig. 4.4: S = shock front, C = contact plane, T = tail rarefaction, H = corresponding head.

The gas in the shaded areas (1,5) of Fig. 4-4 is at rest, ahead and behind the shock. The gas in region 2 moves forward while that in region 3 moves in part in both directions. The gas in region 4 moves to the rear.

When the various wave fronts (S,C,H,T) reach the ends of the tube, they will be reflected back upon themselves. The velocity of the rarefaction wave

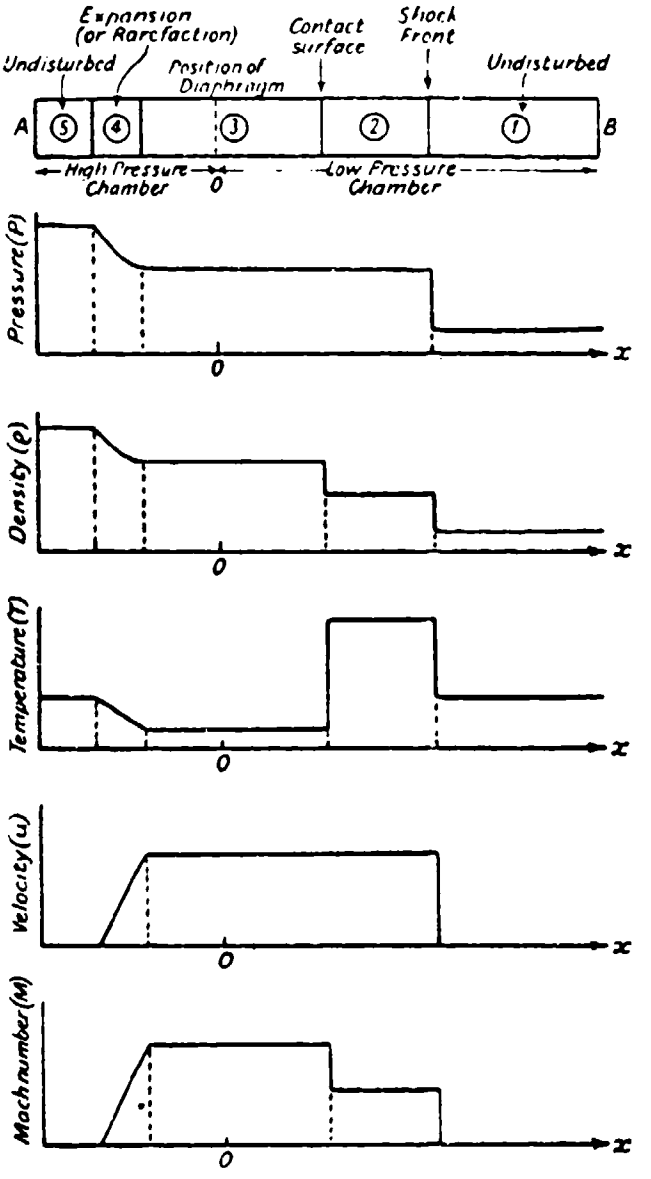

Figure 4-3.–Distribution of various parameters in a shock tube (from Stephens and Bate [1], p. 496).

the front H is greater than that of the shock front, so that it will ultimately catch up with the shock.

In such a reflection, the characteristics of this reflected wave are modified as it successively overtakes the trailing edge of the rarefaction and the contact surface, as well as its final termination at the shock front itself.

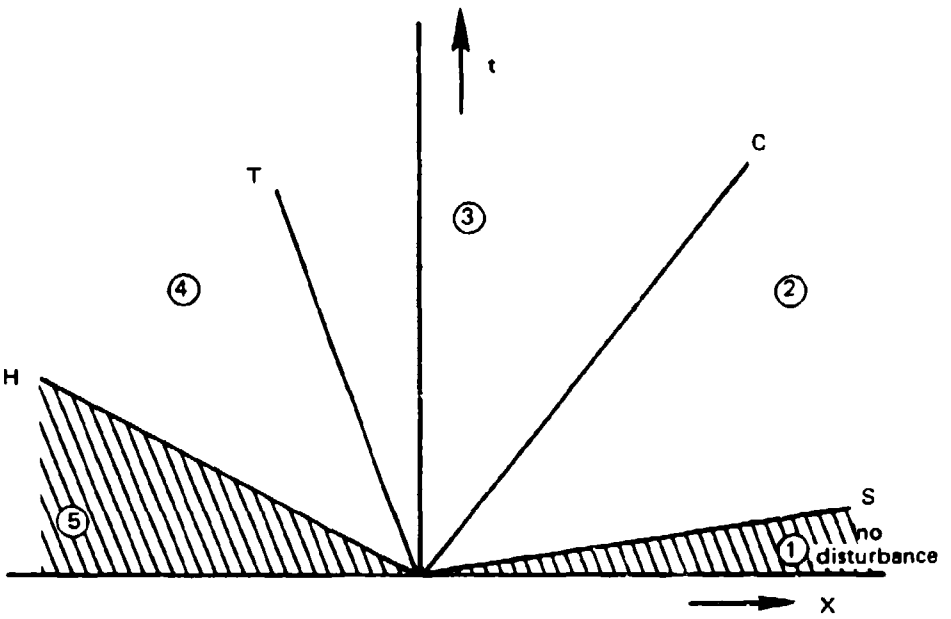

Figure 4-4.–Space-time plot of shock wave: S = shock front, C = contact plane, T = tail rarefaction, H = corresponding head. The numbers correspond to those of Fig. 4-3.

4.3 Reflections of Shocks.

The reflection of a shock wave from a rigid wall is considerably more complicated than simple acoustic reflection. We consider the case of normal incidence, as is illustrated in Fig. 4-5. The dashed lines indicate the behavior of particles at several points in the medium.

The air in region O is at rest, with downstream parameters $v_0 = 0$, ρ_0, p_0, c_0. As the incident shock approaches the wall, the air particles are pushed toward the wall (region 1). This is the upstream region of the incident wave, with $v = v_1$. Finally, region 2 is the region behind the reflected shock, with the air again at rest, so that $v_2 = 0$.

We carry out the analysis of each shock wave separately:

1) *Incident shock.* In this region, the original equations [(4.10) and (4.12)] remain valid and we can write (ref. 2, p. 53)

$$v_1^2 = \frac{\rho_1 - \rho_0}{\rho_1 \rho_0}(p_1 - p_0) = (\pi - 1)^2 \frac{p_0}{\rho_0} \frac{(1 - \mu^2)}{\pi + \mu^2} \tag{4.20}$$

where

$$\mu^2 = \frac{(\gamma - 1)}{(\gamma + 1)} \qquad \pi = \frac{p_1}{p_0}. \tag{4.21}$$

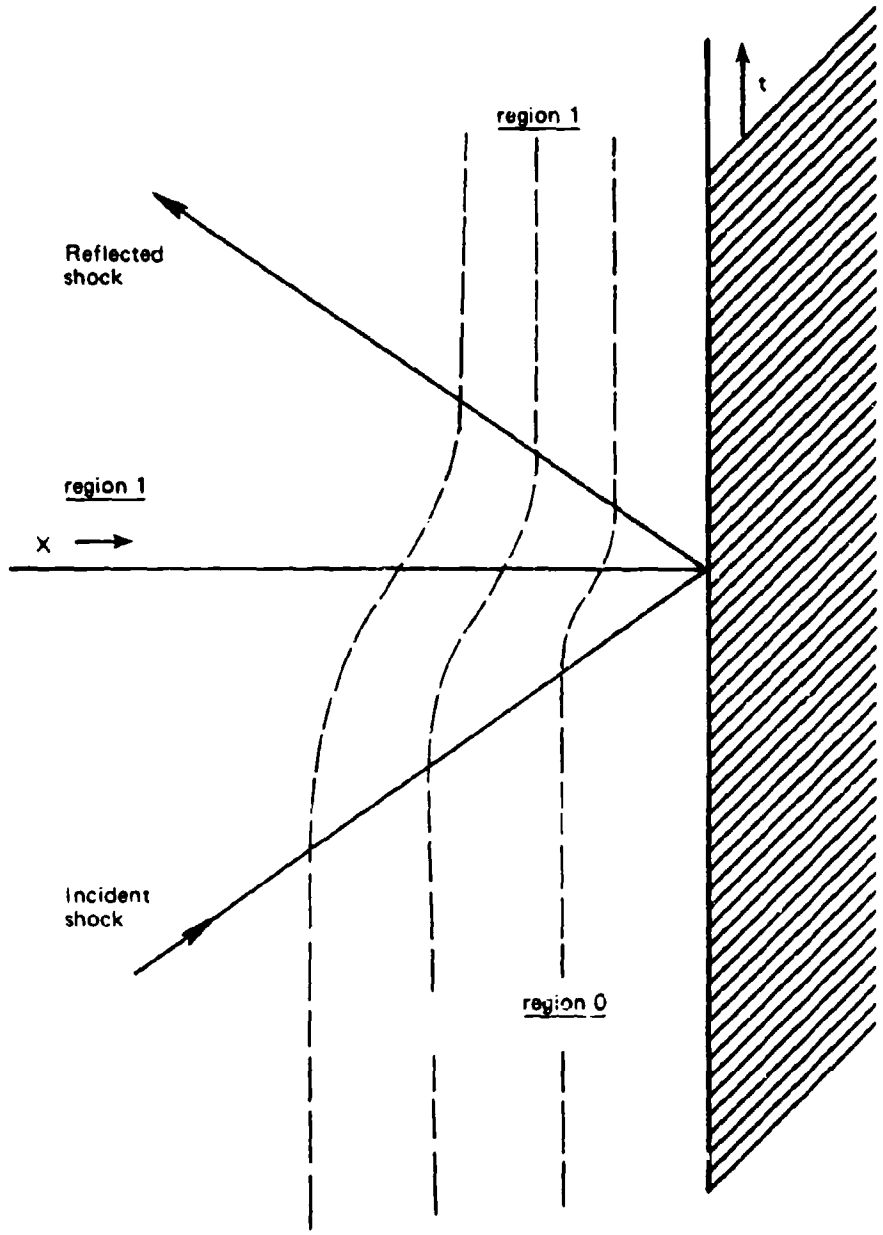

Figure 4-5.–Space-time plot of shock wave reflection at normal incidence.

2) *Reflected shock.* The flow velocity $u_2 = 0$ will be given by an equation similar to (4.20)

$$u_2^2 = (\pi' - 1)^2 \frac{p_1}{\rho_1} \frac{(1 - \mu^2)}{\left[\frac{1}{\pi} + \mu^2\right]} \tag{4.22}$$

where now $\pi' = p_2/p_1$, while the other symbols are the same as before.

Equations (4.20), (4.22) can be solved for the ratio of the excess pressures after and before reflection $(p_2 - p_0)/(p_1 - p_0)$. Physically, this represents the ratio of pressure increase in the reflected shock to the pressure increase in the incident shock. We solve (4.20) for π'

$$\pi' = \frac{p_2}{p_1} = \frac{(2\mu^2 + 1)\pi - \mu^2}{\mu^2\pi + 1}, \tag{4.23}$$

whence it follows that

$$\frac{p_2 - p_0}{p_1 - p_0} = 1 + \frac{1 + \mu^2}{\dfrac{p_0}{p_1} + \mu^2}. \tag{4.24}$$

For a sound wave, the pressure doubles upon reflection, which follows here also in the weak shock limit $p_1 \to p_0$. In general, however, the ratio approaches

$$2 + \frac{1}{\mu^2} = 2 + \frac{\gamma + 1}{\gamma - 1}$$

as p_1 becomes large, and the resulting ratio can be quite large (= 8 for air).

4.4 Method of Characteristics.

Riemann's method of characteristics, introduced in Section 3.3, is very useful in the treatment of shock waves. Let us consider the case of a uniform tube in which a piston is accelerated instantaneously to a constant velocity. This is the idealized behavior of the shock tube.

For an ideal polytropic gas (i.e., a gas for which γ is constant), $\ell(\rho)$ [Eq. (3.36a)] can easily be evaluated in the isentropic case. Using $c^2 = \gamma p/\rho$, $p/\rho^\gamma = p_0/\rho_0^\gamma$, we obtain

$$\ell = \int_{\rho_0}^{\rho} \frac{c}{\rho}\, d\rho = \sqrt{\frac{\gamma p_0}{\rho_0^\gamma}} \int_{\rho_0}^{\rho} \rho^{\frac{\gamma - 3}{2}}\, d\rho$$

$$= \frac{2}{\gamma - 1}\left[\frac{\gamma p_0}{\rho_0^\gamma}\right]^{1/2} \frac{\gamma - 1}{\rho^{\frac{2}{2}}}\Bigg|_{\rho_0}^{\rho} = \frac{2c}{\gamma - 1} - \frac{2c_0}{\gamma - 1}. \tag{4.25}$$

Since we are only interested in the representation $u \pm \ell = \text{const}$ (along the characteristics), the constant term is usually equated to zero so that Eqs. (3.36a) become

$$P = u + \frac{2c}{\gamma - 1} = \text{const}$$
$$Q = u - \frac{2c}{\gamma - 1} = \text{const}. \tag{4.26}$$

If a wave disturbance starts from $x = 0$, $t = 0$, it can clearly be broken up into the two simple waves, P, Q, traveling in opposite directions. If we follow the P wave (Fig. 4-6) we see that $P = u + 2c/(\gamma - 1)$ along its characteristics. In the same region ($x > 0$) Q will remain what it was at $x, t = 0$, i.e., $u = 0$, $Q = -2c_0/(\gamma - 1)$. We can thus evaluate P. From (4.26), $P - Q = 4c/(\gamma - 1)$. Using the value of Q above, we then obtain

$$P = \frac{4c}{\gamma - 1} - \frac{2c_0}{\gamma - 1} \quad (\text{along } dx/dt = u + c)$$
$$Q = \frac{-2c_0}{\gamma - 1} \quad (\text{everywhere}). \tag{4.27}$$

A similar pair can be deduced for the Q wave.

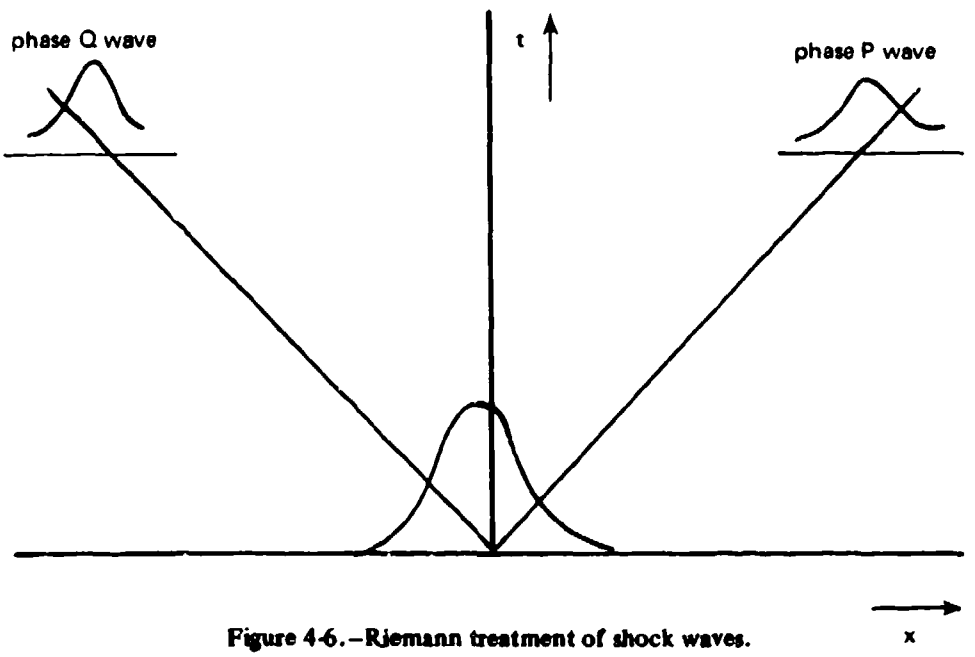

Figure 4-6.–Riemann treatment of shock waves.

We now turn our attention to the characteristics for a wave undergoing steady acceleration so that its velocity increases from 0 at $x = 0$, $t = 0$ to some final value.

For the Q waves in this case,

$$\begin{aligned} \frac{dx}{dt} &= u - c \\ P &= u + \frac{2c}{\gamma - 1} = + \frac{2c_0}{\gamma - 1} \text{ everywhere} \\ Q &= u - \frac{2c}{\gamma - 1} = \text{const.} \end{aligned} \tag{4.28}$$

Again making use of Eqs. (4.26), we obtain

$$Q = P - \frac{4c}{\gamma - 1} = \frac{2c_0}{\gamma - 1} - \frac{4c}{\gamma - 1} \tag{4.29}$$

on the curve $dx/dt = u - c$ and, using the form of Q in (4.28) we can write

$$Q = u - \frac{2c}{\gamma - 1} = \frac{2c_0}{\gamma - 1} - \frac{4c}{\gamma - 1} \tag{4.30}$$

or, solving for u

$$u = \frac{2(c_0 - c)}{\gamma - 1}. \tag{4.31}$$

This enables us to write for c and u

$$\begin{aligned} c &= \frac{2}{\gamma + 1} c_0 - \frac{\gamma - 1}{\gamma + 1} \frac{dx}{dt} \\ u &= \frac{2}{\gamma + 1} c_0 + \frac{2}{\gamma + 1} \frac{dx}{dt} \end{aligned} \tag{4.32}$$

or

$$\frac{dx}{dt} = \frac{\gamma + 1}{2} u - c_0.$$

The resultant characteristics are shown in Fig. 4-7.

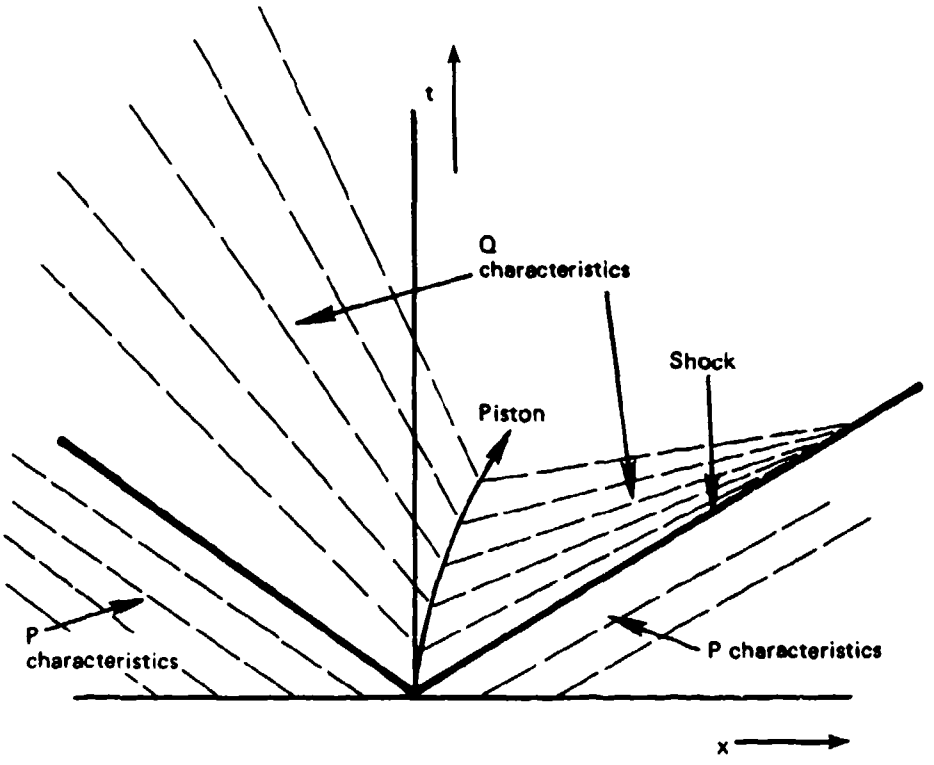

Figure 4-7.–Wave pattern due to steady acceleration of a piston in uniform tube (after Bradley [1], p. 40).

In the region to the left of the line defined by $dx/dt = u_0 - c_0$ ($u_0 = 0$, $x = 0$, at $t = 0$), the fluid is always at rest, so that all the Q characteristics will be straight lines with slope $-1/c_0$.

The path traveled by the piston has the parabolic shape shown. The other Q characteristics will be found from (4.32). As the piston gains speed, dx/dt becomes a smaller negative number, so that the slopes in the t,x plane become steeper.

For the P waves,

$$P = u + \frac{2c}{\gamma - 1} = \frac{4c}{\gamma - 1} - \frac{2c_0}{\gamma - 1}$$

$$Q = -\frac{2c_0}{\gamma - 1}$$

$$\frac{dx}{dt} = u + c.$$

In front of the wave $u = 0$, and we have the characteristics defined by

$$\frac{dx}{dt} = u(= 0) + c_0 .$$

The slopes of these characteristics decrease as the piston increases in speed. Hence a "focusing" of the characteristics takes place—i.e., a shock wave is formed.

Let us now take the limiting case of instantaneous acceleration of the piston. The shock is formed at the origin. In the case of Q characteristics, the situation is the same as in the previous case, except that the piston now moves with a constant velocity u_p (Fig. 4-8). All the characteristics between the head of the rarefaction wave in Fig. 4-8 and the piston now terminate at $x = 0$, $t = 0$, and the shock wave is formed instantaneously at the same point. There are then 5 portions in our diagram. In areas 1 and 5, there is no motion of the fl. . and all Q characteristics have the form $dx/dt = -c_0$. In region 4, the characteristics have the form $x = (u - c_0)t$ and fan out as shown.

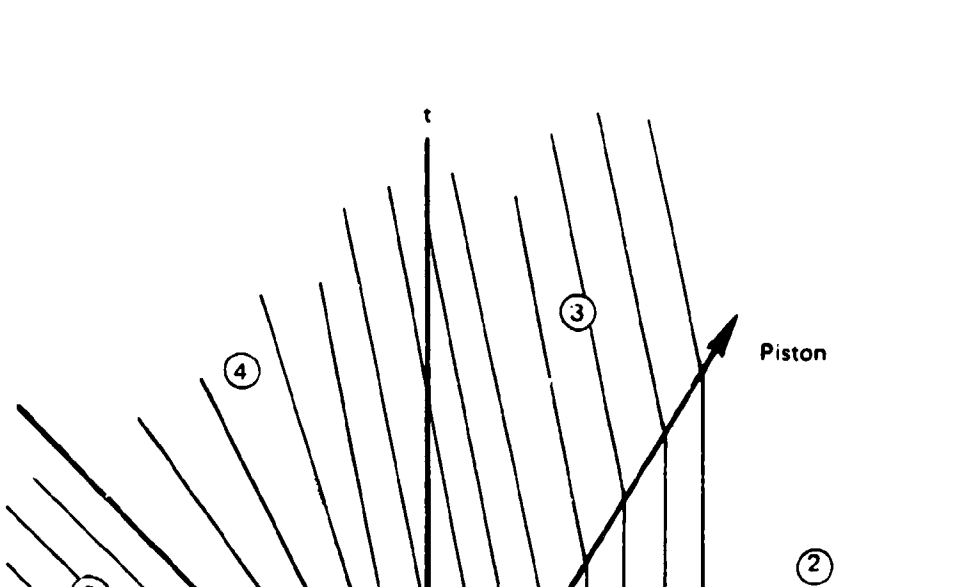

Figure 4-8.—Wave pattern (Q waves) due to instantaneous piston acceleration. Numbers correspond to those of Figure 4-3 (after Bradley [2], p. 42).

We note that when the piston reaches a speed $u_L \geq 2c_0/(\gamma - 1)$, the rarefaction pulls away from the piston, leaving a vacuum behind, between the tail and the piston. For such a condition

$$t = \frac{x}{u_L - c_0}.$$

This equation defines the tail of the wave.

The tail of the wave will have a slope defined by the speed u_L attained by the piston. This also defines a set of parallel characteristics that fill region 3.

The last region to be considered is 2, between the piston and the shock. Here $dx/dt = 0$ and the characteristic curves are vertical lines. This corresponds to sonic flow, i.e., $u = c = 2c_0/(\gamma + 1)$.

It should also be noted that the tail of the rarefaction wave may move to the left or right (Fig. 4-8) depending on whether the flow in region 3 is subsonic or supersonic.

The similarity of Fig. 4-8 to Fig. 4-4 should be remarked. They are in fact the same.

A photograph of the development of the waves in a shock tube, taken by means of the schlieren technique, [2] is shown in Fig. 4-9. Most of the characteristics discussed above can clearly be seen; in particular, the head and tail of the rarefaction waves, the contact surface (split in two) and the shock

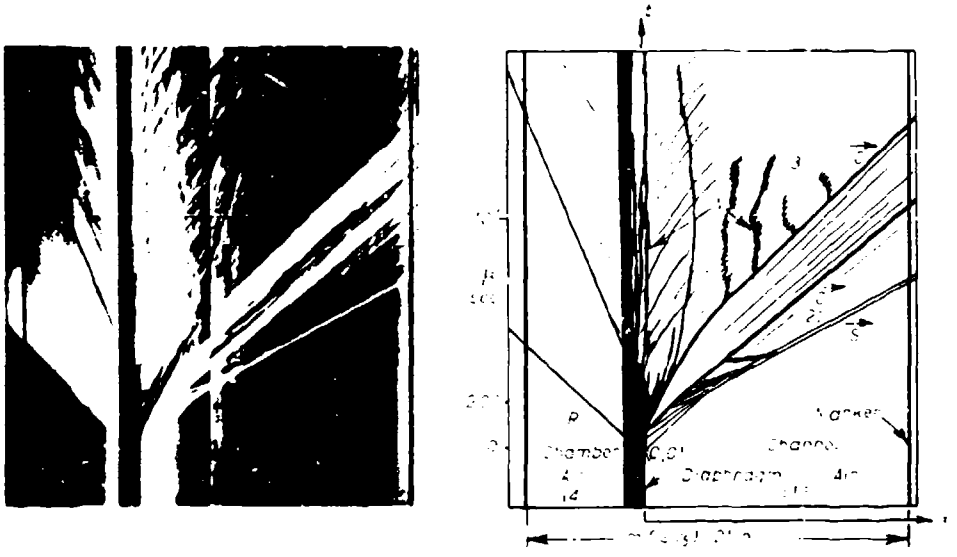

Figure 4-9.–Development of shock wave in tube. Photograph taken by schlieren photograph at Institute of Physics, University of Toronto (from Bradley [2], p. 50).

front are all visible. The wave is not a *centered* one, i.e., the characteristic lines do not extrapolate back to a single point as in Fig. 4-8, but are spread out as in Fig. 4-7, indicating the finite time of acceleration of the piston.

4.5 Shock Wave Structure.

The previous section described various aspects of the fluid flow behind the shock. The behavior of the fluid in the immediate vicinity of the shock front should also be of special interest to us since its features are most closely related with those of nonlinear acoustics.

Thus far we have idealized our shock as a mathematical surface of zero thickness. To proceed further, and to consider finite thickness, it is necessary to refer back to the conservation equations of a continuous medium (see Sections 1.6, 3.1). For the one-dimensional case, these are

$$\frac{d}{dx}(\rho u) = 0 \text{ (continuity)}$$

$$\rho u \frac{du}{dx} = -\frac{dp}{dx} + \frac{d}{dx}\left[b\eta \frac{du}{dx}\right] \text{ (momentum)} \tag{4.33}$$

$$\frac{d}{dx}\left[-pu + b\eta u \frac{du}{dx}\right] + \frac{d}{dx}\left[\kappa \frac{dT}{dx}\right]$$

$$= \frac{\rho u}{\gamma - 1}\frac{d}{dx}\left[\frac{p}{\rho}\right] + \rho u \frac{d}{dx}\left[\frac{u^2}{2}\right] \text{ (energy).}$$

In the second of the equations above (the one-dimensional Stokes-Navier equation), the viscosity term is included as a variable rather than the constant quantity used in Eq. (3.43). The early analysis of shock wave thickness by Becker [4] did not include the possible variation of the viscosity at the high temperatures achieved in the shock zone. Therefore, his results are valid only for weak shocks. (See also the paper by Thomas. [5])

Our analysis follows in part that of Shapiro and Kline. [6] The continuity equation can be integrated immediately to give

$$\rho u = m_t, \text{ a constant.} \tag{4.34}$$

After substitution of $u = m_t$ in the first term of the Navier-Stokes equation, we can integrate it immediately, obtaining

$$m_t u + p - b\eta \frac{du}{dx} = F, \text{ a constant.} \tag{4.35}$$

The constant F can be evaluated upstream, where the flow is uniform, so that $du/dx = 0$. Then $F = m_t u_1 + p_1$.

Proceeding in the same fashion, we integrate the third of Eqs. (4.33) to get

$$\begin{aligned} pu - b\eta u \frac{du}{dx} - \kappa \frac{dT}{dx} + \frac{m_t}{\gamma - 1} \frac{p}{\rho} + m_t \frac{u^2}{2} \\ = G = \text{constant} \\ = p_1 u_1 + \frac{m_t}{\gamma - 1} \frac{p_1}{\rho_1} + m_t \frac{u_1^2}{2}, \end{aligned} \tag{4.36}$$

where the constant G has also been evaluated upstream.

If we make use of the ideal gas law $p = \rho RT$, the energy equation can be rearranged to read

$$\frac{\gamma}{\gamma - 1} pu - \frac{1}{2} b\eta \frac{d(u^2)}{dx} - \frac{\kappa}{Rm_t} \frac{d}{dx} (pu) + \frac{m_t u^2}{2} = G, \tag{4.37}$$

while the Stokes-Navier equation can be written

$$pu - Fu - m_t u^2 + \frac{1}{2} b\eta \frac{du^2}{dx}. \tag{4.38}$$

If we eliminate pu from these equations, we get the nonlinear differential equation

$$\begin{aligned} -\frac{1}{2} \frac{\kappa u}{Rm_t} \frac{d^2}{dx^2} (u^2) + \left[\frac{1}{2} \frac{b\eta}{\gamma - 1} + \frac{\kappa}{R} \right] \frac{d(u^2)}{dx} \\ - \frac{\kappa}{Rm_t} F \frac{du}{dx} - \frac{\gamma + 1}{\gamma - 1} m_t \frac{u^2}{2} + \frac{\gamma}{\gamma - 1} Fu = G \end{aligned} \tag{4.39}$$

which is of rather formidable appearance.

This equation has been solved by Becker [4] for the case of constant viscosity, and for the specific value of the Prandtl number $P_r = c_p\eta/\lambda = 0.75$.

The flow velocity has a number of requirements built into it. Upstream it must have the value u_1, downstream, u_2. In the Becker theory, the velocity at the inflexion point ($d^2u/dx^2 = 0$) is required to be $c^* = \sqrt{u_1 u_2}$.

To satisfy these conditions, Shapiro and Kline expressed u in terms of the error function

$$\begin{aligned} x \leqslant 0 \quad & u = c^* + (u_1 - c^*)\ \mathrm{erf}\ (-x/x_0) \\ x \geqslant 0 \quad & u = c^* + (u_2 - c^*)\ \mathrm{erf}\left[\sqrt{\frac{u_1}{u_2}}\,\frac{x}{x_0}\right] \end{aligned} \tag{4.40}$$

where

$$\mathrm{erf}\ (z) = \sqrt{\frac{2}{\pi}}\int_0^z e^{-t^2/2}\,dt \tag{4.41}$$

and x_0 is a constant still to be determined.

We define the shock thickness δ as

$$\delta = \frac{u_2 - u_1}{(du/dx)|_{x=0}} \tag{4.42}$$

and determine x_0 by requirement that Eq. (4.40) be an exact solution of (4.39). At the inflexion point $x = 0$, we get the result

$$\frac{\delta}{x_0} = \sqrt{\frac{\pi}{2}}\,\frac{M_1^* + 1}{M_1^*} \tag{4.43}$$

where $M_1^* = u_1/c^*$ is the ratio of the upstream flow velocity to the inflexion point velocity.

We now proceed to eliminate x_0. Making use of Eqs. (4.39)-(4.43), and denoting the values of the transport parameters at the inflexion point by asterisks, we obtain the following expression for the shock thickness δ:

$$\begin{aligned} \delta = {} & \frac{\eta^*}{\rho_1 u_1}\,\frac{D}{\gamma + 1}\,\frac{M_1^* + 1}{M_1^* - 1} \\ & \times \left\{1 \pm \left[1 + \frac{8\gamma(\gamma - 1)}{3Pr^*}\,\frac{1}{D^2}\,\frac{(M_1^* - 1)^2}{M_1^*}\right]^{1/2}\right\} \end{aligned} \tag{4.44}$$

where

$$D = \frac{4}{3} + \frac{2\gamma}{Pr^*} - \left[\frac{\gamma + 1}{2Pr^*}\right] \frac{M_1^{*2} + 1}{M_1^*} \tag{4.45}$$

$$M^* = \frac{u_1}{c^*} = \sqrt{\frac{\gamma + 1}{2}}\, \frac{u_1}{c_0} . \tag{4.46}$$

A comparison of the curve (4.40) and Becker's solution is shown in Fig. 4-10.

Typical thicknesses computed by Shapiro and Kline are shown in Fig. 4-11. It should be noted that the evaluation of T presents some difficulty. Becker found that the adiabatic stagnation temperature T_0 remained constant throughout this region and that $T^* = 2T_0/(\gamma + 1)$ in this gas. Shapiro and Kline used this value and the standard expressions for the temperature dependence of η and κ.

The shock thickness is often expressed in terms of the Reynolds number

$$\mathrm{Re} = \frac{\rho_1 u_1 \delta}{\eta^*} . \tag{4.47}$$

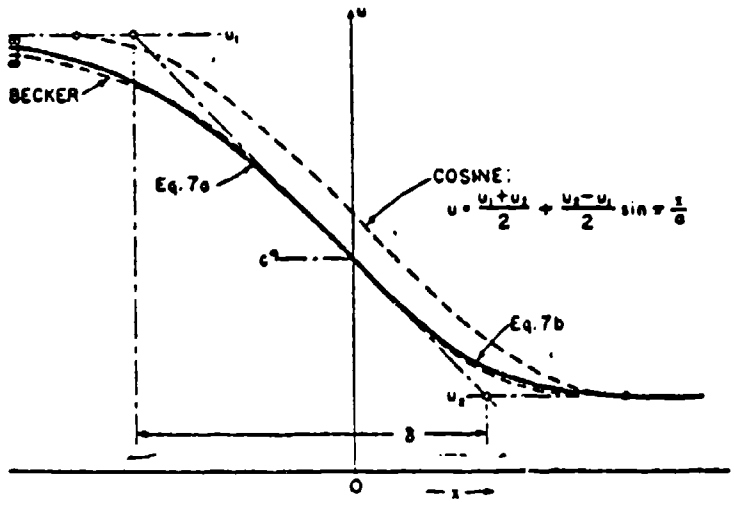

Figure 4-10.–Comparison of Becker's exact velocity distribution (for $P_r = 3/4$, $M_1 = 2.0$ and $k = 1.4$) with arbitrary error curve, symmetric cosine curve and Eq. (4.40) (from Pain and Rogers [7]).

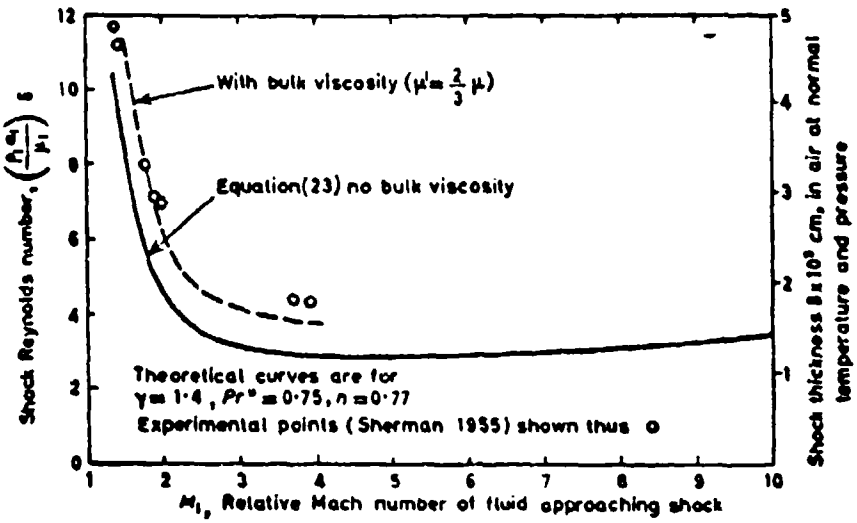

Figure 4-11.–Effect of shock Mach number in front thickness for diatomic gases (from Pain and Rogers [7]).

For weak shocks ($M_1^* \to 1$), Eq. (4.44) reduces to

$$\mathrm{Re} \simeq \frac{4}{\gamma + 1}\left[\frac{4}{3} + \frac{\gamma - 1}{Pr^*}\right]\frac{1}{M_1^* - 1} . \tag{4.48}$$

The thickness δ should be compared with the thickness of the finite amplitude wave as given by Eq. (3.87).

A calculation based on Eq. (4.44), valid for diatomic gases is shown in Fig. 4-11. The solid curve represents the case of zero bulk viscosity, the dashed curve that for a bulk viscosity arbitrarily set at 2/3 the shear viscosity. Experimental points by Sherman [7] are also given. The agreement is quite satisfactory.

The agreement shown in the figure suggests that the measurement of shock wave thickness would be suitable for the determination of the bulk viscosity coefficient.

4.6 Shock Thickness in Liquids.

In liquids, as the equivalent to (4.40), one usually employs the hyperbolic tangent curve

$$p = \frac{1}{2}(p_1 + p_2) + \frac{1}{2}(p_2 - p_1)\tanh\frac{2x}{\delta} \tag{4.49}$$

where p_1, p_2 are the pressures up and downstream and δ is again the shock thickness. If we use pressure as our variable, Eq. (4.42) becomes

$$\delta = \frac{p_2 - p_1}{(dp/dx)_{max}}. \tag{4.50}$$

This can in turn be related to thermodynamic parameters

$$\delta = \frac{\left[16b\eta + \kappa\left(\frac{1}{c_V} - \frac{1}{c_p}\right)\right]}{\beta} \cdot \frac{c_0}{\Delta p}. \tag{4.51}$$

where β, b have the values defined by Eqs. (3.33) and (3.44).

Experimental measurements of this thickness were reported by Flook and Hornig in 1955. [8] Their technique may be understood by reference to Fig. 4-12.

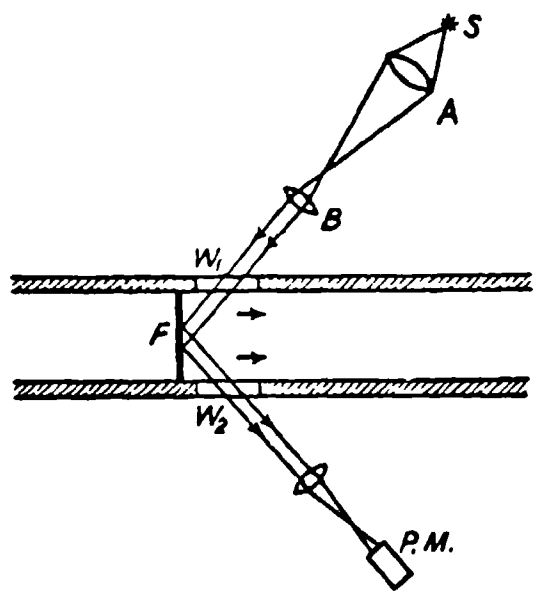

Figure 4-12.–Optical system for measuring shock thickness in liquids: S = source, A,B = focusing system, W_1, W_2 = windows, F = shock front, $P.M.$ = photomultiplier (after Flook and Hornig [8]).

A monochromatic light is passed through a window in the shock tube, is reflected out through a second window and focussed on a photomultiplier.

The reflectivity of the advancing shock front could be measured and then related to the density variation. Such a technique had been widely used in gases, but its success in liquids has been limited.

In 1964, Eisenmenger [9] presented a new technique. In his experiment, shock wave microphones were used to measure the rise time of the incident pressure pulse. The times were determined by a frequency analysis (in the 100-1000 MHz range) of the output signal from the piezoelectric transducer.

A comparison of Eisenmenger's data with those of Flook and Hornig for acetone is shown in Fig. 4-13.

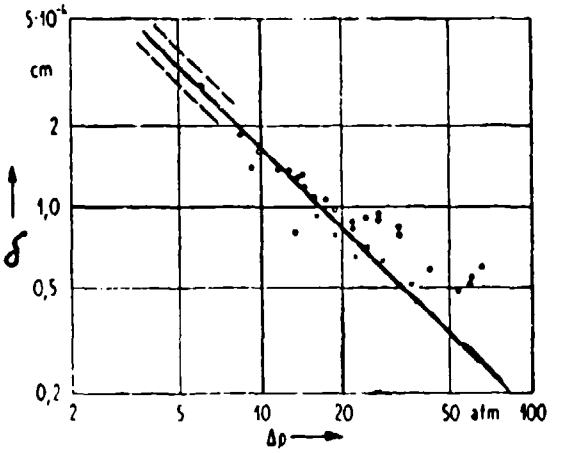

Figure 4-13.–Shock front thickness in acetone as a function of pressure jump: ●●● 26°C [7], ○○○ 19°C [8], ××× 50.5°C [8], _____ theoretical curve (from Eisenmenger [9]).

Table 4-1

(largely from Eisenmenger [9])

	T_c	c, 10^5 cm/sec	α/ν^2, 10^{-17} cm^{-1}/sec^2	B/A	$\Delta p\delta$, 10^{-3} cm-atm	
					Theoret.	Exper.
water	16	1.46	27.5	4.9	7.7	7.1
acetone	19	1.19	30	9.2	1.74	1.64
CCl_4	20	0.925	500	8.5	23.2	21.1
Toluene	20	1.328	80	5.6	11.5	7.3
				7.9	8.8	
Methanol	20	1.12	34	9.6	1.49	1.74
Ethanol	20	1.117	52	10.5	2.50	2.8

The results of Eisenmenger's work for a number of liquids are shown in Table 4-1. The calculations here are an interesting blending of acoustic absorption theory (the role of the bulk viscosity) and nonlinear acoustics (in particular the nonlinear parameter B/A). At the time of the Flook-Hornig work, the theory of ultrasonic absorption in liquids was very imperfectly known, while quantitative knowledge of B/A was almost entirely lacking. The agreement that now exists between the experimental values of the shock thickness and the values computed by means of the better established values of α and B/A is reasonably satisfactory.

4.7 *N* Waves. The Sonic Boom.

As has already been observed, the rapid passage of fluid over the surface of a solid body can give rise to a shock wave. In a study of "ballistic" shock waves in 1946, Dumond, Cohen, Panofsky and Deeds [10] introduced the term *N waves* for this phenomenon, since the pressure profile of the wave is approximately that shown in Fig. 4-14.

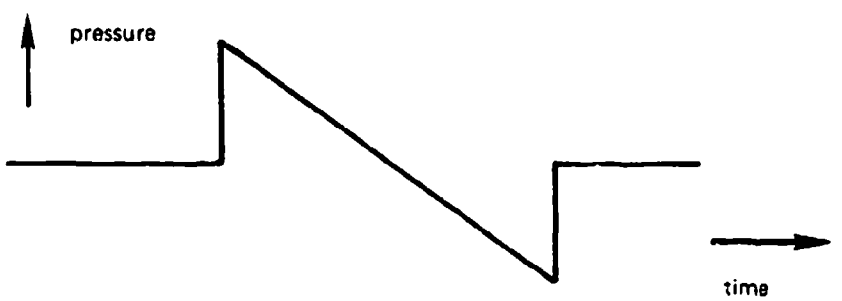

Figure 4-14.–*N* wave.

The buildup of a shock in the neighborhood of a speeding projectile in air (or the formation of the analogous bow wave in the case of a fast moving boat on the surface of the water) is a direct consequence of the medium's inability to move the wave fast enough out of the way of the oncoming source, so that there is a substantial compression of the medium just ahead of the projectile. The form of the wave front in this case can be obtained from a consideration of Fig. 4-15.

In the figure, a source of sound is moving to the right with velocity $v = 1.6\ c_0$. The points A,B,C,D,E are the positions of the source as observed after each of a series of equal time intervals Δt.

The spherical waves set up by the source when it was located at each of these points are shown at corresponding later times. Thus, when the source reaches B, the sound from point A will lie along the curve B', of radius $c_0 \Delta t$. When the source reaches C, the sound from A lies along the curve C'

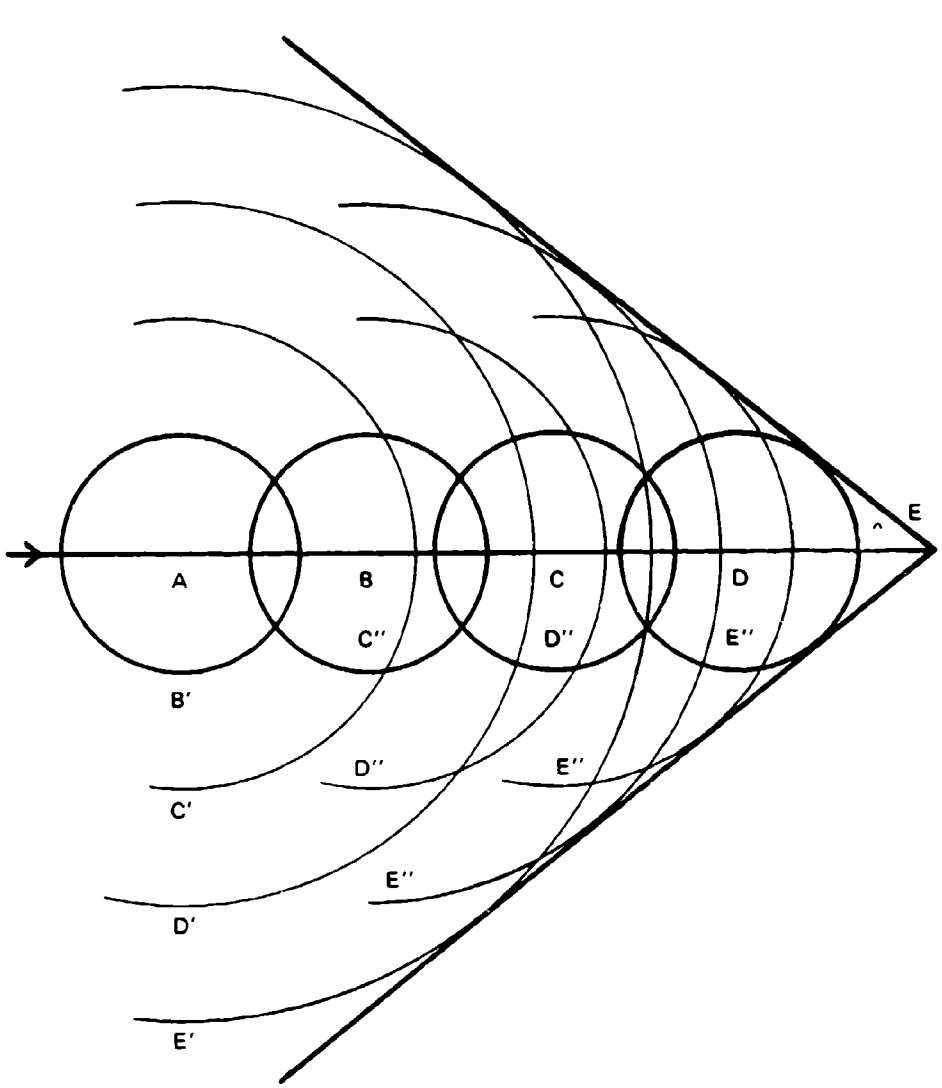

Figure 4-15.–Generation of sonic boom.

[radius $c_0(2\Delta t)$], while the sound from B lies along C'' (radius $c_0\Delta t$). The other curves are similarly drawn when the source is at D,E.

The trace of the resulting wavefront is then given by the tangent curve shown. The angle θ made by the front with the direction of motion of the source is then

$$\sin\theta = \frac{AE'}{AE} = \frac{c(4\Delta t)}{v(4\Delta t)} = \frac{c}{v} = \frac{1}{M}, \tag{4.52}$$

where M is the Mach number. The front of the N wave therefore moves out over a conical surface.

The N wave differs from the shock waves discussed previously in that the pressure is not constant behind the shock front. Therefore, some of the formulas applying to that case require modification. In the elementary treatment of Dumond et al., this was not taken into account.

If we write the Earnshaw relation (3.25a) in terms of $\gamma = (B/A) + 1$, we have

$$u - u_0 = \frac{2c_0}{(\gamma - 1)\left[1 + \frac{\partial \xi}{\partial x}\right]^{\frac{\gamma-1}{2}}}$$

or, since

$$\frac{\rho}{\rho_0} = \left[\frac{p}{p_0}\right]^{\frac{1}{\gamma}} = \left[1 + \frac{\partial \xi}{\partial x}\right]^{-1},$$

we obtain

$$u - u_0 = \frac{2c_0}{\gamma - 1}\left[\frac{p}{p_0}\right]^{\frac{\gamma-1}{2\gamma}}. \tag{4.53}$$

If we consider a coordinate system moving with the speed of sound c_0, then $u = -c_0$ when $p = p_0$, then Eq. (4.53) yields

$$u_0 = -\frac{\gamma + 1}{\gamma - 1} c.$$

Dumond et al. combined the equations of continuity (3.10) and motion (3.16) in Eulerian form and substituted Eq. (4.55) to obtain a rather cumbersome equation for the pressure. This can be simplified by writing $p = p_0(1 + \phi)$, expanding and neglecting terms of order ϕ^2. The final result is

$$-\frac{\gamma + 1}{2\gamma} c\phi \frac{\partial p}{\partial x} = \frac{\partial p}{\partial t}$$

or

$$\left.\frac{\partial x}{\partial t}\right|_{p=\text{const}} = -\frac{\partial p/\partial t}{\partial p/\partial x} = \frac{\gamma + 1}{2\gamma} c_0\phi. \tag{4.54}$$

This is the speed with which the pressure p moves relative to the center of the N wave (where $p = 0$, $u = c_0$). Hence two points with pressures corresponding to the values ϕ_1, $-\phi$, will separate at a rate twice that of Eq. (4.54) or $[(\gamma + 1)/\gamma]c_0\phi$. If we go back to Eq. (4.15) we see that the value of (4.54) is just twice that for the elevation of the speed of a weak shock above that of the speed of sound. The reason for this apparent discrepancy may be understood from Fig. 4-16 and is associated with the weakening of the shock front.

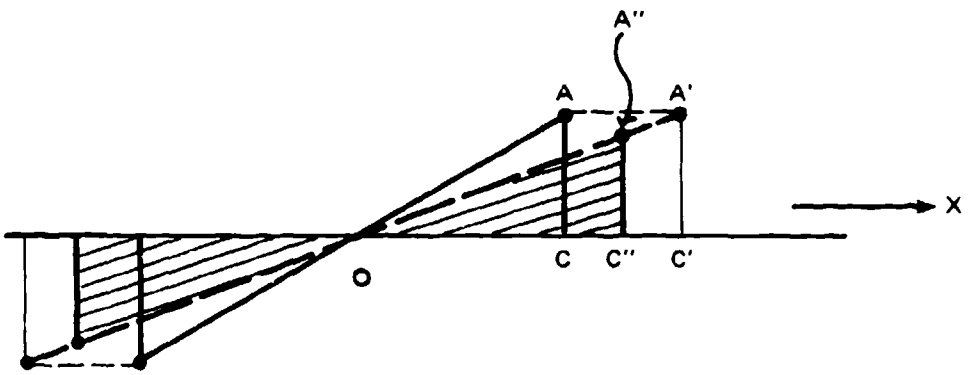

Figure 4-16.–Degradation of N wave.

In Fig. 4-16, the discontinuity AC moves to the right, with a speed $[(\gamma + 1)/4\gamma]c_0\phi_A$ relative to the forward motion of the point 0. In some small time interval δt, it therefore moves to the x position C''. Now, the excess pressure $p_0\phi_A$ moves to the right at twice this velocity, reaching the line AC'. The peak of the front has therefore moved only to the point A''–i.e., the peak pressure in the shock has fallen to the value $p_0\phi_{A''}$. Since the reverse holds at the tail of the wave, the rate at which the entering wave increases in length is given by

$$\frac{dL}{dt} = \frac{\gamma + 1}{2\gamma} c_0\phi. \tag{4.56}$$

The rate at which the amplitude decreases can also be determined from the geometry of Fig. 4-16. From the similarity of triangles $OA''C''$ and $OC'C'$, we obtain

$$\frac{\phi_{A''}}{\phi_{A'}} = \frac{OC''}{OC'} = \frac{\frac{1}{2}L + \frac{\gamma + 1}{4\gamma} c_0\phi_A\delta t}{\frac{1}{2}L_0 + \frac{\gamma + 1}{2\gamma} c_0\phi_A\delta t} \simeq 1 - \frac{\gamma + 1}{2\gamma}\frac{c_0}{L}\phi_A\delta t$$

and in the limit as $\delta t \to 0$

$$\frac{d\phi}{dt} = -\frac{\gamma + 1}{2\gamma} \frac{c_0}{L} \phi^2. \tag{4.57}$$

The energy E in the N wave is proportional to the length of the wave L and to the square of its amplitude ϕ. Hence the logarithmic derivative of E with respect to time is given by

$$\frac{1}{E} \frac{dE}{dt} = \frac{1}{L} \frac{dL}{dt} + \frac{2}{\phi} \frac{d\phi}{dt} = -\frac{(\gamma + 1)\phi}{2\gamma L} \tag{4.58}$$

which is the rate at which energy is lost per unit distance in a direction normal to the shock front.

The usual problem presented by a sonic boom is the strength of the shock as perceived by an observer on the ground when a supersonic plane has flown by on a horizontal trajectory. Equations (4.56)-(4.58) applied strictly only to a plane N wave, but will serve as reasonable approximations if the radius of curvature of the wavefront is large compared with the wavelength L.

The geometry of our problem is shown in Fig. 4-17. In the time interval considered the airplane flies from the position OO' to the position AA'. The sound emitted from position OO' is contained in the N wave that has reached the shaded region by the time the airplane has reached AA'. (The "head" wave lies along HA', the tail along TA.) The perpendicular distance y from the center of the N wave to the line of flight is known as the *miss distance.*

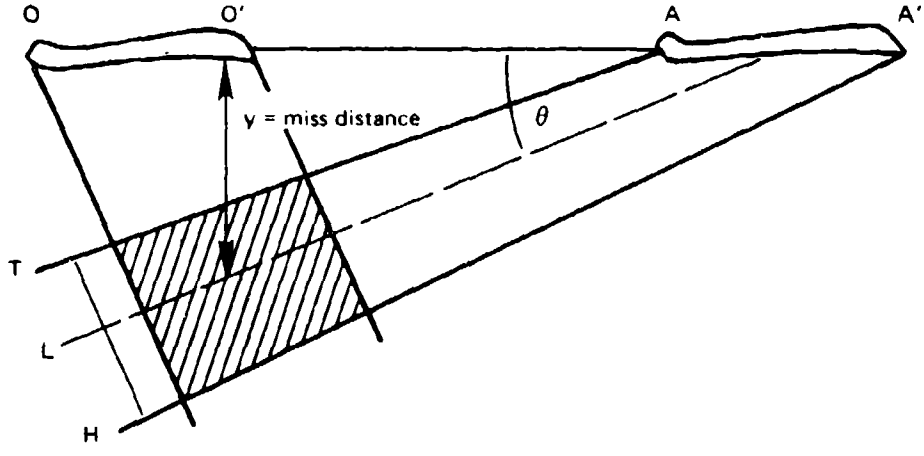

Figure 4-17.–Geometry of the sonic boom

By the application of some tedious algebra, Dumond et al. obtained expressions for the N-wavelength L and the amplitude factor ϕ as a function of the miss distance that are valid for relatively large miss distances.

$$L = \frac{2c_1c_2(\gamma + 1)}{\gamma \cos\theta} y_0^{1/4}(1 - y_0^{-1/2})^{1/2} \tag{4.59}$$

$$\phi = c_2 y_0^{-3/4}(1 - y_0^{-1/2})^{-1/2}. \tag{4.60}$$

Here $y_0 = y/c_1$, and c_1, c_2 are constants which depend on the geometry of the shock source. At large miss distances then,

$$\begin{aligned} \phi &= \text{const } y^{-3/4} \\ L &= \text{const } y^{1/4}. \end{aligned} \tag{4.61}$$

A more sophisticated analysis by Whitham [11] leads to the farfield bow-shock pressure generated by bodies of revolution:

$$2p_0\phi = \Delta p_{max} = \frac{pK_r(M^2 - 1)^{1/8}}{(H/\ell)^{3/4}} K_s \frac{D}{\ell}. \tag{4.62}$$

Here D is the equivalent body maximum diameter, K_S a shape factor, K_r a reflection factor for amplification by ground reflection; K_r is theoretically equal to 2. M is the Mach number, ℓ the length of the aircraft, p the local pressure, h the miss distance; h has the same dependence on the miss distance in Eq. (4.61).

An experimental verification of Eqs. (4.61) is shown in Fig. 4-18 which shows actual recorded pressures (*flight signatures*) from flights of a fight airplane at various altitudes. The dashed lines indicate the theoretical dependence, in line with Eqs. (4.61).

The detail of the near field signature ($h = 60$ ft) is due to shock fronts from various separate parts of the plane. These gradually blend into the characteristic N wave for the far field. [12]

It is of interest to compare the decay of the N wave with that of the sawtooth [Eq. (3.52)]. The pressure step Δp_{saw} for the sawtooth is given by that equation

$$\Delta P_{saw} = p_{10} \frac{2\ell\pi}{\ell + x} \tag{3.52}$$

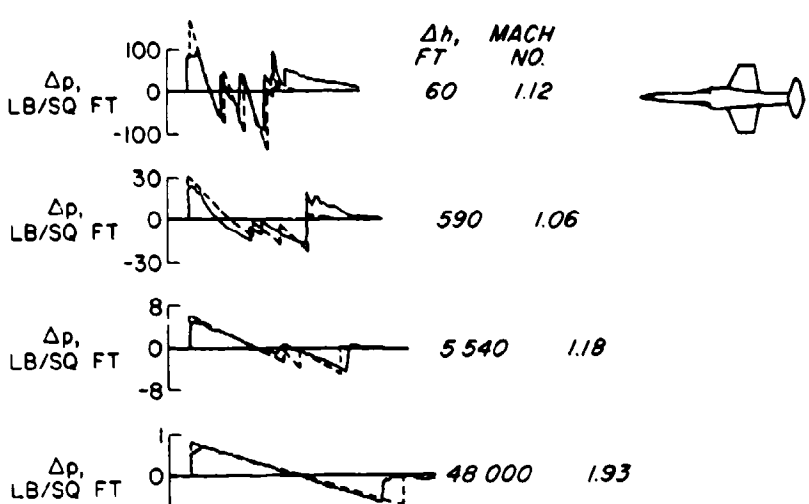

Figure 4-18.–Flight signature. _____ Experiment; - - - - - Theory (from Carlson, Mack and Morris [12]).

where ℓ is the discontinuity length. For the N wave, we rewrite Eq. (4.57) in terms of the pressure step $\Delta p_N = 2p_0\phi$:

$$\frac{d\Delta p_N}{(\Delta p_N)^2} = -\frac{\gamma + 1}{2\gamma}\frac{c_0}{L}\frac{dt}{2p_0}$$

or

$$(\Delta p_N)^{-1} = \frac{\gamma + 1}{2\gamma}\frac{c_0 t}{L 2p_0} + \text{const.}$$

with $c_0 t = x$. At $t = 0$, the pressure step Δp_N is maximum, Δp_{max}, so that

$$(\Delta p_N)^{-1} = \frac{\gamma + 1}{2\gamma}\frac{x}{2p_0 L} + (\Delta p_{max})^{-1}$$

or

$$\Delta p_N = \frac{1}{\frac{\gamma + 1}{2}\frac{x}{2\gamma p_0 L} + \frac{1}{\Delta p_{max}}}. \tag{4.63}$$

If we regard the length L of our N wave as the effective wave length λ_N, so that the discontinuity length ℓ can be interpreted as

$$\ell = \frac{2}{\gamma + 1} \frac{2\rho_0 c_0^2}{\Delta p_{max}} \frac{L}{2\pi}, \tag{4.64}$$

then Eq. (3.52) may be written ($\gamma p_0 = \rho_0 c_0^2$)

$$\Delta p_N = \frac{\Delta p_{max} 2\pi\ell}{x + 2\pi\ell} \tag{4.65}$$

which corresponds to Eq. (3.52) for $x \gg 2\pi\ell$.

The major difference between the phenomenon of the N wave and that of the finite amplitude sawtooth waves discussed in Chapter 3 is that the "wavelength" L increases as the N wave propagates, while the wavelength of the sawtooth remains fixed at the value for its fundamental component. While the result is rather obvious, it is perhaps not without merit to consider the effect briefly. An instantaneous picture of the profiles of the two types of waves is shown in Fig. 4-19.

In the case of the N wave (Fig. 4-19a), the wave B moves forward relative to the midpoint 0 at the speed given by Eq. (4.54), speed which is one-half the value of dL/dt in Eq. (4.56). Similarly, the tail wave T drops back (behind 0) at the same numerical rate. As has been pointed out previously, the lengthening of the shock coincides with a weakening of its intensity from the same mechanism.

For a periodic wave of nearly sawtooth shape (Fig. 4-19b) the spreading out of the length of the wave is not possible. As Blackstock has demonstrated in his treatment of the range of finite amplitude propagation between those governed by the Fubini and Fay solution (Section 3.8), the maximum particle velocity moves forward within the wave, but is cut off in its further motion upon its approach to the discontinuity. The waveform therefore stabilizes in the pattern shown in Fig. 4.19b and decays while remaining in approximately that shape.

4.8 Underwater Explosions.

The explosion of TNT or similar material underwater produces a shock wave with special features of its own. Besides its obvious practical military significance, the study of such explosions has provided insight into shock wave propagation, involved the interrelation of viscosity and finite amplitude effects, and the explosions themselves can serve as acoustic sources in long-range propagation studies.

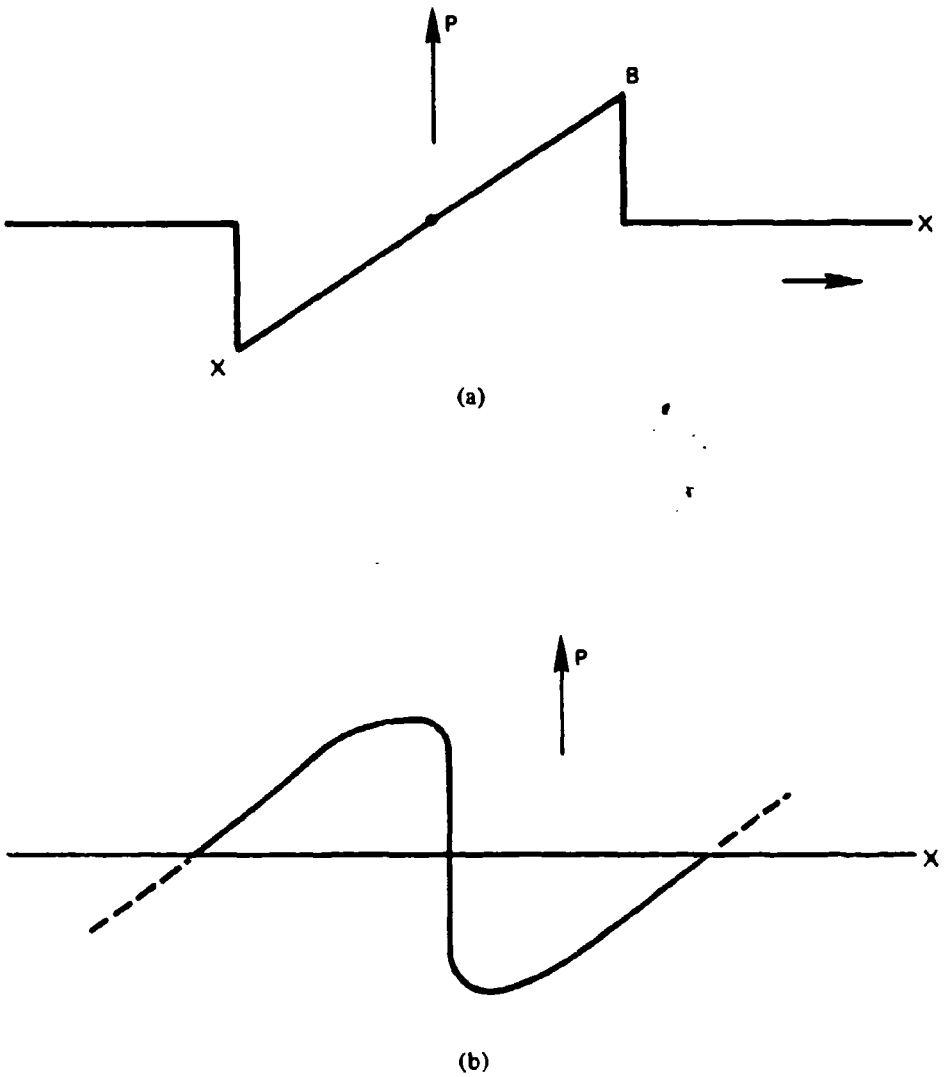

Figure 4-19.–Comparison of *N* wave and the nearly sawtooth sound wave.

For these reasons, it is appropriate to discuss the phenomenon briefly here. For the mathematical details, the reader should consult the works of Arons [13] and Cole. [14]

When an explosive charge is detonated underwater, the initial solid material of the charge is converted rapidly into a sphere of gaseous products at high temperature and pressure. Since the water offers only the relatively low hydrostatic pressure as resistance, the sphere expands rapidly. This expansion lowers the pressure in the bubble so that the bubble reaches maximum size and then contracts under the hydrostatic pressure. This in turn causes a buildup of pressure outside the bubble, so that it is ultimately compressed to minimum size, and then expands once again, repeating the original oscillation.

During this oscillation, however, several events take place which cause the oscillation to be attenuated so that no more than 5-10 pulsations occur. First, the bubble rises (migrates) under the influence of gravity. This converts some of the potential energy of the bubble into kinetic energy of the water, so that there is a steady loss of energy from the bubble.

Next, a pressure pulse (shock wave) is emitted from the bubble each time it passes through its minimum size. This also extracts energy from the source.

Major success in treating explosion phenomena has come from the development of scaling laws. In 1947, Friedman [15] pointed out that the following scale factors are appropriate for length L and time T:

$$L = \left[\frac{3E}{4\pi P^*}\right]^{1/3}$$
$$T = L\left[\frac{3\rho}{2P^*}\right]^{1/2} \tag{4.66}$$

where E is the total energy to be associated with the bubble oscillation, P^* the absolute hydrostatic pressure at the location of the explosion and ρ the equilibrium density of the liquid. These can also be expressed in terms of the bubble energy per unit mass of explosion ϵ (in cal/gm), the weight of the explosive W (in pounds) and the equivalent water depth of the pressure p^*– $Z^* = Z + 33$ (in feet). In terms of these rather bizarre units, we have

$$L = 1.733\epsilon^{1/3}\left[\frac{W}{Z^*}\right]^{1/3}$$
$$T = 0.373\epsilon^{1/3}\frac{W^{1/3}}{(Z^*)^{5/6}}. \tag{4.67}$$

A fundamental theory of explosion shock wave propagation has been developed by Kirkwood and Bethe [16] and is developed in some detail in the book by Cole. The results of this theory give the following relationship for the pressure pulse amplitude at the distance R (ft from explosive source of W lbs.)

$$P_R = K_1\left[\frac{W^{1/3}}{R}\right]^{1.13} \tag{4.68}$$

where K_1 is a constant characteristic of the explosive, equal to 2.16×10^4 for TNT in the units used.

A graph of experimental results [17] is shown in Fig. 4-20, indicating substantial agreement with the theory over variations in explosive charge and depth by a factor of 1000 or more.

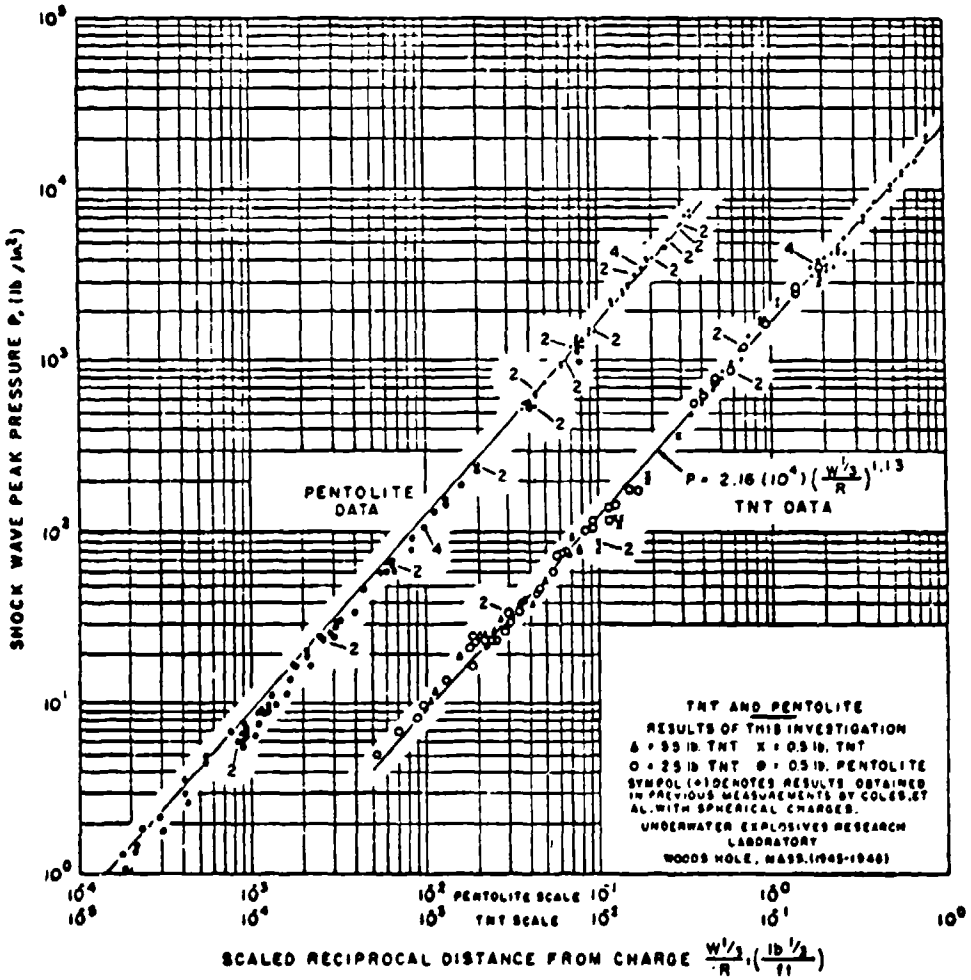

Figure 4-20.–Shock wave in underwater explosion. The peak pressure is plotted as a function of the reciprocal distance (from A. B. Arons [17]).

The shape of the shock pulse is also predicted by the Kirkwood-Bethe theory. The relation of the period T of the first oscillation from an explosion at a depth d is given by

$$T_p = K_2 \frac{W^{1/3}}{(Z^*)^{5/6}} \tag{4.69}$$

which is of the same form as Friedman time dimension [Eq. (4.67)]. Experimental results [18] (Fig. 4-21) also confirm this dependence.

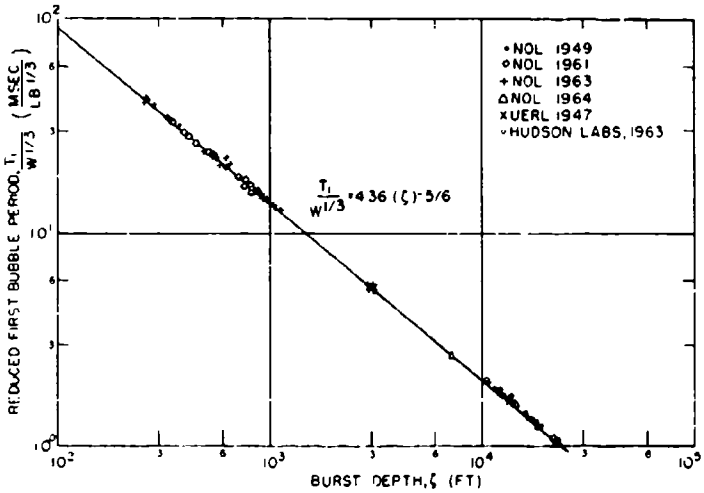

Figure 4-21.–First bubble period as a function of total hydrostatic depth. $\xi(\equiv z^*)$. • (1949), ◇ 1961, + (1963), △ (1964), (all Naval Ordnance Laboratory); × Underwater Explosives Research Laboratory (1947); ○ Hudson Labs (1963) (from Blaik and Christian [18]).

The interconnection of viscosity and shock propagation has been studied by Arons. As in our discussion of finite-amplitude wave propagation in Chapter 3, we found that the role of viscosity in blunting the steepness of the rise and decay times of the pressure peak is counteracted by the role of finite amplitude which tends to sharpen the pressure peak as it passes through the medium. A comparison of the results of this theory with experimental charges at two depths is shown in Fig. 4-22.

Weston [19] has pointed out that the Fourier energy spectrum of an exponentially decaying pulse can be written as

$$E(\omega) = \frac{2P_0^2}{\rho c_0 \left[\frac{1}{t_0^2} + \omega^2\right]}$$

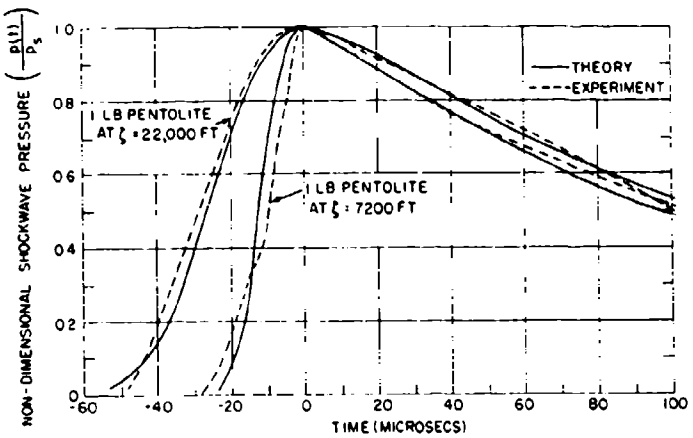

Figure 4-22.–Comparison of measured and theoretic shock wave pressures, normalized to the maximum pressure. ζ is the total hydrostatic depth ($\equiv z^*$) (from Blaik and Christian [18]).

where P_0 is the initial peak pressure and t_0 measures the initial decay of the pulse. For t_0, Arons used

$$t_0 = 58W^{1/3}\left[\frac{W^{1/3}}{R}\right]^{-0.22}$$

while Weston employed a slightly larger value.

Each succeeding bubble pulse has an energy spectrum as does the original shock wave. The combined effects of the shock wave and the first two bubble pulses is shown in Fig. 4-23 for a 1-lb charge at 20 fathoms. The oscillations near the center of the curve are due to the bubble oscillations.

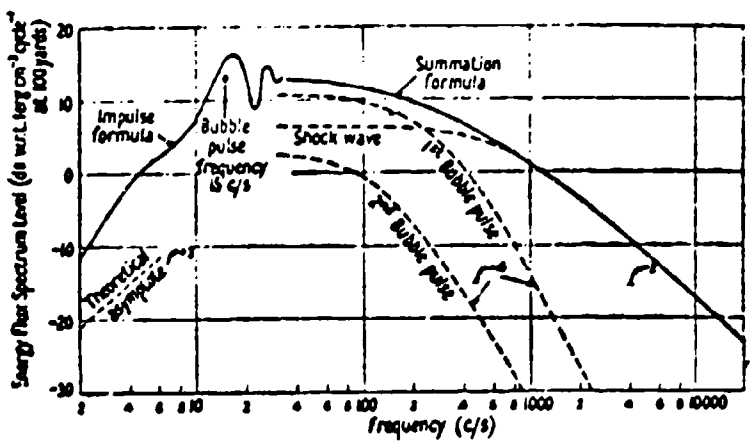

Figure 4-23.–Theoretical energy spectrum of explosion for a 20-fathom 1-lb depth charge (from D. E. Weston [19]).

The propagation of this energy spectrum will be modified by the presence of absorption in the medium. On the other hand, the detection of this explosive material can serve as a measurement of sound absorption in the medium.

This technique has been used widely in connection with the SOFAR channel to measure α at low frequencies. Figure 4-24 shows a variety of results by this technique, while reference 20 gives a critique of some theoretical aspects of the problem.

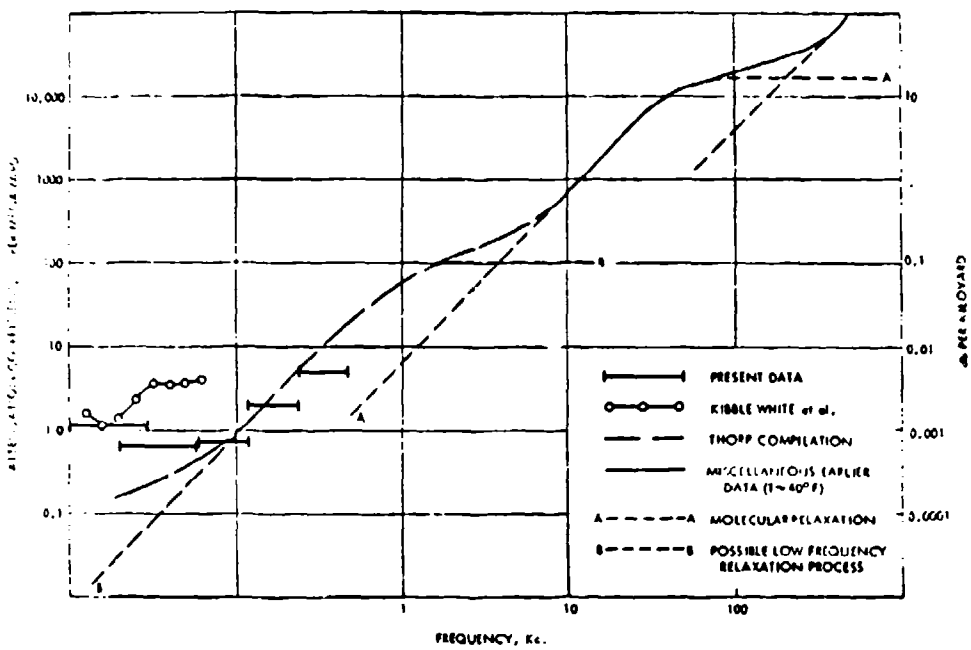

Figure 4-24.–Sound attenuation coefficients obtained from analysis of underwater explosions (from R. J. Urick [10]).

REFERENCES

Chapter 4

1. J. N. Bradley, *Shock Waves in Chemistry and Physics*, Methuen, London (1962). See also, R.W.B. Stephens and A. E. Bate, *Acoustics and Vibrational Physics*, 2nd. ed., E. Arnold, London, 1966, Chapter 19.
2. J. N. Bradley, *op. cit.*, Chapter 10.
3. J. J. Lacey, Jr., *Shock Tubes*, I. G. Glass, ed., University of Toronto Press, 1970, pp. 126ff.

4. R. Becker, Z. Physik 8, 321 (1922).
5. L. H. Thomas, J. Chem. Phys. 12, 449 (1944).
6. A. H. Shapiro and S. J. Kline, J. Appl. Mech. 21, 185 (1954).
7. H. J. Pain and F.W.E. Rogers, Rpts. on Prog. in Phys. 25, 287 (1962).
8. W. N. Flook, Jr. and D. F. Hornig, J. Chem. Phys. 23, 816 (1955).
9. W. Eisenmenger, Acustica 14, 187 (1964).
10. J.W.M. DuMond, E. R. Cohen, W.K.H. Panofsky and E. Deeds, JASA 18, 97 (1946).
11. G. B. Whitham, J. Fluid Mech. 1, 290 (1956).
12. H. W. Carlson, R. J. Mack and O. A. Morris, JASA 39, S10 (1966). For more recent treatments, see H. W. Carlson and D. J. Maglieri, JASA 51, 675 (1972); A. D. Pierce and D. J. Maglieri, JASA 51, 702 (1972).
13. A. B. Arons et al., JASA 20, 271, 277 (1948); Rev. Mod. Phys. 20, 519 (1948); Nav. Ord. Rpt. 478, 1949.
14. R. H. Cole, Underwater Explosions, Princeton, 1948.
15. B. Friedman, Inst. for Math. Mech. N.Y.U., Rep. 166, 1947, "Theory of Underwater Explosion Bubbles," Underwater Explosion Research, (USONR, Washington, 1950), pp. 229-376.
16. See Cole, op. cit., pp. 28-33; J. G. Kirkwood and H. A. Bethe, OSRD 588 (1942).
17. A. B. Arons, JASA 26, 343 (1954).
18. M. Blaik and E. A. Christian, JASA 38, 50 (1965).
19. D. E. Weston, Proc. Phys. Soc. (London) 76, 233 (1960).
20. R. J. Urick, JASA 39, 906 (1966).

Chapter 5

AEROACOUSTICS

5.1 The Lighthill Equations.

It was pointed out in the Introduction that Rayleigh [1] had developed an equation for the scattering of a plane wave from small inhomogeneities in which the d'Alembertian of the pressure was placed on the left side of the equation and all other terms were placed on the right side, where they formed an equivalent distributed monopole source strength. In his subsequent argument, Rayleigh retained only the principal terms, which involved the degree of inhomogeneity of the medium and the strength of the original sound wave:

$$\Box^2 p = -\frac{2\Delta c}{c_0^2}\frac{\partial^2 p_s}{\partial t^2} - \frac{\partial}{\partial y}\left(\frac{\Delta\rho}{\rho_0}\frac{\partial p_s}{\partial y}\right). \tag{5.1}$$

Hence p_s is the pressure amplitude of the original beam in the Rayleigh formulation.

Lighthill, in his classic work, [2] began at this point and noted that the vanishing of the two terms on the right in the absence of an external sound source ($p_s = 0$) made it necessary to reexamine the terms that Rayleigh had quite justifiably neglected in his scattering investigation.

In his analysis, Lighthill considered a fluctuating fluid flow that occupied a limited part of a large volume of fluid, the rest of which was at rest (Fig. 5-1). He then made a comparison between that system (a) and a similar one, (b) whose density values were those appropriate to a uniform acoustic medium at rest. Outside the zone of flow fluctuations, the two systems were therefore identical. Lighthill then stated that the difference between the two systems was to be "considered as if it were the effect of a fluctuating external force field, known if the flow is known, acting in the said uniform acoustic medium at rest and hence radiating sound in it according to the ordinary laws of acoustics."*

To begin the mathematical analysis, we first write out conservation equations. The momentum in a fixed region of space changes as the result of the combined effect of (1) the stresses on its boundary and (2) the momen-

*M. J. Lighthill, I, p. 566.

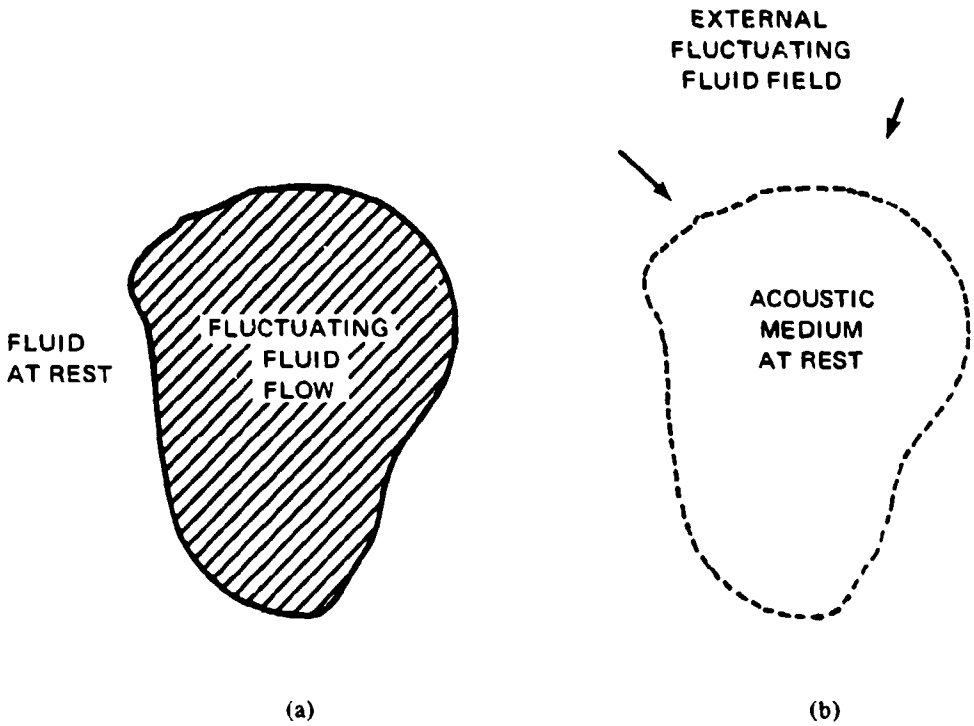

Figure 5-1.–Lighthill concept of fluctuating fluid flow (a) and equivalent acoustic system (b).

tum flow across the boundary. The boundary stresses are expressed by the Reynolds stresses $\rho v_i v_j$ while p_{ij} gives the real stress. Hence the contribution to the rate of momentum changes in the shaded area of Fig. 5-1a is of the form

$$T'_{ij} = p_{ij} + \rho v_i v_j. \tag{5.2}$$

A uniform acoustic medium at rest (5-1b) would have stresses only in the form

$$T''_{ij} = \rho c_0^2 \delta_{ij} \tag{5.3}$$

where δ_{ij} is the Kronecker delta–that is, only a simple hydrostatic pressure would be present. The difference between these two terms then is the equivalent external stress acting on the uniform acoustic medium of Fig. 5-1b:

$$T_{ij} = T'_{ij} - T''_{ij} = \rho v_i v_j + p_{ij} - \rho c_0^2 \delta_{ij}. \tag{5.4}$$

Under such conditions, the equation of motion takes the form

$$\Box^2 p = -\frac{\partial^2 T_{ij}}{\partial y_i \partial y_j} = c_0^2 \Box^2 \rho = c_0^2 \nabla^2 \rho - \frac{\partial^2 \rho}{\partial t^2}. \tag{5.5}$$

Actually, Eq. (5.5) derives from the equation of continuity

$$\frac{\partial \rho}{\partial t} + \frac{\partial}{\partial x_i}(\rho v_i) = 0$$

and the momentum equation

$$\frac{\partial}{\partial t}(\rho v_i) + c_0^2 \frac{\partial \rho}{\partial x_i} = -\frac{\partial T_{ij}}{\partial x_j}, \tag{5.7}$$

which combine to yield

$$\nabla^2 \rho - \frac{1}{c_0^2}\frac{\partial^2 \rho}{\partial t^2} \equiv \frac{1}{c_0^2}\Box^2 \rho = \frac{\partial^2 T_{ij}}{\partial x_i \partial x_j}. \tag{5.8}$$

The effect of viscosity on the processes involved here may be taken into account in the stress tensor p_{ij}. For a *Stokesian gas* (for which the bulk viscosity $\eta' = 0$)

$$p_{ij} = p_0 \delta_{ij} + \eta\left[-\frac{\partial v_i}{\partial x_j} - \frac{\partial v_j}{\partial x_i} + \frac{2}{3}\left(\frac{\partial v_k}{\partial x_k}\right)\delta_{ij}\right] \tag{5.9}$$

where p_0 is the equilibrium pressure.

Equation (5.5) is a rather complicated one, but it can be reduced for the problems at hand. First, the stresses T_{ij} can be neglected outside the flow region. There $v_i = 0$ and one has only the motions of the medium due to sound waves. Next, the viscous stresses in p_{ij} constitute small scale absorption effects which can be neglected except for large scale phenomena. Finally, for low Mach numbers, T_{ij} can be approximated by $\rho_0 v_i v_j$.

5.2 Monopole, Dipole, Quadrupole Sources.

Before proceeding further, a brief discussion of the mathematics of acoustic sources is desirable. The simplest possible sound source is that of a small pulsating sphere whose radius varies sinusoidally with time ($u_s = u_0 e^{i\omega t}$).

By small here we mean $ka \ll 1$, where a is the mean radius of the sphere. In such a case, the pressure at a distance r will be

$$p = i\omega\rho a^2 \frac{u_0 e^{j(\omega t - kr)}}{r}. \tag{5.10}$$

We now define S as the *simple* or *point source strength.* It is equal to the amplitude of the volume rate of expansion of our sphere, i.e., $S = 4\pi a^2 u_0$. Hence the pressure can also be written as

$$p = \frac{i\omega\rho S e^{j(\omega t - kr)}}{4\pi r}. \tag{5.11}$$

The variations of the density can be found from Eq. (5.11), since the excess pressure $p = c_0^2 \Delta\rho$ or

$$\rho - \rho_0 = \frac{i\omega\rho S e^{j(\omega t - kr)}}{4\pi c_0^2 r} \tag{5.12}$$

while the intensity will be given by

$$I = \frac{|p|^2}{2\rho c} = \frac{\rho c_0 k^2}{32\pi^2 r^2} S^2 \tag{5.13}$$

Such a simple source is an example of a *monopole source.* Monopole sources usually involve the introduction of new fluid into the source region (explosions or gas combustions), but they can also originate from the introduction of heat into a localized region or from the presence of turbulence.

If the source emits more generalized radiation than sinusoidal, we may describe the density fluctuation, say, by the expression

$$\rho - \rho_0 = \frac{1}{4\pi c_0^2} \frac{q'\left(t - \frac{r}{c_0}\right)}{r} \tag{5.14}$$

where q is the rate at which a point source adds mass to the medium, and $q'(z) = \partial q(z)/\partial z$.

In the notation of Eq. (5.12), $q[(t - (r/c_0)]$ replaced $\rho S e^{i(\omega t - kr)}$. For an extended distribution of sources of matter, we need to replace our point equation (5.14) by a volume integral, i.e., rewrite Eq. (5.14) as

$$\rho - \rho_0 = \frac{1}{4\pi c_0^2} \int \frac{\partial}{\partial t} Q\left[\mathbf{R}, t - \frac{|\mathbf{r} - \mathbf{R}|}{c_0}\right] \frac{dV_R}{|\mathbf{r} - \mathbf{R}|} \tag{5.15}$$

where $Q dV_R$ represents the time rate of mass production in the volume element dV_R marked out by the vector $\mathbf{R}$ (Fig. 5-2). The integration in Eq. (5.15) is over all space, but in practice is carried out only over the region in which there are sources. The quantity $q'(t)$ is called the *instantaneous strength* of the point source, and $\partial Q/\partial t$ the (mass) *source strength per unit volume* or more briefly, the (monopole) *source density*.

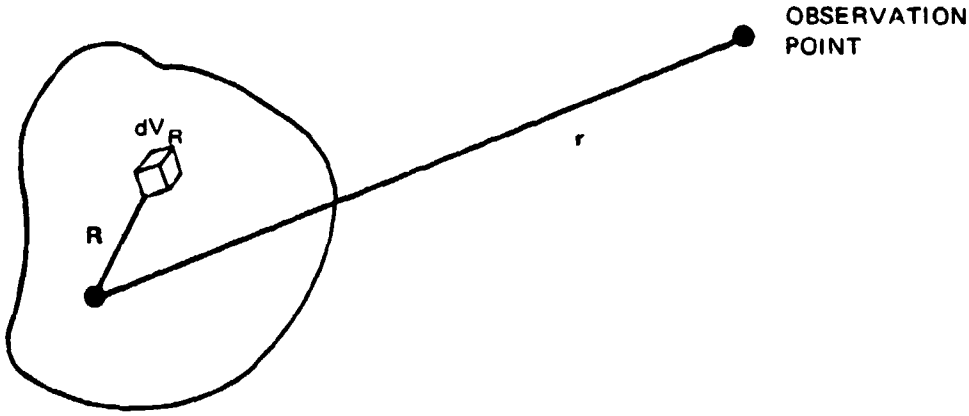

Figure 5-2.–Geometry corresponding to Eq. (5.15).

In most acoustical situations, one is more interested in the pressure rather than the density. The result of Eq. (5.15) (and others following below), can always be put in the form of the pressure by the pressure-density relationship studied in Chapter 3, the linear form of which is

$$p - p_0 = c_0^2(\rho - \rho_0). \tag{5.16}$$

While there are many acoustic sources (such as pulsed jets) which are effectively monopole, in most physical situations, the monopole strength vanishes, and attention must be focused on the next higher level of sources–dipoles.

Lighthill makes the following instructive analysis. If there are no matter sources, then the sound is generated by a fluctuating force field F_i per unit volume in some part of the medium ($i = 1,2,3$ corresponding to the vec-

tor components x,y,z). Such a force would appear as F_i on the right side of Eq. (5.7) and as $-(\partial F_i/\partial x_i)$ on the right side of Eq. (5.8). A comparison of Eqs. (5.7), (5.12), (5.15), (5.16) indicates that this force field would be equivalent to a source distribution with strength per unit volume = $-(\partial F_i/\partial x_i)$.

Lighthill goes on to point out that a specific component of this equivalent source distribution–say, $-(\partial F_1/\partial x_1)$ is itself equivalent to a distribution

$$\frac{1}{\epsilon}F_1(x_1,x_2,x_3) - \frac{1}{\epsilon}F_1(x_1 + \epsilon,x_2,x_3),$$

in the limit as $\epsilon \to 0$, by the definition of a derivative. That is, we are already dealing with a field of dipole sources of strength F_i per unit volume. Thus, "a force field F_i per unit volume emits sound like a volume distribution of dipoles whose strength vector per unit volume is F_i".*

We can therefore generate a pair of equations analogous to (5.15), (5.16), (i) for the force $f_i(t)$ concentrated at a point:

$$\rho - \rho_0 = -\frac{1}{4\pi c_0^2}\frac{\partial}{\partial x_i}\left[\frac{f_i\left(t - \dfrac{r}{c_0}\right)}{r}\right] \tag{5.17}$$

and (ii) for a volume distribution of dipoles:

$$\rho - \rho_0 = -\frac{1}{4\pi c_0^2}\frac{\partial}{\partial x_i}\int F_i\left(\mathbf{R},t - \frac{|\mathbf{r}-\mathbf{R}|}{c_0}\right)\frac{dV_R}{|\mathbf{r}-\mathbf{R}|}. \tag{5.18}$$

Equation (5.18) can be written differently for the far field. Since the derivatives of F_i with respect to the x_i fall off with $|\mathbf{r}-\mathbf{R}|^{-1}$ while those of $|\mathbf{r}-\mathbf{R}|^{-1}$ fall off as $|\mathbf{r}-\mathbf{R}|^{-2}$, the latter can be neglected in far field. Then

$$\rho - \rho_0 \simeq \frac{1}{4\pi c_0^2}\int\frac{r_i - R_i}{|\mathbf{r}-\mathbf{R}|^2}\frac{1}{c_0}\frac{\partial}{\partial t}F_i\left(\mathbf{R},t - \frac{|\mathbf{r}-\mathbf{R}|}{c_0}\right)dV_R. \tag{5.19}$$

Thus the density changes at the point of interest depend on the time rate of change of the dipole strength F_i, and are not due to simultaneous time changes in the local density but depend on their time of arrival at the distant point.

*M. J. Lighthill, I, p. 573.

Lighthill again emphasizes the point: while the fluctuating stresses T_{ij} in Eq. (5.8) produce a force per unit volume equal to their inward flux $-(\partial T_{ij}/\partial x_j)$, so that they generate like a dipole field of strength $-(\partial T_{ij}/\partial x_j)$ per unit volume, the sound radiated is not to be computed from the total dipole strength per unit volume, since this is in fact zero at any instant of time. Rather, the sound will come from the next higher order of terms, i.e., it will be the equivalent quadrupole field, a field that is the limiting case of four simple sources which obey the inverse square law of radiation. This can be seen by paralleling the development given above for a field of distributed monopoles. In the limit as $\epsilon \to 0$, the term $-(\partial T_{i1}/\partial x_1)$ is equivalent to the combination of dipole fields at the two points x_1 and $x_1 + \epsilon$:

$$-\frac{\partial T_{i1}}{\partial x_1} = \lim_{\epsilon \to 0}\left[\frac{1}{\epsilon} T_{i1}(x_1, x_2, x_3) - \frac{1}{\epsilon} T_{i1}(x_1 + \epsilon, x_2, x_3)\right]. \tag{5.20}$$

The total quadrupole field can then be regarded as the combination of three suc' 'ds. However, they may also be regarded as a single quadrupole field with s..ength per unit volume given by the stress tensor T_{ij}.

We therefore write the expression for the density variations due to a continuous distribution of quadrupoles with strength density T_{ij} by analogy with Eqs. (5.17), (5.18) for the dipole field:

$$\rho - \rho_0 = \frac{1}{4\pi c_0^2} \frac{\partial^2}{\partial x_i \partial x_j} \int T_{ij}\left(\mathbf{R}, t - \frac{|\mathbf{r} - \mathbf{R}|}{c_0}\right) \frac{dV_R}{|\mathbf{r} - \mathbf{R}|}. \tag{5.21}$$

Also, at large distances from the quadrupoles producing the radiation, arguments similar to those preceding Eq. (5.19) justify the approximation

$$\rho - \rho_0 \cong \frac{1}{4\pi c_0^2} \int \frac{(R_i - r_i)(R_j - r_j)}{|\mathbf{R} - \mathbf{r}|^3} \frac{1}{c_0^2} \frac{\partial^2}{\partial t^2} T_{ij}\left(\mathbf{R}, t - \frac{|\mathbf{r} - \mathbf{R}|}{c_0}\right) dV_R. \tag{5.22}$$

One other approximation is useful: when the origin of the coordinate system is taken within the flow region, and the dimensions of the latter are small when compared with $\mathbf{r}$ (Fig. 5-2), we can then disregard $\mathbf{R}$ and R_i in the difference terms of the integrand of Eq. (5.22), obtaining

$$\rho - \rho_0 \cong \frac{1}{4\pi c_0^2} \frac{r_i r_j}{r^3} \int \frac{1}{c_0^2} \frac{\partial^2}{\partial t^2} T_{ij}\left(\mathbf{R}, t - \frac{|\mathbf{r} - \mathbf{R}|}{c_0}\right) dV_R. \tag{5.23}$$

Equations (5.22), (5.23) form the starting point for investigations of problems involving the scattering of sound by sound, as we shall see in Chapter 9.

The sound intensity represented by a given fluctuation of the density can now be found by multiplying the average of the square of the fluctuation by c_0^3/ρ_0 [recall Eqs. (5.13), (5.16)]

$$I(\mathbf{r}) = \frac{c_0^3}{\rho_0} \langle (\rho - \langle \rho \rangle)^2 \rangle. \tag{5.24}$$

In Eq. (5.22), ρ_0 is the mean density. One can also write down the expression for $I(\mathbf{r})$ directly by substituting Eq. (5.22) in (5.24).

By integrating once over the surface containing the radiation field, it is possible to give a relatively simple form for the total acoustic power output P under the conditions of Eq. (5.23), i.e., in the far field:

$$P = \frac{1}{60\pi\rho_0 c_0^5} \left\{ \sigma^2 \left[\int \frac{\partial^2}{\partial t^2} T_{ij} \left(\mathbf{R}, t - \frac{|\mathbf{r} - \mathbf{R}|}{c_0} \right) dR \right] \right.$$

$$\left. + 2 \sum_{i=1}^{3} \sum_{j=1}^{3} \sigma^2 \left[\int \frac{\partial^2}{\partial t^2} T_{ij} \left(\mathbf{R}, t - \frac{|\mathbf{r} - \mathbf{R}|}{c_0} \right) dR \right] \right\}. \tag{5.25}$$

Here σ^2 is the variance, defined by

$$\sigma^2(z) = \langle (z - \langle z \rangle)^2 \rangle. \tag{5.26}$$

5.3 Sound from Changes in Vortex Strength.

The discussion of Section 5.2 represents only the foundations of Lighthill's theory. We shall not pursue its ramifications further in this chapter. Particular application of the Lighthill equation will be made in Chapters 9 and 10, and there is no need here of the more sophisticated treatment of mathematical theory.

There are, however, a number of aeroacoustical effects that it is appropriate to treat at this point, and we shall follow the analysis of Powell, [3] an analysis which gives a graphic quality to the description of the phenomena.

It has been pointed out in the INTRODUCTION that interest in flow-induced sound dates back to the Aeolian harp of antiquity, which was later

generalized to the study of the flow past a cylinder. Such a flow gives rise to the well-known alternate eddy pattern known as the von Karman street (Fig. 5-3). If Γ is the circulation ($= \int v \cdot \delta \ell$) around the cylinder, the eddies that are cast off have circulation of $\pm 2\Gamma$. As each eddy removes itself from the cylinder, it changes the circulation about the cylinder by an equal, opposite amount, so that the circulation about the cylinder alternates between $+\Gamma$ and $-\Gamma$.

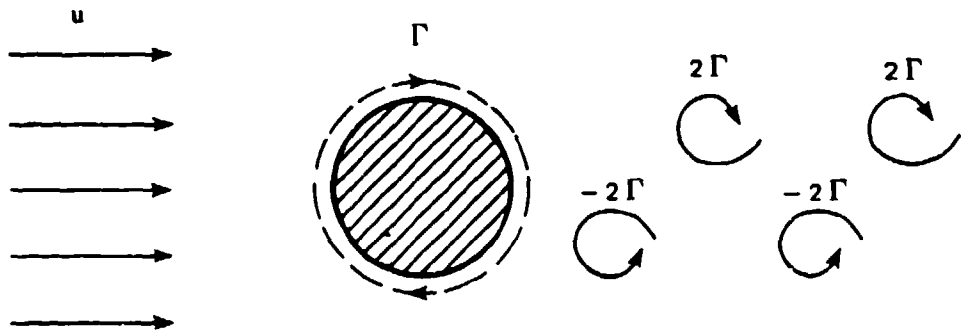

Figure 5-3.–Generation of a von Karman street.

This alternating circulation is suggestive of a dipole phenomenon and, indeed, both Rayleigh [4] and Lamb have shown how a dipole field will be created by the vibration of a cylinder. Lamb [5] in fact proved that the incompressible field induced by a closed vortex loop with constant circulation Γ is equivalent to that produced by a uniform distribution of dipoles of strength Γ per unit area, distributed over any surface with a single boundary of the same shape as the vortex loop. This behavior is illustrated in Fig. 5-4. The equivalent source here is a long rectangular dipole sheet filling the space between the space between the two vortices.

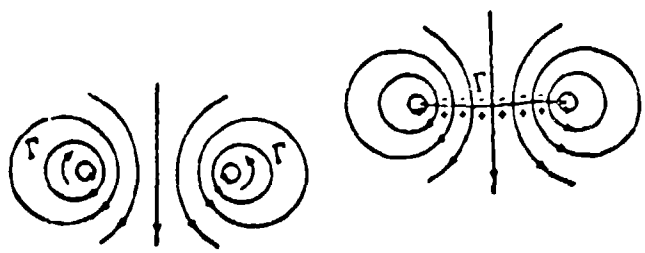

Figure 5-4.–The streamlines resulting from a rectangular vortex ring of great length normal to the page (at left) are identical to those of the corresponding vortex sheet at the right (from Powell [3]).

In mathematical terms, this means that the particle velocity at the point $\mathbf{x}$, which is given by the relation

$$u(\mathbf{x}) = -\frac{\Gamma}{4\pi} \oint \frac{\hat{\mathbf{r}} \times d\ell(\mathbf{R})}{r^2} \tag{5.27}$$

can also be written as

$$u(\mathbf{x}) = -\frac{1}{4\pi}\nabla \times \left[\int \Gamma \hat{\mathbf{s}}\, \nabla_x\left(\frac{1}{r}\right) ds(\mathbf{y})\right] \tag{5.28}$$

where $\mathbf{r} = \mathbf{x} - \mathbf{y}$, and $\hat{\mathbf{r}}, \hat{\mathbf{s}}$ are unit vectors (see Fig. 5-5, where the vectors $\mathbf{s}, \hat{\mathbf{s}}$ are perpendicular to the plane of the drawing).

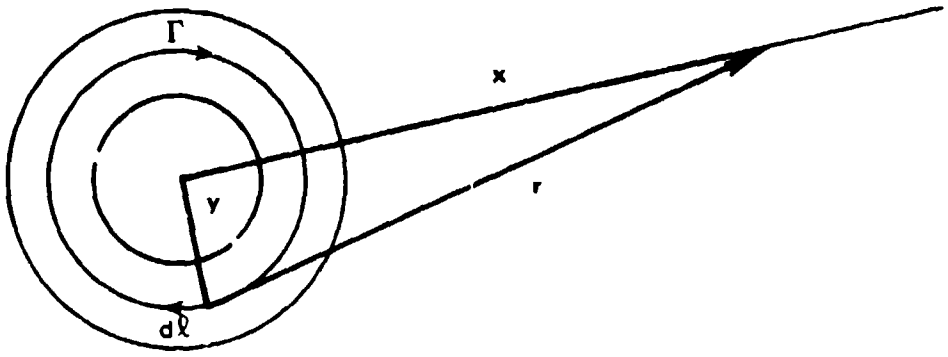

Figure 5-5.–Geometry corresponding to Eq. (5.28).

In regions of zero vorticity, the velocity $u(\mathbf{x})$ can be set equal to the gradient of a velocity potential ϕ:

$$u(\mathbf{x}) = -\nabla_x \phi. \tag{5.29}$$

Then (5.28) can be integrated to obtain

$$\phi = \frac{1}{4\pi}\int \Gamma \hat{\mathbf{s}} \nabla_x\left(\frac{1}{r}\right) ds(\mathbf{y}) \tag{5.30}$$

which corresponds to the potential due to a "point" dipole source of strength $\mathbf{D} = \Gamma \hat{\mathbf{s}}$.

For distances x that are large in comparison with the size of the vortex loop, Eq. (5.28) can now be written

$$u(\mathbf{x}) = \frac{1}{4\pi}\nabla_x\left[\mathbf{D} \cdot \nabla_x\left(\frac{1}{x}\right)\right]. \tag{5.31}$$

This is the expression for an incompressible fluid, for which there will be no retardation of the field. For a slightly compressible fluid, it can be shown that Eq. (5.31) can be replaced by

$$u_x = \frac{1}{4\pi}\nabla_x\left[\mathbf{D} \cdot \nabla_x\left(\frac{1^*}{r}\right)\right] \tag{5.32}$$

where $\mathbf{I}^{\star}$ is a time delay operation, such that

$$\mathbf{D}(t)\mathbf{I}^{\star} \equiv D\left(t - \frac{r}{c_0}\right) = [D(t)]^{\star}. \tag{5.33}$$

[For a sinusoidal time dependence, $D(t) = D_0 e^{i\omega t}$, the effect of $\mathbf{I}^{\star}$ is equivalent to multiplication by $e^{-i\omega(r/c_0)}$.]

If we now expand (5.33) and keep only the terms for which $r \simeq x$, then

$$u(\mathbf{x}) = \frac{\mathbf{x}}{4\pi {c_0}^2} \frac{\partial^2}{\partial t^2} (\hat{\mathbf{x}} \cdot \mathbf{D})\left[\frac{\mathbf{I}^{\star}}{x}\right] = \frac{\hat{\mathbf{x}}}{4\pi x {c_0}^2}\left(\frac{d^2 D_x}{dt^2}\right)^{\star} \tag{5.34}$$

where $D_x = \Gamma s_x = D \cos(\mathbf{x}, \mathbf{s})$.

If the area s remains constant, Eq. (5.34) reduces to

$$u(\mathbf{x}) = \frac{\hat{x}}{4\pi {c_0}^2} s_x \left(\frac{d^2\Gamma}{dt^2}\right)^{\star} \tag{5.35}$$

for a single vortex. For a distribution of vortices, summation or integration would be necessary.

If the circulation remains constant, we need $d^2 s_x/dt^2$. If each part of the vortex loop moves with a velocity $\mathbf{u}$, in the time δt, the area increase will be $\delta \mathbf{s} = (\mathbf{u} \times \delta \ell)\delta t$, where the length increase is $\delta \ell = 2\pi u \delta t$. As a result, we obtain

$$u(x) = \frac{\hat{x}}{4\pi x {c_0}^2}\left[\frac{d}{dt}\oint \Gamma(\mathbf{u} \times d\ell)_x\right]^{\star} = -\frac{\hat{x}}{4\pi x {c_0}^2}\left[\frac{d}{dt}\oint (\Gamma \times \mathbf{u})_x d\ell\right]^{\star}. \tag{5.36}$$

In the more general case of a *vorticity* distribution $\boldsymbol{\zeta} = \nabla \times \mathbf{u}$ we use $\boldsymbol{\mathcal{L}} = \boldsymbol{\zeta} \times \mathbf{u}$ and obtain

$$u(x) = -\frac{\hat{x}}{4\pi x {c_0}^2} \int \frac{\partial \mathcal{L}_x}{\partial t} dV(\mathbf{y})^{\star}. \tag{5.37}$$

Finally, if the surface moves normal to itself, one can develop the expression

$$u(x) = \frac{x}{4\pi x {c_0}^2} \int_s y_x \frac{\partial^2 u_n}{\partial t^2} ds(\mathbf{y})^{\star}. \tag{5.38}$$

Equations can also be derived that give the pressure instead of the velocity. If we use the equation of motion in the form

$$\Box^2 p = \nabla \cdot \nabla p + \nabla \cdot \frac{\partial(\rho \mathbf{u})}{\partial t}$$

and use

$$p = -\nabla \cdot \left(\rho \mathcal{L} + \nabla \frac{1}{2} \rho u^2 - \mathbf{u} \frac{\partial \rho}{\partial t} - \frac{1}{2} u^2 \nabla \rho \right)$$

we can make approximations in the nonlinear terms on the right of the inhomogeneous differential equation, so that it reduces to

$$p = -\nabla \cdot \left(\rho \mathcal{L} + \Delta \frac{1}{2} \rho u^2 \right).$$

In the presence of a closed surface s_0 within the flow, the general solution of (5.39) can be written

$$\begin{aligned} p(\mathbf{x}) = {} & \frac{1}{4\pi} \int_{v_0} \rho \mathcal{L} \cdot \nabla_x \frac{1^\star}{r} dV(\mathbf{y}) + \frac{1}{4\pi c_0^2} \frac{\partial^2}{\partial t} \int_{v_0} \frac{1}{2} \rho u^2 \left(\frac{1^\star}{r} \right) dV(\mathbf{y}) \\ & + \frac{1}{4\pi} \int_{s_0} \left(p + \frac{1}{2} \rho u^2 \right) \left[\nabla_x \left(\frac{1^\star}{r} \right) \right]_n ds(\mathbf{y}) \\ & - \frac{1}{4\pi} \int_{s_0} \frac{\partial(\rho u_n)}{\partial t} \left(\frac{1^\star}{r} \right) ds(\mathbf{y}). \end{aligned} \tag{5.40}$$

These four terms have the following interpretation:

(1) a volume distribution of dipoles, whose strength is proportional to $\mathcal{L}$;

(2) a volume distribution of nondirectional sources, of monopole strength per unit volume proportional to

$$\frac{1}{c_0^2} \frac{\partial^2}{\partial t^2} \left(\frac{1}{2} \rho u^2 \right);$$

(3) a surface distribution of dipoles, whose strength is proportional to the Bernoulli pressure $[p + (1/2)\rho_0 u^2]$;

(4) a monopole distribution over the surface due to its motion normal to itself.

In the far field approximation, Eq. (5.40) can be reduced to the form

$$p(\mathbf{x}) = \frac{\rho_0}{4\pi x c_0}\frac{\partial}{\partial t}\int_V \mathcal{L}_x dV(\mathbf{y})^\star - \frac{1}{4\pi x c_0}\frac{\partial}{\partial t}\int_{s_0}\left(p + \frac{1}{2}\rho_0 u^2\right) n_x ds(\mathbf{y})^\star - \frac{\rho_0}{4\pi x}\frac{\partial}{\partial t}\int_{s_0} u_n ds(\mathbf{y})^\star. \tag{5.41}$$

Here the second integral of Eq. (5.40) has been neglected as of higher order. Again, one may interpret the first term as the motion of vorticity in the volume of flow, and the second as relating to vorticity at the boundaries of the flow, while the third indicates the flow across the boundary, or the motion of the boundary if there is no such flow.

Let us now consider the case of flow past a circular cylinder. The behavior as the flow increases is shown in Fig. 5-6a.

If a vortex forms, the picture is equivalent to the insertion of free vortex of circulation -2Γ in the flow and a vortex of circulation $+2\Gamma$ at the inverse point of the circle, plus one of the same strength and sign at the center. The total effect is that shown in Fig. 5-6b.

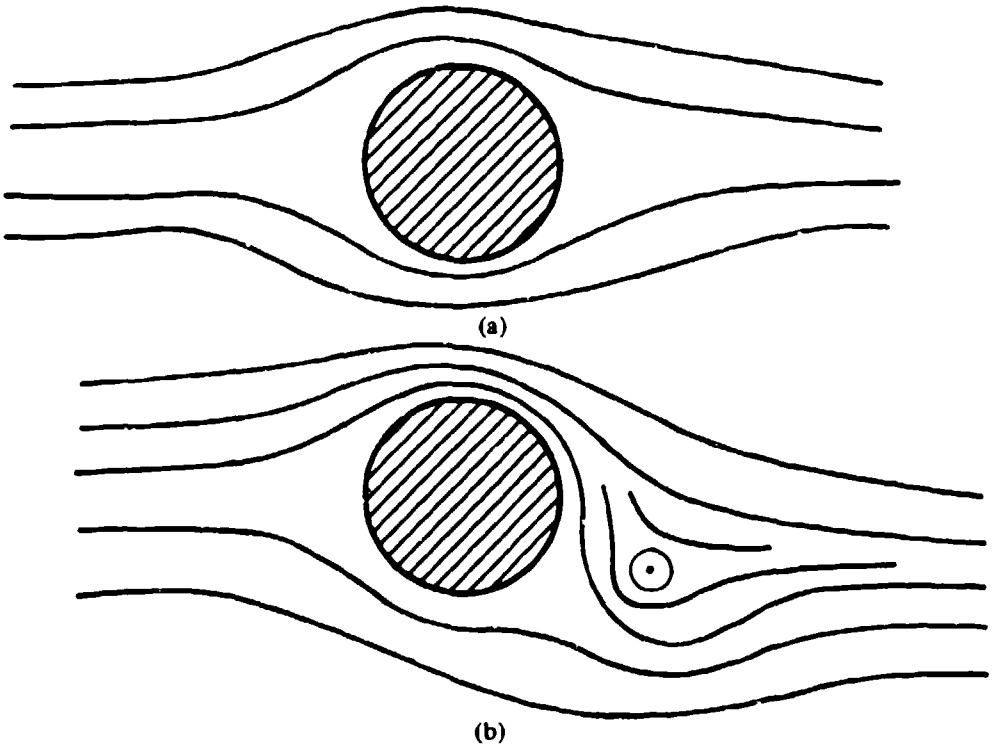

Figure 5-6.—Flow past a rigid circular cylinder (a) low velocity, (b) higher velocity with generation of vortex at the right.

The sound produced can be obtained by means of this analysis. For an order of magnitude dependence, one can use the similarity approach. For high Reynolds numbers, we can assume that the dependent variables do not depend on the Reynolds number. Then $\mathbf{u}(\mathbf{y}) \sim U, r \sim Ud, \partial/\partial t \sim \omega \sim U/d$. From Eq. (5.40),

$$p(x) \sim \langle u^2(x) \rangle \rho_0 c_0 x^2 \sim \rho_0 U^3 d^2 \left(\frac{U}{c}\right)^3 \left(\frac{b}{d}\right)^2.$$

Here b is the length of the cylinder and d its diameter.

5.4 Sound from Movement of Vorticity in Free Flow.

For an inviscid liquid in the absence of impressed forces, we can write the equations of continuity and motion in the form

$$\begin{aligned} &\frac{\partial \rho}{\partial t} + (\mathbf{u} \cdot \nabla)\rho + \rho(\nabla \cdot u) = 0 \\ &\frac{\partial \mathbf{u}}{\partial t} + (\mathbf{u} \cdot \nabla)\mathbf{u} + \frac{1}{\rho}(\nabla p) = 0. \end{aligned} \tag{5.42}$$

These can be combined to produce the form

$$\begin{aligned} \Box^2 \mathbf{u} = &-\nabla \times \nabla \times \mathbf{u} + \frac{1}{c_0^2} \frac{\partial}{\partial t}(\mathbf{u} \cdot \nabla)\mathbf{u} - \nabla\left[\left(\frac{1}{\rho}\right)\mathbf{u} \cdot \nabla \rho\right] \\ &+ \frac{\partial}{\partial t}\left[\left(\frac{c^2}{c_0^2} - 1\right)\nabla(\ln \rho)\right] + \frac{\partial}{\partial t}\left[\left(\frac{\rho - \rho_0}{\rho}\right)\nabla\left(\frac{c^2}{c_0^2}\right)\right]. \end{aligned} \tag{5.43}$$

As we have done before, we can interpret the terms on the right hand side as source terms driving the linear system represented by the left hand side. If we start with a sinusoidal disturbance for u, it is easy to rank the orders of magnitude of the five terms on the right in terms of the Mach number $M = u_0/c_0$ and the *Strouhal number* $S = \omega L/u$ (recall INTRODUCTION), where L is some typical length in the flow. The terms are of the respective order

$$1: SM^2: M^2: SM^4: SM^4. \tag{5.44}$$

If the flows are for low Mach numbers ($M \ll 1$), and if the condition $SM \ll 1$ holds, the last two terms can safely be neglected.

We now rewrite Eq. (5.42), dropping the last two terms and making some simple transformations

$$\Box^2 u = -\nabla \times \boldsymbol{\zeta} + \frac{1}{c_0^2}\frac{\partial \mathcal{L}}{\partial t} + \frac{1}{c_0^2}\nabla\left[\left(\frac{d}{dt} + \frac{\partial}{\partial t}\right)\frac{u^2}{2}\right]$$

where $\boldsymbol{\zeta}, \mathcal{L}$ have been defined previously. The solution to this equation has the form

$$u(x) = \frac{1}{4\pi}\int_{V_0} \nabla \times \boldsymbol{\zeta}\frac{1^*}{r}\,dV(\mathbf{y}) - \frac{1}{4\pi c_0^2}\int_{V_0}\frac{\partial \mathcal{L}}{\partial t}\frac{1^*}{r}\,dV(\mathbf{y})$$

$$-\frac{1}{4\pi c_0^2}\int_{V_0}\nabla\left[\left(\frac{\partial}{\partial t} + \frac{d}{dt}\right)\frac{u^2}{2}\right]\frac{1^*}{r}\,dV(\mathbf{y}) \qquad (5.46)$$

which can be used to obtain the sonic power from turbulent flow.

We shall not pursue this study, which opens up into the entire field of turbulence-produced sound, but shall only make some summarizing observations.

In the case of the aeolian tone, the sound was produced through changes in area of the vortex rings. In such a case, a dipole source exists, as shown in Section 5.2. In the case of free flow however, there is no change of momentum and any dipole radiation is eliminated. In such a case, the motion of a vortex in one place may be accompanied by an opposite vortex motion elsewhere. Each of these generates a dipole sound, but they are of equal strength and opposite sign, so that the dipole effect is zero. However, because of path differences to the field point, their net contribution at that point will not be zero but will be that of a quadrupole.

Powell has given a simple picture of this quadrupole action. Consider two opposite flows of velocity $(1/2)\,u$ and examine the disturbance of a thin, plane layer subject to shear. The layer will be distorted as shown in Fig. 5-7. The circulation $\delta\Gamma$ is given by $\zeta\delta A$. The rate of momentum change δM is then

$$\frac{d}{dt}\delta M = \rho_0 \delta\Gamma \times \mathbf{u}d\ell = \rho_0 \mathcal{L}\delta V. \qquad (5.47)$$

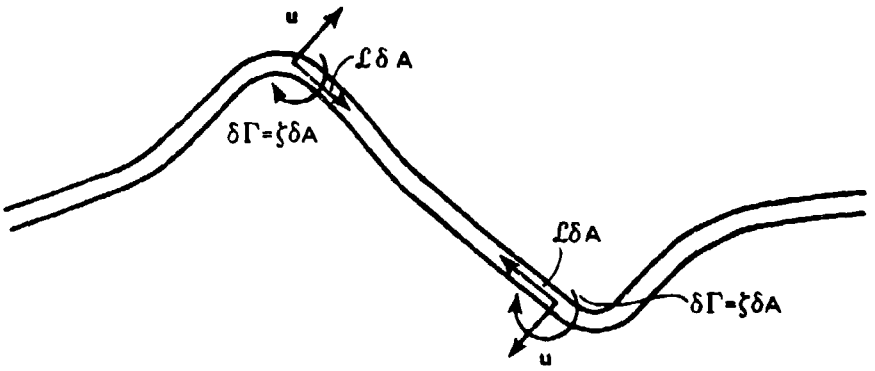

Figure 5-7.–Quadrupole action of thin plane layer subject to shear (from Powell [3]).

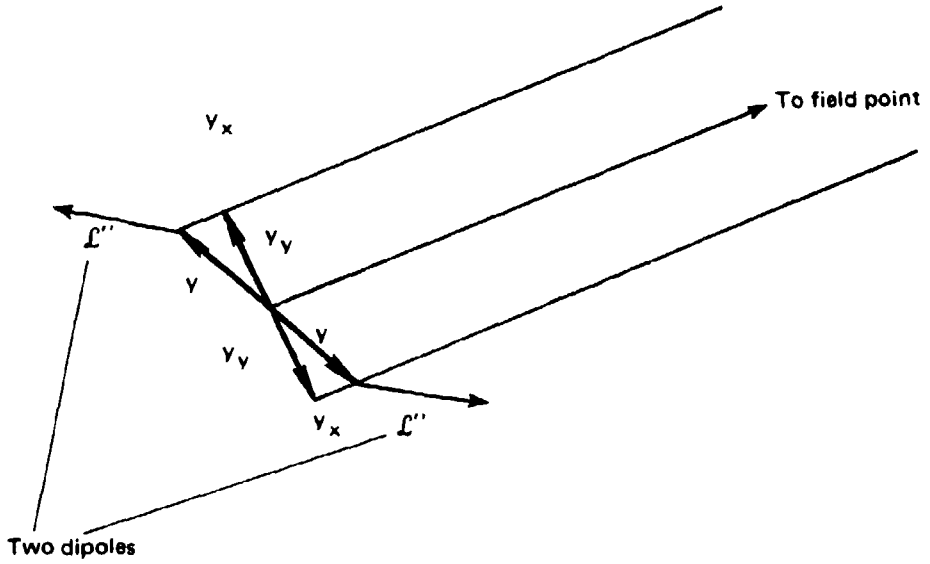

Figure 5-8.–Resolution of y and $\mathcal{L}$ in the direction of the distant observation point x (from Powell [3]).

This is a free vortex, so that no force is applied to it. Therefore

$$\rho_0 \int \mathcal{L} dV(\mathbf{y}) = 0 \tag{5.48}$$

and no dipole results.

That is, the movement of vorticity at one point is simultaneously counterbalanced by an opposite motion elsewhere. However, the contributions to the sound at some field point from the two vorticities have generally trav-

eled different distances and therefore originated at different times. Thus the two signals will have an initial time difference of $2y_x/c_0$. This yields, for Eq. (5.37) a net velocity difference

$$\delta \mathbf{u}(\mathbf{x}) = \frac{2y_x}{c_0} \frac{\partial}{\partial t}\left[\frac{\hat{x}}{4\pi x c_0^2} \frac{\partial \mathcal{L}_x}{\partial t} \delta V^{\star}\right] \tag{5.49}$$

so that the velocity perturbation in the far field, due to quadrupole action, will be

$$\mathbf{u}(\mathbf{x}) = \frac{\hat{x}}{4\pi x c_0^3} \int_{V_0} y_x \frac{d^2 \mathcal{L}_x}{dt^2} dV(\mathbf{y})^{\star}. \tag{5.50}$$

Finally, the sound intensity at the point x has the form

$$I(x) = \rho_0 c_0 \langle u^2(x) \rangle = \frac{\rho_0}{16\pi^2 x^2 c_0^5} \iint_{V_0} y_x z_x \left\langle \frac{d^2 \mathcal{L}_x}{dt^2} (\underset{\sim}{y}) \frac{d^2 \mathcal{L}_x}{dt^2} (\mathbf{z}) \right\rangle dV(\mathbf{y}) dV(\mathbf{z}). \tag{5.51}$$

REFERENCES

Chapter 5

1. Rayleigh, *Theory of Sound*, reprinted by Dover Publications, N.Y., 1945, vol. II, p. 150.
2. M. J. Lighthill, Proc. Roy. Soc. (London) I. A211, 564 (1952); II. A212, 1 (1954).
3. A. Powell, JASA 36, 177 (1964).
4. Rayleigh, Phi. Mag. 7, 161 (1879).
5. H. Lamb, *Hydrodynamics*, 6th ed., Dover, New York, 1945, p. 212.

Chapter 6

RADIATION PRESSURE

The small size of the steady forces involved in the phenomenon of the acoustic radiation pressure, the differences between theoretical conceptions and experimental procedures, and the overly long devotion of acousticians to the linear view have all combined to make obscure this relatively small point in the theory of nonlinear acoustics.

In the analysis that follows, we shall abandon the traditional quasi-linear analysis, (i.e., analysis in which nonlinear distortion of the wave is entirely neglected, but a nonlinear relation between p and ρ is employed) but shall endeavor to point out where errors have been committed in the past.

Some of this confusion regarding radiation pressure stems from the various ways in which this pressure can be defined. Two particular definitions predominate–those due to Rayleigh and Langevin, and we shall now turn our attention to these.

6.1 The Rayleigh Radiation Pressure.

In the previous chapters, we have had occasion to distinguish between Lagrangian (material) and Eulerian (spatial coordinates). This distinction plays an important role in our ideas about radiation pressure. Let us first describe the processes for an ideal gas, obeying the adiabatic law

$$p = p_0(\rho/\rho_0)^\gamma \qquad (6.1)$$

and make the usual transfer to the liquid case later.

In the Lagrangian representation, the pressure ratio ρ/ρ_0 is given by Eq. (3.7)

$$\frac{\rho}{\rho_0} = \frac{1}{1 + \xi_a} \qquad (3.7)$$

where we use the reduced notation $\partial\xi/\partial x \equiv \xi_x$, $\partial^2\xi/\partial x^2 \equiv \xi_{xx}$, etc. Then Eq. (6.1) can be rewritten

$$p^L = p_0(1 + \xi_a)^{-\gamma}$$

and then expanded in powers of $\partial\xi/\partial a$ (the superscript L denotes the Lagrangian form):

$$p^L = p_0\left[1 - \gamma\xi_a + \gamma\frac{(\gamma+1)}{2}\xi_a^2 - \cdots\right]. \tag{6.2}$$

If we assume a plane progressive wave of moderate amplitude, the displacement velocity $\dot{\xi}$ can be found from the first terms of Eq. (3.47)

$$\dot{\xi} = \dot{\xi}_0 \sin(\omega t - ka) + \frac{\dot{\xi}_0 a}{2\ell}\sin 2(\omega t - ka) \tag{6.3}$$

where $\dot{\xi}_0 = \omega\xi_0 = Mc_0$ and $1/\ell = [(\gamma+1)/2]Mk = \beta Mk$.

If we integrate $\dot{\xi}$ with respect to t and apply the boundary condition that $\xi = \dot{\xi} = 0$ when $\omega t - ka = 0$, then

$$\xi = \xi_0[1 - \cos(\omega t - ka)]$$

$$+ k_0^2\frac{\xi_0^2 a}{8}(\gamma+1)[1 - \cos 2(\omega t - ka)] \tag{6.4}$$

and

$$\xi_a = -M\sin(\omega t - ka) - M^2 ka\frac{(\gamma+1)}{4}\sin 2(\omega t - ka)$$

$$+ M^2\frac{\gamma+1}{8}[1 - \cos 2(\omega t - ka)]. \tag{6.5}$$

We now substitute (6.5) in (6.2), keeping only terms up to M^2 and also assuming $ka \gg 1$:

$$p^L - p_0 = \gamma p_0\left\{M\sin(\omega t - ka) - M^2 ka\frac{(\gamma+1)}{4}\sin 2(\omega t - ka)\right.$$

$$\left. + M^2\frac{(\gamma+1)}{8}[1 - \cos 2(\omega t - ka)]\right\}. \tag{6.6}$$

The time average of p^L is then given by

$$\langle p^L \rangle = p_0 + \gamma p_0 \left[-\frac{(\gamma + 1)}{8} M^2 + \frac{\gamma + 1}{2} \cdot \frac{M^2}{2} \right]$$

$$= p_0 + \gamma p_0 M^2 \frac{(\gamma + 1)}{8} = p_0 + \rho_0 c_0^2 M \frac{(\gamma + 1)}{8} \tag{6.7}$$

(here $\langle \cdots \rangle$ indicates the time average).

It is to be noted in the square brackets of Eq. (6.7) that the second term derives from the ξ_a^2 term of Eq. (6.2) and is frequently the only one given (the quasilinear case). The first term is developed from a consideration of the nonlinear term in ξ_a. Thus, even in the simplest analysis here, the nonlinearity cannot be neglected. This fact was pointed out long ago by Fubini, [1] but it has often been overlooked. [2]

Equation (6.7) can be written in simpler form by introducing the mean energy density, which is given by Eq. (1.33)

$$\langle E \rangle = \frac{1}{2} \rho_0 \dot{\xi}_0^2 = \frac{1}{2} \rho_0 c_0^2 M^2 \tag{1.33}$$

so that the average Lagrangian pressure—the pressure at the position of a vibrating particle that is located at rest at the point a, averaged a complete cycle—is

$$\langle p^L \rangle = p_0 + \frac{\gamma + 1}{4} \langle E \rangle. \tag{6.8}$$

The *Rayleigh radiation pressure* can be defined as the difference between the average pressure at a surface moving with the particle (i.e., the mean Lagrangian pressure $\langle p^L \rangle$) and the pressure that would have existed in the fluid of the *same mean density* at rest [p_0 in Eq. (6.2)]. [3] Therefore, the Rayleigh radiation pressure p_R is given by

$$p_R = \langle p^L \rangle - p_0$$

$$= \frac{\gamma + 1}{4} \langle E \rangle \text{ (for an ideal gas)} \tag{6.9}$$

under the assumptions thus far made (note that the quasilinear theory gives $[(\gamma + 1)/2]\langle E \rangle$ in this case).

Special difficulties have been added to the problem of the Rayleigh radiation pressure in a liquid by the introduction of the concept of a "linear liquid." This case has been treated in detail in the literature. [3-5] Such a liquid is one of constant compressibility κ. The relation between p^L and κ would then be

$$p^L - p_0 = -\frac{1}{\kappa}\frac{V - V_0}{V_0} = -\frac{1}{\kappa}\xi_a. \tag{6.10}$$

For the case of a plane harmonic wave just discussed,

$$p^L = p_0 + \frac{k}{\kappa}\xi_0 \sin(\omega t - ka) \tag{6.11}$$

so that

$$\langle p^L \rangle = p_0 \tag{6.12}$$

and the Rayleigh pressure p_R vanishes.

The case of constant compressibility is a false one, however, since no such liquid exists. To solve the actual problem, we must use terms of second order. The Lagrangian pressure p^L will then be [Eq. (3.20)]

$$\begin{aligned} p^L &= p_0 + A\left(\frac{\rho}{\rho_0} - 1\right) + \frac{B}{2}\left(\frac{\rho}{\rho_0} - 1\right)^2 + \cdots \\ &= p_0 + A\left(\frac{1}{1 + \xi_a} - 1\right)^2 + \frac{B}{2}\left(\frac{1}{1 + \xi_a}\right)^2 + \cdots \\ &= p_0 + A(-\xi_a + \xi_a^2) + \frac{B}{2}(\xi_a)^2 + \text{higher order terms} \\ &= p_0 + A\left[-\xi_a + \left(1 + \frac{B}{2A}\right)\xi_a^2\right] + \text{higher order terms.} \end{aligned} \tag{6.13}$$

If we parallel steps (6.2) to (6.8) (with the substitution $Ak^2\xi_0^2 = \rho_0^2\omega^2 c_0^2 = 2\langle E \rangle$), we finally obtain

$$\langle p^L \rangle = p_0 + \frac{1}{2}\langle E \rangle\left(1 + \frac{B}{2A}\right) \tag{6.14}$$

so that

$$p_R = \frac{1}{2}\left(1 + \frac{B}{2A}\right)\langle E\rangle. \tag{6.15}$$

Equations (6.13)-(6.15) could have been obtained from (6.2), (6.8), (6.9) by the usual method [see discussion preceding Eq. (3.15)] of replacing the nonlinear form for gases, $\gamma + 1/2$, by $1 + B/2A$. They were rederived in detail, however, to emphasize the falseness of the "constant compressibility" condition. Even if the liquid were linear in behavior, so that $B = 0$, there would still be a quadratic term in $\partial\xi/\partial a$ in Eq. (6.12) and the Rayleigh pressure would not vanish.

Now let us follow the Eulerian approach to find the mean pressure at a point in a fluid. In the Eulerian system, the density (ρ^E) is given by the general transformation rule (see Section 3.1)

$$\rho^E = \rho^L\Big|_{x=a} - \frac{\partial\rho^L}{\partial a}\Big|_{x=a}\xi = \rho_0(1 - \xi_x + \xi_x{}^2 + \xi_{xx}\xi). \tag{6.16}$$

Then, for the adiabatic process in an ideal gas,

$$p^E = p_0\left(\frac{\rho}{\rho_0}\right)^\gamma = p_0 + \gamma p_0\left[1 - \xi_x + \frac{\gamma+1}{2}\xi_x{}^2 + \xi\xi_{xx}\right]. \tag{6.17}$$

Substituting for the case of a plane harmonic wave, and averaging over time, we finally obtain

$$\langle p^E\rangle = p_0 + \gamma p_0\,\frac{\gamma-3}{8}M^2$$

$$= p_0 + \frac{\gamma-3}{4}\langle E\rangle \tag{6.18a}$$

while, for a liquid,

$$\langle p^E\rangle = p_0 + \frac{1}{4}\left(\frac{B}{A} - 2\right)\langle E\rangle. \tag{6.18b}$$

All of these cases have presumed the existence of a plane wave of infinite extent as well as an undissipated monochromatic wave. As we shall see below, the growth of harmonics, the absorption by the medium and the presence of boundaries on the wave will alter the form of these equations.

The fact that the pressure at a fixed point in a fluid is altered by the passage of a sound wave indicates that the density at a fixed point can also change. This was first pointed out by Langevin [7] and plays a role in the determination of the *Langevin radiation pressure*, to which we now turn our attention.

6.2 The Langevin Radiation Pressure.

The Langevin radiation pressure p_L is defined as the difference between the mean pressure at an absorbing or reflecting wall and in the same acoustic medium, at rest, behind the wall.

Let us consider a collimated plane wave of circular cross section. The mean pressure at a point on the side of the beam is the Eulerian pressure $\langle p^E \rangle$, given, under the approximation used thus far, by Eq. (6.18) [with account of (6.15)]:

$$\langle p^E \rangle = p_0 + \frac{1}{4}\left(\frac{B}{A} - 2\right)\langle E \rangle = p_R - \langle E \rangle + p_0. \tag{6.19}$$

But this value of the mean pressure differs from that just outside the beam, which is p_0. The fluid on the outside will therefore move in or out. Its behavior can be understood by a consideration of the following model experiment, which is taken from Hertz and Mende. [5]

We consider a cylinder, equipped with two frictionless pistons, entirely enclosing the sound beam. The fluid in the cylinder also occupies the region outside the cylinder. The piston X is a perfect absorber, so that the only sound in the medium is the plane wave traveling from left to right. We distinguish two cases.

Case I. Let X and Y be fixed, and let ρ_0, p_0 be the density and pressure in the fluid (at rest) outside the cylinder (see Fig. 6-1a).

The pressure inside the chamber at the end piston X will be the Rayleigh radiation pressure given by Eq. (6.15),* superposed on the mean pressure

$$\begin{aligned} p_X &= p_R + p_0 \\ p_X &= \frac{1}{2}\left(1 + \frac{B}{2A}\right)\langle E \rangle + p_0. \end{aligned} \tag{6.20}$$

*The case discussed by Hertz and Mende was the artificial one of a liquid of constant compressibility. Under those conditions $p_X = p_0$, and the piston X could be free to move as a whole.

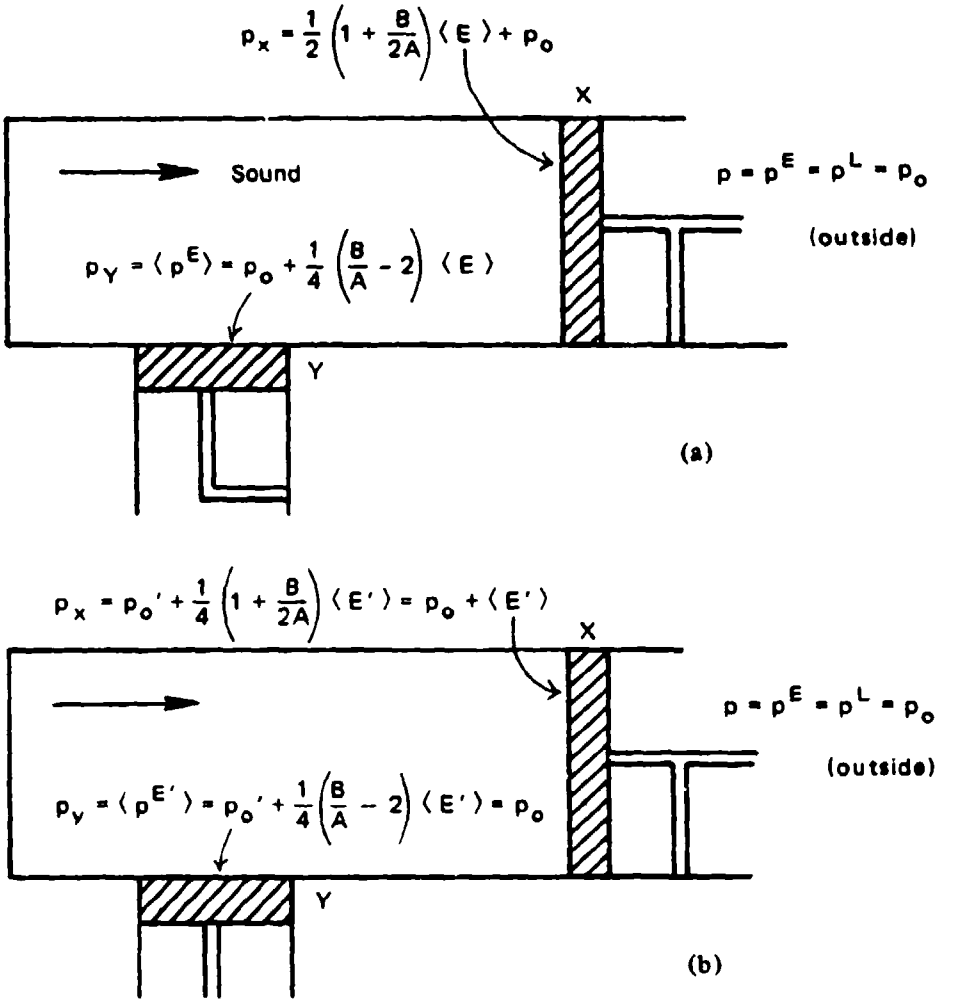

Figure 6-1.–Illustration of Rayleigh (a) and Langevin (b) radiation pressures (after Hertz and Mende [5]).

The fact that the piston is held fixed does not prevent the use of the Lagrangian expression here because the surface of the piston must move back and forth with the adjacent fluid, by the law of continuity.

In this same case, the mean pressure at any point on the piston Y will be the Eulerian pressure from Eq. (6.18):

$$p_Y = \frac{1}{4}\left(\frac{B}{A} - 2\right)\langle E\rangle + p_0. \tag{6.21}$$

Case II. Now let X continue to be fixed but let Y be movable (Fig. 6-1b). The pressure difference Δp between the opposite faces of Y in Case I,

$$\Delta p = p_0 + \frac{1}{4}\left(\frac{B}{A} - 2\right)\langle E\rangle - p_0 = \frac{1}{4}\left(\frac{B}{A} - 2\right)\langle E\rangle \tag{6.22}$$

will cause the piston to move outward until the net pressure at the upper face of the piston Y becomes equal to p_0, i.e.,

$$\langle p^{E'} \rangle = p_0$$

or

$$p_0' + \frac{1}{4}\left(\frac{B}{A} - 2\right)\langle E' \rangle = p_0 \tag{6.23}$$

where the primes on p_0 and E indicate the altered state of the fluid. Then the Lagrangian pressure at the face of the piston X becomes [Eq. (6.14)]

$$p_X = \langle p^L \rangle = \frac{1}{2}\left(1 + \frac{B}{2A}\right)\langle E' \rangle + p_0'$$

$$= p_0' + \frac{B}{4A}\langle E' \rangle + \frac{1}{2}\langle E' \rangle$$

$$= p_0 + \langle E' \rangle. \tag{6.24}$$

Since there is no sound beam behind the piston X, so that the pressure there is p_0, we have the conditions for the *Langevin pressure* p_L. That is,

$$p_L = p_X - p_0 = \langle E' \rangle. \tag{6.25}$$

The modified energy density $\langle E' \rangle$ differs only very slightly from $\langle E \rangle$, so that it is safe to discard the prime in the final result.

If we now remove the cylinder and piston Y, keeping only the piston X, the situation will remain unchanged, except that the beam will not now be so sharply bounded. In such a case, there will be a gradual change from maximum beam intensity in the axis to no beam at some distant point. Between these two points a variation in the hydrostatic pressure of the type indicated in Case II must occur, leading to the same result as in Eqs. (6.21)-(6.25).

In summary then, we have, for our four pressures,

$\langle p^E \rangle = \frac{1}{4}\left(\frac{B}{A} - 2\right)\langle E \rangle$ — time-average pressure at a fixed point (Eulerian)

$$\langle p^L \rangle = p + \frac{1}{2}\left(1 + \frac{B}{2A}\right)\langle E \rangle \qquad \text{time-average pressure at a vibrating particle of the medium (Lagrangian)}$$

$$p_R = \langle p^L \rangle - p_0 = \frac{1}{2}\left(1 + \frac{B}{2A}\right)\langle E \rangle \qquad \text{Rayleigh pressure}$$

$$p_L = \langle p^L(E', p_0') \rangle - p_0 = \langle E \rangle \qquad \text{Langevin pressure} \tag{6.24}$$

where p_0 is the pressure in the fluid at rest, in the absence of sound and

$$\langle p^L(E', p_0') \rangle = p_0' + \frac{1}{2}\left(1 + \frac{B}{2A}\right)\langle E' \rangle. \tag{6.27}$$

A recent paper by Rooney and Nyborg reviews much of this same material with substantially similar conclusions. [8]

6.3 Higher Order Effects.

The relations in the previous section are valid up to terms of order M^2. To find the effect of the next higher order terms, we repeat the substitution of Eq. (6.5) in (6.2) keeping terms up to M^2 there, and also the condition $ka \gg 1$. The result for $\langle p^L \rangle$ is

$$\langle p^L \rangle = p_0 + \gamma p_0 \left[\frac{\gamma + 1}{8} M^2 + \frac{\gamma + 1}{8} M^2 \right.$$

$$\left. \cdot \frac{M^2(\gamma + 1)^2}{8}\left(k^2 a^2 + \frac{3}{4}\right)\right]. \tag{6.28}$$

Retaining the assumption that $ka \gg 1$ and introducing the relation $\langle E \rangle = (1/2)\rho_0^2 c^2 M^2$, $1/\ell = [(\gamma + 1)/2]Mk$, we have

$$\langle p^L \rangle = p_0 + \frac{\gamma + 1}{4}\langle E \rangle \left(1 + \frac{a^2}{2\ell^2}\right). \tag{6.29}$$

However, the correct energy density $\langle E_t \rangle$ to second order is given by $\langle \rho_0 \dot{\xi}^2 \rangle$, where ξ is given by Eq. (6.3). [9] Hence

$$\langle E_t \rangle = \langle \rho_0 \dot{\xi}^2 \rangle = \frac{1}{2} \rho_0 \dot{\xi}_0^2 + \frac{1}{2} \rho_0 \xi_0^2 \cdot \frac{a^2}{4\ell^2} = \langle E \rangle \left(1 + \frac{a^2}{4\ell^2}\right). \quad (6.30)$$

and (6.29) reduces to the same form as Eq. (6.8).

6.4 Effect of Reflection.

Throughout our previous treatment, we have assumed the existence of a perfect absorber of the radiation. Let us now consider the case of a partially reflecting surface (Fig. 6-2).

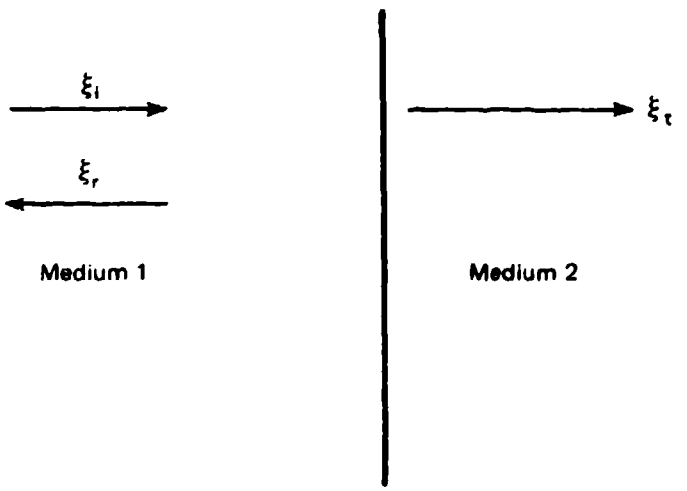

Figure 6-2.–Geometry of beam passing through an interface.

We follow the treatment of Sec. 6.1, but now assume the presence of incident, reflected and transmitted waves

$$\xi_i = K_1 \cos(\omega t - ka)$$

$$\xi_t = K_2 \cos(\omega t - ka) \quad (6.31)$$

$$\xi_r = L_1 \cos(\omega t - ka).$$

Following standard theory [9] we obtain

$$K_2 = \frac{2K_1}{1 + \dfrac{\rho_2 c_2}{\rho_1 c_1}}$$

$$L_1 = \frac{\rho_2 c_2 - \rho_1 c_1}{\rho_2 c_2 + \rho_1 c_1} K_1 \equiv mK \tag{6.32}$$

where m is the reflection coefficient.

In terms of the previous analysis, $K_1 = -\xi_0$. The Lagrangian pressure in medium 1 is then

$$\langle p_1^L \rangle = p_{01} + \frac{1}{2}\left(1 + \frac{B_1}{2A_1}\right)\langle E_1 \rangle (1 + m^2 - 2m \cos 2k_1 a) \tag{6.33}$$

while the corresponding pressure in the second medium will be

$$\langle p_2^L \rangle = p_{02} + \frac{1}{2}\left(1 + \frac{B}{2A}\right)\langle E_2 \rangle \tag{6.34}$$

where $\langle E_2 \rangle$ can be evaluated from the intensity $I = cE$ in the two media:

$$I_1 = m^2 I_1 + I_2$$

$$c_1 \langle E_1 \rangle = c_1 m^2 \langle E_1 \rangle + c_2 \langle E_2 \rangle$$

or

$$\langle E_2 \rangle = \frac{c_1}{c_2}(1 - m^2)\langle E_1 \rangle. \tag{6.35}$$

Similarly, the Eulerian pressure will be (from Eq. (6.17))

$$\langle p_1^E \rangle = p_{01} + \frac{1}{4}\left(\frac{B_1}{A_1} - 2\right)\langle E_1 \rangle (1 + m^2 - 2m \cos 2k_1 x)$$

$$- \langle E_1 \rangle 4m \cos k_1 x$$

$$\times \langle p_2^E \rangle = p_{02} + \frac{1}{4}\left(\frac{B_2}{A_2} - 2\right)\langle E_2 \rangle \tag{6.36}$$

so that the pressure change in each medium will be

$$(p_0' - p_0)_1 = -\frac{1}{4}\left(\frac{B}{A} - 2\right)\langle E\rangle(1 + m^2 - 2m\cos 2k_1 x)$$

$$+ \langle E_1\rangle m\cos 2k_1 x$$

$$\times (p_0' - p_0)_2 = -\frac{1}{4}\left(\frac{B}{A} - 2\right)\langle E_2\rangle. \tag{6.37}$$

We now encounter a difficulty in attempting to establish the Langevin pressure. In the previous section, we set the Eulerian pressure at the boundary of our beam equal to p_0, the quiescent pressure in the medium. In the real case, the change from beam to no beam as we move away from beam axis is a gradual one, but the effect is the same: the medium at the center of the beam is compressed. Now however, we are dealing with time averages of the pressure in the beam that vary periodically along the beam. Borgnis pointed out that a reasonable assumption would be that, by reaction of the surrounding medium, the space and time average of the pressure in the beam be brought to p_0. This in turn requires the taking of space averages of Eq. (6.33), (6.36), (6.37). The Langevin pressure on either side of the interface is then given by

$$(p_L)_1 = \langle\langle p_1{}^L\rangle\rangle + \langle\langle p_0' - p_0\rangle\rangle_1 = \langle E_1\rangle(1 + m^2)$$

$$(p_L)_2 = \langle E_2\rangle = \frac{c_1}{c_2}(1 - m^2)\langle E_1\rangle. \tag{6.38}$$

6.5 Radiation Stress Tensor

In his book on tensors, Brillouin discusses at some length the tensor nature of the radiation stress. [10] He considers, in the case of a solid, an imaginary fixed plane through the solid. The stresses acting through this motionless, undisturbed surface are given by

$$S_{ij} = -p_{ij} - \rho v_i v_j \tag{6.39}$$

where the p_{ij} represents real stress and $\rho v_i v_j$ represents Reynolds stresses [recall Eq. (5.2)]. In this notation a tension is positive, a compression negative, which is opposite to that of Chapter 5.

For a fluid, (6.42) reduces to

$$S_{ij} = -p\delta_{ij} - \rho v_i v_j \tag{6.40}$$

where p is the pressure of the quiescent fluid.

We now consider a sound wave with particle displacements in the x direction only (subscript 1). If we take the mean values of the tension (6.40) at some point x, then

$$(S_{ij}) = \begin{pmatrix} -\overline{p(x_1)} - \overline{\rho v_1^2} & 0 & 0 \\ 0 & -\overline{p(x_1)} & 0 \\ 0 & 0 & -\overline{p(x_1)} \end{pmatrix}. \tag{6.41}$$

Now $\overline{\rho v_1^2}$ is twice the kinetic energy density in the sound wave and is equal to the total energy density $\bar{E}$. Brillouin also demonstrates that $\overline{p(x_1)} = -\bar{E}(v/c)\,(dc/dv)$ so that the final radiation stress tensor can be written as

$$\begin{pmatrix} -\bar{E}\left(1 - \frac{v}{c}\frac{dc}{dv}\right) & 0 & 0 \\ 0 & +\bar{E}\,\frac{v}{c}\frac{dc}{dv} & 0 \\ 0 & 0 & +\bar{E}\,\frac{v}{c}\frac{dc}{dv} \end{pmatrix}. \tag{6.42}$$

Let us apply this to the case of the sound beam of Fig. 6-1b. The pressure at the lateral faces will be $+E(v/c)(dc/dv)$ but the pressure at an absorbing face at x will be $-\bar{E}[1 - (v/c)(dc/dv)]$ from inside the cylinder, but $\bar{E}(v/c)(dc/dv)$ from right to left on the outside, giving the net radiation pressure of $P_{\text{rad}} = \bar{E}$ as before.

6.6 Interface Between Two Nonmiscible Liquids.

Suppose that a beam of sound falls normally in the plane interface of two nonmiscible liquids. We take the hydrostatic pressure p_0 to be the same in both liquids. The arrangement is that of Fig. 6-3. We suppose a signal is generated by the source at the bottom with energy density in the first liquid equal to E_1. Because of the interface there will be partial reflection and par-

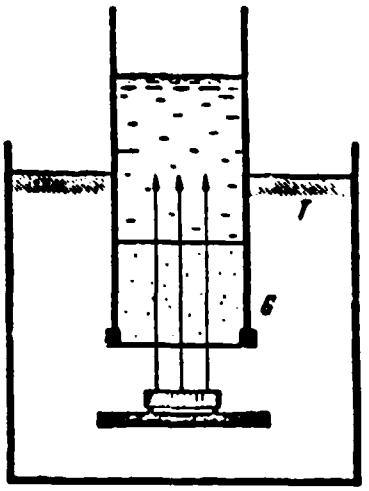

Figure 6-3.–Experimental arrangement for observation of radiation pressure at an interface (from Hertz and Mende [3]).

tial transmission with the energy density E_2 in the second medium given by Eq. (6.35).

The next pressure at the interface in the upward (forward) direction will then be the difference of the two pressures in Eq. (6.38):

$$P_{\text{net}} = E_1(1 + n^2) - E_2$$

$$= E_1 \left[1 - \frac{c_1}{c_2} + n^2 \left(1 + \frac{c_1}{c_2}\right)\right]. \tag{6.43}$$

As can be seen from the equation, the net force acting on the interface can be either positive or negative, depending on the choice of fluids.

This fact has been very clearly demonstrated by Hertz and Mende in terms of the acoustic fountain. [4] It might be observed parenthetically that, if the second medium is air, $m \simeq 1$ and Eq. (6.43) becomes $P_{\text{net}} \simeq 2E$, i.e., a considerable force is exerted on the free surface, resulting in a jet of liquid being forced upward into the air, an effect known as the acoustic fountain (Fig. 6-4).

The beam of sound rises vertically through an oil bath and is incident on the base of a glass tube that is closed at its bottom by a 0.03-mm sheet of copper foil. Two nonmiscible liquids are poured carefully into the glass container. Figure 6-5a shows the case of water over CCl_4. Here $\rho_1 = 1.594$ g/cm^3, $c_1 = 938$ m/sec, $\rho_2 = 1$ gm/cm^2, $c_2 = 1483$ m/sec, $m = -0.004$. By Eq. (6.35), the net force $= SP_{\text{net}} \simeq +0.367 \langle E_1 \rangle$, i.e., the force is in the direction $CCl_4 \rightarrow H_2O$, the direction of the sound beam.

Figure 6-4.–Example of acoustic fountain [from L. Bergmann, Der Ultraschall (6th ed.) S. Hirzel, Stuttgart, 1954, p. 208].

Figure 6-5b shows the case of water over anilin. Here $\rho_1 = 1.022$ g/cm^3, $c_1 = 1659$ m/sec, $m = -0.07$, net force = $-0.364\ \langle E_1 \rangle$, or counter to the direction of the sound beam.

The fact that the direction of the net force is independent of the direction of the sound beam is brought out even more clearly by experiments with the same pairs of liquids, in which reflection system, schematically depicted in Fig. 6-6 is used.

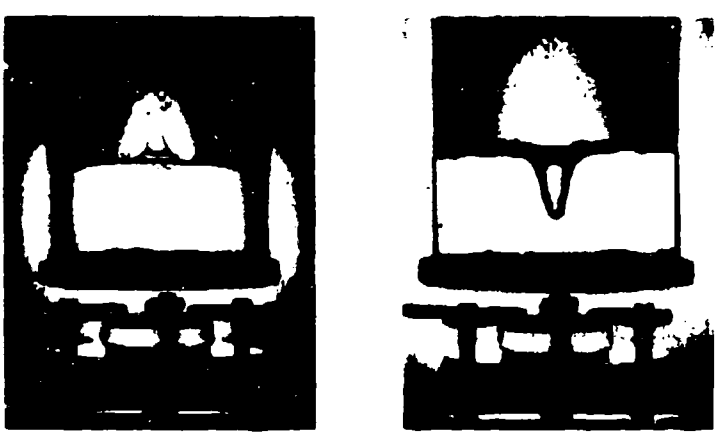

Figure 6-5.–Radiation pressure effects at an interface. (a) water over CCl_4. (b) water over aniline. The sound source is at the bottom in both cases (from Hertz and Mende [3]).

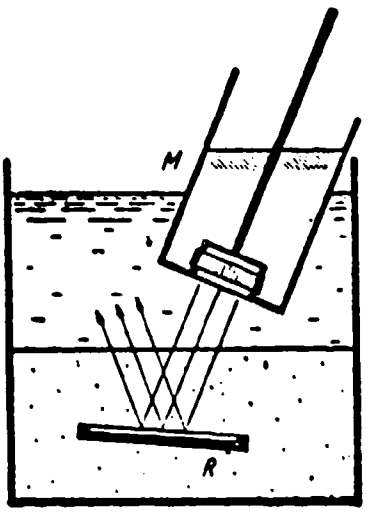

Figure 6-6.–Arrangement for observing independence of net force at interface in direction of the beam (from Hertz and Mende [3]).

Figure 6-7a shows the case for water over carbon tetrachloride and Fig. 6-7b that of water over anilin.

6.7 Radiation Pressure Devices.

The pressure of radiation has been used in several techniques for measuring sound intensity.

Figure 6-7.–Observation of independence of net force on direction of beam. Arrangement is that of Figure 6-7. (a) water over CCl_4; (b) water over aniline (from Hertz and Mende [3]).

The first instrument for sound intensity measurements by means of radiation pressure was due to Altberg. [11] The basic principle is shown in Fig. 6-8.

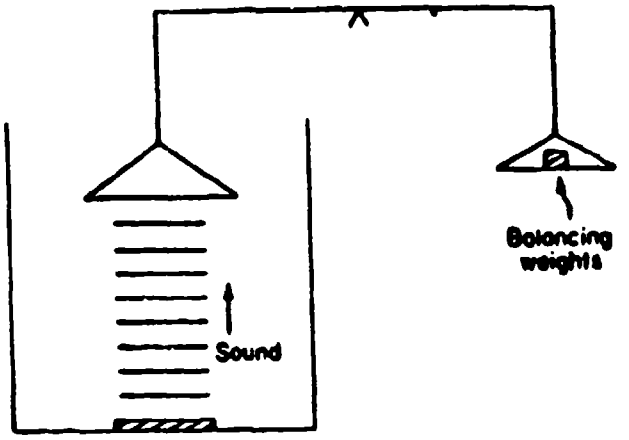

Figure 6-8.–Use of radiation pressure to measure sound intensity.

A continuous beam of sound is propagated upward in a liquid. A flat plate is suspended in the liquid to intercept the beam. The plate also forms one pan of a microbalance. To avoid standing waves, the bottom of the plate is usually roughened so as to produce diffuse reflection.

The balance is first adjusted in the absence of sound. When the sound beam is turned on, the pan will be pushed upward by a force given by

$$F = \int_{\text{beam}} p_L \, dS.$$

If the beam approximates a uniform one of cross sectional area S, and if the entire beam is absorbed by the detecting surface,

$$F = p_L S = \langle E \rangle$$

$$= I \frac{S}{c}.$$

For a beam in water of one atmosphere initial pressure amplitude and cross sectional area 3 cm^2, $F = 6.7$ dynes, which is equivalent to the weight of a 7-mg mass. Thus the accurate measurement of the mass difference gives a measurement of the sound intensity.

To obtain absolute values, it would, of course, be necessary to know the reflection coefficient m. However, one generally needs only to know that the radiation pressure force is proportional to the energy density.

This method of detection was frequently used in measuring sound absorption in early days. [12] More recently it has been incorporated into sound intensity meters.

A more sophisticated technique of "chopping" the radiation pressure by square wave modulation has also been used in absorption measurements. [13-15] The resulting radiation pressure becomes a square wave with an amplitude proportional to the intensity of the initial beam.

The device has the advantage that it measures the total energy density present, rather than that of a particular harmonic, and can be used with success in finite amplitude work.

REFERENCES

Chapter 6

1. E. Fubini, Rev. d'Acoustique 6, 118 (1937).
2. See discussion in the paper by P. J. Westervelt, JASA 22, 319 (1950).
3. For the original discussions, see Rayleigh, Phil. Mag. **3**, 338 (1902); **10**, 364 (1910).
4. F. M. Borgnis, Revs. Mod. Phys. 25, 653 (1953).
5. G. Hertz and H. Mende, Z. Physik 114, 354 (1939).
6. R. T. Beyer, Am. J. Phys. **18**, 25 (1950).
7. P. A. Langevin, Rev. d'Acoust. **1**, 93 (1932); **2**, 315 (1933).
8. J. A. Rooney and W. L. Nyborg, Am. J. Phys. **40**, 1825 (1972).
9. R. B. Lindsay, Mechanical Radiation, McGraw-Hill, N.Y., 1960, p. 76.
10. L. Brillouin, *Tensors in Mechanics and Elasticity*, Academic Press, N.Y., 1964, Ch. XI. For the original reference, see L. Brillouin, Ann. de Phys. **4**, 528 (1925).
11. W. Altberg, Ann. Phys. Lpz. (4) **11**, 405 (1903).
12. R. T. Beyer and M. C. Smith, JASA **18**, 424 (1946).
13. A. B. Barone and M. Nuovo, Ricerca Sci. **21**, 516 (1951).
14. F. L. McNamara and R. T. Beyer, JASA **25**, 259 (1953).
15. R. P. Barnes, Jr. and R. T. Beyer, JASA **36**, 1371 (1964).

Chapter 7

STREAMING

The term streaming is given to the bulk flow of fluid that results whenever a sound wave is present in the medium, and was first observed by Faraday in 1831. [1] Under certain circumstances, (high intensity, presence of surfaces from walls or impurities) the effects of streaming can be quite marked.

7.1 Basic Equations.

In order to treat the phenomenon quantitatively, we first consider a homogeneous isotropic fluid. We focus our attention on a small volume δV of such fluid and suppose that the only forces acting in it are the forces of elasticity ($-\nabla p$) and viscosity ($b\eta\ \nabla\nabla\cdot\mathbf{u} - \eta\nabla\times\nabla\times\mathbf{u}$), where the terminology has all been introduced previously. That is, our equation of motion is the Stokes-Navier relation

$$\mathbf{f} = -\nabla p + \nabla\left[\left(\frac{4}{3}\eta + \eta'\right)\nabla\cdot\mathbf{u}\right] - \eta\nabla\times\nabla\times\mathbf{u}$$

$$= \rho\frac{d\mathbf{u}}{dt} = \rho\left[\frac{\partial\mathbf{u}}{\partial t} + (u\cdot\nabla)\mathbf{u}\right]. \tag{7.1}$$

We can rewrite this equation somewhat differently by making use of the equation of continuity

$$\frac{\partial\rho}{\partial t} + \nabla\cdot\rho\mathbf{u} = 0 \tag{7.2}$$

to yield

$$\frac{\partial(\rho\mathbf{u})}{\partial t} + \rho(\mathbf{u}\cdot\nabla)\mathbf{u} + \mathbf{u}\nabla\cdot\rho\mathbf{u}$$

$$= -\nabla p + \nabla\left[\left(\frac{4}{3}\eta + \eta'\right)\nabla\cdot\mathbf{u}\right] - \eta\nabla\times\nabla\times\mathbf{u}. \tag{7.3}$$

As in our perturbation analysis of Chapter 3, we introduce expansions of p, ρ, $\mathbf{u}$ in terms of successively higher order approximations:

$$\begin{aligned} p &= p_0 + p_1 + p_2 + \cdots \\ \rho &= \rho_0 + \rho_1 + \rho_2 + \cdots \\ \mathbf{u} &= \mathbf{u}_1 + \mathbf{u}_2 + \cdots . \end{aligned} \tag{7.4}$$

The quantities p_0, ρ_0 are the static or quiescent values of the pressure and density, respectively. The corresponding value of $\mathbf{u}$ is of course zero.

A complicating problem is the presence of the viscosity under the ∇ operator in the second term on the right of Eq. (7-3). In some of the standard references (Rayleigh, [2] Eckart [3]) both η and η' are assumed to be independent of the density, so that they can be removed from under the ∇. In the research of Medwin and Rudnick, [4] these authors assumed the shear viscosity η to be constant, but wrote the bulk viscosity η' as

$$\eta' = \eta'_0 + \left(\frac{\partial \eta'}{\partial \rho}\right)_{\rho_0} \rho_1 \equiv \eta'_0 + \eta'_1 . \tag{7.5}$$

A very general form of the acoustic equation in a fluid has been developed by Hunt. [5] For the present we shall neglect all variations in viscosity, returning to them in Section

The equation of continuity has been written in its most general form in (7.2). The conservation of momentum yields

$$\begin{aligned} \rho \frac{\partial \mathbf{u}}{\partial t} = \rho \mathbf{F}_e &- \rho(\mathbf{u}\cdot\nabla)\mathbf{u} - \nabla p + (\lambda + 2\eta)\nabla(\nabla\cdot\mathbf{u}) \\ &- \eta\nabla\times(\nabla\times\mathbf{u}) + (\nabla\cdot\mathbf{u})\nabla\lambda \\ &+ 2(\nabla\eta\cdot\nabla)\mathbf{u} + \nabla\lambda\times(\nabla\times\mathbf{u}) \end{aligned} \tag{7.6}$$

where $\mathbf{F}_e$ is any external vector body force per unit mass acting on the system, η, λ are the two viscosity coefficients, η is the shear viscosity, while λ is the dilatational viscosity. The bulk viscosity η' is given by

$$\eta' = \lambda + \frac{2\eta}{3} . \tag{7.7}$$

If no forces act from outside the system and the variation of viscosity is neglected, Eq. (7.6) reduces to the form

$$\rho \frac{\partial \mathbf{u}}{\partial t} = -\rho(\mathbf{u}\cdot\nabla)\mathbf{u} - \nabla p + (\lambda + 2\eta)\nabla(\nabla\cdot\mathbf{u}) - \eta\nabla\times(\nabla\times\mathbf{u}) \quad (7.8)$$

or, since

$$\frac{\partial(\rho\mathbf{u})}{\partial t} = \rho\frac{\partial\mathbf{u}}{\partial t} + \mathbf{u}\frac{\partial\rho}{\partial t},$$

which, by application of (7.2), becomes

$$\frac{\partial(\rho\mathbf{u})}{\partial t} = \rho\frac{\partial\mathbf{u}}{\partial t} - \mathbf{u}(\nabla\cdot\rho\mathbf{u}),$$

we can obtain the following expression for the mass transport velocity $\rho\underset{\sim}{u}$:

$$\frac{\partial(\rho\mathbf{u})}{\partial t} = -\mathbf{u}(\nabla\cdot\rho\mathbf{u}) - (\rho\mathbf{u}\cdot\nabla)\mathbf{u} - \nabla p$$

$$+ (\lambda + 2\eta)\nabla(\nabla\cdot\mathbf{u}) - \eta\nabla\times(\nabla\times\mathbf{u}), \quad (7.9)$$

which is the same as (7.3) when we identify the second viscosity coefficient λ with $3\eta' - 2\eta$ as in Eq. (7.7).

It should be evident by now that the first rule of calculation of nonlinear acoustics is to keep the minimum number of additional varying quantities that is needed for the consideration of any problem. If the results of calculation with these give good experimental agreement all is well. If not, or if the calculations result in zero effect, we then must look for additional terms.

In application of this second rule, we place all known or solvable terms on the left of the equation and the new, unknown and nonlinear terms on the right as small perturbations.

The treatment of the bulk viscosity has long been a controversial one in the field of linear acoustics. For example, the quantity can be, and often is, used as a catch all, to account for excess absorption beyond that predicted by the Stokes theory. The discovery of relaxational processes in fluids required the bulk viscosity to be a function of the frequency. This has disturbed many researchers (see Markham [6]) who preferred to introduce an empirical dynamic equation connecting the pressure and the density. The resolution of this difficulty is found in the application of irreversible thermodynamics. [7]

In his treatment of the problem, Nyborg [8] introduced a dynamical relation between pressure and density with a frequency-dependent parameter, writing the first order relation between p_1 and ρ_1 as

$$p_1 = c_0^2 \rho_1 + R_\omega \dot{\rho}_1 . \tag{7.10}$$

If we insert Eq. (7.10) in (7.1), we obtain a first order expression for the stress force per unit volume

$$\mathbf{f} = -c_0^2 \nabla \rho_1 - R_\omega \nabla \dot{\rho}_1 + \left(\frac{4}{3}\eta + \eta'\right) \nabla\nabla \cdot \mathbf{u}_1 - \eta \nabla \times \nabla \times \mathbf{u}_1 \tag{7.11}$$

Now the continuity equation in first order is

$$\dot{\rho}_1 + \rho_0 \nabla \cdot u_1 = 0, \tag{7.12}$$

so that the term $-R_\omega \nabla \dot{\rho}_1 = \rho_0 R_\omega \nabla\nabla \cdot \mathbf{u}_1$, i.e., a quantity $\rho_0 R_\omega$ has in effect been added to the bulk viscosity η'. In using R_ω, one must therefore keep it in mind that η' used here does not have a frequency dependent component.

We have already reviewed the simple solutions of Eq. (7.10) in Chapter 2. Of particular importance to our work is the fact that the absorption coefficient

$$\alpha = \left(\frac{4}{3}\eta + \eta'\right) \frac{\omega^2}{2\rho_0 c^3}$$

{or

$$\left[\frac{4}{3}\eta + \eta' + R_\omega \rho_0\right] \left(\frac{\omega^2}{2\rho_0 c_0^3}\right)$$

in the work of Nyborg} is much smaller than k in virtually all fluids.*

Equation (7.9) can be conveniently rewritten in first order (for harmonic waves with the time dependence $e^{i\omega t}$) in terms of the wave number k and the absorption coefficient α:

$$\nabla\nabla \cdot \mathbf{u}_1 + (k - i\alpha)^2 \mathbf{u}_1 = i(k - i\alpha)^2 \frac{2\eta_0}{\rho_0 \omega} \nabla \times \nabla \times \mathbf{u}_1 . \tag{7.13}$$

*An exception is provided by fluids of extremely high viscosity, such as methyl metacrylate, where η is thousands or millions of times greater than for common liquids.

This equation has two distinctive types of solution:

(a) Irrotational motion. Here $\nabla \times \mathbf{u}_{1a} = 0$ and

$$\nabla\nabla \cdot \mathbf{u}_{1a} = \nabla^2 \mathbf{u}_{1a} = -(k - i\alpha)\mathbf{u}_{1a}. \tag{7.14}$$

This is the standard acoustics equation for damped harmonic waves, and will be used for the case of an unbounded medium.

(b) Incompressible motion. Here $\nabla \cdot \mathbf{u}_{1b} = 0$ and

$$-\nabla \times \nabla \times \mathbf{u}_1 = \nabla^2 \mathbf{u}_{1b} = \frac{i\omega\rho_0}{2\eta_0}\mathbf{u}_{1b}. \tag{7.15}$$

Equation (7.13) gives a solution in the case of thin sheets of fluid along interfaces between phases.

The complete solution $\mathbf{u}$, is of course given by the sum $\mathbf{u}_{1a} + \mathbf{u}_{1b}$ as a simple inspection will show.

Now let us return to the streaming problem. We restrict ourselves to the case where the motion is irrotational *to first order* and choose as our first order solution

$$u_1 = u_0 e^{-\alpha x} \sin(\omega t - kx)$$

where $u_0 = \dot{\xi}_0$ is the particle velocity amplitude, and look again at Eq. (7.3). This now takes the form

$$\frac{\partial(\rho\mathbf{u})}{\partial t} - \mathbf{F}' = -\nabla p + \left(\frac{4}{3}\eta + \eta'\right)\nabla\nabla \cdot \mathbf{u} - \eta\nabla \times \nabla \times \mathbf{u} \tag{7.3'}$$

where

$$-\mathbf{F}' = +(\rho\mathbf{u} \cdot \nabla)\mathbf{u} + \mathbf{u}\nabla \cdot \rho\mathbf{u}.$$

If we substitute the expansions (7.4) in (7.3') and sort out terms of corresponding order, we obtain

zeroth order

$$-\nabla p_0 = 0 \quad (p_0 = \text{constant}) \tag{7.16}$$

first order

$$\rho_0 \frac{\partial \mathbf{u}_1}{\partial t} - \nabla p_1 + b\eta \nabla\nabla \cdot \mathbf{u}_1 - \eta \nabla \times \nabla \times \mathbf{u}_1$$

[This is essentially Eq. (7.11)]

(7.16)

second order

$$\frac{\partial}{\partial t}(\rho_1 \mathbf{u}_1 + \rho_0 \mathbf{u}_2) + (\rho_0 u_1 \cdot \nabla)\mathbf{u}_1 + \rho_0 u_1 \nabla \cdot \mathbf{u}_1$$

$$= -\nabla p_2 + b\eta \nabla\nabla \cdot \mathbf{u}_2 - \eta \nabla \times \nabla \times \mathbf{u}_2.$$

Let us look at the second order equation in (7.16). We first denote the mass flow rate through some area S by M_t; then

$$M_t = \int_s \rho \mathbf{u} \cdot d\mathbf{S}.$$

If we now substitute for ρ and $\mathbf{u}$ from Eq. (7.4), keep only terms up to second order, and form the time average, then

$$\langle M_t \rangle = \int_s \langle \rho_0 \mathbf{u}_2 + \rho_1 \mathbf{u}_1 \rangle \cdot d\mathbf{S}.$$

We now introduce the symbols $\mathbf{U}$ and $\mathbf{u}_T$ such that

$$\mathbf{U} = \mathbf{u}_2 + \frac{1}{\rho}\langle \rho_1 \mathbf{u}_1 \rangle \equiv \mathbf{u}_2 + \mathbf{u}_T.$$

Then

$$\int \mathbf{U} \cdot d\mathbf{S} = \langle M_t \rangle / \rho_0.$$

In the steady state $\int \mathbf{U} \cdot d\mathbf{S} = 0$.

The quantity $\mathbf{U}$ is known as the *mass transport velocity.*

The time average of the first term of the second order equation can then be written

$$\frac{\partial}{\partial t}\langle (\rho_1 \mathbf{u}_1 + \rho_0 \mathbf{u}_2) \rangle = \frac{\partial}{\partial t}\left(\frac{d\langle M_t \rangle}{dS}\right)$$

which must vanish in the steady state.

The remaining portion of the equation, when averaged over an integral number of cycles, is therefore

$$-\mathbf{F} = -\nabla\langle p_2\rangle + b\eta\nabla\nabla\cdot\langle\mathbf{u}_2\rangle - \eta\nabla\times\nabla\times\langle\mathbf{u}_2\rangle \tag{7.17}$$

with

$$-\mathbf{F} = \rho_0\langle(u_1\cdot\nabla)\mathbf{u}_1 + \mathbf{u}_1(\nabla\cdot\mathbf{u}_1)\rangle.$$

It should be noted that F depends entirely on first order quantities and therefore is a known function, while the right hand side of (7.17) contains the unknown second order terms. Nyborg refers to $-\mathbf{F}$ as the vector giving the "time average (over a number of sonic cycles) of the time rate of increase of momentum in a fluid element."* The force is then equivalent to a known external force driving the second order system.

We shall now look at $\mathbf{F}$ for some special cases.

7.2 Plane Waves in an Unbounded Medium.

We begin with the usual expression for a damped harmonic wave as the first order solution

$$u_1 = u_0 e^{-\alpha x}\sin(\omega t - kx).$$

Then $\mathbf{F}$ reduces to the single component

$$F_x = -2\rho_0\left\langle u_1'\frac{\partial u_1}{\partial x}\right\rangle = \rho_0\alpha u_0^2 e^{-2\alpha x}. \tag{7.18}$$

One sees immediately that the artificiality of the bounded plane is going to cause trouble. Suppose that we have a beam of circular cross section (Fig. 7-1). Then F_x is a constant over the surface x = constant so long as the radius $\rho \leq a$, and is zero elsewhere. The force must therefore produce a flow of fluid to the right in the central cylinder of Fig. 7-1. Clearly the most elementary application of conservation principles requires that the fluid must return to the left in the region outside the central cylinder. That this return is necessary for maintenance of the flow can be seen from a consideration of

*Nyborg, Op. cit., p. 271.

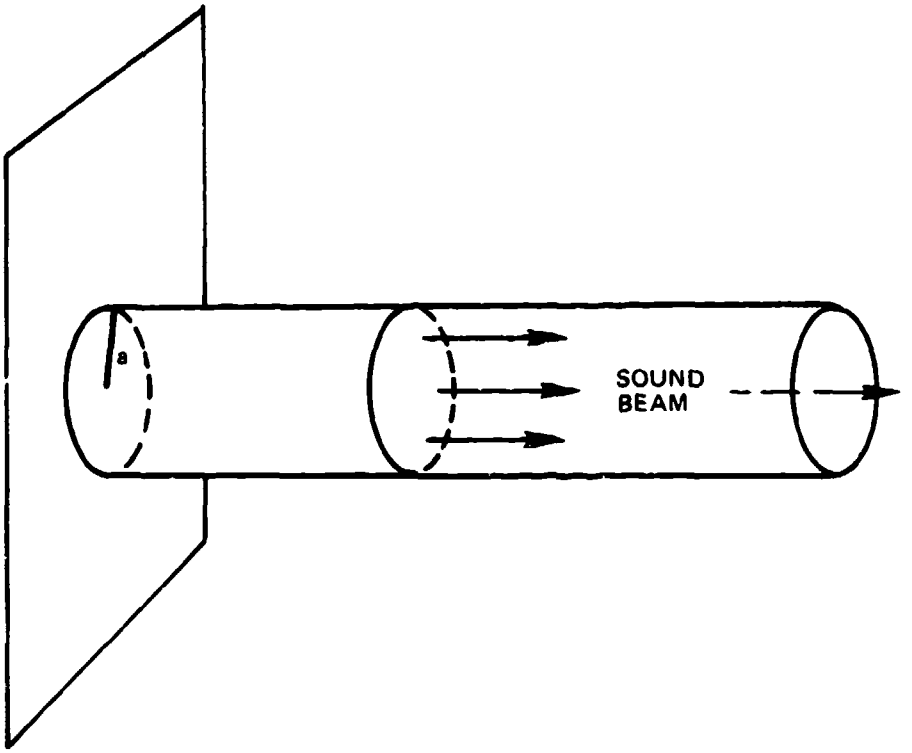

Figure 7-1.–Geometry of a bound sound beam of circular transverse cross section in an unbounded container.

the flow in a cylinder where the entire cross section of the cylinder is radiating sound, so that there is no place for a fluid return. There is then no fluid flow. In that case (7.17) reduces to

$$-\frac{d\langle p_2\rangle}{dx} = \rho_0 \alpha u_0^2 e^{-2\alpha x} \tag{7.17'}$$

or

$$\langle p_2\rangle = \frac{1}{2}\rho_0 u_0^2 (1 - e^{-2\alpha x}).$$

That is, the force F_x is everywhere counterbalanced by the pressure gradient and no net force exists to induce a fluid flow.

The effect of the second order terms in the case of an unbounded medium is then to produce vortical streaming. This can be made more evident

by taking the curl of the second order equation of (7.16) and considering steady state conditions. If we introduce the second order *vorticity* $\Omega_2 = \nabla \times \mathbf{u}_2$, then our equation becomes

$$\nabla^2 \Omega_2 = -\frac{1}{\rho_0^2} b \nabla \rho_1 \times \nabla \frac{\partial \rho_1}{\partial t} - \frac{\rho_0}{\eta} \nabla \times (\mathbf{u}_1 \times \mathbf{R}_1)$$

$$-\frac{1}{\rho_0} \nabla \times (\rho_1 \nabla \times \mathbf{R}_1) \equiv S_E + S_R \; S_T, \tag{7.19}$$

where $b = (4/3) + (\eta'/\eta)$. The identification of the three S terms was pointed out by Medwin and Rudnick. [4] The term S_E is that found by Eckart, [3] S_R that studied by Rayleigh, [9] and S_T a third term which exists only in the case of a rotational field (as is true also for the Rayleigh term S_E).

Medwin and Rudnick pointed out that the quantities S_E, S_R and S_T may be regarded as vorticity for which there is a first order vorticity: $\nabla \times \mathbf{u}_1 = \Omega_1 \neq 0$.

Such sources (S_R and S_T) will be strong in the vicinity of solid surfaces (e.g., near the walls of a tube), where viscous forces are important and $\nabla \times \mathbf{u}_1$ may be large.

The term "volume source" is applied to a source (S_E) in which the first order flow is irrotational. Such sources should predominate in an unbounded fluid or far removed from the walls in the case of a confined one. It can be seen from (7.19) that only the Eckart term depends on the bulk viscosity.

7.3 Case of a Cylindrical Tube.

Let us apply Eq. (7.18) to the case of a cylindrical tube in which a bounded plane beam of sound is progressing (Fig. 7-2). The radius of the beam r_1 is less than that of the tube r_0 and the tube is of sufficient length that we can neglect any returning acoustic signal.

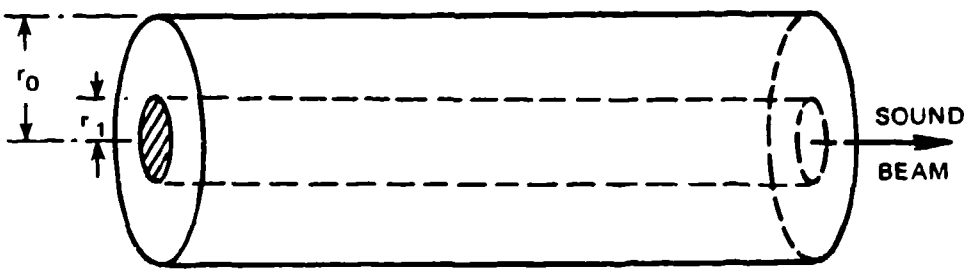

Figure 7-2.–Geometry for bounded sound beam in a walled container (from L. Liebermann [11]).

We rewrite the first order solution for irrotational flow in the form

$$u_1 = U(r)e^{-\alpha x} \sin(\omega t - kx) \tag{7.20}$$

where $U(r)$ allows for radial variation of the particle displacement velocity.

We now consider only the first term on the right in Eq. (7.19) and make use of the first order continuity Eq. (7.12) obtaining

$$\nabla^2\Omega_2 = -\frac{b}{\rho_0^2}\nabla\rho_1 \times \nabla\left(\frac{\partial\rho_1}{\partial t}\right) = \frac{b}{\rho_0}\nabla\rho_1 \times \nabla\nabla \cdot \underline{u}_1. \tag{7.21}$$

If we now identify Ω_2 with the steady vorticity so that $\Omega_2 = \nabla \times \langle \mathbf{u}_2 \rangle$, then time averaging of (7.21) and some vector manipulation (see [10]) gives the result

$$\nabla^2\Omega_2 = \frac{\rho_0}{\eta}\nabla \times \nabla\langle \mathbf{u}_1 \cdot \mathbf{u}_1 \rangle. \tag{7.22}$$

Substituting Eq. (7.20) in (7.21), we get

$$\nabla^2\Omega_2 = -\frac{\alpha\rho_0}{\eta_0}\frac{\partial^2}{\partial r \partial x}\langle u_1^2 \rangle (-\mathbf{i}\sin\phi + \mathbf{j}\cos\phi)$$

$$= -\frac{\alpha\rho_0}{\eta_0}e^{-\alpha x}\frac{\partial U^2}{\partial r}(\mathbf{i}\sin\phi - \mathbf{j}\cos\phi). \tag{7.23}$$

It follows immediately for Eq. (7.21) that there can be no second order circulation if $\alpha = 0$. Further, if we have a plane wave filling the tube, so that $U = u_0$ everywhere, then $\partial U^2/\partial r = 0$ and again no flow results.

To find the streaming velocity, it is useful to take the curl of both sides of Eq. (7.17):

$$-\nabla \times \mathbf{F} = -(\nabla \times \nabla)p_2 + b\eta(\nabla \times \nabla)(\nabla \cdot \mathbf{u}_2) - \eta\nabla \times \nabla \times \nabla \times \mathbf{u}_2. \tag{7.24}$$

But the operator $\nabla \times \nabla$ is identically zero, so that the first two terms on the right vanish and the third reduces to

$$-\eta\nabla \times (\nabla\nabla \cdot \mathbf{u}_2 - \nabla^2\mathbf{u}_2) = -\eta\nabla \times \nabla^2\mathbf{u}_2,$$

and we have, finally,

$$-\nabla \times \mathbf{F} = -\eta \nabla \times \nabla^2 \mathbf{u}_2. \tag{7.25}$$

Let us now consider the circular cylinder of fluid shown in Fig. 7-2. The radius of the transducer r_1 is less than that of the cylinder r_0. It is assumed that the cylinder is a long one and that there is no reflection of the sound from the far end. Furthermore, it will be assumed in calculations that

$$u_1 = u_0 e^{-\alpha x} \sin(\omega t - kx) \qquad 0 < r < r_1$$

$$= 0 \qquad r_1 \leqslant r \leqslant r_0.$$

Then F is given by the expression in (7.18)

$$F_x = \rho_0 \alpha u_0^2 e^{-2\alpha x}. \tag{7.18}$$

Eckart [3] used Eqs. (7.25) and (7.17) to obtain the following solution for the flow in the axial direction, subject to the condition of zero net mass flow through any cross section:

$$u_2(r) = K_1(r_0^2 - r^2) + K_2 \int_0^{r_0} \Gamma(s,r) P(s)\, ds \tag{7.26}$$

where

$$K_2 = \frac{1}{2} b\eta k^2 / \rho_0^2 c_0^3$$

$$\Gamma(s,r) = s \ln(r_0/r) \qquad s \leqslant r$$

$$= s \ln r_0/s \qquad s \geqslant r$$

$$K_1 = K_2 r_0^{-4} \int_0^{r_0} (s r_0^2 - s^3) P^2(s)\, ds.$$

For the specific geometry of Fig. 7-3, Eckart obtained the result

$$u_2 = U = G\left[\frac{1}{2}\left(1 - \frac{r^2}{r_1^2}\right) - \left(1 - \frac{r_1^2}{2r_0^2}\right)\left(1 - \frac{r^2}{r_0^2}\right) - \ln\frac{r_1}{r_0}\right] \qquad 0 < r < r_1$$

$$= -G\left[\left(1 - \frac{r_1^2}{2r_0^2}\right)\left(1 - \frac{r^2}{r_0^2}\right) + \ln\frac{r}{r_0}\right] \qquad r_1 < r < r_0$$

where

$$G = \frac{b\eta}{c_0}\left(\frac{ku_0r_1}{2}\right)^2.$$

Plots of u_2 vs r are shown in Fig. 7-3 for three cases, for which $r_1 = 1.5$ cm and the ratio r_1/r_0 is successively 1/3, 1/2, 2/3. From these calculations, it is evident that the cross sectional area of flow in the positive direction is greater than that of the sound beam for a relatively large tube, but becomes smaller than that of the sound beam in the case of a narrower cylinder.

7.4 Experimental Studies.

A number of interesting experiments have been performed indicating the qualitative validity of the theory just sketched. Figure 7-4 shows that streaming in the case of a geometry similar to that employed in the Eckart theory. [11] Fine particles of aluminum were suspended in a xylol filled glass cylinder. The circulatory nature is clearly indicated.

In another technique, Zarembo and Shklovskaya-Kordi [12] used a container half filled with glycerine and then a layer of vaseline oil (immiscible in glycerine) was added. A beam of sound enters the container parallel to the interface, with its axis lying in the interface.

A drop of colored water is then released in the vaseline. It gradually falls to the level of the interface, where it spread out, due to surface tension forces. The motions of streaming at the level of the interface carry the drop along the stream lines, so that a flow pattern gradually emerges (Fig. 7-5).

A modification of the analysis of Eckart has been given by Statnikov (1967) [13] for the case of sawtooth-like wave [Eq. (3.49)]. In essence, Statnikov begins with Eq. (7.3′) and writes $\mathbf{u}$ in the form $\mathbf{u} = \mathbf{u}_0 + \mathbf{u}_{ac}$, where $\mathbf{u}_0$ is the streaming velocity and $\mathbf{u}_{ac}$ the oscillating particle velocity. He then

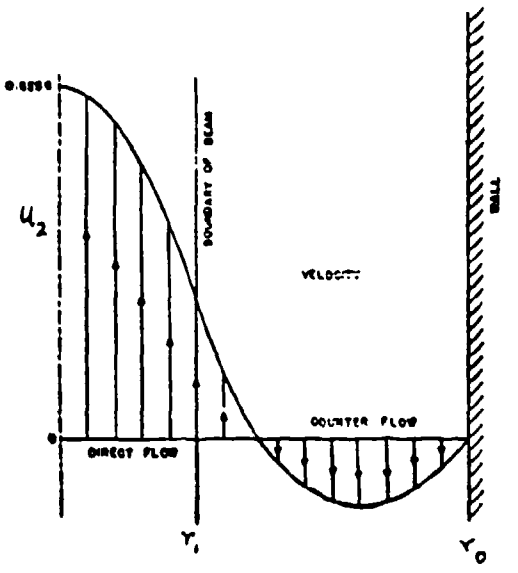

(a)

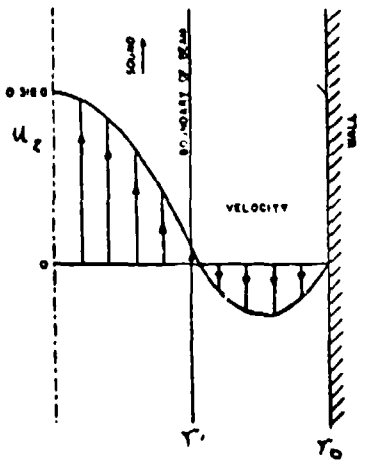

(b)

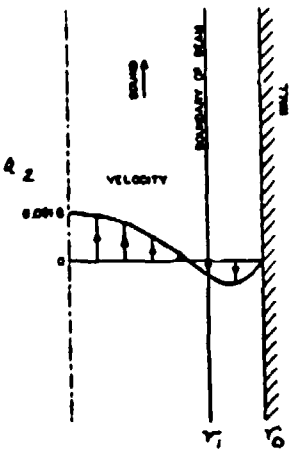

(c)

Figure 7-3.–Plots of theoretical values of streaming velocity as function of radius r. (r_1 = radius of beam, r_0 = radius of cylinder.) (a) $r_1/r_0 = 1/3$; (b) $r_1/r_0 = 1/2$; (c) $r_1/r_0 = 2/3$ (from C. Eckart [3]).

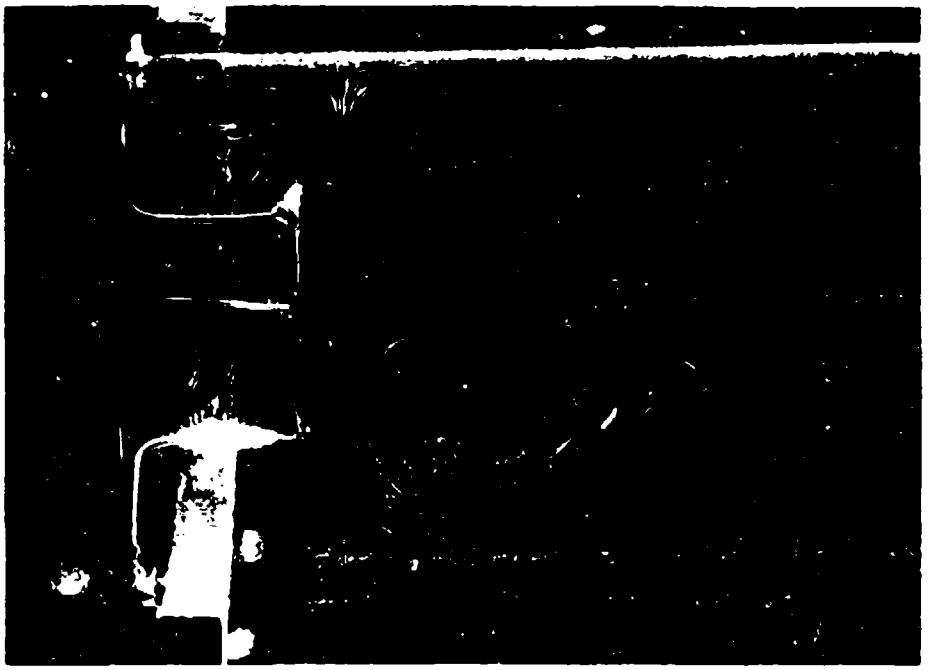

Figure 7-4.—Acoustic streaming from a sound source in water. The motion is made visible by a suspension of finely divided aluminum (from Liebermann [11]).

uses Eq. (3.49) for u_{ac}, under the assumption that the cross sectional area of forward streaming is identical to the area of the sound beam (Fig. 7-6). No attempt was made to determine the reverse motion.

After some mathematical transformations, the same solution as Eckart's is obtained except that the amplitude function G is given by

$$G = \frac{b^2\eta^2\omega^2k^2r_1^2}{\beta^2 4\rho_0^2 c_0^3} \sum_{n=1}^{\infty} \frac{n^2}{\sinh^2 n\alpha_0} \tag{7.28}$$

Here α_0 is the small-amplitude absorption coefficient and β the nonlinearity parameter. If the acoustic Reynolds number $\mathrm{Re}_{ac} = p_{ac}/b\eta\omega \ll 1$ (and $\Gamma \ll 1$), G reduces to

$$\frac{\rho_0\alpha}{2b} \frac{(p_{ac})^2 r_1^2}{\rho^2 c^2} \tag{7.29}$$

which coincides with the Eckart value. For high intensities,

$$G \cong 10^{-4}\,\mathrm{Re}_{ac} \frac{(u_{ac})^2}{c_0} \beta(kr_1)^2. \tag{7.30}$$

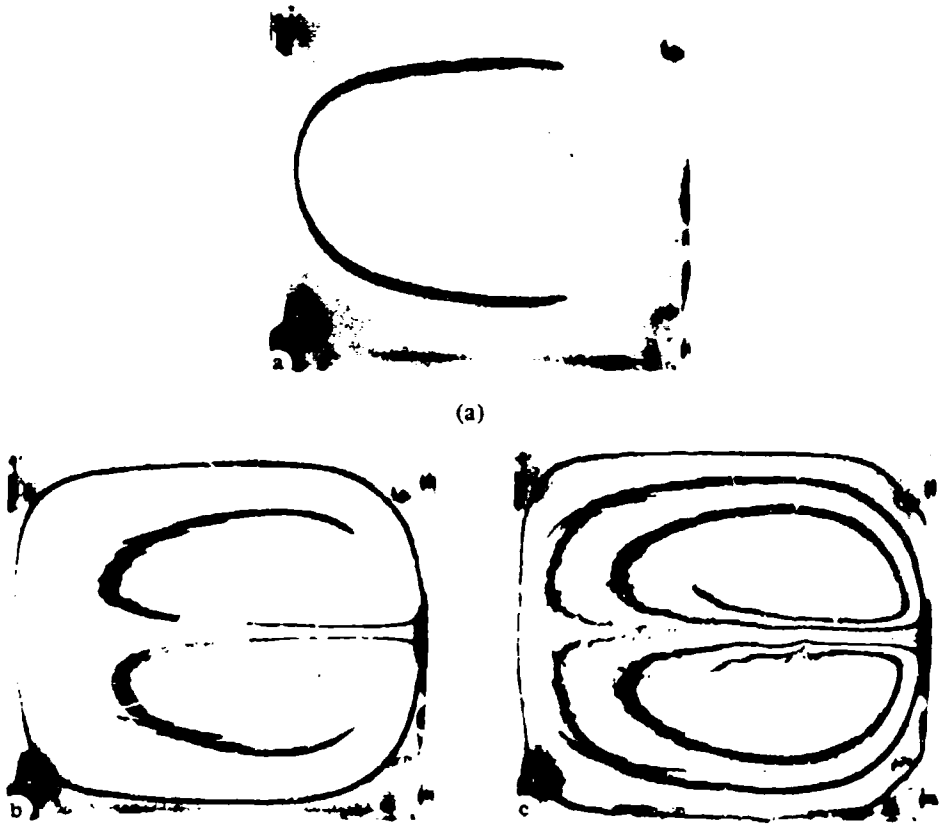

Figure 7-5.–Motion of a colored film of water at an interface between glycerine and vaseline for increasing time after start of experiment. Source is at the left (from Zarembo and Skhlovskaya-Kordi [12]).

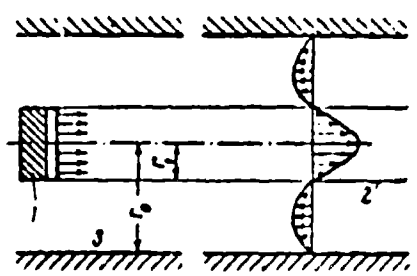

Figure 7-6.–Acoustic streaming for a sawtooth wave (from Statnikov [13]).

Experimental results are shown in Fig. 7-7 for streaming in water. [14] The measurements were made on a 1.2 MHz beam with the receiver 17 cm from the source. Aluminum-magnesium alloy filings were illuminated in the water and photography with intermittent illumination served to measure the velocity.

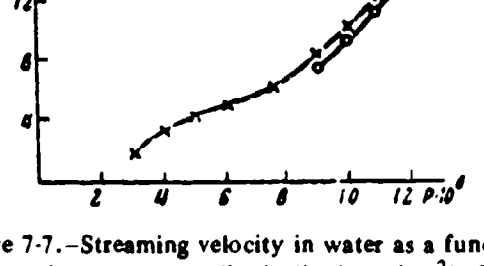

Figure 7-7.–Streaming velocity in water as a function of acoustic pressure amplitude (in dynes/cm^2). Curve (1) experimental data of Romanenko [14]; curve (2) theoretical data of Statnikov [13].

It is estimated that Re_{ac} ranged from 28-145. The inflection on the curve corresponds to the formation of sawtooth. Both upper and lower portions of the curve are parabolic in the pressure. The Statnikov theory for the upper region is indicated by curve 2. The agreement of theory and experiment appears to be quite satisfactory.

7.5 Plane Wave Traveling Between Parallel Walls

We shall follow here the analysis given by Nyborg. [15] The geometry is that sketched in Fig. 7-8. The quantity F of Eq. (7.17) is directed mainly along x and we take F_x to be approximately a function of z only.* We first assume that the surfaces are infinitely rigid, and that there is no slipping of the fluid at the walls. Under these circumstances, Eq. (7.17) reduces to

$$-\eta \frac{\partial^2 u_2}{\partial z^2} - \frac{\partial p_2}{\partial x} + F_x = 0 \tag{7.31}$$

(all the variables are averaged quantities) where $\partial p_2/\partial x = K$ is a constant.

*Although we know that the fluid must return somewhere, so that there will be some point at which the main flow must turn and therefore be in the z direction, we defer the location of this turning to some distant point out of the range of our immediate consideration. Nyborg makes the comparison with an express highway – heavy traffic in both directions, but no U turns are permitted except at some far distant location.

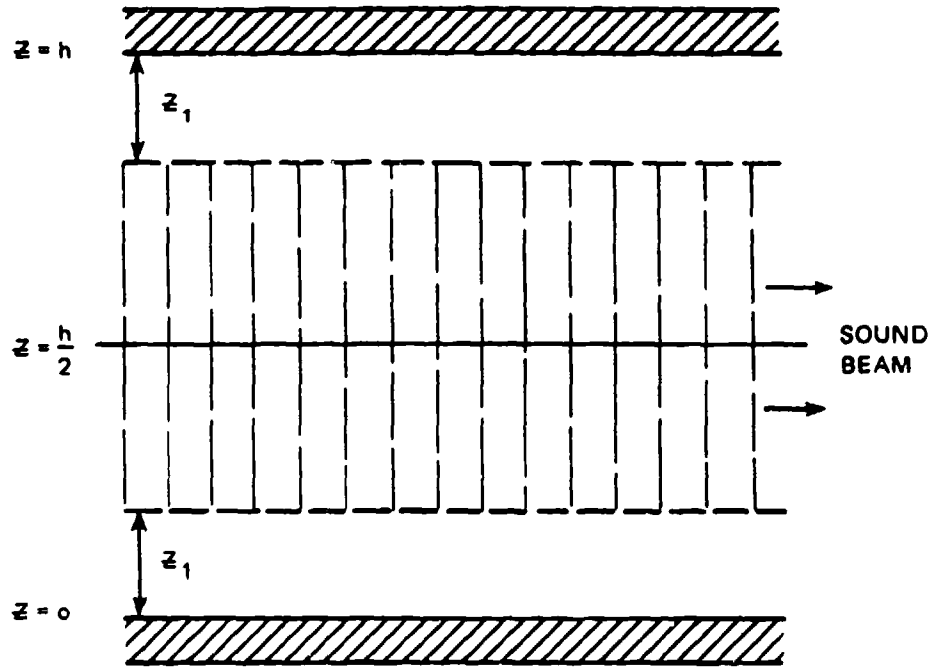

Figure 7-8.–Geometry for plane wave between parallel walls.

We further particularize the sound beam to be symmetric about the plane $z = 0$, and to be cut off sharply at $z = z_1, h - z_1$. Three major cases can now be distinguished.

(a) $z_1 > 0, K = 0$. This corresponds to a sound beam whose edges do not reach the walls, one in which the ends of the beam are not terminated (open channel).

The first order velocity will be given by

$$u_1 = Ae^{-\alpha x + i(\omega t - kx)} \qquad z_1 \leqslant z \leqslant h - z$$

$$= 0 \text{ elsewhere.}$$

Then $F_x = \rho_0 \alpha A^2 e^{-2\alpha x} \simeq \rho_0 \alpha A^2$ over the cross section of the beam [Eq. (7.18)].

Equation (7.31) then has the solution

$$u_2 = B(h - 2z_1)z \qquad 0 < z < z$$

$$= B(hz - z^2 - z_1^2) \qquad z_1 < z < \frac{1}{2}h \quad (7.32)$$

where $B = \rho_0 \alpha A^2 / 2\mu$.

The same curve will be repeated in the opposite half of the channel.

(b) $z_1 > 0, K \neq 0$. This corresponds to the case in which the flow is altered by a closing or partial closing of the ends so that a pressure gradient exists. This in effect alters the constant in Eq. (7.31). However, we shall have $K \neq 0$ over the whole cross sectional area. The result is therefore a flow velocity u_2' to be added to the u_2 of Eq. (7.32), given by

$$u_2' = \frac{2}{\eta} Kz(z - h). \tag{7.33}$$

The alteration produced in the flow pattern here is shown in Fig. 7-9.

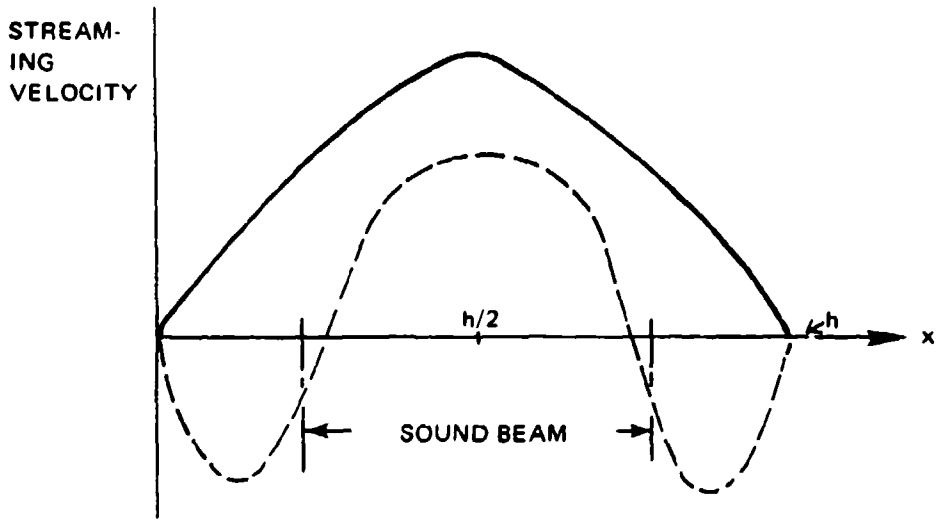

Figure 7-9.–Distribution of streaming velocity in propagation of sound between parallel walls. The geometry is that of Figure 7-8. _____: open channel, $z_1 = h/4$; – – – –closed channel.

The solid curve gives the streaming velocity u_2 for an open channel for the case in which $z_1 = h/4$. The dashed curve shows the velocity $u_2 + u_2'$ for a closed channel. In the latter case, the mass flow rate M_t must vanish:

$$M_t = \rho_0 \int_0^h (u_2 + u_2')dz$$

$$= \rho_0 h \left| \bar{u}_2 - \frac{Kh^2}{12\mu} \right| = 0 \tag{7.34}$$

Here $\bar{u}_2$ is the average of the quantity u_2 across the channel.

Equation (7.34) therefore represents the mean forward flow of case (a), $\bar{u}_2$, plus the reverse flow, characterized by the potential gradient K. The value of $\bar{u}_2$ can be found from Eq. (7.32):

$$\bar{u}_2 = \frac{2}{h}\int_0^{h/2} u_2 dz = \frac{Bh^2}{12}(2 - 3Z_1^2 + Z_1^3). \tag{7.35}$$

Here $Z_1 = \dfrac{z_1}{h/2}$ measures the relative width of the sound beam in the channel. (When $z_1 = 0$, the sound beam fills the entire channel.)

(c) $z_1 = 0$. Nonslip condition. If we allow $Z_1 = 1$ in Eq. (7.35) so that the sound beam fills the entire channel, $\bar{u}_2 = K = M = 0$, i.e., no flow can occur. However, this result is based on an unlikely physical situation—that the fluid particles can move freely at the wall (i.e., we have allowed the magnitude of u_1 to be constant over the cross section of the channel, even at the wall). A more realistic assumption would be that the tangential component of the particle velocity is zero at the walls, i.e., a *nonslip condition*. The solution of this program involves the problem of boundary layer behavior, a problem that has had enormous attention in fluid dynamics (see Schlichting [16]) and one into which we should like to enter as little as possible.

If one has a sound beam that extends to the wall, the first order solution $\mathbf{u}_1$ that satisfies the nonslip condition is given by the following equation (Nyborg, p. 314):

$$\begin{aligned} u_1 \ &\text{(longitudinal component)} \\ &= u_0 e^{-\alpha x}(1 - e^{-mz}) \cos(\omega t - kx) \\ w_1 \ &\text{(transverse component)} \\ &= -\frac{u_0 e^{-\alpha x}}{m}(1 - e^{-mz})\left[\alpha \cos(\omega t - kx) - k \sin(\omega t - kx)\right]. \end{aligned} \tag{7.36}$$

These lead to a force field F dominated by an x component that consists of two separate terms

$$F_x = F_{xa} + F_{xs}$$

where

$$F_{xa} = \rho_0 \alpha u_0^2 e^{-2\alpha x}$$

$$F_{xb} = \frac{1}{2}\rho_0 A^2 e^{-2\alpha x}\,[k f_1(\beta z) + \alpha f_2(\beta z)]\,. \tag{7.37}$$

The functions $f_1(\beta z), f_2(\beta z)$ are defined as follows

$$f_1(\beta z) = e^{-\beta z}\cos\beta z + e^{-\beta z}\sin\beta z - e^{-2\beta z}$$

$$f_2(\beta z) = -3e^{-\beta z}\cos\beta z + e^{-\beta z}\sin\beta z + e^{-2\beta z} \tag{7.38}$$

where $\beta^2 = \omega\rho/2\mu$.* These relations can be put in a neater form by introducing the substitution $C = e^{-\beta z}\cos\beta z, S = e^{-\beta z}\sin\beta z$ so that

$$f_1(\beta z) = C + S - e^{-2\beta z}$$

$$f_2(\beta z) = -3C + S + e^{-2\beta z}. \tag{7.39}$$

The variation of $f_1(\beta z), f_2(\beta z)$ with βz is shown in Fig. 7-10.

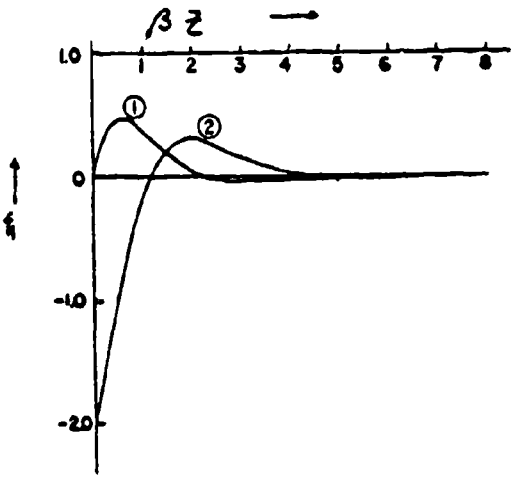

Figure 7-10.–Force field functions of Eq. (7.39): ①–$f_1(\beta z)$; ②–$f_2(\beta z)$ (from Nyborg [8]).

It is clear from the figure that both f_1 and f_2 vanish for z greater than $5/\beta$.

*The *ac* thickness parameter β is used only in Secs. 7.5-7.7, and should not be confused with the nonlinear parameter β used elsewhere in the book.

The distance β^{-1} is given the name of the *ac boundary layer thickness*. For water at 10 kHz, $1/\beta \simeq 5$ microns, so that the ac boundary layer will be extremely thin.

We shall not go into the details of further calculations but only cite the result.

The average flow velocity U in the channel that is capped at both ends (valid for distances $>5\beta^{-1}$ from the walls) is

$$U = \frac{3u_0^2}{4c}\left[1 - \frac{6z}{h}\left(1 - \frac{z}{h}\right)\right]. \tag{7.40}$$

A graph of (7.39) is shown in Fig. 7-11. This is a complete turnaround from case (b). The forward flow of the fluid will occur near (but not at) the walls, with reverse flow in the center.

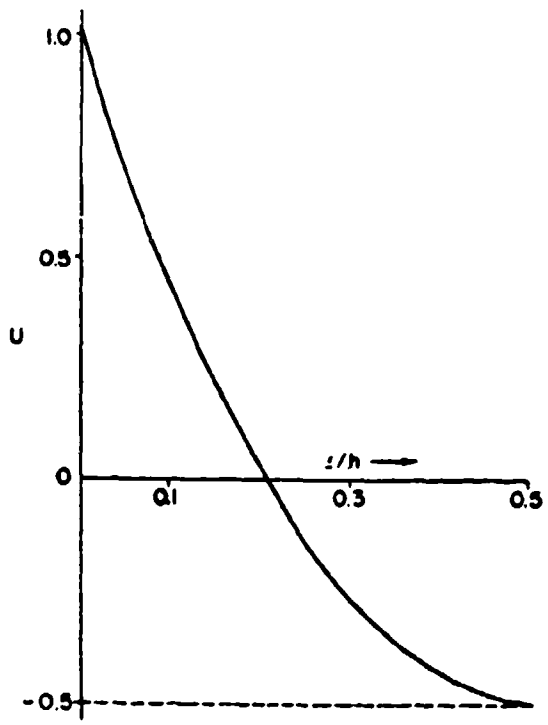

Figure 7-11.--Average flow velocity U for closed channel with nonslip condition on side wall. Units of U arbitrary (from Nyborg [8]).

In the case of an open channel, the flow is given by Eq. (7.31) for $z_1 = 1$ provided that the width of the channel is large compared with the sound wavelength ($kh \gg 1$).

7.6 Standing Waves Between Parallel Walls.

As pointed out in the INTRODUCTION, streaming in the case of standing waves was observed a hundred years ago in Kundt's tube experiments and here as almost everywhere else in acoustics, Lord Rayleigh presented much of the basic theory. [17] Using the geometry and notation of the previous section, we follow the Rayleigh treatment and introduce the stream function ψ. This function was used by Stokes to express the average for the second order, or streaming, velocity $\mathbf{u}_2$. The quantity $\nabla \cdot \mathbf{u}_2$ is essentially zero and we define the *stream* function such that the x, z components of $\mathbf{u}_2$ (u,w) are given by

$$u = \frac{\partial \psi}{\partial z}$$
$$w = -\frac{\partial \psi}{\partial x}. \tag{7.41}$$

Then the associated vorticity $\Omega_2 = \nabla \times \mathbf{u}_2$ will take on the value (for the case of Fig. 7-7)

$$\Omega_2 = \nabla \times \mathbf{u}_2 = \mathrm{j}\left(\frac{\partial u}{\partial z} - \frac{\partial w}{\partial x}\right) = \mathrm{j}\left(\frac{\partial^2 \psi}{\partial z^2} + \frac{\partial^2 w}{\partial z^2}\right). \tag{7.42}$$

Then, taking the curl of Eq. (7.17) (with $\nabla \cdot \langle \underset{\sim}{u}_2 \rangle \simeq 0$),

$$\nabla \times \mathbf{F} = +\eta \nabla \times \nabla \times \mathbf{u}_2 = +\eta \nabla \times \nabla^2 \mathbf{u}_2$$
$$= \eta \nabla^2 \nabla \times \mathbf{u}_2 = \eta \nabla^2 \Omega_2. \tag{7.43}$$

Rayleigh derived the solution for standing waves in a channel with the nonslip boundary condition as

$$u_1 = u_0 \cos kx \left[\cos \omega t - e^{-\beta z} \cos (\omega t - \beta z)\right]$$
$$w_1 = -\frac{k}{\beta\sqrt{2}} u_0 \sin kx \left[\cos\left(\omega t - \frac{\pi}{4}\right) - e^{-\beta z} \cos\left(\omega t - \beta z - \frac{\pi}{4}\right)\right].$$

Here β^{-1} is the *ac* boundary layer thickness, as before.

As in the case of a traveling wave, the force F_1 along the direction of propagation will be given by the sum of two terms,

$$F_x = F_{xa} + F_{xs}$$

where

$$F_{xa} = \rho_0 k u_0^2 \sin 2kx$$

$$F_{xs} = \frac{1}{4}\rho_0 k u_0^2 f_2(\beta z) \sin 2kx \tag{7.45}$$

with $f_2(\beta z)$ given by Eq. (7.38).

The patterns of u_1, F_x, and the average particle velocity $\mathbf{U} = [\mathbf{u}_2 + (1/\rho_0)\langle \rho_1 \mathbf{u}_1 \rangle]$ are shown in Fig. 7-12.

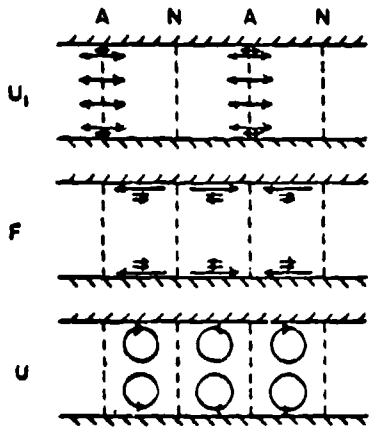

Figure 7-12.–Distribution of u_1, F_{xs} and V for standing waves in a channel (from Nyborg [8]).

The combination of Eqs. (7.42), (7.43) yields the equation

$$\nabla^4 \psi_2 \cong \frac{d^4\psi}{dz^2} = \frac{1}{2\eta}\beta\rho_0 k u_0^2 \sin 2kx\,(2C + S - e^{-2\beta z}) \tag{7.46}$$

where the nonvanishing of $\nabla \cdot \mathbf{u}$ has been taken into account. The solution of this equation with the boundary conditions

$$u_2 = w_2 = 0 \text{ at } z = 0$$

$$\frac{\partial u_2}{\partial z} = w_2 = 0 \text{ at midchannel } (z = (1/2)h)$$

has the following form for $\beta h \gg 1$:

$$\psi = G \sin kx \left[4C + 2S + \frac{1}{2}e^{-\beta z} - \frac{9}{2} + 3\beta z \left(1 - \frac{h}{z}\right)\left(1 - \frac{2h}{z}\right)\right]$$

where $G = u_0^2/8\beta c$.

Equation (7.47) can then be used to find the velocity components u_2, w_2. By further manipulation, we can derive the expression for the x and z components of the average particle velocity U and W:

$$\begin{aligned} U &= -3\beta G \sin kx \left[e^{-2\beta z} + 2S - 1 + 6\frac{h}{z}\left(1 - \frac{h}{z}\right)\right] \\ W &= -3kG \cos 2kx \left[e^{-2\beta z} + 2(S + C) - 3\right. \\ &\quad \left. + 2\beta\frac{h^2}{z}\left(1 - \frac{h}{z}\right)\left(1 - 2\frac{h}{z}\right)\right]. \end{aligned} \tag{7.48}$$

If we assume $\beta z \gg 1$ (i.e., positions in the channel well outside the boundary layer) then

$$\begin{aligned} U = u_2 &= 3\beta G \left[1 - 6\frac{h}{z}\left(1 - \frac{h}{z}\right)\right] \sin 2kx \\ W = w_2 &= -(6kh\beta G)\left[\frac{h}{z}\left(1 - \frac{h}{z}\right)\left(1 - 2\frac{h}{z}\right)\right] \cos 2kx. \end{aligned} \tag{7.49}$$

These are the values obtained by Rayleigh.

Expressions can also be derived for U and W near the walls, say near $z = 0$. These take the form

$$\begin{aligned} U &= -(3\beta G)(e^{-2\beta z} + 2S - 1) \sin 2kx \\ W &= -(3kG)[e^{-2\beta z} + 2(S + C) - 3 + 2\beta z] \cos 2kx \end{aligned} \tag{7.50}$$

$$\frac{h}{z} \ll 1.$$

The behavior of all these relations can be made somewhat clearer by defining limiting values of U and W:

$$U_L = 3\beta G \sin 2kx$$
$$W_L = -6k\beta zG \cos 2kx. \tag{7.51}$$

Figure 7-13 shows plots of U/U_L as a function of βz. If βh is sufficiently large ($>10^4$), the streaming rises rapidly to the limiting value.

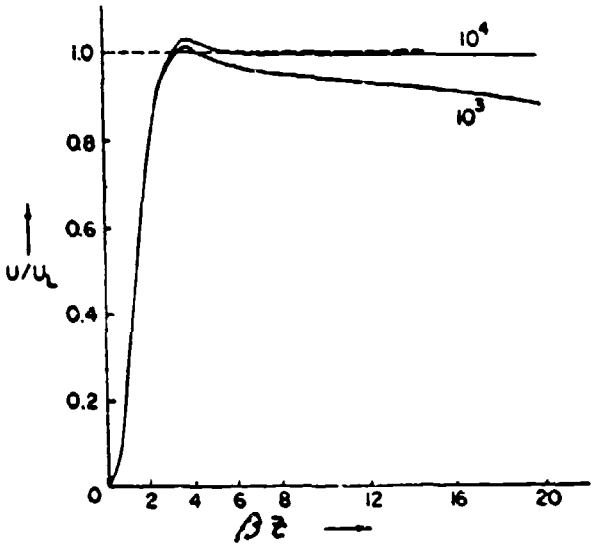

Figure 7-13.–Distribution of streaming velocity near wall for standing waves in a channel. Upper curve: $\beta h = 10^4$; lower curve: $\beta h = 10^3$ (from Nyborg [8]).

Many other relations can be obtained for the streaming for various specific situations and the reader is referred to Nyborg for further details.

7.7 Oscillatory Flow Near A Cylinder.

The streaming field in the neighborhood of a cylinder has been widely studied. The basic acoustic problem is that of streaming in the presence of a sound field. It has been shown by Westervelt [18] that, to terms of second order, the streaming past a fixed cylinder in an oscillating fluid is the same as in the case of a cylinder that is oscillating in a fluid that was previously at rest.

The first of these cases was solved in detail by Holtzmark, et al., [19] and we shall summarize the main points of their analysis.

The geometry is that indicated in Fig. 7-14.

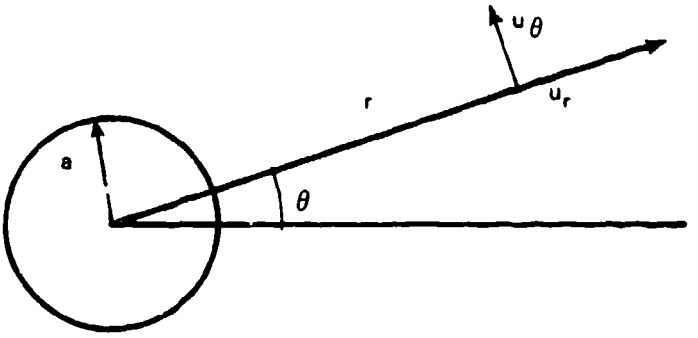

Figure 7-14.–Geometry for oscillatory flow near cylinder.

We assume that the fluid at large distances from the cylinder is oscillating sinusoidally and apply the usual boundary conditions on u_r and u_θ.

$$\begin{aligned} u_\theta &= \frac{\partial \psi}{\partial r} = 0, \quad r = a \\ &= -A \cos \omega t \sin \theta, \quad r = +\infty \\ u_r &= \frac{1}{r}\frac{\partial \psi}{\partial \theta} = 0, \quad r = a \\ &= A \cos \omega t \cos \theta, \quad r = +\infty. \end{aligned} \tag{7.52}$$

As in virtually all scattering problems of this type, the solutions are most effectively written in terms of the Hankel functions of the first kind (recall Section 1.8). We therefore define

$$X = \frac{H_0^{(1)}(kr)}{H_0^{(1)}(ka)} \qquad Y = \frac{H_1^{(1)}(kr)}{H_0^{(1)}(ka)} \qquad Z = \frac{H_2^{(1)}(kr)}{H_0^{(1)}(ka)} \tag{7.53}$$

where k is the wave number of the shear wave:

$$k = i^{1/2}\sqrt{\omega\rho/\eta} = (1 + i)\beta. \tag{7.54}$$

X, Y and Z are therefore the Hankel functions of order 0, 1, 2, normalized to the value of the zero order Hankel function on the surface of the cylinder.

The first order solution of the problem with the boundary conditions (7.52) is

$$\psi_1 = Aa \sin\theta \left[\frac{Y}{ka} - \frac{1}{2}\frac{r}{a} - \frac{1}{2}Z(a)\frac{a}{r}\right] e^{-i\omega t} + \text{complex conjugate.} \tag{7.55}$$

If βa is large, as it usually is, Eq. (7.55) can be greatly simplified. This form, first given by Schlichting [16], can be written as the real part of

$$\psi_{1S} = \frac{\sqrt{2}}{\beta} A \sin\theta\, e^{-i\pi/4}[1 - e^{-(1+i)\beta(r-a)} - \sqrt{2}\,\beta(r-a)]\, e^{-i\omega t}. \tag{7.56}$$

The solution of (7.55) and (7.56) is divergence free. For $r > a$ and $\beta a \gg 1$, one can consider ψ_{1S} in the limit of large βr. In such a case, the tangential component u_θ is much greater than the radial component u_r. The actual relations are

$$\begin{aligned} u_\theta &= -2A \sin\theta\,[\cos\omega t - e^{-n}\cos(\omega t - n)] \\ u_r &= \frac{\sqrt{2}}{\beta r} A \cos\theta \left[\cos\left(\omega t - \frac{\pi}{4}\right) - e^{-n}\cos\left(\omega t - n - \frac{\pi}{4}\right) - \sqrt{2}\, n \cos\omega t\right] \end{aligned} \tag{7.57}$$

where $n = \beta(r - a)$.

For large βr and far from the boundary layer ($n \gg 1$), Eq. (7.57) reduces to

$$u_\theta = -2A \sin\theta \cos\omega t$$

$$u_r = \frac{\sqrt{2}}{r} A \cos\theta \cos\left(\omega t - \frac{\pi}{4}\right).$$

We now attempt to determine the streaming velocity. To do this, Holtzmark et al. begin with the first order streaming function and obtained the equation analogous to Eq. (7.44):

$$\nabla^4 \psi_2 = \rho(r) \sin 2\theta. \tag{7.58}$$

Here $\rho(r)$ is an involved function of the Hankel functions:

$$\rho(r) = \frac{i\omega A^2}{4\eta^2}\left[Z + \frac{a^2}{r^2}Z(a)X^* + 2XZ^* - Z^* - \frac{a^2}{r^2}Z^*(a)X - 2X^*Z\right]$$

where the asterisk indicates the complex conjugate.

We shall not write down the solutions of Eq. (7.58), which are even more involved, but limit ourselves to reproducing the calculated streamlines for the first quadrant (Fig. 7-15) in a particular case.

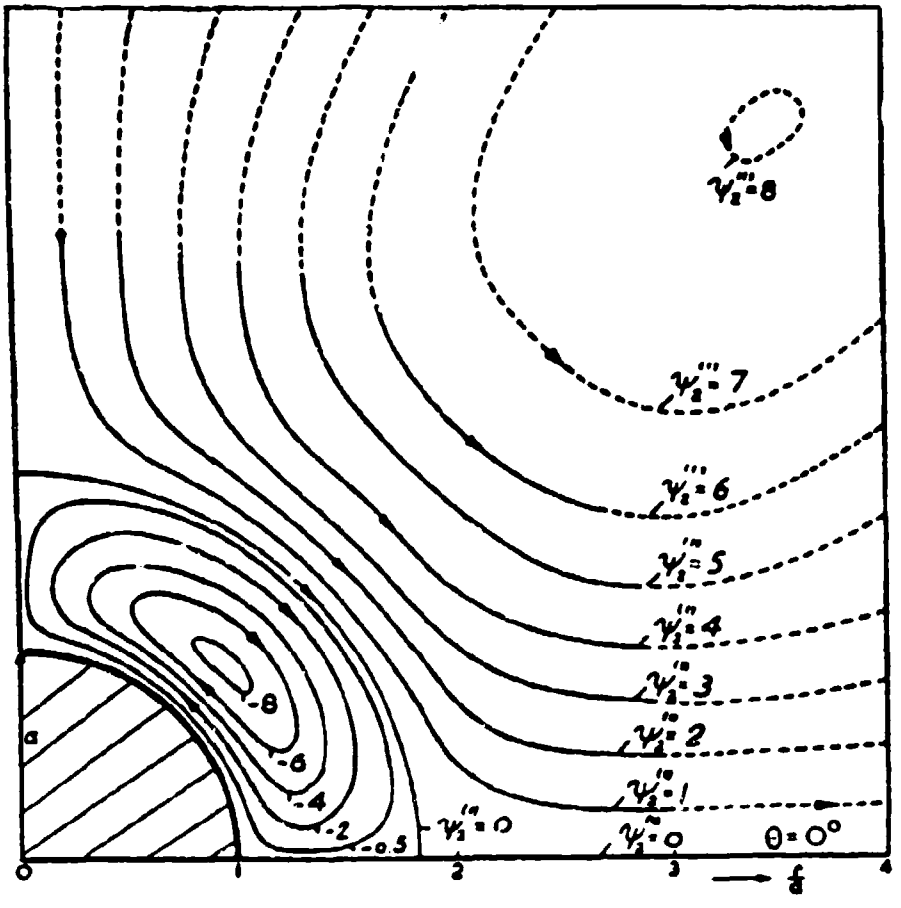

Figure 7-15.–Streamlines in quadrant of field near circular cylinder in oscillating fluid. Oscillation occurs in horizontal direction (from Holtzmark [19]).

7.8 Some Further Experimental Work.

The connection between sound absorption and acoustic streaming which was noted by Rayleigh in a remark on Eckart's work, [20] has been subjected to further experimental test. In 19[illegible] Nolinson and Tjötta [21] made experi-

mental studies of the streaming velocity profiles that were in good agreement with theory. From the values of the axial streaming velocity, they computed the ratio of the viscosity coefficients η', η for water and ethanol and propanol and obtained values within 10% of the accepted values. While this was not a precise method of measuring the sound absorption, it did give substantial experimental confirmation of streaming theory.

Piercy and Lamb [22] also used the streaming technique to determine the absorption. Their experimental arrangement is indicated in Fig. 7-16.

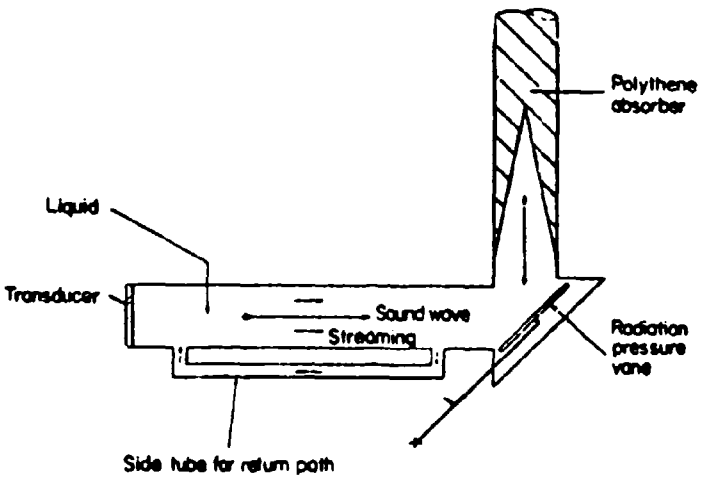

Figure 7-16.–Arrangements for streaming measurements (from Piercy and Lamb [22]).

A tube of approximately L shape with a side arm is filled with the test liquid. A 1-MHz quartz transducer terminates at the end of the vessel so that a traveling wave fills the main body of the vessel. This wave is incident on and reflected from a radiation pressure vane at the corner of the L. This vane measures the initial acoustic pressure by determining the radiation pressure.

As the sound wave reflects into the leg of the L, it is substantially absorbed by the polythene material surrounding the terminal cone of the liquid.

Since the transducer fills the main channel, there is negligible streaming in it. The static pressure is then that of Eq. (7.16)

$$\langle p_2 \rangle = \frac{1}{2} \rho_0 u_0^2 (1 - e^{-2\alpha x})$$

and the pressure difference between points $x = 0$ and $x = \ell$ marking the ends of the side arc will be

$$\Delta p = \frac{1}{2} \rho_0 u_0^2 (1 - e^{-2\alpha \ell}). \tag{7.59}$$

If the flow in the side arm is then assumed to follow Poiseuille's law, it follows that the velocity u_a measured along the axis of the tube will be

$$u_a = \frac{a^2}{4\eta\ell}\Delta p \tag{7.60}$$

where Δp is given by Eq. (7.59). Hence the measurement of u_a was sufficient to determine the absorption coefficient α. This method was used by Lamb and his colleagues for the measurement of the absorption coefficient of a considerable number of liquids.

REFERENCES

Chapter 7

1. M. Faraday, Phil. Tran. Rev. Soc. (London) **121**, 229 (1831).
2. Rayleigh, Theory of Sound, Ch. 29, reprinted by Dover, N.Y., 1945.
3. C. Eckart, Phys. Rev. **73**, 68 (1948).
4. H. Medwin and I. Rudnick, JASA **25**, 538 (1953).
5. F. V. Hunt, JASA **27**, 1019 (1955).
6. J. J. Markham, Phys. Rev. **86**, 497 (1952).
7. R. T. Beyer and S. V. Letcher, *Physical Ultrasonics*, Academic Press, N.Y., 1969, especially pp. 69-106.
8. W. L. Nyborg, "Acoustic Streaming," *Physical Acoustics*, Vol. IIB (W. Mason, ed., Academic Press, 1965).
9. Rayleigh, op. cit., Vol. II, p. 333.
10. P. J. Westervelt, JASA **25**, 60 (1953).
11. L.N. Liebermann, Phys. Rev. **75**, 1415 (1949).
12. L. K. Zarembo and V. V. Shklovskaya-Kordi, Sov. Phys. Acoustics **3**, 401 (1957).
13. Yu. G. Statnikov, Sov. Phys. Acoustics **13**, 122 (1967).
14. E. V. Romanenko, Sov. Phys. Acoustics **6**, 87 (1960).
15. W. L. Nyborg, op. cit., p. 282.
16. H. Schlichting, Boundary Layer Theory, McGraw-Hill, 1955.
17. Rayleigh, Phil. Trans. Roy. Soc. (London) **175**, 1 (1883).
18. P. J. Westervelt, JASA **25**, 60, 799, 1123 (1953); **27**, 379 (1953).
19. J. Holtzmark, I. Johnson, T. Sikkeland and S. Skavlem, JASA **26**, 26 (1954).
20. J. J. Markham, Phys. Rev. **86**, 497 (1952).
21. I. Johnson and S. Tjötta, Acoustics **7**, 7 (1957).
22. J. E. Piercy and J. Lamb, Proc. Roy. Soc. (London) **A226**, 43 (1954).

Chapter 8

CAVITATION

8.1 The Nature of Cavitation.

The name cavitation has been applied to the phenomenon of the appearance of holes in liquids. This appearance is usually due to the stress of tensile forces of some kind. These later may, in turn, be due to high speed flow, the rapid motion of a solid (such as a propeller blade) through the liquid, or to high intensity sound. At the same time, the nature and behavior of the holes can be quite varied. Depending on circumstances, these holes will be filled either by gases previously dissolved in the liquid or, in the absence of such dissolved gases, by the vapor of the liquid itself. Some authors have distinguished between these two types of behavior by calling the first *gaseous cavitation* or *pseudocavitation* and the second, *vapor cavitation* or *true cavitation.* In his very detailed study of the cavitation process, Flynn [1] (1964) noted that the first phenomenon has also been called "soft," "weak," "degassing," and "false" cavitation, while the second bears the labels "hard," "strong," "pure," and "real." The terminology certainly suggests that we are dealing here with the "bad guys" and the "good guys," and in an effort to avoid prejudicial language, Flynn has suggested the name *stable bubble field* for the first of these phenomena and *transient bubble* or *cavitation field* for the second. This shifts the distinction between two general types from the nature of the content of the bubble, or from a description of the characteristic manifestation of the bubble, to the ability of the bubble to survive for any appreciable length of time.

The subject of cavitation is a large one and could easily fill up a whole book, as the article by Flynn can testify. We shall be interested here only in a few aspects of cavitation that bear most closely on the field of nonlinear acoustics. These include acoustic means of cavitation generation, nonlinear behavior of the cavity, and sound produced by the collapsing cavity.

8.2 Static Bubble Theory.

When we observe a cavitation event in detail, we note that we first see a very minute bubble which grows very rapidly and then collapses with a distinctive sound. What we do not see is the process in which the little bubble

came to be. Qualitatively, most of cavitation theory presumes that the little bubble was already there, clinging to some bit of impurity in the medium. If we begin with this hypothesis, postponing the discussion of the origination of the little bubble, we must ask the question as to what conditions are necessary to bring about the rapid growth and collapse of this bubble. This begins with the study of the equilibrium theory of a bubble nucleus in a static pressure field.

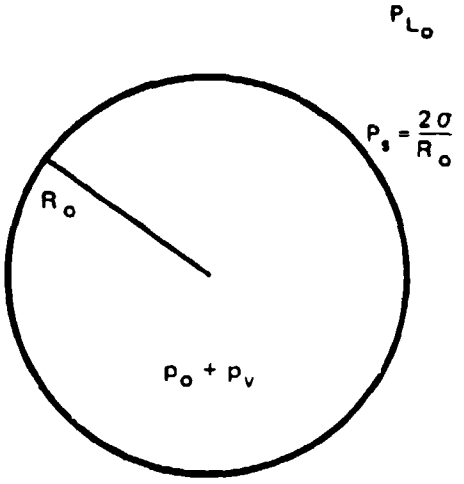

Figure 8-1.–Pressures in cavitation bubble.

In such a bubble (Fig. 8-1), the total pressure p_c inside the bubble, due to the gas pressure p_0 and the vapor pressure p_v, will be counterbalanced by the hydrostatic pressure of the liquid p_{L0} plus the contribution of surface tension $p_s = 2\sigma/R_0$, where σ is the surface tension and R_0 the radius of the bubble. Therefore

$$p_v + p_0 = p_{L0} + \frac{2\sigma}{R_0}. \tag{8.1}$$

If the external pressure is changed to some new p_L, so that the bubble radius becomes R, the new equilibrium relation will be

$$p_v + p = p_L + \frac{2\sigma}{R}. \tag{8.2}$$

If the pressure change inside the bubble is isothermal, then $pR^3 = p_0R_0^3$ or

$$p_v + p_0\left(\frac{R_0}{R}\right)^3 = p_L + \frac{2\sigma}{R}. \tag{8.3}$$

Equation (8.3) defines the equilibrium condition, but does not guarantee stability. Given $p_L < p_v$, R may be so large that the left side of the equation cannot equal the right side and the bubble will grow steadily. If we take the differential of both sides of (8.3) with respect to R and require the two sides to be equal, we define a critical radius R_c:

$$3p_0 \frac{R_0^3}{R_c^3} = \frac{2\sigma}{R_c}$$

If $R < R_c$, the bubble will be in stable equilibrium. Substituting this relation for R_c in Eq. (8.3), we obtain the result

$$R_c = \frac{4\sigma}{3|p_L - p_v|} \tag{8.4}$$

If $p_L = -1$ bar, then the critical radius in water at 20°C is 9.5×10^{-5} cm or 95 microns.

Of course, one does not usually maintain static negative pressures. Instead, one deals with an acoustic wave where the pressure is oscillating, with periods of negative pressure being less than half the period of the sound wave. We therefore seek, first, an expression for the value of the acoustic pressure amplitude needed to enlarge a bubble of initial size R_0 to the critical size R_c. We must then study the time interval necessary to bring about this growth.

The first of these questions was answered by Blake, [2] using simple equilibrium theory. If p_{ac} is the acoustic pressure amplitude, then the most negative pressure in a medium in which the static pressure is p_{L0} will be

$$p_L = -p_{ac} + p_{L0}.$$

Since this is a negative quantity, the expression $(p_L - p_v)$ of (8.4) can be written $p_{ac} - p_{L0} + p_v$ so that (8.4) becomes

$$R_c = \frac{4\sigma}{3(p_{ac} - p_{L0} + p_v)}. \tag{8.5}$$

In the absence of sound, we have Eq. (8.1)

$$p_0 + p_v = p_{L0} + \frac{2\sigma}{R_0}$$

while in the presence of a sound beam that just achieves critical size of the bubble, we can write Eq. (8.3) as

$$p_0\left(\frac{R_0}{R_c}\right)^3 + p_v = -p_{ac} + p_{L0} + \frac{2\sigma}{R_c}. \tag{8.6}$$

The original bubble size R_0 can now be eliminated between the last two equations, achieving the result for the Blake threshold for vapor cavitation as

$$p_t^B = p_{L0} - p_v + \frac{4\sigma}{3\sqrt{3R_0}}\left[1 - (p_{L0} - p_v)\frac{R_0}{2\sigma}\right]^{-1/2}. \tag{8.7}$$

According to this analysis, the radius of the bubble nucleus of original size R_0 will grow at an explosive rate whenever the acoustic amplitude reaches the value p_t^B.

Under normal conditions, and in the absence of sound, bubbles of gas can disappear by reason of diffusion of the gas through the gas-liquid interface. This will occur even though the liquid is itself saturated with the gas. The reverse process, known as rectified diffusion, occurs when a sound field is present, and may cause gas to go from the liquid into the cavity. This phenomenon was first suggested by Harvey et al. [3] in 1944 and has been developed in the researches of Blake, [2] Hsieh and Plesset [4] and Strasberg. [5] The theory involves the existence of a threshold pressure amplitude p_t^{HP}, for which the nucleus will grow under rectified diffusion. When the pressure in the liquid is below this threshold value, the bubble will lose its gas by normal diffusion and disappear. The expression for p_t^{HP} is given by

$$p_t^{HP} = \sqrt{\frac{2}{3}}\,p_{L0}\left(1 + \frac{2\sigma}{R_0 p_{L0}} - \frac{c_\infty}{c_0}\right)^{1/2} \tag{8.8}$$

where c_0 is the saturation concentration of the gas at the pressure p_{L0} and c_∞ is the actual concentration of the gas in the liquid at great distances from the nucleus.

Figure 8-2 is a graph taken from Flynn of the two thresholds just discussed. We restrict our attention to the case of p_{L0}. The effect of an increase in p_{L0} is to shift the entire set of curves upward.

If we are to take both theories seriously, the nucleus bubble will grow sometimes by one mechanism and sometimes by the other. For example, a bubble of radius less than 2×10^{-5} cm would grow by rectified diffusion as soon as p_{ac} reached the threshold p_t^{HP}. If the acoustic pressure remained constant, the bubble would increase in size until it reached the line of the Blake

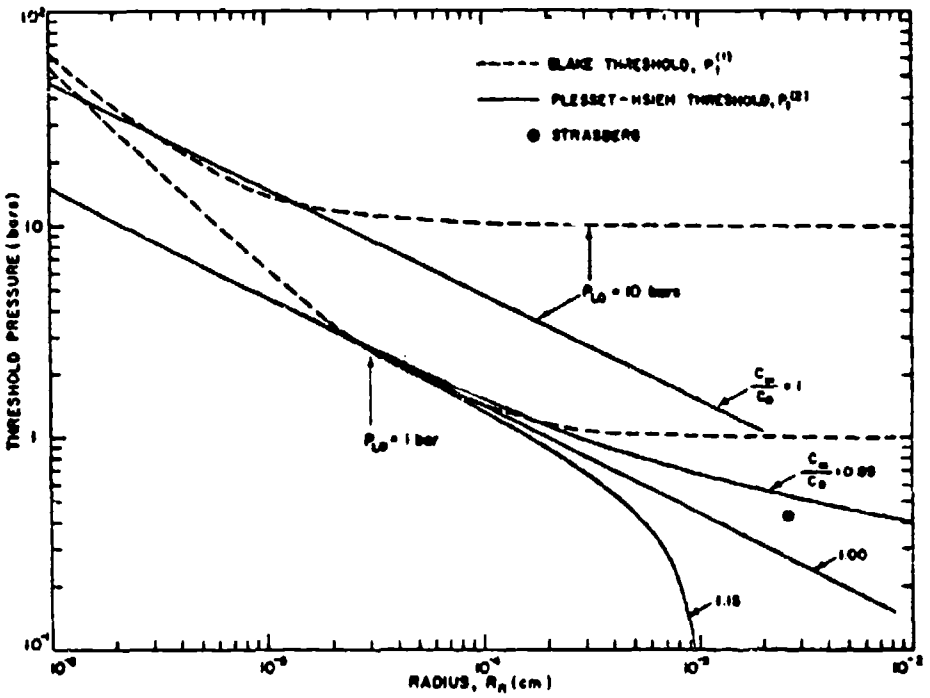

Figure 8-2.–Theoretical cavitation thresholds (from H. Flynn [1]).

threshold, whereupon it would grow explosively. For bubbles of initial radius greater than $(1\text{-}2) \times 10^{-4}$ cm, the growth must be entirely by rectified diffusion, while those in the intermediate range, for which the threshold pressures are about the same for the two mechanisms, the growth will be dominated by the very rapid Blake process.

All of this theory suggests that the growth process will be independent of frequency. Since many experimental measurements exist that demonstrate a frequency dependence the application of Eqs. (8.6), (8.7) must be limited to cases in which the sound frequencies are far below the resonance frequencies of the bubbles.

One experimental point has been plotted, that of Strasberg for bubble growth under rectified diffusion. It can be seen to be in good agreement with the theory.

8.3 Dynamic Bubble Theory.

The previous section dealt only with the equilibrium states of the cavitation bubble. Since we are primarily interested in the growth and collapse of cavitation bubbles, a study of the dynamics of bubbles is necessary.

In reviewing the large literature on the subject, Flynn distinguishes four major approximations, each leading to a somewhat different differential equation. To quote Flynn, we have

"I. The *incompressibility approximation* in which the density of the liquid is assumed to be constant and the speed of sound is infinite. This approximation leads to a differential equation (DE I) most useful in giving us semiquantitative information about stable cavities that can be simply interpreted.

II. The *acoustic approximation* in which the speed of sound is a finite constant but in which there is inadequate account taken of energy storage by compression of the liquid. This approximation leads to a second differential equation (DE II) most useful in giving us more precise statements about stable cavities and the dissipative effects of sound radiation on transient cavities.

III. The *Herring approximation* [6] in which the speed of sound is a finite constant, and a more adequate account is taken of energy storage by compression of the liquid. This approximation leads to a differential equation (DE III) that should be most useful in describing the motions of transient cavities that only expand to several times their initial radius.

IV. The *Kirkwood-Bethe approximation* [7] in which the speed of sound is a function of the motion. This approximation leads to a fourth differential equation (DE IV) most useful in this context in describing the final stage of collapse of a transient cavity that expanded to many times its initial radius." [8]

It should be clear that all of these treatments represent approximations and that qualitative agreement with experiment, for certain ranges of variable, is probably the most that can be hoped for.

We begin with an isolated bubble of radius R undergoing oscillations in an ideal incompressible liquid. The equation of motion can be written for the velocity u at the point r as

$$\frac{\partial u}{\partial t} + u \frac{\partial u}{\partial r} = -\frac{1}{\rho_0} \frac{\partial p}{\partial r} \tag{8.9}$$

for all points in the liquid, i.e., $r \geqslant R$.

Similarly, the continuity equation is

$$\frac{\partial}{\partial r} (r^2 u) = 0. \tag{8.10}$$

Since we have irrotational flow, we can introduce the velocity potential ϕ:

$$u = \frac{\partial \phi}{\partial r}. \tag{8.11}$$

We now integrate (8.9) from r to infinity, obtaining

$$\frac{\partial \phi}{\partial t} + \frac{u^2}{2} + \int_{p_\infty}^{p(r)} \frac{dp}{\rho} = 0. \tag{8.12}$$

We have assumed here that $\phi = 0$, $u = 0$ and $p(r) = p_\infty$ for $r = \infty$. Since we are dealing with an incompressible liquid, $\rho = \rho_0$ and Eq. (8.12) becomes

$$-\frac{\partial \phi}{\partial t} - \frac{u^2}{2} - \frac{p(r) + p_\infty}{\rho_0} = 0. \tag{8.13}$$

Integration of Eq. (8-10) from r to ∞ gives

$$r^2 u = \text{constant}.$$

If we designate the velocity at the surface of the bubble (radius R) to be U, then the constant $= R^2 U$ or

$$u = U\frac{R^2}{r^2} = \frac{\partial \phi}{\partial r}. \tag{8.14}$$

Then $\phi = -U(R^2/r)$ and (8.13) becomes

$$\frac{1}{r}\frac{d}{dt}\left(UR^2\right) - \frac{1}{2}\frac{U^2R^4}{r^4} + \frac{1}{\rho_0}\left[p_\infty - p(r)\right] = 0$$

or

$$\frac{1}{r}R^2\frac{dU}{dt} + \frac{2}{r}RU\frac{dR}{dt} - \frac{1}{2}\frac{U^2R^4}{r^4} + \frac{1}{\rho_0}\left[p_\infty - p(r)\right] = 0.$$

If we now set $r = R$, and recall that $U = dR/dt$ in this case, we have

$$R\frac{d^2R}{dt^2} + \frac{3}{2}\left(\frac{dR}{dt}\right)^2 + \frac{1}{\rho}\left[p_\infty - p(R)\right] = 0. \tag{8.15}$$

or

$$\frac{dU}{dt} + \frac{3}{2}\frac{U^2}{R} + \frac{1}{\rho R}\left[p_\infty - p(R)\right] = 0.$$

Equation (8.15) was the equation used by Rayleigh [9] for the case of a collapsing bubble, in which he assumed a constant hydrostatic pressure $p_{\ell 0}$ at infinity and a vacuum inside the bubble. Under such conditions, it can easily be verified that the solution of (8.15) is

$$U^2 = \frac{2}{3}\frac{p_0}{\rho_0}\left(\frac{R_0^3}{R^3} - 1\right). \tag{8.16}$$

The value of U is zero at $R = R_0$ and becomes rapidly more negative as $R \to 0$. The time required for the collapse of such a bubble was found by Rayleigh to be

$$t_c = 0.915\, R_0 \sqrt{\frac{\rho_0}{P_0}}\,. \tag{8.17}$$

Thus, for $p = 1$ atm, $\rho_0 = 1$ g/cm^3, $R_0 = 10^{-4}$ cm, $t_c = 91.5$ nanoseconds. Such a bubble would indeed have a short life! If R_0 is the radius of any bubble as it starts its final collapse, this expression gives a very accurate estimate of the collapse time.

In the presence of a harmonic sound field, the pressure at infinity would be written

$$p_\infty = p_{\ell 0} - p_m \sin \omega t. \tag{8.18}$$

The pressure inside the cavity will be due to the pressure of any residual gas, water vapor and surface tension [as in the equilibrium pressure relation (8.3)]. The pressure due to the gas will be

$$p_g = p_{g0}\left(\frac{R_0}{R}\right)^{3\gamma} \tag{8.19}$$

where P_{g0} is the gas pressure at $R = R_0$ and $\gamma = 1$ for isothermal expansion. For a simple adiabatic expansion, γ would be the ratio of specific heats of the gas. In general, the actual behavior is neither one nor the other, so that it is perhaps better to define an effeotive Γ (see Zwick, [10]).

The pressure of the gas in the bubble will also be sensitive to the surface tension and can be written

$$P_{g0} = p_0 + \frac{2\sigma}{R_0}$$

so that $p(R)$ now becomes

$$p(R) = p_v + \left(p_0 + \frac{2\sigma}{R_0}\right)\left(\frac{R_0}{R}\right)^{3\Gamma} - \frac{2\sigma}{R}. \tag{8.20}$$

We now substitute (8.18) and (8.20) in Eq. (8.15), obtaining the Noltingk-Neppiras equation, [11] labeled DE I by Flynn:

$$R\frac{d^2R}{dt^2} + \frac{3}{2}\left(\frac{dR}{dt}\right)^2 = \frac{1}{\rho_{\ell 0}}\left[\left(p_0 + \frac{2\sigma}{R_0}\right)\left(\frac{R_0}{R}\right)^{3\Gamma} + p_v - \frac{2\sigma}{R} - p_0 + p_m \sin \omega t\right]. \tag{8.21}$$

or

$$\frac{dU}{dt} + \frac{3}{2}\frac{U^2}{R} = \frac{1}{\rho_{\ell 0} R}\left[\left(p_0 + \frac{2\sigma}{R_0}\right)\left(\frac{R_0}{R}\right)^{3\Gamma} + p_v - \frac{2\sigma}{R} - p_{\ell 0} + p_m \sin \omega t\right].$$

We shall spend most of the time on this equation, but it must be that it assumes an incompressible liquid and is inadequate for description of the final stages of collapse of the cavity. Before proceeding to its consideration, however, let us turn to the other three equations delineated by Flynn.

If the compressibility of the liquid is taken into consideration, Eq. (8.10) must be replaced by

$$\frac{1}{\rho c_0^2}\frac{\partial p}{\partial t} + \frac{u}{\rho c_0^2} + \frac{\partial p}{\partial r} + \frac{2u}{r} = 0 \tag{8.22}$$

where we have used the sound velocity relation $c_0^2 = \partial p/\partial \rho$.

By a development parallel to that of Eqs. (8.9)-(8.15) we then obtain the result

$$R\frac{d^2R}{dt^2} + \frac{3}{2}\left(\frac{dR}{dt}\right)^2 \equiv \frac{1}{\rho_{\ell 0}}\left[p_\ell(t) - p_\infty(t) + \frac{R}{c_0}\left(1 - \frac{1}{c_0}\frac{\partial R}{\partial t}\right) \times \frac{dp_\ell}{dt}\right] = 0. \tag{8.23}$$

When the values of p_ℓ and p_∞ given above are substituted we obtain DE II

$$\frac{dU}{dt} + \frac{3}{2R}U^2 = \frac{1}{\rho_{\ell 0}R}\left[p_g + p_u + p_m \sin \omega t + \left(1 - \frac{U}{c_0}\right)\left(\frac{R}{c_0}\frac{dp_\ell}{dt} - \frac{2\sigma}{R} - \frac{4\eta U}{R}\right)\right] \tag{8.24}$$

with $p_g = p_n(e^{S/c_v}/R^{3/\gamma})$, η = shear viscosity, S = entropy, $U = dR/dt$.

This equation has been solved numerically by high-speed computer techniques. It can be used to study the effect of sound radiation and viscosity on bubbles of moderate amplitude.

The third form, due to Herring, [6] introduced compressibility of the fluid. In its general form it is quite similar to (8.23):

$$\left(1 - \frac{2U}{c_0}\right)\frac{dU}{dt} + \frac{3}{2}\left(1 - \frac{4}{3}\frac{U}{c_0}\right)\frac{U^2}{R} = \frac{1}{\rho_{\ell 0}R}\left[p_\ell(t) - p_\infty(t) + \frac{R}{c_0}\left(1 - \frac{1}{c_0}U\right)\frac{dp_\ell}{dt}\right]. \tag{8.25}$$

Akulichev refers to Eq. (8.26) as the Herring-Flynn equation. [12] Since it has taken the compressibility of the liquid into rough account, it is a better source of quantitative information on the rate of collapse of the bubbles than the Noltingk-Neppiras equation. It is not accurate however, if U/c_0 approaches or becomes greater than unity.

In such a case, the finite amplitude theory of spherical waves must be used. This method was developed by Kirkwood-Bethe [7] in the theory of underwater explosions, and leads to DE IV—the Kirkwood-Bethe equation.

Their theory postulates that the quantity $r\phi$ propagates with a velocity $c_f = c + u$ where c is the local sound velocity.

In Eq. (8.12), the integral is the specific enthalpy h of the liquid for the case of constant entropy that we are considering. The quantity $\partial\phi/\partial t$ also has the dimensions of enthalpy and is called the kinetic enthalpy Ω. Then

$$\bar{r}\,\Omega = r\left(\frac{u^2}{2} + h\right). \tag{8.26}$$

It can be demonstrated that

$$\left(\frac{\partial}{\partial t} + c_f \frac{\partial}{\partial r}\right)(r\Omega) = 0 \tag{8.27}$$

which in turn implies that $r\Omega$ also propagates with the finite amplitude velocity c_f. Thus if the value of $r\Omega$ is known on the surface of sphere of radius R, and time t_R, its value can be deduced elsewhere in the fluid at a later time t by use of the generalized retarded time

$$t - t_R = \int_R^r \frac{dr}{c_f}. \tag{8.28}$$

When these relations are applied to our problem of the radiating bubble, we obtain the result

$$\left(1 - \frac{u}{c}\right)\frac{dU}{dt} + \frac{3}{2}\left(1 - \frac{U}{3c}\right)\frac{U^2}{R} = \left(1 + \frac{U}{c}\right)H + \frac{U}{c}\left(1 - \frac{U}{c}\right)\frac{dH}{dR} = 0 \tag{8.29}$$

with

$$H = \int_{p_\infty}^{p(R)} \frac{dp}{\rho}. \tag{8.30}$$

Equation (8.29) is the Kirkwood-Bethe equation. It is deceptively simple; the sound velocity here is a variable and H is a very involved parameter.

We make use of the Tait relation for the pressure-density relation [Eq. (3.17)]

$$p = P\left(\frac{\rho}{\rho_0}\right)^{\gamma} - Q. \tag{8.31}$$

The quantity H can then be expressed in the form

$$H = \frac{\gamma}{\gamma - 1}\frac{P^{1/\gamma}}{\rho_0}\left[\left(P_0 + \frac{2\sigma}{R_0}\right)\left(\frac{R_0}{R}\right)^{\Gamma} - \frac{2\sigma}{R} + Q\right]^{\frac{\gamma-1}{\gamma}} - (P_0 - P_m \sin \omega t + Q)^{\frac{\gamma-1}{\gamma}}. \tag{8.32}$$

A comparison of the numerical solutions of Eqs. (8.21), (8.25) and (8.30) indicates that they all give identical results in the early stages of bubble growth. This is shown in Fig. 8-3. The ordinate a is the reduced bubble

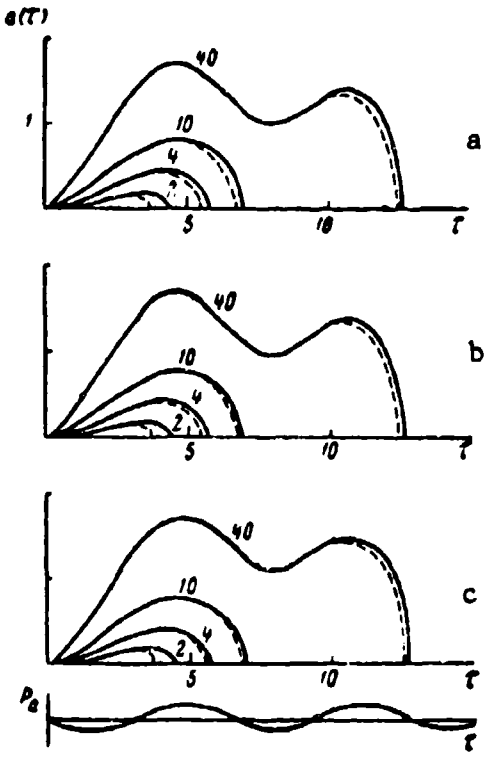

Figure 8-3.–Solutions of the bubble equations of (a) Noltingk-Neppiras, (b) Herring-Flynn, and (c) Kirkwood-Bethe (from Akulichev [12], p. 219).

radius, $= (\omega/\omega_0)(R/R_0)$ while the abscissa is the reduced time $\tau = \omega t$. The frequency ω_0 is the linear resonance frequency of an equilibrium bubble of radius R_0.

$$\omega_0 = \frac{1}{R_0}\left[\frac{P_0 + \frac{2\sigma}{R_0}}{\rho_0}\right]^{1/2} . \tag{8.33}$$

In terms of these units, the Noltingk-Neppiras equation can be written

$$a\frac{d^2a}{dt^2} + \frac{3}{2}\left(\frac{da}{dt}\right)^2 - \frac{1}{\rho_0\omega_0^2R_0^2}\left[\frac{2\sigma}{R_0}\left(1 - \frac{\omega}{\omega_0 a}\right) + P_v + P_m \sin t\right] + \left[1 - \left(\frac{\omega}{\omega_0 a}\right)^{\Gamma}\right] = 0. \tag{8.34}$$

Figure 8-3 represents the results of the numerical solution of (a) the Noltingk-Neppiras equation (8.21), (b) the Herring-Flynn equation (8.25) and the Kirkwood-Bethe equation (8.30) for a bubble of initial radius $R_0 = 10^{-5}$ cm for adiabatic behavior in water at a hydrostatic pressure of 1 atm. The solid curve represents behavior at 10 kHz while the broken curve indicates 500 kHz. The numbers on the curves indicate the values of the sound pressure in atmospheres. The sine wave at the bottom of the drawing represents the applied acoustic signal. The value of ω_0 for this bubble is 4×10^8/sec, so that $\omega = 2\pi f$ is much smaller than ω_0 in each case.

It can easily be seen from these curves that the three results are virtually identical. The basic characteristic of all curves at low acoustic pressure is the growth of the bubble radius to a maximum and then rapid collapse. The total time required for this process is roughly one acoustic period.

When the pressure reaches some critical value, the bubble does not immediately collapse after passing its maximum radius but instead expands again, reaching a second maximum and then collapsing.

This behavior is shown in greater detail in Figs. 8-4. These figures apply to Eq. (8.21) and are for the same case as Fig. 8-3 (500 kHz) except that the initial bubble size is varied (a -10^{-4} cm; b -5×10^{-4} cm and c -10^{-3} cm).

The calculations have been extended to higher acoustic pressures, and the ordinate is plotted in terms of the radius ratio R/R_0. The resonant frequencies of the bubbles are $\omega_0 = 15.8 \times 10^6$/sec, 2.28×10^6/sec and 1.07×10^6/sec, respectively. Since $\omega = 2\pi f = 3.14 \times 10^6$/sec, these three cases correspond to a bubble radius smaller than resonance (a), approximately equal to resonance (b), and greater than resonance (c).

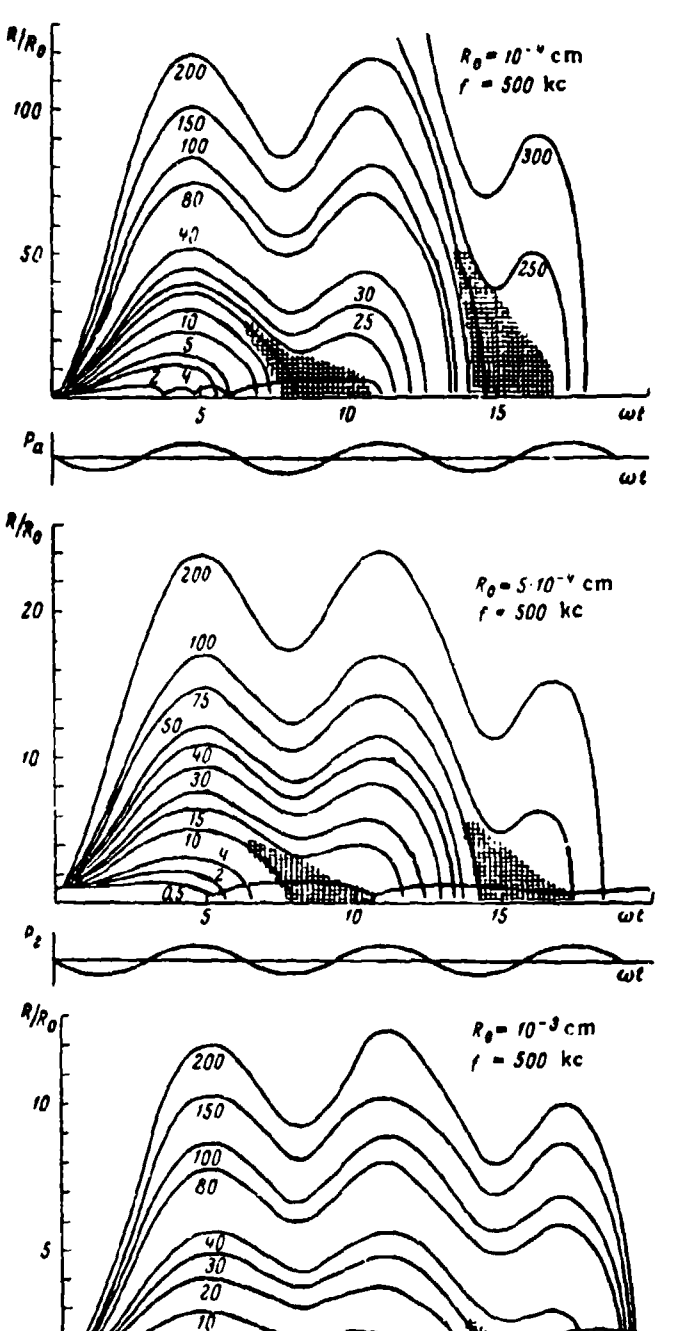

Figure 8-4.–Pulsations of cavitation bubble at 500 kHz for (a) $R_0 = 10^{-4}$cm, (b) $R_0 = 5 \times 10^{-4}$ cm, (c) $R_0 = 10^{-4}$ cm. Sine wave at bottom indicates sound signal (from Akulichev [12], pp. 222-223).

The shaded areas on the figures indicate instability of the solution, since a very small change in the acoustic pressure produces a qualitative change in the shape of the solution, i.e., a new pulsation of the bubble.

We can also see that there exists an acoustic pressure amplitude p_{mc}, below which the bubbles do not collapse, but fluctuate in size with roughly the period of the applied acoustical signal. This can be interpreted as the cavitation threshold for bubbles of the given size.

An extraordinary experimental confirmation of the theory of bubble growth and collapse has been carried out by Akulichev. [12] Cavitation bubbles were formed under the action of 15-kHz sound and photographed by a camera system capable of a film speed of 200,000 per second. A series of such photographs is shown in Fig. 8-5 for a sound pressure of about 2 atm. It was inferred by curve fitting that the initial bubble size was $R_0 = 10^{-4}$ cm.

The comparison of theory and experiment is shown in Fig. 8-6. The solid curve is Herring-Flynn and Kirkwood-Bethe, the broken curve Noltingk-Neppiras and the circles are experimental points based on the data of Fig. 8-5.

A somewhat paralleling set of investigations have been carried out by Lauterborn, [17a] including detailed photographic studies of tearing of a water column by a centrifuge [17b] and laser-induced cavitation. [17c]

8.4 Experimental Evidence of Cavitation Thresholds.

The material of the previous section indicates that cavitation effects depend critically on the size of ambient bubbles, which in turn must depend on the purity of the medium and the physical conditions under which it is examined.

There exists a long history in the literature of attempts to measure a cavitation threshold. Such measurements of course require some criterion for judging the appearance of cavitation. In the earliest measurements, cavitation was described as the appearance of vigorous bubble activity. Blake described three stages in the process. [13] At low acoustic pressures, relatively large bubbles were produced without appreciable sound emission. At higher pressures, streams of bubbles appeared in the liquid, accompanied by a hissing sound. These bubbles rose as stable bubbles to the surface of the liquid. Blake found a critical pressure for these streams to form and called that his threshold. Since his liquid was nearly saturated with air in these measurements, he regarded these bubble streamers as evidence of gaseous cavitation.

When Blake increased the pressure still further, he found that new bubbles would appear suddenly, and just as suddenly disappear. These short-lived bubbles appeared irregularly and singly, and were accompanied by a click or snap as they went through their stage of growth and collapse. He identified this process with "vaporous" cavitation.

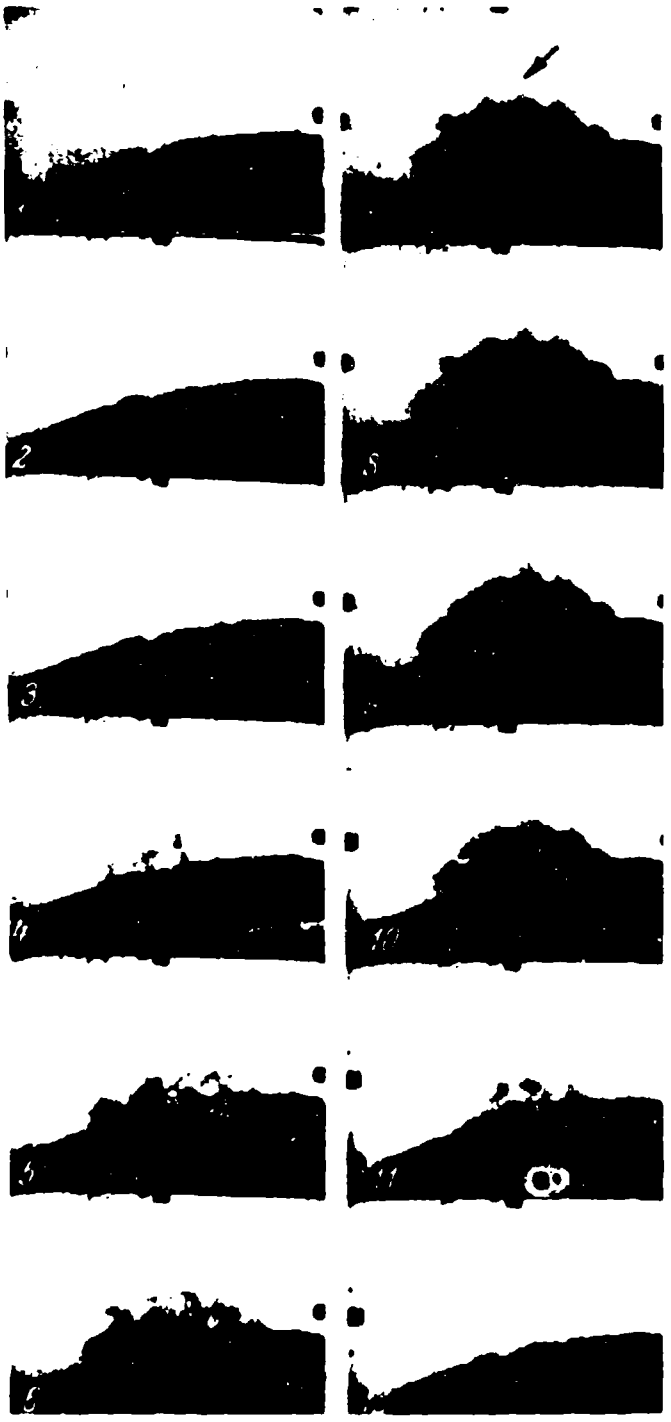

Figure 8-5.–Bubble growth and collapse. Ultrasonic frequency is 15 Hz, film speed 200,000 frames/sec and sound pressure amplitude 2.0 atm (from Akulichev [12], p. 235).

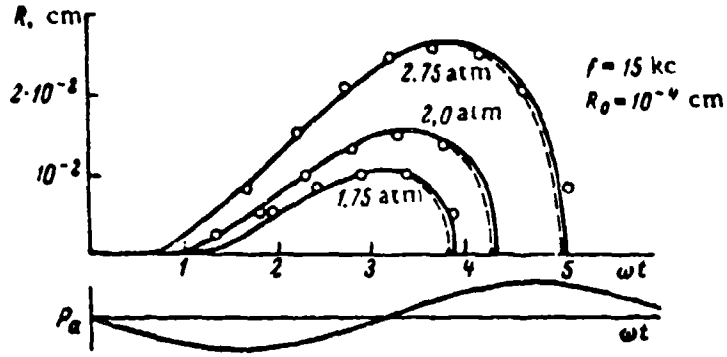

Figure 8-6.–Comparison between the pulsations of experimentally observed cavitation bubbles and the calculated pulsations (from Akulichev [12], p. 236).

While Blake made threshold measurements, he did not report information on size of bubbles in the medium or of the bubbles produced. (This is true of many other observers also.) Other observers have, however, studied size distribution, so that some remarks can be made. [14] In freshly drawn tap water, the commonest ambient bubble radius is near 2×10^{-3} cm. After it has stood for several hours, the water was found to have the largest nuclei with radius of 8×10^{-4} cm. Such bubbles are somewhat larger than those of Fig. 8-4a and are capable of serving as cavitation nuclei.

Blake's experiments relied mainly on the visual. One can also use the acoustical evidence for the appearance of cavitation. This has been done by Meyer and coworkers at Göttingen. [15] They noted that very small bubbles could grow to a size of 50×10^{-4} without being visible to the naked eye, and could then collapse. While such transient cavities would never be noted visually, they could be detected acoustically.

The problem of the presence of dissolved gas in the water was especially studied by Galloway. [16] He worked with a large liquid-filled sphere driven by a magnetostrictive element at a resonant frequency of the sphere.

At this resonance, the acoustic pressure at the center of the sphere could attain values as high as 200 atm. As the acoustic pressure was increased to a threshold value, a cavitation bubble would appear at the center of the sphere, grow to about a 1-cm radius and collapse violently. The appearance of the bubble was taken as the evidence of cavitation, which would be of Blake's third or vaporous type. In his measurements (Fig. 8-7), the limiting value of the pressure threshold for water was approximately 200 atm. Theoretical estimates of the tensile strength of a homogeneous liquid lead to values of the order of a thousand atmospheres or more, while an experimental value of −275 atm has been obtained by Briggs in a static measurement. The agreement is quite respectable, since Galloway's figure must be highly sensitive to the presence of minute impurities in the liquid.

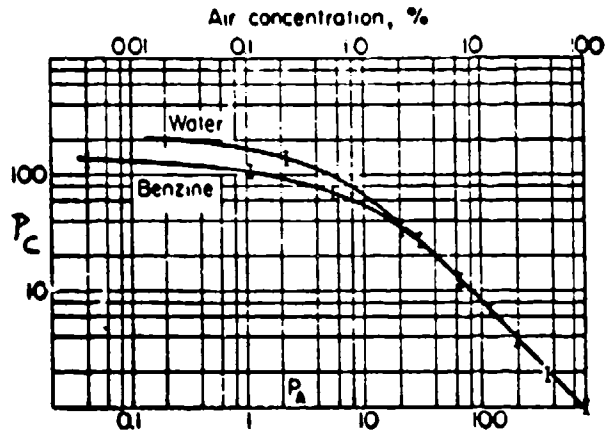

Figure 8-7.–Cavitation threshold for water and benzene as a function of percent air concentration for a hydrostatic pressure of 1 atm and T = 22°C. P_C = cavitation threshold in bars, P_A = hydrostatic pressure in Torr (from W. Galloway [16]).

In a further experiment, Galloway measured the cavitation threshold of air-saturated water as a function of the hydrostatic pressure (Fig. 8-8). These results, together with those of other observers, indicate clearly that gaseous cavitation can occur (for sound of about 30 kHz) whenever the total pressure (hydrostatic plus instantaneous acoustic) reaches zero during the acoustic cycle.

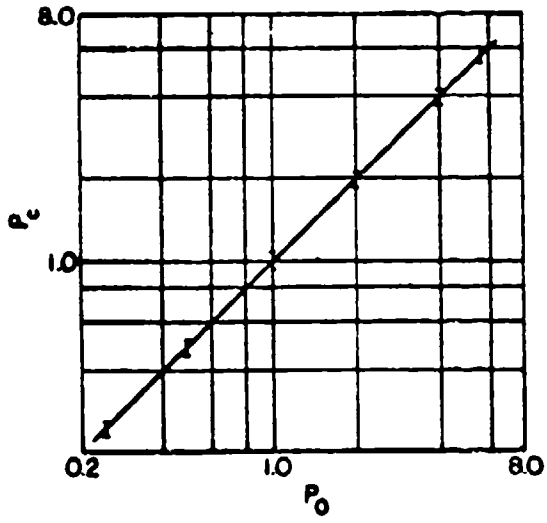

Figure 8-8.–Cavitation threshold of air-saturated water as a function of hydrostatic pressure: P_c = cavitation threshold in bars, P_A = atmospheric pressure in bars, T = 22°C (from Galloway [16]).

The measurements thus far discussed have not been concerned with the time required to produce cavitation. It is clear from other measurements that the instantaneous pressure must remain above the threshold value for some time interval in order to produce the cavitation phenomenon. Esche (1952) measured the onset of cavitation in gassy water at a number of frequencies from 3 kHz to 3.3 MHz, and found a steady increase in the pressure required. While his results are rather qualitative, they are supported by various finite amplitude studies, which indicate that the gaseous type of cavitation does not occur even at acoustic pressures of several atmospheres, when the measurements are performed in the megahertz range.

Figure 8-9 summarizes experimental work in cavitation threshold in water. The three values given by Rozenberg, [17] correspond to water

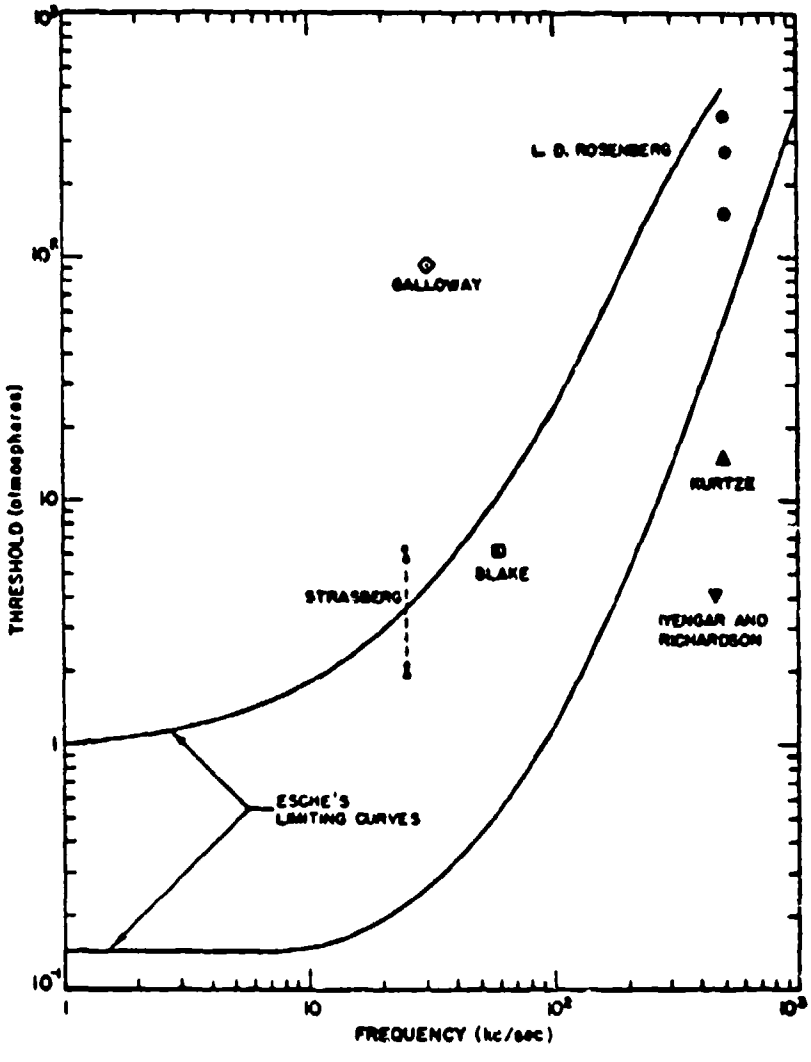

Figure 8-9.–Cavitation threshold measurements (data from Refs. 13-18, curve from Flynn [17], p. 126).

"clarifée et dégazée" (150 atm), water "distillée et degazée" (270 atm) and the latter "in certain cases", (380 atm). In his research Esche [18] estimated that the threshold for cavitation should lie between the two continuous curves shown (depending on the bubble and dissolved gas content).

Another view of the frequency dependence of the cavitation threshold, due to Sirotyuk, [19] is shown in Fig. 8-10. The size of ambient bubbles was carefully controlled in the case of curve 2, but allowed to vary up to $R_0 = 10^{-3}$ in case 1.

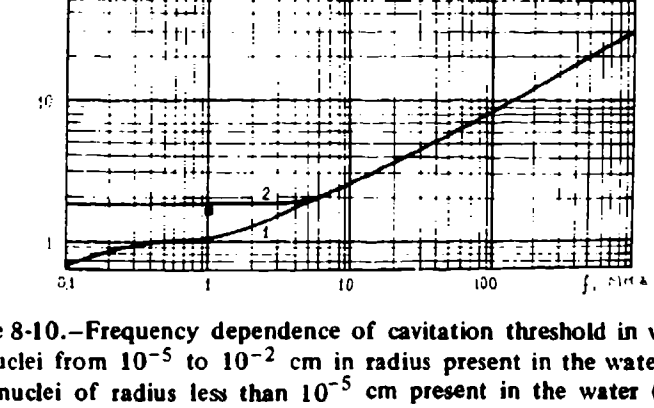

Figure 8-10.–Frequency dependence of cavitation threshold in water; (1) nuclei from 10^{-5} to 10^{-2} cm in radius present in the water; (2) only nuclei of radius less than 10^{-5} cm present in the water (from Sirotyuk [19].

In summary then, meaningful quantitative information on the cavitation cannot be had until one knows the size of the ambient bubbles. In most cases, the cavitation threshold increases as the frequency increases, although the presence of large bubbles may mask this effect.

8.5 Origin and Stability of Cavitation Nuclei.

Throughout the previous sections we have talked about the growth of bubbles already present in the liquid without explaining why bubbles might be there in the first place. In fact the history of cavitation research includes a large number of articles describing attempts to find the cavitation threshold for pure or clean water.

Such a search is largely illusory. It has been well described by M. G. Sirotyuk:

"The production of absolutely pure water is impossible. One of the strongest of existing solvents, it dissolves the walls of the container and, on coming into contact with any gas, dissolves that gas." [20]

In fact then, any sample of water will contain some dissolved materials. It may also contain minute particles of solid matter, not dissolved in the chemical sense, too small to be seen, but large enough to trap vapor or gas within their crevices. These trapped microbubbles are then available to serve as nucleation centers.

Another possible sort of cavitation nuclei may be found in nuclear radiations or cosmic radiation. The passage of energetic charged particles through a liquid can lead to the formation of microbubbles (of size 0.1 to 10 μ). If these bubbles can be stabilized in some way in the liquid, then the passage of a sound wave can initiate the bubble growth processes discussed in the previous section. Thus the presence of nuclear or cosmic radiation could serve to lower the threshold pressure for cavitation in a given liquid.

Evidences of this behavior have been reported by a number of authors. In 1958, D. Lieberman [21] irradiated a liquid filled sphere with a sound beam. He failed to achieve cavitation with a sound beam maximum pressure at 22 atm. He then irradiated the sphere with a neutron beam and found that the threshold fell to 6.5 bars in acetone and 3.5 bars in pentane.

This work was followed by experiments by Sette and Wanderlingh [22] on the influence of cosmic radiation. In their apparatus, lead screens could be placed around a tank of distilled water. Typical results are shown in Fig. 8-11. As the thickness of the screen is increased (up to about 15 mm), the threshold of acoustic pressure required for cavitation increased.

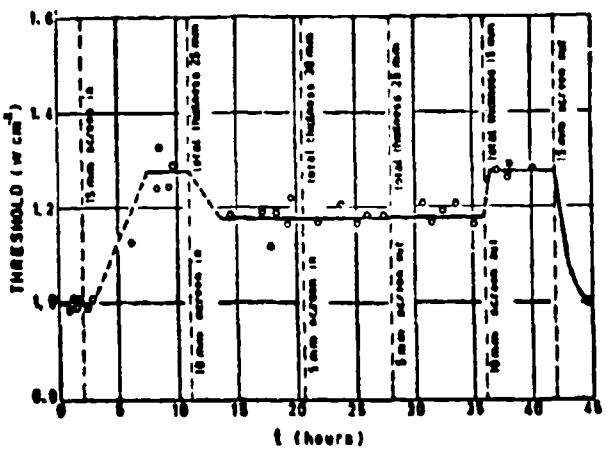

Figure 8-11.–Cavitation threshold in distilled water shielded by lead screens of various thicknesses (from Sette and Wanderlingh [22]).

When the screen was removed, the cavitation level returned to its original value.

In a second experiment, a Ra-Be neutron source was used. Figure 8-12 shows the results. The following sequence of steps was used: (1) no screen (0-8 *h*); (2) 15 mm lead screen (at 8 *h*); (3) neutron source added (at 27 *h*);

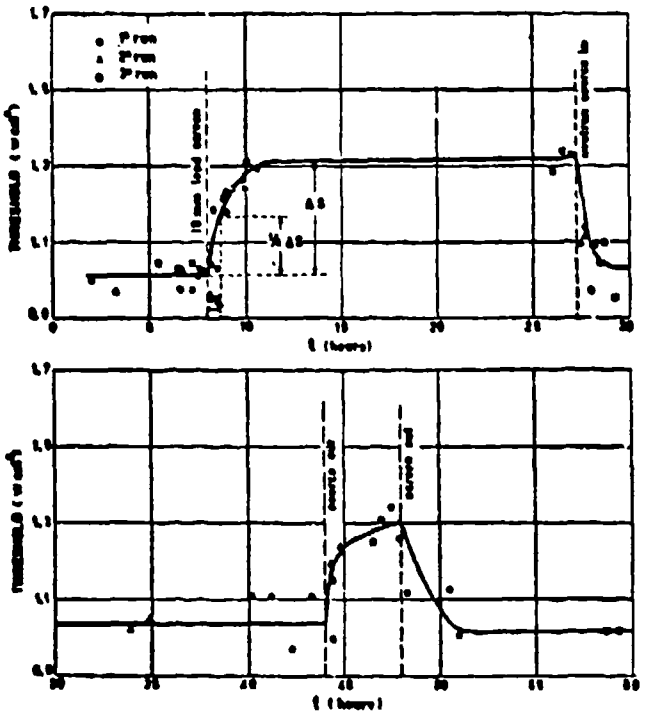

Figure 8-12.–Cavitation threshold in distilled water surrounded by a 15-mm lead screen and in the presence of a *Ra-Be* neutron source (from Sette and Wanderlingh [22]).

(4) neutron source removed (44 *h*); (5) lead screen removed (48 *h*). This shielding from cosmic radiation raised the cavitation threshold; insertion of a neutron source in the medium lowered it again. Removal reversed the two processes.

The water used in these experiments was distilled but not degassed. Subsequent experiments by Finch [23] gave similar results for degassed water.

In his theory of nucleation in bubble chambers, Seitz [24] suggested that the energy from the incident charged particle is transferred first to the electron system of an atom of the medium and then to atomic and nuclear vibrations, which can be communicated to immediate neighbors. This "thermal spike" can result in the production of a vapor bubble if the energy is sufficient to overcome surface tension forces and supply energy for evaporation. The analysis indicated that the chief agents for nucleation were knocked-on electrons of about 1 keV. Later, Lieberman and Rudnick [25] used Seitz's theory with C and O recoil nuclei (in pentane and acetone) as the nucleation agents. However, Sette and Wanderlingh conclude that the maximum energy deposited by the ionizing particle in traveling a distance equal to the diameter of a critical-size bubble is insufficient to establish that bubble. Sette and

his coworkers therefore suggest that the energizing particle makes two contributions:

(1) it heats up a small region of the liquid beyond its critical temperature so that a bubble originates;

(2) it warms the surrounding region sufficiently that the minute bubble can continue to grow.

Even these are apparently insufficient in a perfectly pure liquid. If however, the liquid is assumed to contain dissolved gases, so that these can act as cavitation embryos, the energy needed reduces to the level of the energy available from processes (1) and (2). Sette and Wanderlingh [26] draw the following conclusions:

"Ultrasonic cavitation in water under normal conditions indicates the presence of microbubbles of 1μ radius. An enormous amount of energy is required for the creation in pure water of such bubbles from a high-energy particle. This value is lowered by the presence of dissolved gases.

It is shown that, if an ionizing particle passes through water containing dissolved gas, a threshold-energy value exists for the initiation of an exoenergetic process. When the particle energy is higher than the threshold, the particle may create a bubble of large size.

It would seem that the process suggested will ensure a statistical lifetime of the microbubbles in the liquid for a time sufficient to reach a condition at which the bubble may remain indefinitely stable: e.g., by adhering to a dust particle, as proposed by Harvey." [27]

The last remark in the passage quoted above reflects a long standing problem in cavitation research. The classical theory of bubbles indicates that small bubbles are not stable; they tend to collapse if below critical size, or they grow if they are above that size and simultaneously rise toward the surface. A suggestion was made by Harvey et al. that air is trapped on the surface of hydrophobic particles suspended in water. Strasberg has given a detailed picture of how gas can be maintained in cracks, and a more complete discussion is provided by Flynn. [28]

There appears to be ample evidence that even distilled water contains large numbers of solid specks or motes, sufficiently small that they can be prevented from sinking to the bottom but large enough to provide the crevices needed to secrete the gaseous embryos. Some support to these ideas is given by Messino, Sette and Wanderlingh, [29] who compared the amount of bubble production for various acoustic fields when distilled water was used and when minute wettable and nonwettable impurities were introduced. They drew the conclusion that these impurities played an active role in altering the distribution of nuclei previously present and raise again an earlier notion of Fox and Herzfeld that the bubbles may have a kind of skin formed from organic impurities. [30] Turner [31] has also made the suggestion that

solid unwettable impurities of very small size may adhere to the surface of the gas nucleus, forming a wall that would prevent further solution. Such a process would apply primarily to larger bubbles and the results of Sette et al. [32] indicated that the use of unwettable teflon particles did in fact increase the number of large nuclei in the liquid. An excellent review of the complexities of this subject has recently been given by Apfel. [33]

8.6 Cavitation Noise.

The phenomenon of cavitation is accompanied by a variety of noises, often given colorful names in the literature. As pointed out in Section 8.4, these noises can be used as a basis of determination of the threshold, since the sounds are usually detectable at very low intensities, before cavitation bubbles can be seen.

There are two main types of cavitation noise. One is the noise due to the collapse of the bubble. The collapse of a transient bubble gives rise to a shock wave which propagates through the medium. Schneider [34] assumed that a shock wave would propagate from the bubble when the inward motion of the collapsing bubble was stopped by an incompressible sphere at the origin. This yielded an exponential decay of the shock pressure in the medium. More precise theoretical calculations by Brand [35] and by Hickling and Plesset [36] indicated that the pressure falls off as $1/r$. The results of the latter's measurements are shown in Fig. 8-13.

The pressure discontinuity in the shock results in a continuous power spectrum with the high frequency end being proportional to f^{-2}, where f is the radiated frequency of the spectral component.

The second source of noise from the bubble is due to oscillations of the stable bubble. That these oscillations will reflect both the harmonics and the subharmonics of the forcing sound frequency can be gathered by a review of Figs. 8-4, although the theoretical problem is a more complex one. An excellent experimental study of these cavitation noises was made by Esche, [18] the results of which are shown in Fig. 8-14. The half-harmonic component is clearly seen in each case, while even lower frequency subharmonics are visible in the higher frequency cases. The low-intensity continuous spectrum is also evident.

The relation of harmonic, subharmonic and continuous components are clearly demonstrated in the work of Akulichev [37] shown in Fig. 8-15. Here fresh tap water was irradiated by 22.5 kHz sound of pressure amplitudes 0.4, 0.6 and 0.8 atm. A detecting system that was practically flat from 8 to 500 kHz was used. At the lowest intensity, only the harmonics and a small continuous spectrum can be observed, but as the pressure amplitude is in-

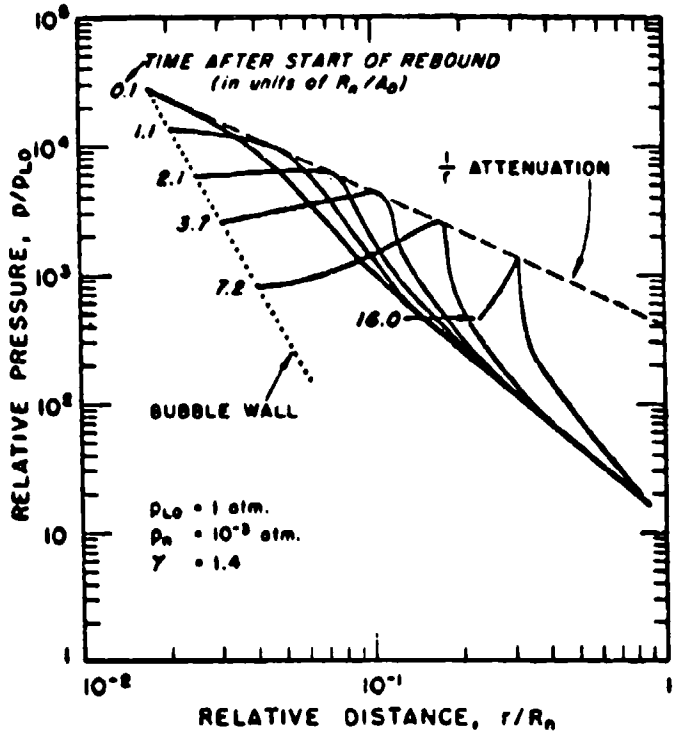

Figure 8-13.–Decay of bubble produced shock wave in water (from Hickling and Plesset [36]).

creased, the subharmonics grow until they are nearly as strong as the harmonics, while the continuous spectrum also increases appreciably.

The case of cavitation noise in dc fluid flow has also been treated. In particular, Boguslavskii, Ioffe and Naugolnykh [38] have applied Lighthill's Eq. (5.8) to the problem, obtaining the modified equation for the liquid density ρ in the case of a liquid containing bubble:

$$\frac{\partial^2 \rho}{\partial t^2} - c^2 \nabla^2 \rho = \rho_0 \frac{\partial^2 v_i v_j}{\partial x_i \partial x_j}$$

$$- \rho_0 \frac{\partial^2 z v_i v_j}{\partial x_i \partial x_j} + \rho_0 \frac{\partial^2 z}{\partial t^2} \tag{8.35}$$

where $z = (4/3)\pi n(R^3 - R_0^3)$, n being the number of bubbles per unit volume, R the bubble radius and R_0 its initial value, as before. That is, z is the volume of all bubbles per unit volume of liquid.

A detailed mathematical analysis of this equation leads to the conclusion that the cavitation noise intensity is proportional to the fourth power of the flow velocity.

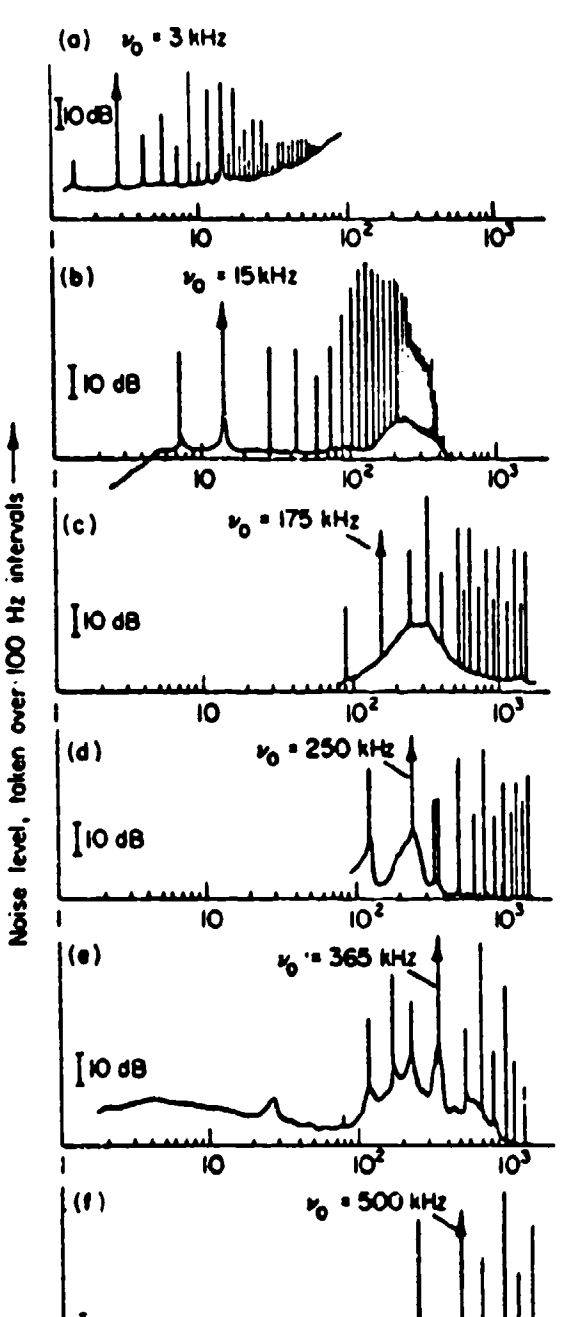

Figure 8-14.–Noise spectrum from cavitating bubbles; ν_0 = exciting frequency (from R. Esche [18]).

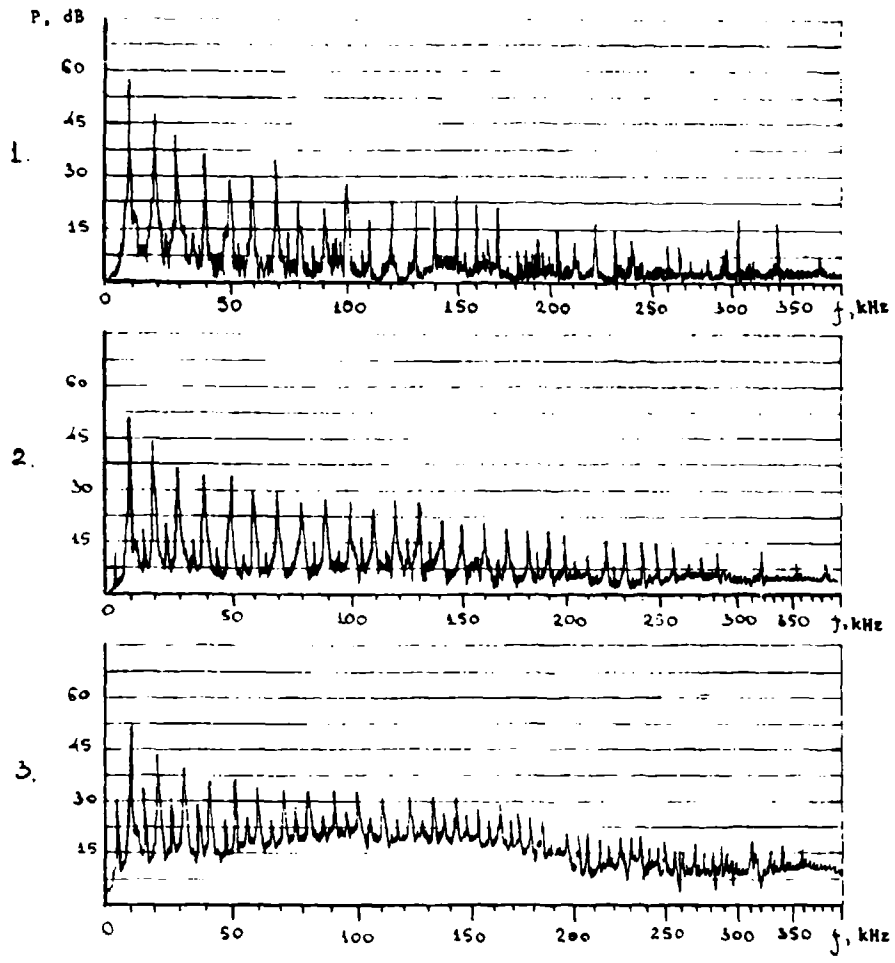

Figure 8-15.–Subharmonic spectral components of cavitation noise (from Akulichev [37]).

8.7 Sonoluminescence.

The phenomenon of cavitation in a sound beam is accompanied by the emission of visible radiation. This optical emission was first reported in 1933 and was later given the name of sonoluminescence. [39] Its qualitative features have by now been reasonably well identified, although the nature of its origin is not yet wholly clear. The intensity of the light is strongly dependent on the nature and temperature of the liquid, being greatest at low temperatures and in materials of high electric dipole moment and viscosity. The spectral content covers the entire visible range and is relatively independent of the material involved.

An early theory of Frenkel, [40] that the sonoluminescence was due to the appearance of nonspherical bubbles which then develop positive and negative charges, with ensuing electrical microdischarges has been largely aban-

doned, since it would apply only to a completely degassed liquid, whereas the sonoluminescent effect is observed mainly in gassy liquids and is indeed highly sensitive to the nature of the dissolved gas.

Tables 8.1 and 8.2 show the effect of different liquids and different gases on the relative intensity of the sonoluminescence. [41]

At the present time, the most acceptable theory of sonoluminescence is that the radiation arises in the microshocks developed in the collapse of the cavitation bubbles, i.e., from the same phenomenon that produces luminescence in the case of cavitation bubbles produced by continuous gas flow, by the study of luminescence from the collapse of a single large bubble, and from the well known phenomenon of luminescence appearing behind a shock wave.

The phenomenon of sonoluminescence is accompanied by some chemical changes which could in turn give rise to chemiluminescence, but apparently this could only account for a very small portion of the luminescence actually observed.

Table 1
Relative intensity of sonoluminescence from various liquids at three different temperatures.*

Liquid	Relative intensity of sonoluminescence 25°C	40°C	55°C
Dimethyl phthalate	16	6.6	2.4
Ethylene glycol	12	3.4	0.5
Tap water	3.6	1.0	...
Chlorobenzene	0.84	0.43	0.20
Isoamyl alcohol	0.54	0.28	0.18
O-Xylene	0.36	0.24	0.14
Secondary butyl alcohol	0.30	0.17	0.086
N. butyl alcohol	0.21	0.10	0.030
Isobutyl alcohol	0.17	0.088	0.046
N. propyl alcohol	0.21	0.076	0.038
Toluene	0.15	0.074	0.050
Benzene	0.23	0.060	0.010
Tertiary butyl alcohol	...	0.050	0.025
Isopropyl alcohol	0.054	0.028	0.012
2*N* NaCl	25		
2*N* KCl	20		
2*N* $MgCl_2$	15		
2*N* $MnCl_2$	5		
1*N* NaCl	10		
Sea water	10		

*From Jarman

Table 2
Effect of dissolved gas on the intensity of sonoluminescence from water.*

Gas	Relative intensity of sonoluminescence	Relative intensity of sonoluminescence divided by the bunsen coefficient of gas
Xenon	28.5	195
Krypton	8.5	120
Oxygen	0.15	4
Xenon	540	
Krypton	180	
Argon	54	
Nitrogen	45	
Oxygen	35	
Air	20	
Neon	18	
Helium	1	

*From Jarman

REFERENCES

Chapter 8

1. H. G. Flynn, "Physics of Acoustic Cavitation in Liquids," *Physical Acoustics* 1B, pp. 265-336, W. P. Mason, ed., Academic Press, N.Y., 1965.
2. F. G. Blake, Jr., Tech. Mem. No. 12, Acoustics Research Laboratory, Harvard University, Cambridge, Mass., 1949.
3. E. N. Harvey, D. K. Barnes, W. D. McElroy, A. H. Whiteley, D. C. Pease and K. W. Cooper, J. Cellular Comp. Physio. **24**, 1 (1944).
4. D. Y. Hsieh and M. S. Plesset, JASA **33**, 206 (1961).
5. M. Strasberg, JASA **33**, 359 (1961).
6. C. Herring, OSRD Report No. 236, 1941.
7. J. G. Kirkwood and H. A. Bethe, OSRD Report No. 588, 1942.
8. H. G. Flynn, op. cit., p. 73.
9. Rayleigh, Phil. Mag. [6], **34**, 94 (1917).
10. S. A. Zwick, J. Math & Phys. **37**, 246 (1958).
11. B. E. Noltingk and E. A. Neppiras, Proc. Phys. Soc. (London) **63B** 675 (1950); **64B**, 1032 (1951).
12. V. A. Akulichev, "Pulsations of Cavitation Voids," in *High Intensity Ultrasonic Fields*, (L. D. Rozenberg, ed.), English translation, Plenum Press, N.Y., 1971, pp. 203-259.

13. F. G. Blake, Jr., Tech Mem. No. 9, Acoustics Research Lab., Harvard University, Cambridge, Mass., 1949.
14. K. S. Iyengar and E. G. Richardson, Brit. J. Appl. Phys. **9**, 154 (1958).
15. G. Kurtze, Nach. Akad. Wiss, Gött. Math. Phys. Kl. IIa No. 1, Jan. 1, 1958. See also the discussion in Flynn, op. cit., pp. 123-125.
16. W. J. Galloway, JASA **26**, 849 (1954).
17. L. D. Rozenberg, Acustica **12**, 40 (1962).
17a. W. Lauterborn, Acustica **20**, 14, 105, 370 (1968); **22**, 48 (1969/70); **23**, 73 (1970).
17b. W. Lauterborn, Acustica **22**, 35 (1969/70).
17c. W. Lauterborn, JASA **52**, 151(A) (1972).
18. R. Esche, Acustica 2, AB208 (1952).
19. M. G. Sirotyuk, "Experimental Investigations of Ultrasonic Cavitation," in *High Intensity Fields*, (L. D. Rozenberg, ed.), English translation, Plenum Press, N.Y., 1971, p. 278.
20. M. G. Sirotyuk, op. cit., p. 267.
21. D. Lieberman, Phys. Fluids 2, 466 (1959).
22. D. Sette and F. Wanderlingh, Phys. Rev. **125**, 409 (1962).
23. R. D. Finch, JASA **36**, 2287 (1964).
24. F. Seitz, Phys. Fluids 1, 2 (1958).
25. D. Lieberman and I. Rudnick, Third ICA Stuttgart, 1959 (unpublished).
26. D. Sette and F. Wanderlingh, JASA **41**, 1074 (1967).
27. E. N. Harvey et al., J. Appl. Phys. **18**, 162 (1947).
28. H. P. Flynn, op. cit., pp. 128-131.
29. C. D. Messino, D. Sette and F. Wanderlingh, JASA **41**, 573 (1966).
30. F. E. Fox and K. F. Herzfeld, JASA **26**, 984 (1954).
31. W. R. Turner, Vitro Lab (Silver Spring, Md) Tech. Note TN-N. 4329-12960 (1960).
32. Ref. 29, p. 581.
33. R. E. Apfel, JASA **48**, 1179 (1970).
34. A. J. R. Schneider, Ph.D. thesis, California Institute of Technology, 1949.
35. R. S. Brand, Report No. 1, School of Engineering, University of Connecticut, 1962.
36. R. Hickling and M. S. Plesset, Phys. Fluids 7, 7 (1964).
37. Ref. 12, p. 254.
38. Y. Y. Boguslavskii, A. I. Ioffe and K. A. Naugol'nykh, Soviet Physics Acoustics **16**, 17 (1970).
39. M. Marinesco and J. J. Trillat, Comp. rend. **196**, 858 (1933).
40. J. Frenkel, Acta Physiochim, USSR **12**, 317 (1940).
41. P. Jarman, Proc. Phys. Soc. (London) **72**, 68 (1959); JASA **32**, 1459 (1960).
42. J. H. Kuttruff, Akust. Beihefte (Acustica) **12**, 230 (1962).

Chapter 9

NONLINEAR INTERACTION OF SOUND WAVES

As has been amply demonstrated in Chapter 3, the passage of a finite-amplitude sound wave through a fluid leads to distortion of the wave, both from the nonlinearity of the equation of motion and the nonlinearity of the equation of state of the medium.

Such a distortion is similar to that in a vacuum tube operated in the nonlinear portion of its characteristic. The question now arises as to whether there is an acoustic analog to the mixing that occurs in the case of such a nonlinear device when two electric signals of different frequency combine to form sum and difference components.

The problem has posed special difficulties, both theoretically and experimentally. In a linear system, there can be no such interaction. In line with the principle of superposition, the solution of two waves passing separately through a region will be equal to the solution of two waves passing simultaneously through the same region. No new terms will appear and the interaction is zero.

Since the effect may be small, the simplifications necessary to produce a solution may eliminate the effect on the one hand, or insert a false positive result on the other. Experimentally, the impossibility of obtaining two perfectly collimated beams, or of plane waves, raises the possibility that any interactions that are measured experimentally may be taking place on the face of the detecting instrument rather than in the "interaction region."

Because of the amount of controversy on this problem, a chronological resume of the various theoretical works will be given.*

9.1 Lighthill, Ingard, Westervelt (1950-60).

All of the theoretical work on nonlinear interaction of two sound beams (or, in different words, the scattering of sound by sound) begins with the papers of M. J. Lighthill on sound produced by turbulence. [3] In these papers, which were discussed in the INTRODUCTION and again in Chapter 5,

*The author acknowledges the usefulness of the survey of this field prepared by J. P. Jones, [1] as well as the summary given by C. A. Al-Temimi. [2]

Lighthill represented the exact equations of motion for an arbitrary fluid in the form

$$\frac{\partial \rho}{\partial t} + \frac{\partial (\rho u_i)}{\partial x_i} = 0$$

$$\frac{\partial}{\partial t}(\rho u_i) + c_0^2 \frac{\partial \rho}{\partial x_i} = -\frac{\partial T_{ij}}{\partial x_j} \qquad (9.1)^{**}$$

$$\frac{\partial^2 \rho}{\partial t^2} - c_0^2 \nabla^2 \rho = \frac{\partial^2 T_{ij}}{\partial x_i \partial x_j}$$

where the stress T_{ij} is defined by the relation

$$T_{ij} = u_i u_j + p_{ij} - \rho c_0^2 \delta_{ij}. \qquad (9.2)$$

Here $\rho u_i u_j$ is the instantaneous Reynolds stress tensor, p_{ij} the compressive stress tensor and δ_{ij} the Kronecker delta. In effect, the sound field radiated by fluid flow (including the interacting sound beams) is equivalent to one produced by a static distribution of acoustic quadrupoles with source strength density given by T_{ij} (cf. Section 5.2).

Lighthill found the solution Eq. (5.22) for the density changes in terms of the retarded potentials. In the far field his expression reduces to Eq. (5.23), which we write out again:

$$\rho - \rho_0 = \frac{1}{4\pi c_0^2} \frac{r_i r_j}{r^3} \int \frac{1}{c_0^2} \frac{\partial^2}{\partial t^2} T_{ij}\left(\mathbf{R}, t - \frac{\mathbf{r} - \mathbf{R}}{c_0}\right) dV_R. \qquad (5.23)$$

In their analysis, Ingard and Pridmore-Brown [4] began with this equation, neglected viscous loss and derived the following expression for the far field magnitude of the pressure at the sum frequency, $p_+(r)$:

$$p_+(r) = \frac{4\pi a^3}{\rho_0 c^4} (\nu_1 + \nu_2)^2 \frac{p_1(I) p_2(I)}{r} \left(\sin 2\theta + 2\frac{B}{A}\right) \frac{\sin \alpha}{\alpha} \frac{\sin \beta}{\beta}. \qquad (9.3)$$

Here ν_1, ν_2 are the primary beam frequencies, a the radius of each source, $p_1(I), p_2(I)$ the primary beam pressure amplitudes at the center of the interaction region, r the distance from the interaction region to the receiver, θ =

**The summation convention is used here; repeated subscripts are summed over.

angle between the first incident beam and the receiver (see Fig. 9-1), and the angles α, β are defined by

$$\alpha = \frac{2\pi a}{c_0}\left[\nu_1 - (\nu_1 + \nu_2)\cos\theta\right]$$

$$\beta = -\frac{2\pi a}{c}\left[(\nu_1 + \nu_2)\sin\theta - \nu_2\right]. \tag{9.4}$$

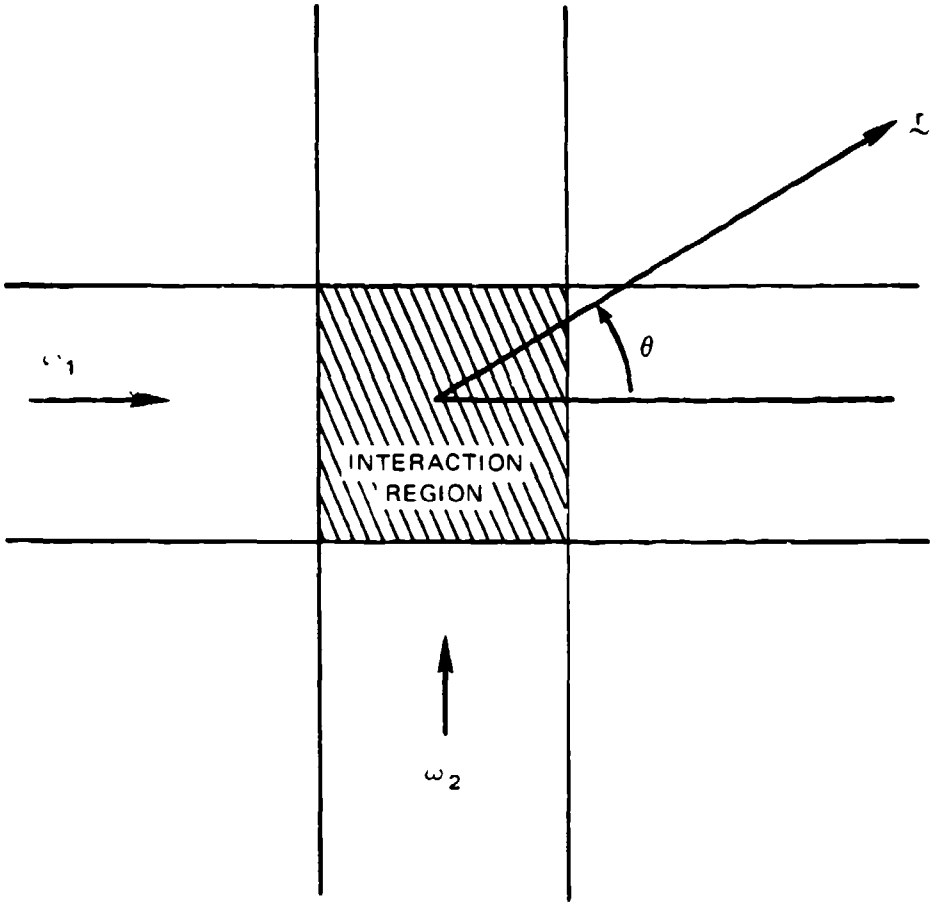

Figure 9-1.–Geometry for interaction of two crossed beams.

The corresponding expression for the difference frequency can be obtained by replacing ν_2 by $-\nu_2$ everywhere in Eqs. (9.3), (9.4).

Ingard and Pridmore-Brown performed an experiment to test their analysis using an electrostatic speaker at 110 or 130 kHz as one source and a horn-equipped electrodynamic speaker drum at 10 kHz for the other. Each was about 10 cm from the center of the interaction region. A 120-kHz $BaTiO_3$ ceramic was used to detect sum and difference frequencies.

Signals were obtained at both these frequencies, with maxima defined by the angles $\alpha = 0, \beta = 0$ (which define the Doppler angle for θ). The intensity of the scattered signals however was about 10 dB below those expected theoretically.

There has been criticism of this work: the theory assumes perfect collimation of the beams, but the low frequency of the sources, especially that at 10 MHz, and the continuous nature of the signals make possible the interaction of the two beams outside the defined interaction region, including the face of the receiving probe ("pseudo-sound"). [5]

Such comments were made by Westervelt, [6] who developed his own theory for the interaction. Westervelt used the expansion of the pressure in terms of the density [Eq. (3.19)] and deduced the following equation for the lowest order in the scattering process:

$$\Box^2 \rho_s = -\frac{1}{c_0^2} \frac{\partial^2}{\partial x_i \partial x_j} \left[\rho_0 u_i u_j + \frac{1}{2} \left(\frac{\partial^2 p}{\partial \rho^2} \right)_{\rho = \rho_0} \rho^2 \delta_{ij} \right]. \tag{9.5}$$

Here $\Box^2 \equiv \nabla^2 - (1/c_0^2)(\partial^2/\partial t^2)$ is the D'Alembertian operator, ρ_s is the density in the scattered wave. From Eq. (3.21),

$$\frac{1}{2c_0^2} \left(\frac{\partial^2 p}{\partial \rho^2} \right)_{\rho = \rho_0} = \frac{B}{\rho_0 A}.$$

Westervelt then recast (9.5) in the following form for harmonic dependence of the initial wave

$$\Box^2 \rho_s = c_0^{-2} \Box^2 E_{12} - \nabla^2 (2T_{12} + qV_{12}). \tag{9.6}$$

Here

$$T_{12} = \rho_0 \mathbf{u}_1 \cdot \mathbf{u}_2$$

$$V_{12} = c_0^3 \frac{\rho_1 \rho_2}{\rho_0}$$

$$E_{12} = T_{12} + V_{12} \tag{9.7}$$

$$W_{12} = \left(\frac{c_0^2}{\rho_0 \omega_1 \omega_2} \right) \left(\frac{\partial \rho_1}{\partial t} \right) \left(\frac{\partial \rho_2}{\partial t} \right)$$

$$q = \rho_0 c_0^{-2} \left(\frac{\partial^2 p}{\partial \rho^2} \right)_{\rho = \rho_0}$$

and the following relation exists among V_{12}, W_{12}, T_{12}:

$$\nabla^2 V_{12} = \frac{1}{2}\left(\omega_1^2 + \omega_2^2\right)\omega_1^{-1}\omega_2^{-2}\Box^2 W_{12} + c_0^{-2}\frac{\partial^2 T_{12}}{\partial t^2}. \tag{9.8}$$

The quantities ρ_1, ρ_2 refer to the excess density in each of the primary beams, while T_{12}, V_{12}, E_{12} are respectively the kinetic, potential and total interaction energies, respectively.

For the case of two mutually perpendicular beams, some reductions result: $v_1 \cdot u_2 = 0, T_{12} = 0, E_{12} = V_{12}$. Equation (9.6) then becomes

$$\Box^2 \rho_s = \Box^2 \psi \tag{9.9}$$

where

$$\psi = \frac{1}{c_0^2}\left[E_{12} - \frac{\rho_0}{2\omega_1\omega_2 c_0^2}\left(\frac{\partial^2 p}{\partial \rho^2}\right)_{\rho=\rho_0}\nabla^2 W_{12}\right]. \tag{9.10}$$

At this point, Westervelt states that $\rho_s = \psi$ is the complete solution of Eq. (9.9). If the two beams involved are perfectly collimated, then W_{12} and E_{12} will vanish everywhere outside of the interaction region, and zero scattering result.

Westervelt attributed the positive theoretical results of Ingard and Pridmore-Brown to the singularities produced by assuming perfect collimation of the waves.

In a review of Westervelt's paper, Lighthill writes

"The reviewer has had the advantage of Pridmore-Brown's collaboration in checking the theory of this paper; both of us agree that it is correct, and that the author correctly explains the wrong theoretical results of Ingard and Pridmore-Brown by referring to the singularities in the assumed primary fields. The author's explanation of their experimental results as due to radiation pressure, is, however, untenable, since the microphone was much farther outside both beams than he supposes. Accordingly, imperfect perpendicularity of the two beams near their edges seems the most probable explanation." [7]

In a subsequent paper, [8] Westervelt considered the more general case of two collimated beams intersecting at an arbitrary angle ϕ. The governing equation is

$$\Box^2 \rho_s = \Box^2 \left\{ \frac{E_{12}}{c_0^2} - \frac{1}{2\omega_1 \omega_2 (\cos\phi - 1)} \left[2\cos\phi + \frac{\rho_0}{c_0^2} \left(\frac{\partial^2 p}{\partial \rho^2} \right) \right] \right.$$

$$\left. \times \nabla^2 W_{12} \right\} \equiv \Box^2 \psi' \tag{9.11}$$

where ψ' is the quantity in the curly brackets of (9.11) and reduces to ψ in the case $\phi = 90°$.

Once again, Westervelt set $\rho_s = \psi'$ as the solution. Since, just as in (9.11), $E_{12} = W_{12} = 0$ outside the interaction region, there can be no scattering at the combination (sum and difference) frequencies.

An exception to this case is the angle $\phi = 0°$ (collinear beams), since the second term in Eq. (9.12) becomes indeterminate in this case. We shall discuss this case in Section 9.5.

In 1960, Bellin and the author attempted to measure the scattering that might result from two CW sources, operating in water at 7.4 and 6.0 MHz. [9] The sources were mutually perpendicular. A receiving crystal tuned to the sum frequency was provided so as to move in a circular path about one foot from the interaction region. Pressure amplitudes of 1.72 and 2.0 atm were maintained in the interaction region. For these amplitudes, the theory of Ingard and Pridmore-Brown predicts a scattered wave of amplitude 10^4 dynes/cm^2 at the angles defined by α and β. Although the apparatus was capable of detecting 0.3 dyne/cm^2 at the sum frequency, the only signal actually received could be explained in the overlap of the two primary waves at the position of the microphone—i.e., a failure of perfect collimation.

9.2 Dean, Lauvstad, Tjötta (1960-66).

In 1962, Dean considered the interaction of two concentric cylindrical waves and two concentric spherical waves. [10] His solutions follow the general method of Westervelt. For cylindrical waves that do not depend on the polar angles, Dean obtained the following result for the sum pressure:

$$p_+ = p_1 p_2 \frac{(1 - \Gamma) k_+ r}{2\rho_0 c_0^2} \mathcal{R}e \frac{H_1(k_1 r) H_0(k_2 r) + H_0(k_1 r) H_1(k_2 r)}{H_1(k_1 a) H_1(k_2 a)} \tag{9.12}$$

Here $\Gamma = (1/2)\rho_0 c_0^4 (\partial^2 \rho / \partial p^2)$, a is the radius of the cylinder and H_n is the nth order Hankel function of the first kind. The subscripts 1, 2, + refer to the two primary beams and the sum-frequency beam.

Referring back to Eqs. (3.20), (3.21), we can form the derivative

$$\left(\frac{\partial p}{\partial \rho}\right) = \frac{A}{\rho_0} + \frac{B(\rho - \rho_0)}{\rho_0^2}$$

from which

$$\left(\frac{\partial^2 \rho}{\partial p^2}\right)\Bigg|_{\rho=\rho_0} = -\frac{1}{\rho_0 c_0^4}\frac{B}{A}$$

so that

$$1 - \Gamma = 1 + \frac{B}{2A}. \tag{9.13}$$

Similarly, for two concentric spherical sources, each of radius a, we have, for the sum frequency pressure amplitude,

$$p_+ = -\frac{p_1 p_2 \left(1 + \frac{B}{2A}\right) k_+ k_1 k_2 a^4}{2\rho_0 c_0 r} \times \mathcal{R}e \frac{i \exp(ik_+ r)}{(1 - ik_1 a)(1 - ik_2 a)} \times \left[\ln \frac{r}{a} - \exp(-2ik_+ r) \int_a^r r^{-1} \exp(2ik_+ r) dr\right]. \tag{9.14}$$

In reviewing the work of Westervelt, and of Bellin and Beyer, Dean solved the inhomogeneous equation for the interaction region. For the analysis of fully collimated beams, Dean argued that the second order pressure wave incident on the plane boundaries of the beam must develop a reflected wave that comes back into the interaction region and a transmitted (scattered) wave that goes outside, thus making the pressure and normal velocities of the secondary field continuous across the boundaries. This analysis leads to maximum scattering at the Doppler angles ($\alpha, \beta = 0$). In the near field, his value for the same frequency in the plane wave case is

$$p_+ = \frac{(\omega_1 + \omega_2)^2}{2\rho_0 c_0^2 \omega_1 \omega_2}\left(\frac{B}{A} + 2\right) p_1(t) p_2(t). \tag{9.15}$$

Equation (9.15) gives smaller values of p_+ than Eq. (9.3) of Ingard and Pridmore-Brown. Dean further inserted a correction for the circular beams (radius a) used by Bellin and Beyer, since the theory was developed for beams of square cross section:

$$\frac{p_+ \text{ (circular c.s.)}}{p_+ \text{ (square c.s.)}} = \left(\frac{2a}{\pi r}\right)^{1/2}. \tag{9.16}$$

Thus with the conditions used by Bellin and Beyer, the expected pressure amplitude should have been about 25 dynes/cm^2 instead of the 10^4 dynes/cm^2 cited. The difference, Dean believed, lay in the fact that real beams are not perfectly collimated so that neither the stipulations of Westervelt nor of Dean conform to the real case.

Lauvstad and Tjötta [11] continued the efforts begun by Dean to avoid the artificialities introduced into the problem by the requirements of perfectly collimated beams. As has been noted above, such a requirement leads to the necessity of introducing fictitious sources. Lauvstad and Tjötta defined the problem in terms of two highly directional spherically spreading sound beams. The interaction volume was taken to be in the Fraunhofer region of ansmitters.

This approach avoids the existence of sharp collimation boundaries and the singularities that result. It also provides for some non-perpendicularity of the two beams.

The result of this analysis was similar to that of Ingard and Pridmore-Brown with the addition of a frequency dependent factor that causes the scattering to vanish as the combination frequency goes to infinity. It was noted by them that if the interaction takes place in the Fresnel near field, the rapid oscillations characteristic of this region would cause the scattering to vanish.

In other papers Lauvstad and coworkers introduced an angle ϕ between the directions of the two primary beams. [12,13] Their resultant expressions gave maximum scattering at two generalized Doppler angles defined by

$$\cos\alpha = \frac{\nu_1 \cos\phi + \nu_2}{\nu_1 + \nu_2}$$

$$\sin\alpha = \frac{\nu_1 + \nu_2 \cos\phi}{\nu_1 + \nu_2} \tag{9.17}$$

for the sum frequency. These reduce to the angles α, β of Eq. (9.4) where $\phi = \pi/2$. For the difference frequency case, one need only replace ν_2 by $-\nu_2$ in Eqs. (9.17).

In a third paper Lauvstad endeavored to take into consideration the dependence of destructive interference between second order sound sources on the frequencies and directions of the primary waves. [12] He found that the destructive interference between the primary waves in the interaction region is enough to eliminate any scattered wave except when the primary sources are collinear.

9.3 Berktay, Al-Temimi.

Thus far, the weight of theory and experiment has been moving in the direction of zero scattered radiation outside the interaction region, except for collinear beams. However, new voices were soon added to the discussion with the report of work by Berktay and his student Al-Temimi. [14]

As a point of departure, they reconsidered Westervelt's solution of Eq. (9.9), namely that the scattered density $\rho_s = \psi$, which is a function that differs from zero only in the interaction region. Westervelt states that $\rho_s = \psi$ is the complete solution of Eq. (9.9), but Berktay and Al-Temimi point out that this is the complete solution only if the interaction region is unbounded. The more general solution is

$$\rho_s = \psi + A \tag{9.18}$$

where A is a homogeneous function satisfying the equation

$$\Box^2 A = 0. \tag{9.19}$$

Thus, Berktay and Al-Temimi then obtain

$$\begin{aligned} \rho_s &= \psi + A_1 \text{ inside the interaction region} \\ \rho_s &= A_2 \text{ outside the interaction region} \end{aligned} \tag{9.20}$$

where $\Box^2 A_1 = \Box^2 A_2 = 0$. Recalling the definition of the D'Alembertian, we recognize that A_1, A_2 are additional sound waves inside and outside the interaction region, respectively. For the case of two beams intersecting at right angles, Berktay concluded that the scattered pressure for the sum frequency $p_+(r)$ at distances that are large when compared with the interaction region is

$$p_+(r) = 4\pi a^3 \frac{(\nu_1 + \nu_2)^2}{\rho_0 c_0^4} \left[\frac{p_1(l) p_2(l)}{r}\right] \frac{B}{A} \frac{\sin \alpha}{\alpha} \frac{\sin \beta e^{-\alpha_+ r}}{\beta} \tag{9.21}$$

where α_+ is the absorption coefficient at the sum frequency. This expression differs but slightly from that of Ingard and Pridmore-Brown [Eq. (9.3)].

In his derivation, Berktay has assumed the two primary beams to be fully collimated and has neglected any amplitude or phase variation across them. This latter is the case only for far field interactions, which is not the usual experimental case.

Berktay and Al-Temimi also consider the case of two non-collimated beams interacting at an arbitrary angle. In the directions of the two Doppler angles α, β (Eqs. 9.4), they found the following relations for the ratio of non-collimated to collimated pressures

$$\frac{p_+(\text{non-collimated})}{p_+(\text{collimated})} = \frac{0.45\pi a}{\alpha}\left(\frac{2\nu_2}{R_2 c_0}\right)^{1/2} \qquad (\beta = 0)$$

$$= \frac{0.45\pi a}{\beta}\left(\frac{2\nu_1}{R_1 c_0}\right)^{1/2} \qquad (\alpha = 0) \tag{9.22}$$

where $R_{1,2}$ are the distances between the appropriate source (1 or 2) and the interaction region. Such a factor would further reduce the scattered pressure to be expected in the Bellin-Beyer experiment.

In their original experiments (in air), Berktay and Al-Temimi were unable to obtain decisive results, since their maximum expected scattered pressure was just above the noise level. In later experiments in water, they did record scattering of sound outside the interaction region for non-collinear beams. [15]

The geometry of their experiment is shown in Fig. 9-2. It should be noted that the two beams are not collinear. In his review, Jones pointed out that their scattering can be accounted for in two ways. [1] First, the fact that the beams are not collimated allows for the possibility that parts of the

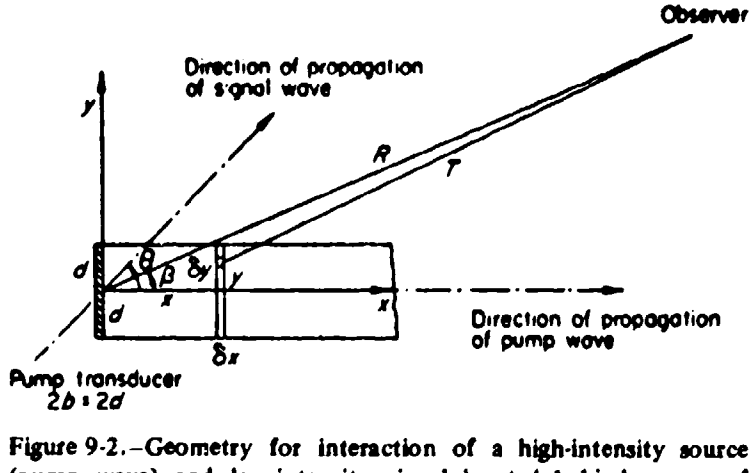

Figure 9-2.–Geometry for interaction of a high-intensity source (pump wave) and low-intensity signal located behind source of pump wave (from Berktay [14]).

two beams may be traveling in the same direction, so that partial collinearity exists (see Section 9.5). Second, some of their measurements apparently took place in the interaction region, where scattering is conceded to exist by all.

In 1970, another paper has appeared in which the authors, Zverev and Kalachev, follow an analysis similar to that of Lauvstad and Tjötta, and with similar results. [16] That is, for two collimated plane waves intersecting at right angles, Zverev and Kalachev obtained the following expression for $p_+(r)$:

$$p_+(r) = \frac{\pi V}{2\rho_0 c_0^4}\left[\frac{p_1(l)p_2(l)}{r}\right]\left[\frac{B}{A}(\nu_1 + \nu_2)^2 + 2\nu_1\nu_2\right]\frac{\sin\alpha}{\alpha}\frac{\sin\beta}{\beta} \tag{9.23}$$

where V is the volume of the interaction region.

This expression differs but little from Eq. (9.5), mainly in that the entire angular dependence lies in the factor $(\sin\alpha/\alpha)(\sin\beta/\beta)$. Indeed, the authors show that if $\nu_1 \gg \nu_2$ (which was the case of Ingard and Pridmore-Brown), the scattered field is a maximum in the direction of propagation of the main beam, i.e., when $\theta = 0$

$$p_+(r) = \frac{\pi V}{2\rho_0 c_0^4}\frac{p_1(l)p_2(l)}{r}\frac{B}{A}\nu_1^2. \tag{9.24}$$

In the same paper, Zverev and Kalachev report an experimental test. Their apparatus consisted of two separated water tanks connected by a copper tube 40 cm in length. Transducers operating at 5.0 MHz and 4.5 MHz were oriented at right angles to each other in the first tank. The copper tube serves as a high pass acoustic filter and the sum frequency was detected in the second tank in the usual fashion. No diagram of the apparatus is available, but it would seem that the system may in fact be measuring the sum frequency in the interaction region.

9.4 Jones and Beyer.

Quite recently, a student of the author attempted to make a definitive experimental study of the problem. [1,17] One major improvement over the experimental set-up of Bellin and Beyer was the use of pulses. Two circular x-cut quartz transducers of resonant frequencies 7 and 5 MHz were used, each

of 0.9525 in radius. They were fixed at right angles to one another at a distance of 21.89 cm from the center of the interaction region (see Fig. 9-3). Pulse lengths of 15 μ sec were used, which produced an interaction region equal in length to the diameter of the sources. Standard pulse-echo techniques were used to ensure simultaneous arrival of the pulses at the interaction region.

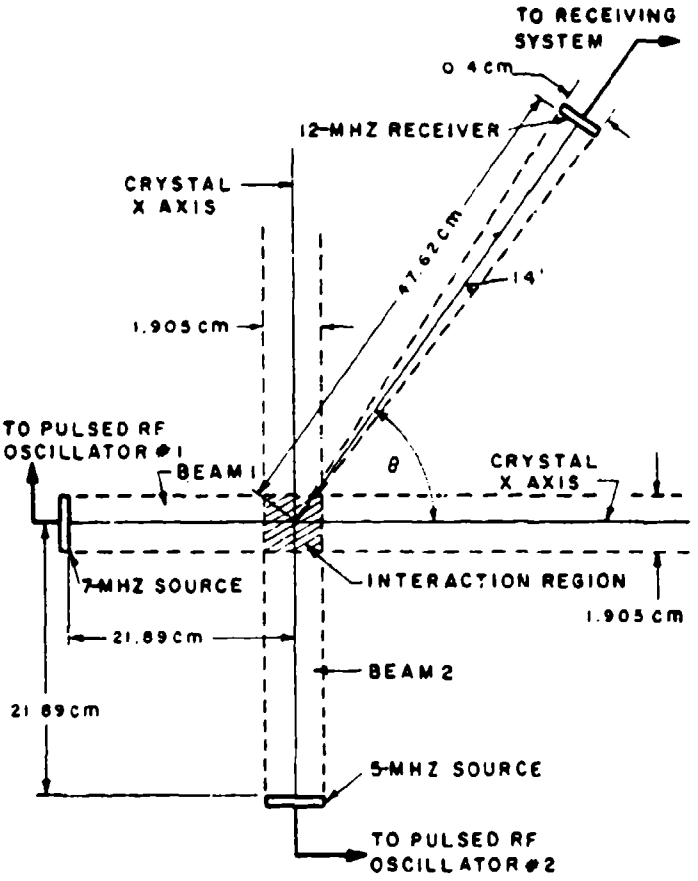

Figure 9-3.–Geometry used in scattering of sound by sound experiment [from Jones and Beyer, JASA 48, 398 (1970)].

The authors considered an additional source of experimental difficulty not noted by previous workers, namely that rapid oscillations in the scattered pressure amplitude are predicted by the factor $(\sin\alpha/\alpha)(\sin\beta/\beta)$ in Eqs. (9.5), (9.23). In previous experiments, the angle subtended by the receiver with the interaction was such that a number of oscillations would be present across the face of the receiver. These oscillations could conceivably cancel each other, thereby producing negative results. In the present arrangement, the angular displacement between a theoretical pressure maximum and the first zero pressure is about $1/2°$; that is, the change in the angle θ between $\beta = 0$ [a

pressure maximum, according to (9.3), (9.23)] and $\beta = \pi$ (a zero in pressure) is about $1/2°$. Since the receiver subtended an angle of 28° as viewed from the interaction region (see Fig. 9-3), any experimental curve would follow the fluctuations in $(\sin \alpha/\alpha)(\sin \beta/\beta)$, rather than smooth them out.

It was estimated that the apparatus was capable of detecting a signal at the combination frequency of 12 MHz as low as 0.07 dyne/cm^2 with a 10-dB signal-to-noise ratio.

In searching for scattering, particular attention was given to the Doppler angles (24°37′, 54°20′ in this case) for which pressure maxima had been predicted. A comparison of predicted values of p_+ for one specific experimental trial is given in Table 1.

Table 1
Various theoretical predictions for Jones-Beyer experiment:
$p_1(f) = 4.5$ atm, $p_2(f) = 1.8$ atm, $R_1 = R_2 = 21.89$ cm, $r = 47.62$ cm.

Research	Equation	$p_+ \max$ ($\beta = 0$, $\theta = 24°57'$) dyn/cm^2
Ingard, Pridmore, Brown	9.3	24,000
Dean		
Correction for receiver in near field	9.15	5,230
Additional correction owing to use of circular instead of square beam	9.16	586
Berktay, Al-Temimi		
Correction for noncollimated	9.21	2,940
Correction for noncollimated plus Dean	–	45.3
Correction for circular beam	–	5.1
Westervelt		0

A number of experimental trials were conducted, in which the distance between the receiver and the interaction region was varied from 7 to 74 cm and the distance between the source and the interaction region from 3 to 30 cm.

The experimental conclusion of Jones and Beyer was, therefore, that no interaction occurred between the two beams under the specified conditions.

It is of interest to note that in the solid state case (Chapter 10) such interactions (called three phonon-interactions) for longitudinal phonons are forbidden except in the case in which both momentum and energy are conserved–i.e., collinear beams. [18]

9.5 Collinear Beams.

Throughout the preceding sections of this chapter we have avoided consideration of the case in which the two beams are collinear. The theoretical

treatment here is due to Westervelt, who noted that the nonlinear terms made the beam act as a distribution of sources for the modulating frequency. [19]

In his analysis, Westervelt returned to the formulation of Lighthill, rearranging the fundamental equations of (9.1) in terms of the pressure

$$\Box^2 p \equiv \nabla^2 p - \frac{1}{c_0^2}\ddot{p} = \frac{\partial^2}{\partial t^2}\left(\rho - \frac{1}{c_0^2}p\right) - \frac{\partial^2}{\partial x_i x_j}(\rho u_i u_j). \tag{9.25}$$

The terms on the right are kept only up to the quadratic. The comparable approximation in the relationship of ρ and p is

$$\rho - \frac{1}{c_0^2}p \simeq -\frac{1}{2c_0^6}\left(\frac{\partial^2 p}{\partial \rho^2}\right)_{\rho=\rho_0} p^2 \tag{9.26}$$

$$\frac{\partial^2}{\partial x_i \partial x_j}(\rho u_i u_j) = \frac{1}{\rho_0 c_0^2}\left[-\Box^2\left(\frac{1}{2}\rho^2 + \frac{1}{2}\frac{\rho_0^2}{c_0^2}u^2\right) + \nabla^2\frac{\rho_0^2}{c_0^2}u^2\right].$$

Now p in (9.25) is the total pressure at a point in the medium. It is made up of the hydrostatic pressure p_0 which is a constant, the pressures of the two primary beams p_1, p_2, and the scattered p_s. Since we are interested here in the sound energy p_s that might be scattered at the sum and difference frequencies, we can omit p_1, p_2 as well as p_0 from the pressure in $\nabla^2 p$, recalling this omission when we calculate the contribution of terms on the right hand side. Putting all this together gives the governing equation for the scattered pressure p_s:

$$\Box^2 p_s = -\frac{1}{2c_0^6}\left(\frac{\partial^2 p}{\partial \rho^2}\right)_{\rho=\rho_0}\frac{\partial^2 p_i^2}{\partial t^2} - \rho_0 \nabla^2 u_i^2 \tag{9.27}$$

where the subscript i refers to the total primary beam. We note also that

$$\left(\frac{\partial^2 p}{\partial \rho^2}\right)_{\rho=\rho_0} = \frac{c_0^2}{\rho_0}\frac{B}{A}. \tag{3.21}$$

The quantity u_i can be reasonably approximated on the right by the linear acoustics relation $u_i = p_i/\rho_0 c_0$. Then

$$\nabla^2 u_i^2 \simeq \frac{1}{\rho_0^2 c_0^2}\nabla^2 p_i^2 = \frac{1}{\rho^2 c_0^2}\Box^2 p_i^2 + \frac{1}{\rho_0^2 c_0^4}\frac{\partial^2 p_i^2}{\partial t^2}.$$

Since we have discarded terms of $\Box^2$ in the source, we can write

$$\nabla^2 u_i^2 \simeq \frac{1}{\rho_0 c_0^3} \frac{\partial^2 p_i^2}{\partial t^2}$$

so that (9.27) becomes

$$\Box^2 p = -\rho_0 \frac{\partial q}{\partial t} \tag{9.28}$$

where

$$q = \frac{1}{\rho_0^2 c_0^4}\left(1 + \frac{B}{2A}\right)\frac{\partial}{\partial t} p_i^2. \tag{9.29}$$

Westervelt notes that q is the "simple source strength density resulting from the primary waves p_i." [20]

Further solution of Eq. (9.28) depends on the character of the interacting beam. For the case of two primary beams,

$$P_1 = P_{10} e^{-\alpha_1 x} \cos(\omega_1 t - k_1 x)$$

$$P_2 = P_{20} e^{-\alpha_2 x} \cos(\omega_2 t - k_2 x)$$

$$\omega_s = \omega_1 - \omega_2,$$

the general solution of (9.29) is (see Fig. 9-4)

$$p_s(r) = -\frac{i\omega_s \rho_0}{4\pi} \int \frac{q e^{ik_s|\mathbf{r} - \mathbf{r}'|}}{|\mathbf{r} - \mathbf{r}'|} dV' \tag{9.30}$$

$$= -\frac{2\omega_s \rho_0 S}{4\pi} \int_0^L \frac{q e^{ik_s r}}{r} dx. \tag{9.30'}$$

The integration in (9.30) is taken over the volume of the sources. Setting $dV' = S dx$, since our effective sources are distributed along the x axis, we obtain the form (9.30'). The quantity L represents the effective length of the array, extending to the point where g becomes negligible. For simplicity of calculation, Westervelt extended the integration to infinity. In the case discussed below, where $\omega_1/2\pi \simeq \omega_2/2\pi \simeq 13.5$ MHz, $\alpha_1 + \alpha_2 \simeq 0.09$/cm so that

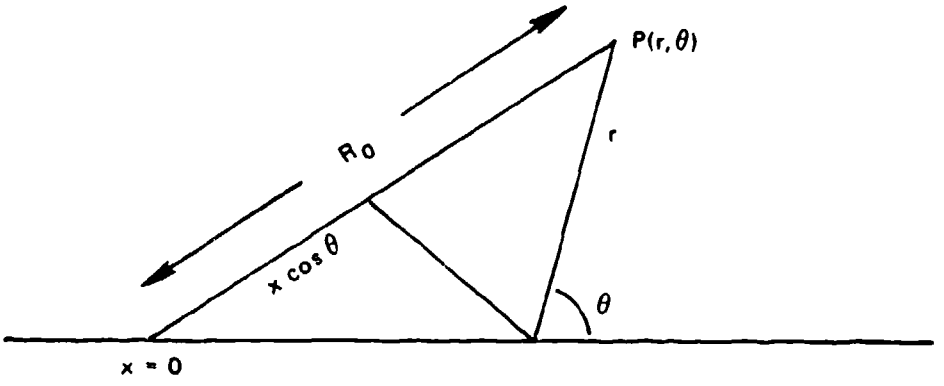

Figure 9-4.–Geometry for parametric array source.

a choice of $L = 30$ would mean a reduction of q by a factor of 15 from its initial value. We need only $L \gg 1/(\alpha_1 + \alpha_2)$.

With the added approximation $R_0 > \omega_s/\alpha^2 c$, the scattered pressure becomes

$$p_s = \omega_s^2 \rho_0 \frac{F}{8\pi R_0} \frac{e^{i(\omega_s t - k_s R_0)}}{i\left(\frac{\alpha_1 + \alpha_2}{2} + k_s \sin^2 \frac{\theta}{2}\right)} \tag{9.31}$$

where

$$F = -\frac{i\omega_s}{\rho_0^2 c_0^4}\left(1 + \frac{B}{2A}\right) p_{10} p_{20}. \tag{9.32}$$

For the case of two collinear beams of equal pressure P_0, Westervelt obtained the following expression for the radiated intensity I_s at a distance R_0 far from the source:

$$I_s = \frac{\omega_s^4 P_0^4 S_0^2 \left(1 + \frac{B}{2A}\right)^2}{2(8\pi)^2 \rho_0^3 c_0^9 R_0^2} \frac{1}{\alpha^2 + k_s^2 \sin^4 (\theta/2)}. \tag{9.33}$$

Here ω_0 is the angular difference frequency, S_0 the cross sectional area of the primary beams, α the acoustic absorption coefficient for the carriers (it is assumed that $\omega_1 \simeq \omega_2$), θ is the angle between the line of R_0 and the axis of the primary beams and $k = \omega_s/c_0$.

This arrangement was called by Westervelt the *parametric end fire array* because of its resemblance to the corresponding sonar array; and in his origi-

nal note, he remarked on the fact that if a single high intensity sound beam is radiated, it behaves as a parametric amplifier for any sound traveling in the direction of the beam and can be used therefore as a highly directional receiver (see Chapter 10).

The qualitative aspects of Westervelt's theory were very quickly confirmed experimentally. Bellin and Beyer [21] drove a 1-in. diameter quartz crystal (resonance frequency 13.5 MHz) by means of two transmitters operating at frequencies of 13.0 and 14.0 MHz. The difference frequency was received on a cylindrical barium titanate probe 1/16" outer diameter, 1/16" long. The results are shown in Figs. 9-5, 9-6 which give the directivity of the difference beam for both the theoretical and experimental cases. The coordinate for each curve is measured in relative units.

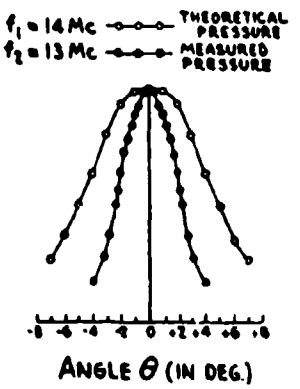

Figure 9-5.–Experimental and theoretical directivity patterns for end-fire radiation in water (from Bellin and Beyer [21]).

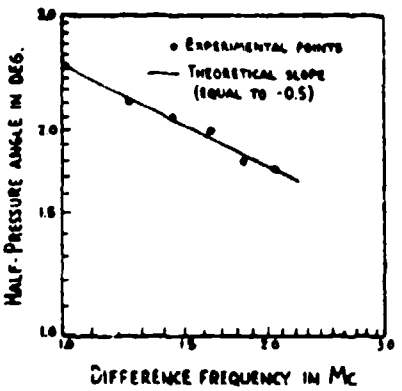

Figure 9-6.–Half pressure angle versus difference frequency for the case of transmission in water (from Bellin and Beyer [21]).

The maximum scattered pressure was measured to be 2×10^4 dyn/cm^2 while theory predicted 3.5×10^4 dyn/cm which was regarded as reasonably satisfactory agreement.

The half-width of the beam $\theta_{1/2}$ at the half pressure point (6 dB down) was measured as a function of the difference frequency, with the results shown in Fig. 9-6. The theoretical value can be obtained from Eq. (9.24):

$$\theta_{1/2} \simeq 2 \cdot 3^{1/4} \left(\frac{\alpha}{k_s}\right)^{1/2}. \tag{9.34}$$

Thus the correct frequency dependence was obtained. However, the narrower form of the directivity pattern in Fig. 9-5 was a surprise; it has been conformed by subsequent measurements of other researchers. In particular, Vestrheim and Hobaek [22] have reported measurements of the variation of $\theta_{1/2}$ with respect to the sound intensity and the distance from the primary source. Figure 9-7a gives the experimental $\theta_{1/2}$ as a function of the acoustic pressure, while Fig. 9-7b gives $\theta_{1/2}$ as a function of distance from the source. In both cases, $\theta_{1/2}$ approaches the calculated value θ_c for collimated sources at large values of the argument.

Further discussion of this problem will be given in Chapter 10.

9.6 Absorption of Sound by Sound.

Recently, Westervelt [23] has made a new approach to the problem of scattering of sound by sound. He begins with the more general form of Eq. (9.11), valid for the angle ϕ between the two beams $\neq 0$: [24]

$$\rho_s = \frac{1}{c_0^2}\left[E_{12} - \frac{1}{2\omega_1\omega_2(\cos\phi - 1)}\left(2\cos\phi + \frac{B}{A}\right)\nabla^2 W_{12}\right]. \tag{9.35}$$

This expression has a singularity at $\theta = 0$. However, by forming the operator

$$D \equiv 1 - \exp\left[\left(\left|\frac{\partial}{\partial t}\right| \left| c_0\nabla\right|^{-1} - 1\right)\right] \mathbf{r} \cdot \nabla \tag{9.36}$$

and applying it to ρ_s, Westervelt was able to exhibit a solution for ρ_s that was valid at $\phi = 0$, and that reduced to axial form of Eq. (9.31) as $\phi \to 0$.

Westervelt then proceeded to apply this solution to the attenuation of a monochromatic plane wave with wave vector $\mathbf{k}_1$ interacting with an isotropic distribution of other waves with arbitrary angular and spectral distributions.

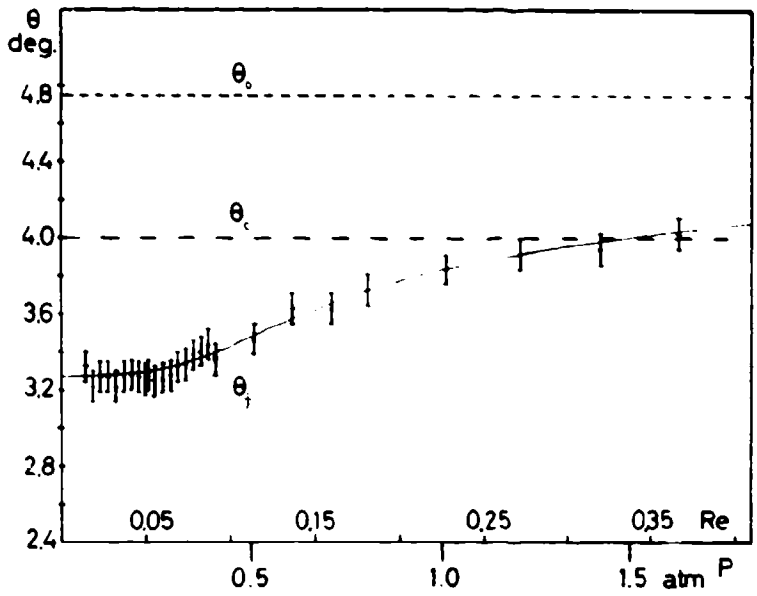

Figure 9-7a.–Variation of half-pressure angle $\theta_{1/2}$ with primary intensity (*Re* = Reynolds number of source, θ_c = corresponding angle for collimated sources, θ_d = angle for direct radiation (from Vestrheim and Hobaek [22]).

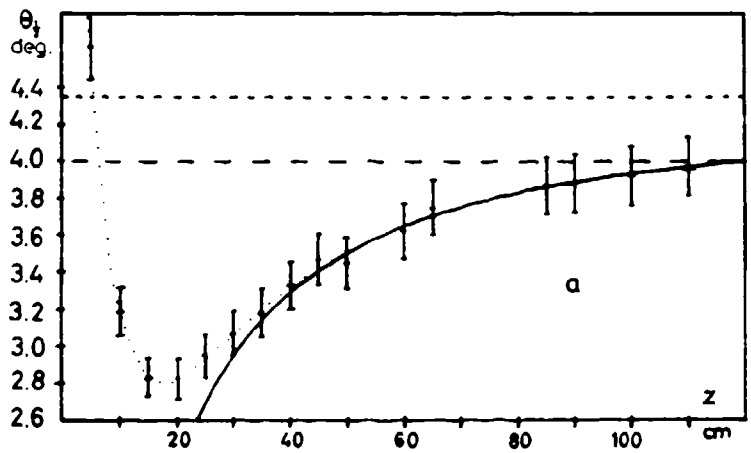

Figure 9-7b.–Variation of $\theta_{1/2}$ with distance for primary source (from Vestrheim and Hobaek [22]).

Using an energy conservation method based on the power absorbed by virtual sources, [24] he obtained the general form of the absorption coefficient resulting from this interaction

$$\alpha = \frac{1}{2\rho_0 c_0^2}\left(1 + \frac{B}{2A}\right)^2 \pi \left| \int_0^{k_1} ku(k)dk \right.$$

$$\left. + 2k_1 \int_{k_1}^{\infty} u(k)dk + k_1^2 \int_0^{k_1} \frac{1}{k} u(k)dk. \right| \tag{9.37}$$

If the range of frequencies in $u(k)$ lies well above that of k_1, this equation reduces to

$$\alpha = \frac{1}{2\rho_0 c_0^2}\left(1 + \frac{B}{2A}\right)^2 \pi k_1 E \tag{9.38}$$

where E is the energy density of this background radiation.

Since Eq. (9.37), (9.38) represent an absorption of sound from the primary beam due to interaction with the secondary (background) radiation, Westervelt has called this the absorption of sound by sound.

A similar phenomenon has already been noted in the absorption of sound in liquid He^4 below 0.6°K. [25] The maximum absorption, due to interaction of the sound beam with the background of phonons, is given by Eq. (9.38) if E is the energy density of the background phonons [26]

$$E = \frac{\pi(k_B T)}{30h^3 c^3} \tag{9.39}$$

(k_B = Boltzmann constant), and if $B/2A$ is replaced by the Grüneisen constant (see Section 11.3). The experimental results are larger than the theory by a factor of about 2, a difference explained by Maris and Massey in terms of anomalous dispersion.

This phenomenon suggests that one might be able to increase the absorption of an unwanted low frequency sound by use of an intense background field at other frequencies.

9.7 Scattering of Sound by Sound in the Presence of Obstacles.

In his early paper on the scattering of sound by sound, Westervelt [6] pointed out that the presence of a solid body in the interaction region would give rise to scattered waves at the combination frequencies. He attributed such an effect to the action of the time-dependent radiation forces exerted on the solid by the primary beams. The reaction of these forces on the me-

dium would generate the sound. He also noted that the primary waves would undergo simple scattering and that such scattered waves might interact with themselves and with the original beams.

These effects were observed by Bellin and Beyer [9] when a #38 wire was introduced in the interaction region. They also noted that interaction could be produced by blowing bubbles through the interaction region, but no quantitative measurements were made at that time. More recently, Jones and Beyer [1,17] have reported a systematic study of both phenomena, a summary of which is given here.

A. *Rigid Cylinder.* The geometry of the arrangement is the same as that described in Section 9.4, except that a metal cylinder is centered on the interaction region (Fig. 9-8). Their analysis begins with the expression for a diverging cylindrical wave from linear acoustics (recall Section 1.9):

$$p_i(r) = p_i(a_c)\left[\frac{H_0(k_i r)}{H_0(k_i a_c)}\right]; \; i = 1,2 \tag{9.40}$$

$p_i(r)$ is the pressure of the ith wave at a distance r from a cylinder of radius a_c, $p_i(a_c)$ is the pressure of that wave on the surface of the cylinder, H_n is the nth order Hankel function of the first kind.

When the pressure $p_i(a_c)$ is gradually increased, nonlinear effects appear and Eq. (9.40) will no longer be strictly correct. However, we shall continue to use it for the large amplitude case (at the fundamental frequency), correcting for finite-amplitude losses by inserting an appropriate factor.

This particular problem was solved by Dean, [10] who obtained Eq. (9.12) for the sum-frequency pressure at a distance r:

$$p_+(r) = \frac{p_1(a_c)p_2(a_c)}{2\rho_0 c_0^2}\left(1 + \frac{B}{2A}\right) \times k_+ r \, \mathrm{Re}\, \frac{H_1(k_1 r)H_0(k_2 r) + H_0(k_1 r)H_1(k_2 r)}{H_1(k_1 a_c)H_1(k_2 a_c)} . \tag{9.12}$$

Lauvstad [12] has noted that this equation applies only when $r \gg a_c$, but such a condition was satisfied in these experiments.

In what follows, it will be desirable for us to express Eq. (9.12) in terms of the primary pressure at the field point r, rather than at the surface of the cylinder. We therefore replace $p_1(a_c), p_2(a_c)$ by $p_1(r), p_2(r)$ through Eq.

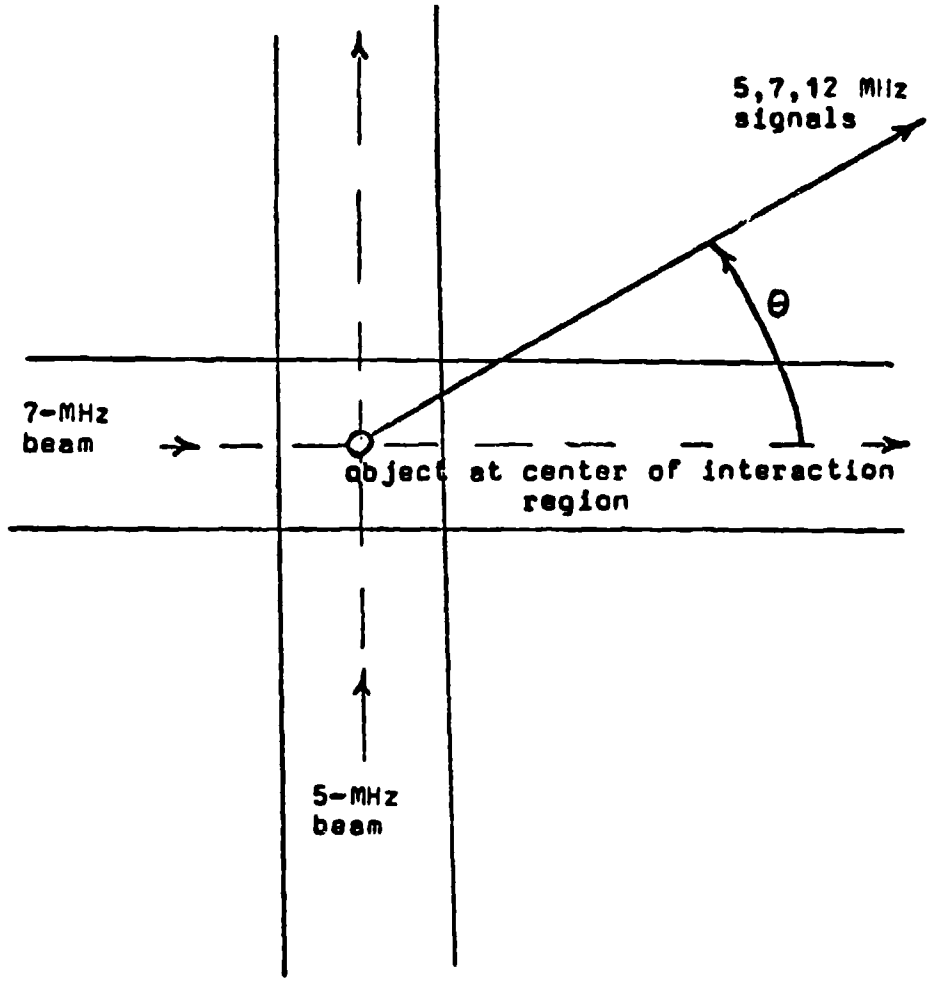

Figure 9-8.–Arrangement for scattering of sound by sound in presence of obstacle.

(9.40). The result is a most unwieldy expression. However, under the approximation $r \gg a_c$, the Hankel functions can be approximated by

$$H_1(k_1 a_c) = -\frac{2}{\pi k_1 a_c}$$

$$H_0(k_i r) = \left(\frac{2}{\pi k_i r}\right)^{1/2} e^{i\left(k_i r - \frac{\pi}{4}\right)} \tag{9.41}$$

$$H_1(k_i r) = \left(\frac{2}{\pi k_i r}\right)^{1/2} e^{i\left(k_i r - \frac{3\pi}{4}\right)}$$

and the revised and approximated (9.12) is given by

$$p_+(r) = \mathrm{Re}\,[p_1(r)] \cdot \mathrm{Re}\,[p_2(r)] \cdot \left[\left(1 + \frac{B}{2A}\right) \frac{k_+}{\rho_0 c_0^2}\right] r. \tag{9.42}$$

What we have done is to make possible a discussion of the scattering amplitude at the field point r in terms of the primary signals that would exist at the same field point in the absence of interaction.

In the experimental arrangement, the cylinder lies at the center of the common region formed by two perpendicularly intersecting plane-wave beams. It is now assumed that the scattered field produced by the plane waves is equivalent to a cylindrical source modulated by the plane wave diffraction pattern. The assumption is illustrated in Fig. 9-9.

Figure 9-9a indicates the classical diffraction pattern plane wave scattered by a rigid cylinder (no attempt has been made to give detail). It is now assumed that the cylinder is acting as a source of cylindrical waves, in accord with Eq. (9.40), but that the amplitude of the waves at a_c is modulated in accord with the diffraction pattern just described. This wave form is indicated for source #2 by the solid line. A similar pattern is also shown for source #1 (dashed curve).

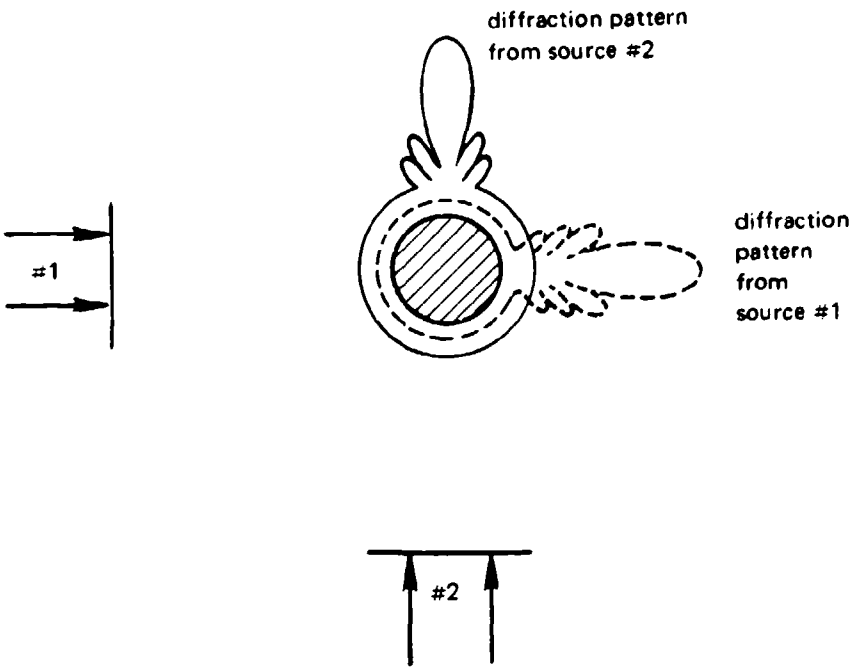

Figure 9-9.–Diffraction pattern from rigid cylinder.
– – – –: source #1; ——: source #2.

The scattering of a plane wave by a rigid cylinder is given in the infinitesimal amplitude case by Morse and Ingard [27]

$$p_s(r) = p(I)\left[\frac{a_c}{r}\sin\frac{\theta}{2} + \frac{1}{\pi kr}\cot^2\left(\frac{\theta}{2}\right)\sin^2(ka_c\sin\theta)\right]^{1/2} \qquad (9.43)$$

where $p(I)$ is the pressure amplitude of the incident plane wave at the face of the cylinder—the interaction region. For this formula to be valid, it is required that $kr \gg 1$ and $a_c \gg \lambda_1$, which are both the case here.

For high amplitudes, of course, this formula is not strictly accurate. However an exponential decay factor can be added in the form

$$\exp\left[-r/(r + \ell_i)\right] \qquad (9.44)$$

where ℓ_i corresponds to the discontinuity length for a plane wave for the appropriate source (in this experiment, $i = 1$ refers to the 7-MHz source, $i = 2$ to the 5-MHz.

We may now identify $\mathcal{R}e[p_i(r)]$ (Eq. (9.37) with $p_{s_i}(s)$ (9.43). This is the step in which we transfer from the classically scattered pressure p_{s_i} to the pressure radiated by a cylindrical source $\mathcal{R}e[p_i(r)]$.

We therefore have two concentric cylindrical waves whose pressure amplitudes depend on the polar angle θ in exactly the same way as two perpendicularly intersecting plane waves scattered by a rigid cylinder. We are in effect rewriting Eq. (9.42) as

$$p_+(r) = p_{s1}(r)p_{s2}(r)\left(1 + \frac{B}{2A}\right)\frac{k_+ r}{\rho_0 c_0^2}. \qquad (9.45)$$

Figures 9-10, 9-11 show results of the scattering by a 1/4" steel cylindrical rod ($a_c = 0.3175$ cm) as a function of angle; $\theta = 0$ corresponds to direct alignment of the receiver with the 7-MHz source, $\theta = 90°$ to similar alignment of the receiver with the 5-MHz source. The distance from both sources to the interaction region was fixed at 21.89 cm.

Figure 9-10 indicates the diffraction scattering from each sound beam alone.

The apparatus was so constructed that the two transmitters could be rotated about the interaction region. This rotation was carried out until a maximum or minimum was recorded.

The theoretical curves have been plotted from Eq. (9.43) with the attenuation factor (9.44) added. The argument on the various maxima is quite satisfactory. The lack of absolute agreement on the level of the minima prob-

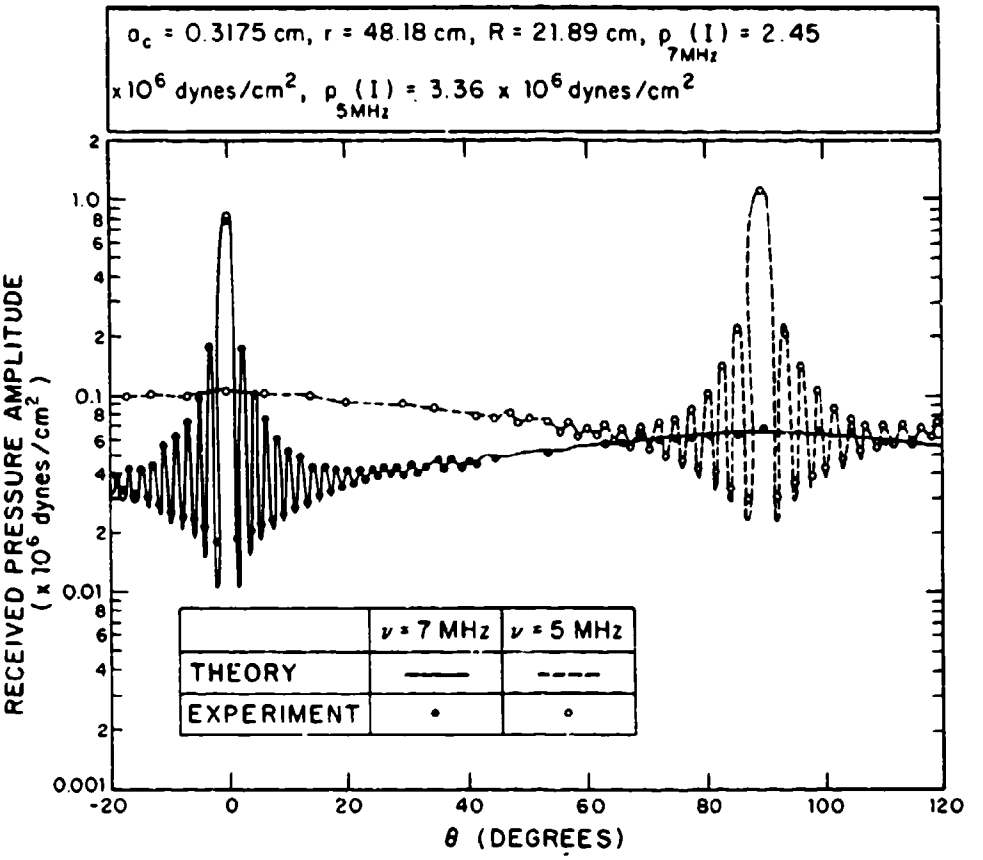

Figure 9-10.–Scattering of sound by a rigid cylinder (from Jones [1], p. 111).

ably results from the fact that the finite sized receiver is averaging over an angle that extends well beyond the width of the crevasse.

The same frequency was examined by means of the same apparatus, with both transmitters in operation. Once again theory and experiment are in good agreement.

Similar measurements were also reported for a 1/16″ cylinder.

In all of these measurements, the interaction distance R was greater than the discontinuity distance ℓ.

In order to study the buildup of the interaction signal, an additional experiment was performed in which the amplitudes of the primary beams were greatly reduced, so that the distance to the receiver r would be smaller than the discontinuity distance. Measurements were then made with the 1/4″ rod at $\theta = i$ over a range of values of r. The results are shown in Fig. 9-12. The discontinuity distances for each primary beam were over 100 cm.

The curve divides into three regions. When r is less than about 20 cm, the amplitude of the received sum frequency increases with r–which is characteristic of the parametric interaction in its building-up phase. In the region

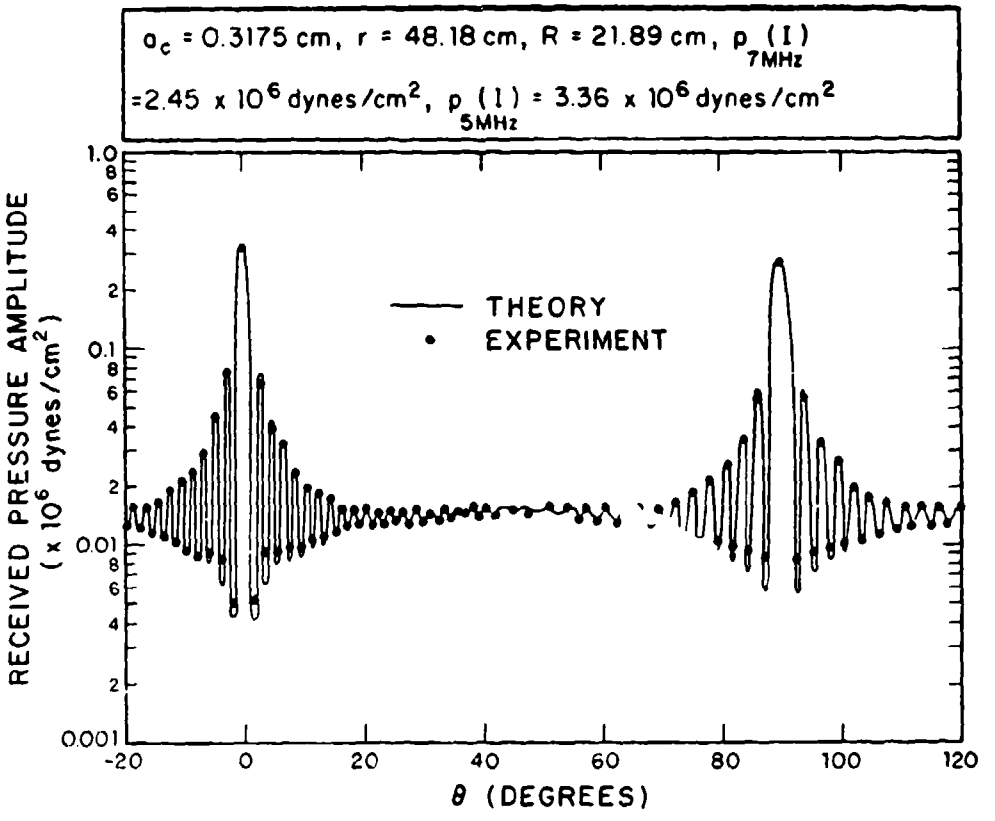

Figure 9-11.–Interaction (at the sum frequency) of sound with sound from scattering by a rigid cylinder (from Jones [1], p. 112).

of r between 20 and 36 cm, the value of p_+ is roughly a constant. This is the region in which the increase in $p_+(r)$ by the factor r in Eq. (9.45) is almost exactly counterbalanced by the cylindrical spreading ($1/r^{1/2}$) in each of the classically scattered beams (the damping of the signal is slight). Finally, in the region where r is greater than 36 cm, the attenuation due to the varying absorption factors becomes dominant and the value of p_+ decreases. When the higher intensities were used for p_1, p_2, only the latter part of the curve could be observed.

B. *Rigid Sphere.* Similar measurements were reported in the same research for rigid spheres. The analysis is completely analogous to the case of a cylinder. We first assume two linear concentric spherical waves, each given by

$$p_i(r) = p_i(a_s) \frac{k_i a_s^2}{r} \exp \frac{ik_i r}{1 - ik_i a_s} \tag{9.46}$$

where the subscript i denotes the particular wave, a_s is the radius of the sphere. As before, we shall add the factor $\exp [-r/(r + \ell_i)]$ to account for finite amplitude attenuation beyond the distance $r = \ell$.

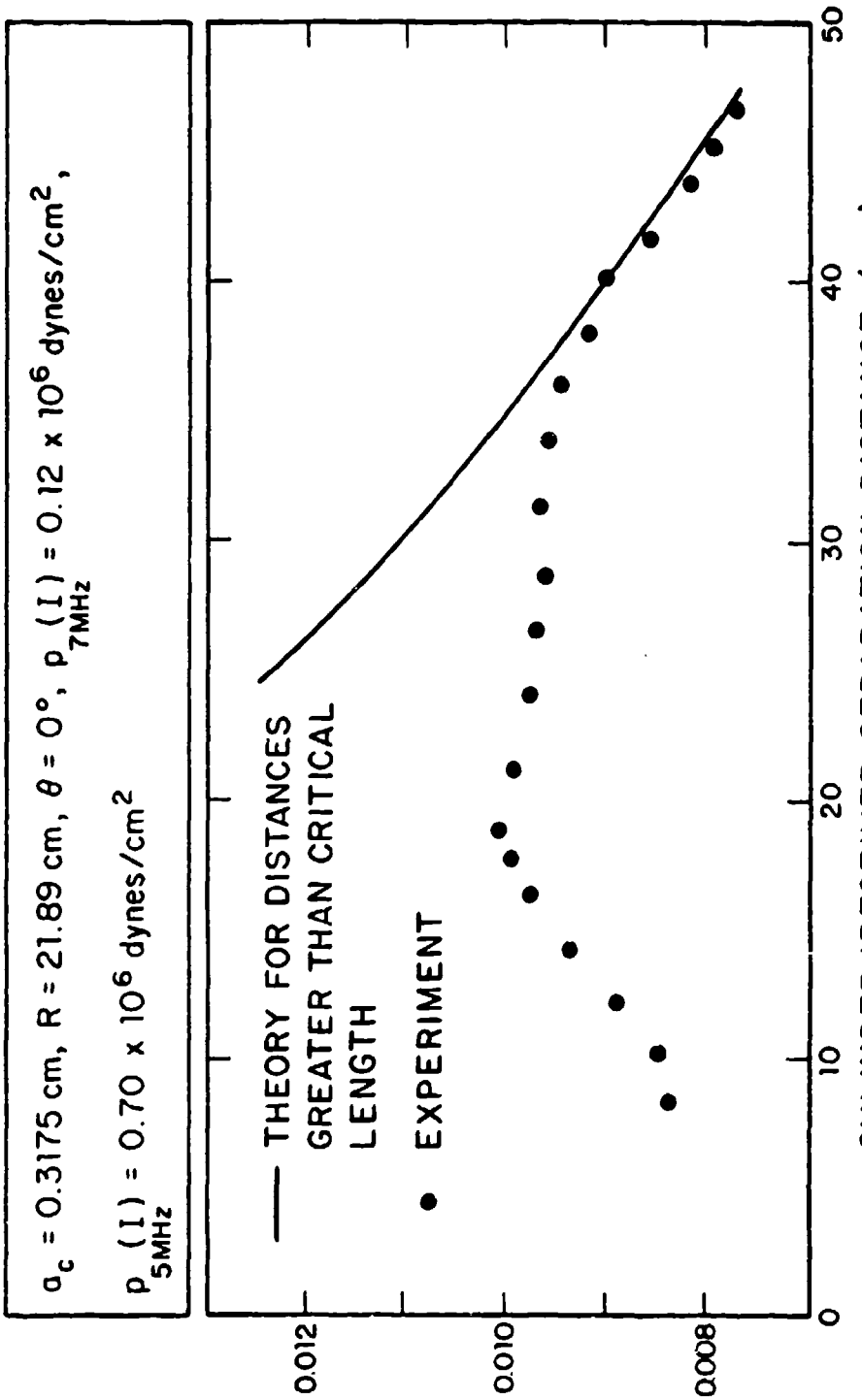

Figure 9-12.–Growth and decay of sum frequency in scattering of two beams from a circular cylinder (from Jones [1], p. 126).

From the work of Dean, [10] we have, for the sum interaction frequency $p_+(r)$,

$$p_+(r) = \frac{p_1(a_s)p_2(a_s)\left(1 + \frac{B}{2A}\right)k_+k_1k_2a_s^4}{2\rho_0c_0^2r} \times \left\{\mathcal{R}e\,\frac{i\exp(ik_+r)}{(1 - ik_1a_s)(1 - ik_2a_s)} \times \left[\ln\frac{r}{a_s} - e^{-i2k_+r}\int_{a_s}^{r} r^{-1}\exp 2ik_+r\,dr\right]\right\} \tag{9.47}$$

for $r \gg a_s$, this reduces to

$$p_+(r) = F\,\ln\left(\frac{k + r}{r}\right)\cdot\mathcal{R}e\left[ie^{i\left(k_+r - \frac{\pi}{2}\right)}\right] \tag{9.48}$$

where F is the factor in front of the expression $\{\ldots\}$ in (9.47).

We now rewrite the $p_i(a_s)$ in terms of $\mathcal{R}e[p_i(r)]$ and substitute the result in (9.48). This gives

$$p_+(r) = \mathcal{R}e[p_1(r)]\cdot\mathcal{R}e[p_2(r)]\left[\frac{\left(1 + \frac{B}{2A}\right)k_+}{\rho_0c_0^2}\right] r\ln(k_+r). \tag{9.49}$$

We again refer to Morse and Ingard [28] for the classical scattering of a plane wave by a rigid sphere,

$$p_{s_i}(r) = p_i(I)\cdot\frac{a_s}{2r}\cdot\left[1 + \cot^2\left(\frac{\theta_i}{2}\right)J_1(k_1a_s\sin\theta_i)\right]^{1/2} e^{-\frac{r}{r+\ell_i}} \tag{9.50}$$

where $i = 1, 2$, $p_i(I)$ is the pressure amplitude of the ith plane wave beam at the center of the interaction region, $p_{s_i}(r)$ is the scattered wave at the distance r from the sphere, θ_i the polar angle of the ith wave, ℓ_i the plane wave critical length for the same wave, J_1 is the Bessel function of order 1. As before, the exponential fraction has been added to account for the decay of the fundamental component of the pressure after an initial sawtooth has been established.

We now make the identification

$$\mathcal{R}e[p_i(r)] \equiv p_{s_i}(r)$$

which is entirely analogous to the step of Eq. (9.44). Then

$$p_+(r) = p_{s1}(r)p_{s2}(r)\left[\frac{\left(1 + \frac{B}{2A}\right)k_+}{\rho_0 c_0^2}\right] r \ln k_+ r. \tag{9.51}$$

The results for the interaction resulting from a 1/4" rigid sphere are shown in Figs. 9-13, 9-14. Figure 9-13 gives the measurement of the 5 and 7-MHz scattered signal (only one transmitter operating at a time). The continuous curves are plots of Eq. (9.50). Figure 9-14 gives the received sum frequency. The continuous curve is a plot of Eq. (9.51).

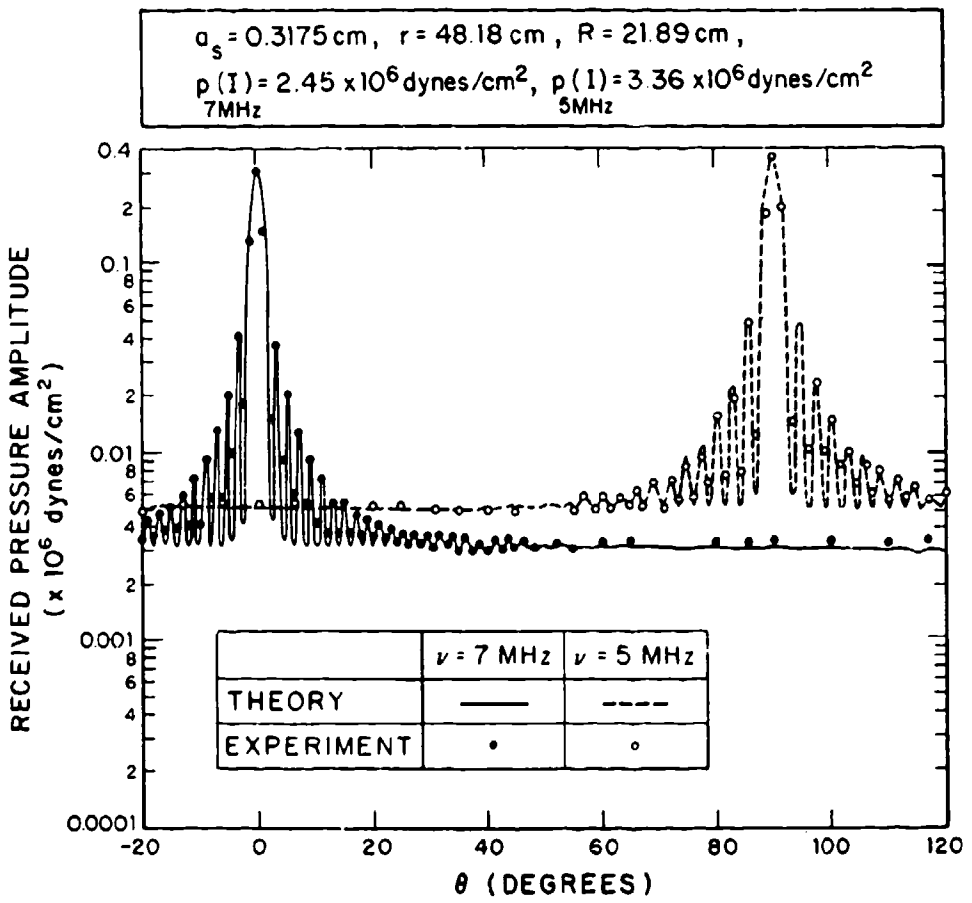

Figure 9-13.–Scattering of sound by rigid sphere (from Jones [1], p. 130).

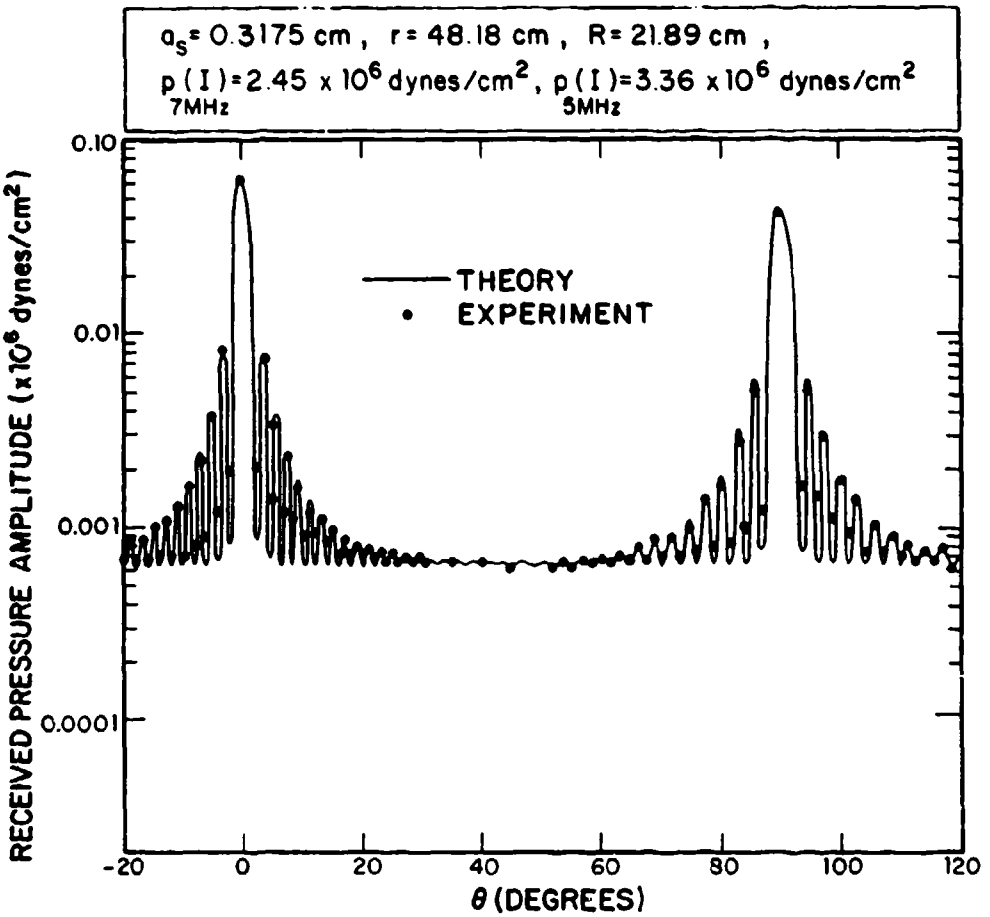

Figure 9-14.–Interaction (at the sum frequency) of sound with sound from scattering by a rigid sphere (from Jones [1], p. 131).

C. *Non-rigid Sphere (air bubble).* We proceed as in the previous paragraph. The classical formula for the scattering of a plane wave by a non-rigid sphere of radius a_B is given in the Born approximation by

$$p_{s_i}(r) + p_i(I)\,\frac{k_i^2 a_B^3}{3r}\left[\frac{\kappa_B - \kappa}{\kappa} + \frac{3\rho_B - 3\rho}{2\rho_B - \rho}\cos\theta_i\right] \tag{9.52}$$

where κ, ρ are the compressibility and density of the medium, κ_B, ρ_B the corresponding values for the sphere (bubble).

Equation (9.52) holds for $\lambda_i > 2\pi a_B$. For a frequency of 7-MHz, this restricts us to bubbles of radius less than 0.02 cm.

For an air bubble in water, Eq. (9.52) reduces to

$$p_{s_i}(r) = p_i(I) k_i^2 a_B^3 r^{-1}\,[10^4 - \cos\theta_i]\, e^{-\frac{r_i}{\ell_i + r_i}} \tag{9.53}$$

cross-sectional area S and possessing an envelope $f[t-(x/c)]$, where f is normalized so as to have a maximum amplitude of unity:

since $\kappa_B \gg \kappa$, $\rho \gg \rho_B$. Here again we have added the exponential sawtooth decay factor. It is obvious for (9.53) that the scattering is nondirectional.

We may now use Eq. (9.51) for the pressure of the sum frequency wave, but with the p_{s_i} given by Eq. (9.53) in place of (9.50).

Experiments were conducted on air bubbles produced by controlling the flow of air under high pressure through a small glass nozzle. The system permitted a steady vertical flow of bubbles whose size could be varied from 3 to 700 microns. Controls were provided so that only a single bubble would be in the interaction region at any one time.

Considerable indeterminancy existed in these experiments. During the passage of the bubble through the interaction region, it scattered numerous pulses of the primary waves, but each from a different vertical position. This led to a blurring of the results. The authors attempted to compensate by averaging over some ten independent readings at each position and frequency, but it was not possible to reproduce the detailed structure.

Figure 9-15 shows the results for bubbles of radius $r = 0.0035$ cm ($35\,\mu$). The solid curves correspond to Eq. (9.53) (the two upper lines) and Eq. (9.51) (the lower line).

Virtually identical results were obtained for bubbles with a mean radius of $95\,\mu$. However, when larger bubbles, of mean radius $283\,\mu$, were used, the scattered signal was far below that given by Eqs. (9.51) and (9.52) (see Fig. 9-16).

In this last case, of course the bubble radius has become larger than the wavelength of one of the primary beams (7-MHz) so that Eq. (9.53) is no longer a valid approximation.

The general conclusion of this section then is that sum frequencies are indeed obtainable when a rod or sphere is located in the interaction region, and that the entire scattering behavior can be accounted for by the Westervelt theory.

9.8 Interaction of Pulses of Finite Amplitude.

Thus far all of the discussion of interaction has been of two separate beams of two distinctive frequency components in a single collinear beam. In a typical ultrasonic pulse, such as that shown in Fig. 9-17, the beginning and ending portions of the pulse have broad frequency spectra, so that large amplitude pulses must possess considerable self-interaction.

Such pulses might be viewed as transient versions of the parametric array discussed in Chapter 9.4. The theory of such an array has been presented by Berktay, [29] who derived an expression for the transient signal pressure $p(x,t)$ generated along the propagation axis of a pulse of initial amplitude P,

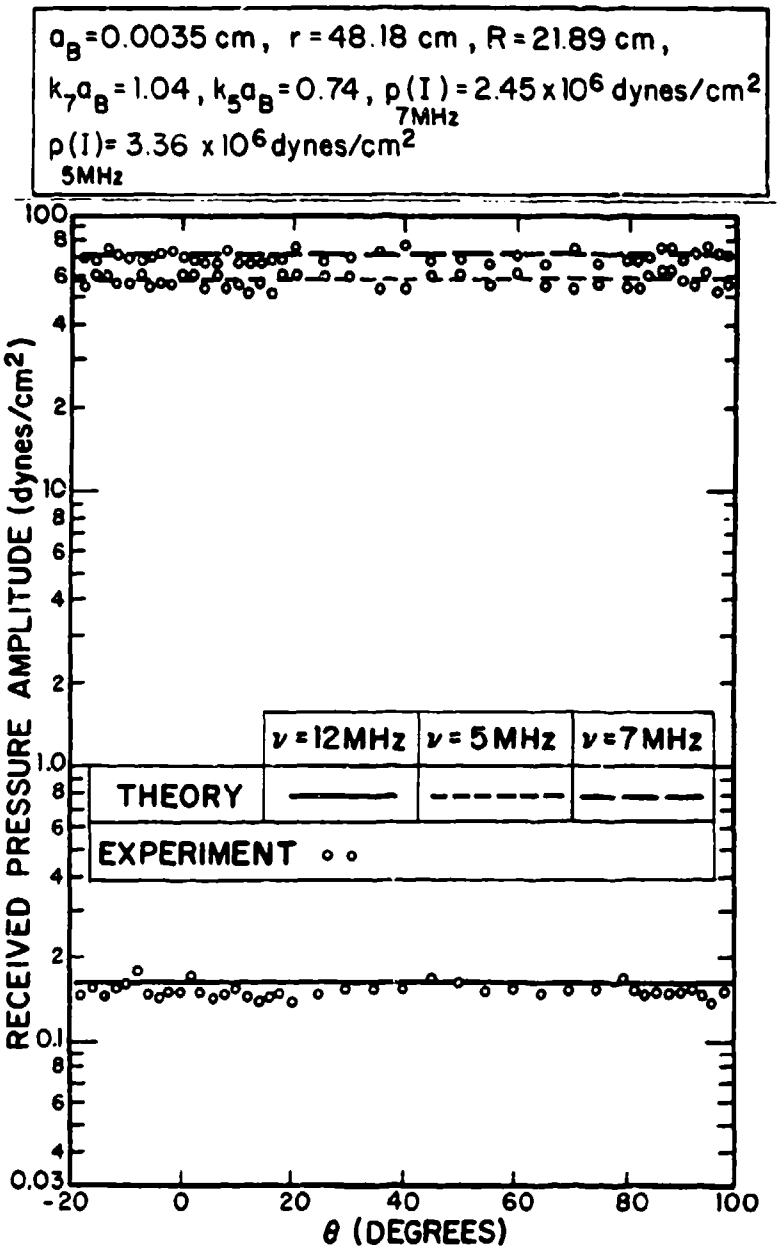

Figure 9-15.–Scattering of sound beams from air bubble of radius 35 microns and the interaction at the sum frequency (from Jones [1], p. 143).

$$p(x,t) = \left(1 + \frac{B}{2A}\right) \frac{P^2 S}{16\pi\rho c^4} \frac{1}{\alpha x} \frac{\partial^2}{\partial t^2} \left[f\left(t - \frac{x}{c}\right)\right]^2 \tag{9.54}$$

Equation (9.54) therefore describes the on-axis generation of sound by a "parametric array" consisting of a propagating high amplitude pulse.

The theory has been accurately confirmed by experiments in carbon tetrachloride. [30] The pulse shown in Fig. 9-17 had a carrier frequency 10

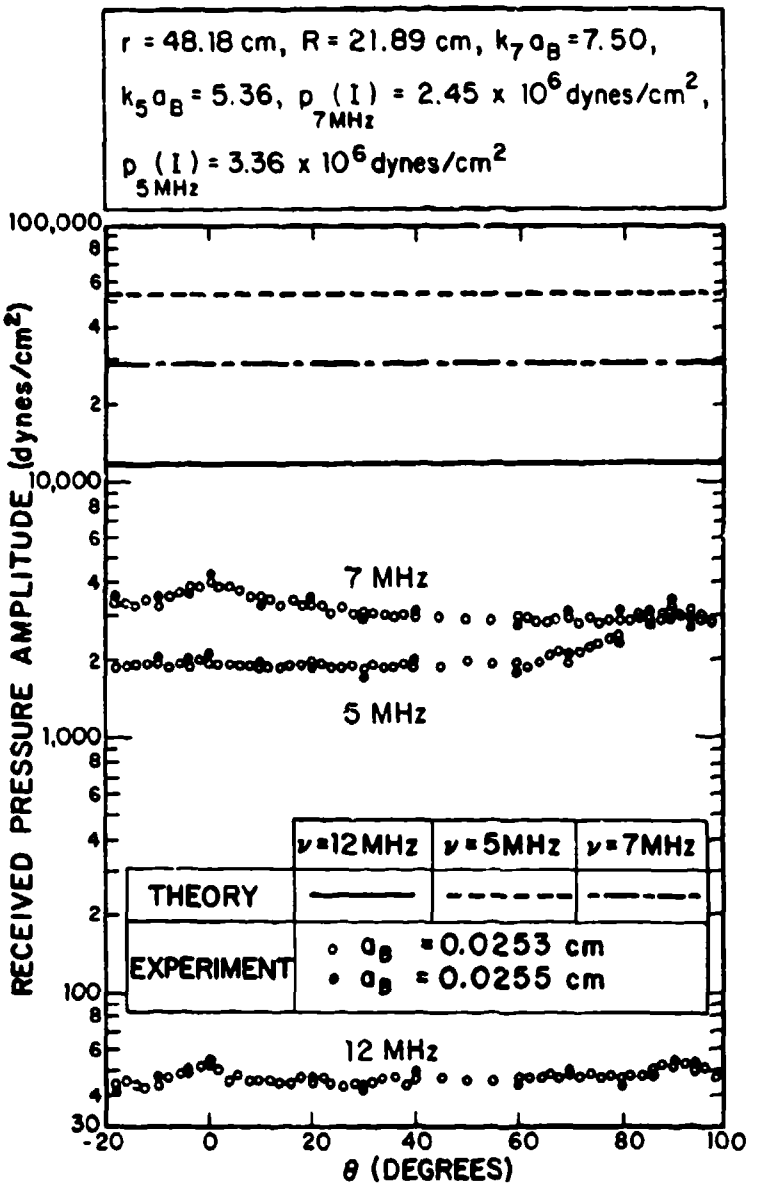

Figure 9-16.–Scattering of sound beams from air bubble of radius 253 microns and the interaction at the sum frequency (from Jones [1]).

MHz and was of about 6-μsec duration. It was fed to an air-backed x-cut quartz crystal with a resonance frequency of 10 MHz. The resultant ultrasonic signal in the CCl_4 had a pressure amplitude of 1.9 atm.

The pulse propagated through the CCl_4 and was detected by a wideband acoustic receiver which consisted of a 30-MHz 0.5-in. quartz transducer bonded to a fused quartz delay line. The crystal output was preamplified within the receiver housing and then fed to external amplifiers and the oscilloscope.

Figure 9-17.–Pulse applied to transducer (from Moffett, Westervelt and Beyer [30]).

Oscillograms showing various stages of the pulse's progress are shown in Fig. 9-18.

The rapid transformation produced by the effect is clearly demonstrated. Berktay has called this process the "self-demodulation of a pulsed

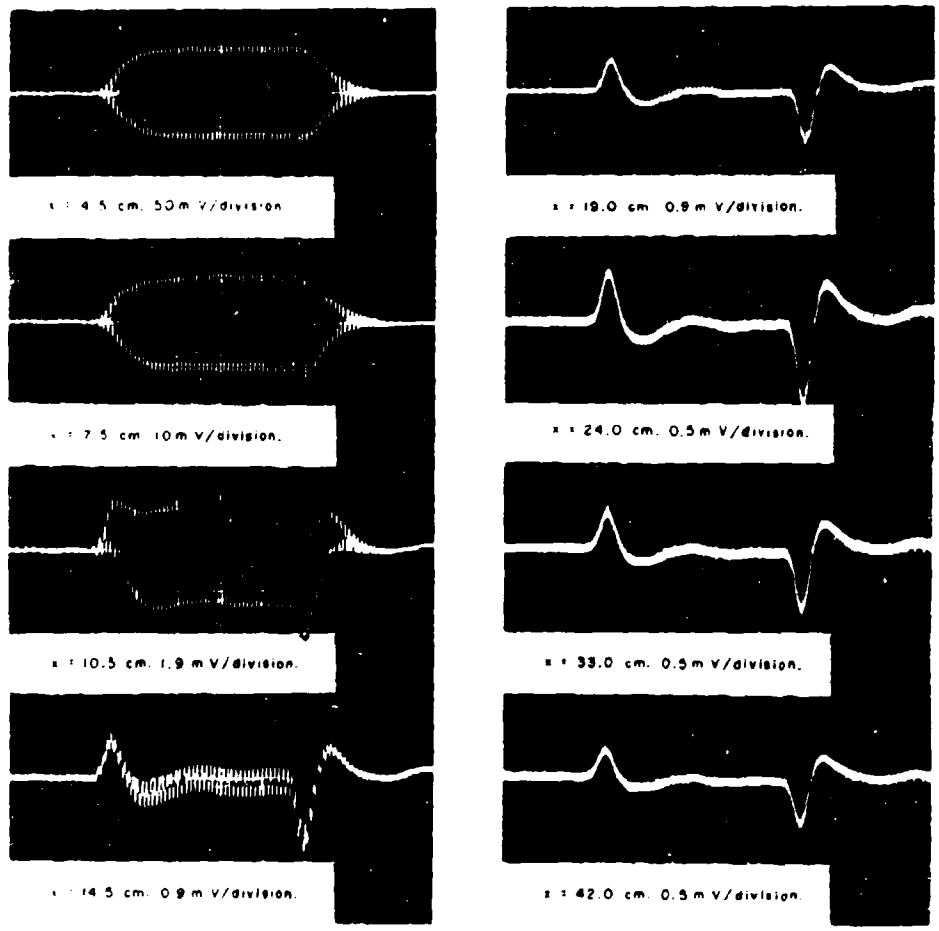

Figure 9-18.–Variation of pulse shape with x, the source receiver separation (from Moffett, Westervelt and Beyer [30]).

carrier." One can also think of the medium as playing the role of an acoustical low-pass filter. The fluctuations of $\partial^2 f^2/\partial t^2$ have an approximate period of 2 μsec or a "frequency" of 500 kHz. The effective absorption coefficient of such a pulse would be $1/20^2 = 1/400$ that of the carrier with its frequency of 10 MHz (at frequencies far removed from any relaxation frequency).

Moffett and his coworkers made further confirmations of the theory. A smoothed version of the envelope of the pulse in Fig. 9-18 at $x = 3.0$ cm was plotted and read into a digital computer, squared and differentiated twice. The computed result for $t^2\partial^2 f^2/\partial t^2$ is shown as the continuous curve in Fig. 9-19. The abscissa τ is the retarded time expressed in periods of the carrier. The experimental points are taken from Fig. 18, $x = 19.0$ cm. The horizontal scale was adjusted to place the first experimental peak at its computed position.

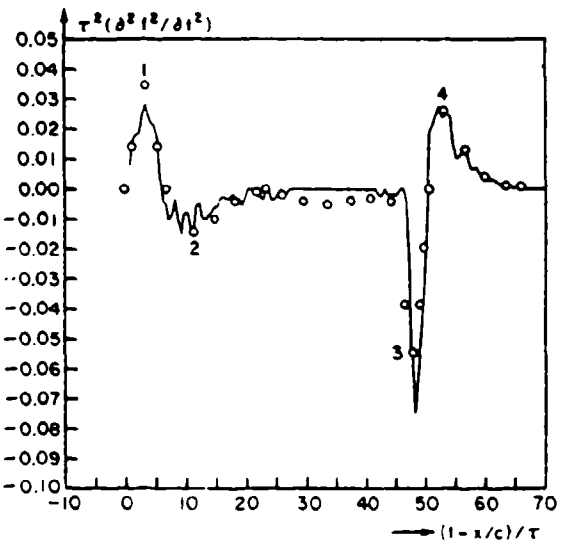

Figure 9-19.–Comparison of transient signal shapes calculated from the pulse envelope similar to that of the first curve of Figure 9-18 (continuous curve) and measured from the photograph of Figure 9-18 at $x = 19.0$ cm (from Moffett, Westervelt and Beyer [30]).

The same effect has been observed in water, where the much smaller absorption coefficient prevents a clearcut separation of the carrier and transient responses. However, it was observed that rotation of a 20-MHz x-cut quartz carrier beam could have the same "filtering" effect as the spatial filter of Fig. 9-18.

The results are shown in Fig. 9-20.

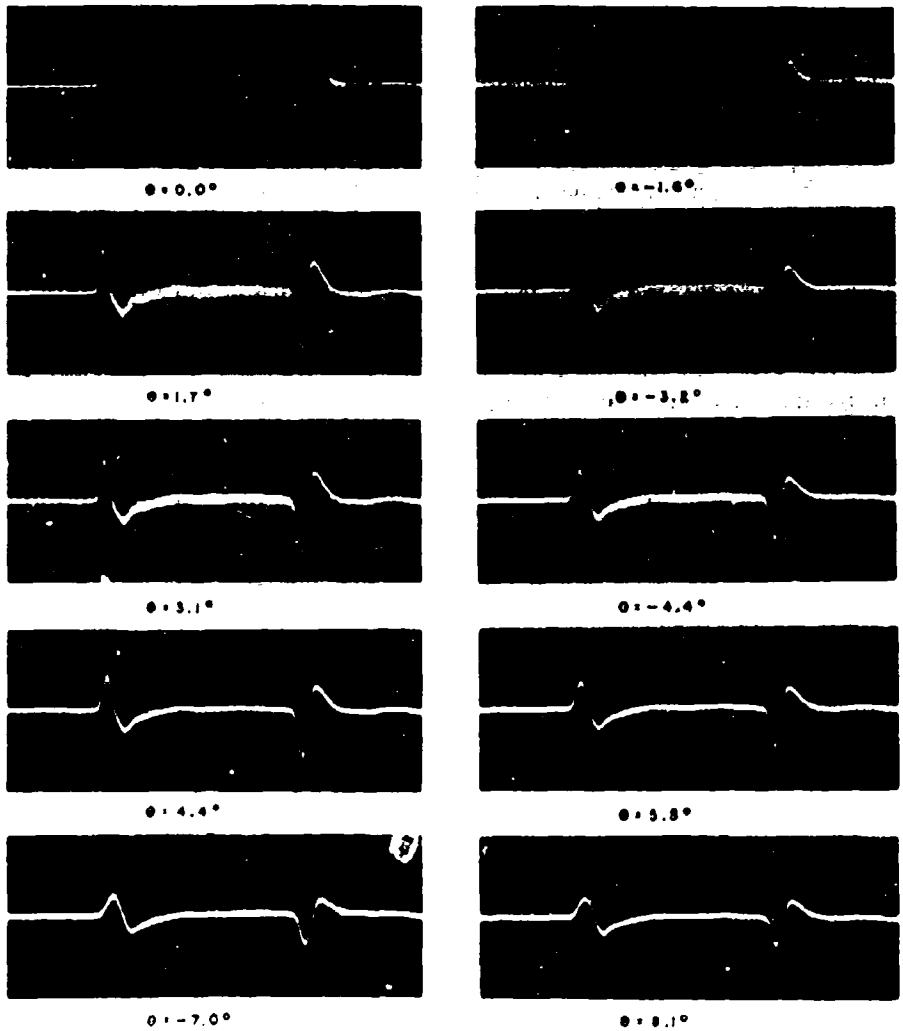

Figure 9-20.–Received pulse at a radius of r = 47.7 cm in tap water for various angles of beam (from Moffett, Westervelt and Beyer [30]).

REFERENCES

Chapter 9

1. J. P. Jones, Ph.D. thesis, Brown University, 1970.
2. C.A. Al-Temimi, J. Sound Vib. 8, 44 (1968).
3. M. J. Lighthill, Proc. Roy. Soc. (London) **A211**, 564 (1952); **A222**, 1 (1954).
4. K. U. Ingard and D. C. Pridmore-Brown, JASA **28**, 367 (1956).

5. See the discussion of pseudo-sound in D. I. Blokhintsev, *The Acoustics of a Moving Inhomogeneous Medium*, Sec. 24, English translation of R. T. Beyer and D. Mintzer, Physics Department, Brown University, 1952.
6. P. J. Westervelt, JASA **29**, 199 (1957).
7. M. J. Lighthill, Math. Rev. **19**, 915 (1958).
8. P. J. Westervelt, JASA **29**, 934 (1957).
9. J. L. S. Bellin and R. T. Beyer, JASA **32**, 339 (1960).
10. L. W. Dean, JASA **34**, 1039 (1962).
11. V. R. Lauvstad and S. Tjötta, JASA **34**, 1645 (1960); **35**, 929 (1963).
12. V. R. Lauvstad, Acustica **16**, 191 (1966).
13. V. R. Lauvstad, J. Naze and S. Tjötta, Arb. Univ. Bergen, Mat. Naturv. Serie No. 12 (1964).
14. H. O. Berktay, J. Sound Vib. **2**, 462 (1965); H. O. Berktay and C. A. Al-Temimi, J. Sound Vib. **8**, 44 (1968).
15. H. O. Berktay and C. A. Al-Temimi, J. Sound Vib. **9**, 295 (1969).
16. V. A. Zverev and A. I. Kalachev, Sov. Phys. Acoustics **15**, 322 (1970); **16**, 204 (1970).
17. R. T. Beyer and J. P. Jones, Seventh International Congress on Acoustics, Budapest, 1971, p. 629.
18. G. L. Jones and D. R. Kobett, JASA **35**, 5 (1963).
19. P. J. Westervelt, 32, 8 (1960).
20. P. J. Westervelt, JASA **35**, 535 (1963).
21. J. L. S. Bellin and R. T. Beyer, JASA **34**, 1051 (1962). See also H. O. Berktay and B. V. Smith, Electronics Letters, March, 1965.
22. M. Vestrheim and H. Hobaek, Proc. Symposium on Nonlinear Acoustics, University of Birmingham (U.K.), April, 1971, p. 159.
23. P. J. Westervelt, JASA **53**, 384 (1973).
24. P. J. Westervelt, Proc. Third International Congress on Acoustics, Stuttgart, p. 316.
25. H. J. Maris and W. E. Massey, Phys. Rev. Lett. **25**, 220 (1970).
26. F. London, Superfluids, Vol. 2, p. 94, John Wiley, New York, 1954.
27. P. M. Morse and K. U. Ingard, Theoretical Acoustics, McGraw-Hill, New York, 1968, p. 404.
28. Ref. 27, p. 419.
29. H. O. Berktay, J. Sound Vib. **2**, 435 (1965).
30. M. B. Moffett, P. J. Westervelt and R. T. Beyer, JASA **47**, 1473 (1970); **49**, 339 (1971).

Chapter 10

APPLICATIONS OF NONLINEAR INTERACTIONS. THE PARAMETRIC ARRAY

The ultrasonic parametric array has now been analyzed and tested over a wide range of conditions. A large number of these researches will be touched on in this chapter. To develop some system for our review, we shall consider first the transmitting applications and subsequently the receiving applications. In each instance the research subdivides further into far-field and near-field operation.

10.1 Far-field Transmission.

Equation (9.33) gave Westervelt's expression for the interaction to be expected from two beams of the same intensity and nearly equal frequency. This analysis assumed the existence of plane waves and was further restricted to the far field of the scattered wave by the condition $k_s R_0 > (k_s/\alpha)^2$. [1] Berktay extended Westervelt's treatment to take into account the finite size of the transducer. [2] Assuming a rectangular transducer of sides $2b$, $2d$, he obtained the following expression for two beams of initial pressure amplitudes P_1, P_2 (Fig. 10-1):*

$$p_s = \frac{\beta P_1 P_2 S \omega_s^2 \exp(-\alpha_s R)\psi(\gamma,0)}{4\pi\rho_0 c_0^4 R_0 \left[A^2 + 4k_s^2 \sin^2\frac{\theta}{2}\right]^{1/2}} \tag{10.1}$$

where

$$\begin{aligned} S &= (2b)(2d) \\ A &= \alpha_1 + \alpha_2 - \alpha_s \cos\theta \\ \psi(\gamma,\theta) &= \frac{\sin(dk_s \cos\gamma)}{dk_s \cos\gamma} \frac{\sin(bk_s \sin\gamma \sin\theta)}{bk_s \sin\theta \sin\gamma} \end{aligned} \tag{10.2}$$

*In his derivations, Berktay made the simplifying assumption that the nonlinear parameter β was equal to unity.

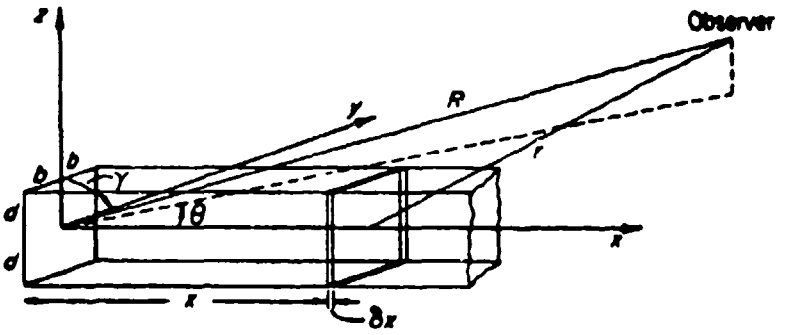

Figure 10-1.–Geometry for two collinear interacting sound beams traveling in the x direction (from Berktay [2]).

$\alpha_1, \alpha_2, \alpha_s$ = absorption coefficients for the two primary waves and the difference frequency wave, respectively.

The results shown in Fig. 10-2 indicate the effect on the beam width of taking the diffraction pattern (10.2) into account.

For practical application, a different transducer geometry is often used, and Berktay has derived expressions for both cylindrical and spherical spreading:

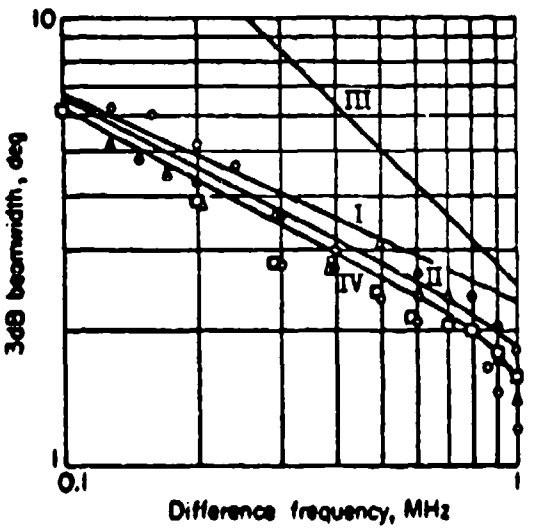

Figure 10-2.–Experimental results of the interaction of two collinear sound beams. Curve I, II derive from Eq. (10.1), curve I without the aperture function ψ, curve II with it; curve III corresponds to the case of radiation from a square aperature of area 9 cm^2; curve IV is the mean experimental curve (from Berktay [2]).

(a) *Cylindrical case* (Fig. 10-3)

The pressure distribution in the far field in the plane $z = 0$ is given by

$$p_s = \frac{\beta P_1 P_2(2\ell)\omega_s^2 e^{-\alpha_s R}}{\rho_0 c_0^4 8\pi R_0 \sqrt{2k_s A}} \sqrt{\Phi^2 + L^2} \tag{10.3}$$

where

$$\Phi = -2\tan^{-1}(\sqrt{2u_1} - 1)^{-1} + \tan^{-1}(\sqrt{2u_1} - 1)^{-1}$$

$$- \tan^{-1}(\sqrt{2u_2} + 1)^{-1} - \tan^{-1}(\sqrt{2u_1} - 1)^{-1}$$

$$e^L = \frac{\left(\theta_0^2 - \psi_d^2 - \sqrt{2}\psi_d\right)^2 + (1 + \sqrt{2}\psi_d)^2}{\left(\theta_0^2 - \psi_d^2 + \sqrt{2}\psi_d\right)^2 + (1 - \sqrt{2}\psi_d)^2} \tag{10.4}$$

$$u = \theta_0 - \psi_0 \qquad \theta_0 = \theta/\theta_d \qquad \theta_d = \sqrt{2\alpha/k_s}$$

$$u_1 = \theta_0 - \psi_d \qquad \psi_0 = \psi/\theta_d$$

$$u_2 = \theta_0 - \psi_d \qquad \psi_d = \psi_1/\theta_d.$$

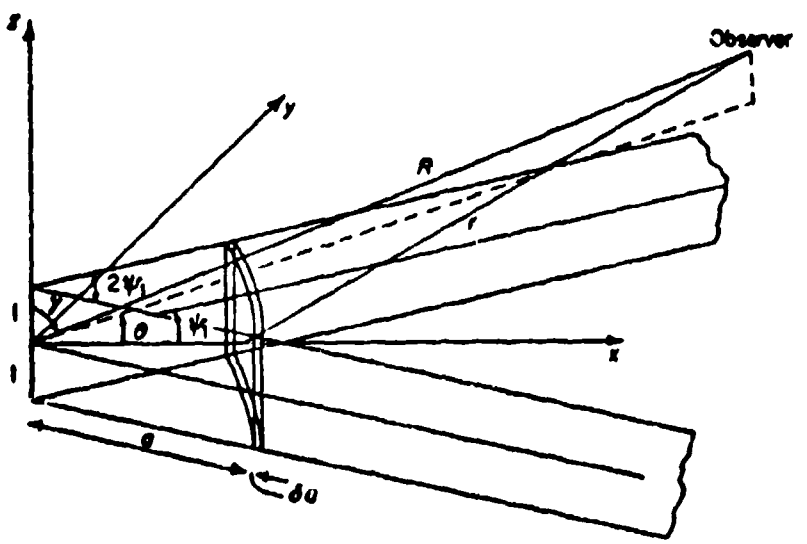

Figure 10-3.–Geometry for an end-fire array formed by cylindrically spreading primary wave (from Berktay [2]).

In this case, one is dealing with a primary beam of two cylindrically spreading waves confined within the limits $z \pm \ell$ and making angles of $\pm\psi_1$ with the x axis. It is also assumed that the radial power flow is uniform over the angular range of 2ψ.

(b) *Spherical spreading*

Here it is assumed that the primary waves are confined to a cone of angular width $2\psi_1$ with the intensity independent of angular position within the cone.

The analysis by Berktay leads to the result

$$p_s = \frac{P_1 P_2 \omega^2 e^{-\alpha_s R}}{2\rho_0 c_0^4 R k_s} \left\{ \left[\frac{1}{2} \ln \left(1 + \psi_d^4 \right) \right]^2 + (\tan^{-1} \psi_d^2)^2 \right\}^{1/2}. \tag{10.5}$$

[Same terminology as in Eq. (10.4).]

The directivity of the array can be considered by comparing the scattered pressure at angle θ with its value at $\theta = 0$. For the bounded plane wave case, in the plane $z = 0$

$$D(\theta) = \frac{p_s(r,\theta)}{p_s(R,0)} = \frac{\sin(bk_s \sin\theta)}{bk_s \sin} \left[1 + \left(\frac{2k_s}{A} \sin^2 \frac{\theta}{2} \right)^2 \right]^{-1/2}.$$

For the problems of interest (waterborne sound) $\sqrt{A/2k_s} = \sin\theta_d/2 \ll 1$. The half power points (3 dB down) of this directivity pattern occur when $(2k/A) \sin^2 \theta/2 = 1$. Hence

$$2\theta_d \simeq 4\sqrt{A/2k_s}. \tag{10.7}$$

The corresponding directivity function for cylindrical waves is given by

$$D_c(\theta_0, \psi_d) = \frac{1}{8\psi_d} \sqrt{\phi^2 + L^2}, \tag{10.8}$$

and for spherical waves

$$D_s(\theta, \psi_d) = \frac{1}{\psi_d^2} \left\{ \left[\frac{1}{2} \ln \left(1 + \psi_d^4 \right) \right]^2 + (\tan^{-1} \psi_d^2)^2 \right\}^{1/2}. \tag{10.9}$$

The relation of the scattered wave to the intensity of the fundamental frequency component in the far field has been established semi-empirically

by Merklinger. [3] He points out that the source function (9.29) can be written in the form

$$q(x,t) = \frac{\beta}{\rho c_0^3} \frac{\partial I}{\partial t}(r,t) \tag{10.10}$$

where I is the total acoustic intensity.

Of several empirical relations between I and the intensity of the fundamental frequency component I_0 proposed by Merklinger, the simplest is

$$\begin{aligned} I &= I_0 e^{-2\alpha x} \qquad x < x_2 \\ &= 1.6\, I_1 \qquad x > x_2, \end{aligned} \tag{10.11}$$

where I_0 is the initial sound intensity and x_2 the distance at which the extra attenuation [Eq. (3.72)] is 2 dB. Working with this and a somewhat more involved approximation, Merklinger obtained an approximate form for p_s:

$$p_s = \frac{\beta}{4\pi c_0^3} \frac{\partial^2}{\partial t^2} \left[\frac{I_0\left(t - \frac{R}{c_0}\right)}{K_1} \tan^{-1} \sqrt{\frac{K_1 I_0\left(t - \frac{R}{c_0}\right)}{16 \alpha_s^2 S^2}} \right] \tag{10.12}$$

where $K_1 = \beta^2 \omega^2 / \rho_0 c_0^2$. At high intensities, Eq. (10.12) becomes independent of β, achieving the form

$$p_s(R,t) = \frac{S}{4\sqrt{2} R c_0 \omega} \frac{\partial^2}{\partial t^2} \left| P_0\left(t - \frac{R}{c_0}\right) \right|. \tag{10.13}$$

Merklinger has applied this analysis to the case of the parametric array to show that the beam pattern will narrow as the nonlinear parameter β is reduced.

In an attempt to be more realistic, Berktay and Leahy [4] considered interaction in the far field of a transducer, the directivity (in the far field) of whose two primary frequencies is known, under the assumption that one can neglect interactions in the near field and also any higher order (than primary-primary) interaction.

In their work, Berktay and Leahy generalize the Westervelt scattering integral Eq. (3.90) to the case of complex waves with known directivity char-

acteristics. The geometry is shown in Fig. 10-4. If the primary waves are given by

$$p_j = \frac{P_j}{r} D_j(\gamma,\phi) \exp\left[-(\alpha_j + ik_j)r\right] \qquad (10.14)$$

$$j = 1,2$$

where $D_j(\gamma,\phi)$ is the directivity index of the jth primary wave, then the difference frequency pressure at the point **R** will be given by

$$p_-(R,\theta,\eta) = \frac{-\omega^2 P_1 P_2 \beta}{4\pi\rho_0 c_0^4} \int \frac{D_1 D_2}{r|\mathbf{r}-\mathbf{R}|} \times \exp\left[-(\alpha_1 + \alpha_2 + ik_-)r - (\alpha_- - jk)|\mathbf{r}-\mathbf{R}|\right] dV \qquad (10.15)$$

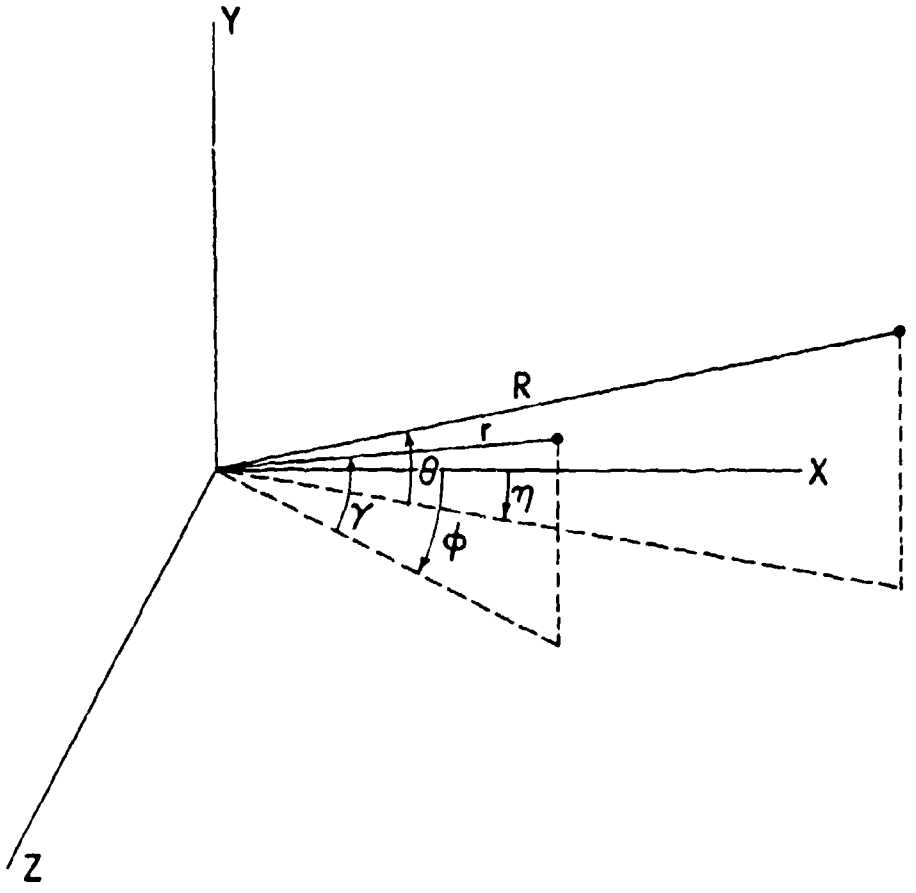

Figure 10-4.–Geometry for interaction of two primary sound waves of known characteristics (from Berktay and Leahy [4]).

where the volume element is

$$dV = r^2 \cos\gamma \, d\gamma \, d\phi \, dr.$$

In the far-field approximation, Eq. (10.15) can be reduced to

$$p_-(R,\theta,\eta) \simeq \frac{\omega_-^2 \beta P_1 P_2}{4\pi\rho_0 c_0^4} e^{-(\alpha_- + ik_-)R} \int_{-\pi/2}^{\pi/2} \int_{-\pi/2}^{\pi/2} \frac{D_1(\gamma,\phi) D_2(\gamma,\phi) \cos\gamma}{\alpha_T + ik(1-u)} \, d\gamma \, d\phi \, e^{-ik_- R(1-u)}$$

$$\left[kR \gg 1, u \simeq 1 - \frac{(\gamma-\theta)^2}{2} - \frac{(\phi-\eta)^2}{2}, \right.$$

$$\left. \alpha_T = \alpha_1 + \alpha_2 + \alpha_- . \right] \tag{10.16}$$

If the directivity functions are the same for each primary beam and if it is assumed that the beams are very narrow, then Eq. (10.16) reduces to the Westervelt solution of two collimated plane waves (9.33).

Berktay and Leahy have applied their analyses to the cases of a rectangular transducer and a circular transducer, both in infinite baffles. We shall review the first of these cases.

We therefore suppose the transducer to be a rectangle of length ℓ, width m. The directivity function is taken to be approximately

$$D(\gamma,\phi) \simeq \frac{\sin \pi L\gamma}{\pi L\gamma} \cdot \frac{\sin \pi M\gamma}{\pi M\gamma}, \tag{10.17}$$

where $L = \ell/\lambda$, $M = m/\lambda$.

The half power points of the two primary beams are defined by

$$\pi L\gamma_1 = \pi M\phi_1 \simeq \sqrt{2}. \tag{10.18}$$

The authors then normalized all angles with respect to the halfpower point of the difference frequency beam θ_d [Eq. (10.4)]

$$\theta_d \simeq 2\sqrt{2\alpha_T/k_-}$$

$$\gamma' = \gamma/\theta_d \qquad \psi_y = \gamma_1/\theta_d \tag{10.4}$$

$$\phi' = \phi/\theta_d \qquad \psi_z = \phi_1/\phi_d.$$

Then

$$D(\gamma',\phi) \simeq \frac{\sin(\sqrt{2}\gamma'/\psi_y)}{\sqrt{2}\gamma'/\psi_y} \frac{\sin(\sqrt{2}\phi'/\psi_z)}{\sqrt{2}\phi'/\psi_z}. \tag{10.19}$$

In these terms, Berktay and Leahy could write a general expression for the difference frequency pressure:

$$p_-(R,\theta,\eta) \simeq p_w(R,0)V(\psi_y,\psi_z,\theta',\eta') \tag{10.20}$$

where

$$p_w(R,0) = \frac{-\omega^2 P_1 P_2 \beta S}{4\pi\rho_0 c_0^4}$$

$$V = LM\theta_d^2 \int_{-\pi/2}^{\pi/2} \int_{-\theta_d}^{+\theta_d} \frac{D^2(\gamma',\phi')d\gamma'\,d\phi'}{1 + i[(\theta' - \gamma')^2 + (\eta' - \phi')^2]}. \tag{10.21}$$

The integration of $V(\psi_y,\psi_z,0,0)$ was carried out and the results are plotted in Fig. 10-5. Curves such as that of Fig. 10-5 can be used to compute the far field behavior of a parametric area for a given set of parameters.

Another approach to the same problem has been made by Mellen and coworkers [5] who have sought scaling parameters for the design of parametric arrays. In particular, Mellen and Moffett considered a model in which the piston transducer was driven at frequencies $f_0 \pm f/2$ so that a difference frequency $f \ll f_0$ is achieved. The beam is assumed to be a collimated plane wave out to $R_0 = \pi a^2/\lambda_0$ (a = radius of transducer, $\lambda_0 = c/f_0$) and then to spread spherically within a cone defined by the half angle $\theta_0 \simeq 0.6\sqrt{\lambda_0/R_0}$.

In their analysis, these authors began with the usual Westervelt interaction formula and computed the far field of the secondary pressure at distances large compared with the dimensions of the interaction volume (which are of the order of $1/2\alpha_0$). At the same time, they described their results in terms of three scaling parameters: 1) the downshift ratio f_0/f, assumed to be greater than about 5; 2) the absorption number $2\alpha_0 R_0$, which is less than unity for most practical systems; 3) the saturation number r_0/ℓ (equivalent to σ of Chapter 3). Finally they defined the *scaled primary source level* L_0^*, equal to the actual source level in dB (re 1 μbar at 1 m) + 20 log f_0, where f_0 is in kHz. Thus scaled levels above 180 dB corresponds to shock formation in the collimated zone.

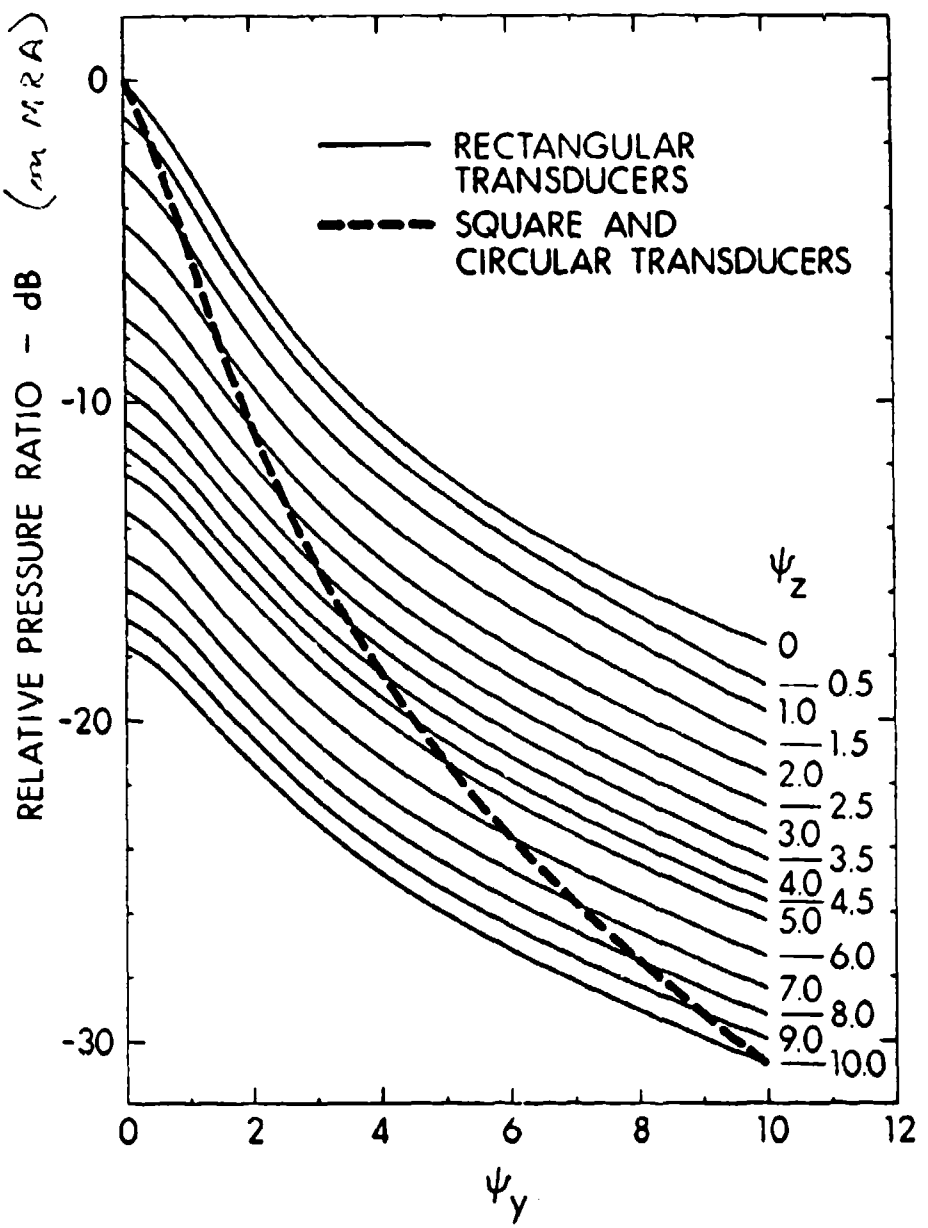

Figure 10-5.–Far-field behavior for given dimensions of transducer in the case of a parametric array (from Berktay and Leahy [4]).

The principal results of their analysis are shown in Fig. 10-6 for a downshift ratio of 10. The quantity labeled parametric gain is the ratio (in dB) of the secondary source level frequency (f) to the primary source level frequency (f_0). For scaled input levels above 180 dB, the formation of shock within the collimated zone flattens the gain curves (saturation limiting).

The lower left of the figure corresponds to the Westervelt situation, in which the gain is limited by the small signal absorption.

As a typical example, the problem is considered of producing a 5-kHz secondary beam from a 50 kHz source with primary level 130 dB re 1 μbar at 1 m. Then $f_0/f = 10$, $L^* = 130 + 20 \log 50 = 164$ db re 1 μbar-m-kHz. If

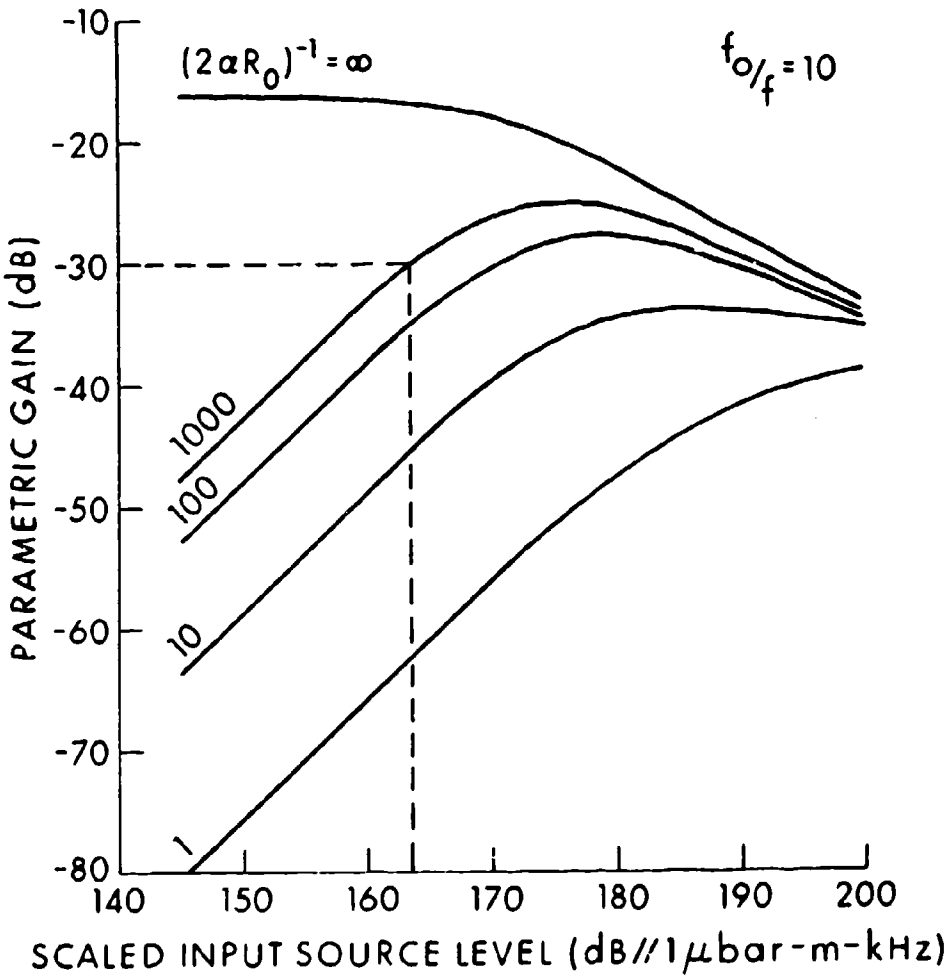

Figure 10-6.–Parametric gain as a function of scaled input source level for various values of the absorption number $2\alpha R_0$. (From Mellen and Moffett [5]).

the diameter of the projection is 3 in., $R_0 \sim 6$ in, and $1/2\alpha_0 R_0 \sim 1000$, the parametric gain can then be read as −30 db re 1 μbar-m (see dashed lines on graph).

Propagation curves have also been studied by Muir and Willette [6] who used the directivity of a low frequency circular plane piston source

$$D(ka \sin\theta) = \frac{2J_1(ka \sin\theta)}{ka \sin\theta}$$

and employed numerical integral of the Westervelt equation for the scattered pressure. Their results are shown in Fig. 10-7 for 418 and 482-kHz primary beams. Theoretical and experimental values of the received signal are given for the carrier beam and for the sum and difference frequency.

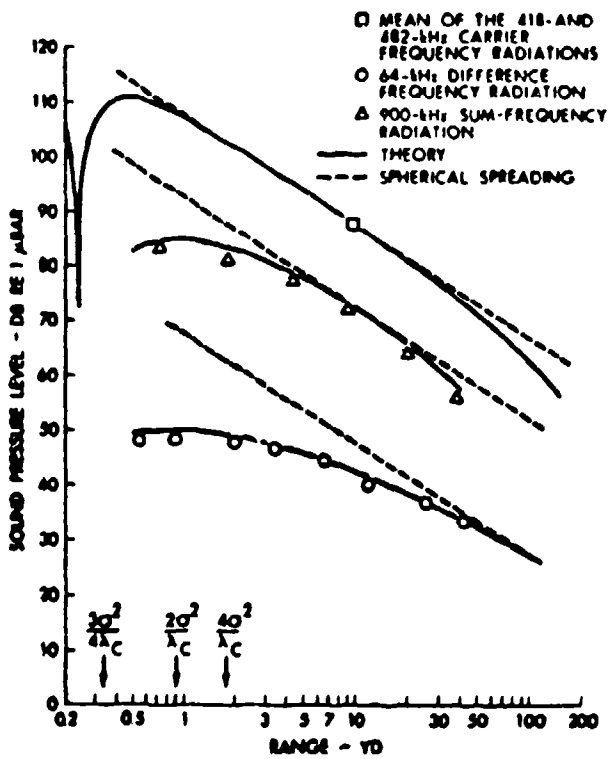

Figure 10-7.–Behavior of primary and difference frequency components in a transmitting array (from Muir and Willette [6]).

The problem of the secondary beam directivity has been treated by a number of authors.

Muir and Willette [6] extended the calculations and measurements to off axis measurements of the scattered pressure. Their results for carrier, sum and difference frequencies are shown in Figure 10-8.

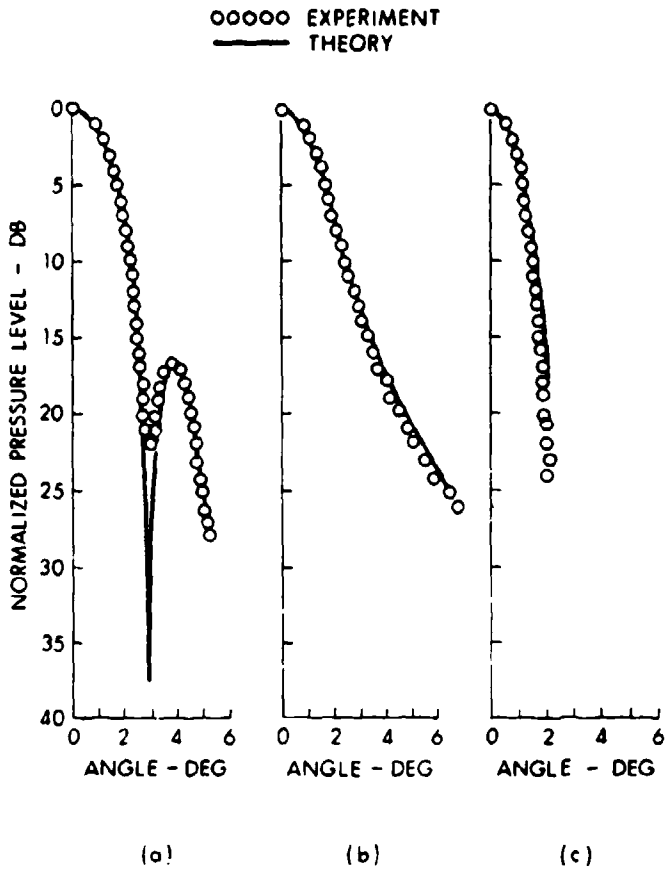

Figure 10-8.–Beam pattern for carrier, sum and difference frequency components in a transmitting array. (a) 482-kHz carrier; (b) 64-kHz difference frequency radiation; and (c) 900-kHz sum frequency radiation (from Muir and Willette [6]).

Mellen, Konrad and Browning [5] also measured the difference frequency obtained by driving a single transducer with two signals of mean frequency 720 kHz. The difference frequency signal is plotted as a function of angle in Fig. 10-9 for difference frequencies from 12.5 kHz to 100 kHz. Somewhat similar results have also been obtained by Pearce and Berktay, [7] who employed a mosaic transducer.

Finally, an operational sonar has been described by Walsh. [8] In this construction, primary beams in the vicinity of 200 kHz were used to produce a difference frequency of 12 kHz. Figure 10-10 shows the beam pattern for the 200-kHz primary and for the 12-kHz difference frequency.

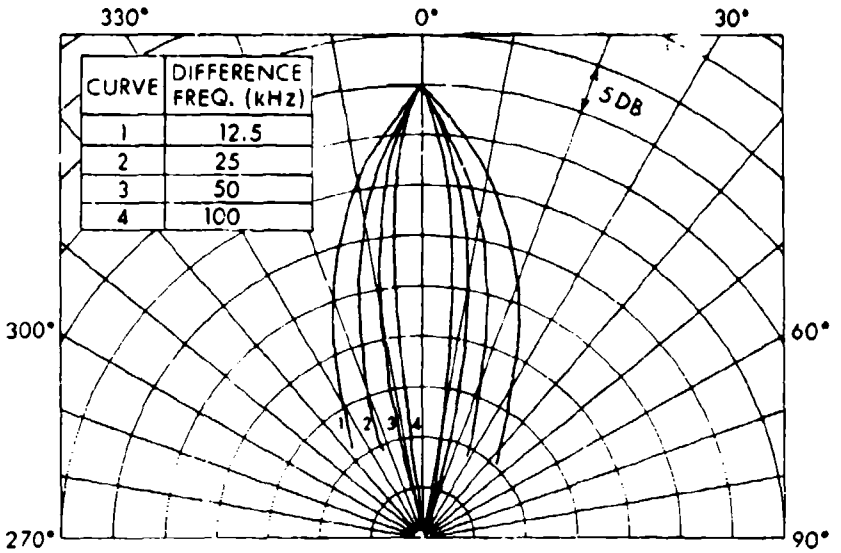

Figure 10·9.–Difference frequency beam patterns. Mean of primary frequencies = 750 kHz (from Mellen, Konrad and Browning [5]).

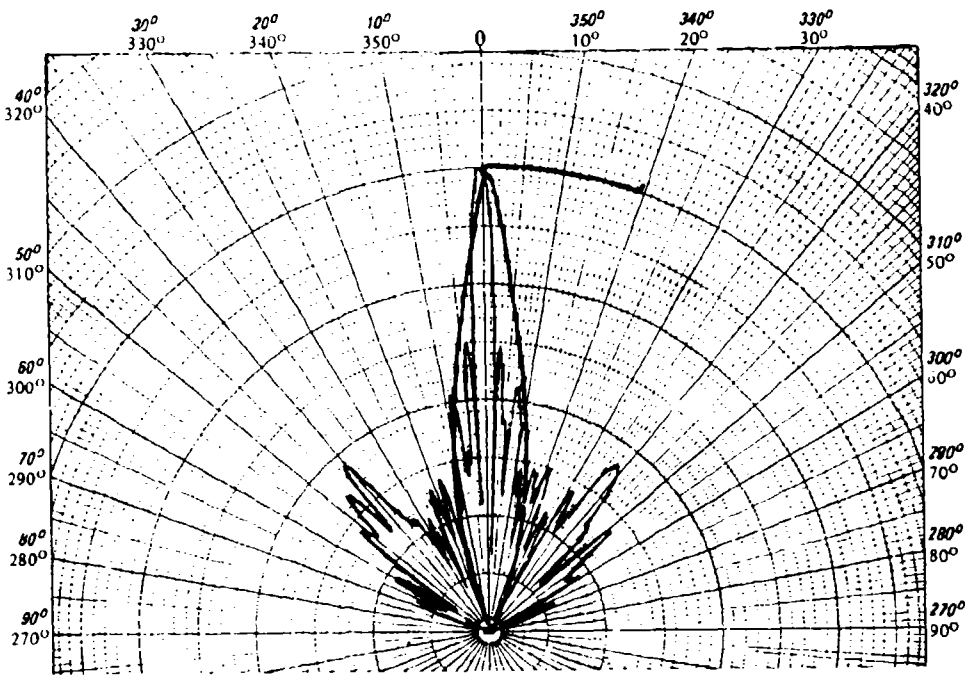

Figure 10·10.–Beam patterns of parametric array sonar. (a) primary beam, 200 kHz; (b) difference frequency beam, 12 kHz. Equivalent source level 87.6 dB re 1 μbar (from G. Walsh [8]).

10.2 Near-Field Transmission.

The problem of the near field of the parametric array has been treated by Berktay and Shooter. [9] They begin with a continuous line array of simple sources (shown in Fig. 10-11) with a strength q per unit length:

$$q(x,t) = Q_0 \exp\,[i(\omega t - kx)] \tag{10.22}$$

for $0 \leqq x \leqq L$, and zero outside the range. The velocity potential at the point r can then be written

$$\phi(z,p) = \frac{Q_0}{4\pi}\int_{x=0}^{L} \frac{1}{r}\exp\,[-ik(x+r)]\,dx$$
$$r^2 = (z-x)^2 + \rho^2. \tag{10.23}$$

By introducing the notation

$$v = k(r + x - \qquad k(r - \sqrt{r^2 - \rho^2}), \tag{10.24}$$

Eq. (10.23) can be ... on as

$$\phi(R,\theta) = \frac{Q_0}{4\pi}\ln\frac{R}{R-L}\exp(-ikR\cos\theta)D(R,\theta) \tag{10.25}$$

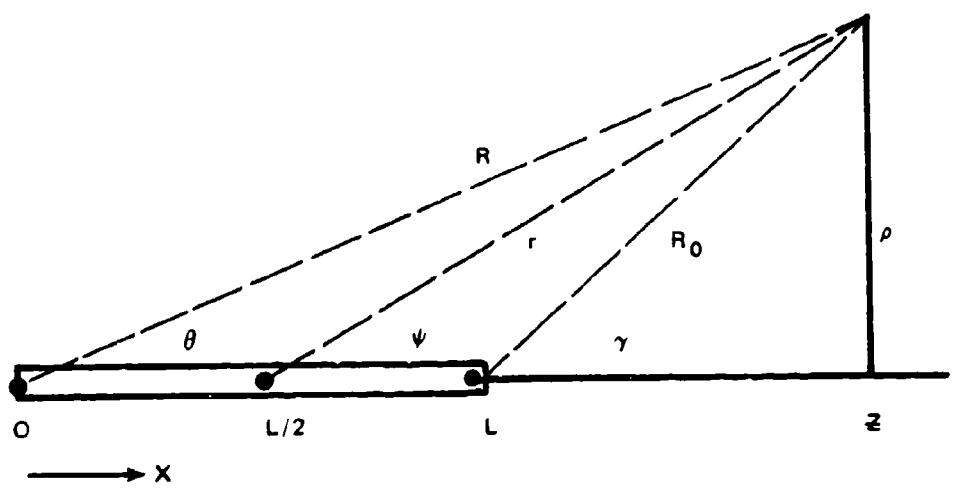

Figure 10-11.–Geometry for near-field transmission.

where

$$D(R,\theta) = \left[\ln \frac{R}{R-L}\right]^{-1} \int_{v_1}^{v_2} \frac{1}{v} \exp(-iv)\, dv$$

$$v_1 = kR(1 - \cos\theta) \tag{10.26}$$

$$v_2 = k[(R^2 + L^2 - 2LR\cos\theta)^{1/2} - (R\cos\theta - L).$$

The function $D(R,\theta)$ is a normalized directivity function. This function is plotted in Fig. 10-12 for various values of R/L, ranging from 1.1 to

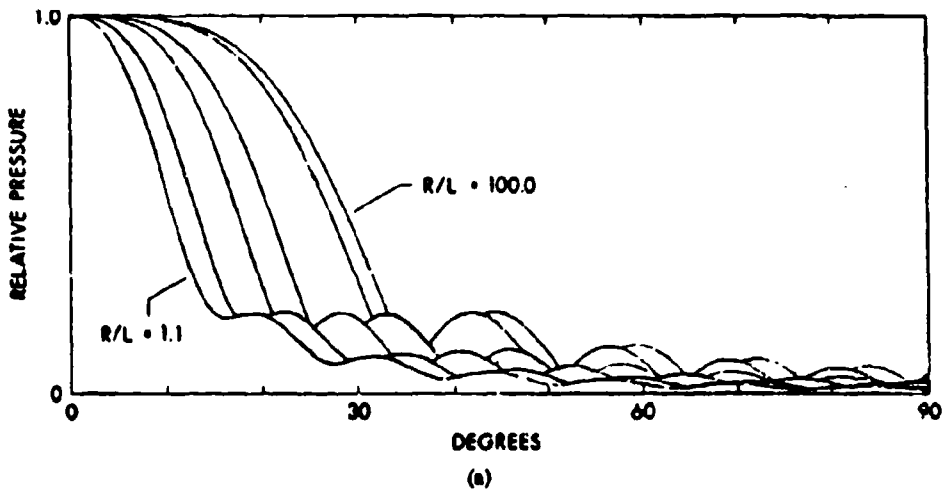

Figure 10-12a.–End-fire array pattern for kL = 31.4 and the ratio R/L = 1.1, 1.2, 1.5, 2.0, 8.0 and 100.0.

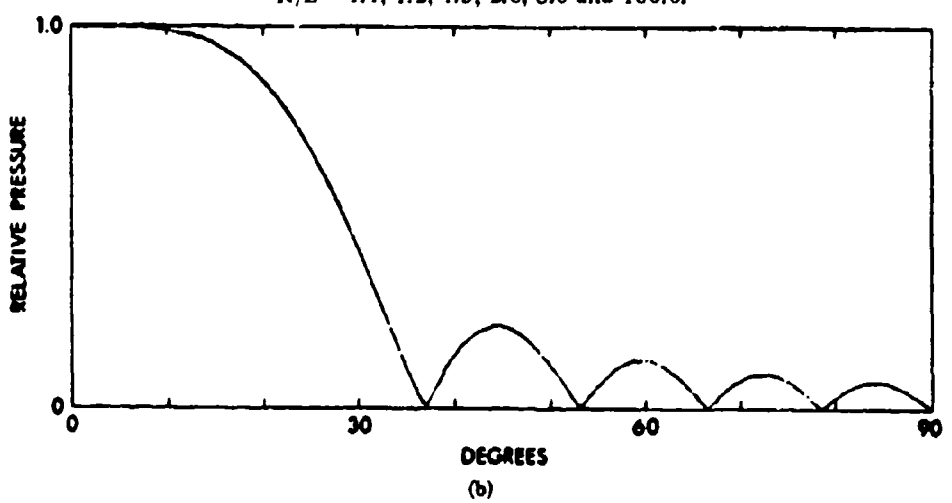

Figure 10-12b.–Far-field end-fire array beam pattern for kL = 31.4 (from Berktay and Shooter [8]).

100, i.e., from the near field to a relatively far field. In all cases $kL = 31.4$. The most interesting feature is the narrowing of the beam as the range is decreased.

While the analysis of Berktay and Shooter is derived in terms of real arrays, it can be used also in the case of the parametric array. In that situation, the effective length of the ray is at least as great as $1/\alpha$ where α is the absorption coefficient at the mean transmitter frequency. In the experiments in water of Bellin and Beyer, [10] described in Sec. 9.5, $1/\alpha = 22$ cm. Since the difference frequency was detected at distances of about 1 foot,* it is clear that $R \sim L$ in Eqs. (10.25), (10.26), so that considerable narrowing should be expected (see Fig. 9.5).

Some further mathematical analysis of Berktay and Shooter is also of interest. If Eq. (10.25) is expressed in terms of the retarded time

$$t' = t - \frac{z}{c_0}$$

and the substitution

$$t = t' - \frac{\rho y}{c_0}$$

is made, Eq. (10.25) becomes

$$\Phi(z,\rho,t) = \frac{1}{4\pi} \int_{\tau_2}^{\tau_1} \frac{q(\tau)\, d\tau}{t' - \tau} \tag{10.27}$$

or, if we introduce the so-called window function $U(\tau_1, \tau_2)$

$$U(\tau_1,\tau_2) = 1, \qquad \tau_2 < \tau < \tau_1$$

$$= 0 \qquad \text{otherwise,}$$

where

$$\tau_i = t' - \frac{\rho y_i}{c_0} \equiv t' - t_i'$$

$$i = 1,2,$$

*These authors neglected to record the distance for posterity, but the dimensions of the tank and this writer's memory suggest 1 foot as the most probable value.

then

$$\Phi(z,\rho,t) = \frac{1}{4\pi}\int_{-\infty}^{\infty} q(\tau)\,\frac{U(\tau_1,\tau_2)}{\tau' - \tau}\,d\tau. \tag{10.28}$$

This integral is the convolution of $q(t')$ with the function $h(t')$, where

$$h(t') = \frac{1}{4\pi}\,\frac{U(t_2',t_1')}{t'}; \tag{10.29}$$

$h(t')$ is known as the *impulse response function* of the end-fire array. [11]

This latter result was actually first obtained by Westervelt in 1965 in a problem on gravitational waves. [12]

Measurements have also been carried out in air by Bellin and Beyer. As in water the directivity pattern was inversely proportional to the difference frequency (Fig. 10-13), but the absolute width was narrower than that predicted by the Westervelt theory, again, presumably because the measurements were carried out in the near field.

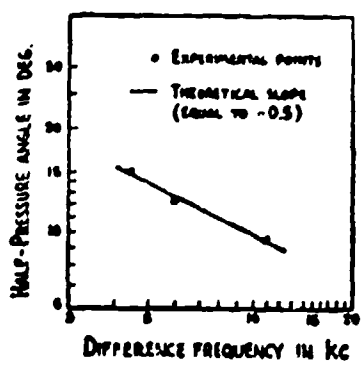

Figure 10-13.–Half-pressure angle for difference frequency in air. Primary frequencies ~ 350 kHz (from Bellin and Beyer [10]).

Recently, Bennett [13] has confirmed the results of Ref. 10 by exciting two elements of a "squirter" transducer at 18.6 kHz and 23.6 Hz. Each of these primary beams has a directivity half width of about 16°. Both the sum and difference frequencies were detected after various false signals resulting from intermodulation distortions in the receiving system had been eliminated. All the Bennett measurements were made in the near field. Re-

sults of the measurements are shown in Fig. 10-14. The solid curves in each case were obtained by numerical integration of the equivalent of Eq. (10.13), where the directivity patterns are those of ideal pistons operating at the two primary frequencies.

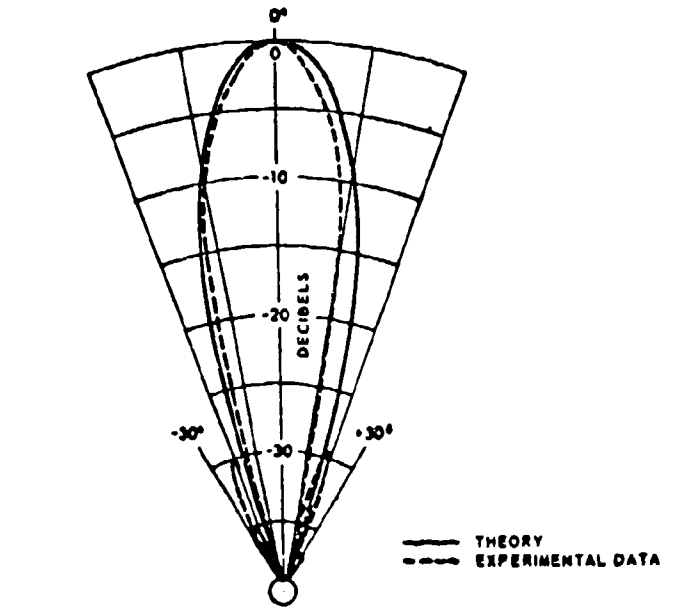

(a) SUM FREQUENCY (47.2 kHz)

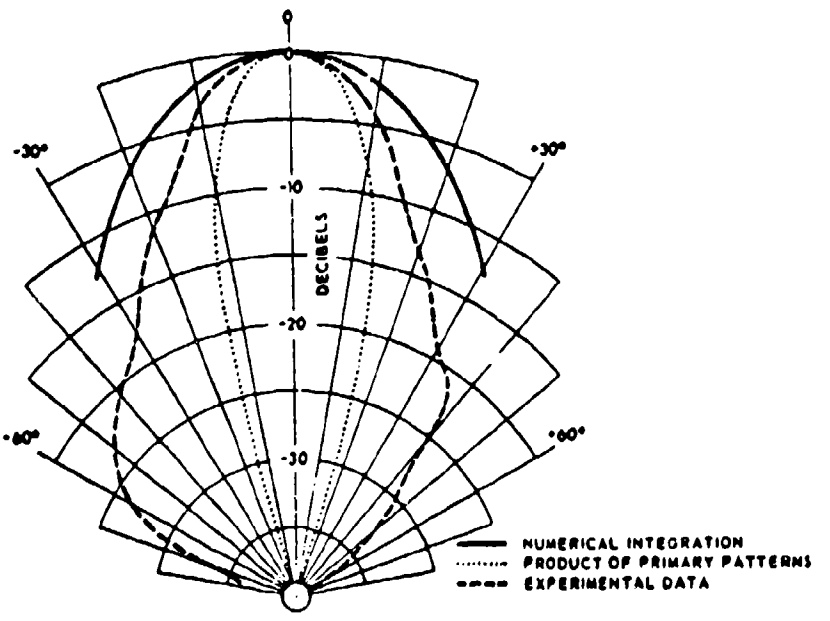

(b) DIFFERENCE FREQUENCY (5 kHz)

Figure 10-14.–Measured and computed beam patterns for parametric area in air. (a) sum frequency (47.2 kHz); (b) difference frequency (5 kHz) (from M. B. Bennett [13]).

10.3 Far-field Receiving

Westervelt's parametric acoustic array [1] can also serve as a receiving array, in which an incoming wave interacts nonlinearly with a local sound source and the scattered sum-or-difference frequency is detected. Such systems have now been examined by a number of authors. [14-16]

The arrangement used in Ref. 16 involved the geometry shown in Fig. 10-15. The first order field consisted of a spherical wave source of angular frequency ω, and a plane wave source of a lower frequency $\omega_2(\omega_1 > \omega_2)$. The spherical wave emanated from a baffled circular piston and both sources were assumed to have harmonic time dependences.

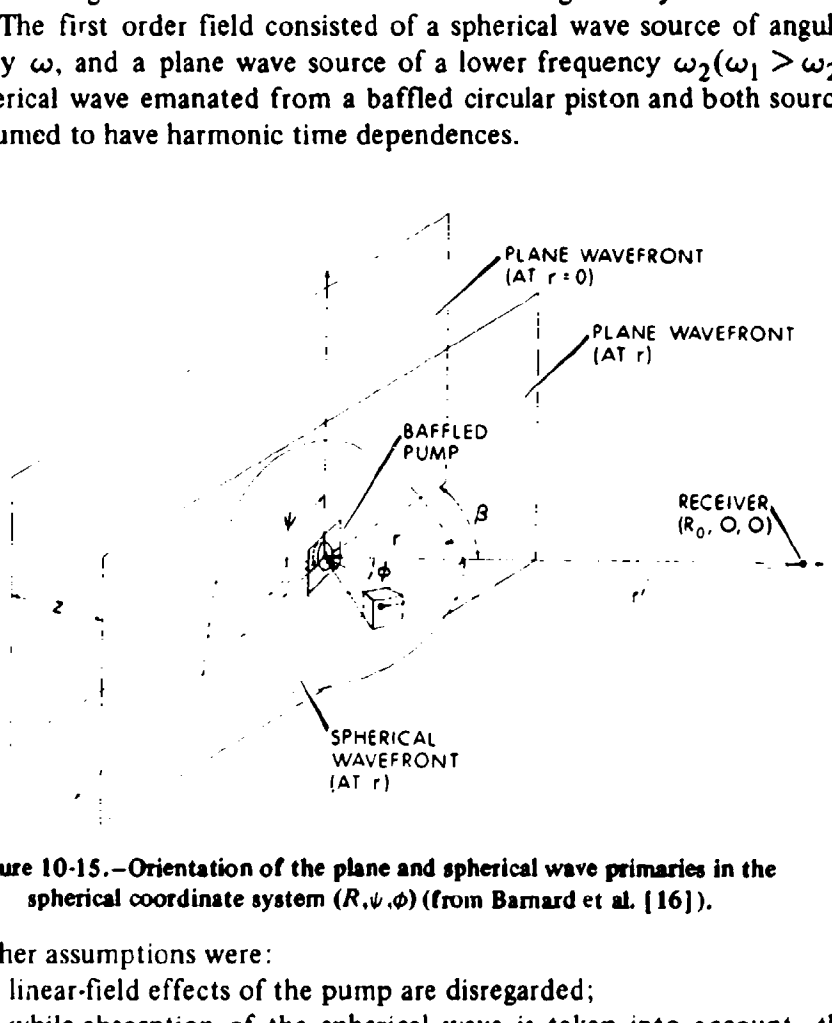

Figure 10-15.–Orientation of the plane and spherical wave primaries in the spherical coordinate system (R,ψ,ϕ) (from Barnard et al. [16]).

Other assumptions were:

1) linear-field effects of the pump are disregarded;

2) while absorption of the spherical wave is taken into account, the absorption in the plane wave is neglected;

3) the amplitudes of the primary waves are such that losses in the primary beams due to finite amplitude effects can be neglected.

Barnard and his coworkers began their analysis with the Westervelt equation for the scattered wave

$$p_s(R_0,t) = -\frac{-\rho_0}{4\pi}\int \frac{\partial q}{\partial t}\,\frac{\exp\,[i(k_s + i\alpha_s)]}{|\mathbf{R}_0 - \mathbf{r}|}\,|\mathbf{R}_0 - \mathbf{r}|\,dV \qquad (10.30)$$

where q is the source strength and the subscript s refers to quantities in the scattered wave. The factor $\exp(-\alpha_s|\mathbf{R}_0 - \mathbf{r}|)$ did not appear in the original Westervelt formulation but was added to take into approximate account the absorption of the secondary radiation.

As before, $q = (\beta/\rho_0{}^2c_0{}^2)(\partial p_f{}^2/\partial t)$ where p_f is the first order sound field and β the nonlinearity parameter.

In the specific case studied in Ref. 16, the pressure p_f is given by

$$p_f = p_1 \frac{r_0}{r}\left[\frac{2J_1(k_1 a \sin\phi)}{k_1 a \sin\phi}\right] e^{-\alpha_1 r} \cos(\omega_1 t - k_1 r) + p_2 \cos(\omega_2 t - k_2 z). \tag{10.31}$$

Insertion of (10.31) into (10.30) and integration over ψ yields

$$p_s \simeq \frac{\beta\omega_0{}^2 P_1 P_2 r_0}{2\rho_0 c_0{}^4 a k_1} \int_0^{R_0} \int_0^{\phi_{\text{eff}}} J(k_1 a \sin\phi) \times J_0(k_2 r \sin\phi \cos\gamma) \exp[i(k_1 \pm k_2 \sin\gamma \cos\phi + i\alpha_1)r] \times \frac{\exp[i(k_s + i\alpha_s)r]}{r'} r\, d\phi\, dr, \tag{10.32}$$

where $\omega_s = \omega_1 \pm \omega_2$ and the upper limit on the ϕ integration, ϕ_{eff}, is the angle from the axis of the acoustic beam to the first zero of the pump far-field radiation pattern.

Equation (10.32) has been solved numerically and the results tested against experiment for the sum-frequency. The results are shown in Fig. 10-16, with good agreement between theory and experiment.

10.4 Near-field Receiving.

The problem of nonlinear parametric reception in the near field of the pump signal has been treated theoretically by Rogers, Williams, and Barber in the case of the difference frequency. [17]

The geometry of the system is shown in Fig. 10-17. The circular piston (pump) of radius a is driven at the frequency $\omega_1 = k_1 c$; $k_1 a \gtrsim 100$. The velocity potential $\phi_p(x,y,z)$ describes the field of this piston. A plane wave of frequency $\omega_2 = k_2 c$ is incident as shown. The authors assume $k_2 a > 1$ and seek the second order velocity potential $\phi_2(x,y,z)$. The perturbation method

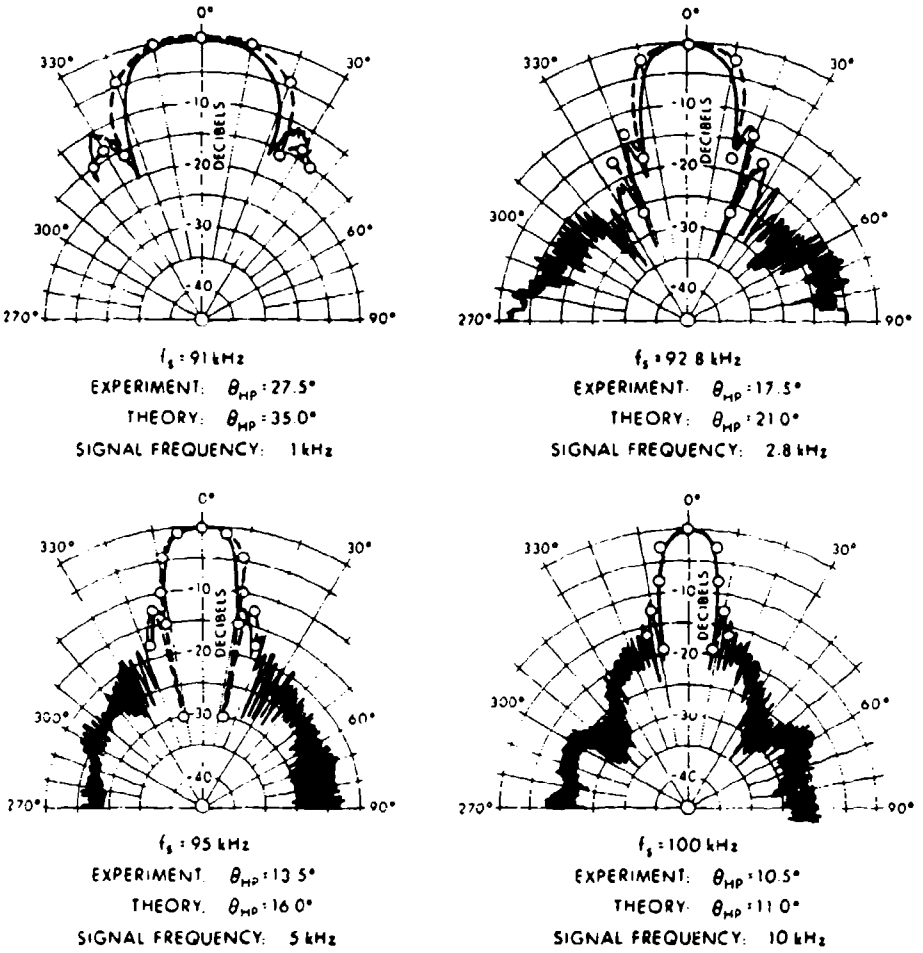

Figure 10-16.–Sum frequency patterns for a pump-receiver separation of 48 ft. Theoretical values ○ — ○, experimental values ——, F_1 = 90 kHz, P_1 = 101 dB re 1 μbar at 1 yd, P_2 = 85 dB re 1 μbar at input to parametric receiving array, f_2 = 1.0, 2.8, 5 and 10 kHz (from Barnard et al. [16]).

of analysis used is similar to that used by Ingenito and Williams [18] and described in Section 3.13. In complex notation the differential equation under study takes the form

$$\left(\nabla^2 + k_s^2\right)\phi_2(x,y,z) = -\frac{i\beta}{c}(k_1 k_2 k_s)P\phi_p(x,y,z)e^{-i\mathbf{k}_2 \cdot \mathbf{R}} \tag{10.33}$$

where R denotes the field position, $\mathbf{k}_s = \mathbf{k}_1 - \mathbf{k}_2$.

By the use of the Green's function

$$G = \frac{1}{4\pi}\sum_{n=0}^{\infty} \epsilon_n \cos\left[n(\theta - \theta_2)\right] \int_0^{\infty} \frac{1}{\mu_{ks}} J_n(\ell r_0)\, e^{-\mu_{ks}|z - z_0|}\ell\, d\ell \tag{10.34}$$

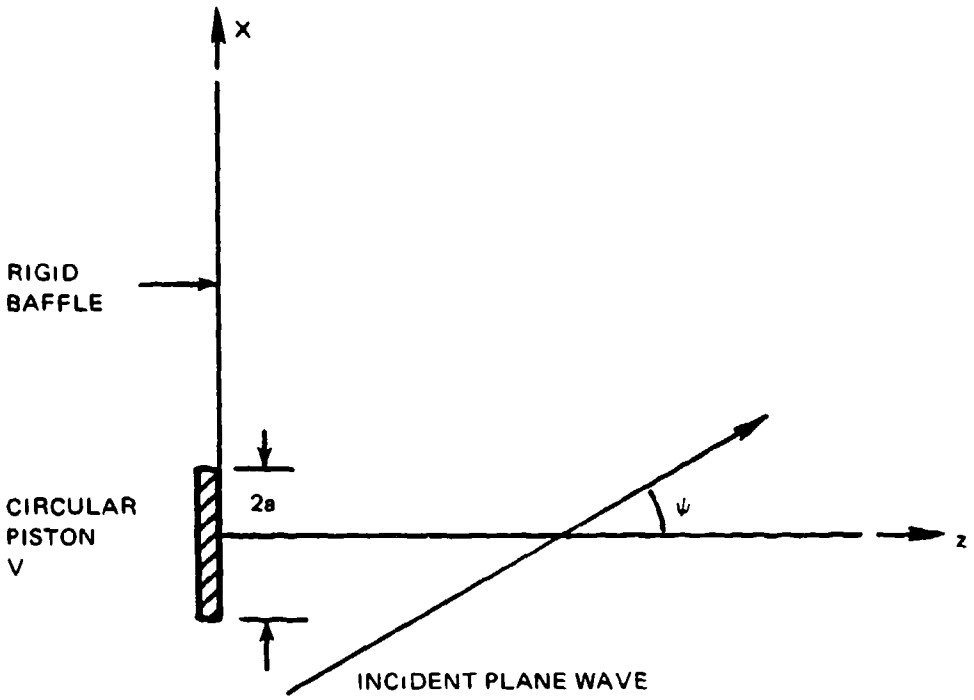

Figure 10-17.–Geometry for near-field receiving system.

where $\mu_{k_s}^2 = \ell^2 - k_s^2$, and a number of approximations, Rogers et al. were able to obtain an expression for the difference-frequency component of the particle velocity in the z direction

$$u_{2z}(r,z,\psi) = -\left[\frac{i\beta}{2c}(k_s^2 k_2)P^*\right]\phi_{pd}(r,z)F(k_2,z,\psi) \tag{10.35}$$

where

$$F(k_2,z,\psi) = \exp\left(-ik_2 z \sin^2\frac{\psi}{2}\right)\sin\left(k_s z \sin^2\frac{\psi}{2}\right)\left(k_2 \sin^2\frac{\psi}{2}\right)^{-1};$$

$\phi_{pd}(r,z)$ is the piston velocity potential calculated at the difference frequency. The quantity $F(k_2,z,\psi)$ is the response function of the end-fire array of length z to a plane wave of wave number k_2, directed at the angle ψ to the array axis.

Thus, the directional characteristic is governed entirely by the response function. This function is plotted in Fig. 10-18 for three different distances from the source.

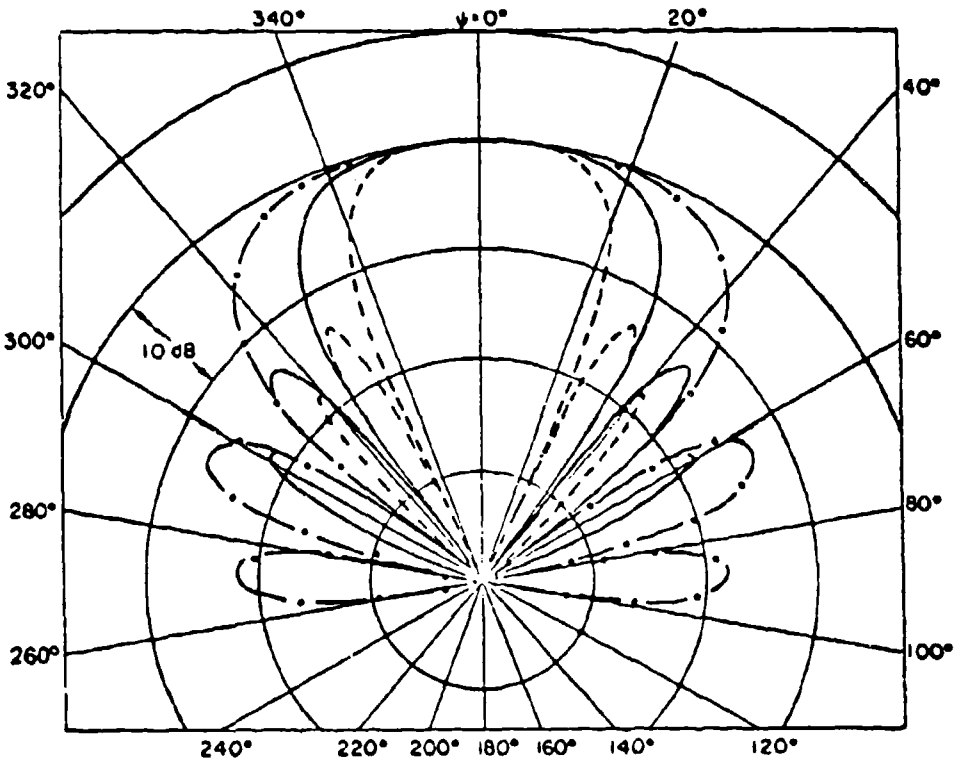

Figure 10-18.–Response curve $|F(k_2 z,\psi)|$ vs ψ. ——: $k_2 a \simeq 1$, $k_1 a = 100$ and $z = k_2 a^2/k$, which corresponds to a value for $k_2 z = 31.83$. – – – –: $k_2 z = 63.66$; —.—.: $k_2 z = 15.915$ (from Rogers et al. [17]).

10.5 Other Applications of the Parametric Array.

It was noted in the paper of Walsh [8] that the parametric array sonar was especially useful in shallow water, subbottom investigations. Two specific variations of this facet of the parametric array have been discussed by Muir, Adair et al.

In the first of these, [19] an array was designed to search for objects buried in the sea bottom, such as materials from sunken ships. Two beams in the neighborhood of 200 kHz, with a 20-kHz difference frequency were obtained from a transducer consisting of eight hollow ceramic cylinders, driven in the thickness mode, four at 210 kHz and four at 190 kHz. The difference frequency directivity pattern is shown in Fig. 10-19.

As a test, a scan was made of the ocean bottom in the absence and in the presence of a 5-in diameter aluminum sphere buried to a depth of six inches in sand. The signal strength of the difference frequency is plotted as a function of the grazing angle in Fig. 10-20. In this particular case, the ball could not be detected by use of carrier beam alone.

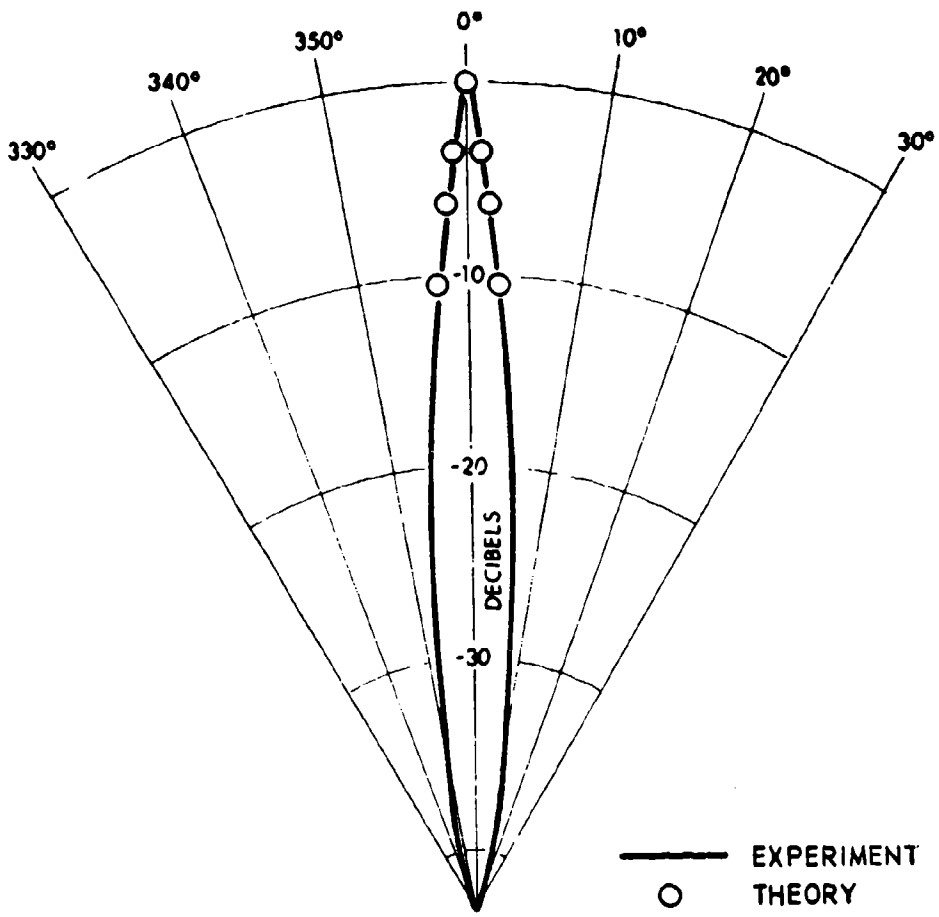

Figure 10-19.–Beam pattern for subbottom investigations (from Muir and Adair [19]).

In the second experiment, the parametric array system is compared with other conventional techniques of ultrasonography. To quote the author, it was found that, "for the range of parameters required in medical diagnostics, the nonlinear parametric array does not usually provide as good an angular resolution as does the strong focussing of large, linear arrays. The parametric array, does however, provide for a large depth of field and as regards angular resolution, it is competitive and in many cases superior to unfocussed transducers commonly used in diagnosis employing contact scanning." [20] Clearly these applications are only in exploratory stages.

10.6 Arrays of Parametric Arrays.

Berktay and coworkers [21] have considered the advantages of extending the parametric receiver to a two dimensional array of simple (single-element) parametric arrays. In the case of a single-element array, the pressure

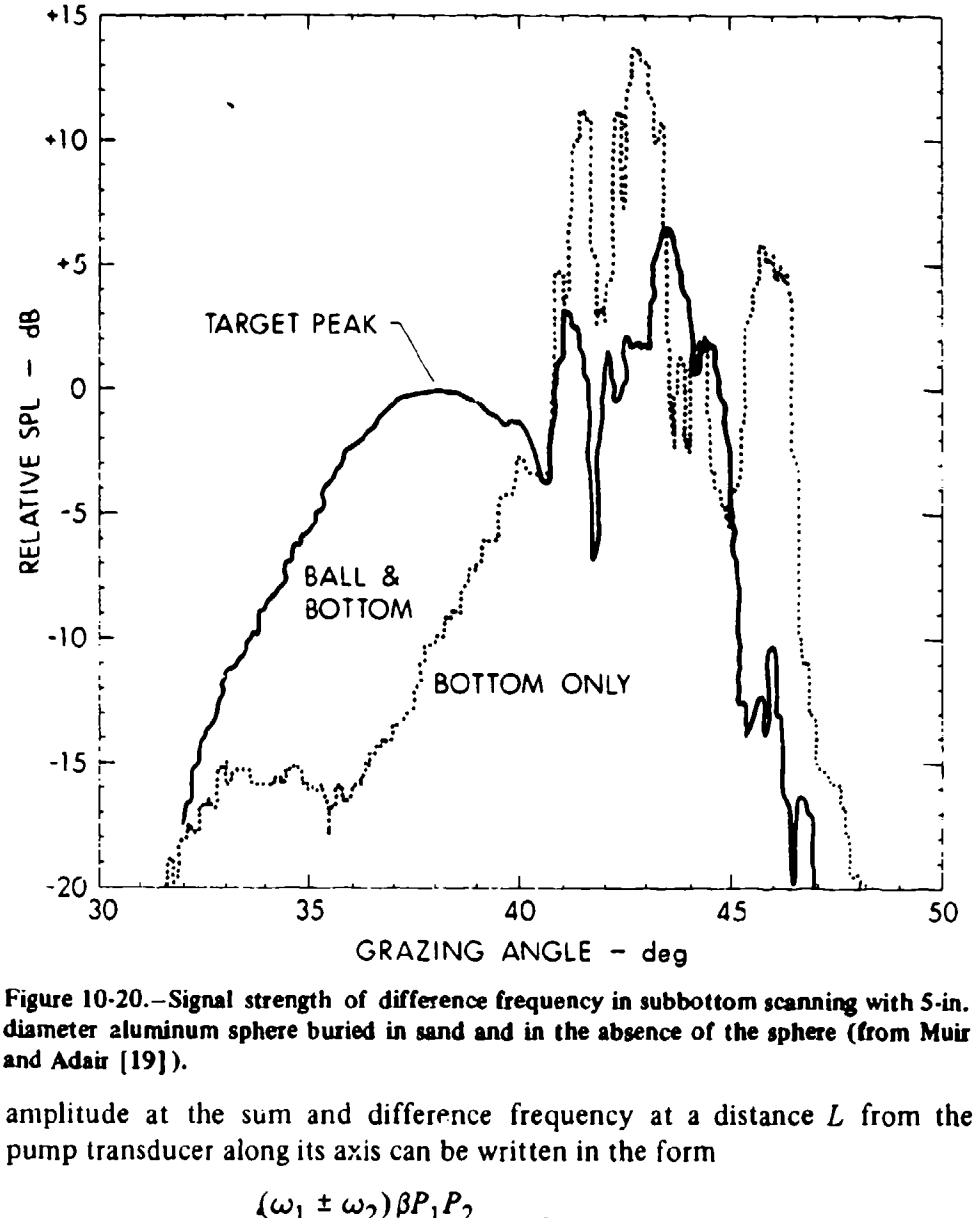

Figure 10-20.–Signal strength of difference frequency in subbottom scanning with 5-in. diameter aluminum sphere buried in sand and in the absence of the sphere (from Muir and Adair [19]).

amplitude at the sum and difference frequency at a distance L from the pump transducer along its axis can be written in the form

$$p_{\pm}(L,\theta) = -\frac{(\omega_1 \pm \omega_2)\beta P_1 P_2}{2\rho_0 c_0^3} \exp\left[-(\alpha_{\pm} + ik_{\pm})L + iM\right] D(\theta) \tag{10.36}$$

where

$$D(\theta) = \frac{\sin M}{M}$$

$$M = k_2 L \sin^2 \frac{\theta}{2}.$$

The half power point for such a beam is given by the relation

$$\theta_{HP} = 4 \sin^{-1}\left[(0.470)\left(\frac{\lambda_2}{L}\right)^{1/2}\right] \simeq 1.88\sqrt{\frac{\lambda_2}{L}},$$

so that the beam width is inversely proportional to the square root of the parameter array length L, whereas the broadside array of primary sources has a beam width proportional to $1/L$.

Now let us consider the array of parameter receivers shown in Fig. 10-21. Each element has the directivity $D(\theta)$ given by Eq. (10.36). If $D_B(\theta)$ is the directivity of an array of elements with the same geometry, but acting

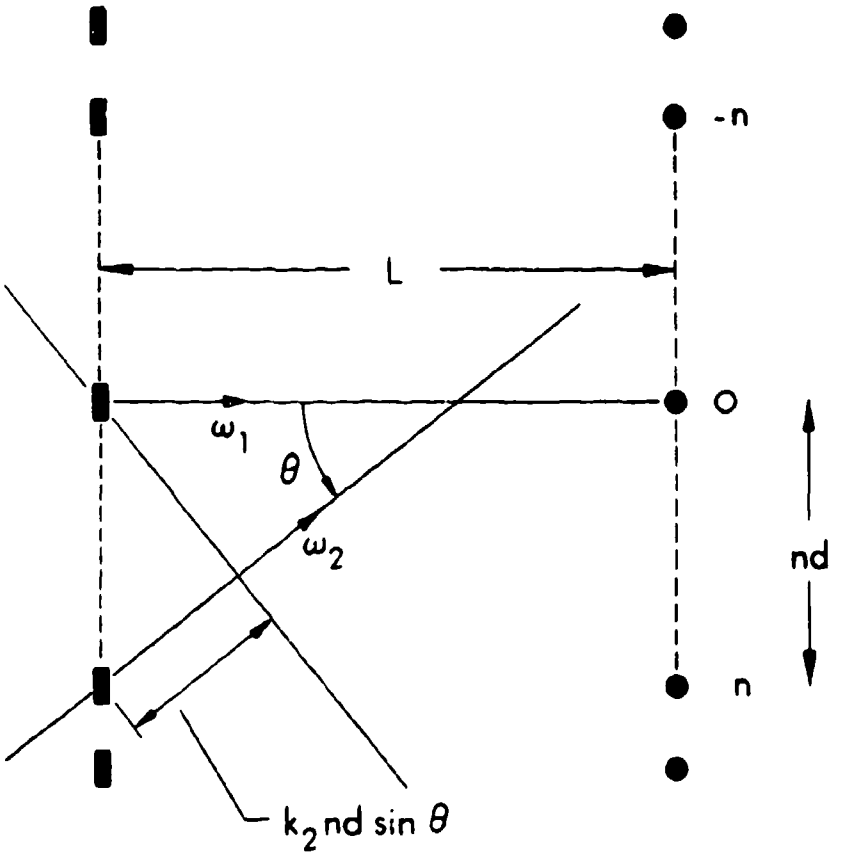

Figure 10-21.—An array of parametric receivers (from Berktay and Muir [21]).

as omnidirectional receivers, then the combined directivity function $D_T(\theta)$ will be [23]

$$D_T(\theta) = D(\theta)D_B(\theta). \tag{10.37}$$

Berktay and Muir first studied an array of two independent parallel parametric receivers placed a distance d apart. The total directivity then becomes

$$D_T(\theta) = \cos\frac{k_2 d \sin\theta}{2}\,\frac{\sin M}{M} \tag{10.38}$$

Thus the beam is further narrowed by the introduction of the second element. Figure 10-22 shows the beam pattern in the case, first for a single element [Fig. 10-22a and Eq. (10.36)] and for the two-element case [Fig. 10-22b and Eq. (10.38)].

Arrays of more than two elements can be treated similarly. It is clear that the parametric array can be manipulated according to the many techniques of sonar arrays of conventional elements, with corresponding improvement of operation.

10.7 A Standing Wave Parametric Source (SWAPS).

Rogers and Van Buren [24] have developed a mathematic model of a standing wave parametric source (SWAPS) that is designed to improve the efficiency.

The proposed SWAPS apparatus consists of a piston transducer at one end of a liquid filled cylinder. The far end of the cylinder is terminated by a pressure release wall. The piston is driven at two neighboring resonance frequencies that lie within the bandwidth of a single resonance. In either case, the difference frequency ω will be much less than either primary frequency ω_1, ω_2.

The walls of the cylinder are sufficiently rigid for all predominantly plane waves to propagate, but they and the end terminations are to be thin enough to be nearly transparent at the difference frequency.

The role of the pressure release surface is to discourage harmonic generation of the primaries. These will, of course, be generated in the forward propagation of the primary beam. Reflection from the pressure-release surface will produce a reverse sawtooth, so that the harmonic generation in the trip back to the transducer will tend to restore the original sinusoidal wave form.

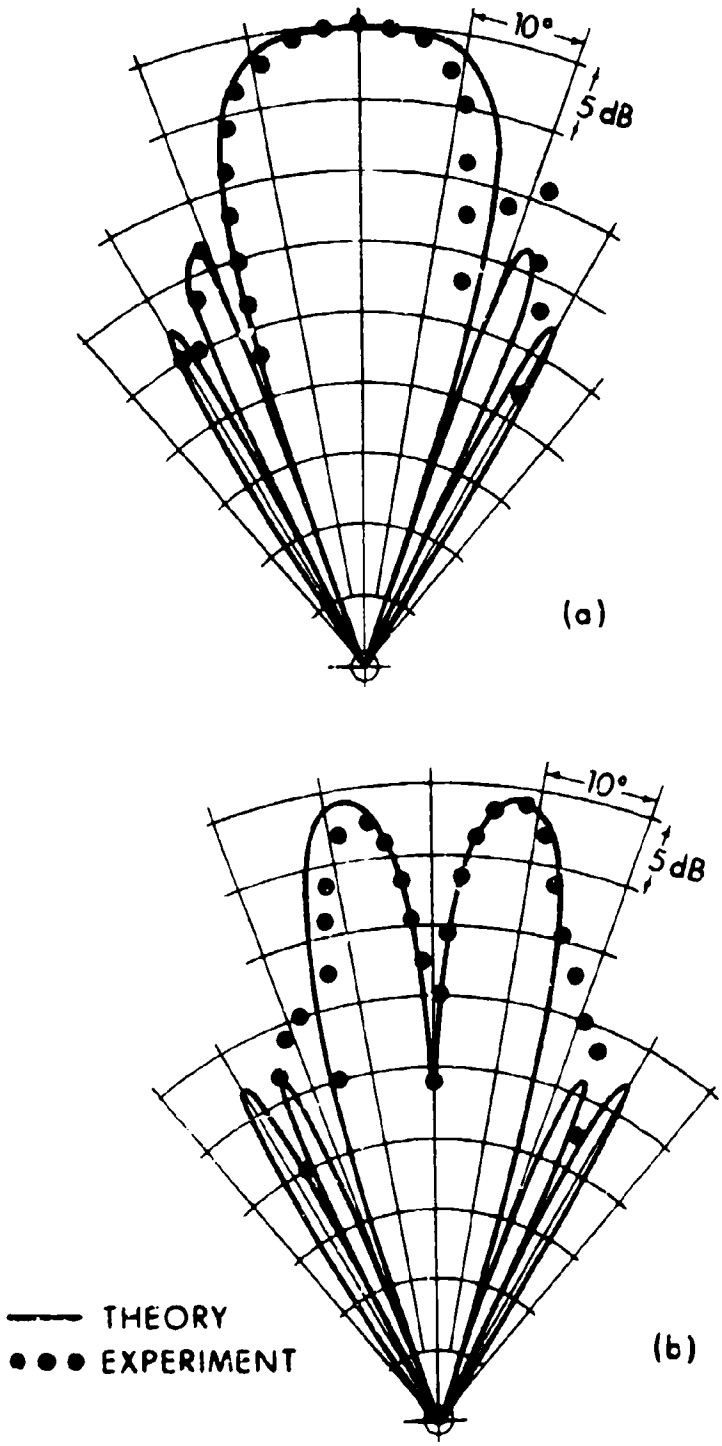

Figure 10-22.—Beam patterns for parametric areas (a) single beam pattern; (b) difference pattern for two-element case (from Berktay and Muir [21]).

The mathematic analysis follows substantially along the lines developed earlier in this chapter, and will not be reproduced here. We shall content ourselves here with giving the principal results. The pressure at the difference frequencies is given in spherical coordinates by

$$p_{-}(R,\theta) = SF(\theta)\exp\left[i(\omega_{-}t - k_{-}R - 2\phi_0)\right] \tag{10.39}$$

where S is the sound level, $F(\theta)$ the far-field pressure distribution and ϕ_0 the plane shift introduced by reflection. We now look at the results for the two special cases:

1) ω_1, ω_2 neighboring resonance frequencies:

$$\begin{aligned} S_{(\lambda/2)} &= \pi\beta_0 P_0^2 Q^2 k_{-}\frac{a^2}{16} \\ |F(\theta)| &= \frac{J_1(k_{-}a\sin\theta)\cos\theta\cos\left(\frac{\pi}{2}\cos\theta\right)}{\frac{1}{2}k_{-}a\sin\theta\cdot\frac{\pi}{4}\sin^2\theta} \end{aligned} \tag{10.40}$$

Here P_0 is the amplitude of the initial signal, β the nonlinear parameter, Q is a quality factor covering the reflection coefficients of the terminating material and the losses in propagation due to finite-amplitude distortion.

The factor $S_{\lambda/2}$ is very close to unity, while $F(\theta)$ is very nearly omnidirectional except close to the 90°-270° axis.

The total power radiated by this system is obtained by numerical integration of $|F(\theta)|^2$ with the result

$$W_{\lambda/2} = \frac{1.64\pi}{2\rho_0 c_0} S_{\lambda/2}^2. \tag{10.41}$$

2) ω_1, ω_2 both within bandwidth of a single resonance:

In this case,

$$S_s \simeq \beta\rho_0 P_0^2 Q^2 k_{-}\frac{a^2\ell}{8} \tag{10.42}$$

where ℓ, the effective length of SWAPS, $\simeq (2m + 1/4)\lambda$, m an integer;

$$W_s \simeq \frac{4\pi S_s^2}{2\rho_0 c_0}. \tag{10.43}$$

The output of SWAPS can be compared with the output of the traveling wave parametric source of Westervelt (TWAPS). For the case (2), with the SWAPS system filled with sea water,

$$\frac{S_s}{S_T} = Q^2 \alpha' \ell \tag{10.44}$$

where the subscript T refers to TWAPS, α' is the absorption coefficient of sea water and

$$\frac{W_s}{W_T} = 2Q^4 \alpha' \ell \frac{k\ell}{\pi} \simeq \left(\frac{S_s}{S_T}\right)^2. \tag{10.45}$$

Here Q is as yet undetermined, but it would appear that the system is a more efficient radiator of the difference frequency, principally because near-resonance conditions can be maintained in the tube and competing nonlinear interactions are inhibited through the use of the pressure-release reflection. In addition, the operating liquid in SWAPS can be chosen with different parameters of nonlinearity and absorption coefficient so as to increase the output of the system.

There is, however, a possible problem that by constraining the interaction to a relatively narrow tube, one has interfered with the phase relations of individual portions of the signal—both primary and scattered—so that the gain may be considerably lessened.

10.8 Nonlinear Interactions in Intense Noise.

The preceding portions of this chapter offer substantial evidence of the powerful role of the source function [Eq. (9.29)] developed by Westervelt in nonlinear interactions and we have indeed reviewed a number of interactions of pairs of sinusoidal waves, as well as the effect of a pulse of finite amplitude [Eq. (9.54)].

These analyses suggest a further extension, to the case of more than two incident frequencies, or to the case of a nondeterministic amplitude variation, such as finite amplitude noise.

Such an extension has not yet been made, but a recent study by Pestorius and Blackstock [25] of finite amplitude noise propagation in tubes views this same problem from the weak-shock point of view. While the subject matter is close to that of Section 3.14, it seemed more appropriate to insert it at this later point in the text, after interactions had been more fully discussed.

The weak shock theory developed in Chapter 3 indicates the progressive distortion of a sinusoid (see especially Fig. 3-10). From Eq. (3.28) we have, for $u \ll c_0$, the rate of propagation dx/dt of a given displacement velocity $u = \dot{\xi}$

$$\frac{dx}{dt} = c_0 + \beta u. \tag{10.46}$$

At the discontinuity of a shock wave, this form becomes

$$\frac{dt}{dx} \simeq \frac{1}{c_0}\left[1 - \frac{\rho}{c_0}\frac{(u_a + u_b)}{2}\right], \tag{10.47}$$

where u_a and u_b are the values of u just ahead of and just behind the shock.

It is convenient to rewrite and approximate Eq. (10.46) in the form

$$\frac{dt}{dx} = \frac{1}{c_0 + \beta u} \simeq \frac{1}{c_0}\left(1 - \frac{\beta u}{c_0}\right). \tag{10.48}$$

Pestorius and Blackstock began with this relation and then proceeded to write Eq. (10.46) in the form of a difference relation, solving the latter by use of a computer. The method is reminiscent of the analysis of a finite-amplitude sine wave by Fox and Wallace. [26] That is, they considered the propagation of the wave through a small distance x. Then the difference in time corresponding to (10.48) is

$$t_{new} = t_{old} - \beta u_{old}\frac{x}{c_0^2}. \tag{10.49}$$

The new wave form is then tested for multivaluedness. If it is still single-valued, the process is repeated. If it becomes multivalued, Eq. (10.47) is used; the shock is located and particle velocities are corrected.

These shocks can overtake other portions of a complex waveform, and as the authors point out: "Through the progression of growing, decaying and merging, the shocks ultimately determine the shape and amplitude of the wave." [27]

The experimental problem to which Pestorius and Blackstock addressed themselves involved propagation in a tube, and required the introduction of a computational procedure to take into account both the attenuation and dispersion that are characteristic of tube propagation.

The algorithms developed made it possible for them to predict the behavior of both single pulses and noise in propagation in an air-filled aluminum tube of 96-ft. length, 2-in. i.d.

To test the apparatus, a sinusoidal source of 2-kHz sound with an initial sound pressure level (SPL) of 160 dB re 0.0002 μbar was employed. Figure 10-23 shows the received pulse shape (both experimental and computed) for distances of 1, 13 and 85 feet from the source. The solid curves were computed by the algorithm mentioned, taking tube effects into account, while the dashed curves are the corresponding results with the omission of wall effects. The most conspicuous feature of these curves is the round off of the positive peak, which is the result of wall-induced dispersion.

The case of intense noise was considered both theoretically and experimentally. The results are shown in Fig. 10-24 for noise with an SPL of 160 dB in the frequency range 500-3520 Hz at a distance of 85 feet from the source. Figure 10-24 (a) is the experimental pulse, (b), that computed from weak shock theory and (c), that computed from weak shock theory taking wall effects into account.

Figure 10-25 shows the experimental and computed (with wall effects) values at various distances from the source.

Two conclusions can be drawn from these data. First, roundedness of the positive peaks is indeed characteristic of tube propagation for noise as well as single pulses. Second, the number of axis crossings decreases with propagation and the overall wave form becomes more regular as portions of the wave are overtaken and "eaten up" by the stronger shocks. Thus the frequency distribution of the noise is significantly altered because of the nonlinear effects, with the upper and lower ends of the spectrum gaining at the expense of the middle. The similarity of this behavior with that of the absorption of sound by sound (Section 9.6) should also be noted.

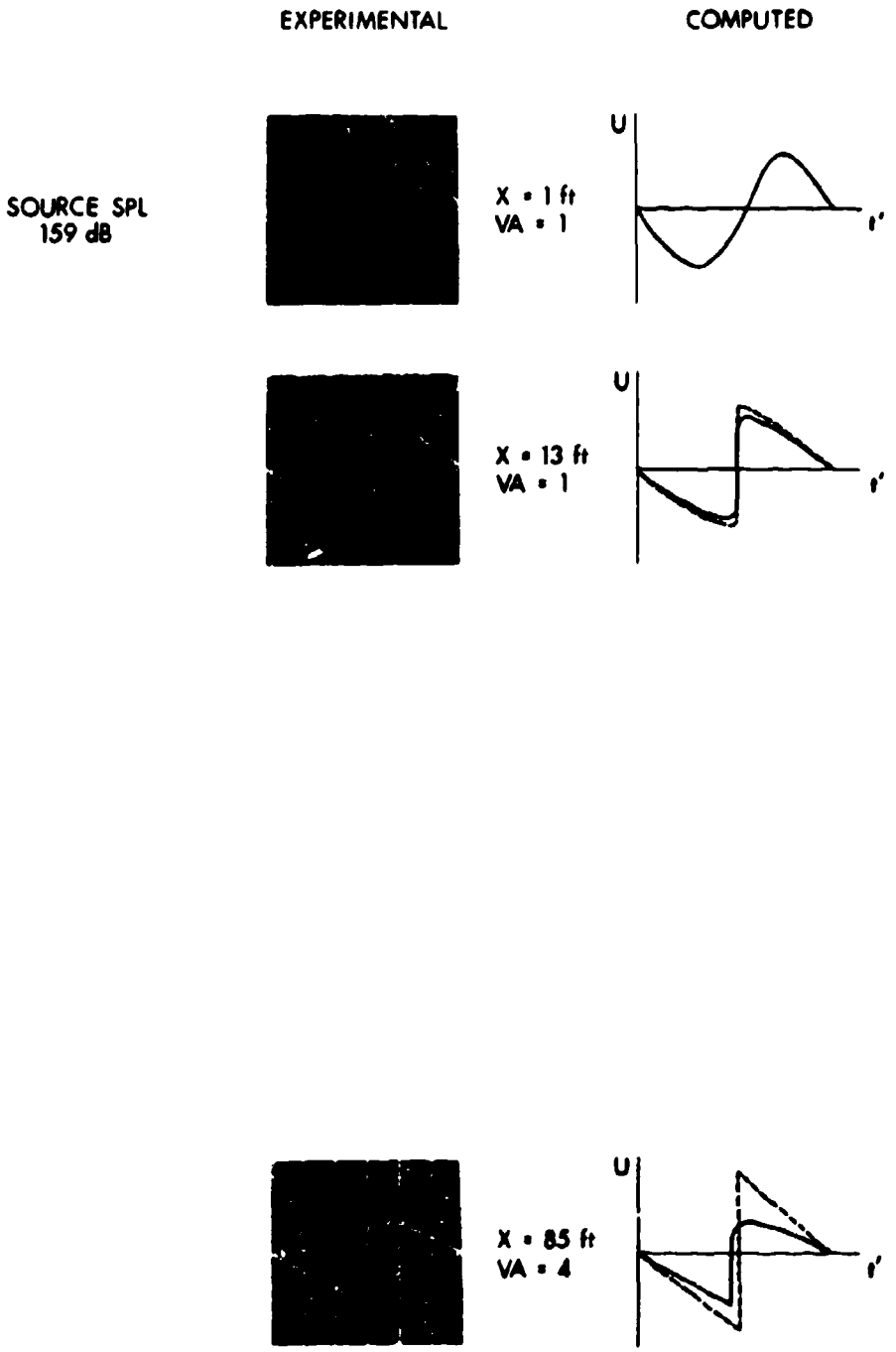

Figure 10-23.–Wave distortion in an air-filled aluminum tube of 2-in. diameter (from Pestorius and Blackstock [27]).

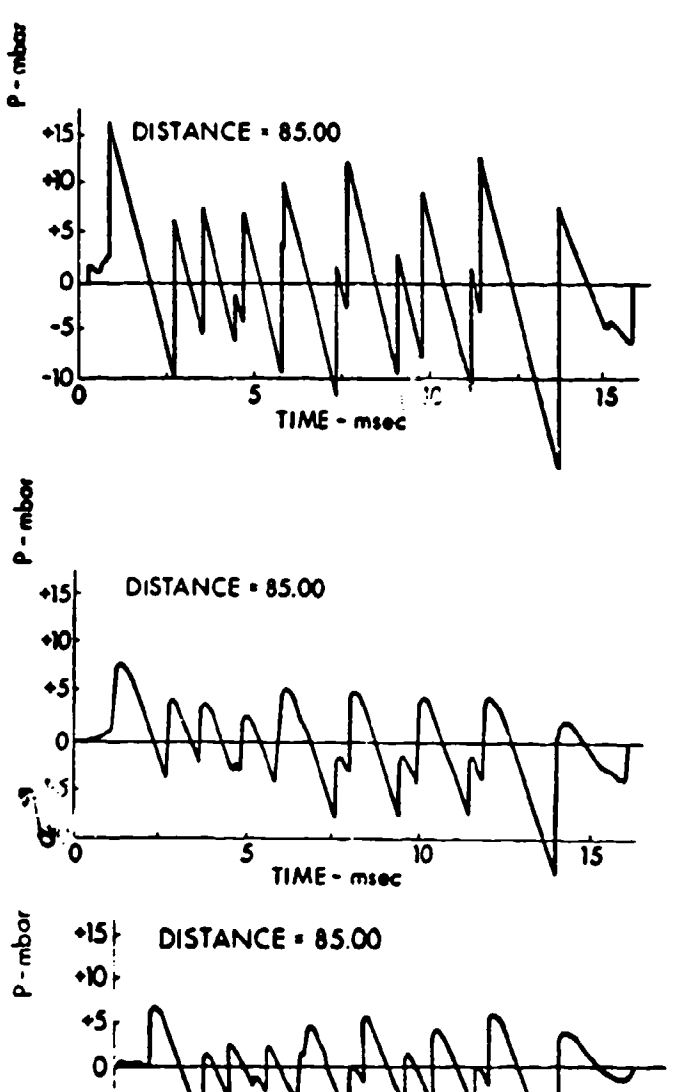

Figure 10-24.—Behavior of noise burst in propagation along 85 feet of a 2-in. diameter aluminum tube. (1) Experimental signal; (b) signal computed from weak shock theory; (c) weak shock theory plus wall effects (from Pestorius and Blackstock [27]).

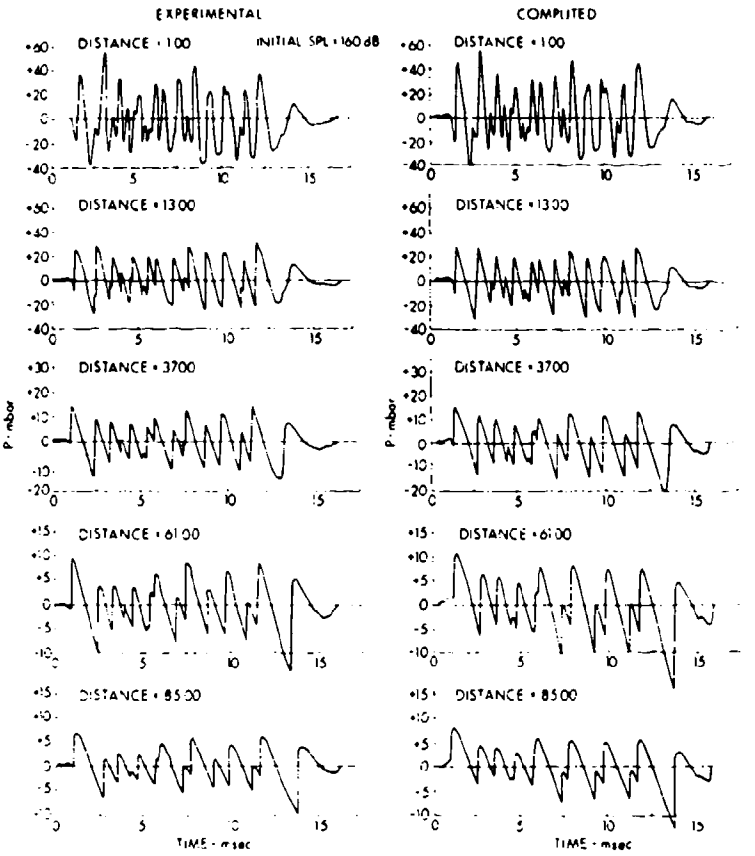

Figure 10-25.–Experimental and computed distortions of a noise pulse in propagation in air-filled aluminum tube (from Pestorius and Blackstock [27]).

REFERENCES

Chapter 10

1. P. J. Westervelt, JASA **35**, 535 (1963).
2. H. O. Berktay, J. Sound Vib. **2**, 435 (1965).
3. H. M. Merklinger, Symposium on Nonlinear Acoustics, University of Birmingham (U.K.), April 1,2, 1971; Ph.D. thesis, University of Birmingham, June 1971; JASA **52**, 122 (1972).
4. H. O. Berktay and D. J. Leahy, Preprint, Electronic and Electrical Engineering Department, University of Birmingham (U.K.), 1972, JASA **55**, 539 (1974).
5. R. H. Mellen, W. L. Konrad and D. G. Browning, Proc. Symposium on Nonlinear Acoustics, Birmingham, U.K., April 1971, pp. 184-193; R. H. Mellen, D. G. Browning and W. L. Konrad, JASA **49**, 932 (1971); R. H. Mellen and M. B. Moffett, JASA **52**, 122 (1972) and private communications to author.

6. T. G. Muir and J. G. Willette, JASA **52**, 1481 (1972).
7. G. Pearce and H. O. Berktay, JASA **52**, 123 (1972) and private communication to author.
8. G. M. Walsh, Electronic Progress **13**, No. 1, 17 (1971).
9. H. O. Berktay and J. A. Shooter, JASA **53**, 550 (1973).
10. J. L. S. Bellin and R. T. Beyer, JASA **34**, 1051 (1962).
11. For a discussion of impulse response, see C. W. Horton, Sr., Signal Processing of Underwater Acoustics Waves, Government Printing Office, 1969, Ch. 2.
12. P. J. Westervelt, Acta Phys. Polonica XXVII, (1965), esp. Eq. 3.6.
13. M. B. Bennett, Ph.D. thesis, University of Texas at Austin, 1973.
14. H. O. Berktay, J. Sound Vib. **2**, 462 (1965); H. O. Berktay and C. A. Al-Temimi, J. Sound Vib. **9**, 295 (1969).
15. W. L. Konrad, R. H. Mellen and M. B. Moffett, Naval Underwater Systems Center Tech. Mem. No. PA4-304-71, Dec. 9, 1971.
16. G. A. Barnard, J. G. Willette, J. J. Truchard and J. A. Shooter, JASA **52**, 1437 (1972).
17. P. H. Rogers, A. O. Williams, Jr. and J. M. Barber, "Nonlinear Detection of a Low-Frequency Plane Wave by a Directional Circular Piston Beam," NRL Report 7484, Dec. 29, 1972.
18. F. Ingenito and A. O. Williams, Jr., JASA **49**, 319 (1971).
19. T. G. Muir and R. S. Adair, "Potential Use of Parametric Sonar in Marine Archaeology," Paper at 83rd Meeting, Acoustical Society of America, April 18-21, 1972: JASA **52**, 122(A) (1972).
20. T. G. Muir, C. M. Talkington, B. S. Shaw, R. S. Adair and J. G. Willette, "Parametric Echoscanner for Biomedical Diagnostics," Paper at 84th Meeting, Acoustical Society of America, Nov. 28-Dec. 1, 1972; JASA **53**, 382(A) (1973).
21. H. O. Berktay and T. G. Muir, JASA **53**, 1377 (1973); H. O. Berktay and C. A. Al-Temimi, J. Sound Vib. **9**, 295 (1969).
22. H. O. Berktay and J. A. Shooter, JASA **54**, 1056 (1973).
23. R. J. Urick, Principles of Underwater Sound for Engineers, McGraw-Hill, N.Y. (1967), p. 45.
24. P H. Rogers and A. L. Van Buren, Preprint.
25. F. M. Pestorius and D. T. Blackstock, JASA **54**, 302(A) (1973) and preprint. For earlier work on finite amplitude noise, see W. A. Burnett and D. Ackerman, "Propagation Distortion of Large Amplitude Acoustic Noise," Wright-Patterson Air Force Base, Ohio. Report No. WADD Tech. RPT, 60-233, May, 1960; D F Pernet and R. C. Payne, "Propagation of Finite Amplitude Sound Waves in Tubes," National Physical Laboratory AERO Report Ac 43, November 1969.
26. F. E. Fox and W. A. Wallace, JASA 26, 994 (1954).
27. F. M. Pestorius and D. T. Blackstock, preprint.

Chapter 11

NONLINEAR PROPAGATION IN SOLIDS

11.1 General Aspects.

Problems in solid state acoustics are not only classified separately, historically, from other branches of acoustics but are generally performed by a different group of researchers, who are interested in the sound wave only as a tool in the study of the properties of matter. This is not wholly the case in nonlinear acoustics, but it still seems appropriate to treat all nonlinear aspects of acoustics in solids as a separate chapter.

The difficulty for the acoustician is one of selection. The concept of the phonon was generated by the Soviet school of theoretical physicists in the early thirties [1] and applied to the analysis of thermal vibrations, or lattice vibrations of the solid. If the totality of thermal vibrations of the lattice is considered as a sea of phonons, then such a classical problem as that of electrical conduction can be solved in terms of "collisions" of the electrons with the lattice, or alternatively, of electron-phonon interaction.

By proceeding in this fashion, one is led to the consideration of thermal conduction in the same manner. But this requires internal adjustment of the phonon population—i.e., of the interaction of different groups of phonons with one another.

Finally then, the passage of a sound beam through a lattice is a special case where the rhythmically advancing phonons (*coherent phonons*) undergo collisions with the lattice phonons, producing a new set of phonons, this time incoherent in nature.

Both thermal conduction and sound dissipation are therefore cases of phonon-phonon interaction. But such interactions have been treated at length in Chapter 9 as instances of nonlinear acoustics. In this sense, then, virtually all of solid state acoustics could be included under the label "nonlinear".

It is, however, not our intention to repeat the extensive surveys of this field given elsewhere. [2] A very brief background survey will suffice. [2a]

We begin with the concept of the phonon. In complete analogy with the photon description of electromagnetic waves, elastic waves can be represented by quasi-particles called *phonons*. A phonon has energy $\hbar\omega$ and acts as if it has momentum $\hbar\mathbf{q}$ (often called the *quasimomentum*). The increase or decrease of the energy of an elastic wave corresponds to the creation or annilation of phonons.

The quasiparticle that is the phonon has some characteristics that differ from that of a true particle. Thus, suppose a phonon (in a crystalline solid) with wavevector $\mathbf{q}$ combines with any system of wavevector $\mathbf{k}$, a phonon with wavevector $\mathbf{q}'$ resulting. Conservation of momentum requires that

$$\mathbf{q} + \mathbf{k} = \mathbf{q}' + \mathbf{G} \tag{11.1}$$

for that process, where $\hbar G$ represents the momentum imparted to the crystal as a whole. If $\mathbf{q}'$ lies outside the first Brillouin zone (see below), then $\mathbf{q}' + \mathbf{G}$ is the wavevector inside the first Brillouin zone that describes the same physical motion as $\mathbf{q}'$. If $\mathbf{k}$ is the wavevector of a phonon, so that three phonons are involved in Eq. (11.1) then $\mathbf{g}$ may be equal to zero (called a *normal* or N-process) or differ from zero (an *Umklapp* or U-process).

11.2 Lattice Vibrations in Crystals. The Debye Approximation.

According to the modern theory of solids, the motions of the atoms of a solid can be described as elastic waves propagated under the action of the nearly elastic interatomic forces. In the classical theory, the medium is treated as an elastic continuum. Both the continuous and elastic properties of such a medium are approximations that need further consideration. The effects of a discrete crystal structure of the propagation of elastic waves are most easily seen from a consideration of the simplest case—a linear chain of identical atoms. The relation between the frequency and the wave number q for this case can be shown to be

$$\omega = \left(\frac{4\beta}{M}\right)^{1/2} \left|\sin\left(\frac{qa}{2}\right)\right| \tag{11.2}$$

where a is the spacing between atoms, each with mass M, and β is the interatomic force constant. The corresponding dispersion curve is shown in Fig. 11-1. When the wavelength is much longer than the atomic spacing a, the

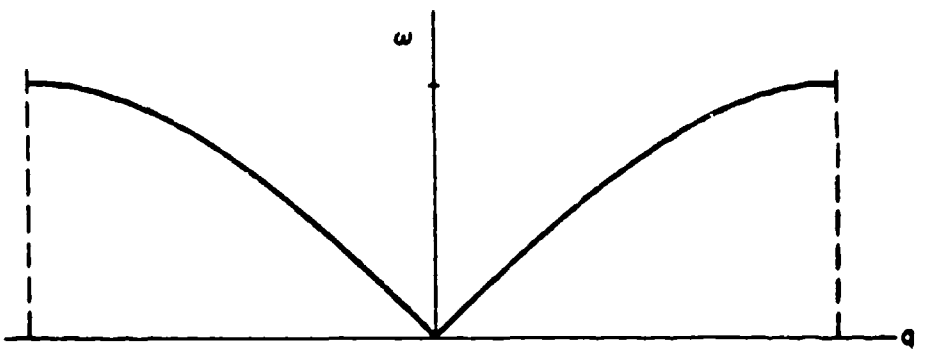

Figure 11-1.–Dispersion curve for a monatomic linear lattice.

chain can be treated as a continuum and $\omega = c_0 q$. The phase velocity c_0 is then the same as the group velocity $\partial\omega/\partial q$, and is independent of frequency—there is no dispersion. As the wavelength becomes shorter, the discrete nature of the lattice produces dispersion. In fact, when $\lambda = 2a$, the wave is no longer a progressive wave, but is a standing wave. The adjacent particles are then 180° out of phase; the group velocity has vanished and no energy is transported.

Since only the motion of the atoms has physical significance, all waves of length shorter than $2a$ describe exactly the same physical motions that can be represented by other waves with wavelength greater than $2a$ (Fig. 11-2). All unique physical motions are then represented by waves with wavenumbers between $q = -\pi/a$ and $q = \pi/a$. This region is called the *first Brillouin zone.* If there are N atoms in the chain, then there are N discrete vibrational states located in the first Brillouin zone.

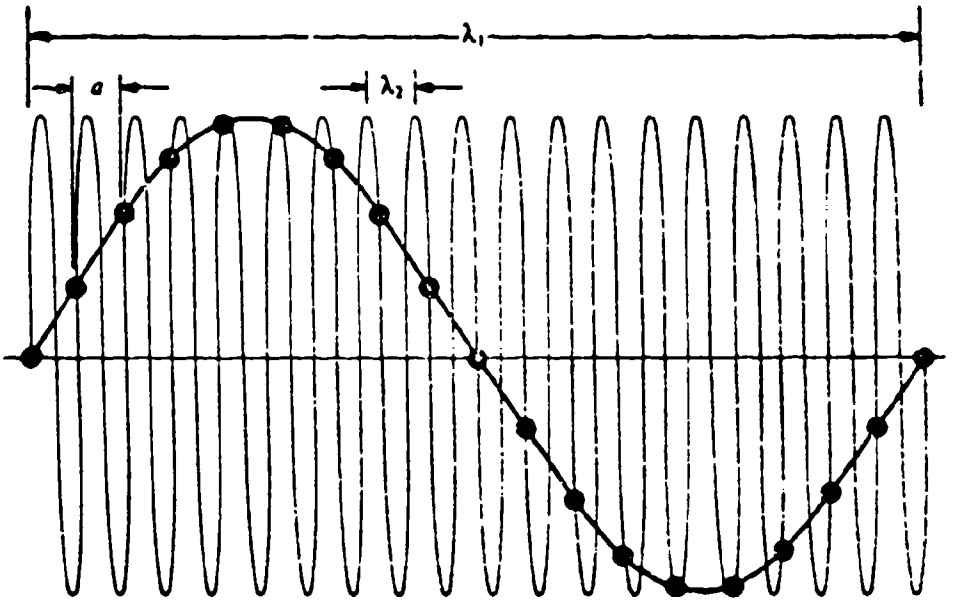

Figure 11-2.—Two different wavelengths that could represent the same physical motion of a linear chain (from Beyer and Letcher [2a]).

In a real, three-dimensional crystal, the waves can propagate in all directions, and for each direction there are three polarizations Each propagation direction and polarization will have its own dispersion curve.

Thus, for any direction of propagation in a solid, three different modes with mutually orthogonal displacements are possible. However, the anisotropy of crystalline solids strongly affects the elastic waves. For an arbitrary propagation direction, the three modes will not be pure longitudinal or pure

transverse waves, and the energy flux will generally not be exactly in the direction of wave propagation.

The fundamental relations for strains in a solid is given by the strain tensor u_{ik}, whose components are (recall Eq. 1).

$$u_{ij} = \frac{1}{2}\left(\frac{\partial \xi_i}{\partial x_j} + \frac{\partial \xi_j}{\partial x_i} + \frac{\partial \xi_\ell}{\partial x_i}\frac{\partial \xi_\ell}{\partial x_j}\right). \tag{11.3}$$

If one deals with small deformations only (the linear case), the third term can be neglected. In such a case, Hooke's law of elasticity applies; this can be written in tensor form

$$T_{ij} = c_{ijk\ell}u_{k\ell} \tag{11.4}$$

where $c_{ijk\ell}$ is the fourth rank elastic modulus tensor.

When the direction of propagation is a pure mode direction, one longitudinal and two transverse polarizations exist. The particle displacement is either parallel or perpendicular to the propagation direction. In other, nonpure-mode directions, the branch with the greatest phase velocity is usually identified as the longitudinal branch.

Debye Approximation.

In order to calculate in detail the thermal properties of a particular crystal lattice and the resultant effect of the thermal lattice vibrations of an ultrasonic wave, one would need to know not only the dispersion curve for all directions of propagation and polarization, but also the density of vibrational states as a function of frequency. This would be a formidable task, but one which can be avoided by using the simple but remarkably successful Debye approximation.

The Debye approximation treats the solid as a continuum. As a result, the two transverse modes become identical and the speeds of propagation are independent of frequency. Although a true continuum has an unlimited number of normal modes of vibration (there being no restriction of the wavelength) the Debye approximation limits the number of normal modes to the number of degrees of freedom of the actual solid. If the crystal contains $N/3$ atoms per unit volume, each with three degrees of freedom, the number of normal modes will be limited to N. If $D(\omega)\,d\omega$ is the number of modes per unit volume with frequency between ω and $\omega + d\omega$, then the cutoff fre-

quency, ω_D, which is characteristic of the Debye approximation, is defined by the relation

$$\int_0^{\omega_D} D(\omega)\, d\omega = N. \tag{11.5}$$

The density of states $D(\omega)$ for a solid continuum can be shown [3] to be

$$D(\omega) = \frac{\omega^2}{2\pi^2}\left(\frac{1}{c_{\text{long}}^3} + \frac{2}{c_{\text{tr}}^3}\right) \tag{11.6}$$

where c_{long} and c_{tr} are the phase velocities for longitudinal and transverse waves, respectively. This is shown in Fig. 11-3. Then, from Eq. (11.5), we have

$$\omega_D = \left[6\pi^2 N\left(\frac{1}{c_{\text{long}}^3} + \frac{2}{c_{\text{tr}}^3}\right)\right]^{1/3}. \tag{11.7}$$

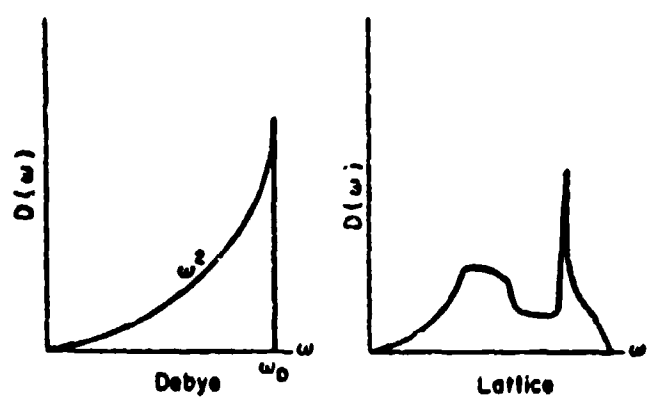

Figure 11-3.–Density of phonon states by the Debye approximation and by a more exact lattice theory (from Levy [3]).

The Debye temperature Θ_D is defined by

$$\Theta_D = \frac{\hbar\omega_D}{k_B} = \left[\frac{6\pi^2\hbar^3 N}{k_B^3}\left(\frac{1}{c_{\text{long}}^3} + \frac{2}{c_{\text{tr}}^3}\right)^{-1}\right]^{1/3} \tag{11.8}$$

where k_B is the Boltzmann constant. For an anisotropic crystal, suitable averaging of c_{long} and c_{tr} over possible directions is needed to obtain a representative Θ_D. If an effective sound velocity c_0 is used, Eq. (11.8) becomes

$$\Theta = \frac{\hbar c}{k_B}(2\pi^2 N)^{1/3} \tag{11.9}$$

where

$$\frac{3}{c_0^3} \equiv \frac{1}{c_{\text{long}}^3} + \frac{2}{c_{\text{tr}}^3}. \tag{11.10}$$

The number of thermally excited phonons in the Debye approximation is given by

$$n = \int_0^{\omega_D} D(\omega)n(\omega)d\omega, \tag{11.11}$$

where $n(\omega) = (e^{\hbar\omega/k_BT} - 1)^{-1}$, which is known as the Bose-Einstein distribution function, is the probability that a phonon is in a state with frequency ω. Then

$$n = \int_0^{\omega_D} \frac{\omega^3}{2\pi^2 c_0^3} \frac{1}{e^{\hbar\omega/k_BT} - 1} d\omega$$

$$= \frac{k_B^3 T^3}{2\pi^2\hbar^3 c_0^3} \int_0^{x_D} \frac{x^2}{e^x - 1} dx \tag{11.12}$$

where $x_D = \hbar\omega_D/k_BT = \Theta_D/T$. In the region $T \ll \Theta$, (11.12) becomes

$$n = 3N\left(\frac{T}{\Theta_D}\right)^3 \int_0^{\infty} \frac{x^2}{e^x - 1} dx. \tag{11.13}$$

In a similar manner, the total thermal energy in the Debye approximation is given by

$$U = \int_0^{\omega_D} \hbar\omega D(\omega)n(\omega)d\omega \tag{11.14}$$

which becomes

$$U = 3Nk_B T\left(\frac{T}{\Theta_D}\right)^3 \int_0^{\Theta_D/T} \frac{x^3}{e^x - 1}\, dx. \tag{11.15}$$

11.3 Nonlinear Lattice Waves.

In an ideally elastic medium, propagating waves are represented by functions that are solutions of the linear wave equation and therefore obey the principle of superposition. Even a very small amplitude wave in a real solid however, will only approximate this linear behavior. Fundamental nonlinearities, as in the definition of strain [Eq. (11.3)] are assumed to be negligible in order to derive the linear wave equation. It is a common occurrence that elastic waves do, in fact, interact with one another. Quantum mechanically, one can speak of phonon-phonon interactions. Such familiar phenomena as lattice thermal resistivity, thermal expansion and the maintenance of an equilibrium distribution of thermal phonons are possible only if the lattice waves behave in a nonlinear way.

A. *Grüneisen Constant.* A particular lattice vibration mode can be characterized by its wave vector $\mathbf{q}$, and its polarization p. The anharmonicity of the lattice can be expressed by the change of sound velocity (or elastic constants) as a function of the strain or, equivalently, by the change in the frequency $\omega = \omega(\mathbf{q},p)$ of the mode $\mathbf{q},p$ with changing strain. This latter change is defined in terms of the *Grüneisen number* for the effect of a strain ϵ_{jk} on the frequency of mode $\mathbf{q},p$. This number, $\gamma_{jk}(\mathbf{q},p)$ is defined to be

$$\gamma_{jk}(\mathbf{q},p) = -\frac{1}{\omega_0(\mathbf{q},p)} \frac{\partial\omega(\mathbf{q},p)}{\partial\epsilon_{jk}} \tag{11.16}$$

where the strains are defined as

$$\begin{aligned} \epsilon_{jk} &= u_{j\ell} = \frac{\partial\xi_j}{\partial x_k} \quad \text{if} \quad j = k \\ &= 2u_{jk} = \frac{\partial\xi_j}{\partial x_k} + \frac{\partial\xi_k}{\partial x_j} \quad \text{if} \quad j \neq k, \end{aligned} \tag{11.17}$$

and where $\omega_0(\mathbf{q},p)$ is the mode frequency for zero strain.

If the strain involved is a pure dilation, Eq. (11.16) becomes

$$\gamma(\mathbf{q},p) = \frac{V}{\omega_0(\mathbf{q},p)} \frac{\partial\omega(\mathbf{q},p)}{\partial V} = \frac{d\ln\omega(\mathbf{q},p)}{d\ln V}. \tag{11.18}$$

If the further, rather unrealistic, assumption is made that all modes have the same γ, and if we use the Debye approximation, Eq. (11.18) becomes

$$\gamma = \frac{d \ln \omega}{d \ln V} = \frac{d \ln \Theta_D}{d \ln V} . \tag{11.19}$$

The quantity γ in Eq. (11.19) is the Grüneisen constant, a single parameter that describes the anharmonic properties of a crystal in much the same way that the Debye temperature describes the elastic properties. The Grüneisen constant can be written in terms of various thermodynamic parameters:

$$\gamma = \frac{3\beta}{\kappa_T C_V} = \frac{3\beta B}{C_V} \tag{11.20}$$

where β is the linear thermal expansion coefficient, κ_T the isothermal compressibility, B the bulk modulus and C_V the heat capacity per unit volume at constant volume.

In the real case, γ is of course a more complicated quantity. For many purposes, however, one can define [4] an average Grüneisen constant from (11.16):

$$\gamma = \frac{\Sigma \gamma (\mathbf{q},p) C(\mathbf{q},p)}{\Sigma C(\mathbf{q},p)} \tag{11.21}$$

This satisfies Eq. (11.20) with the heat capacity of the mode $(\mathbf{q},p)$ serving as the weighting factor.

B. *Finite Deformation of Solids.* We have already noted the form of Hooke's law [Eq. (11.4)]. In the same notation, the elastic potential energy is given by

$$V = \frac{1}{2} c_{ijk\ell} \epsilon_{ij} \epsilon_{k\ell} . \tag{11.22}$$

The $c_{ijk\ell}$ are commonly called the second-order elastic constants, for the reason that they appear in an expression that is second order in the strains. Nevertheless, they represent linear elastic phenomena.

Expressions such as (11.4) and (11.22) can be modified to describe nonlinear effects by letting $c_{ijk\ell}$ (and, therefore, the speed of sound) be dependent on the strain. Then the stress will no longer be directly proportional to the strain, and the potential energy will no longer be merely quadratic in the strain. A convenient form for the generalization is in terms of higher order elastic constants.

A point at position vector **a** in the unstrained solid is moved to point **x** by a finite strain. This displacement of the particle is $\boldsymbol{\xi} = \mathbf{x} - \mathbf{a}$ or, for each component, $\xi_i = x_i - a_i$. The strain, which is given by Eq. (11.3), can also be written

$$u_{ij} = \frac{1}{2}\left(\frac{\partial x_\varrho}{\partial a_i}\frac{\partial x_\varrho}{\partial a_j} - \delta_{ij}\right) \tag{11.23}$$

where δ_{ij} is the Kronecker delta.

The ratio of a volume element in the new coordinate system (**x**) to the volume element in the unstrained system (**a**) is the Jacobian determinant. Hence the ratio of the unstrained density to the density in the strained state is given by

$$\frac{\rho_0}{\rho} = \det\left(\frac{\partial x_i}{\partial a_j}\right) \equiv \frac{\partial(x_1, x_2, x_3)}{\partial(a_1, a_2, a_3)}. \tag{11.24}$$

The equation of motion of the system, if we ignore body forces, is

$$\rho \ddot{x}_i = \frac{\partial T_{ji}}{\partial x_j}. \tag{11.25}$$

A change in the internal energy of a solid is given by the thermodynamic relation

$$dU = TdS + \frac{1}{\rho_0} t_{ij} d\xi_{ij} \tag{11.26}$$

where T is the temperature, S the entropy per unit mass, and t_{ij} the thermodynamic tension, given by

$$t_{ij} = \rho_0 \left(\frac{\partial U}{\partial \epsilon_{ij}}\right)_s. \tag{11.27}$$

Then quantity t_{ij} is related to the stress T_{ij} by

$$T_{ij} = \frac{\rho}{\rho_0}\frac{\partial x_i}{\partial a_k}\frac{\partial x_j}{\partial a_m} t_{km}. \tag{11.28}$$

11.4 Third Order Elastic Constants.

We are now in a position to generalize the relation between the internal energy of a system and the strains ϵ_{ij}. We expand the internal energy $U(S,\xi)$ about the point of zero strain $\epsilon = 0$ in the isentropic case:

$$\rho_0 U(S,\xi) - \rho_0 U(S,0) = \frac{1}{2!} c_{ijk\ell}\epsilon_{ij}\epsilon_{k\ell} + \frac{1}{3!} c_{ijk\ell mn}\epsilon_{ij}\epsilon_{k\ell}\epsilon_{mn} + \cdots \tag{11.29}$$

where the nth order ($n \geq 2$) isentropic elastic constants are defined by

$$c^S_{ijk\ell\ldots} = \rho_0 \left(\frac{\partial^n U}{\partial\epsilon_{ij}\partial\epsilon_{k\ell\ldots}}\right)_S . \tag{11.30}$$

In cases where Hooke's law is valid, only the first term on the right hand side of Eq. (11.29) differs from zero, and the left hand side becomes the elastic potential energy.

Because of inherent symmetries in crystal systems, it is possible to simplify the subscripts on the elastic constants. In this reduction of the multiplicity of the first four subscripts on the $c^S_{ijk\ell mn\ldots}$, we condense them unambiguously according to the following scheme:

$$\begin{array}{ll} 11 \rightarrow 1 & 23 \rightarrow 4 \\ 22 \rightarrow 2 & 13 \rightarrow 5 \\ 33 \rightarrow 3 & 12 \rightarrow 6 \end{array} \tag{11.31}$$

(In the case of an elastic crystal, this reflects the fact that the most general crystalline form has 21 elastic constants rather than 81). Then, for example, we have

$$\begin{aligned} c^S_{111111} \equiv C_{111} &= \rho_0 \frac{\partial^3 U}{\partial\epsilon_{11}^3} \\ c^S_{112323} \equiv C_{144} &= \rho_0 \frac{\partial^3 U}{\partial\epsilon_{11}\partial\epsilon_{23}^2} . \end{aligned} \tag{11.32}$$

The term "third-order elastic constant" is rather self-contradictory, since the original connotation of an elastic body was that it obeyed Hooke's law, i.e., that all the higher order constants $c^S_{ijk\ell mn\ldots}$ vanished. However, here, as is often the case in physics, the concept has been generalized along with the equation.

A cubic crystal has three independent second-order elastic constants. In the reduced notation, they are c_{11}, c_{12}, c_{44}. For the third-order constants, symmetry rules again restrict the number, this time to six, as follows

$$\begin{aligned} &C_{111} = C_{222} = C_{333} \\ &C_{114} = C_{255} = C_{366} \\ &C_{112} = C_{223} = C_{133} = C_{122} = C_{233} = C_{113} \\ &C_{155} = C_{244} = C_{344} = C_{166} = C_{266} = C_{355} \\ &C_{123} \\ &C_{456} \end{aligned} \tag{11.33}$$

all others being zero.

For an isotropic medium, the third-order constants have the same representation as a cubic crystal, with the additional relationships

$$\begin{aligned} C_{112} &= C_{123} + 2C_{144} \\ C_{155} &= C_{144} + 2C_{456} \\ C_{111} &= C_{123} + 2C_{144} + 8C_{456}. \end{aligned} \tag{11.34}$$

Thus, an isotropic medium, which has two independent second-order constants [c_{11} and $c_{44} = (1/2)(c_{11} - c_{12})$], has three independent third-order constants.

By means of this scheme, the elastic energy Eq. (11.30) for an isotropic solid is found to be

$$\begin{aligned} \rho_0 U(S,\xi) - \rho_0 U(S,0) = {} & \frac{1}{2} c_{12} \epsilon_{ii} \epsilon_{jj} + c_{44} \epsilon_{ij} \epsilon_{kj} + \frac{1}{6} C_{123} \epsilon_{jj} \epsilon_{kk} \\ & + C_{144} \epsilon_{jj} \epsilon_{jk} \epsilon_{ik} + \frac{4}{3} C_{456} \epsilon_{ik} \epsilon_{ij} \epsilon_{kj} \\ & + \text{higher order terms.} \end{aligned} \tag{11.35}$$

The corresponding expressions for anisotropic crystals are considerably more complicated.

11.5 Ultrasonic Determination of Third Order Elastic Constants.

Third-order elastic constants of crystals can be found by measuring the change in the sound velocity caused by the application of hydrostatic pressure or uniaxial stress. [5] The appropriate relationships for cubic crystals are given in Table 11.1. These give 17 different relationships directions when the solid is undergoing either hydrostatic pressure or uniaxial compression along the [001] or [110] directions. Fourteen of these velocities (6-8 excepted) can be measured with a single sample cut with [001] and [110] faces exposed (Fig. 11-4). This allows several independent checks on the values of the elastic constants. Usually the hydrostatic pressure results are given extra weight because of the relative confidence in the uniformity of the stress.

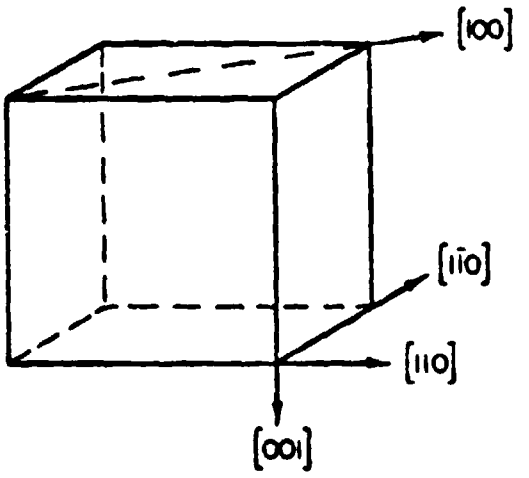

Figure 11-4.–Crystalline directions for a cubic crystal.

A system for applying uniaxial stress is shown in Fig. 11-5. A steel ball bearing is inserted to make the stress as uniform as possible. It is also helpful to reduce shear stresses at the specimen-piston interfaces by matching their mechanical properties.

Certain crystals, particularly metals, will not sustain a large stress without permanent deformation, because of dislocation motion. In this case, the third order elastic constants can be found by methods that are similar to those used for nonlinear effects in liquids (see Section 11.5). Breazeale and Ford [6] have shown that the third-order elastic constants of cubic crystals

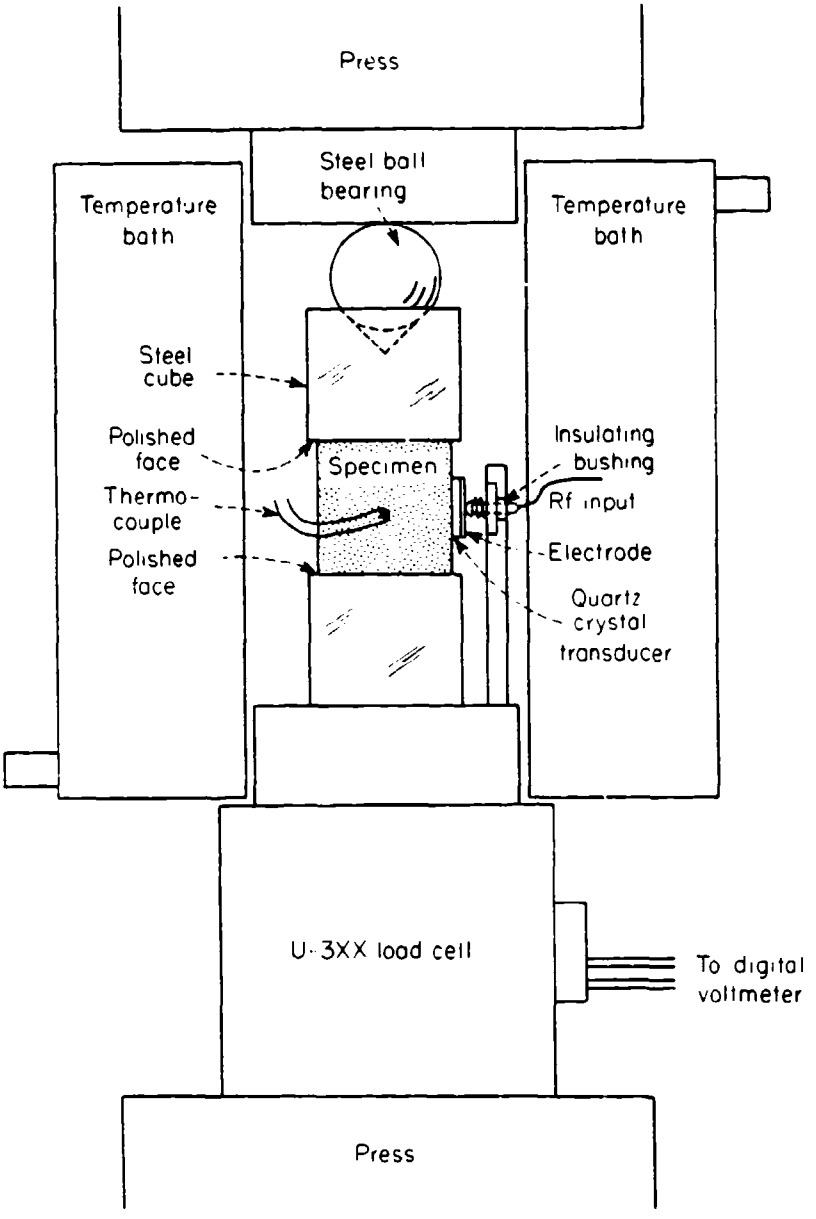

Figure 11-5.–Arrangement for uniaxial stress experiments (from McSkimin and Andreatch [5a]).

can also be obtained by measuring the discontinuity distance of finite amplitude longitudinal waves. Some measured third order elastic constants are shown in Table 11-2.

One can single out two major causes of nonlinear behavior in a crystal–the anharmonicity due to a departure of the medium from the simple linear behavior of Hooke's law and the phenomenon of dislocation displacements.

Table 11.1
Relations for third-order moduli, derived by Thurston and Brugger.[a,b]

Propagation direction	Displacement direction	$w \equiv (\rho_0 c_0^2)_{p=0}$	F_{U0}	$(\rho_0 W^2)'_{p=0}$
		A. Cubic crystals under hydrostatic pressure		
1. [100]	[100]	c_{11}^S		$-1-(2w/3B)-(1/3B)(C_{111}+2C_{112})$
2. [100]	Any ⊥ direction	c_{44}		$-1-(2w/3B)-(1/3B)(C_{144}+2C_{166})$
3. [110]	[110]	$\frac{1}{2}(c_{11}^S+c_{12}^S+2c_{44})$		$-1-(2w/3B)-(1/3B)\left(\frac{1}{2}C_{111}+2C_{112}+C_{144}+2C_{166}+\frac{1}{2}C_{123}\right)$
4. [110]	[001]	c_{44}		$-1-(2w/3B)-(1/3B)(C_{144}+2C_{166})$
5. [110]	$[1\bar{1}0]$	$\frac{1}{2}(c_{11}^S-c_{12}^S)$		$-1-(2w/3B)-(1/3B)\left(\frac{1}{2}C_{111}-\frac{1}{2}C_{123}\right)$
		$B \equiv \frac{1}{3}(s_{11}^T+2s_{12}^T)^{-1}=\frac{1}{3}(c_{11}^T+2c_{12}^T)$ = isothermal bulk modulus at $p=0$		
		B. Cubic crystals under uniaxial compression along [001]		
6. [100]	[100]	c_{11}^S	a	$2wF_{U0}+aC_{111}+C_{112}(a-b)$
7. [100]	[010]	c_{44}	a	$2wF_{U0}-bC_{144}+2aC_{166}$
8. [100]	[001]	c_{44}	$-b$	$2wF_{U0}+aC_{144}+C_{166}(a-b)$
9. $[1\bar{1}0]$	$[1\bar{1}0]$	$\frac{1}{2}(c_{11}^S+c_{12}^S+2c_{44})$	a	$2wF_{U0}+\frac{1}{2}aC_{111}+\frac{1}{2}C_{112}(3a-b)+2aC_{166}-bC_{144}-\frac{1}{2}C_{123}$
10. $[1\bar{1}0]$	[110]	$\frac{1}{2}(c_{11}^S-c_{12}^S)$	a	$2wF_{U0}+\frac{1}{2}aC_{111}-\frac{1}{2}C_{112}(a+b)+\frac{1}{2}bC_{123}$

11.	[110]	[001]	c_{44}	$-b$	$2wF_{U0} + aC_{144} + C_{166}(a-b)$

$$a \equiv -s_{12}^T = c_{12}^T/3B(c_{11}^T - c_{12}^T),\ b \equiv s_{11}^T = (c_{11}^T + c_{12}^T)/3B(c_{11}^T - c_{12}^T),\ B = \tfrac{1}{3}(c_{11}^T + 2c_{12}^T)$$

C. Cubic crystals under uniaxial compression along [110]

12.	[001]	[001]	c_{11}^S	a	$2wF_{U0} + aC_{111} + (a-b)C_{112}$
13.	[001]	[110]	c_{44}	$\frac{1}{2}(a-b-2c)$	$2wF_{U0} + \frac{1}{2}(a-b)C_{144} + \frac{1}{2}C_{166}(3a-b) - 2cC_{456}$
14.	[001]	[110]	c_{44}	$\frac{1}{2}(a-b+2c)$	$2wF_{U0} + \frac{1}{2}(a-b)C_{144} + \frac{1}{2}C_{166}(3a-b) + 2cC_{456}$
15.	$[1\bar{1}0]$	$[1\bar{1}0]$	$\frac{1}{2}(c_{11}^S + c_{12}^S + 2c_{44})$	$\frac{1}{2}(a-b+2c)$	$2wF_{U0} + \frac{1}{4}(a-b)C_{111} + \frac{1}{4}C_{112}(5a-3b) + C_{166}(a-b+4c) + aC_{144} + \frac{1}{2}aC_{123}$
16.	$[1\bar{1}0]$	[110]	$\frac{1}{2}(c_{11}^S - c_{12}^S)$	$\frac{1}{2}(a-b-2c)$	$2wF_{U0} + \frac{1}{4}(a-b)C_{111} + \frac{1}{4}C_{112}(a+b) - \frac{1}{2}aC_{123}$
17.	$[1\bar{1}0]$	[001]	c_{44}	a	$2wF_{U0} + \frac{1}{2}(a-b)C_{144} + \frac{1}{2}C_{166}(3a-b) + 2cC_{456}$

$$c = \frac{1}{4}s_{44} = 1/4c_{44}$$

[a] Thurston and Brugger [5].

[b] c_0 is the velocity of sound in the unstrained state; $(\rho_0 W^2)'$ is the stress derivative of the unstrained density and the "natural" velocity W, which is the unstrained path length divided by the acoustic time of flight under stressed conditions.

Table 11.2
Measured third-order elastic constants of some cubic crystals at room temperature[a] (from Ref. 2a)

Crystal	C_{111}	C_{112}	C_{123}	C_{144}	C_{166}	C_{456}
Ge	−7.10	−3.89	−0.18	−0.23	−2.92	−0.53
Si	−8.25	−4.51	−0.64	+0.12	−3.10	−0.64
GaAs	−6.22	−3.87	−0.57	+0.02	−2.69	−0.39
GaAs	−6.72	−4.02	−0.04	−0.70	−3.20	−0.69
InSb	−3.14	−2.10	−0.48	+0.09	−1.18	+0.002
Cu	−15.0	−8.5	−2.5	−1.35	−6.45	−0.16
Cu	−12.71	−8.14	−0.50	−0.03	−7.80	−0.95
Ge	−7.32	−2.90	−2.2	−0.08	−3.03	−0.41
Ge	−7.16	−4.03	−0.18	−0.53	−3.15	−0.47
MgO	−48 9	−0.95	−0.69	+1.13	−6.6	+1.47
NaCl	−8.3					
KCl	−7.1					
NaCl	−8.80	−0.57	0.284	0.257	−0.611	0.271
KCl	−7.01	−0.224	0.133	0.127	−0.245	0.118
BaF_2	−5.84	−2.99	−2.06	−1.21	−0.889	0.271
Approx. Accuracy	±5%	±10%	±50%	±50%	±3%	±15%

[a] All elastic constants $\times 10^{12}$ dyn/cm^2.

The first of these leads primarily to a small shift in the sound propagation velocity. The accurate measurement of this velocity therefore provides for the measurement of the third-order elastic constants.

The effect of dislocation displacements is associated with the *p* defects present in any crystal. A dislocation is a linear imperfection in a crystal, such as the edge dislocation pictured in Fig. 11-6. Such dislocations can move easily under stress within a crystal, thus facilitating the propagation of the lattice vibrations that are sound waves. The motion of the dislocations is hindered by the presence of point defects and by other dislocations. Internal stresses surrounding dislocations and point defects are both relieved by their interaction, so that they tend to attract one another, causing the dislocations to be *pinned* at certain points.

In passing through a real crystal, a sound wave will be attenuated by interaction with the dislocations. The theory for such dislocations damping is based on the concept of the motion of dislocations between the two pinning points as analogous to the motion of a vibrating string, equal in length to the distance between pinning points. The small amplitude oscillations of such dislocation loops leads to an attenuation that has been well confirmed by experiment. [7] This corresponds to the first three portions of Fig. 11-7.

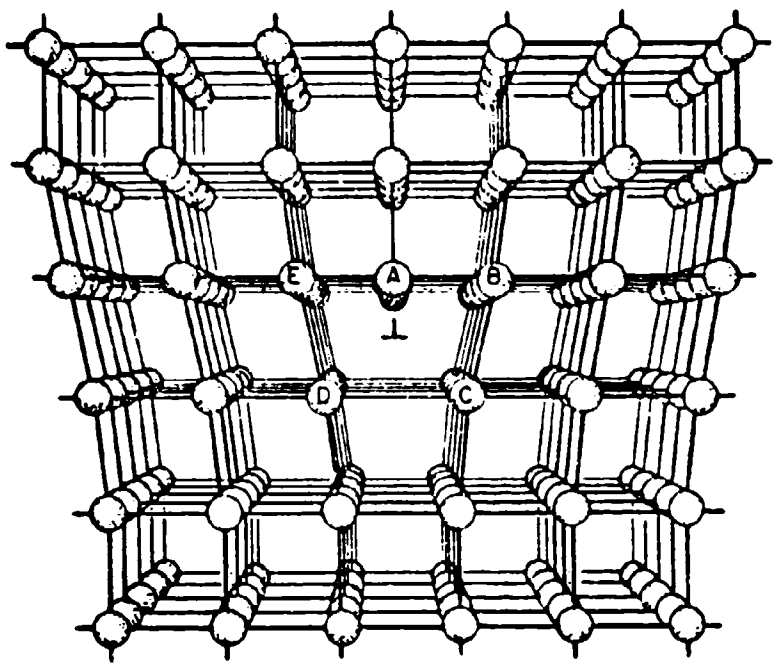

Figure 11-6.–Structure of an edge dislocation. The imperfection can be regarded as the insertion of an extra half plane of atoms in the top half of the crystal (from Kittel [3]).

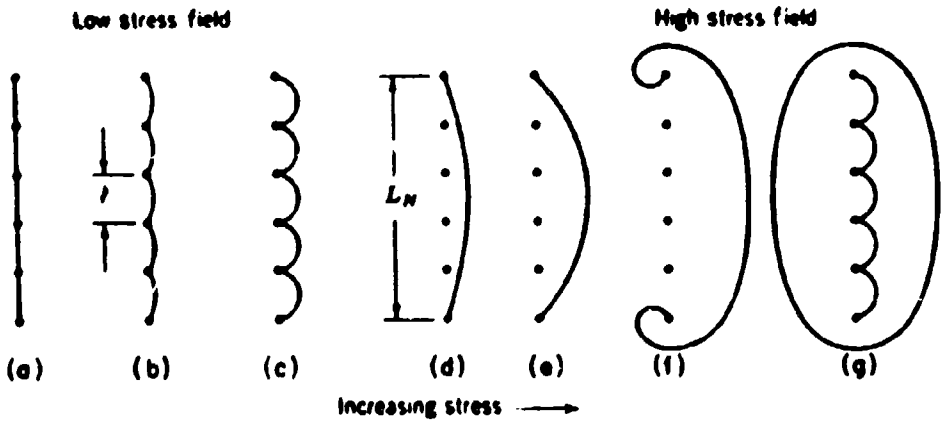

Figure 11-7.–Bowing out of a pinned dislocation line by an increasing applied stress. The loop length, determined by the impurity pinning is ℓ and the network length L_N. At (d) the stress is large enough to cause the dislocation to break away from the impurity pinning sites (from Granato and Lücke [7]).

As the amplitude of the oscillation becomes larger, however, the dislocation loop will break away from many of the pinning points, producing the bowing out shown in the latter stages of the drawing.

In these latter instances, the bowing out becomes nonlinear. An ultrasonic wave propagating through a crystal containing movable dislocations will therefore become distorted and harmonics of the fundamental frequency will be generated. This is in addition to the same effects caused by the anharmonic nature of the crystal lattice itself. By use of the vibrating string model, Hikata and Elbaum have cast the equations of motion of the dislocation into normal coordinate form. Concentrating their attention on the equation for the first coordinate ξ_0, they obtained the result

$$A\frac{\partial^2\xi_0}{\partial t^2} + B\frac{\partial\xi_0}{\partial t} + \frac{\eta^2}{\ell_0{}^2}C\xi_0 - \frac{3\pi^4}{8\ell_0{}^4}C\xi_0{}^3 - \frac{3\pi^4}{4\ell_0{}^4}\xi_0{}^3 = \frac{4}{\pi}b\sigma R. \tag{11.36}$$

In this equation, C is the line tension of the dislocation, given by the product of the shear modulus and the square of the Burgers vector $\mathbf{b}$, ℓ_0 is the equilibrium distance between pinning points, R is an orientation factor, A the effective mass of dislocation per unit length (see Ref. 2, p. 222) and B is the damping coefficient per unit length, σ = applied stress.

For small dislocations displacements, ξ will be a linear function, given approximately by

$$\xi = \xi_0 \sin\frac{\pi y}{\ell_0}. \tag{11.37}$$

Equation (11.36) can be solved by iteration. If one neglects the cubic term, one obtains the first order solution

$$\xi' = \frac{4bR\sigma_0}{\pi p} + \frac{4bRA_1}{\pi}\frac{\cos(\omega t - kx - \delta_1)}{[(-\omega^2A + p)^2 + \omega^2B^2]^{1/2}}$$

$$\delta_1 = \tan^{-1}\left[\frac{\omega B}{(-\omega^2A + p)}\right] \tag{11.38}$$

$$p = \frac{\pi^2}{\ell^2}C$$

for a driving stress $\sigma = \sigma_0 \cos(\omega t - kx)$. This value of ξ' is introduced in Eq. (11.36) and the resultant linearized equation is solved. The resulting solution is a lengthy one and will not be given here (see Ref. 2, p. 224).

The results indicate that dislocation displacements can produce second harmonics that are comparable to those resulting from lattice inharmonicity, while the corresponding contribution to the third harmonic is enormously greater. Experimental investigations of the nonlinear behavior of dislocations is therefore most conveniently carried out by use of the third harmonic. Hikata and Elbaum [8] derived the term for the third harmonic amplitude in the form

$$A_3 \propto NA_{10}^3 f_1(\ell_0) f_2(\alpha, x) \tag{11.39}$$

where N is the dislocation density, A_{10} the initial amplitude of the fundamental, $f_1(\ell_0)$ a function of the loop length and $f_2(\alpha,x)$ a function that depends on the distance x traveled by the wave and on the absorption coefficients of the fundamental and the third harmonic. Although this equation was derived for the pre-breakaway region, experiments have shown that the breakaway from point defect pinning points also contributes to third harmonic generation.

11.6 Interaction of Sound with Sound.

A theoretical study of the interaction of elastic waves in an isotropic solid has been made by Jones and Kobett. [9] The cubic terms in the particle displacements are included in the equation of motion and perturbation analysis has been carried out for the case of an initial signal consisting of two sinusoidal waves of arbitrary direction and frequency. A set of resonance conditions has been worked out for primary waves of three different types: (1) both transverse, (2) both longitudinal, and (3) one transverse and one longitudinal. Table 11.3, taken from their article, indicates the allowed contributions. Here $\mathbf{k}_1, \mathbf{k}_1, \omega_1, \omega_2$, refer to the wave vectors and frequencies of the primary waves. In each case, the resonance occurs for a sum or difference frequency propagated along a particular direction.

It is of interest to note that the combination of two longitudinal waves produces an interaction wave that is transverse. The corresponding case cannot arise for a normal fluid, which does not support a shear wave.

Such a result is consistent with our earlier discussion of the fluid case.

Experimental verifications of these results has been reported by Rollins (9a). Two pulses with frequencies between 3 and 15 MHz were applied to a hexagonal specimen of fused quartz, polycrystalline aluminum and polycrystalline magnesium. The specimen was of such a shape as to satisfy the resonant conditions of Table 11.3. Each of the five cases noted in the table has been observed experimentally.

Table 11.3
Interaction cases which produce a scattered wave.[a]

Primary waves	Resonant wave type and frequency	Direction of scattered wave	$\cos\phi$[b]	Frequency limits[c]
Two transverse	Longitudinal $(\omega_1 + \omega_2)$	$\mathbf{k}_1 + \mathbf{k}_2$	$c^2 + \frac{(c^2-1)(a^2+1)}{2a}$	$\frac{1-c}{1+c} < a < \frac{1+c}{1-c}$
Two longitudinal	Transverse $(\omega_1 - \omega_2)$	$\frac{\mathbf{k}_1 - \mathbf{k}_2}{\omega_1 - \omega_2}$	$\frac{c^2}{1} + \frac{(c^2-1)(a^2+1)}{2ac^2}$	$\frac{1-c}{1+c} < a < \frac{1+c}{1-c}$
One longitudinal and one transverse[d]	Longitudinal $(\omega_1 + \omega_2)$	$\mathbf{k}_1 + \mathbf{k}_2$	$c + \frac{a(c^2-1)}{2c}$	$0 < a < \frac{2c}{(1-c)}$
One longitudinal and one transverse[d]	Longitudinal $(\omega_1 - \omega_2)$	$\frac{\mathbf{k}_1 - \mathbf{k}_2}{\omega_1 - \omega_2}$	$c + \frac{a(1-c^2)}{2c}$	$0 < a < \frac{2c}{(1+c)}$
One longitudinal and one transverse[d]	Transverse $(\omega_1 - \omega_2)$	$\frac{\mathbf{k}_1 - \mathbf{k}_2}{\omega_1 - \omega_2}$	$\frac{1}{c} + \frac{(c^2-1)}{2ac}$	$\frac{1-c}{2} < a < \frac{1+c}{2}$

[a] From Jones and Kobett [9].
[b] ϕ is the angle between $\mathbf{k}_1$ and $\mathbf{k}_2$ at resonance; a is the frequency ratio ω_2/ω_2; c is velocity ratio c_{tr}/c_{long}.
[c] When a is within the limits shown, it is possible to choose an angle ϕ that will give a scattered wave.
[d] The frequency of the longitudinal primary wave is ω_1.

11.7 Nonlinear Surface Waves.

The simple phenomenon of surface waves, described in Chapter 1, has recently been widely exploited in signal processing. [10,11,12] The first surface wave transducer using interdigital electrodes was developed by White and Voltmer. [13]

In a typical arrangement, [Fig. (11-8)] metallic "fingers" are deposited on a piezo-electric substrate by photolithographic techniques. For a 100-MHz transducer, for example, the aluminum fingers would be 0.2 x 9 microns. The fingers are spaced a half wavelength apart. If the rf voltage is between one set of fingers, Rayleigh waves will be excited on the surface, traveling at a velocity given approximately by (recall Sec. 1.10)

$$c_R = \left(\frac{0.87 + 1.12\nu}{1 + \nu}\right) c_S \tag{11.40}$$

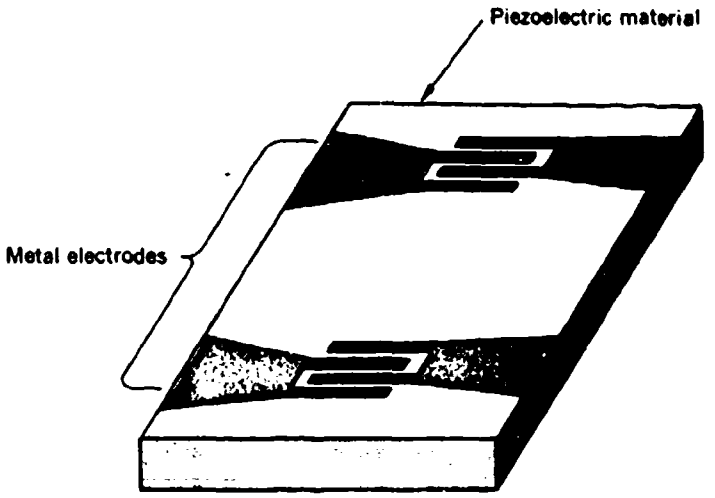

Figure 11-8.–Schematic representation of a typical piezoelectric device with interdigital electrodes ("fingers") (from Kino and Matthews [11]).

where ν is the Poisson ratio and c_S the shear velocity in the bulk medium. When these waves reach the second group of fingers, an rf signal will be detected.

The first use of such a circuit was in delay lines. By varying the numbers and spacing of the electrodes, various pulse compression and phase coding techniques have also been developed.

The velocity expression (11.40) is of course based on linear elasticity theory. When the strain exceeds $10^{-5} - 10^{-4}$, nonlinear effects appear, similar to those described for bulk waves in solids.

In 1970, Lean and Tseng [14] developed a phenomenological theory for the generation of harmonics of surface waves, using the method of coupled amplitude equations, taking losses into account. If A_i is the (complex) amplitude of the ith harmonic and α_i the corresponding absorption coefficient, these equations take the form

$$\frac{dA_i}{dZ} = \Gamma_{ijl} A_j A_l - \Gamma_{imn} A_m A_n^* + \alpha_i A_i \tag{11.41}$$

$$\text{for } i = j + l \qquad i, j, l, m, n = 1,2,3\ldots .$$

$$i = m - n$$

The asterisk denoted the complex conjugate. The nonlinear coefficients are related to the wavenumber. If dispersion effects can be neglected, then

$$\Gamma_{ij\ell} = \gamma_{ij\ell} k_j k_\ell$$
$$\Gamma_{imn} = \gamma_{imn} k_m k_n \tag{11.42}$$

where the γ's are analogs of the Grüneisen constant.

In their theory, Lean and Tseng assumed that a single γ would suffice and obtained the value experimentally. As a refinement, adjustments were made to fit the individual experimental curve. As a result, a set of ∂'s ranging from 0.81 to 5.20 were obtained. The comparison of theory and experiment for a specific case is shown in Fig. 11-9.

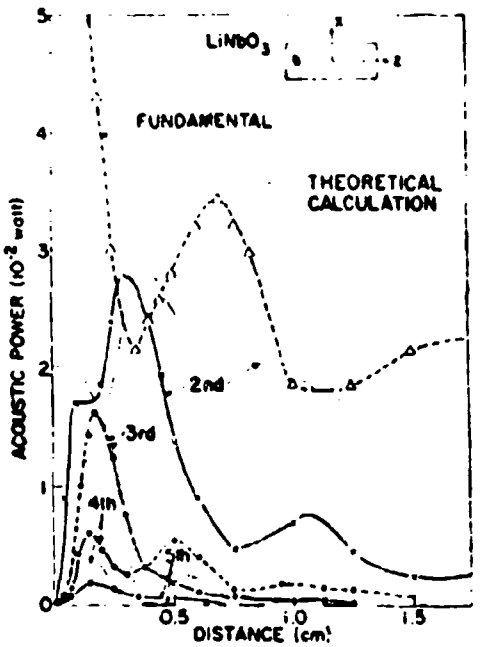

Figure 11-9.–Experimental results of Rayleigh-wave harmonic generation on a *YZ Li bO*$_3$ substrate as a function of interaction length. The fundamental frequency is 615 MHz. Also shown are the theoretical calculations based on coupled amplitude equations (from Lean and Tseng [14]).

Just as in the cases of fluids and bulk waves in solids, nonlinear mixing of finite amplitude waves can take place. Typical experimental schemes are

shown in Fig. 11-10. [15] Two pulses of center frequency ω_1, ω_2 travel in opposite directions along the surface. The nonlinearity will produce a combination wave with frequency $\omega_3 = \omega_1 + \omega_2$ and wave number $\mathbf{k}_5 = \mathbf{k}_1 + \mathbf{k}_2$. Since the spacing of the electrodes is based on the relation $k_3 \ell = 2\pi$, the "pitch" of the figure must necessarily be relatively coarse (see Fig. 11-10b). If the two primary frequencies are identical, so that $k_3 = 0$, $\omega_3 = 2\omega$, two continuous metal films, one on each side of the acoustic substrate, are used (Fig. 11-10a).

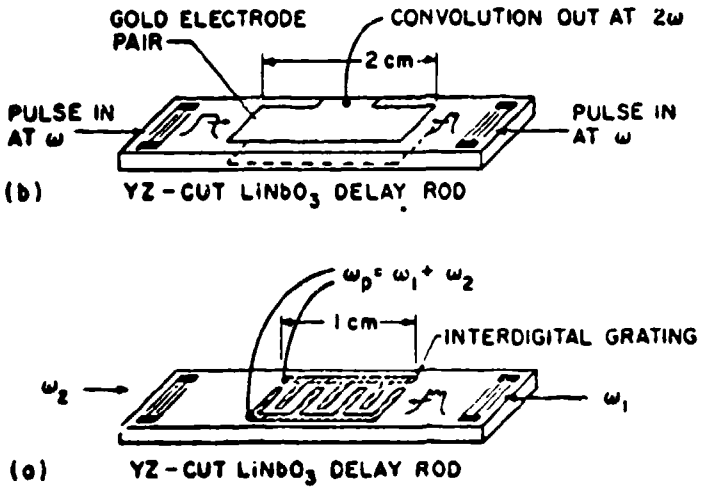

Figure 11-10.–The two different electrode configuration referred to in the text (from Luukkala and Kino [15]).

Quate and Thompson [16] have obtained the convolution of two modulated rf signals through an application of this technique. If two are modulated in the form

$$F(t)\cos\omega_1 t,\ G(t)\cos\omega_2 t$$

and passed in opposite directions in the arrangement of Fig. 11-10b, with the pickup signal driving a microwave cavity resonator, the output signal will be proportional to the convolution integral

$$K(t) = \int_{-\infty}^{\infty} F(\tau)G(2t-\tau)\,dt. \tag{11.43}$$

The correlation function can also be obtained from the relations above if one of the two signals is inverted in time. This has been done by applying an input signal to the left transducer in Fig. 11-10b, and a spike to the central

transducer. The output is then the time inversion of the original signal and can be used without a convolution step to obtain the correlation function. A sketch of the time inversion step and a set of oscilloscope traces are shown in Fig. 11-11.

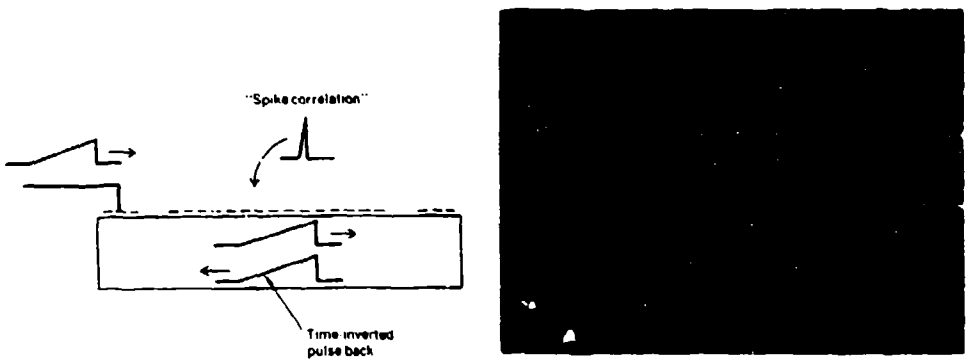

Figure 11-11.–Time inversion step (a) and oscilloscope trace of stop (b) in surface wave circuitry (from Kino and Matthews [11]).

REFERENCES

Chapter 11

1. H. Maris and R. T. Beyer, Physics Today **23**, 19 (February, 1970).
2. R. Truell, C. Elbaum and B. B. Chick, *Ultrasonic Methods in Solid State Physics*, Academic Press, New York, 1969.

2a. Much of this review is taken from R. T. Beyer and S. V. Letcher, *Physical Ultrasonics*, Academic Press, New York, 1969.

3. e.g., A. J. Dekker, *Solid State Physics*, Prentice-Hall, Englewood Cliffs, New Jersey, 1957; C. Kittel, *Introduction to Solid State Physics*, 3rd ed, Wiley, New York, 1966; R. A. Levy, *Principles of Solid State Physics*, Academic Press, New York, 1968.
4. K. Brugger and T. C. Fritz, Phys. Rev. **157**, 524 (1967).
5. R. N. Thurston and K. Brugger, Phys. Rev. **133A**, 1604 (1964).

5a. H. J. McSkimin and P. Andreatch, Jr., J. Appl. Phys. **35**, 3312 (1964).

6. M. A. Breazeale and J. Ford, J. Appl. Phys. **36**, 3486 (1965).
7. A. V. Granato and K. Lücke, J. Appl. Phys. **27**, 583 (1956).
8. A. Hikata and C. Elbaum, Phys. Rev. **144**, 469 (1966). See also A. Hikata, F. A. Sewell, Jr. and C. Elbaum, Phys. Rev. **151**, 442 (1966).

9. G. L. Jones and D. R. Kobett, JASA 35, 5 (1963).
9a. F.R. Rollins, Jr., Appl. Phys. Lett. 2, 47 (1963); JASA 35, 799 (1963).
10. R. M. White, Proc. IEEE 58, 1238 (1970).
11. G. S. Kino and H. Matthews, Spectrum 8, 22 (August, 1971).
12. J. de Klerk, Physics Today 25, 32 (November, 1972).
13. R. M. White and F. W. Voltmer, Appl. Phys. Lett. 7, 314 (1965).
14. E. G. Lean and C. C. Tseng, J. Appl. Phys. 41, 3912 (1970).
15. M. Luukkala and G. S. Kino, Appl. Phys. Lett. 18, 393 (1971).
16. C. F. Quate and R. B. Thompson, Appl. Phys. Lett. 16, 404 (1970).

AUTHOR INDEX

SUBJECT INDEX

© U. S. GOVERNMENT PRINTING OFFICE : 1975 O - 596-215